Vol. 200 No. 1, September 1, 1987
Complete in one issue

ISSN 0003-2670

ANALYTICA CHIMICA ACTA

International journal devoted to all branches of analytical chemistry

200

ELSEVIER

ANALYTICA CHIMICA ACTA

International journal devoted to all branches of analytical chemistry
Revue internationale consacrée à tous les domaines de la chimie analytique
Internationale Zeitschrift für alle Gebiete der analytischen Chemie

PUBLICATION SCHEDULE FOR 1987

	J	F	M	A	M	J	J	A	S	O	N	D
Analytica Chimica Acta	192	193	194	195	196	197	198	199	200/1 200/2	201	202	203/1 203/2

Scope. *Analytica Chimica Acta* publishes original papers, short communications, and reviews dealing with every aspect of modern chemical analysis both fundamental and applied.

Submission of Papers. Manuscripts (three copies) should be submitted as designated below for rapid and efficient handling:

Papers from the Americas to: Professor Harry L. Pardue, Department of Chemistry, Purdue University, West Lafayette, IN 47907, U.S.A.

Papers from all other countries to: Dr. A. M. G. Macdonald, Department of Chemistry, The University, P.O. Box 363, Birmingham B15 2TT, England. Papers dealing particularly with computer techniques to: Professor J. T. Clerc, Universität Bern, Pharmazeutisches Institut, Baltzerstrasse 5, CH-3012 Bern, Switzerland.

Submission of an article is understood to imply that the article is original and unpublished and is not being considered for publication elsewhere. Papers in English, French and German are published. There are no page charges. Manuscripts should conform in layout and style to the papers published in this Volume. See inside back cover for "Information for Authors".

Reprints. Fifty reprints will be supplied free of charge. Additional reprints (minimum 100) can be ordered. An order form containing price quotations will be sent to the authors together with the proofs of their article.

Publication. *Analytica Chimica Acta* appears in 12 volumes in 1987. The subscription for 1987 (Vols. 192–203) is Dfl. 2700.00 plus Dfl. 300.00 (p.p.h.) (total approx. US $1463.40). All earlier volumes (Vols. 1–191) except Vols. 23 and 28 are available at Dfl. 243.00 (US $118.50), plus Dfl. 18.00 (US $8.80) p.p.h., per volume.

Our p.p.h. (postage, packing and handling) charge includes surface delivery of all issues, except to subscribers in the U.S.A., Canada, Australia, New Zealand, P.R. China, India, Israel, South Africa, Malaysia, Thailand, Singapore, South Korea, Taiwan, Pakistan, Hong Kong, Brazil, Argentina and Mexico, who receive all issues by air delivery (S.A.L. — Surface Air Lifted) at no extra cost. For Japan, air delivery requires 50% additional charge; for all other countries airmail and S.A.L. charges are available upon request.

Subscription. Subscription should be sent to: Elsevier Science Publishers B.V., Journals Department, P.O. Box 211, 1000 AE Amsterdam, The Netherlands. Tel: 5803 911, Telex: 18582, to which requests for sample copies can also be sent. Claims for issues not received should be made within three months of publication of the issues. If not they cannot be honoured free of charge.

Readers in the U.S.A. and Canada can contact the following address: Elsevier Science Publishing Co. Inc., Journal Information Center, 52 Vanderbilt Avenue, New York, NY 10017, U.S.A., Tel: (212) 916-1250, for further information, or a free sample copy of this or any other Elsevier Science Publishers journal.

Advertisements. Advertisement rates are available from the publisher on request.

0003-2670/87/$03.50

Printed in The Netherlands

ANALYTICA CHIMICA ACTA

International journal devoted to all branches of analytical chemistry

bstracted, Indexed in: Anal. Abstr.; Biol. Abstr.; Chem. Abstr.; Curr. Contents Phys. Chem. Earth Sci.; 'e Sci.; Index Med.; Mass Spectrom. Bull.; Sci. Citation Index; Excerpta Med.)

)L. 200 NO. 1 CELEBRATION ISSUE CONTENTS SEPTEMBER 1, 1987

(Continued overleaf)

(*Contents continued*)

ANALYTICA CHIMICA ACTA
VOL. 200 (1987)

ANALYTICA CHIMICA ACTA

International journal devoted to all branches of analytical chemistry

ELSEVIER Amsterdam–Oxford–New York–Tokyo

Anal. Chim. Acta, Vol. 200 (1987)

Editorial

The appearance of Volume 200 of Analytica Chimica Acta only ten years after Volume 100, but some forty years after the introduction of the journal, reflects the greatly expanded demand for fast reliable analytical methods in recent years. The contents of this issue mirror the changes in direction that have taken place. The traditional methods of chromatography, spectrometry and electroanalysis are still the mainstays; novel designs, chemistry and applications are constantly being reported. But now, far more attention is given to less conventional areas: to flow methods, for their speed, efficiency and versatility; to environmental analysis, particularly speciation; to applications of computers, both to get data efficiently and to make the most of the data obtained; and to process monitoring, for more economic production.

Scientific research is an impersonal discipline. In this particular issue, some biographies of the authors are included to provide a glimpse of the people behind the work reported.

The editorship of Analytica Chimica Acta has expanded in recent years, to relate more closely to the different sorts of expertise now considered essential for analytical chemists. Yet the spirit of the journal continues to be as stated by Professor Paul Wenger forty years ago: "les Analytica Chimica Acta acceuilleront tous ceux qui, de loin ou de près, travaillent au progrès de la chimie analytique moderne". We still welcome all those, from near or far, who work for the progress of modern analytical chemistry.

A. M. G. Macdonald

Analytica Chimica Acta, 200 (1987) 1—19
Elsevier Science Publishers B.V., Amsterdam — Printed in The Netherlands

CHEMICAL KINETICS WITH REAGENT DISPERSION IN SINGLE-LINE FLOW-INJECTION SYSTEMS

JAMES M. HUNGERFORD and GARY D. CHRISTIAN*
Department of Chemistry, BG-10, University of Washington, Seattle, WA 98195 (U.S.A.)
(Received 2nd April 1987)

SUMMARY

Simultaneous chemical kinetics and dispersion kinetics in single-line flow-injection manifold can be modeled by using total rate laws for dispersion and chemical reaction. The model combines a (non-equilibrium) mass-transfer rate coefficient with residence-time theory based on extended tanks-in-series. Reagent dispersion is found to play a key role in defining a zone of mixing. Double product peaks and narrow analyte peaks observed in the literature are predicted by the model. When applied to a slow chemical reaction under conditions of constant length of mixing, predicted and experimentally observed response curves agree well.

In flow-injection analysis (FIA), chemical reaction need not be complete to ensure good precision. The same is true for any kinetic method; however, the one feature of FIA which sets it apart from other kinetic methods is that incomplete reaction is always accompanied by incomplete, inhomogeneous mixing. These conditions are acceptable in FIA because the mixing patterns and mixing rates are entirely reproducible. Sample and reagent are mixed at a rate governed by the dynamics of radial mass transfer and axial dispersion. The mixing processes and the reaction time are thus easily held constant by controlling flow rate, temperature, and sample volume [1].

In this work, the kinetic aspects of FIA are examined, kinetic theories for FIA are critically reviewed and a theoretical treatment is developed for dispersion with slow chemical reaction. Predicted response curves are compared with those obtained experimentally for the permanganate oxidation of crotonic acid.

*Gary D. Christian received his B.S. degree in 1959 from the University of Oregon and his M.S. degree and Ph.D. from the University of Maryland in 1962 and 1964, respectively. He was a research analytical chemist at the Walter Reed Army Institute of Research from 1961 to 1967. He joined the University of Kentucky in 1967, and in 1972 moved to the University of Washington as professor of chemistry. Christian's research interests include electroanalytical chemistry, new ion selective electrodes, atomic spectroscopy, fluorimetry, clinical chemistry, immunochemical techniques, and flow injection analysis. He is the author of some 200 papers and has authored books on atomic absorption spectroscopy, analytical chemistry, instrumental analysis, and trace analysis, as well as an ACS shortcourse on atomic absorption spectroscopy.

0003-2670/87/$03.50

REVIEW OF KINETICS THEORY FOR FIA

Most studies of simultaneous dispersion and reaction [2—7] have considered only the dispersion of the sample [3—6]. Haagensen [2] reported a differential equation describing simultaneous chemical reaction and dispersion. While his equation was never solved, Haagensen's work represents an important step in the right direction, because it includes both sample dispersion [1] and reagent dispersion [8]. Furthermore, pseudo-first-order reaction conditions are not assumed; instead, the full, overall second-order rate law is included, modified to include dispersion of sample, reagent, and product.

Since Haagensens' work, several other interesting papers have appeared addressing chemical kinetics theory for FIA [3—7]. Painton and Mottola [4] used numerical methods to solve differential equations for convection, molecular diffusion, and pseudo-first-order reaction kinetics. They found that observed response curves could not be predicted by any single rate coefficient. However, experimental response curves could be fitted by allowing periodic variations in the rate coefficient. Painton and Mottola then postulated that these apparent variations in the pseudo-first-order rate coefficient were indicative of different dispersion processes in the leading, central, and trailing regions of the sample zone [4].

Reijn et al. [5] used a pseudo-first-order model to develop a tanks-in-series treatment of chemical kinetics in a single-bead string reactor (SBSR). For conditions of slow chemical reaction and very small injection volume, these workers obtained reasonable agreement between theory and experiment. Under these conditions, their assumption of pseudo-first-order conditions is a good approximation. However, their assumption of adequate mixing is not valid immediately after injection or when large sample volumes are used because, under either condition, much of the sample is isolated from the reagent. By definition, no reaction can occur at any point where $D = 1$ [1].

These pioneering studies have done much to expand our knowledge of simultaneous dispersion and reaction in FIA. Two of them [4, 5] assume rapid axial mixing and pseudo-first-order kinetics, while Haagensen's model [2] does not. A critical examination of the pseudo-first-order condition and the mixing process now follows.

A well known axiom of chemical engineering states that, with first-order kinetics, the yield of product is independent of the details of the mixing process [9, 10]. Implicit in this statement is the assumption that the majority of the conversion process can be described by a well-defined first-order process. In light of this, it is worthwhile to point out that first-order and pseudo-first-order reactions differ in that mixing is required in the latter. The extension from first-order to pseudo-first-order thus requires that mixing is instantaneous [5] or at least much faster than the chemical reaction. Both of these requirements are easily met in the impulse/response

experiments of chemical engineering [10], where it is assumed that the tracer is injected as an infinitesimal, delta impulse. In these engineering studies, the volume of injected tracer is so small compared to the reactor volume that an impulse is at least approximated. Under these conditions, it is reasonable to assume rapid mixing because the narrow impulse of tracer occupies a length of the reactor which is even shorter than the length of mixing.

Even if mixing is instantaneous, there is an additional requirement which must be met to allow the definition of meaningful pseudo-first-order rate coefficient: the reagent concentration must be maintained at a constant level. This requirement is easily met in homogeneous solution by using a reagent concentration far in excess of sample. In FIA, the situation is different, because the reagent is often significantly diluted by the injected sample [8]. The effective rate law will then change as a result of reagent dilution, as can be predicted from Haagensen's equation [2]. Injection of a small sample volume approximates a zero width, delta injection [1] where the sample does not displace a significant volume of reagent. This leads to minimal reagent dilution, and so the reagent dilution problem is diminished in the classic delta injection (impulse/response) experiment of chemical engineering. While all of the necessary requirements appear to be met in the engineering studies, there is no reason to assume that the same can be said of a flow-injection experiment. Differences in both scale and purpose imply that the sample-introduction process in FIA will not necessarily meet the requirements of a delta (impulse) injection. Indeed, the sample volume used in a flow-injection assay is often increased so that dilution is minimized. In this case, a delta injection will not be realized, and so the chemical kinetics occurring in the channel(s) of a flow-injection manifold are often more complex than pseudo-first-order.

Two recent theoretical treatments of kinetics in single-line flow-injection manifolds avoid the delta injection and pseudo-first-order assumptions altogether. The first, a computer simulation by Betteridge et al. [6] is based on a random-walk model. Their treatment incorporates chemical kinetics using a probabilistic approach. For this reason, their results cannot be related to a specific rate law. In the context of the present discussion, the most important aspect of their work is the flexibility of the model; the random-walk model imposes no limits on the magnitude of the sample volume. This flexibility allows simulation of important aspects of axial mixing. For example, the simulation makes the very reasonable prediction that mixing occurs first in the leading and trailing edges of the sample zone. Many other predictions of the simulation are qualitatively consistent with outside work. Most recently, Wada et al. [7] used a numerical calculation method to generate response curves for laminar flow and second-order chemical reaction in a straight tube. Like the above simulation, their model does not require that the sample volume be small. Furthermore, they considered not only dispersion of sample and product, but also dispersion of

reagent, as in the original work of Haagensen [2]. Any of the above single qualities of their model [7] are important. In combination they are a powerful reminder of two basic differences between purely physical models of dispersion and a chemically reacting system. In physical dispersion the carrier fluid is no more than a medium for conveying and dispersing the solute, while in a chemically reacting system the carrier is often reactive, and so the state of mixing between sample and carrier solutions is crucial. Furthermore, because chemical reaction is a dynamic process, the rate of mixing is also important. Because their model includes the full second-order rate law and because changes in reagent concentration were included in the dispersion calculations, their treatment automatically includes both of these important aspects of flow-injection kinetics. While it is somewhat less obvious, the same can be said of the random-walk simulation [6].

Kinetic dispersion

Mixing by dispersion is a kinetic process. Early in the development of FIA, the research groups of Mottola [11, 12] and Růžička and Hansen [13] were aware of analogies between mixing in FIA and kinetic processes. Later, Pardue and Fields [14, 15] strongly suggested a kinetic approach to axial dispersion, and applied their model to flow-injection systems which use gradient chambers. Pardue and Jager [16] continued to stress dispersion kinetics.

Physical dispersion dynamics in a reactor can be described by combining empirically determined or theoretically derived mass-transfer terms with theories of residence-time distribution such as the tanks-in-series model. The rationale behind this approach is the following: the peak shape, or exit age distribution, is the result of both residence time and a redistribution process [10]. The constant length of mixing required in the tanks-in-series model and chromatographic plate theory [17] is itself a reflection of a radial mass transfer rate. To yield a constant length of mixing, the rate of radial mass transfer must be sufficiently rapid, on the time scale of the experiment, to randomize the solute distribution. The following discussion will show that this link between radial mass-transfer rate and mixing length in the tanks-in-series residence time model is the same link that exists between the non-equilibrium [18] and plate theories of chromatography.

Mass-transfer rate

A kinetic description of dispersion based on mixing rates will benefit from a parameter which characterizes the mass transfer dynamics in a flow-injection reactor. In the work of Reijn et al. [5], a tanks-in-series, dispersion mass balance was written using an a term which was defined as the reciprocal of the residence time for an individual tank. Their approach has several implications. Primarily, back-transformation of their Laplace-domain equations to give chi-square functions [5] requires (by definition [19]) the Gamma function, and so the Gamma function extension [10] to the tanks-

in-series model must be used. Nauman and Buffham [10] have pointed out that the Gamma function extension removes the interpretation of the model as a series of discrete mixing stages. This change in interpretation imposes no serious limitations, because the tanks-in-series model by itself is not physically meaningful; it does not specify a mechanism of dispersion. The tanks are only a convenient means of relating differences in axial dispersion to particle residence time. Empirically, this is done by measuring the residence time and peak width to determine the number of tanks (N), the mixing length or plate height (H) or by measuring a, as defined below and by Reijn et al. [5]. Theoretical approaches to bridging the gap between dispersion and residence time require theories relating mass-transfer dynamics and flow [18].

A survey of the literature shows that a can be defined in the following ways:

$$a = 1/t_i = q/V_i = U_{ave}/H = N/t_R \tag{1}$$

where q and U_{ave} are the volumetric flow rate and the average linear velocity, respectively, V_i is the individual tank volume [10], t_i is the individual tank residence time [10] or tank time constant [5], and t_R is the sum of all t_i [5]. Equation 1 indicates a striking similarity between t_i, and Giddings' [18] mass-transfer term, C:

$$C = H_{chrom}/U_{ave} \tag{2}$$

$$t_i = H/U_{ave} = a^{-1} \tag{3}$$

where H_{chrom} is the chromatographic plate height [17, 18].

Equations 2 and 3 recall well-known similarities between residence time theory based on tanks-in-series and plate theory [18]. This parallelism is revisited here only to shed further light on dispersion dynamics in FIA and to better understand the a term. The C term that describes mass transfer in the mobile phase of an open tubular chromatography column is [18]:

$$C_m = (1/24)(6r^2 - 16r + 11) R^2/D_m \tag{4}$$

where the m subscript refers to the mobile phase, r is the fraction of solute in the mobile phase, R is the column radius, and D_m is the solute diffusion coefficient in the mobile phase. In FIA, no partition occurs, and so $H_{chrom} = H$ and $r = 1$. In this case, C_m is given by

$$C_{m,1} = R^2/24D_m \tag{5}$$

where the 1 subscript indicates that $r = 1$. By combining Eqn. 3 with the (zero retention) expression for H in open capillaries [18] that includes the longitudinal diffusion term, one obtains

$$t_i = 2D_m/U_{ave}^2 + R^2/24D_m = a^{-1} \tag{6}$$

The first term in this expression accounts for longitudinal diffusion, and the second is a radial mass-transfer term. Because the first term in Eqn. 6 is

much smaller than the second, then

$$t_i = R^2/24D_m \tag{7}$$

Thus, $a = C_{m,1}^{-1}$. The constant a is now identified as a mass-transfer rate constant, just as C is a mass-transfer time constant. This means that all of the mixing characteristics of the reactor, including the reactor radius and other parameters affecting mass transfer, such as packed-bed geometry [18] or secondary flow [20], are contained in a. In the context of the tanks-in-series model, a determines N, because $N = at_R$ and t_R is fixed by other considerations, such as chemical reaction rate.

Mass transfer in FIA has two dimensions, axial and radial. Axial mass transfer in FIA is very rapid because of convection, and so the radial process is mass transfer rate-limiting. Thus, a will mainly reflect the rate of radial mass transfer in the reactor.

SINGLE-LINE FIA KINETICS

Tanks-in-series

The starting point in the tanks-in-series kinetic treatment is a mass balance for the analyte product, and reagent in the first, second, and Nth imaginary tanks [5]. Assuming an overall second-order reaction, the resulting differential equations are simply the sum of the mass transfer rate law, the chemical kinetics rate law, and the appropriate input functions. When the analyte and product have similar radial mass transfer rates, so that the radial mass-transfer rate constant (a) for product (P) and analyte (A) are identical, and when the stoichiometry for reaction of product with analyte is 1:1, the dispersing zone containing analyte and product is described by a series of total rate laws:

$$dC_{A1}(t)/dt = -a_{AP}C_{A1}(t) + a_{AP}C_A(0)I_p(t,t_0,\mu) - k_2C_{A1}(t)C_{R1}(t) \tag{8}$$

$$dC_{A2}(t)/dt = -a_{AP}C_{A2}(t) + a_{AP}C_{A1}(t) - k_2C_{A2}(t)C_{R2}(t) \tag{9}$$

$$dC_{AN}(t)/dt = -a_{AP}C_{AN}(t) + a_{AP}C_{AN-1}(t) - k_2C_{AN}(t)C_{RN}(t) \tag{10}$$

$$dC_{P1}(t)/dt = -a_{AP}C_{P1}(t) + k_2C_{A1}(t)C_{R1}(t) \tag{11}$$

$$dC_{P2}(t)/dt = a_{AP}C_{P1}(t) - a_{AP}C_{P2}(t) + k_2C_{A2}(t)C_{R2}(t) \tag{12}$$

$$dC_{PN}(t)/dt = a_{AP}C_{PN-1}(t) - a_{AP}C_{PN}(t) + k_2C_{AN}(t)C_{RN}(t) \tag{13}$$

where a_{AP} is the mass-transfer rate constant (in s^{-1}) for analyte and/or product. Other terms are defined below.

When the reagent has similar mass-transfer properties to the analyte and product, the mass transfer and chemical kinetics for the reagent are described by

$$dC_{R1}(t)/dt = -a_R C_{R1}(t) + a_R C_R(0) I_{P,C}(t,t_0,\mu) - k_2C_{A1}(t)C_{R1}(t) \tag{14}$$

$$dC_{R2}(t)/dt = -a_R C_{R2}(t) + a_R C_{R1}(t) - k_2C_{A2}(t)C_{R2}(t) \tag{15}$$

$$dC_{RN}(t)/dt = -a_R C_{RN}(t) + a_R C_{RN-1}(t) - k_2 C_{AN}(t) C_{RN}(t) \quad (16)$$

where a_R is the reagent mass-transfer rate constant in s^{-1}, and $C_{Ai}(t)$, $C_{Pi}(t)$, and $C_{Ri}(t)$ denote molar concentrations, at time t, in the ith tank, of analyte, product, and reagent, respectively; $C_A(0)$ is the concentration of analyte injected, $C_R(0)$ is the reagent concentration pumped into the channel, k_2 is the second-order rate constant in l mol^{-1} s^{-1}, and $I_P(t, t_0, \mu)$ is the injection (pulse) function [19] for injection of a sample slug with a time width of μ seconds, at injection time t_0 and $I_{P,C}(t, t_0, \mu)$ is the pulse-function complement, which accounts for the vacancy in the reagent stream caused by sample injection. These input functions are illustrated and related to manifold and solution conditions in Fig. 1 (note that β here is identical to α in [5]). The Laplace transforms of the pulse function and pulse-function complement are

$$\begin{aligned} I_P(s, t_0, \mu) &= \{\exp(-t_0)[1 - \exp(-\mu s)]\}/s \\ I_{P,C}(s, t_0, \mu) &= \{1 - \exp(-t_0)[1 - \exp(-\mu s)]\}/s \end{aligned} \quad (17)$$

where s is the Laplace variable. The pulse function is used in place of the usual plug injection function [5, 21] so that the reagent concentration is defined upstream of the injector. By summing Eqn. 8 with 11, Eqn. 9 with 12, and Eqn. 10 with 13, a set of equations is obtained for the sum of $dC_{Ai}(t)/dt$ and $dC_{Pi}(t)/dt$ in any tank, i. After their Laplace transforms have been taken, the resulting algebraic equations are then solved to yield

$$C_{AN}(s) + C_{PN}(s) = C_A(0) a_{AP}^N \exp(-t_0 s)(1 - \exp(-\mu s)/s(s + a_{AP})^N) \quad (18)$$

where $C_{AN}(s)$ and $C_{PN}(s)$ are the Laplace transforms of the analyte and product concentrations, respectively. This function defines the dispersing zone composed of analyte and product. Note that this function is independent of reaction rate; this is because, at 1:1 product/analyte stoichiometry, each analyte molecule consumed by reaction is replaced by a product molecule, and because their a values are assumed identical, the dispersion process does not distinguish between analyte and product.

Because Eqn. 18 is easily back-transformed, the time-domain product-formation curve, $C_{PN}(t)$, can be solved from knowledge of either $C_{AN}(s)$ or $C_{AN}(t)$. Inspection of Eqn. 10 reveals that neither can be solved without knowledge of $C_{RN}(t)$.

Equations 14—16 can be simplified by assuming that $k_2 C_{Ai}(t)$ is much smaller than a_R. This requirement is easily met for slow reactions (small k_2), low concentrations of analyte, or systems with very rapid radial mass transport of reagent (large a_R). In effect, this means that the most significant changes in reagent concentration must be caused by dispersion of reagent rather than by consumption of reagent. If these conditions are satisfied, the chemical kinetic terms in Eqns. 14—16 can then be dropped. The boundary conditions for the reagent stream require that, at time $t = 0$, each tank has reagent concentration $C_R(0)$. On applying the boundary conditions, dropping the chemical kinetic terms, and taking the Laplace trans-

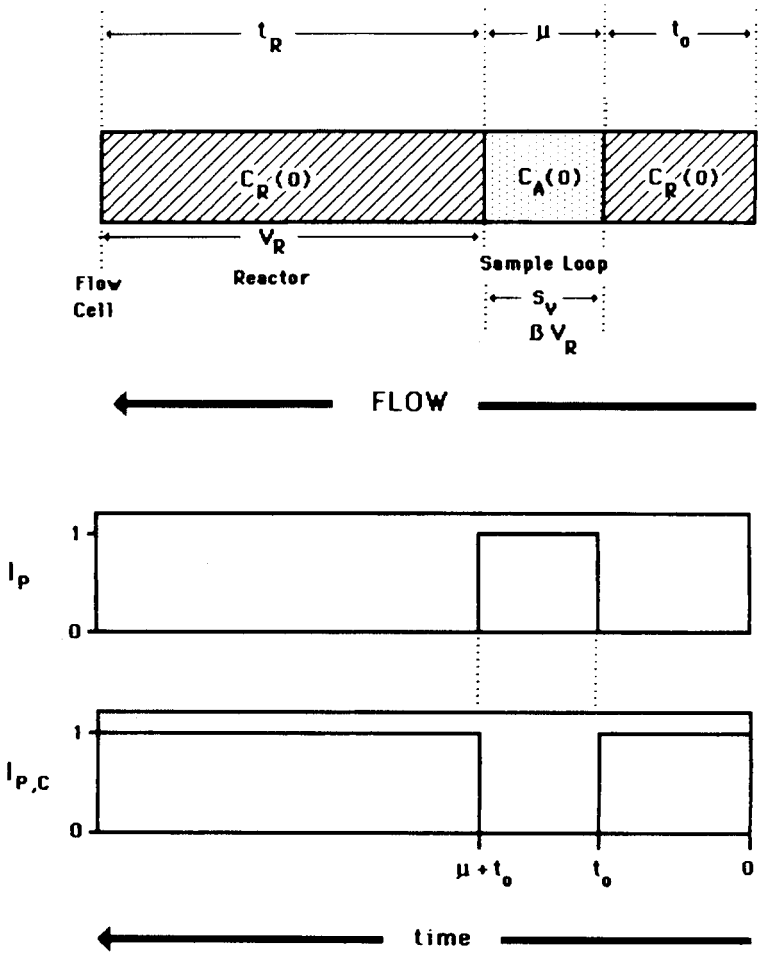

Fig. 1. Illustration of pulse and pulse-complement input functions. The injection parameter (β) is the sample volume, S_V, divided by the reactor volume, V_R. The injection time, μ, is the time analog of S_V, while t_0 is the time at injection. Other parameters are defined in the text.

forms, a set of geometric equations is obtained:

$$(s + a_R)C_{R1}(s) = a_R C_R(0)[1 - \exp(-t_0 s)[1 - \exp(-\mu s)/s] + C_R(0)] \quad (19)$$

$$(s + a_R)C_{R2}(s) = a_R C_{R1}(s) + C_R(0) \quad (20)$$

$$(s + a_R)C_{RN}(s) = a_R C_{RN-1}(s) + C_R(0) \quad (21)$$

where C_{Ri} is the Laplace transform of the reagent concentration in tank i.

The solution of Eqns. 19—21 is straightforward:

$$C_{RN}(s) = C_R(0)\left\{ \sum_{X=0}^{N-1} [a_R^{N-x-1}/(s + a_R)^{N-x}] + a_R^N/s(s + a_R)^N \right.$$

$$\left. - a_R^N \{[\exp(-t_0 s)(1 - \exp(-\mu s))]/s(s + a_R)^N\} \right\} \quad (22)$$

where x is an integer. In the summation term, let $N - x - 1 = i$ and back-transform the result. The time domain form of the summation term now yields the normalized washout function, $W(\theta)$, for a delta injection [10]:

$$W(\theta) = \exp[-N(\theta)] \sum_{i=0}^{N-1} [N^i(\theta)^i/i!] \tag{23}$$

where θ is a dimensionless time variable [10]. Also, the second term (by applying the division by s, or integration theorem [22] of Laplace transforms) is readily shown to be the Laplace transform of the integral of the differential distribution function for a delta injection [10]. The time domain form of this function is $F(\theta)$, the residence-time distribution function [10]. The sum of $F(\theta)$ and $W(\theta)$ is, by definition, unity [10] so that the first two terms in Eqn. 22 can be replaced by $1/s$, the Laplace transform of unity [22]. Equation 22 is now written:

$$C_{RN}(s) = C_R(0)\{(1/s) - a_R^N\{\exp(-t_0)[1 - \exp(-\mu s)]\}/s(s + a_R)^N\} \tag{24}$$

The negative term following $1/s$ is back-transformed as before [5]. Briefly, the convolution, shift, and integration theorems of Laplace transformation reveal chi-square terms. The latter are approximated by error functions, assuming large N, and the $1/s$ term back-transforms as unity. Following complete back-transformation, all N terms are replaced with $a_R t_R$. The time-domain function giving the reagent concentration reads

$$C_R(t) = (C_R(0)/2)\{1 - \mathrm{erf}[(a_R/2t_R)^{1/2}(t - t_0 - t_R)] + \mathrm{erf}[(a_R/2t_R)^{1/2} (t - t_0 - \mu - t_R)]\} \tag{25}$$

Equation 25 is now substituted into Eqn. 10 and t_0 is set equal to zero. The resulting equation, and the boundary conditions that when $t = 0$, $C_A = C_A(0)$, $C_R = 0$, and when $t = \infty$, $C_A = 0$, and $C_R = C_R(0)$, strongly suggest a solution based on an exponentially modified error function. The new form of Eqn. 10 is then used directly to verify the proposed $C_{AN}(t)$ function. Because N can be eliminated by $a_{AP} t_R$, the N subscripts are dropped. In the abbreviated form, the solution is

$$C_A(t) = C_A(0) D_{AP}(a_{AP},t)^{-1} \exp[-k_2 t C_R(0) D_R(a_R,t)^{-1}] \tag{26}$$

where $D_R(a_R,t)$ and $D_{AP}(a_{AP},t)$ are functions defining reagent and analyte dispersion, respectively. These are obtained by substituting $a_{AP} t_R$ for N in the time-domain form of Eqn. 18, dividing by $C_A(0)$, and by dividing Eqn. 21 by $C_R(0)$. Both equations are then inverted:

$$D_{AP}(a_{AP},t) = \tfrac{1}{2}[\mathrm{erf}[(a_{AP}/2t_R)^{1/2}(t - t_R)] - \mathrm{erf}[(a_{AP}/2t_R)^{1/2}(t - \mu - t_R)]]^{-1} \tag{27}$$

$$D_R(a_R,t) = [1 - \tfrac{1}{2}\{\mathrm{erf}[(a_R/2t_R)^{1/2}(t - t_R)] + \mathrm{erf}[(a_R/2t_R)^{1/2}(t - \mu - t_R)]\}]^{-1} \tag{28}$$

Reagent dispersion

From Eqns. 27 and 28, it can be readily shown that if $a_{AP} = a_R = a$, then $D_R(a,t)^{-1}$ is the complement of $D_{AP}(a,t)^{-1}$. This complementary relationship between analyte and reagent dispersion has also been proposed in the literature [8].

The complementary nature of sample and reagent dispersion is not as general as has been suggested [8]. The complementary relationship collapses when the reagent and analyte have different a terms. For example, when a straight open tube is used as the reactor and Taylor-Aris dispersion predominates, Eqn. 6 predicts that a high-molecular-weight reagent such as a protein will have an a value about 100 times smaller than a low-molecular weight analyte. This wide disparity is a direct result of their different diffusion coefficients. Thus, the rate of penetration of reagent into the vacancy caused by sample injection reflects the mass-transfer properties of the reagent, while the rate of dispersion of the analyte into the reagent stream reflects the mass-transfer properties of the analyte. In some reactors, such as knotted reactors [23] and SBSRs [24], a is only a weak function of the intrinsic mass-transfer properties of the solutes. Under such conditions, the two processes will appear to be complementary but strictly speaking, only the boundary conditions and input functions of analyte and reagent dispersion are complementary in all cases.

Reversed dispersion

In order to describe the dispersion process acting on the reagent in more general terms, it is much more useful to redefine reagent dispersion as a special case of a process to be termed reversed dispersion. In the literature, the term reversed-FIA has been used to describe FIA schemes in which the reagent is injected into the sample [25]. Redistribution of the sample in reversed-FIA is caused by the same dispersion process which acts on the reagent in conventional FIA. The complementary relationship between conventional and reversed dispersion is entirely general:

$$D(a,t)_{rev}^{-1} = 1 - D(a,t)^{-1} \tag{29}$$

where $D(a,t)_{rev}$ is a dispersion coefficient or function for the reversed process, demonstrated in Fig. 2 (data adapted from Tyson [8]). The top curve, generated by injecting a dye, represents conventional dispersion. The bottom curve, showing reversed dispersion, was obtained by injecting a transparent buffer solution into a carrier stream of the same dye used to give the peak. Thus, both curves were generated using the same dye, and so each had the same a value. As predicted by the above treatment, these curves are exactly complementary. If the conventional dispersion curve at the top is folded into the reversed dispersion curve at the bottom, the peak exactly fills the trough. By using Eqn. 29, this can be explained by the following

$$\begin{aligned} C_T(t,a)_{peak} + C_T(t,a)_{trough} &= C_T(0)D(t,a)^{-1} + C_T(0)D_{rev}(t,a)^{-1} \\ &= C_T(0)D(t,a)^{-1} + C_T(0)[1 - D(t,a)^{-1}] = C_T(0) \end{aligned} \tag{30}$$

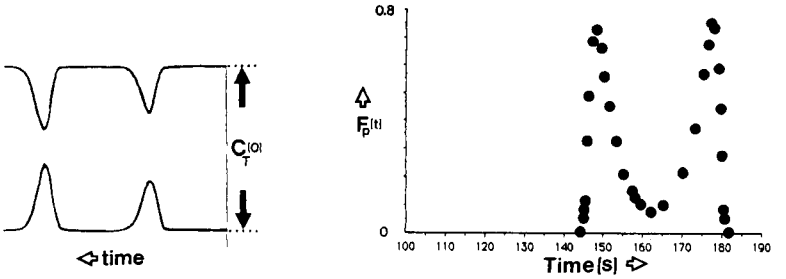

Fig. 2. Illustration of relationship between reversed and conventional dispersion. Top peaks generated by injections of tracer dye into transparent buffer; bottom troughs generated by injection of same buffer into carrier consisting of the same tracer. The tracer concentration injected is $C_T(0)$. Adapted from Tyson [8].

Fig. 3. A predicted double product peak caused by incomplete mixing. Conditions used in calculation are given in the text.

Returning to the kinetics problem, the product response function can be obtained by back-transformation of Eqn. 18 (as described by Reijn et al. [5]) followed by subtraction of Eqn. 26. Under the above conditions (identical product and analyte a values, 1:1 product/analyte stoichiometry) the product function is written:

$$C_P(t) = C_A(0)D_{AP}(a_{AP},t)^{-1}\{1-\exp[-k_2 t C_R(0)D_R(a_R,t)^{-1}]\} \quad (31)$$

The exponential term in Eqn. 31 describes the chemical kinetics of the system. This term also shows, by virtue of the reagent dispersion term, $D_R(a_R,t)$, that the chemical kinetics in a single-line flow-injection manifold are a function of dispersion kinetics. As a result, slow chemical kinetics in a single-line flow-injection manifold are not pseudo-first-order. This is because reagent dispersion prevents a constant reagent concentration from being maintained; only when the reagent dispersion term is near unity will the reaction appear to be pseudo-first-order. As is often the case in FIA, the complexity and nonlinearity of the above kinetic process does not prevent a linear response. In the calibration process, every term in Eqn. 31 except $C_A(0)$ is held constant. A dimensionless product distribution curve, or product response function, $F_P(t)$, can be defined by eliminating $C_A(0)$ from Eqn. 31:

$$F_P(t) = C_P(t)/C_A(0) = D_{AP}(a_{AP},t)^{-1}\{1-\exp[-k_2 t C_R(0)D_R(a_R,t)^{-1}]\} \quad (32)$$

The mixing zone

The system is considered to be mixed when the (no-reaction) concentrations of both reactants are non-zero. Using this definition, the reciprocal dispersion coefficients of the reactants can be used to determine which elements of solution are mixed. If either $D_{AP}(a_{AP},t)^{-1}$ or $D_R(a_R,t)^{-1}$ is zero in a solution element, then the reactants A and R are unmixed at that

time, t. Conversely, any solution element in which both A and R have non-zero reciprocal D values is mixed and will react. This definition is consistent with observed [1] and predicted [6] axial mixing behavior. Axial mixing will occur at the leading and trailing edges first because, immediately following injection, the only regions where both $D_{AP}(a_{AP},t)^{-1}$ and $D_R(a_R,t)^{-1}$ are non-zero are at the leading and trailing edges of the peak. Closer to the center, $D_R(a_R,t)^{-1}$ is zero. This "hole" in the reagent stream has a center where $D_R(a_R,t)^{-1}$ reaches a minimum value, and this defines the solution element which is last to mix. Taken together, those elements of the solution which give non-zero values of Eqn. 32 define a mixing zone, the outer borders of which are defined by the dispersed analyte where $D_{AP}(a_{AP},t)^{-1}$ goes to zero.

Double product peaks

The mixing zone is an integral part of the product formation solution given in Eqn. 32. When the sample volume is made large enough to delay or prevent axial mixing in some areas, Eqn. 32 predicts double peaks. An example of such a peak is shown in Fig. 3. The mixing zone boundaries are set by the function defining $D_{AP}(a_{AP},t)^{-1}$, and this influence dominates the rising part of the first peak and the falling portion of the second peak. The falling portion of the first peak and the rising portion of the second peak are defined by the rate of axial mixing and the rate of chemical reaction. This peak was calculated using mass-transfer and chemical-reaction conditions similar to those found in the experimental work presented below: $a_{AP} = a_R = 1.29\ s^{-1}$, $t_R = 127.7$ s, $k_2 = 232\ l\ mol^{-1}\ s^{-1}$, and $C_R(0) = 1.00 \times 10^{-4}$ M. An injection parameter (β) value of 0.40 was chosen for the purpose of illustration. Note that the double peaks have somewhat different heights; this is because the large β value (corresponding to a large sample volume) leads to significant differences in both dispersion and reaction time between the leading and trailing elements of the zone. Luque de Castro and Valcárcel [26] recently proposed the use of large injection volumes to utilize such a time delay as the basis for a novel differential kinetic assay.

Chemical kinetics

Crotonic acid (2-butenoic acid) is oxidized by permanganate ion [27] with the following stoichiometry:

$$3\ C_4H_6O_2 + 4\ MnO_4^- \rightarrow \text{Oxidation products} + 4\ MnO_2$$

In the experimental work below, a potassium permanganate solution is injected into a carrier solution of crotonic acid. For the sake of consistency with the above treatment, subscripts used in the above treatment indicate analyte and reagent are retained. Permanganate is treated as if it were the analyte, and crotonate as if it were the reagent. The permanganate/crotonate reaction is overall second-order [27], and so the rate law is consistent with Eqn. 10.

Rather than product, the analyte (permanganate) was measured. The response curves resulting from dispersion and consumption of permanganate are obtained by multiplying the concentration, $C_A(t)$, (predicted by Eqn. 26) by the cell path length and molar absorptivity. These last two factors can be eliminated by dividing Eqn. 26 by $C_A(0)$:

$$F_A(t) = C_A(t)/C_A(0) = D_{AP}(a_{AP},t)^{-1} \exp[-k_2 t\, C_R(0)\, D_R(a_R,t)^{-1}]$$
$$= A_A(t)/A_A(0) \qquad (33)$$

where $A_A(0)$ is the absorbance of the stock permanganate solution injected, and $A_A(t)$ is the permanganate absorbance measured at time t after dispersion and reaction. The dispersions $D_{AP}(a_{AP},t)$ and $D_R(a_R,t)$ terms can be predicted after determining a_{AP}, a_R, t_R, and β. In this work, crotonate is assumed to have an identical a value to permanganate, based on their similar molecular weights and charge [28], and so $a_{AP} = a_R = a$.

EXPERIMENTAL

Reagents, solutions and apparatus

All chemicals used were analytical-reagent grade. Crotonic acid was checked for purity by ^{1}H-NMR and infrared spectroscopy and used without further purification. Phosphate buffer solutions were prepared as described by Wiberg and Geer [27]. Filtration of stock potassium permanganate solutions after the experiments gave no residue, and their absorbance readings were reproducible for 1 week. Crotonic acid solutions were prepared immediately before use.

In all experiments, a single-line flow-injection manifold was used. An Ismatec peristaltic pump (8 roller, 60 rpm) was used to propel the carrier stream. The reactor was made of teflon tubing (0.50 ± 0.01 mm i.d., as measured by microscope), and for convenience was gently coiled (10-cm coil diameter). The injector was a Rheodyne 6-port Teflon valve, with all connecting tubes and sample loops removed and replaced by sections of the above tubing. Connections were made by using short sections of tight-fitting, thick-walled silicone tubing to sleeve the tubes to be joined. Teflon tubing was carefully cut at right angles to minimize dead volumes at the connections (the translucent silicone sleeve allowed visual observation of connector integrity after pumping dye through the manifold).

The stainless-steel flow cell used was from a Varian Varichrome detector. This cell has an 8-μl illuminated volume and 10-mm path length. The flow cell was mounted within a Beckman DU-7 spectrophotometer, which was used to monitor the permanganate absorbance at 525 nm with an 8-nm bandpass.

A remote (camera) shutter cable was positioned near the injector. The other end of the cable was attached to the front control panel of the spectrophotometer. In this way, data were always acquired over the same time inter-

val by allowing the injector to trigger the spectrophotometer mechanically. A series of injections showed that absorbance measurements (at fixed times) were reproducible to better than 0.3 r.s.d. using this arrangement.

Procedure

Pumping rates were calibrated volumetrically at the beginning and end of a series of experiments. First, permanganate solutions were repeatedly injected into buffer to confirm reproducibility. The reactor length chosen was 405 cm, so that conditions in the experiments were similar to those used by Painton and Mottola [4]. If the precision of these injections was 0.5% or better, response curves were then determined: 100 μl of $C_A(0) = 1.10 \times 10^{-5}$ M potassium permanganate dissolved in buffer was injected into a carrier stream composed of crotonic acid dissolved in buffer at 1.01×10^{-5}, 2.02×10^{-5}, and 1.01×10^{-4} M concentrations. The flow rate was measured volumetrically. In one experiment, the above concentration of permanganate solution was injected but the crotonate was made more concentrated (1.01×10^{-3} M) so that all permanganate was converted to product. The absorbance at peak maximum was about 5% of the peak absorbance obtained by injection of permanganate into buffer only.

Response curves were obtained and the experiments were repeated twice more. Peak arrival times were measured ($t_{max} = t_{ave}$, the peaks were highly symmetric). From the sample volume and the reactor dimensions, β was calculated (α in [5]). Together with t_{ave} from the "no reaction" peak, this allowed calculation of t_R [5]. The peak widths at 61% peak height were also measured to evaluate σ_t [29]. From the "no-reaction" σ_t value and t_R, a was evaluated [5].

Permanganate solution of concentration $C_A(0)$ was continuously pumped to measure $A_A(t)$. This was used to convert the recorded $C_A(t)$ curves to $F_A(t)$ curves, and to measure D_{max}. The $F_A(t)$ curves were then predicted by using Eqns. 19, 20, 27, a, t_R, β, $C_R(0)$, and a literature [27] value of k_2 (232 l mol^{-1} s^{-1}). A program was written using a power series [19] to expand the error function terms. Fifteen terms were sufficient to give error functions which were identical with tabulated [19] values to at least 4 significant figures.

RESULTS AND DISCUSSION

In Fig. 4A, the observed dispersion curve of permanganate is shown, along with predicted $D_{AP}(t)^{-1}$ points calculated as described above. Very good agreement between experiment and theory is clearly evident. Deviations between predicted and experimental data are strongest at the leading and trailing edges of the peak. It should be noted that this comparison of the observed and predicted peak only provides peak shape information, such as whether the peak is accurately represented as an error function (and whether

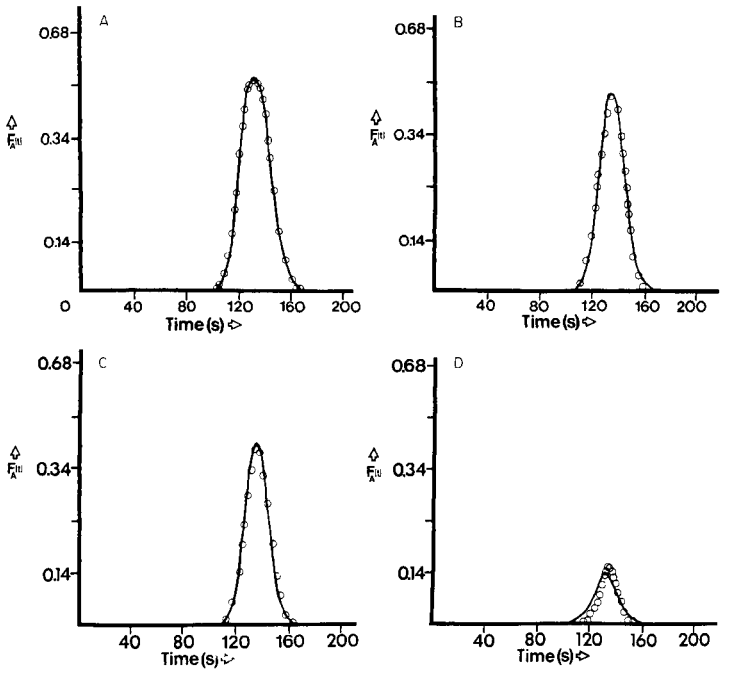

Fig. 4. Predicted and observed curves: (A) permanganate dispersion curves; (B—D) analyte response functions at $C_R(0) = 1.01 \times 10^{-5}$ M crotonate (B), $C_R(0) = 2.02 \times 10^{-5}$ M crotonate (C), and $C_R(0) = 1.01 \times 10^{-4}$ M crotonate (D). In all cases, the solid line indicates the observed peak and the theoretical curve is given by circles. Other conditions are given in the text.

$D_{AP}(t)$ can be predicted from σ_t); this is because a was determined empirically from σ_t and t_R. From the empirical a value and Eqn. 7, the apparent diffusion coefficient of permanganate ion is 3.39×10^{-5} cm^2 s^{-1}. This is substantially larger than a literature value from conductivity data (in water at infinite dilution) of 2.0×10^{-5} cm^2 s^{-1} [30]. Mild secondary flow in the gently coiled reactor could be responsible for this discrepancy in the diffusion coefficient [31].

Observed and predicted analyte response curves ($F_A(t)$, Eqn. 33) are shown in Fig. 4B—D at three crotonate (reagent) concentrations. These curves were generated for crotonate concentrations of 1.01×10^{-5} M, 2.02×10^{-5} M, and 1.01×10^{-4} M, respectively. Agreement between the observed and predicted curves is generally very good, although the observed peak in Fig. 4D is shorter and shifted forward in time from the predicted peak. This disparity may reflect the fact that the earliest stages of the mixing process, which take place at the boundaries of the sample zone [1, 6], do not occur under conditions of constant mixing length. Dispersion theory [29, 32] predicts that the solute distribution is skewed positive during these early stages, and the chemical reaction may serve as a marker of early mixing events. At the lower reagent concentrations, $C_R(0)$, used in the data for

Fig. 4B and C, the chemical reactions are so slow compared to the mixing process that the peak shape is less affected by early mixing events.

Comparison of the analyte peaks in Fig. 4B—D shows that the permanganate peak width is very sensitive to reaction rate (or to the extent of reaction). It is instructive to compare the observed and predicted peak widths from this work with values predicted by a pseudo-first-order treatment. If the second-order reaction terms given in Eqns. 8—10 are replaced by pseudo-first-order rate constants, k_1', as in work by Reijn et al. [5], the following expression for the Laplace transform of the analyte distribution is readily derived [5]:

$$C_{AN}(s) = C_T(0)\, a^N [1 - \exp(-\mu s)]/[s(s + a + k_1')^N] \quad (34)$$

In comparing peak widths (temporal standard deviations), the second moment is required, and this is readily obtained from the above equation and its zero and first moments [5, 10]. In the present notation, the second moment of Eqn. 34 is

$$\sigma_{t,A}^2 \ (\text{at } k_1') = N/(a + k_1')^2 + (N/a^2)(\beta^2/12) \quad (35)$$

The second term on the right side of Eqn. 35 is negligible compared with the other term, and so it can be dropped. By setting $k_1' = 0$, a no-reaction expression is readily obtained. Dividing the reaction second moment by the no-reaction second moment and then taking the square root yields a dimensionless term for the peak temporal standard deviation:

$$\sigma_{t,A} \ (\text{at } k_1')/\sigma_{t,A} = a/(a + k_1') \quad (36)$$

In Table 1, the pseudo-first-order predicted ratio, as calculated from Eqn. 36, is compared with the ratio predicted from curves generated by using Eqn. 33, and with the experimentally observed ratio. The experimental peak widths are accurately predicted by the present work, but not by the model assuming pseudo-first-order kinetics. Similar decreases in analyte peak width have been observed by Painton and Mottola [4]. The progressively narrower analyte distributions with faster reaction can be understood by considering the mixing process. As noted above, mixing occurs first in the leading and trailing regions of the sample zone. This differential mixing effect means that analyte in these regions will be consumed over longer reaction times than the analyte in more central parts of the zone. At the same time, these are also the regions where the analyte is least concentrated. The net result is a large relative drop in analyte concentration in these areas, and this produces narrow analyte peaks. The effect is most pronounced at higher reagent concentrations, $C_R(0)$, because the reaction is faster and so more analyte is consumed. This occurs early, in the peak leading and trailing edges, before mixing occurs all along the zone, and the analyte distribution (peak) becomes even narrower.

The narrowing in peak width cannot be explained by differences in reaction rate along the zone (even though they do exist) because this is

TABLE 1

Predicted and observed changes in analyte peak widths[a]

k_1' (s^{-1})	$[\sigma_{t,A}$ (at $k_1')/\sigma_{t,A}]$[b]		
	Predicted		Observed
	Pseudo-first-order[c]	This work	
0.00232	0.998	1.00	1.00
0.00464	0.996	0.87	0.83
0.0232	0.982	0.64	0.68

[a]With a = 1.29 s^{-1} (empirical). [b]$\sigma_{t,A}$ and $\sigma_{t,A}$ (at k_1') are the time widths (standard deviations) of sample peaks, at time t, in the absence of chemical reaction and at a given k_1', respectively. The pseudo-first-order rate coefficient (k_1') is defined here, as in [5], as $k_1' = k_2 C_R(0)$. [c]Calculated from Eqn. 36.

actually expected to decrease the above effect, since the product of the reagent and analyte concentrations [based on $D_R(t)^{-1}$ and $D_{AP}(t)^{-1}$], and thus the instantaneous reaction rate, is actually maximum at the peak center.

As shown in Fig. 5, the product curves predicted by the reagent dispersion model (Eqns. 27, 28 and 32) show distorted peak maxima at the two slowest reaction rates (curves A and B, the lowest reagent concentrations, 1.01×10^{-5} M and 2.02×10^{-5} M crotonate). This is consistent with observed response curves [33] at low dispersion ($D < 3$ [1]) where axial mixing is slow. The region corresponding to D_{max} is the last part of the sample to mix and so, when reaction is slow, less product is formed in this late-mixing region. However, when reaction is faster, product is formed rapidly enough to make up for the late mixing and a fully formed peak is predicted (as in curve C, Fig. 5).

Scaling laws

The above model predicts very favorable chemical kinetic scaling laws. Figure 6 shows predicted $F_{P,max}$ values as a function of the injection parameter (β) at three values of a from 0.76 s^{-1} to 76 s^{-1}. All other conditions are identical to those given in the text for Fig. 3. At the optimum β, all three yield about the same peak product response, but the higher a values reach their maximum response at much lower β. Because a in straight open tubes scales inversely with the square of the channel radius, the change from a = 0.76 s^{-1} to a = 76 s^{-1} corresponds to a ten-fold reduction in channel diameter. The sample volume is directly proportional to β, and so the mass sensitivity of the flow system is improved by the effect of downscaling on the chemical kinetics.

Conclusions

When chemical reaction occurs at constant mixing length, simultaneous chemical and dispersion kinetics in single-line FIA can be modeled by

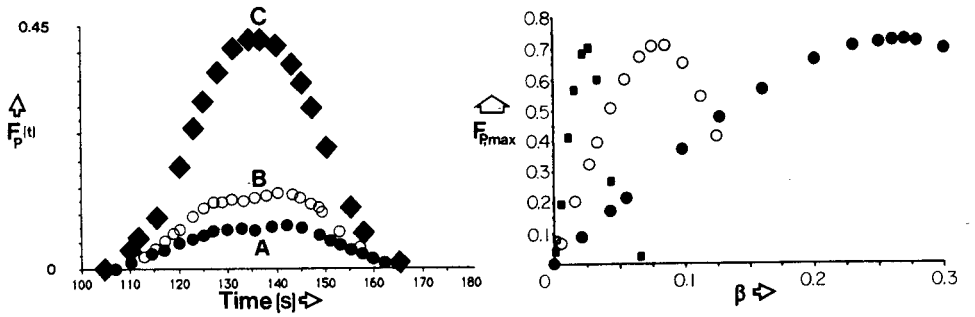

Fig. 5. Predicted product response curves at three reagent concentrations. Curve A was generated assuming $C_R(0) = 1.01 \times 10^{-5}$ M crotonate, while the B and C curves assume 2.02×10^{-5} M and 1.01×10^{-4} M crotonate, respectively. Other conditions are identical to those for Fig. 4B—D.

Fig. 6. Maximum product response, $F_{P,max}$, as a function of the injection parameter, β, at three values of a: (•) 0.76 s^{-1} ; (○) 7.6 s^{-1} ; (▪) 76 s^{-1} . Other conditions given in text. All other conditions are identical to those given for Fig. 3.

developing total rate laws for reaction and dispersion. The treatment is based on a modified tanks-in-series residence time model combined with an empirical mass-transfer term. A dynamic model of the mixing process is formulated. This is done by including the reagent concentration in the rate law, and developing a reversed dispersion concept based on the vacancy in reagent solution caused by sample injection. This treatment can explain narrow analyte peaks and double product peaks observed in the literature.

REFERENCES

1 J. Růžička and E. H. Hansen, Flow Injection Analysis, Wiley, New York, 1981.
2 P. Haagensen, unpublished work, cited in ref. 1, p. 26.
3 D. J. Hooley and R. Dessey, Anal. Chem., 55 (1983) 313.
4 C. C. Painton and H. A. Mottola, Anal. Chim. Acta, 158 (1984) 67.
5 J. M. Reijn, H. Poppe and W. E. van der Linden, Anal. Chem., 56 (1984) 943.
6 D. Betteridge, C. Z. Marczewski and A. P. Wade, Anal. Chim. Acta, 165 (1984) 227.
7 H. Wada, S. Hiraoka, A. Yuchi and G. Nakagawa, Anal. Chim. Acta, 179 (1986) 181.
8 J. F. Tyson, Anal. Chim. Acta, 179 (1986) 131.
9 J. C. Sternberg, Adv. Chromatogr., 2 (1966) 206.
10 E. B. Nauman and B. A. Buffham, Mixing in Continuous Flow Systems, Wiley-Interscience, New York, 1983.
11 H. A. Mottola and A. Hanna, Anal. Chim. Acta, 100 (1978) 167.
12 H. A. Mottola, Crit. Rev. Anal. Chem., 229 (1975) 4.
13 J. Růžička and E. H. Hansen, Anal. Chim. Acta, 99 (1978) 37.
14 H. L. Pardue and B. Fields, Anal. Chim. Acta, 124 (1981) 39.
15 H. L. Pardue and B. Fields, Anal. Chim. Acta, 124 (1981) 65.
16 H. L. Pardue and P. Jager, Anal. Chim. Acta, 179 (1986) 169.
17 A. J. P. Martin and R. L. M. Synge, Biochem. J., 35 (1941) 1358.
18 J. C. Giddings, Dynamics of Chromatography, M. Dekker, New York, 1965.
19 M. Abramowitz and I. A. Stegun, Handbook of Mathematical Functions, Dover, New York, 1963.

20 R. Tijssen, Anal. Chim. Acta, 114 (1980) 71.
21 J. C. Sternberg, Adv. Chromatogr., 2 (1966) 206.
22 M. R. Spiegel, Laplace Transforms, McGraw-Hill, New York, 1965.
23 U. Neue, Chromatographia, 15 (1981) 403.
24 J. M. Reijn, W. E. van der Linden and H. Poppe, Anal. Chim. Acta, 123 (1981) 229.
25 K. S. Johnson and R. L. Petty, Anal. Chem., 54 (1984) 1185.
26 M. D. Luque de Castro and M. Valcárcel, Trends Anal. Chem., 5 (1986) 71.
27 K. B. Wiberg and R. D. Geer, J. Am. Chem. Soc., 88 (1966) 5827.
28 A. Hines and R. N. Maddox, Mass Transfer, Prentice-Hall, Englewood Cliffs, NJ, 1984.
29 J. G. Atwood and M. J. E. Golay, J. Chromatogr., 218 (1981) 97.
30 R. Parsons, Handbook of Electrochemical Constants, Butterworths, London, 1959.
31 H. Soeberg, personal communication.
32 J. T. Vanderslice, K. K. Stewart, A. G. Rosenfeld and D. J. Higgs, Talanta, 28 (1981) 11.
33 T. D. Yerian, personal communication.

Analytica Chimica Acta, 200 (1987) 21—33
Elsevier Science Publishers B.V., Amsterdam — Printed in The Netherlands

THE TRACE DETERMINATION OF SOME HEAVY METALS IN WATERS BY FLOW-INJECTION SPECTROPHOTOMETRY AND POTENTIOMETRY

YU. A. ZOLOTOV*, L. K. SHPIGUN, I. YA. KOLOTYRKINA, E. A. NOVIKOV and O. V. BAZANOVA

Vernadsky Institute of Geochemistry and Analytical Chemistry, U.S.S.R. Academy of Sciences, Moscow 117975 (U.S.S.R.)

(Received 16th March 1987)

SUMMARY

Three automated flow-injection systems are proposed for the determination of traces of manganese(II), lead and copper(II) in waters. The first system utilizes the catalytic effect of manganese(II) on the oxidation of *N,N*-diethylaniline by potassium periodate at pH 6.86—7.10 (30°C) and is used for spectrophotometric determination at 475 nm in the range 0.02—1.00 $\mu g\ l^{-1}$; the system involves reagent injection and stopped flow. The determination of lead in the range 0.7—100 $\mu g\ l^{-1}$ is based on spectrophotometric detection of the lead 4/(2-pyridylazo)resorcinol complex at 525 nm after on-line preconcentration of the sample (5—50 ml) on a minicolumn filled with Chelex-100 or Dowex 1-X8 resin. A potentiometric flow-injection system with a copper ion-selective electrode is applied for the determination of 0.5—1000 $\mu g\ l^{-1}$ copper(II) after on-line preconcentration of 50—500 ml of sample on Chelex-100 resin. The procedures are tested on synthetic and real water samples, including sea water and waste-waters.

Rapid, sensitive and accurate methods of determining dissolved heavy metals in water are essential in environmental chemistry, geochemistry and oceanography. Recently, the concept of flow injection analysis (FIA) has been applied successfully to trace determinations of heavy metals in natural and industrial waters using various techniques [1, 2]. In most of the described flow-injection systems, low concentrations of ions (in the $\mu g\ l^{-1}$ range) such as lead, copper(II) or manganese(II) were measured with the help of electrochemical stripping analysis [3, 4], laser-induced fluorescence detection [5], inductively-coupled plasma/atomic emission spectrometry (ICP/AES) [6] or flame atomic absorption spectrometry (AAS) [7, 8] after concentration and separation of the trace metals from the interfering matrix.

*Prof. Yu. A. Zolotov is a head of laboratory for solvent extraction in the Vernadsky Institute of Geochemistry and Analytical Chemistry and a head of laboratory for preconcentration in Lomonosov Moscow State University. He is an Associate (Corresponding) member of the USSR Academy of Science. His main fields are trace analysis especially preconcentration of trace elements, solvent extraction, ion chromatography and general aspects of modern analytical chemistry.

0003-2670/87/$03.50

The importance of automatic routine analysis and monitoring of heavy metals in natural waters and industrial effluents is increasing. Therefore, FIA methods have been considered which, by using simple and inexpensive instrumentation such as a spectrophotometer or ion-selective electrode (ISE) for detection, have allowed rapid and effective automatic procedures to be developed for the determination of heavy metals at the trace level. In this context, flow-injection manifolds are described below for the determination of dissolved ionic (or weakly associated) forms of copper(II), lead and manganese(II) in various waters.

EXPERIMENTAL

Reagents, solutions and minicolumns

A manganese(II) stock solution (100 μg ml^{-1}) was prepared from 0.4384 g of $MnSO_4 \cdot 5H_2O$ dissolved in 1 l of water containing 13 ml of concentrated nitric acid. A copper stock solution (1000 μg ml^{-1}) was prepared by dissolving 3.930 g of $CuSO_4 \cdot 5H_2O$ in 1 l of water or 0.5 M nitric acid. A lead stock solution (1000 μg ml^{-1}) was prepared by dissolving 0.3312 g of $Pb(NO_3)_2$ in 1 l of water. All stock solutions were standardized by titration with EDTA. Working standard solutions of metal ions were prepared daily by appropriate dilution of the stock solutions. Mineral acids and salts were high-purity chemicals; other reagents were of analytical grade. All solutions were prepared in double-distilled/deionized water and stored in polyethylene bottles.

The packed minicolumns for on-line ion-exchange preconcentration of metals were made from silicone rubber tubing (2-mm inner diameter). A thin layer of glass wool was put at both ends of the column to prevent movement of the resin particles by the carrier stream. The first minicolumn (22 mm long, volume 69 μl) was filled with Chelex-100 chelating resin (50—100 mesh) in the NH_4^+-form. The second minicolumn (12 mm long, volume 38 μl) contained the strongly basic anion-exchange resin Dowex 1-X8 (100—200 mesh) in the OH^--form.

Apparatus

A FIAStar system 5020-003 (Tecator, Sweden) was used with a model 5023 spectrophotometer (provided with a 18-μl flow-through cell), connected to a model 5032 detector controller. Tecator Chemifolds I—III were used.

All potentiometric measurements were made with an Orion Research 811 digital pH/mV meter interfaced to a chart recorder (Linear 1200 Instruments). The copper sulfide/silver sulfide membrane electrode (Crytur, C.S.S.R.) was used in conjunction with an Orion 90-02-00 double-junction reference electrode with 10% (w/v) potassium nitrate in the outer chamber. Both electrodes were placed in a laboratory-made cascade-type potentiometric cell, similar to one described by Růžička et al. [9].

The different manifolds investigated are described in detail below for the various determinations.

RESULTS AND DISCUSSION

The determination of heavy metals at trace levels in waters requires the development of flow-injection systems with very low detection limits. In some cases, this can be achieved in conjunction with on-line metal preconcentration methods. Recent publications on FIA have reported that methods such as liquid/liquid extraction [10] and ion-exchange [11] show considerable promise for the automated determination of traces of heavy metals by flame AAS. The use of flow-injection spectrophotometry or potentiometry with an ISE in combination with ion-exchangers in the form of packed reactors in FIA has hardly been mentioned. The limit of spectrophotometric detection in such a flow-injection system is likely to be controlled by the refractive-index perturbations associated with differences between the sample and carrier solutions and their effect on the response signals. This leads to the appearance of blank signals. In potentiometric detection, the difference in the pH of the eluate zone and the carrier stream can also produce a blank signal. So for optimum performance in such trace level determinations, considerable attention is required to the design of the flow-injection manifold.

In order to reach much better detection limits in trace metal determinations with spectrophotometric detection, the use of some kinetic methods adapted to FIA has been suggested [1, 2, 12].

The present investigations were directed towards examining the general possibilities of the above-mentioned approaches for increasing sensitivity in spectrophotometric and potentiometric measurements of trace metals, and illustrating their potential in automated water analysis. Procedures for manganese(II), lead and copper(II) were designed and examined for application to samples of natural, potable and waste waters.

Catalytic determination of manganese

Several procedures for the spectrophotometric determination of manganese by FIA have been described. The best-known method is based on the catalytic effect of manganese(II) on the oxidation of succinimide in alkaline medium. It has been applied to the determination of manganese in the 0.2—10 $\mu g\ l^{-1}$ range in food products [13]. The inhibitory effect of Mg^{2+} and other interferences from Co^{2+}, Fe^{3+}, Ni^{2+}, Cd^{2+} and Pb^{2+} make the method useless for water analysis. A promising approach to determining traces of manganese(II) in water is provided by the catalytic oxidation of *N,N*-diethylaniline (DEA) by potassium periodate in the presence of manganese(II) [14]. This reaction appears to be well suited to flow-injection spectrophotometry, and was investigated further.

A three-channel flow-injection manifold was used, which utilizes the potassium periodate/DEA reaction by using reagent-injection. This mode is most convenient for automated water analysis because the plentiful water sample is used as the carrier stream and a reagent is injected into it. Such a flow-injection system based on kinetic measurements would provide an

increase in sensitivity and a decrease in the number and level of interferences and would require much smaller quantities of reagents than conventional methods.

A schematic diagram of the manifold is shown in Fig. 1a. The sample or standard manganese(II) solution is pumped at 2.0 ml min^{-1} through the channel towards the flow cell of the detector. It merges with a flowing reagent solution (0.001 M DEA) pumped at 0.6 ml min^{-1}.

A 30-μl portion of oxidant (a saturated aqueous solution of potassium periodate) is injected into the phosphate buffer stream (pH 6.86, pumped at 1.2 ml min^{-1}) and later merges with the mixture of the sample and DEA. The catalyzed oxidation proceeds while the reaction zone moves forward through coil L_3. The peak height which corresponds to the increase in absorbance of the yellow product is monitored at 475 nm. The reaction could be started by injection of either DEA or potassium periodate. The latter approach was chosen because of the better precision obtained.

The catalytic oxidation of DEA was found to be relatively slow. In such cases, the transient signal height in FIA depends mainly on the extent of the reaction, the physical dispersion in the flowing system being less significant. The optimum values of the variables in the flow-injection system were found to be as follows: flow rates of sample, DEA and buffer streams, 2.0, 0.6 and 1.2 ml min^{-1}, respectively; $L_1 = L_2 = 60$ cm and $L_3 = 180$ cm. The residence time in such a system was 30 s. It was increased to 90 s when the pumps P_1 and P_2 were operated as shown in Fig. 1b (mode 1). After 15 s, pump P_1 was stopped for 75 s so that the reaction zone was propelled only by pump P_2, which worked continuously. In this case, a linear relationship between peak height and manganese(II) concentration was obtained in the 0.2—1.0 μg l^{-1} range with a sample throughput of 40 h^{-1} (Fig. 2, curve 1).

A much higher sensitivity was achieved when the absorbance measurements were based on the stopped-flow principle. The reaction zone was stopped in the flow cell as soon as the recorded signal reached its maximum. The stop period was 99 s (Fig. 1B, mode 2). Figure 2 shows the calibration graph for manganese(II) for pure manganese(II) solutions (curve 3) and for an artificial

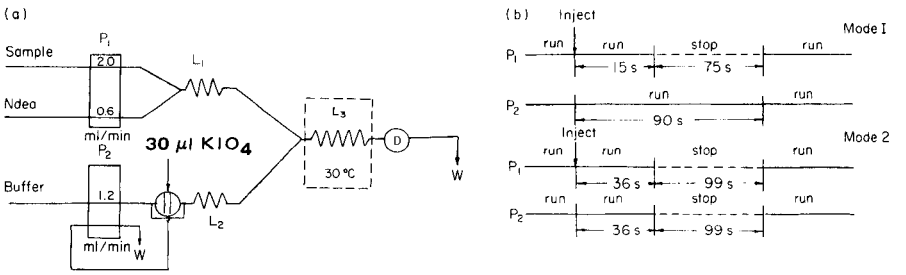

Fig. 1. (a) Schematic diagram of the flow-injection manifold for the catalytic determination of manganese(II): P_1, P_2, peristaltic pumps; L_1, L_2, mixing coils; L_3, reaction coil; D, detector at 475 nm; W, waste. (b) The two operation modes of the pumps; the stop/go sequences are controlled by a microprocessor.

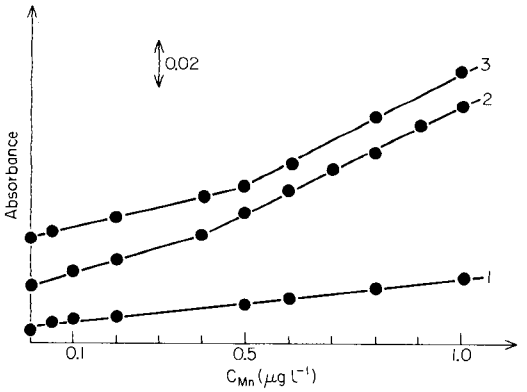

Fig. 2. Calibration graphs for manganese(II) determination. The manifold used was as shown in Fig. 1 with pumps operating in mode 1 (curve 1) and mode 2 (curves 2, 3). Curves 1 and 3 were obtained for working pure manganese standards and curve 2 for a manganese standard prepared in artificial sea water.

sea water (curve 2). The slopes of the graphs decrease in the range 0.01—0.4 $\mu g\ l^{-1}$. The graphs do not pass through the origin because of the contribution of the uncatalyzed reaction and of manganese contamination in the reagents. Colour development for sea water samples was slower than that for pure manganese solutions of the same manganese concentration.

The blank signal increases as the temperature in the reaction coil increases. The reaction temperature chosen was 30°C. It will be seen that stopped-flow measurements allow manganese(II) to be determined down to 20 ng l^{-1}. The sample throughput was ca. 25 h^{-1}.

The proposed system for the determination of manganese is the most sensitive of those based on flow-injection techniques. The effect of most other ions on the determination of manganese(II) was negligible. Iron(III) interference was eliminated by using phosphate (pH 6.86) or citrate/phosphate buffer (pH 7.10). Any substance that oxidizes DEA or reduces periodate constitutes a potential interference and should be eliminated prior to the measurements, or a standard-addition method should be used.

Spectrophotometric determination of lead

In some flow-injection methods described for the determination of traces of lead, a preliminary on-line preconcentration was required, both to concentrate lead and to separate it partly from interfering elements. Nord and Karlberg [10] proposed a flow-injection extraction system with flame AAS detection, which was capable of achieving a 15—20-fold enhancement in sensitivity for lead determination. Olsen et al. [7] and recently others [11, 15, 16] successfully used a small ion-exchange column to preconcentrate on-line lead and other heavy metals from sea water with flame AAS or ICP/AES detection. Preconcentration of lead in sea water has been improved

to 50—100-fold min^{-1}. However, the potential of this technique in flow-injection systems is far from being fully explored.

This lead enrichment technique was adapted for spectrophotometric measurements. The formation of a complex between lead and 4-(2-pyridylazo)-resorcinol (PAR) in an alkaline medium was chosen as the indicator reaction (maximum absorption wavelength, 520 nm; molar absorptivity = 4×10^4 l mol^{-1} cm^{-1}) [17]. The optimum values of the flow-injection variables and the manifold used are shown in Fig. 3. In this manifold, the injection valve is connected to an ion-exchange minicolumn instead of a sample loop. The sample stream, pumped at 4.3 ml min^{-1} is mixed with a flowing buffer solution (at 0.6 ml min^{-1}) in order to obtain the pH suitable for the metal ion preconcentration and then pumped through the column to waste. There is also a selection valve in the sample channel for the exchange of water samples and washing solution, placed prior to the peristaltic pump. The washing step is necessary when samples with a high salt concentration are analyzed. Simultaneously, the carrier-eluent (0.5 M nitric acid) and the chromogenic reagent solution (5×10^{-4} M PAR in 9 M ammonia/ammonium chloride buffer, pH 9.8, at 0.8 ml min^{-1}) are pumped through separate channels in the manifold and merged before flowing through a reaction coil (45 cm long) placed prior to the flow cell. At the end of the preconcentration time and washing period, the injection valve is automatically turned to the elution position. The eluent passes through the column, thus eluting the lead directly into the buffered reagent stream. The optimum elution flow rate was found to be 2.8 ml min^{-1}.

The lead ions react with PAR in the reactor coil to give the coloured lead/PAR complex. Maximum colour was found to develop immediately. The

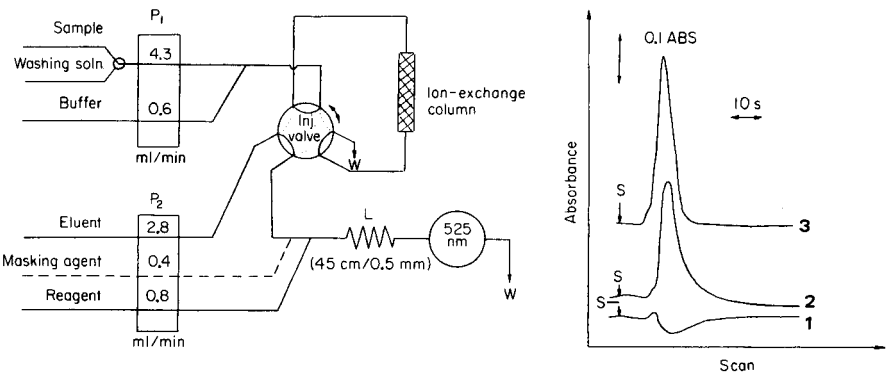

Fig. 3. Schematic diagram of the flow-injection manifold for the determination of lead. Symbols as for Fig. 1; L is a 45-cm mixing coil (0.5 mm i.d.); detection at 520 nm.

Fig. 4. Signals obtained in the flow-injection system for lead determination with different minicolumns: (1, 2) Chelex-100; (3) Dowex 1-X8. Signals: (1) blank; (2, 3) for 5 ml of lead standard solution pumped.

elution was stopped after 10—15 s and another turn of the injection valve commenced the next preconcentration cycle. During elution, the sample flowed to waste.

Previous studies have shown that the type of ion-exchange resin is important in the overall performance of these flow-injection systems [11, 16]. Therefore, different types of resin were compared. It was found that best efficiency was achieved with the chelating resin Chelex-100 or the strongly basic anion-exchanger Dowex 1-X8. Under the optimum flow-injection conditions, the degree of on-line preconcentration of lead on the column of Chelex-100 (1 M acetic acid/1 M ammonia, pH 8.5) and Dowex 1-X8 (1 M ammonia, pH 11.3) was found to be 70% and 44%, respectively. Figure 4 indicates typical transient signals obtained in the system with both ion-exchangers. It should be noted that the peak for the column filled with Chelex-100 was wider and lower than that for Dowex 1-X8, owing to differences in the kinetic behavior of the sorbents and the faster exchange rate for Dowex 1-X8.

Table 1 provides an evaluation of the performance of the proposed system, including the equations of the calibration graphs, linear concentration range for lead and limit of detection. The system has high sensitivity, good reproducibility and a sample throughput of 6—30 h^{-1}. The values of the enrichment factors, which were calculated by comparing the peak height obtained during elution with the response of standard solutions injected into the manifold without any preconcentration, vary from 25 to 150 depending mainly on the sample volume, which was varied from 5 ml to 50 ml, respectively. For a 50-ml sample, the limit of detection for lead was 0.7 $\mu g\ l^{-1}$.

Neither the resin used nor PAR is very selective for lead, so that many other metal ions interfere. To overcome these interferences, a masking solution was pumped at 0.4 ml min^{-1} in another channel and merged with the eluate zone; the mixture was passed through a coil (120 cm long, 0.7 mm i.d.) placed before the entry point of the PAR reagent stream. It was found that when 10% (w/v) potassium cyanide (or acetone cyanohydrin) solution was

TABLE 1

Performance of the proposed flow-injection system for the spectrophotometric determination of lead

Ion exchanger	Sample volume (ml)	Linear range ($\mu g\ ml^{-1}$)	Calibration eqn.[a] ($n = 30$; $p = 0.95$)	r[b]	Limit of detection[c] ($ng\ ml^{-1}$)	Sample throughput (h^{-1})
—	0.200	0.5—7.0	$A = (-0.006 \pm 0.002) + (0.0975 \pm 0.0006)$ [Pb]	0.9998	80	180
Chelex 100	5.0	0.01—0.1	$A = (0.032 \pm 0.004) + (2.18 \pm 0.07)$ [Pb]	0.9964	3.6	30
Dowex 1-X8	5.0	0.01—0.1	$A = (0.032 \pm 0.002) + (2.65 \pm 0.03)$ [Pb]	0.9994	1.4	30
Dowex 1-X8	50.0	0.001—0.01	$A = (0.059 \pm 0.005) + (13 \pm 0.9)$ [Pb]	0.9927	0.7	6

[a] A = absorbance, [Pb] in $\mu g\ ml^{-1}$. [b] Correlation coefficient. [c] Twice the mean blank signal.

used as the masking agent, the interferences of Ag(I), Cd, Co(II), Cu(II), Hg(II), Ni and Zn were largely eliminated. The alkaline earth metals posed a more difficult problem. Their interference could be removed by washing the column of Chelex-100 with 1 M ammonium acetate buffer (pH 5.5) before elution. Because the main constituents of natural waters (calcium, magnesium, alkali metals and iron) are not retained on Dowex 1-X8, it would be more suitable to on-line preconcentration of lead from water samples with high salt contents.

Potentiometric determination of copper

In recent years, various flow-injection procedures have been developed for copper. These include AAS [7,11], potentiometry [18], chemiluminescence measurements [19] and ultraviolet/visible spectrophotometry based on various chromogenic reagents [20]. Among these methods, the use of potentiometric detection in FIA offers some advantages such as wide concentration range, high selectivity, fast response, low-cost instrumentation and little sample pretreatment [21]. The possibilities of direct potentiometric measurements with a copper ion-selective membrane electrode (Cu-ISE) in the flow-injection systems with on-line copper preconcentration on a chelating ion-exchanger were therefore investigated.

The manifold used is described in Fig. 5a. The sample and 0.5 M acetate buffer streams were mixed to give pH 3.5—6.0 and passed via pump P_1 through the column filled with Chelex-100 resin to waste. Similarly, a carrier stream, which was an 0.5 M acetate buffer of the same pH, was transported by pump P_2 to the channel connected to the potentiometric cell with the Cu-ISE. After a suitable preconcentration time, pump P_1 was stopped (Fig. 5b) and the metal ions were eluted by injection of 500 μl of 0.5 M nitric acid. The eluate zone was mixed sequentially with two acetate buffer streams, generated by pump P_2, to provide the necessary pH, and then passed through the cell.

A series of preliminary experiments was conducted to optimize the flow-injection variables as well as the analytical performance of the Cu-ISE itself.

Curve 1 in Fig. 6 shows the calibration graph obtained for 300-μl injections of copper standards in 0.5 M potassium nitrate in the two-line manifold without an ion-exchange column. It indicates that the Cu-ISE can measure the copper(II) ion concentration down to a detection limit of 1.5×10^{-5} M. The calibration graph was linear over the range 5.0×10^{-5}—0.1 M copper and was expressed by the equation ΔE(mV) = (142.9 ± 1.6) + (29.8 ± 0.5) log [Cu], with a correlation coefficient of 0.9998. The effect of the acidity of the sample on the electrode response was examined. A calibration graph (Fig. 6, curve 2) was obtained for 300-μl injections of copper standards in 0.5 M nitric acid. It can be seen that the addition of acid has no marked effect on the peak height and sensitivity compared to solutions in 0.5 M potassium nitrate but the linear range is reduced somewhat. The linear relation between peak height (electrode response) and logarithm of copper ion concentration

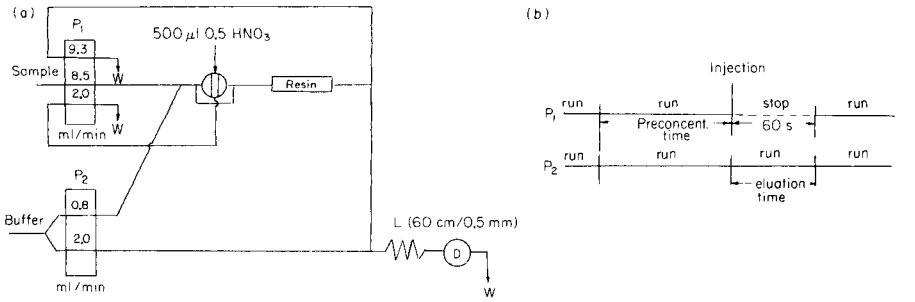

Fig. 5. (a) Flow-injection manifold for potentiometric determination of copper(II) with preconcentration on a minicolumn of Chelex-100 resin; L, 60-cm coil (0.5 mm i.d.); D, cascade-type potentiometric flow cell with Cu-ISE. (b) Pump program.

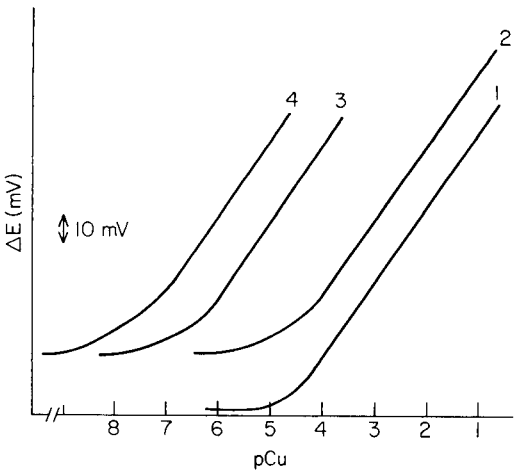

Fig. 6. Calibration curves for the Cu-ISE in the flow-injection system: (1, 2) 300-µl injections of copper solutions in 0.5 M KNO_3 (1) or 0.5 M HNO_3 (2); (3, 4) after preconcentration of 50 ml (3) or 500 ml (4) of copper solutions on the minicolumn and elution with 500 µl of 0.5 M HNO_3.

is expressed by the equation $\Delta E(\text{mV}) = (169.5 \pm 2.2) + (29.8 \pm 0.7) \log [\text{Cu}]$ with a correlation coefficient of 0.9996.

A series of experiments was conducted in order to find a buffer pH which would decrease the blank signal obtained for injections of 0.5 M nitric acid alone. The influence of the pH of the buffer carrier on the electrode response is shown in Fig. 7. The peak height for a 300-µl injection of 0.001 M copper ion in 0.5 M nitric acid increased with increasing pH from 3.7 to 4.7 and then did not change. A tendency to split-peak formation was seen at pH $\leqslant$4.0, because the pH changes along the flowing sample zone. The size of the blank (acid) peak increased slightly with increasing pH from 3.7 to 6.0. These

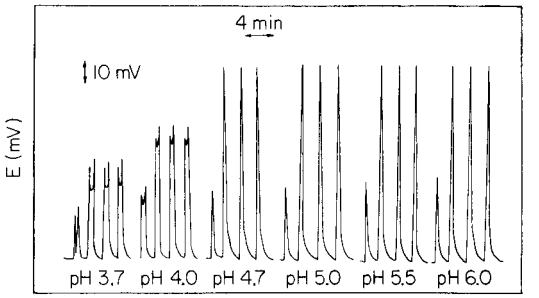

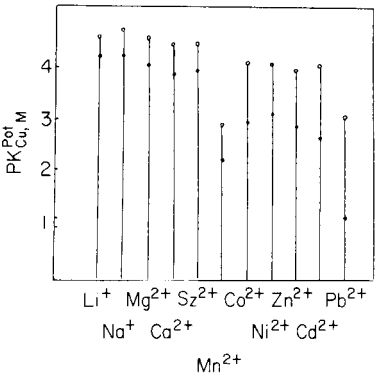

Fig. 7. Peaks for one injection of 0.5 M HNO_3 followed by triplicate injections of 1×10^{-3} M copper solution into acetate buffer carrier stream with different pH values. Sample volume, 300 μl.

Fig. 8. Graphic comparison of the potentiometric selectivity coefficients, $K^{pot}_{Cu,M}$, for the Cu-ISE: (○) in the flow-injection system; (●) under steady-state conditions. The other metal ion was at a concentration of 0.1 M in these tests.

data clearly demonstrate that the highest signals and optimum sensitivity are obtained when the pH of the 0.5 M acetate buffer carrier is 4.7.

The incorporation of the Cu-ISE in the flow-injection system with the ion-exchange column (Fig. 5) extended the concentration range of the electrode to lower concentrations. Figure 6 (curve 3) shows the calibration graph obtained for 50 ml of the working standards after preconcentration on the chelating resin. The linear concentration range was then 5.0×10^{-7}—1.0×10^{-4} M and the calibration equation was ΔE(mV) = (217.6 ± 6.1) + (29.6 ± 1.2) log [Cu] with a correlation coefficient of 0.9989. The limit of detection was 1.0×10^{-7} M copper. Curve 4 in Fig. 6 is the corresponding plot for 500 ml of the working standards. In this case, the detection limit was 5.0×10^{-9} M. The results shown in Fig. 6 demonstrate that the enrichment factor for copper can be varied from 50 to 1000 depending on the sample volume and can be selected to give the most favorable conditions. The sample throughput was 1—50 h^{-1}, depending on the volume of sample pumped through the resin cartridge.

The main drawback of this flow-injection system in its present form is the need for large sample volumes, but for water analysis this is not a limiting factor. Additionally, the responses of Cu-ISE are affected by most anions and the matrix exchange obtained in the proposed system allows these interferences to be removed. The influence of other metal ions on the electrode transient response in the flow-injection system was less than under steady-state conditions (Fig. 8).

Analysis of water samples

The designed systems were tested by analyzing both synthetic and real water samples. Results are presented in Tables 2—5. The data shown in Table 2 indicate that trace levels of manganese(II) added to double-distilled water can be determined in the range 0.02—1.0 $\mu g\ l^{-1}$ by direct use of a calibration graph, with relative standard deviations (RSD) of 10—1%, respectively. As a rule, the manganese or its yellow product is adsorbed on the teflon tubing used and all conduits should be cleaned regularly with a wash solution (1 M HNO_3), followed by repeated rinsing with deionized water. The calibration graph should be checked every 2 h. The determination of manganese in natural water is an exceedingly delicate analysis and large errors are commonly obtained. The content of manganese in a sea-water sample, measured by the standard addition technique, was found to be 20 ng l^{-1}, with RSD 18.9%. The proposed system was successfully applied to the determination of manganese in ocean water, when the FIAStar equipment was tested aboard ship in order to get fast analytical data. Samples were taken by means of a Rosette water sampler at depths down to 5000 m and analyzed immediately. The flow-injection system was found to be very useful for discovering anomalously high concentrations of manganese (up to $\mu g\ ml^{-1}$ levels), which is considered to be one of the main indicator elements for finding hydrothermal fields of mineral deposits (polymetallic sulfides) on the sea floor [22].

The results obtained for the determination of copper in various water samples are summarized in Tables 3 and 4. The data obtained by the flow-injection procedure compared well with those found by flame AAS (Table 4). It is obviously possible to analyze waters with good sensitivity and reproducibility. For example, 0.51 $\mu g\ l^{-1}$ copper was found in a sea-water sample with an RSD of 5.2%, for a sample volume of 500 ml.

Table 5 shows results of the determination of lead in a synthetic water sample prepared by adding known amounts of different inorganic salts. The sensitivity and the reproducibility of the proposed flow-injection procedure are generally satisfactory.

TABLE 2

Results for the determination of manganese(II) in water samples

Sample	Concentration of manganese ($\mu g\ l^{-1}$)		RSD (%)
	Added	Found ($n = 4; p = 0.95$)	
Deionized water	0.05	0.056 ± 0.009	9.8
	0.20	0.207 ± 0.009	3.2
	1.00	0.980 ± 0.015	1.1
Sea water (Atlantic Ocean)	0.00	0.020 ± 0.005[a]	18.9
	0.10	0.11 ± 0.01	5.7
	0.20	0.19 ± 0.01	3.3
	0.40	0.39 ± 0.01	1.6

[a]Standard-addition technique used ($n = 8; p = 0.95$).

TABLE 3

Results for the determination of copper(II) in various water samples with the flow-injection Cu-ISE system (Fig. 5)

Sample	Volume (ml)	Copper added	Copper found ($n = 4; p = 0.95$)	RSD (%)
Deionized water[a]	50	0.063	0.064 ± 0.009	9.6
		0.630	0.630 ± 0.030	2.9
		6.300	6.290 ± 0.065	1.5
Sea water[b]	500	0.00	0.51 ± 0.04	5.2
		3.10	3.05 ± 0.14	2.8
		6.30	6.14 ± 0.23	2.4

[a]Concentrations are given in $\mu g\ ml^{-1}$. [b]Concentrations are given in $ng\ ml^{-1}$.

TABLE 4

Comparison of copper(II) concentrations found in tap and waste waters by the flow-injection method (Fig. 5) and by AAS

Sample	Copper(II) concentration ($\mu g\ ml^{-1}$)	
	FIA[a]	AAS
Tap water	0.020 ± 0.002 (6.2)	0.02
Waste water A	0.030 ± 0.003 (6.3)	0.03
Waste water B	0.120 ± 0.010 (5.2)	0.11
Waste water C	0.250 ± 0.020 (5.0)	0.23

[a]Sample volume 80 ml; mean ($n = 4$) and probability limits ($p = 0.95$) are given with RSD (%) in parentheses.

TABLE 5

Performance and reproducibility for the determination of lead in a synthetic water sample by the proposed flow-injection system (Fig. 3)

Sample content[a] ($\mu g\ ml^{-1}$)	Lead concentration ($\mu g\ ml^{-1}$)		RSD (%)
	Added	Found ($n = 3; p = 0.95$)	
Fe (0.5), Zn, Cu, Co, Ni, Al (0.1 each),	0.01	0.011 ± 0.003	12.0
Cd (0.01), Na (200),	0.03	0.028 ± 0.004	6.0
K (20), Ca (80), Mg (50),	0.05	0.048 ± 0.008	7.0
Cl^- (593), SO_4^{2-} (36)	0.07	0.070 ± 0.004	2.0

[a]Sample volume, 12 ml.

Conclusions

The proposed flow-injection systems for the determination of manganese, lead and copper demonstrate that the sensitivities of the developed procedures are satisfactory for the analysis of natural and waste waters in most cases. Compared with earlier flow-injection methods for these purposes, both the schemes and the chemical systems reported here are simple, the reagent consumption is minimal and the instrumentation is inexpensive. The automatic procedures should be attractive for routine water laboratories. They also promise to be of considerable practical interest in on-line process control.

REFERENCES

1 J. Růžička and E. H. Hansen, Flow Injection Analysis, Wiley-Interscience, New York, 1981.
2 J. Růžička and E. H. Hansen, Anal. Chim. Acta, 179 (1986) 1.
3 J. Janata and J. Růžička, Anal. Chim. Acta, 139 (1982) 105.
4 W. Frenzel and P. Brätter, Anal. Chim. Acta, 179 (1986) 389.
5 T. A. Kelly and G. P. Christian, Anal. Chem., 54 (1982) 1444.
6 E. A. G. Zagatto, A. O. Jacintho, F. J. Krug, B. F. Reis, R. E. Bruns and M. G. U. Araujo, Anal. Chim. Acta, 15 (1983) 169.
7 S. Olsen, L. C. R. Pessenda, J. Růžička and E. H. Hansen, Analyst, 108 (1983) 905.
8 Z. Fang, S. Xu and S. Zhang, Anal. Chim. Acta, 164 (1984) 41.
9 J. Růžička, E. H. Hansen and E. A. G. Zagatto, Anal. Chim. Acta, 88 (1977) 1.
10 L. Nord and B. Karlberg, Anal. Chim. Acta, 145 (1983) 151.
11 Z. Fang, J. Růžička and E. H. Hansen, Anal. Chim. Acta, 164 (1984) 23.
12 T. Deguchi, A. Higashi and I. Sanemasa, Bull. Chem. Soc. Jpn., 59 (1986) 295.
13 S. Maspoch, M. Blanco and V. Cerda, Analyst, 111 (1986) 69.
14 T. P. Hadjiiannou and T. A. Kephalas, Mikrochim. Acta, (1969) 1215.
15 F. Malamas, M. Bengtsson and G. Johansson, Anal. Chim. Acta, 160 (1984) 1.
16 Z. Fang, S. Xu, X. Wang and S. Zhang, Anal. Chim. Acta, 179 (1986) 325.
17 R. M. Dagnall, T. S. West and P. Young, Talanta, 12 (1965) 583.
18 L. Risinger, Anal. Chim. Acta, 179 (1986) 509.
19 M. Yamada and S. Sazaki, Chem. Lett., 11 (1982) 1747.
20 A. T. Faizullah and A. Townshend, Anal. Chim. Acta, 172 (1985) 291.
21 K. Toth, J. Fucsko, E. Lindner, Zs. Feher and E. Pungor, Anal. Chim. Acta, 179 (1986) 359.
22 K. L. Von Damm, J. M. Edmond, B. Grant, G. I. Measures, B. Walden and R. F. Weiss, Geochim. Cosmochim. Acta, 49 (1985) 2197.

Analytica Chimica Acta, 200 (1987) 35—49
Elsevier Science Publishers B.V., Amsterdam — Printed in The Netherlands

FUNDAMENTAL AND PRACTICAL CONSIDERATIONS IN THE DESIGN OF ON-LINE COLUMN PRECONCENTRATION FOR FLOW-INJECTION ATOMIC SPECTROMETRIC SYSTEMS

ZHAOLUN FANG*, SHUKUN XU and SUCHUN ZHANG
Institute of Forestry and Soil Science, Academia Sinica, Box 417, Shenyang (China)
(Received 2nd April 1987)

SUMMARY

Fundamental considerations and practical points in the development of on-line preconcentration flow-injection with atomic spectrometric detection are discussed, with emphasis on overall efficiency and accuracy. The terms concentration efficiency (CE) expressed as the enrichment factor achieved per minute by the system, and retention efficiency (%E), together with recovery studies on real samples, are recommended as criteria for the evaluation of the efficiency and reliability of such systems. Time-based sampling and double-column systems without intermediate column washing are recommended for improving efficiency. Large columns (3 mm i.d., 45 mm long) with high sample-loading rates of 9.5 ml min^{-1} are proposed for achieving high efficiency and accuracy with atomic absorption detection; more careful optimization of column dimensions is needed for detection with inductively-coupled plasma/atomic emission spectrometry. A procedure for the on-line preconcentration of cobalt in water samples was developed under the guidelines presented. An enrichment factor of 48 was achieved at a sampling frequency of 60 h^{-1} with good recoveries for all the water types studied. The precision was 1.7% r.s.d. at the 40 $\mu g\ l^{-1}$ level, and the detection limit (3σ) was 0.2 $\mu g\ l^{-1}$.

In recent years, flow injection analysis (f.i.a.) has been repeatedly proved to be a powerful means of extending the capabilities of conventional atomic spectrometry, particularly flame atomic absorption spectrometry (a.a.s.) and inductively coupled plasma/atomic emission spectrometry (i.c.p./a.e.s.) in trace analysis [1]. Improvements in terms of sample throughput, economy in sample and reagent consumption, tolerance of salt content and interferences, calibration procedures and pretreatment procedures have been reported [1]. In the last category, the on-line preconcentration of trace metals by using micro-columns has been shown to enhance the sensitivity of trace

*Zhaolun Fang, Research Professor of Analytical Chemistry in Soil Science and Environmental Sciences at the Institute of Forestry and Soil Science of the Chinese Academy (Academia Sinica) is a graduate of Beijing University. He is author of over 60 research papers. His main research interests include development of atomic spectrometric and flow-injection methods and their applications to soil science and environmental sciences. He is chairman of the Chinese Society for Development of Flow Injection Analysis.

0003-2670/87/$03.50

element determinations by flame a.a.s. and i.c.p./a.e.s. by factors of 10—100 at sampling frequencies of 10—60 h^{-1}. Extensive interest was stimulated by the first publication on the subject by Olsen et al. [2] in 1983, and there has been a roughly exponential increase of related publications per annum in the ensuing years [1—17]. Various modifications have been proposed to improve the performance of the system [5] and the detection system has been gradually extended from flame a.a.s. to i.c.p./a.e.s. The technique has been successfully applied to the determination of trace elements in a large variety of real samples including tap water [3, 8], natural waters [4, 6, 11], soil extracts [1], plants [14—16], bovine liver [14], and steels [10], and also in synthetic sea water [2, 5] and EPA quality-control water samples [8].

Before the advent of on-line column preconcentration, numerous papers reported on the preconcentration of trace elements by off-line batch procedures either with columns or by static equilibration prior to atomic spectrometric determination [18]. Such methods offer prominent advantages in achieving a large gain in sensitivity as well as separation of the interfering sample matrix, but they are tedious to operate, especially when compared to the final atomic spectrometric step, and several litres or hundred millilitres of sample are often required for each determination. These shortcomings have largely been overcome by using on-line column preconcentration whilst the advantages of the off-line procedures are preserved.

The advantages of on-line column preconcentration over conventional batch procedures can be summarized as follows. First, the columns offer much greater efficiency; enrichment factors are one or two orders of magnitude higher for a defined time interval, or a larger number of samples can be processed to achieve a certain enrichment factor in a fixed time period. Secondly, sample consumption is usually 5—10 ml per determination for enrichment factors of 10—100, while reagent consumption is usually only a few hundred microlitres of eluant per sample with <100 mg of column packing; the latter will normally last for hundreds of samples. Thirdly, the closed preconcentration system decreases the risks of contamination from the laboratory environment. Finally, the continuous monitoring of the baseline provides better checks on the column performance.

However, the application of on-line column preconcentration is not without problems. In some cases, the improvement in efficiency is only marginal and, occasionally, interference effects seem even to be enhanced. In this paper, an attempt is made to assess fundamental and secondary aspects of the design of on-line column preconcentration flow-injection systems with atomic spectrometric detection. The scattered information on the technique is at least partially integrated in order to present some guidelines for future improvements. Recent developments of the technique in this laboratory serve to support some of the viewpoints.

EXPERIMENTAL

Apparatus

The atomic absorption spectrometer was a Nippon Jarrell-Ash AA-1 MK II model connected to a Yanaco YR-101 chart recorder. The sample uptake rate of the nebulizer was adjusted to 4 ml min^{-1}. The wavelengths used for cobalt and cadmium were 240.8 and 228.8 nm, respectively.

A Gilson Minipuls 8-channel peristaltic pump was used with tygon pump tubes. A two-layer multi-functional valve following a previous design [5] was used, but the push-fit tube connections were replaced by connections with threaded fittings and flanged tube-ends furnished with silicone rubber washers to form a seal at the ends. This improved the reliability of the connections under the slightly elevated hydrodynamic pressures caused by the incorporation of a packed column in the line. A pneumatic system similar to that described by Jørgensen et al. [9] controlled by an electronic timer was used to operate the valve automatically. A two-way pneumatic cylinder (Festo DSN, 8-mm diameter, 40-mm stroke) and two solenoid valves (Festo MFH-3-M5) were used to construct the automated system.

The columns were made from plexiglas with threaded fittings at both ends (Fig. 1), teflon washers with conical holes were inserted at both ends to ensure a streamlined flow through the column. The teflon tubes for connection were flanged at the ends and furnished with silicone rubber washers as in the connections for the valve. The tube and washers were slipped through the threaded fitting and connected to a column with a piece of nylon gauze inserted between the flanged tube-end and teflon washer to keep the column packing in position. The column design is more complex than a previously reported version with push-fit connections but the reliability is much improved, completely avoiding leakages and severance at the connections.

The manifold for the on-line preconcentration system was basically the same as that used previously [5] except that a single pump was used without timing. The loading (preconcentration) and elution periods were governed by settings on the timer which controlled the operation of the multifunctional valve via the pneumatic system. A simple two-way valve was included in the eluant line and operated manually to switch the eluant from one column to the other to permit sequential elution of the columns during the elution stage (Fig. 2).

Reagents and procedures

All chemicals were of analytical-reagent grade. Deionized water was used throughout.

Standard solutions of cobalt and cadmium were made by two- or three-stage dilutions of aqueous 1000 mg l^{-1} stock solutions. The ammonium acetate buffer solutions were prepared by diluting a 2 M ammonium acetate solution adjusted to the appropriate pH with 25% ammonia solution.

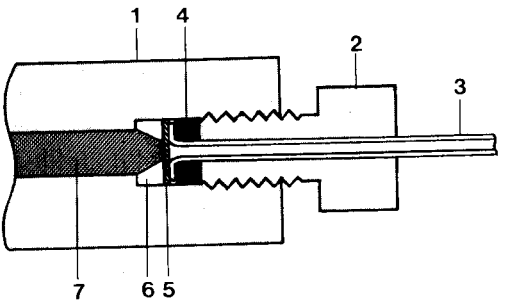

Fig. 1. Construction of on-line preconcentration column: (1) plexiglas column body; (2) plexiglas fitting; (3) teflon tube with flanged end; (4) silicone rubber washer; (5) nylon gauze; (6) teflon washer with conical hole; (7) column packing.

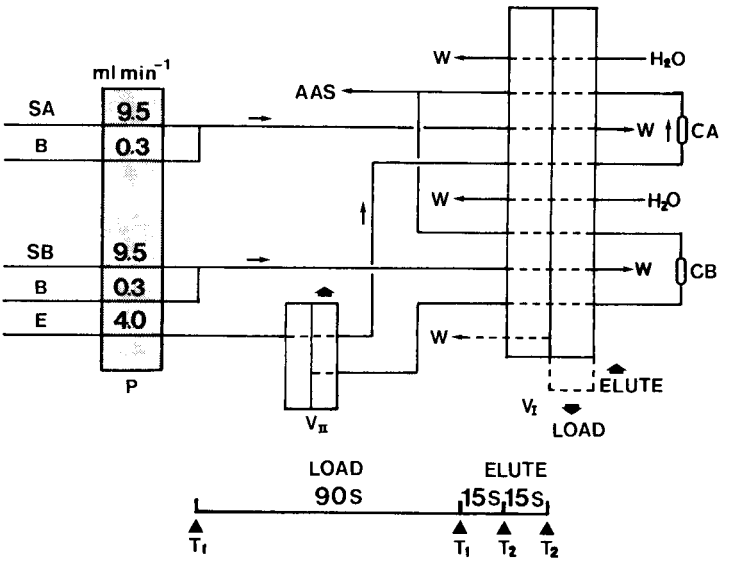

Fig. 2. Schematic diagram of flow-injection atomic absorption spectrometric system with on-line ion-exchange: P, pump; V_I, multifunctional valve; V_{II}, elution-stage column selection valve; SA, SB, samples A and B; CA, CB, columns A and B; B, buffer solution; E, eluant; W, waste; AAS, atomic absorption spectrometer; T_1, T_2, turning points for valves V_I and V_{II}.

The Chelex-100 and 8-quinolinol chelating exchangers were as previously reported [5]; the weakly acidic 122 resin in the previous report [5] was replaced by a 501 resin, which has the same properties as the 122 resin.

Procedures were as reported previously [5], except that the timer was used to control the valve instead of the pump and 2 M hydrochloric acid was used as eluant. Samples were buffered to pH 8 for the CPG-8Q column and to pH 9 for the other columns.

PRIMARY CONSIDERATIONS IN THE DEVELOPMENT OF ON-LINE COLUMN PRECONCENTRATION SYSTEMS

The ultimate purpose of developing an on-line column preconcentration system for flame a.a.s. or i.c.p./a.e.s. must be considered in relation to the particular application involved. In principle, each of the advantages for on-line preconcentration cited in the introductory section might be regarded as part of the purpose; however, the advantages in material consumption, lack of contamination and baseline monitoring, taken individually, may not stimulate enough interest to construct an on-line preconcentration system, as they might either be achieved in other ways or be considered of minor importance. Low sample consumption can be an important feature which could prompt the use of an on-line system, either when only limited amounts of samples are available or to save effort in collection and/or transportation of large sample loads; but in such situations, some workers might prefer to use electrothermal atomization methods. Thus, it is safe to say that for most applications the efficiency offered by the on-line system will be the principal purpose of adopting the procedure. This does not imply that the other merits are unimportant and can be ignored in designing on-line preconcentration systems but that they show their real value only when they are combined in an efficient system.

It is important therefore to set some criterion for evaluating the efficiency of different on-line ion-exchange systems, so that the favourable aspects from different designs may be located and integrated or enhanced, providing stimulation for further development. Commonly, both the enrichment factors and the sampling frequencies are mentioned in evaluating the efficiency of on-line preconcentration systems. This is reasonable, as both criteria are equally important in the assessment of efficiency and neither is independent of the other. Fang et al. [5] proposed the integration of the two criteria by using the term "concentration efficiency", which was defined as the product of enrichment factor (EF) and the sampling frequency in number of samples analyzed per minute; they used this term to compare different on-line column preconcentration systems for illustration of the development of the technique [5]. In the present paper, the term is abbreviated as CE, expressed in EF min^{-1}. Thus, a system capable of attaining 25-fold enrichment at a sampling frequency of 25 h^{-1} (0.417 min^{-1}) will have a CE value of 10.4, whilst one achieving 100-fold enrichment at 60 h^{-1} will have a CE value of 100 EF min^{-1}. The CE value of a typical manual batch procedure is usually less than 4 even when operated in batches of ten, and so is obviously much less efficient than an on-line system. It should be taken into account, however, that with conventional batch preconcentrations the spectrometer will be required for measurements only after completion of the preconcentration step, whereas with on-line column preconcentration, the spectrometer will be working full-time. As the preconcentration step normally takes longer than the elution stage, the spectrometer

is not in use for a large percentage of the total working period, even when two columns are used alternately for preconcentration (see, e.g. [4, 9]). Thus, an assessment of the overall efficiency of this type of on-line preconcentration system will not be complete without consideration of the most efficient usage of the spectrometer involved. This is especially important when a multichannel i.c.p. spectrometer capable of delivering large amounts of analytical data and consuming large amounts of argon is used for detection. Therefore it is suggested here that the CE value for an on-line preconcentration system based on atomic spectrometry should be at least twice as high as the conventional batch procedure in order to outweigh the loss in efficient usage of the spectrometer. In practice, this means that an on-line system with CE < 8 probably will not show much advantage over conventional batch procedures in terms of overall efficiency of the system. Of course, even with the most inefficient on-line system, the analytical readout will be available within a few minutes, which is much faster than any efficient conventional batch method, yet this favourable feature may have little significance except in process control. In most circumstances, the sample throughput per day and overall costs are of greater concern. Conventional batch procedures are then favoured because numerous columns can be processed in parallel; simultaneous use of more than 3—4 columns in an on-line preconcentration system would require highly sophisticated control.

Obviously, any trace method requires not only sensitivity and efficiency but also reasonable accuracy. This is a vital factor in considering the selection of a system because a careful balance between efficiency and accuracy is often necessary. An effective measure for improving efficiency might also degrade the accuracy through deterioration of retention efficiency, defined by Hartenstein et al. [7] as the percentage of total amount of analyte retained on the column and abbreviated as %E. Under the controlled conditions of a flow-injection system, low retention efficiencies do not necessarily imply a serious loss in precision, but effective control over matrix effects and interferences from competing trace elements cannot be guaranteed if the separation cannot be considered reasonably "clean". Even for trace elements which show 100% retention efficiency, there may be large drops in %E when matrices contain significant amounts of interfering species. Unlike the retention efficiency, the elution efficiency, defined as the percentage elution of the retained analyte from the column, is normally high, particularly with chelating ion-exchangers, provided that the appropriate eluant is chosen. Hence, for critical evaluation of an on-line column preconcentration system, the features to be considered are not only the concentration efficiency CE but also the retention efficiency %E, recovery data obtained in the presence of the sample matrix, and sometimes also the elution efficiency.

SECONDARY CONSIDERATIONS IN THE DEVELOPMENT OF AN ON-LINE COLUMN PRECONCENTRATION SYSTEM

In this section, some tactical considerations on the development of on-line column preconcentration spectrometric systems which are both efficient and interference-free will be discussed. The various factors involved are often supplementary and sometimes even contradictory, so that care is needed not to overemphasize some favourable aspect as it might often lead to harmful effects in other factors.

Time-based vs. volume-based sample loading

The process of sample loading on packed columns is a key link in the entire preconcentration procedure. Proper choice of manifold design and operational parameters in relation to sample loading are essential for achieving good efficiency and accuracy.

Different modes involving either the injection of a defined volume of sample from a sample loop on to the column (volume-based loading) or the pumping of sample at a definite flow rate through the column for a defined time interval (time-based loading) have been proposed by different workers. When other factors are similar (e.g., number of columns, column-packing material, etc.), time-based loading systems [3, 5, 7, 9, 13] usually give higher CE values than volume-based systems. Obviously, it is simpler and more straightforward to load the sample directly on to a column without prior introduction into a loop. This also obviates the need for a washing stage to remove the somewhat dispersed sample completely from the loop, which is necessary for volume-based loading. Admittedly, with time-based loading, the sample remaining in the pump tube at the end of the loading period will have to be washed out of the pump tube by the next sample, but this can be done during the elution state and will not require extra time as in the volume-based mode [4, 8]. Samples can normally be changed in 10—20 s, depending on the sample flow rate, during the elution period so that the next sample-loading cycle can be initiated immediately after the elution period without appreciable carry-over.

A disadvantage of time-based sample loading is its larger dependence on the stability of the flow rate. Because of the relatively large back-pressures produced in flow systems incorporating packed columns compared to open tube systems, the flow rates obtained with the commonly used peristaltic pumps tend to be sensitive to pressure changes in the flow system, created by partial line blockages (e.g., from accidentally released resin particles, etc.) and also by swelling and shrinking of certain ion-exchangers such as Chelex-100. Thus, with time-based loading, regular checks of the sample flow rate are needed, particularly when a new column of different column dimensions or different packing material is used for the first time or when large fluctuations in sensitivity are observed.

Single-column vs. double-column on-line preconcentration systems

Both single and double column systems have been proposed. The obvious advantage for a single-column system is its simple construction; the simplest version can be built with a few pieces of basic flow-injection hardware [2, 8, 10]. Yet when other factors are considered, such as reversal of flow direction during elution, intermediate washing of the column between elution and sample-loading sequences, avoiding discharge of sample waste into the nebulizer, etc., the system becomes more complicated [2, 3, 13]. A double-column system was proposed by Fang et al. [4] to enhance the efficiency of an on-line preconcentration system. Sample loading and elution were performed on the two columns alternately, i.e., while one column was being loaded, the other was being eluted, using a multifunctional valve (commutator). In this way, a CE value of 13—18 was attained for Ni, Cu, Pb, Cd even when the relatively inefficient volume-based sample loading was used. The double-column system was later improved by using time-based sample loading and more efficient column packing; furthermore, with the consideration that the elution period (15—20 s) is usually much shorter than the sample-loading period, a double-column system which allowed simultaneous sample loading and sequential elution of the analyte from the two columns was proposed and CE was increased to 50—100 [5]. Such a system with 90-s loading period and 15-s elution period takes 120 s to complete a cycle (two samples analyzed), whilst an alternately operated double-column system with the same loading period will take 180 s for a complete cycle, and a single-column system will take 210 s to analyze two samples. Thus the efficiency of the preconcentration system can be almost doubled by using a double-column system. Operation is not complicated if suitable valves with adequate timing facilities are available.

A possible drawback of double-column systems is that, although elution peaks from a single column are usually reproducible, often with precisions of better than 2% r.s.d., columns which give identical peak heights are difficult to prepare because the peak heights are extremely sensitive to variations in tightness of packing materials and differences in the geometry of the flow systems. Yet this difficulty can be overcome either by using the average of the peak heights or by constructing separate calibration curves for each of the columns. It was even suggested that two columns with different packing materials can be used to provide a cross-check on the accuracy [5].

The effect of intermediate washing of columns

In conventional batchwise column preconcentration, it is common practice that after each elution the column is washed with water and equilibrated with a buffer solution to restore the pH to that optimized for the retention of the analyte or separation of matrix elements. This policy has been adopted in most on-line column systems either by using the buffer as the carrier for the eluant [2, 3, 8] or by using a separate line for the

equilibration [13, 15]. This was considered to be necessary because elution by a strong acid or alkali immediately followed by introduction of the next sample to the column will result in loss of analyte in the initial stage of loading owing to unsuitable pH conditions. Yet, in some on-line column preconcentration systems, the washing stage was completely omitted to simplify the flow system and improve the efficiency [5, 7]. No degradation in the preconcentration capability or precision was observed in these systems.

It is, therefore, essential to consider if the washing (equilibration) of columns is really necessary in an on-line column preconcentration system, and if omitting the washing degrades sensitivity or precision. A detailed study of these points was made in this laboratory with the system outlined in Fig. 2. The columns were packed with CPG-8Q exchanger and an ammonium acetate buffered (0.025 M, pH 8) sample containing 0.6 mg l^{-1} cobalt was pumped through the columns immediately after the elution of the previous sample with 2 M HCl. The outlet from the column was connected to the nebulizer of the atomic absorption spectrometer, and the cobalt signal recorded. A peak appeared in the initial stage of sample loading which lasted for a total of 12 s. The area of this peak was compared to that of the sample aspirated in the conventional mode at an identical pumping rate for a period of 90 s. The short duration of the peak show that the columns can be rapidly equilibrated by the buffer in the sample under the flow conditions used. The area of the peak, which was considered to be the amount of cobalt lost because of the lack of an equilibration sequence, constituted only 5% of the total amount. Ten replicate recordings of the breakthrough peak gave an r.s.d. of 2%, which shows that the leakage is reproducible. The percentage leakage may vary with different elements and column-packing materials and the duration of the sample loading period. But with sample-loading periods of over 1 min, which is the case with most on-line column systems, the omission of a washing/equilibration sequence seems not seriously to affect the sensitivity or precision of the determination, whereas the advantages gained by simplifying the manifold and improving the overall efficiency are obvious.

Washing the CPG-8Q columns with deionized water after sample loading before elution with 2 M HCl also did not show any advantage in terms of sensitivity and precision for cobalt. On the contrary, the lowering of pH during the washing caused some loss of cobalt so that the elution peak was lower than when no washing was done.

Optimization of sample-loading rate and column dimensions

As stated above, the sample-loading sequence is the key link in the entire procedure for achieving high efficiency and accuracy. The principal factors to be optimized for this key link are the loading (flow) rate and column dimensions including the ion-exchange capacity, although pH and eluant composition can also be important in some situations. A joint evaluation of the concentration efficiency CE and retention efficiency %E of an ana-

lyte, together with recovery studies of real samples and potential interferents is recommended for the optimization of the factors. This is important because pursuance of efficiency without simultaneous consideration of its effects on accuracy is rarely justifiable in the context of real samples.

Optimization studies have shown that an increase in sample-loading rate within an upper limit enhances the enrichment factor by increasing the sample volume passing through the column within a certain time interval [7, 13, 16]. However, the effects of sample-loading rate on the tolerance for interferences in relation to column dimensions and capacity seem not to have been studied hitherto.

Such an investigation was undertaken in this laboratory, and the results are tabulated in Tables 1 and 2. Cobalt, which forms medium-strong complexes with the functional groups of the chelating ion-exchangers studied, was used as a model element, and cadmium, representing the metals which form the weakest complexes, was used for comparison. Although high loading rates are expected to yield better concentration efficiencies, their optimum values are limited by the column dimensions and the capacity of the ion-exchanger. Ignoring factors associated with tolerance capacity of interferences, the loading rate should not be so high as to produce excessive back-pressure in the system, because this will create problems in leakages and fluctuations in the flow rate; nor should it produce excessively low retention efficiencies. Considering these factors and the range of column dimensions often used for on-line preconcentrations, a loading rate of 9.5 ml min^{-1} was chosen for these studies. For the larger columns (3 × 45 mm), this is close to the upper limit of ensuring a uniform flow; for the smaller columns (2.3 × 12 mm), this is also the upper limit before the preconcentration process becomes counterproductive, with retention efficiencies below 50% [7]. Columns with different dimensions, representative of those reported earlier, were compared, with CPG-8Q as the packing. The largest columns (3 × 45 mm) were also packed with Chelex-100 and Resin 501 for comparison.

The results of these tests (Tables 1 and 2) allow some conclusions to be drawn. With the sample-loading rate at its highest practicable limit, the concentration efficiency of the on-line system remains relatively constant within a factor of 2, for different column dimensions, sample residence times, exchange capacities and even with different ion-exchangers and analyte metals, provided of course that reasonably strong complexes are formed between the metals and the functional groups at the pH used. It is inferred, therefore, that other factors in the design of an on-line preconcentration system (time-based or volume-based sampling, single or double columns, etc.) will have more influence on the concentration efficiency of the system.

An explanation for this behaviour could be that the higher retention efficiencies obtained with larger columns, and hence with larger exchange capacities and longer residence times, were counteracted by losses in peak height during elution because of increased dispersion in the larger dead volume of the columns. With the smaller columns, lower dispersion in

TABLE 1

The effects of column dimensions and capacity of CPG-8Q ion-exchange columns and effect of different ion-exchangers on concentration efficiency retention efficiency and recoveries of cobalt and cadmium in water samples

Column packing	Column[a]		Residence time (s)	CE (EF min^{-1})	E[b] (%)	Recovery[c] (%)			
	i.d.	length				Sea water	Tap water[d]	Tap water	Waste water
Cobalt									
CPG-8Q	3.0	45	1.0	48	95	96	99	102	98
	2.3	20	0.3	58	95	90	66	98	83
	2.3	12	0.15	50	80	73	56	98	72
Resin 501	3.0	45	1.0	35	96	37	89	100	99
Chelex-100	3.0	45	1.0	34	87	98	101	—	105
Cadmium									
CPG-8Q	3.0	45	1.0	55	98	95	42	104	60
	2.3	20	0.3	55	87	58	30	100	50
	2.3	12	0.15	56	65	46	18	85	32
Resin 501	3.0	45	1.0	52	97	28	87	102	81
Chelex-100	3.0	45	1.0	28	81	68	88	100	94

[a]Dimensions in mm. [b]%E evaluated by passing 1 mg l^{-1} (each) Co and Cd solution through column. [c]Loading rate 9.5 ml min^{-1}; 90-s preconcentration period; samples spiked with 100 μg l^{-1} Co and 20 μg l^{-1} Cd. [d]Tap water collected from a new pipeline with high zinc content.

TABLE 2

The effects of sample-loading rate, column dimensions and capacity of CPG-8Q ion-exchange column on recoveries of cobalt and cadmium in a tap-water sample with high zinc content[a]

Loading rate (ml min^{-1})	9.5	9.5	9.5	1.5	1.5	1.5
Column i.d. (mm)	3.0	2.3	2.3	3.0	2.3	2.3
Column length (mm)	45	20	12	45	20	12
Residence time (s)	1	0.3	0.15	6	2	1
Recovery (%)						
Cobalt	99	66[b]	56	59[b]	58	31
Cadmium	42	30	18	29	12	8

[a]The water samples were spiked with 100 μg l^{-1} cobalt and 20 μg l^{-1} cadmium. A 14-ml aliquot of sample was taken in each case for the preconcentration. The zinc content of the sample was 8 mg l^{-1} unless stated otherwise. [b]Sample, collected on a separate day, contained 12 mg l^{-1} zinc.

elution would be counteracted by losses of analyte caused by insufficient contact time (as low as 0.15 s) with the column packing. The relatively low retention efficiency for cadmium with the smaller columns was probably compensated by the faster elution producing a high narrow peak. The

relatively low retention efficiency and concentration efficiency for the Chelex-100 columns is attributed to the swelling and shrinking properties as well as the coarser particle size of the Chelex-100 (50—100 mesh compared to 90—120 mesh for the CPG-8Q exchanger). The %E measurements were made with pure aqueous standards at a relatively high concentration of 1 mg l^{-1}; the situation will be different with lower concentrations, and could be extremely different in the presence of certain sample matrices which would influence the concentration efficiency.

The column dimensions and exchange capacity have a strong influence on the tolerance for interferences of the on-line preconcentration system. This can be seen from the recovery studies on the water samples in Table 1. Whereas the large column (3 × 45 mm) of CPG-8Q produced good recoveries of 90—99% for cobalt in all the samples studied, few of the recoveries with the smaller column (2.3 × 12 mm) could be considered satisfactory. The same tendency can be seen in the case of cadmium, but the recoveries are worse. A study on the retention efficiencies for cobalt and cadmium in the water samples (not included in the table) showed that the low recoveries were almost without exception due to breakthrough of the analyte during the loading stage. This behavior was at first attributed mainly to the short residence time of the sample in the column which would be unfavourable for retention of the analyte in the presence of a large population of competing ions from the sample matrix. The flow rate was therefore varied to produce identical or longer residence times with the smaller columns without altering the total volume of sample loaded on the columns. The results are shown in Table 2. The tap-water sample showing the most serious interfering effects in Table 1 was used for the study. Surprisingly, the recoveries at the lower flow rate were even worse than those at the higher flow rate, although the elution peaks for both standards and samples were 20—50% taller than at the higher flow rate with 2.3 × 12 mm columns. The increase in peak height showed that the retention efficiency was definitely improved but at the expense of poorer concentration efficiency. Yet the increased residence time seemed to favour retention of the competing ions, which apparently is the reason for the low recovery. Analysis of the tap-water sample, which was from a new pipeline, revealed an extraordinarily high zinc content of 8 mg l^{-1}; this was suspected to be the main interferent creating the low recovery. A separate study conducted by adding similar amounts of zinc to standard solutions of cobalt and cadmium confirmed this suspicion. The stability constants of the zinc complexes of the functional groups studied are similar to those of cobalt and higher than those of cadmium. Thus, if insufficient exchange capacity is reserved for the competition, recovery of the more weakly complexed metals will be low. This phenomenon was also observed by Malamas et al. [3] in a study on the interfering effects of copper on cadmium also with a CPG-8Q column. These observations further emphasize the importance of column capacity in the design of on-line column preconcentration systems.

Although columns with higher ion-exchange capacities are more tolerant to chemical interferences in the sample solution, this may not be true in relation to spectral interferences in the eluate, particularly when i.c.p./a.e.s. is used for detection. A high column capacity is also beneficial for the collection of matrix elements such as calcium and magnesium which usually form weak complexes with chelating ion-exchangers. Although a sample buffered at a pH favouring the analyte is generally used for preconcentration, considerable amounts of the alkaline earth metals are still retained on the columns which are later eluted with the analyte metals. Hirata et al. [13] recently reported spectral interferences from magnesium and manganese in the determination of chromium(III), using an on-line column preconcentration/i.c.p. system.

The effect of column capacity on the concentration of calcium and magnesium in the elution peak maxima was studied here by passing a solution containing 1000 mg l^{-1} magnesium and 500 mg l^{-1} calcium through CPG-8Q columns with different capacities. The results are shown in Table 3. Much less of the alkaline earth metals was collected on the smaller columns, so that spectral interferences would be less. Clearly, the tolerance capacity of interferences in both the sample-loading stage and in the elution/detection stage must be carefully balanced in the optimization of column capacity.

The primary and secondary considerations presented above were used as guidelines for the optimization of experimental parameters for the determination of trace amounts of cobalt in water samples by a.a.s. after on-line column preconcentration, with special emphasis on the overall performance, including preconcentration factor, speed, precision and accuracy. The recommended procedure involves on-line preconcentration of cobalt with time-based sampling and a double-column system. Columns (3 mm i.d., 45 mm long) of CPG-8Q ion-exchanger are used with a loading rate of 9.5 ml min^{-1} and a loading period of 90 s. An enrichment factor of 48 is thus achieved at a sampling frequency of 60 h^{-1}. Good recoveries were obtained for all the water sample types studied (see Table 1). The precision was 1.7% r.s.d. (n = 11) at the 40 $\mu g\ l^{-1}$ level, and the detection limit (3σ) was 0.2 $\mu g\ l^{-1}$,

TABLE 3

The effects of dimensions of a CPG-8Q column on the retention of calcium and magnesium[a]

Column i.d. (mm)	2.3	2.3	3.0
Column length (mm)	12	20	45
Ca (mg l^{-1})	2.0	13.2	77
Mg (mg l^{-1})	4.7	21	138

[a]Concentrations given refer to those of the eluate peak maxima. Original concentrations in sample were 500 mg l^{-1} Ca and 1000 mg l^{-1} Mg. Sample loading rate 9.5 ml min^{-1}; preconcentration period 90 s.

which is close to that of electrothermal atomization a.a.s. with a 10-μl sample.

Preliminary attempts to develop an efficient and reliable preconcentration procedure for cadmium were not as successful, as can be seen from Table 1. Although fairly satisfactory results can be obtained with a Chelex-100 column for most of the sample types studied, the concentration efficiency is not impressive, and a better chelating ion-exchanger is needed. The Japanese chelating ion-exchanger Muromac A-1, which exhibits the same chelating properties as Chelex-100 but without its swelling properties, was used successfully by Japanese workers [13, 14] in on-line preconcentration systems, and seems to be a good choice.

CONCLUSIONS

One of the principal drawbacks of on-line column-preconcentration flow-injection spectrometric systems in comparison to electrothermal atomization spectrometric systems is their relatively large sample consumption of 10—20 ml per determination for a 20—100 fold signal enhancement, although this volume is much smaller than that needed for conventional batch preconcentration. A study of a typical elution curve for on-line column preconcentration shows that the eluate zone containing the highest concentration of analyte and corresponding to over 90% of the peak maximum, is often only 30—50 μl. As an injection of a 30-μl sample via the shortest possible connection into the nebulizer of an atomic absorption or i.c.p. spectrometer will produce only about 30% of the stable-state signal, decreased dispersion by improvement of the nebulization system would obviously also improve the performance of the overall system. The direct injection nebulizer, recently introduced by Fassel and coworkers [19, 20] and designed for f.i.a./i.c.p./a.e.s. systems, is capable of attaining a peak response almost equivalent to the stable state signal by injecting 30-μl samples. Thus, a dramatic increase in concentration efficiency could be expected if such a system were coupled to an on-line column preconcentration system. This direct injection nebulizer should also permit further miniaturization of the on-line preconcentration system so that concentration efficiencies of 20—50 EF min^{-1} may be achieved with 1—2 ml of sample.

Gosnell et al. [21] have recently shown that controlled-pore glass can be plastic-embedded on the walls of teflon or tygon tubing to construct open tubular reactors with immobilized enzymes. The back-pressure in such reactors is greatly reduced, permitting higher flow rates and longer column lengths. Chelating agents such as 8-quinolinol might be immobilized similarly for use in on-line preconcentration.

Financial support for this work was provided by the Research Foundations of Academia Sinica. The authors are grateful to Pierce Chemicals for the donation of a sample of the CPG-8Q ion-exchanger.

REFERENCES

1 Z. Fang, S. Xu, X. Wang and S. Zhang, Anal. Chim. Acta, 179 (1986) 325 (and references therein).
2 S. Olsen, L. C. R. Pessenda, J. Růžička and E. H. Hansen, Analyst, 108 (1983) 905.
3 F. Malamas, M. Bengtsson and G. Johansson, Anal. Chim. Acta, 160 (1984) 1.
4 Z. Fang, S. Xu and S. Zhang, Anal. Chim. Acta, 164 (1984) 41.
5 Z. Fang, J. Růžička and E. H. Hansen, Anal. Chim. Acta, 164 (1984) 23.
6 Z. Fang, S. Xu and S. Zhang, Fenxi Huaxue, 12 (1984) 997.
7 S. D. Hartenstein, J. Růžička and G. D. Christian, Anal. Chem., 57 (1985) 21.
8 M. A. Marshall and H. A. Mottola, Anal. Chem., 57 (1985) 729.
9 S. S. Jørgensen, K. M. Petersen and L. A. Hansen, Anal. Chim. Acta, 169 (1985) 51.
10 C. W. McLeod, I. G. Cook, P. J. Worsfold, J. E. Davies and J. Queay, Spectrochim. Acta, Part B, 40 (1985) 57.
11 A. G. Cox, I. G. Cook and C. W. McLeod, Analyst, 110 (1985) 331.
12 I. G. Cook, C. W. McLeod and P. J. Worsfold, Anal. Proc., 23 (1986) 5.
13 S. Hirata, Y. Umezaki and M. Ikeda, Anal. Chem., 58 (1986) 2602.
14 T. Kumamaru, H. Matsuo, K. Okamoto and M. Ikeda, Anal. Chim. Acta, 181 (1986) 271.
15 S. Hirata, Y. Umezaki and M. Ikeda, J. Flow Inject. Anal., 3 (1986) 8.
16 S. Hirata, Y. Umezaki and M. Ikeda, Bunseki Kagaku, 35 (1986) 106.
17 Z. Fang, S. Xu, X. Wang and S. Zhang, Guangpuxue yu Guangpu Fenxi, 6 (1986) 31.
18 A. Mizuike, Enrichment Techniques for Inorganic Trace Analysis, Springer, Berlin, 1983.
19 K. E. Lawrence, G. W. Rice and V. A. Fassel, Anal. Chem., 56 (1984) 289.
20 K. E. LaFreniere, G. W. Rice and V. A. Fassel, Spectrochim. Acta, Part B, 40 (1985) 1495.
21 M. C. Gosnell, R. E. Snelling and H. A. Mottola, Anal. Chem., 58 (1986) 1585.

Analytica Chimica Acta, 200 (1987) 51—59
Elsevier Science Publishers B.V., Amsterdam — Printed in The Netherlands

EFFECTS OF ULTRASONIC IRRADIATION IN FLOW-INJECTION SYSTEMS

P. LINARES, F. LÁZARO, M. D. LUQUE DE CASTRO** and M. VALCÁRCEL*
Department of Analytical Chemistry, Faculty of Sciences, University of Córdoba, Córdoba (Spain)

(Received 26th March 1987)

SUMMARY

The effects of ultrasonic irradiation on transport and reactions in several flow-injection manifolds are described. The influence of ultrasound on the physical dispersion of the injected plug is considered. Its effects on systems involving homogeneous (catalytic and non-catalytic) and heterogeneous (liquid/liquid extraction, precipitation) reactions are critically evaluated. In general, greater sensitivity is obtained, especially for heterogeneous systems, slow reactions and low analyte concentrations. Finally, practical considerations and potential uses of the combination of ultrasonic irradiation with flow-injection analysis are discussed.

The propagation of ultrasonic waves, characterized by a minimum frequency of 16 kHz, results in rapid fluid movement through compression and rarefaction, and the waves generated give rise to cavitation, i.e., the formation and collapse of microbubbles. Thus, regular temperature and pressure waves are generated which, in general, facilitate and accelerate chemical reactions. Free radicals and ions may be generated, chemical layers are dispersed and the contact between the ingredients of the reaction mixture is dramatically facilitated. Usually, ultrasonic effects are much greater in heterogeneous than in homogeneous chemical systems, because emulsification is favoured and mass and heat transfer in two-phase systems is increased [1]. Organic chemistry has been the discipline exploiting to a greater extent the systematic use of ultrasounds to facilitate, improve and accelerate a large variety of reactions [2, 3].

*Miguel Valcárcel has been Professor of Analytical Chemistry of the University of Córdoba (Spain) since 1976. He is currently Head of the Department of Analytical Chemistry. His present research interests are in automatic methods of analysis, with emphasis on continuous-flow systems and advanced fluorimetric techniques. He is co-author of several monographs and textbooks, as well as of over 200 papers. He was appointed President of the Spanish Society of Analytical Chemists in 1985.

**María Dolores Luque de Castro obtained her Ph.D. degree from Seville University in 1976 and was appointed Assistant Professor of Analytical Chemistry by the University of Córdoba in 1979. She is the co-author of a monograph on flow-injection analysis and of over 100 papers.

0003-2670/87/$03.50

The involvement of sound in analytical chemistry occurs in three areas. One is sound generation by light irradiation in photoacoustic spectroscopy [4, 5]. A second is the use of acoustic emissions from chemical reactions as analytical signals [6, 7]. Recently, an ultrasonic gas-chromatographic detector was reported for the determination of the absolute weight of an unknown analyte without the need for calibration [8]. The application of ultrasound to on-line analysis has been discussed by Asher [9]. The third is the use of ultrasound to enhance one or more of the properties of an analytical system. In a recent paper [10], three extraction procedures (Soxhlet, alkaline digestion and ultrasonication) were critically compared for removal of petroleum hydrocarbons in sediments. The system based on ultrasound was found to be much faster, though it also resulted in poorer reproducibility. A similar study was reported on the determination of chlorobenzenes in bottom sediments [11] and on the extraction of thirteen trace elements from atmospheric particulates collected on glass-fibre high-volume sampler filters [12]. A sonication system has been used for the direct extraction of metals from plants with hydrochloric acid [13]. Recently, an ultrasonic procedure for liberating trihalomethanes from granular activated carbon was described [14]. An application of growing interest is in the design of interfaces in hybrid techniques, as in reverse-phase liquid chromatography/mass spectrometry [15] and liquid chromatography with flame photometric detection [16].

The sole application of sonication in flow-injection analysis (f.i.a.) so far reported involves the chemiluminescence of aqueous alkaline solutions of luminol containing dissolved oxygen, catalyzed by cobalt at the sub-pg level [17, 18].

This paper is concerned with a study of the effects of ultrasonic treatment on various flow-injection systems involving homogeneous or heterogeneous chemical reactions, as well as on the physical dispersion of an injected zone.

EXPERIMENTAL

A Pye Unicam SP6-500 single-beam spectrophotometer equipped with a Hellma 178.12QS flow-cell (inner volume 18 μl) and a Perkin-Elmer LS-1 fluorimeter furnished with a 4-μl flow-cell were used as detector, the chart recorder being a Radiometer REC80. Gilson Minipuls-2 pumps, variable-volume Tecator L100-1 valves, Tecator TMI and II "chemifolds" and teflon tubing of various diameters were used to construct the manifolds, which are described in detail below. The ultrasound source was a Bandelin Sonorex TK52 ultrasonic cleaner (60 kHz, 80 W) in which all reaction coils, etc., were placed; it was fed with water from a Selecta S-382 circulating thermostat bath.

All reagents were of analytical-reagent grade.

RESULTS AND DISCUSSION

The procedures used entailed parallel studies in the presence and absence of ultrasound to compare critically the results obtained.

Influence of ultrasound on dispersion

A single-channel flow-injection configuration was used through which a 10^{-2} M sodium borate solution circulated and into which a dye (0.0025% bromocresol green in 10^{-2} M borate) was injected. The influence of flow-injection variables (flow rate, reactor length, injected volume, inner diameter of the tubing and coil diameter) and other variables (viscosity, temperature) was systematically studied. In general, ultrasound decreased the dye dispersion slightly ($\leqslant 30\%$). The effects are plotted in Fig. 1.

The dependence of the signal on the reactor length can be explained as follows. The residence time increases with reactor length, so that the time of exposure to the ultrasound and hence the radial dispersion are increased. When the length is great, there is already much axial dispersion so the effect of ultrasound is less pronounced. For small injected volumes, the effect of ultrasound on dispersion is smaller because the degree of dilution of the plug is higher; with large injected volumes, the dilution is so small that the positive effect of ultrasound is more evident. As increased flow rates decrease the residence time and hence the time of exposure of the zone to sonication, the effect ultimately decreases with the increase in flow rate. From the observation

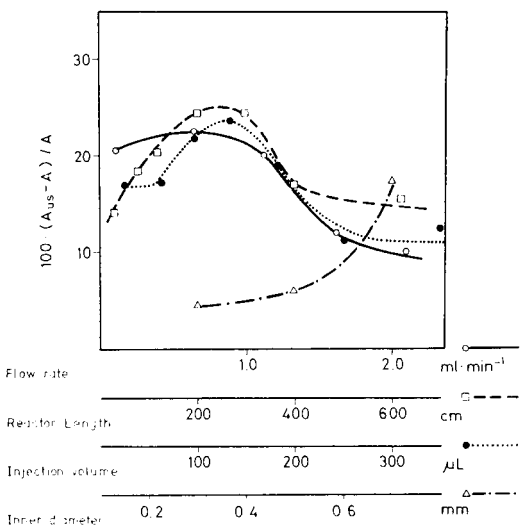

Fig. 1. Plots of the percentage increase in the analytical signal (100 $(A_{us} - A)/A$) vs. flow rate (○), reactor length (□), injected volume (●), and inner diameter (△) obtained in the study of the influence of sonication on the dispersion of a dye. (A, absorbance in the absence of ultrasound; A_{us}, in its presence.)

(Fig. 1) that ultrasound decreases dispersion at increasing reactor tubing diameter, it can be inferred that sonication exerts a positive influence on radial dispersion thus limiting linear dispersion so that its enhancing effect on the peak height increases with increasing diameter. A similar effect was observed on increasing the coil diameter. For viscosity values (carrier and sample) below 0.1 and above 0.95 cp, respectively, the effect of sonication on the system is almost nil; yet, for intermediate values, an increase in the signal of about 20% is observed in the presence of ultrasound. Increasing the temperature between 10 and 50°C shows a gradual increase in the enhancing effect of sonication from 2% to >15%.

The effect on the dispersion in single-bead-string reactors of various lengths was studied by using the same single-channel configuration. Sonication had no effect on the peak height, probably because the effective diameter of the reactor was very small (this is in agreement with the change in the sonication effect with the diameter of the open reactor tubing).

Finally, the effect of ultrasound on dispersion in configurations with splitting and confluence points along channels with the same or different lengths [19] was studied by applying this effect to one or both channels. No appreciable differences were observed with or without ultrasound. The same behaviour was observed in a cyclic configuration [20].

Influence on homogeneous reactions

The application of sonication to aqueous solutions increases the oxidizing rate [1]. To study the influence on an uncatalyzed homogeneous reaction in a flow-injection system, the complex formation between cobalt and salicylaldehyde thiosemicarbazone (SAT) was selected because this requires the prior oxidation of cobalt(II) to cobalt(III) by dissolved oxygen [19]. The configuration used is shown in Fig.2A.

This system yields an almost linear relationship between reaction rate and pH between 4.5 and 6.0. Within this pH interval, the effect of sonication at low pH values is noticeably greater than at high values, the rate being 37% greater at pH 4.5 but only 6% greater at pH 6.0, as shown in Fig. 3A. Likewise, the effect is greater, the smaller the injected volume. However, reactor length has little effect. Lengthening the residence time of the reactant zone in the system increases the effect of sonication, i.e., increasing the flow rate decreases the effect (Fig. 3B).

The calibration graph obtained under the most favourable conditions with sonication (for 2.0—20.0 μg ml^{-1}) had the equation, absorbance = 0.025 + 0.0248 [Co(II)] (in μg ml^{-1}) with r^2 = 0.999. This provides 44% more sensitivity than the calibration equation obtained without sonication: for 2—40.0 μg ml^{-1}, absorbance = 0.0091 + 0.0172 [Co(II)] with r^2 = 0.998. Some of the increase arises because the sample plug undergoes increased radial dispersion, as described for the dye. This increase results in a 28% increase of the analytical signal (calculated from the peak height obtained by injecting a dye under the same working conditions with and without ultrasound. Thus, the

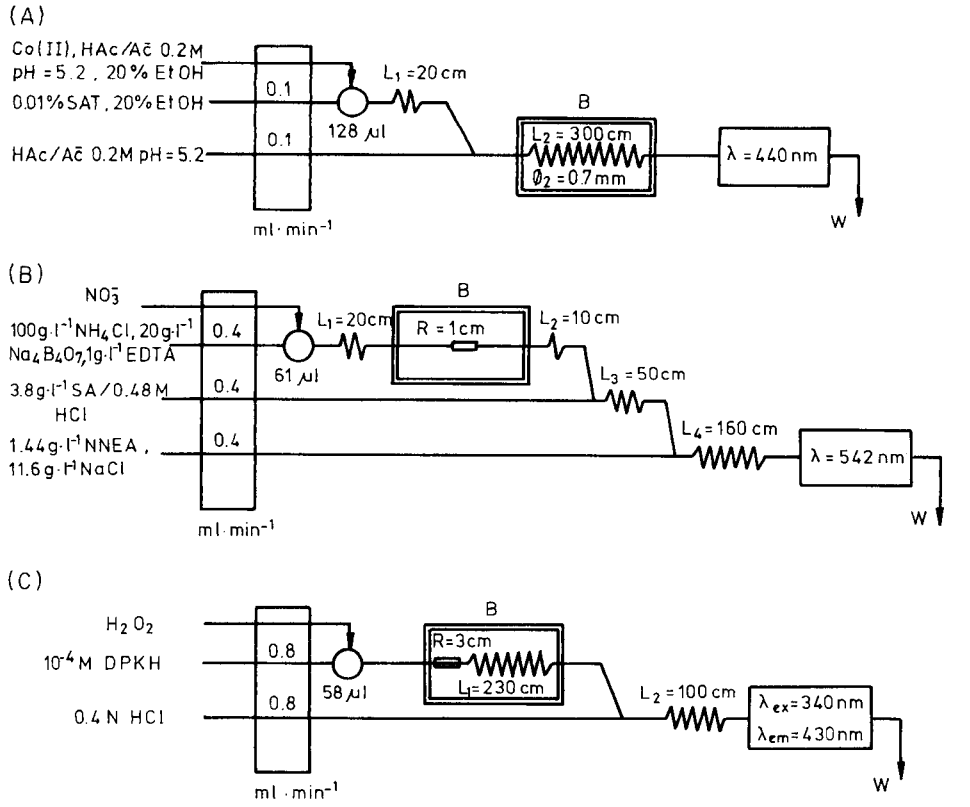

Fig. 2. Flow-injection configurations used for the study of: (A) an uncatalyzed homogeneous reaction; (B) a heterogeneous redox reaction; (C) a heterogeneous catalyzed reaction. SAT, SA, NNEA, and DPKH denote salicylaldehyde thiosemicarbazone, sulphanilamide, *N*-(1-naphthyl)-ethylenediamine dihydrochloride and 2,2′-dipyridylketone hydrazone, respectively; B is the thermostatted ultrasonic bath. All teflon tubes had an inner diameter of 0.5 mm unless stated otherwise.

effect of ultrasound on the reaction rate is to increase the signal by 16%; this is rather small, as is usual for uncatalyzed reactions.

Tests were also conducted on a homogeneous catalyzed reaction, namely, the copper-catalyzed oxidation of 2,2′-dipyridylketone hydrazone by hydrogen peroxide [21]. The reaction yield increased by 200—300% when the reaction tubing was ultrasonically irradiated, especially at small catalyst concentrations (a few ng ml^{-1}). This effect introduces interesting possibilities.

Influence on heterogeneous reactions

As stated above, those chemical systems involving interfaces are the most favourably influenced by ultrasound. Several types of flow-injection system in which the interface is permanently in the system (e.g., a redox or catalytic reactor) or is formed during the dynamic process (turbidimetry or liquid/liquid extraction) were studied.

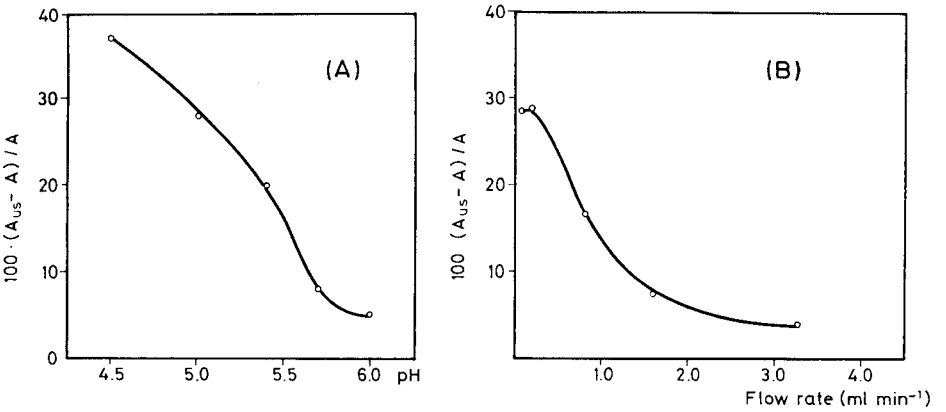

Fig. 3. Influence of pH and flow rate on the percentage increase in the analytical signal resulting from the use of ultrasonic radiation on the cobalt(II)/SAT system. Symbols as in Fig. 1.

The use of redox reactors in f.i.a. has attracted especial attention for obtaining strong but unstable oxidants and reductants [22]. Another interesting application of these reactors is the change in the oxidation state of the analyte before its measurement and/or speciation, as in the use of a copperized-cadmium reactor for determination of nitrate after reduction to nitrite (modified Griess reaction) [23]. To show the effect of ultrasonic radiation on this type of heterogeneous reaction, the redox reactor in this system was subjected to the action of ultrasound (Fig. 2B). Among the variables studied, the sample volume scarcely affected the influence of ultrasound. The plot of the relative increase in peak height in the presence of ultrasonic radiation as a function of the flow rate was a curve with a maximum at 1.1 ml min^{-1} (1-cm long reductor column) because at lower flow rates the solid/liquid interaction time is longer and the reaction in the absence of ultrasound also proceeds to an appreciable extent. At higher flow rates, the time of exposure to sonication is much shorter and so its effect is rather small. The increased reaction yield resulting from the use of ultrasonic radiation is much more noticeable when the length of the redox reactor is short, as is shown in Table 1. The calibration graphs obtained in the range 1.6×10^{-6}—3.2×10^{-5} M nitrate in the presence of sonication (absorbance = $-0.006 + 24700[NO_3^-]$ (M) with $r^2 = 0.999$) and in its absence (absorbance = $-0.009 + 15340[NO_3^-]$ (M) with $r^2 = 0.995$) showed an increase in sensitivity of ca. 60% when ultrasonic radiation was applied, although the relative standard deviation was also somewhat increased (from 1.5 to 2.7%).

To study the influence of ultrasonic radiation on catalytic reactors incorporated in a flow-injection system, a copper wire was used to catalyze the oxidation of 2,2′-dipyridylketone hydrazone (DPKH) by hydrogen peroxide. This system was used previously to develop a flow-injection stopped-flow fluorimetric procedure [21]. In this investigation, it was used to determine

TABLE 1

Enhancement of the yield of a copperized-cadmium redox reactor for reducing nitrate to nitrite, by using ultrasound

Reactor length (cm)	Reduction yield (%)[a]		Enhancement
	Without ultrasound	With ultrasound	
0.5	11.6	39.3	3.4
1.0	47.5	86.0	1.8
2.0	73.0	97.4	1.3

[a]Calculated by comparing peak heights for equimolar concentrations of nitrate and nitrite.

traces of oxidant. The configuration used is shown in Fig. 2C. A study of variables similar to that done for the redox reactor was carried out; the influence of sonication was similar to that described for nitrate determination. The calibration graphs for hydrogen peroxide in the range 5×10^{-5}—3×10^{-4} M in the presence of sonication and in its absence showed a sensitivity enhancement of 43% when ultrasound was used.

The effect of ultrasonic radiation on a flow-injection system involving continuous precipitation and turbidimetric measurements was considered by using classical chemical systems for the determination of anions. The features of the determination of sulphate by injection of the sample into an aqueous stream merging with a barium chloride solution in hydrochloric medium and in the presence of polyvinyl alcohol, were not appreciably modified when the reactor (300 cm long, flow rate 1.8 ml min^{-1}) was subjected to ultrasonic radiation. However, in the determination of oxalate by injecting the sample into an aqueous solution of calcium chloride in an ammoniacal medium, sonication of the reactor (200 cm long, flow rate 1.0 ml min^{-1}) increased the turbidimetric signal by about 20%. The different behaviour of these continuous systems on ultrasonic irradiation may be due to the different initial particle sizes of the precipitates, which are quite large for barium sulphate but much smaller for calcium oxalate. The coagulating effect of sonication [1] would therefore be more advantageous in the latter case.

One aspect of interest in the use of continuous liquid/liquid extraction without phase separation in f.i.a. involves continuous measurements made on emulsions, which normally are only possible by fluorimetry. Two approaches have been described in the literature. Kina et al. [24] in 1978 indicated the possibility of determining potassium, which was injected with an anionic fluorophore into an organic solution of a crown ether. Recently, however, Memon and Worsfold [25] proposed the use of microemulsions for the determination of analytes; this has significant advantages over the use of normal emulsions. Here, preliminary experiments were done to demonstrate the viability of ultrasound in a flow-injection design with two immiscible phases and direct measurement of the fluorescence intensity of the emulsified

zone. A merging-zones configuration was utilized for the simultaneous injection of microlitre volumes of aqueous solution of aluminium (0.5 μg ml^{-1}) and a 0.5% 8-quinolinol solution in chloroform (60 and 30 μl, respectively) into a 1:1 water/ethanol carrier (flow rate = 0.6 + 0.6 = 1.2 ml min^{-1}). Single-bead-string reactor (100 cm) was incorporated after the confluence point and placed in the ultrasonic bath. The signals obtained were enhanced by 35—100%, depending on the analyte concentration, when ultrasound was applied.

DISCUSSION

To demonstrate the possibilities of the use of ultrasonic radiation in analytical continuous-flow systems involving homogeneous or heterogeneous reactions, different procedures previously described for applications of conventional f.i.a. were investigated, and the results obtained with and without the use of ultrasound were critically compared for the same manifolds and reagents. From these studies, it can be concluded that in most of the systems studied the analytical features are more or less enhanced, particularly when interfaces or catalyzed reactions are involved. In general, the effect of sonication is more marked when detection takes place during the initial development of the reaction on which the measurements are based.

The results obtained for the large variety of systems considered in this paper allow the following practical conclusions to be drawn. To minimize problems related to the effect of ultrasonics on laboratory personnel, it is advisable to use a simple electronic timer synchronizing injection with the start of the ultrasonic system, which must act only during the residence time of the plug in the reactor. To distinguish the effect of sonication from that of the increase in temperature which it causes in the thermostat bath, thermal control by recirculation is advisable, especially in fundamental studies. The use of temperatures above 30° C in these systems give rise to bubble formation, which makes measurements difficult; thus, prior degassing of sample and carrier is mandatory. The use of an ultrasonic cleaning bath is inadvisable for analytical purposes, owing to the lack of stability of the radiation and the difficulty involved in controlling the radiation frequency and intensity.

The application of ultrasonic radiation to the transport and reaction zone of a flow-injection system has a number of prospective applications of great interest. These include ultratrace determinations of catalysts by homogeneous chemical reactions, enhancement of the yield of redox and catalytic reactors and development of continuous liquid/liquid extraction without phase separation based on fluorimetric detection. Other possibilities are in the design of continuous solid(sample)/liquid extraction which would be of interest in the automation of processes such as the determination of essential elements in soil, and trace metals in vegetable material and the desorption of pollutants from "filtration" systems.

REFERENCES

1 D. Bremner, Chem. Br., 22 (1986) 633.
2 P. Boudjouk, Nachr. Chem. Tech., 32 (1983) 798.
3 S. Toma and V. Kaliska, Chem. Listy, 79 (1985) 578.
4 M. J. Adams, J. G. Highfield and G. F. Kirkbright, Anal. Chem., 49 (1977) 1850.
5 M. J. Adams, G. F. Kirkbright and K. R. Memon, Anal. Chem., 51 (1979) 508.
6 D. Betteridge, M. T. Joslin and T. Lilley, Anal. Chem., 53 (1981) 1064.
7 M. T. Joslin, Anal. Proc., (1982) 330.
8 K. J. Skogerboe and E. S. Yeung, Anal. Chem., 56 (1984) 2684.
9 R. C. Asher, Anal. Proc., (1985) 180.
10 S. Sporstøl, R. G. Lichtenthaler and F. Oreld, Anal. Chim. Acta, 169 (1985) 343.
11 F. I. Onuska and K. A. Terry, Anal. Chem., 57 (1985) 801.
12 S. L. Harper, J. F. Walling, D. M. Holland and L. J. Pranger, Anal. Chem., 55 (1983) 1553.
13 D. M. Kumina, A. V. Karyakin and I. F. Gribovskaya, Zh. Anal. Khim., 40 (1985) 30.
14 K. T. Alben and J. H. Kaczmarczyk, Anal. Chem., 58 (1986) 1817.
15 R. G. Christensen, E. White, V. S. Meiselman and H. S. Hertz, J. Chromatogr., 271 (1983) 61.
16 J. F. Karnicky, L. T. Zitelli and S. van der Wal, Anal. Chem., 59 (1987) 327.
17 M. Yamada and S. Suzuki, Chem. Lett., (1983) 783.
18 T. Komatsu, M. Ohira, M. Yamada and S. Suzuki, Bull. Chem. Soc. Jpn., 59 (1986) 1849.
19 A. Fernández, M. D. Luque de Castro and M. Valcárcel, Anal. Chem., 56 (1984) 1146.
20 A. Ríos, M. D. Luque de Castro and M. Valcárcel, Anal. Chem., 57 (1985) 1803.
21 F. Lázaro, M. D. Luque de Castro and M. Valcárcel, Anal. Chim. Acta, 165 (1984) 177.
22 R. C. Schothorst, O. O. Schmitz and G. den Boef, Anal. Chim. Acta, 179 (1986) 299 (and references therein).
23 M. F. Giné, H. Bergamin F°, E. A. G. Zagatto and B. F. Reis, Anal. Chim. Acta, 114 (1980) 191.
24 K. Kina, J. Shiraishi and N. Ishibashi, Talanta, 25 (1978) 295.
25 M. H. Memon and P. J. Worsfold, Anal. Chim. Acta, 183 (1986) 179.

Analytica Chimica Acta, 200 (1987) 61—72
Elsevier Science Publishers B.V., Amsterdam —Printed in The Netherlands

CONTINUOUS-FLOW ENZYMATIC DETERMINATION OF CREATININE WITH IMPROVED ON-LINE REMOVAL OF ENDOGENOUS AMMONIA

M. E. COLLISON and M. E. MEYERHOFF*
Department of Chemistry, University of Michigan, Ann Arbor, MI 48109 (U.S.A.)
(Received 31st March 1987)

SUMMARY

A new continuous-flow automated enzymatic method suitable for the direct determination of creatinine in physiological samples is described. The proposed system utilizes an on-line gas predialysis unit in conjunction with a flow-through enzyme reactor coil and a potentiometric ammonia detector. The enzyme reactor contains immobilized creatinine iminohydrolase (EC 3.5.4.21) which converts creatinine to ammonia and *N*-methylhydantoin. Ammonia liberated from this reaction is detected downstream with the membrane electrode-based detector. The novel gas predialysis unit effectively removes >99.8% of endogenous ammonia (up to 1 mM) present in the sample. Thus, final peak potentials recorded by the electrode detector are directly proportional to the logarithm of creatinine concentrations present. The method is shown to be precise (< 3%), selective, and capable of accurately determining creatinine in serum and urine samples containing abnormally high endogenous ammonia levels. Determinations of creatinine in serum samples (n = 30) using this new method correlate well with an existing Technicon AutoAnalyzer colorimetric method (r = 0.996).

In recent years, various selective enzymes have been coupled with ammonia detection methods to measure important amino acids and metabolites in physiological samples [1—6]. In such assays, ammonia liberated from the enzymatic reaction should be directly proportional to the concentration of analyte initially present in the sample. In reality, problems arise from the background levels of ammonia nitrogen (NH_3—N) found in many biological samples. Indeed, normal blood ammonia levels are generally in the same concentration range as most amino acids and metabolites (10—100 μmol l^{-1}) [7, 8]. Moreover, any delay in analysis of the blood sample will result in large increases in background ammonia levels because of hydrolysis of labile glutamine and aspargine residues in proteins [9]. The problem is further

*Mark E. Meyerhoff obtained his B.A. (Chemistry) at the Herbert H. Lehman College (CUNY system), and his Ph.D. in 1979 at the State University of New York at Buffalo under the direction of Prof. G. A. Rechnitz. After postdoctoral work at the University of Delaware, Newark, DE he moved to Michigan in 1979 and became an Associate Professor of Chemistry at the University of Michigan in 1985. His research interests are in the areas of ion-selective electrodes, gas sensors, bioanalytical chemistry, enzyme-labelled competitive binding assays, and novel toxicity bioassays.

0003-2670/87/$03.50

compounded when samples are drawn from patients with disease states that result in hyperammonemia (e.g., hepatic coma, Ryes syndrome, etc.), where ammonia can reach levels as high as 1 mmol l^{-1} in fresh serum [10].

Various methods have been proposed to alleviate or correct for the endogenous ammonia problem in blood and particularly urine. Time-consuming manual pretreatment steps including cation-exchange [11, 12] and distillation [13, 14] have been used. Difference measurements in which background ammonia is first determined and then subtracted from the total ammonia present after the enzyme reaction have been proposed for blood analysis [11]. Unfortunately, the accuracy of this latter method decreases when the ratio of endogenous ammonia to analyte levels increases. Recently, several researchers [2, 15—17] have used glutamate dehydrogenase (GLDH) to remove endogenous ammonia enzymatically

$$NH_4^+ + \alpha\text{-ketoglutarate} + NADH \rightarrow NAD^+ + \text{L-glutamate} + H_2O$$

from physiological samples. The method requires the use of NADH or NADPH, and soluble or immobilized GLDH, making the system less attractive for adaptation to high throughput autoanalyzer-type systems. In order to reduce the cost, the amount of NADH used per assay can be lowered; however, this severely limits the concentration of endogenous ammonia which can be tolerated [10].

In 1983, a novel flow-through on-line gas predialyzer was introduced, which was capable of removing approximately 90% of endogenous ammonia in serum and plasma samples [18]. The original concept was demonstrated in an automated system for the determination of asparagine in plasma samples. While such a system could adequately reduce normal background ammonia levels, errors greater than 10% could still occur if samples contained abnormally high ammonia concentrations. In this paper, a simple temperature modification to the original on-line gas predialyzer design is described; it enables greater than 99.8% of the ammonia to be removed from serum and urine samples containing up to 1 mM ammonia. Additionally, this predialyzer is used in conjunction with immobilized creatinine iminohydrolase enzyme (EC 3.5.4.21) to develop an automated system for the direct determination of creatinine in serum and urine samples.

Creatinine levels in blood and urine are the most widely accepted indicators of kidney function. The classical Jaffé colorimetric method is known to suffer many interferences [19]. Consequently, the accuracy and precision requirements of clinical creatinine assays require the development of non-Jaffé methods [20]. Among alternative techniques it is well recognized that enzymatic methods can greatly enhance the selectivity of creatinine determinations [19, 21]. Towards this end, the new system (Fig. 1) contains a tubular enzyme reactor coil to convert creatinine to *N*-methylhydantoin and ammonia. The ammonia is detected downstream with an improved membrane electrode-based detector [22]. The on-line predialyzer is placed ahead of the enzyme coil where it removes endogenous ammonia from the

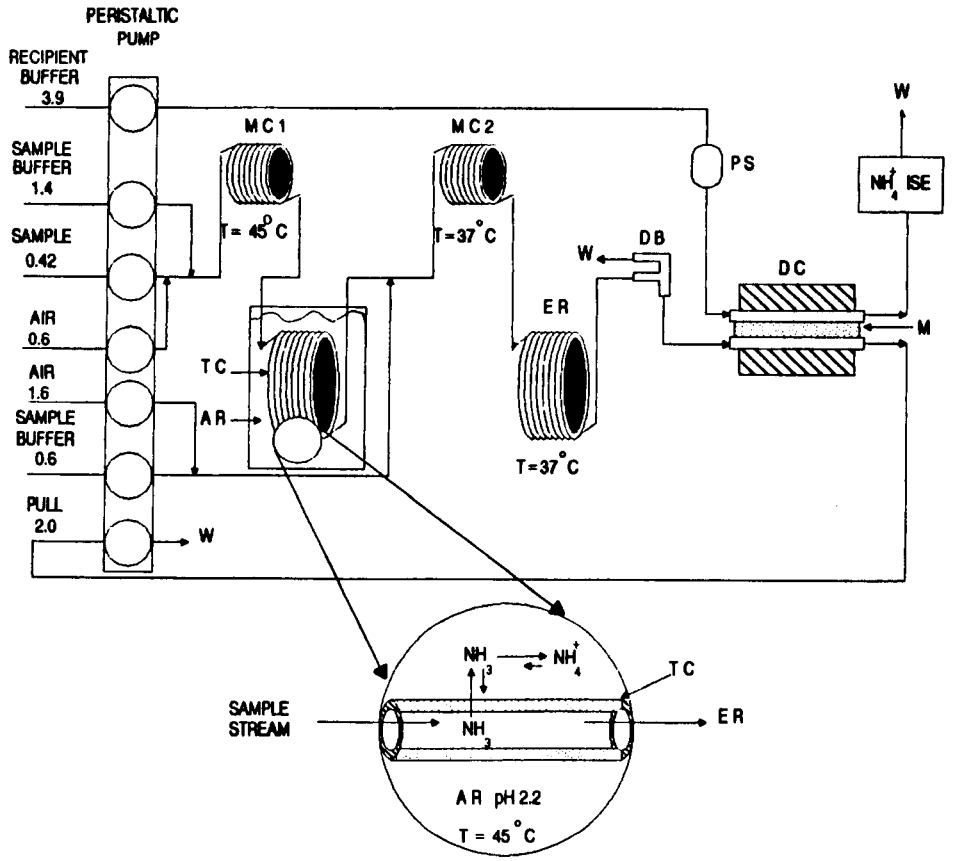

Fig. 1. Flow diagram of automated creatinine system: (MC) mixing coil; (TC) on-line teflon predialyzer coil; (AR) acid reservoir trap; (ER) enzyme reactor coil; (DB) debubbler; (PS) pulse suppressor; (DC) gas dialysis chamber; (M) porous gas permeable membrane; (W) waste. Numbers represent flow-rates in ml min^{-1}.

sample before it enters the enzyme coil. Consequently, detected ammonia is directly proportional to the concentration of creatinine, regardless of the initial ammonia level present in the sample.

EXPERIMENTAL

Apparatus

A schematic diagram of the automated creatinine system is shown in Fig. 1. A Rainin (Woburn, MA) peristaltic pump was used to deliver the sample, reagents and air through the system. A Technicon Sampler II served as the autosampler, and was operated at a throughput of 30 samples per hour, with a 1:2 sample/wash ratio.

The ammonia predialysis unit consisted of a 4.2-m length of teflon gas-permeable tubing [poly(tetrafluoroethylene), 1-mm i.d., 50% porosity, Anspec Company, Ann Arbor, MI]. The tubing was coiled and placed in a 250-ml acid reservoir (0.2 mol l^{-1}, pH 2.2, H_3PO_4, NaOH buffer). The predialyzer was thermostated at temperatures ranging from 25 to 45°C, with optimal ammonia removal being obtained at 45°C. The predialyzer was preceded by a 40-s (1.5 ml) mixing coil that was also thermostated at the predialyzer temperature. The sample residence time in the predialysis coil was 110 s.

The enzyme-reactor coil consisted of creatinine iminohydrolase immobilized on the inner walls of a 1-m length of 1.0-mm i.d. nylon tubing. The enzyme was obtained from G.D.S. Technology (Elkhart, IN) and was immobilized by established procedures [23]. The specific activity of this enzyme coil was evaluated by the method described by Hornby and Noy [24]. The method was applied in the range 3—85 mmol l^{-1} creatinine where the fractional conversion varied, i.e., where the enzyme activity was rate-limiting. The apparent Michaelis-Menten constant, K', was found to be 2.8×10^{-2} mol l^{-1}. The specific activity of the enzyme coil was 0.84 μmol min^{-1} cm^{-1}. When stored as described below (see Reagents) the activity of this enzyme coil remained essentially constant for 1 year and several thousand creatinine samples.

For certain preliminary experiments, commercial enzyme-reactor coils obtained from Farmitalia Carlo Erba (Milan, Italy) were used. The various enzyme reactors were thermostated at 37°C and preceded by a 25-s (1.5 ml) mixing coil maintained at the same temperature. Sample residence times in the enzyme reactor were usually 10—12 s.

The potentiometric ammonia detection system used in this work was similar in design to those described previously [22, 25]. An improvement in response to low levels of ammonia was achieved by using a custom-designed gas dialysis chamber (for details, see [26]) which enhances the efficiency of gas transfer between the sample and recipient streams. The final configuration was further modified to reduce extensive streaming potential oscillations (±1—2 mV) caused by the relatively high recipient buffer flow rate used in this particular work (3.9 ml min^{-1}). This was accomplished by using two Ag/AgCl electrodes, rather than a single reference and stainless steel nipple, in a circuit arrangement analogous to that suggested by van den Winkel et al. [27]. With this change, oscillations in baseline potentials were reduced to ±0.2 mV.

Potentiometric measurements were made with a Fischer Accumet pH Meter (Model 620) and were recorded on a Linear (Irvine, CA) Model 1201 strip-chart recorder. The recorder output of the Fisher pH meter was also monitored by a computer-based data acquisition system. The data acquisition system consisted of a Keithley Model 179 TRMS-A Digital Multimeter with IEEE-488 interface connected to a Commodore Pet Model 8032 microcomputer. Appropriate software was used to detect and record auto-

matically the baseline, peak potentials and ΔE values (peak minus baseline potentials).

Reagents

All chemicals used were analytical-reagent grade. Standard solutions and buffers were prepared with reverse-osmosis deionized water. Buffer concentrations refer to total ionic strength. Reagents were stored in sealed glass containers to minimize absorption of atmospheric ammonia.

The sample stream diluent was 0.1 mol l^{-1} boric acid/sodium hydroxide, pH 9.50, containing 2 mmol l^{-1} EDTA. The recipient stream buffer at the detector was a 0.01 mol l^{-1}, HCl/Tris [tris(hydroxymethyl)aminomethane] buffer, pH 7.50.

Enzyme-reactor coils were stored refrigerated (4°C) between experiments and filled with a 0.1 mol l^{-1} phosphate storage buffer, pH 7.0, containing 0.1% (w/w) EDTA and 0.05% (w/w) sodium azide.

Weekly, a fresh 5×10^{-2} mol l^{-1} creatinine stock solution (prepared in 0.01 mol l^{-1} HCl) was diluted with deionized water to prepare working creatinine standards in the range of 25—5000 μmol l^{-1} (0.28—56.6 mg dl^{-1}).

Procedures

Evaluation of predialyzer unit. Initially, the predialysis unit and enzyme-reactor coil of Fig. 1 were removed so that the ammonia response could be calibrated and the ammonia content of serum and urine samples could be determined. Aqueous ammonium chloride standards (5—5000 μmol l^{-1}) were sampled and corresponding ΔE values recorded. Following the standards, ammonium chloride-spiked pooled serum (undiluted) and urine samples (1 + 99 diluted) were aspirated into the system and the resulting ΔE values were recorded. The predialysis unit was then reincorporated into the system and the same series of ammonium chloride standards and ammonium chloride-spiked serum and urine samples were analyzed.

The pooled serum used for these experiments was obtained from healthy members of our research group. Reconstituted Fisher Level 1 Control Urine (lot 258-074) was used to prepare the ammonium chloride-spiked urine samples. These latter samples were prepared by diluting (with deionized water) 1 ml of reconstituted urine plus microliter amounts of 0.1 mol l^{-1} ammonium chloride to a final volume of 100 ml. All serum and urine samples were stored frozen (—21°C) between experiments.

Creatinine determinations. The complete flow configuration was used for creatinine determinations (Fig. 1). An initial series of aqueous creatinine standards ranging from 25 to 5000 μmol l^{-1} (0.28—56.6 mg dl^{-1}) were sampled. The potential was then allowed to return to baseline before serum or urine samples were analyzed. Following the serum and/or urine samples, the potential was again allowed to return to baseline before a second series of creatinine standards was sampled. Unknown creatinine levels were determined from a linear least-squares fit of the combined initial and final aqueous calibration data in which peak-height potentials (ΔE) were plotted vs. the logarithm of creatinine concentrations.

RESULTS AND DISCUSSION

The basic operating principles of the proposed creatinine system are straightforward. Samples are pumped from the autosampler, immediately air-segmented, and diluted with an alkaline buffer to convert partially ammonia in the sample to free ammonia gas. The samples then pass through the on-line gas predialyzer. The insert in Fig. 1 shows an expanded view of the predialysis unit and the chemical processes that take place within. As the sample passes through the predialyzer, free ammonia gas in the sample diffuses through the walls of the gas-permeable teflon tubing and is trapped as ammonium ions by the acid reservoir. Thus, as the sample traverses the length of the coiled tubing, the ammonia content of the sample is reduced while the creatinine level remains unchanged. Following the predialyzer, additional air-segmentation and buffer are added to the sample prior to its passage through the enzyme reactor. In the enzyme reactor, immobilized creatinine iminohydrolase catalyzes the following reaction:

creatinine + $H_2O \rightarrow$ *N*-methylhydantoin + NH_3

Following the enzyme reactor, the sample stream is debubbled and passed through the flow-through potentiometric ammonia detector. The recorded potential changes (ΔE) are proportional to the logarithm of the creatinine concentration in the sample.

In the design of the final automated arrangement, numerous studies were done to optimize sample ammonia removal and to maximize the response of the system to creatinine. The results of these studies are detailed below.

Optimization of ammonia and creatinine response

Initial experiments with the enzyme reactor coils demonstrated that approximately 50% conversion of creatinine to ammonia could be achieved with a sample-stream diluent pH of 9.50 and a total sample/diluent ratio of 1:5. Consequently, the ammonia detection system was optimized under these conditions. For ammonia response studies, the gas predialyzer and the enzyme reactor were removed and the response was monitored as a function of varying flow rate combinations through the detector gas dialysis chamber. In all, 22 combinations of flow rates for the sample and recipient streams were examined. The flow-rate combination shown in Fig. 1 (3.9 ml min^{-1} recipient; 2.0 ml min^{-1} sample stream in the dialysis chamber) provided a good compromise for reasonably fast detector washout times and nearly optimal potential response for given ammonia concentrations.

Typical calibration curves for aqueous ammonia and creatinine standards obtained by using this combination of flow rates are shown in Fig. 2. The creatinine curve was obtained by adding the enzyme reactor coil to the flow system while still leaving the predialyzer unattached. Response to creatinine paralleled that obtained for ammonia but was shifted to higher concentrations owing to the incomplete conversion of creatinine to ammonia in the

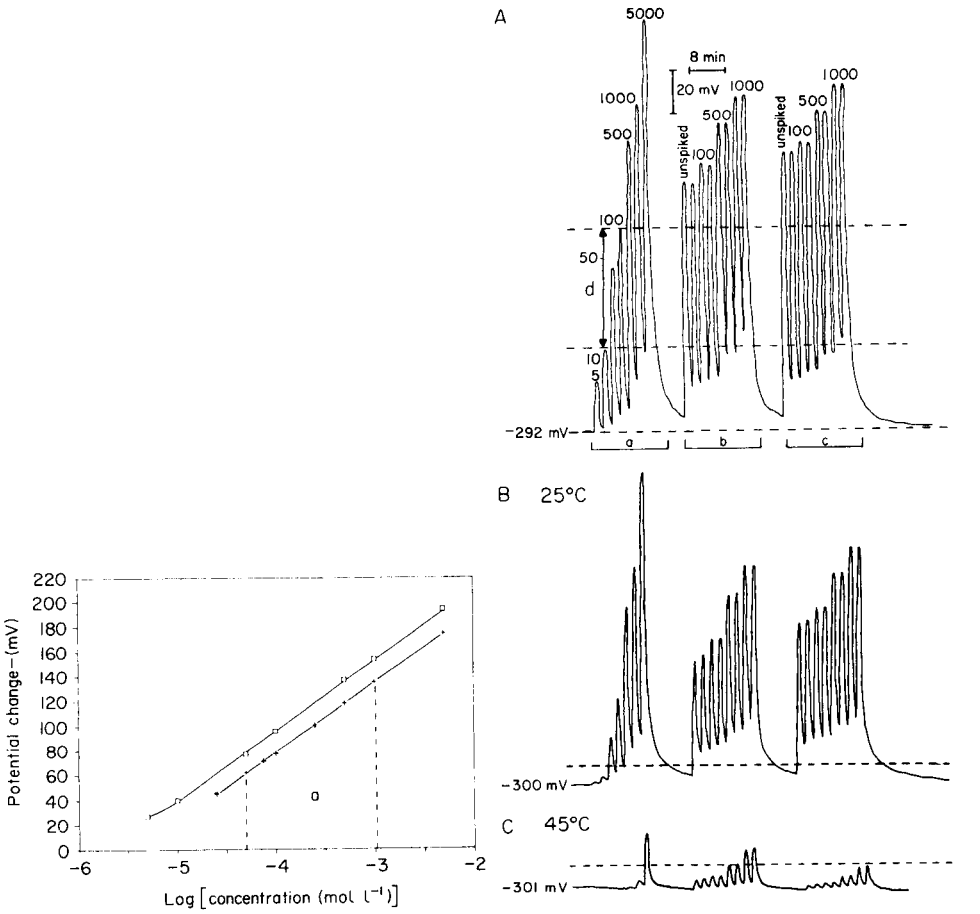

Fig. 2. Typical calibration curves obtained for ammonia (□) and aqueous creatinine standards (+) with the system shown in Fig. 1 without gas predialyzer in place. Range (a) is the clinical range (50—1000 μmol l^{-1}, 0.56—11 mg dl^{-1}).

Fig. 3. Strip-chart recordings illustrating the effectiveness of the on-line gas predialyzer coil in removing endogenous ammonia at two different predialyzer temperatures: (A) without predialyzer in place; (B) with predialyzer maintained at 25°C; (C) with predialyzer maintained at 45°C. Samples were aqueous ammonium chloride standards (a), ammonium chloride-spiked serum (b), and ammonium chloride-spiked (1 + 99) diluted urine (c). The range labeled (d) is the normal range of serum ammonia (10—100 μmol l^{-1}). Numbers above peaks in (A) refer to μmol l^{-1} ammonia in standards or added to serum and urine samples.

reactor. Nevertheless, the creatinine response is nearly Nernstian (58 mV/decade) in the range of 25—5000 μmol l^{-1}, a range which extends well below and above that required for clinical applications (50—1000 μmol l^{-1}). It should be noted that, given the ammonia detection capabilities of the proposed system, creatinine conversion efficiencies as low as 20% can be tolerated while still maintaining calibration linearity in the low end of the clinically important creatinine range.

Optimization of predialyzer efficiency

Hydrochloric acid solutions (1.0 and 0.1 mol l^{-1}), citric acid buffer (0.2 mol l^{-1}, pH 3.2) and phosphoric acid buffer (0.2 mol l^{-1}, pH 2.2) were each studied as potential solutions for the acid-trap reservoir. Though hydrochloric acid was used successfully in the previous predialyzer configuration [18], its use in the current system was not possible. At the elevated predialyzer temperatures used in these studies, hydrogen chloride readily diffused through the walls of the gas-permeable predialyzer coil and caused large changes in the sample stream pH. Of the two non-volatile buffers studied, the phosphoric acid buffer with lower pH (pH 2.2) proved to be the more efficient trapping medium because of the larger pH difference between the sample-stream buffer inside the coil and the external acidic reservoir.

The most critical parameter with regard to the efficiency of on-line ammonia removal is the temperature of the predialysis unit. As shown in Fig. 3, for a given predialysis residence time, dramatic improvements in efficiency can be realized when the temperature of the unit is increased. Figure 3A shows a strip-chart recording obtained when aqueous ammonium chloride standards along with serum and urine samples spiked with varying levels of ammonium chloride were passed through the system without the predialyzer and enzyme reactor in place. Figure 3B and 3C show the response of the system toward the same standards and samples after the predialyzer is added and thermostated at 25°C and 45°C, respectively. The baseline potential of the system also changes upon addition of the predialyzer. This is a result of the removal of trace levels of ammonia in the diluent buffer. Taking this baseline shift into account, removal of ammonia is approximately 90% for all samples when the predialyzer is thermostated at 25°C. In contrast, elevating the predialysis temperature to 45°C results in efficiencies greater than 99.8%, even for serum samples spiked to contain more than 1 mmol l^{-1} ammonia (10 times the highest levels normally found in serum). This dramatic temperature effect may be rationalized in terms of decreasing sample stream viscosity, increasing ammonia diffusion coefficient and decreasing ammonia solubility in the sample stream with increasing predialyzer temperature.

Determinations of creatinine in physiological samples

With the various components optimized, the performance of the complete continuous-flow arrangement was assessed. The response to creatinine in physiological samples (control serum and control urine) was studied with and without the predialyzer in place. Figure 4A shows the tracing obtained for a series of aqueous creatinine standards followed by serum and diluted urine (1 + 99) samples spiked with varying amounts of ammonium chloride. As can be seen, without removal of endogenous ammonia, the "creatinine" response closely follows the levels of ammonium chloride added. When the predialyzer is in place (Fig. 4B), regardless of the amount of ammonium chloride added, the response towards creatinine remains constant and

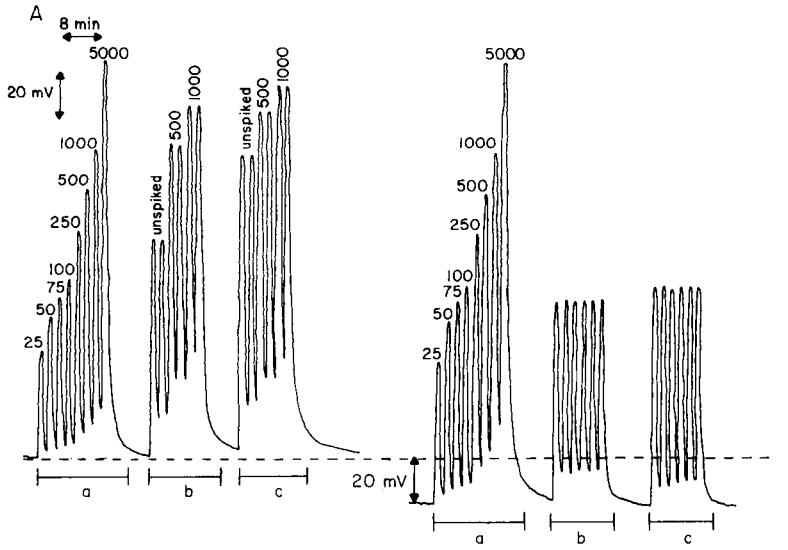

Fig. 4. Strip-chart recording showing the creatinine response of the automated system: (A) without gas predialyzer coil in place; (B) with predialyzer maintained at 45°C. Samples were aqueous creatinine standards (a), ammonium chloride-spiked control serum (b), and ammonium chloride-spiked (1 + 99) diluted control urine (c). The numbers above the creatinine standard peaks indicate μmol l^{-1} creatinine. Those above the serum and urine samples indicate μmol l^{-1} added ammonia. Reported creatinine values for control serum and urine were 92 ± 1 and 106 ± 4 μmol l^{-1}, respectively.

closely correlates with the control values reported for these samples (see legend to Fig. 4). Additionally, it can be seen from Fig. 4 that within-run precision is excellent (s.d. less than ±0.5 mV, corresponding to a concentration reproducibility of 2%) even for samples containing constant creatinine but varying ammonia. In subsequent experiments, between-run precision was evaluated by analyzing 30 different serum samples in each of three successive runs (see Experimental section for calibration and analytical procedures corresponding to a single run). The observed between-run relative standard deviation was 3% or less over the entire concentration range of the samples (0.5—12 mg dl^{-1}; 44—1060 μmol l^{-1}).

Recovery studies were performed on pooled serum and control urine samples to which known amounts of creatinine were added. These samples were further divided into lots which were spiked with varying levels of ammonium chloride. As shown in Tables 1 and 2, added creatinine could be quantitatively recovered regardless of the background of added ammonia.

The proposed creatinine method was further evaluated by conducting a correlation study with the existing Technicon SMAC method number SG4-0011B83 (Jaffé reaction) using unidentifiable serum samples obtained from the University of Michigan Hospital (n = 30). Prior to creatinine determinations, the range of endogenous ammonia in these serum samples was found to be 5.7×10^{-5}—3.3×10^{-4} mol l^{-1}. Figure 5 shows a com-

TABLE 1

Recovery of creatinine added to urine at two background ammonia levels

Creatinine added[a] (mg dl^{-1})	Recovery[b] (%)	
	Endogenous ammonia	1.0 mM ammonia added
1.13	106.7	113.5
2.83	100.9	100.9
5.66	99.3	103.8
11.31	103.7	99.9
Average	102.7 ± 3.3	104.5 ± 6.2

[a]To a (1 + 99) dilution of urine. The unspiked urine creatinine level was 1.21 mg dl^{-1}. [b]Average of three determinations.

TABLE 2

Recovery of creatinine added to serum at three different background ammonia levels

Creatinine added[a] (mg dl^{-1})	Recovery[b] (%)		
	Endogenous ammonia	0.5 mM NH_3 added	1.0 mM NH_3 added
1.13	93.7	104.2	103.8
2.82	98.5	98.3	102.2
5.60	96.1	102.7	101.8
11.09	95.0	95.9	102.5
Average	95.8 ± 2.0	100.3 ± 3.9	102.6 ± 0.9

[a]Unspiked serum creatinine level was 0.91 mg dl^{-1}. [b]Average of three determinations.

parison of results with the proposed method and the SMAC method for different ammonia levels in the samples. The negative y-intercept is expected in view of the known chromophoric interferences with Jaffé methods [19]. The slope of <1.0 suggests that the efficiency of the enzymatic creatinine conversion and/or the detection of ammonia is decreased somewhat in the serum samples relative to the aqueous standards used in these studies. Thus, before routine clinical use, further characterization of this bias will be required.

Conclusions

These studies demonstrate that the proposed on-line gas predialysis method can be used to remove virtually 100% of normal and elevated levels of endogenous ammonia from physiological samples. This approach offers significant advantages over other ammonia abatement methods in that no additional reagents or secondary enzyme systems are required. In view of

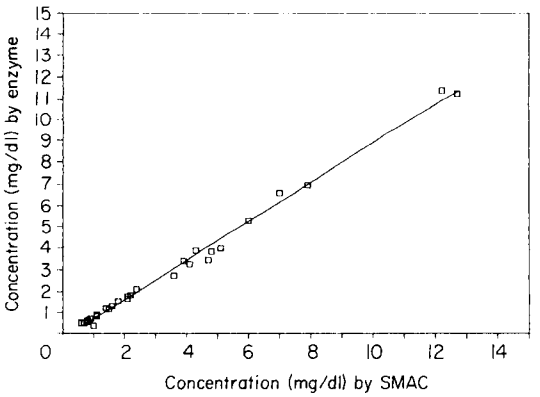

Fig. 5. Results from correlation study between the enzyme-based continuous-flow method and the Technicon SMAC colorimetric method. The SMAC assays were run at the Chemical Pathology Laboratory, University of Michigan Hospital. N = 30; slope = 0.91 ± 0.02; intercept = −0.20 ± 0.07; correlation coefficient = 0.9966; standard error of estimate = ±0.24 mg dl^{-1}.

the large number of selective enzymes which liberate ammonia, the system described here should offer a general approach for the selective determination of a variety of biomolecules. Furthermore, it is likely that this concept could be extended to the removal of endogenous carbon dioxide from biological samples thereby enabling the adaptation of decarboxylating enzymes to the development of analogous bioanalytical systems.

The authors gratefully acknowledge the preliminary experimental work performed by Dr. Heung Lark Lee (Kyungpook National University, Korea), and the helpful discussions with Mr. David Allan (University of Michigan). This work was supported by a grant from the National Institutes of Health (GM-28882-06). In addition, M. Collison acknowledges support from the Samuel Baer and Herman Sokol fellowships administered by the Rackham Graduate School of the University of Michigan.

REFERENCES

1 R. K. Kobos, Trends Anal. Chem., 6 (1987) 6.
2 M. Mascini, S. Fortunati, D. Moscone and G. Palleschi, Anal. Chim. Acta, 171 (1985) 175.
3 M. A. Arnold and R. L. Solsky, Anal. Chem., 58 (1986) 84R.
4 G. G. Guilbault and P. R. Coulet, Anal. Chim. Acta, 152 (1983) 223.
5 G. G. Guilbault, Analytical Uses of Immobilized Enzymes, Dekker, New York, 1984.
6 M. A. Arnold, Am. Lab., 15 (1983) 34.
7 F. A. Ibbot, in R. J. Henry, D. C. Cannon and J. W. Winkleman's (Eds.), Clinical Chemistry, Principles and Techniques, 2nd edn., Harper and Row, Haggerstown, MD, 1974, Chap. 18.
8 J. I. Routh, in N. W. Tietz (Ed.), Fundamentals of Clinical Chemistry, W. B. Saunders, Philadelphia, PA, 1976, Chap. 16.
9 T. L. Perry and S. Hansen, Clin. Chem. Acta, 25 (1969) 53.

10 E. Tanganelli, L. Prencipe, D. Bassi, S. Cambiaghi and E. Murador, Clin. Chem., 28 (1982) 1461.
11 M. Mascini and G. Palleschi, Anal. Chim. Acta, 136 (1982) 69.
12 D. M. Matthews, G. G. Muir and D. M. Baron, J. Clin. Pathol., 17 (1964) 150.
13 J. F. Goodwin, Clin. Chem., 14 (1968) 1080.
14 N. S. Constantsas and C. Danelatau-Athanassiadon, Clin. Chim. Acta, 9 (1964) 1.
15 S. P. Chen, S. S. Kuan and G. G. Guilbault, Clin. Chim. Acta, 100 (1980) 21.
16 M. Tabata, T. Kido, M. Totani, et al., Anal. Biochem., 134 (1983) 44.
17 K. Kihara and E. Yasukawa, Anal. Chim. Acta, 183 (1986) 75.
18 Y. M. Fraticelli and M. E. Meyerhoff, Anal. Chem., 55 (1983) 359.
19 K. Spencer, Am. Clin. Biochem., 23 (1986) 1.
20 L. D. Bowers and E. T. Wong, Clin. Chem., 26 (1980) 555.
21 S. K. Gerard and H. Khayam-Bashi, Am. J. Clin. Pathol., 84 (1985) 659.
22 Y. M. Fraticelli and M. E. Meyerhoff, Anal. Chem., 53 (1981) 992.
23 L. Campanella, M. Tomassetti, B. Rappuoli and M. R. Bruni, Am. Clin. Products Rev., June (1986) 42.
24 W. E. Hornby and G. Noy, in K. Mosbach (Ed.), Immobilized Enzymes, Academic Press, London, 1976, p. 633.
25 Heung Lark Lee and M. E. Meyerhoff, Analyst (London), 110 (1985) 371.
26 G. B. Martin and M. E. Meyerhoff, Anal. Chim. Acta, 186 (1986) 71.
27 P. van den Winkel, J. Mertens and D. L. Massart, Anal. Chem., 46 (1974) 1765.

Analytica Chimica Acta, 200 (1987) 73—78
Elsevier Science Publishers B.V., Amsterdam — Printed in The Netherlands

APPLICATION OF AN ENZYME THERMISTOR FOR THE DETERMINATION OF GLUCOSE IN COMPLEX FERMENTATION MEDIA

G. WEHNERT, A. SAUERBREI, TH. BAYER, TH. SCHEPER and K. SCHÜGERL*
Institut für Technische Chemie der Universität Hannover, Callinstr. 3, D-3000 Hannover 1 (Federal Republic of Germany)
TH. HEROLD
Sartorius GmbH, Göttingen (Federal Republic of Germany)
(Received 16th March 1987)

SUMMARY

An enzyme thermistor was used for on-line glucose determination during cultivation of *Cephalosporium acremonium* for a period of 160 h. The complex medium consisted of 100 g l^{-1} peanut meal. Automatic control and data registration were achieved by interfacing a process computer with the thermistor unit. Problems caused by long-term application are discussed. On-line and off-line data obtained with the enzyme thermistor are compared with the results obtained with a commercial glucose analyzer. The results of these experiments show that an enzyme thermistor can be used to determine glucose concentrations in complex fermentation media under real cultivation conditions for about 60 h.

The operational principle of the enzyme thermistor is the measurement of heat generated by enzyme-catalyzed reactions. The extent of heat generation depends on the quantity of converted substance. The resulting temperature changes are small because of the small amount of converted substance, but they can be detected with a highly sensitive temperature probe, i.e., a thermistor. A thermistor (thermally sensitive resistor) is an oxide semiconductor which converts temperature changes, even <0.001 K, to detectable changes of electrical resistance. The enzyme thermistor combines the universal calorimetric method with the selectivity of enzymes, thus allowing the selective detection of one substrate in a complex mixture. Such an enzyme thermistor was first described in 1974 by Mosbach and Danielsson [1].

*Karl Schügerl is Professor and Chairman of Technical Chemistry, and Director of the Institute of Technical Chemistry at the University of Hannover. His research interests include biochemical reaction engineering, measuring and control, and separation processes.

0003-2670/87/$03.50

EXPERIMENTAL

The enzyme thermistor

The design of an enzyme thermistor is shown schematically in Fig. 1. A small plastic column (total length 44 mm, diameter 8 mm) contains immobilized enzyme in a chamber with a volume of ca. 0.5 ml. A thermistor is located on the top of this column. The enzyme column and thermistor are situated in a cylindrical aluminium block, which can be thermostated. The cylinder is protected from external temperature influences by polyurethane insulation. A constant stream of buffer solution is fed through the enzyme thermistor at 50 ml h^{-1}. A four-way valve allows the injection of the sample into the buffer stream. The sample volume was 0.5 ml. The buffer stream first passes through a heat-exchange coil in the enzyme thermistor before entering the enzyme column, where the enzymatic reaction takes place. The resulting changes in the resistance of the thermistor are measured by a Wheatstone bridge. The amplified signals are shown on a chart recorder or stored in a computer. A detailed description of the enzyme thermistor has been given [2]. The enzyme thermistor used here was constructed in the Chemical Center of the University of Lund, Sweden.

Materials

An enzyme system consisting of glucose oxidase (EC 1.1.3.4) and catalase (EC 1.11.1.6) was used for the determination of glucose with the enzyme thermistor, because this system converts glucose with generation of a relatively large amount of heat [3]. A glucose oxidase preparation with a high content of catalase (glucose oxidase III, Boehringer Mannheim) was immobilized on an oxirane acrylic resin (Eupergit C; Röhm Parma, Weiterstadt, F.R.G.) as described previously [4]. This resin is available in the form of small beads (diameter ca. 0.15 mm). Numerous free epoxy groups on the

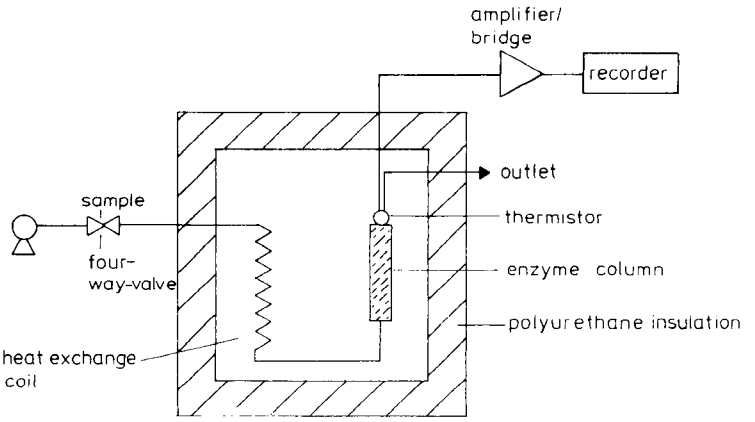

Fig. 1. Design of a single-column enzyme thermistor.

surface of the polymer allow covalent attachment of enzymes. Former studies showed the advantage of Eupergit C as a support material for glucose oxidase/catalase [4].

Procedures

It was necessary to find the correlation between glucose concentration and thermistor signal before analytical measurements were started. For that purpose, solutions with known glucose concentrations were injected and the corresponding temperature responses were measured. During the fermentation process, such a calibration had to be repeated every 24 h because of changes in the enzyme activity.

The enzyme thermistor was used to monitor cultivation of the fungus *Cephalosporium acremonium* (W.53.2.53, Ciba Geigy, Basel, Switzerland) in a 20-l stirred tank reactor in order to optimize the production and yield of cephalosporin C [5]. The medium consisted of the following components: peanut meal (low fat), 100.0 g l^{-1}; ammonium acetate, 6.0 g l^{-1}; methyl oleate, 5.0 g l^{-1}; DL-methionine, 3.0 g l^{-1}; glucose monohydrate, 5.0 g l^{-1}; magnesium sulfate heptahydrate, 5.0 g l^{-1}; calcium carbonate, 5.0 g l^{-1}; calcium sulfate dihydrate, 5.0 g l^{-1}; SAG 471 (antifoaming agent), 0.5 g l^{-1} [5]. Because of the complexity of the medium, especially the high content of solid particles (peanut meal), it was impossible to utilize conventional methods for glucose determination without special preparation of the sample. The scheme for sample injection into the enzyme thermistor is shown in Fig. 2.

Samples were continuously filtered with a hollow-fiber microfiltration module constructed in-house (membranes from Enka, Wuppertal, F.R.G.). The samples were automatically injected into the enzyme thermistor via a four-way motor-driven valve (Latek, Heidelberg) into a 0.1 M sodium phosphate buffer solution (pH 7.0). The valve control and the on-line data recording of the output from the enzyme thermistor were performed by a PDP-11/34 process computer (Digital Equipment Corporation). The switching

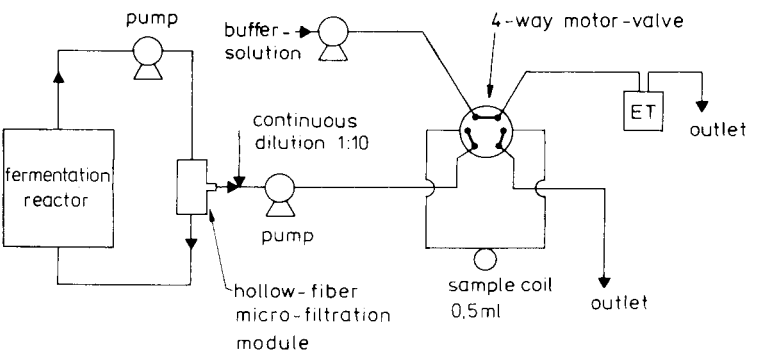

Fig. 2. Automatic sample injection.

sequences of the magnetic valve (e.g., 13 min position "load", 2 min position "injection"), and the data processing were performed with the flexible software package CASFA (Computer Automation System for Fermentation Plants), developed at this Institute. This package allows simultaneous control of the entire data acquisition, data processing and data analysis of up to 10 fermentation plants [6].

In addition to on-line samples, off-line samples were taken, frozen and analyzed with the enzyme thermistor at the end of the fermentation. These measurements were compared to data obtained with a commercial glucose analyzer (YSI-23A; Yellow Springs Instruments, Yellow Springs, OH).

RESULTS AND DISCUSSION

The on-line data obtained from the enzyme thermistor were monitored and converted to the corresponding glucose values by the computer, using a correlation function obtained from the previous calibration. The results are shown in Fig. 3A. In addition, the results from off-line analysis (measured with the enzyme thermistor and the glucose analyzer) are presented in Fig. 3B.

Comparison between the results measured on-line and off-line shows good correlation between both methods during the first 60 h of cultivation. During these 60 h, about 240 samples were injected automatically. Peaks 2—4, which appear after addition of the concentrated glucose nutrient solution, are clearly visible in the on-line as well as in the off-line detection. The on-line peaks appear with an average delay of 1 h. This delay refers to the dead volume of the sample-collecting system, the filling time of the sample coil and the response time of the enzyme thermistor. The results of on-line and off-line measurements differ considerably after ca. 60 h, so that peaks 5 and 6 of the on-line measurement cannot be explained. After that, the on-line values reach a level of ca. 4 g l^{-1}, although the glucose concentration is low, as shown by the off-line data. This deviation is due to alterations in the enzyme column after a large number of sample injections. Components of the complex medium, such as protein, deposit on the enzyme support material during the course of time. The deposits affect measurements by generating additional temperature changes which are superimposed on the glucose signal. Further difficulties resulted from occasional clogging of the sample-collecting system. Figure 3A shows these occurences indicated as points 7—10. Clogging may result in an incompletely filled sample coil. However, it was possible to flush away the clogging material from the hollow-fiber module.

The off-line glucose values obtained with the enzyme thermistor showed good correlation with the values detected with the glucose analyzer YSI-23A (Fig. 3B). Most of the values from the enzyme thermistor are ca. 1.1 g l^{-1} higher than the values from the YSI-23A. This discrepancy is due to non-specific heat generation caused by mixing of the buffer solution and sample

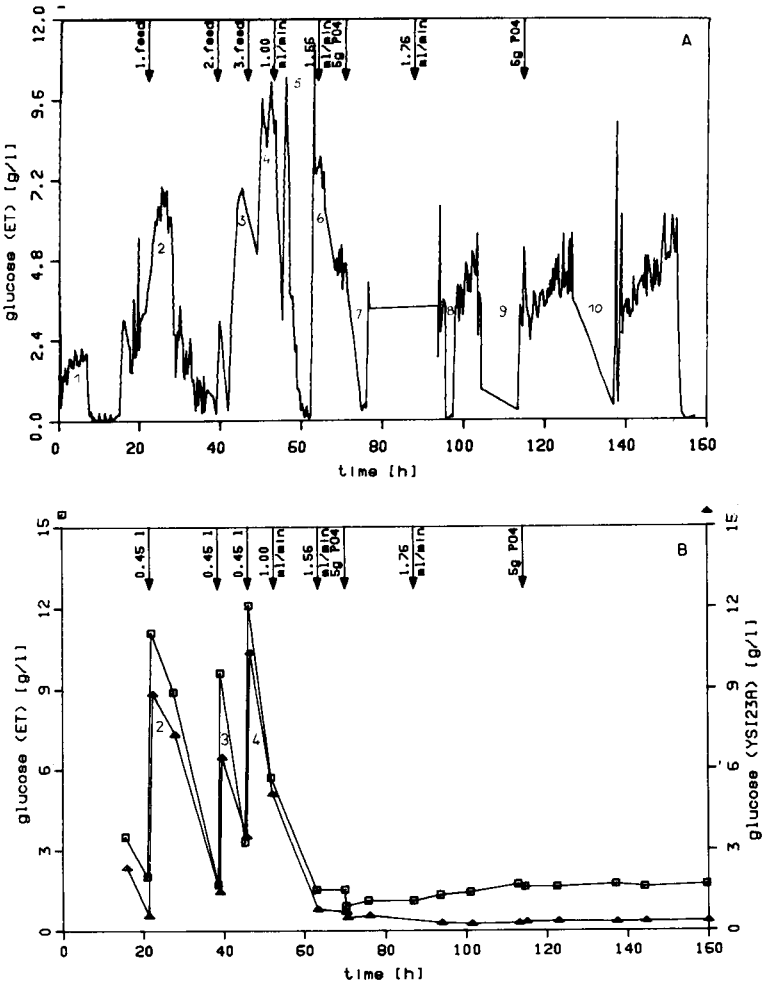

Fig. 3. (A) Glucose concentration on-line detected with the enzyme thermistor (ET) during cultivation for 160 h; (B) glucose concentration off-line detected with the enzyme thermistor and the Glucose Analyzer YSI-23A. Arrows 1, 2 and 3 indicate the addition of 450 ml of a nutrient solution consisting of 500 g l^{-1} glucose monohydrate and 24.75 g l^{-1} methionine. Arrows 4, 5 and 7 indicate the start of continuous addition of this nutrient solution at a volumetric flow rate of 1.00 ml min^{-1}, later increased to 1.56 ml min^{-1} and 1.76 ml min^{-1}. Arrows 6 and 8 indicate two additions of 5 g of phosphate to maintain the optimal phosphate concentration.

in the enzyme column. The samples pass through the heat-exchange coil in the form of segregated zones in the buffer stream. Mixing does not occur before the enzyme column is reached because of the laminar flow. Thus, mixing enthalpies cannot be eliminated by previous heat exchange. Elimination of such enthalpies should be possible by using a mixing column located ahead of the heat-exchange coil. But this arrangement would include a

dilution of the sample and, therefore, would result in a loss of sensitivity.

The extent of non-specific enthalpies can be measured with a column filled with inactive support material, but without the enzyme. Experiments showed that the injection of a sample in an enzyme thermistor with such an inactive column leads to a detectable temperature response. In a normal column containing immobilized enzyme, this non-specific temperature response is superimposed on the signal for the enzymatic reaction and, therefore, results in erroneously increased substrate concentrations. The consequences are high errors at low substrate concentrations. Such erroneous results might be avoided by using an additional inactive column as a reference. Non-specific enthalpies are then generated in both columns, but the reaction heat is only produced in the enzyme column. Subtraction of the measured reference signal from the main signal should eliminate the non-specific effect and give the correct result. More extensive investigations to test the practicability of measurements with an additional thermistor reference column will be made.

REFERENCES

1 K. Mosbach and B. Danielsson, Biochim. Biophys. Acta, 364 (1974) 140.
2 B. Danielsson, Appl. Biochem. Biotechnol., 7 (1982) 127.
3 K. Mosbach and B. Danielsson, Anal. Chem., 53 (1981) 83A.
4 G. Wehnert, A. Sauerbrei and K. Schügerl, Biotechnol. Lett., 7 (1985) 827.
5 Th. Herold, Dissertation, University of Hannover, 1986.
6 K. Früh, R. Hiddessen, J. Niehoff, A. Lübbert and K. Schügerl, Biotech-Forum, 3 (1986) 203.

Analytica Chimica Acta, 200 (1987) 79—88
Elsevier Science Publishers B.V., Amsterdam — Printed in The Netherlands

SPECIATION OF TIN IN LEMON JUICE: AN EXAMPLE OF TRACE METAL SPECIATION IN FOOD

G. WEBER*

Institut für Spektrochemie und angewandte Spektroskopie, Bunsen-Kirchhoff-Str. 11, D — 4600 Dortmund 1 (Federal Republic of Germany)

(Received 14th February 1987)

SUMMARY

A scheme is presented for the separation and identification of different tin species in lemon juice. Soluble tin species are separated from other constituents by means of column-switching liquid chromatography and detected by electrothermal atomic absorption spectrometry (AAS). Other metals (copper, zinc, iron, calcium and magnesium) are detected in the same fraction by on-line flame-AAS. Gas chromatography/mass spectrometry of the organic ligands after derivatization confirmed that citric acid is the important ligand for metal binding in lemon juice. Tin is also partly bound to particulate matter, which is investigated by infrared spectroscopy and model experiments. It is shown that tin is most probably bound to carboxylic groups of pectin (analogously to calcium). Investigations of different lemon juices showed large variations of total tin, but few differences between tin species. Only one sample contained organotin compounds at a detectable level.

Food is probably the main source of trace elements entering the human body; other sources are water and air. There is strong evidence for a correlation of effects on health (e.g., essentiality or toxicity) with the concentrations and chemical forms of many trace elements. The species dependence of effects on health is now well established for the absorption and metabolism of elements by the human organism. Knowledge of elemental species in food is therefore of great importance [1]. To date, few analytical procedures have been published for the determination of different species of an element in food [2, 3]. In the case of tin, for example, most of the available data refer to total tin, with the exception of some investigations on organotin species which are used in plastics manufacture and in paints and can migrate from packing materials into food [4, 5]. The total tin content of foods varies over a wide range and differences between canned and packaged or fresh foods are apparent [6]. But there is no possibility of relating such data to uptake

*Günther Weber studied chemistry at the University of Göttingen and obtained his doctoral degree in 1983 with work on the speciation of trace metals under the direction of Prof. Dr. G. Schwedt. Since 1983 he has worked at ISAS in Dortmund in the research group of Prof. Dr. G. Tölg. His main interests are trace analysis and speciation of metals by chromatographic, spectroscopic and electrochemical methods.

0003-2670/87/$03.50

of tin from food unless actual compounds are identified. For example, organic coordination compounds of tin are absorbed to a much greater extent than inorganic salts [7, 8]. Biological effects of absorbed tin have been reported not only at real toxic levels, but also at sub-toxic levels (i.e., some mg kg^{-1} of food) and include interactions with other essential elements or with enzyme systems [9, 10].

It has been shown that high-performance liquid chromatography (HPLC) is valuable for the separation of soluble coordination compounds of trace metals in blood [11], food [3] and environmental samples [12]. The combination of HPLC with element-specific detection is very useful in the case of complex matrices, because the highly selective detector eliminates interferences by other organic constituents which are present at a much higher level than the trace metal species. For this purpose, combinations of HPLC with atomic absorption spectrometry (AAS) are often used [3, 11, 12], but detection by atomic emission spectrometry after excitation with inductively coupled plasmas [13, 14], d.c. plasmas [15] or microwave-induced plasmas [16] is also possible. In this paper, lemon juice is taken as an example, and combined procedures are presented for the identification and determination of different tin species. The influence of other metals, which may take part in complex-formation equilibria and thus change the distribution of tin species, is also discussed.

EXPERIMENTAL

Total-element determinations

Digestion of the samples was done with a mixture of nitric and sulfuric acids (10:1). Tin was determined by electrothermal AAS with a Perkin-Elmer 4000/HGA 500 instrument at 224.6 nm with zirconium-impregnated graphite tubes [17]; the charring and atomization temperatures were 800 and 2700°C, respectively. It is also possible to determine total tin without digestion directly in the extract after extraction with tropolone/toluene [18]. Additionally, this procedure allows the determination of organotin compounds, which are extracted under slightly different conditions. Other metals investigated were calcium, magnesium, zinc, iron and copper, which were measured, after digestion, by flame AAS (nitrous oxide/acetylene for calcium and air/acetylene for the other elements). Measurements were done by using the injection method [19] and a Pye-Unicam SP9 instrument.

Chromatography of soluble species

Samples were filtered (0.45-μm filter, precleaned with tropolone/HBr [6]) and then directly injected. The HPLC system consisted of a Milton-Roy ConstaMetric III pump, a Rheodyne 7125 injection valve with 100-μl loop, a 250 × 4.6 mm stainless-steel column packed with Spherisorb S5 ODS-I and a 30 × 4 mm pre-column with the same material. This pre-column was used for column-switching by means of a Rheodyne 7000 valve, which was

activated 36 s after sample injection (see Fig. 1). Detection was done with a Knauer ultraviolet/fluorescence detector (at 254 nm for absorption or fluorescence excitation and measurement of emission at >370 nm) or with on-line flame AAS for zinc, magnesium and iron. For the latter purpose, a Varian 1000 spectrometer was coupled to the HPLC column with an aspiration rate equal to the HPLC flow rate. No background correction was necessary. Tin was determined in HPLC fractions by electrothermal AAS. The mobile phase was 0.1 mol l^{-1} sodium dihydrogen phosphate adjusted to pH 2.5 with phosphoric acid. The flow rate was 0.5 ml min^{-1}. The metal peak areas were measured by using a Milton-Roy CI-10 integrator coupled to the spectrometer.

Analysis for organic ligands by mass spectrometry

For the identification of organic ligands, HPLC fractions were collected, freeze-dried, derivatized with freshly prepared diazomethane in ether and then examined by gas chromatography/mass spectrometry (GC/MS); a DANI GC was interfaced to a Finnigan MAT ion trap. Artefacts produced by sample preparation or reagent impurities were identified by running a blank of pure HPLC eluent treated in the same way as the sample fractions.

Investigation of tin bound to particles

Isolation of this fraction was achieved by precipitation with ethanol and filtration (0.45-μm PVC filter). Infrared spectra of the dried residue and also of pure pectin (Riedel de Haen) were obtained by using KBr pellets and a Perkin-Elmer 180 spectrometer. Tin determinations were possible either after digestion or after extraction with tropolone/toluene by electrothermal AAS.

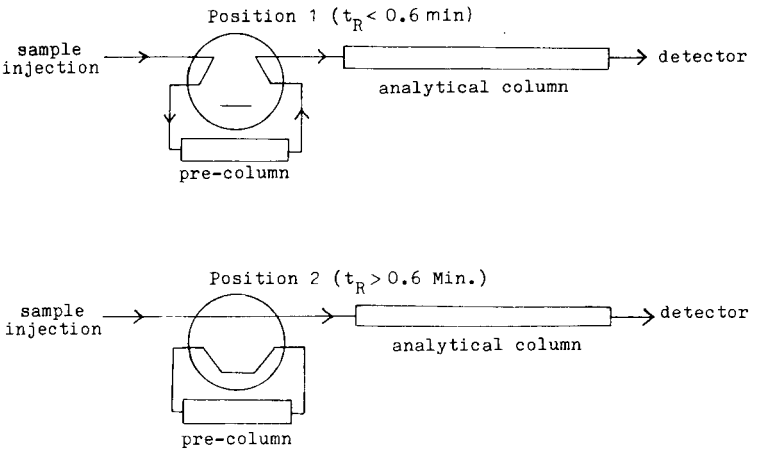

Fig. 1. Diagram for column-switching HPLC. In position 2, for t_R >0.6 min, the valve is turned so that the mobile phase passes directly to the analytical column.

RESULTS AND DISCUSSION

For investigation of the tin species in lemon juice, a commercially available sample was chosen with a total tin content of 142.5 ng ml^{-1}. The pH was 2.5; 82.7 ng ml^{-1} (58%) of the tin was soluble and 59.8 ng ml^{-1} (42%) bound or adsorbed to particles (filtered on 0.45-μm filters).

Identification of soluble tin species

For the separation of lemon juice by HPLC, different chromatographic conditions were tested involving different reversed-phase columns and various aqueous buffer systems or methanol/water mixtures. Figure 2 shows a typical example of such a separation. Trace metals were always found in the front zone of the chromatogram, whereas the retention times of most of the other compounds were much longer. That means that the metals are present as relatively polar substances, exhibiting only weak absorption at 254 nm and no fluorescence. From literature data on the HPLC separations of juices and from the retention times of single compounds, it can be concluded that this front zone consists mainly of organic acids, which are potential ligands. Therefore, the chromatographic conditions were altered to those suggested by Coppola [20], who used phosphate buffer for the separation of organic acids in fruit juice. Additionally, a front-cutting technique was used (see Experimental), which enabled the acids to be separated on the analytical column, while all the other components were retained on a small pre-column. Use of the phosphate buffer of pH 2.5 has the advantage of maintaining the natural pH of the juice and avoiding methanol addition, which could possibly alter metal/ligand equilibria.

The resulting chromatogram of this "organic acid fraction" is shown in Fig. 3 with detection at 254 nm (no fluorescence was measured). The AAS signals for magnesium, zinc and tin are also given. These signals correspond to 600, 30 and 14 ng of the metals, respectively. There is only one tin species present (at t_R = 5.3 min) and at the same retention time magnesium and iron (not shown) are also found. The zinc peak is separated from these metals (t_R = 7.1 min). The reproducibility of this separation is good; the relative standard deviations (N = 5) were 1.9% for retention times and 3.8% for peak areas. The recovery of the metals with respect to the injected sample was between 95% and 103%.

For identification of the metal-binding ligand or ligands, HPLC fractions were collected from t_R = 5.0 to 5.4 min (fraction 1), from 5.4 to 6.2 min (fraction 2) and from 6.2 to 8.0 min (fraction 3). Fraction 1 contained the metal species of magnesium, iron and tin, fraction 3 contained the zinc species and fraction 2 was an intermediate fraction. The three fractions were freeze-dried and then treated with diazomethane in ether to yield the methyl esters of the acids. The reaction products of the samples and a blank HPLC fraction were analysed by GC/MS, because the HPLC fractions were still mixtures of similar compounds. For the identification of the metal-binding

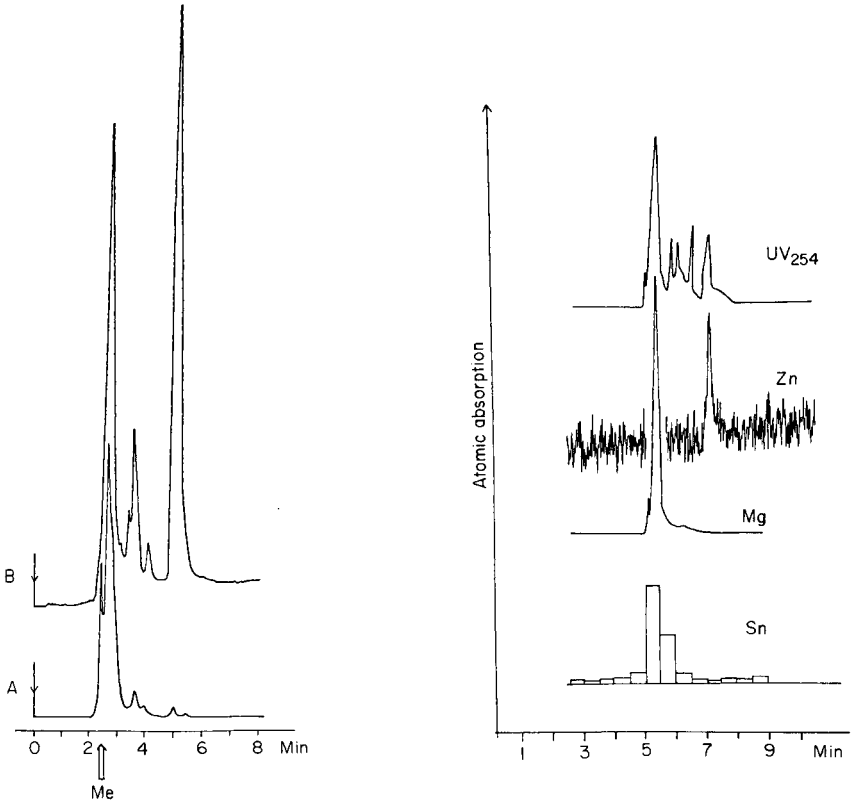

Fig. 2. Chromatographic separation of lemon juice: (A) UV detector at 254 nm; (B) fluorescence detector. Mobile phase, 0.1 M ammonium acetate in methanol/water (70 + 30); pH 4.6; 1.1 ml min^{-1}. Me, retention time of metals (Sn, Fe, Zn, Mg).

Fig. 3. HPLC of lemon juice with column switching. For chromatographic conditions, see Experimental. Signals for Zn and Mg were recorded on-line (flame AAS) and tin was measured in fractions by electrothermal AAS.

ligands, the following steps were used. First, fractions 1 and 3 were searched for a compound; if none was found in these metal-containing fractions, the zinc species and the other metal species must be of different type and must therefore be treated separately. Secondly, any compound found was identified from its mass spectrum. Thirdly, the metal/ligand compounds were prepared and examined by using the HPLC/AAS system for direct comparison with the sample.

Only one compound was found to be present in both fractions 1 and 3. From its mass spectrum (Fig. 4) it was identified as citric acid trimethylester. The mass chromatogram of the molecular ion cluster was used to construct a histogram (Fig. 5a) specific for citric acid, although it is only semiquantitative without any standardization. Nevertheless, it can be seen that citric acid

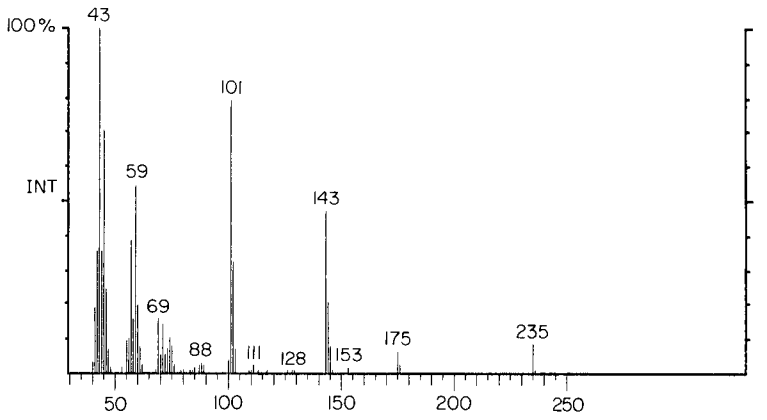

Fig. 4. Mass spectrum of the trimethyl ester of citric acid.

is present at two different retention times. The second peak at 7.1 min coincides with that of citric acid alone and the first one at 5.3 min is present only together with metal ions. This is illustrated by the two ultraviolet chromatograms in Fig. 5, which were obtained for a citric acid solution of pH 2.5 (Fig. 5c) and for the same solution after addition of 1 μg ml^{-1} each of magnesium and zinc (Fig. 5b). The influence of metal ions on the retention behaviour of organic acids by complex formation is well known and in organic trace analysis it is often recommended to add EDTA to the sample for reproducible results [21].

Model experiments with metal citrates were conducted at different concentrations for tin, iron, magnesium and zinc. With the exception of zinc, the metals were always found quantitatively at the retention time of 5.3 ± 0.1 min. The chromatographic behaviour of zinc citrate depended on the presence of other elements; if no other metals were present, zinc was found at 5.3 min. When a mixture of zinc and magnesium citrates was examined, a second zinc peak appeared at 7.1 min. This means that at least two different zinc citrates are formed depending on the matrix composition. This is in accordance with the results of Capone et al. [22], who found that citrate species of zinc and cadmium are strongly dependent on absolute concentrations and metal/ligand ratio. In particular, equilibria of 1:1 and 1:2 complexes (metal/citrate) could be responsible for the chromatographic behaviour. According to data of Gutierrez et al. [23], tin should be present at the citrate concentration in lemon juice as its 1:2 complex with the proposed formula $[Sn(H_2Cit)_2(OH)]^+$.

Investigation of tin bound to particles

In contrast to other metals such as zinc or magnesium, tin is also present bound to particles. However, it can be extracted by tropolone/toluene or partly released by treatment with 1 M hydrochloric acid (15% released) or 1 M ammonia solution (51% released) [18]. Particles found in fruit juice

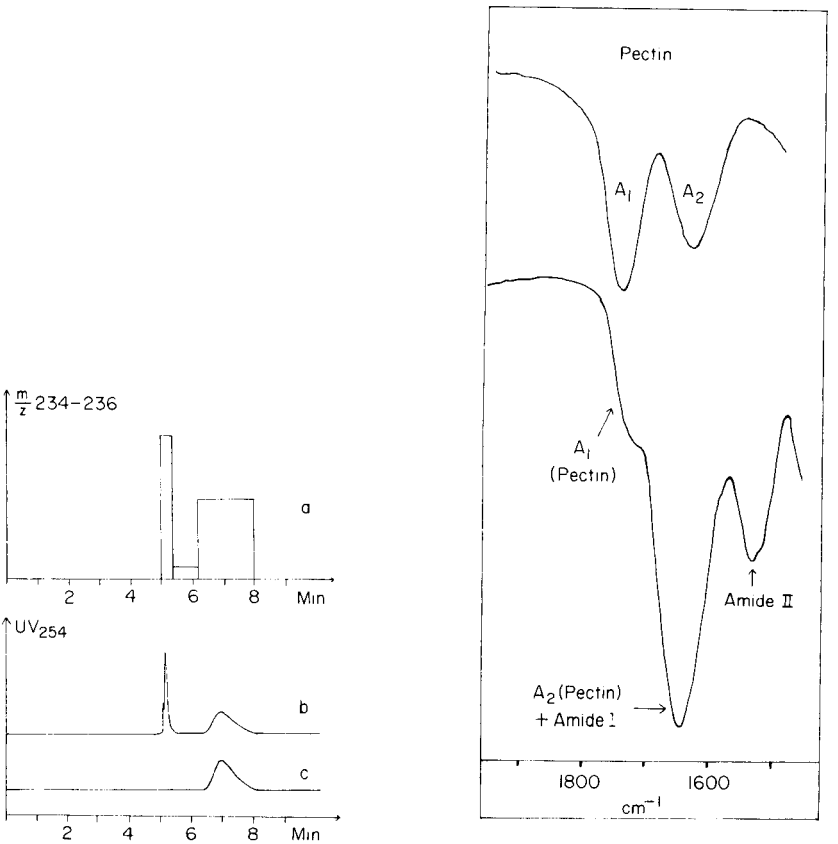

Fig. 5. Chromatographic behaviour of citric acid: (a) histogram of citric acid found in HPLC fractions of lemon juice; (b) UV detection of citric acid + Zn and Mg citrates; (c) UV detection of citric acid alone.

Fig. 6. Infrared carbonyl bands of pectin and particles isolated from lemon juice. See text for explanation.

contain a lot of pectin material, which is able to bind metal ions such as calcium and is also more sensitive to alkaline attack than to acid treatment. Therefore, the possibility of tin-binding to pectin was investigated. In Fig. 6, a part of the infrared spectrum of isolated particles of the juice is shown together with the corresponding spectrum of pectin. Pectin has two characteristic carbonyl bands (A_1 and A_2) in this region at about 1620 cm^{-1} (mainly metal-bound carboxyl groups) and at about 1740 cm^{-1} (non-ionized and methylated carboxyl groups). In juice these are overlapped by the amide bands of proteins (amide I at 1630—1680 cm^{-1} and amide II at 1515—1570 cm^{-1}). This is in agreement with the statement that particles in juice at about pH 3 consist of associates of negatively charged pectins around a nucleus of positively charged proteins [24].

To test if tin can be bound to pectin (without protein), a model experiment was carried out with a suspension of pectin in 5% (w/v) citric acid of pH 2.5 containing 100 ng ml^{-1} tin and 10 μg ml^{-1} each of magnesium and zinc. After one hour, only 21% of the tin was soluble and 79% was bound to pectin even in the presence of citrate as a strong complexing agent. It is difficult, however, to investigate the nature of the binding at such low concentrations of metals. Tin could be bound to the carboxyl groups of pectin in the same way as calcium or it could simply be adsorbed to particles. To investigate the possibility of direct binding of tin to pectin carboxyl groups, the method of Filippov was applied [25]; in this method, the two carbonyl bands of pectin mentioned above were used for the determination of metal-bound, methylated and non-ionized carboxyl groups. For a citrus-pectin values of 22% metal-bound, 58% methylated and 20% non-ionized carboxyl groups were given by Filippov, calculated from the infrared spectra of pure pectin and pectin after calcium treatment. With the present pectin standard, the values obtained were 23%, 61% and 16%, respectively. When tin was used instead of calcium, these values changed to 15%, 61% and 24%, but this experiment was done at pH 1.2 to avoid precipitation of tin (0.1 mol l^{-1}). Clearly, at this low pH the amount of non-ionized carboxyl groups increases and the metal-bound fraction decreases. When this point is taken into account, the values are similar to those obtained with calcium. This means that tin is bound to pectin in a similar way to calcium, because the method of Filippov assumes conversion of non-ionized to metal-bound carboxyl groups after treatment with the metal. This tin-binding at the 0.1 M level is no definite proof for tin-binding at the ng g^{-1} level, but it illustrates the possibility of such binding. Additionally, adsorptive effects or mixed-ligand complexes (e.g., pectin and citrate) may be involved. In contrast, pure adsorption without chemical binding is unlikely because in this case tin should be released by treatment with hydrochloric acid.

Comparison of different lemon juices

To compare the distribution of tin species in different lemon juices, six commercially available juices were analysed; these differed in packing material and origin. Soluble and particulate tin was determined and the presence of organotins was checked by toluene extraction. Additionally, the total contents of calcium, magnesium, zinc, iron and copper were determined, because many of these metals (especially Ca and Mg) are present at relatively high concentrations and therefore may influence complex-formation equilibria. The pH of all the juices was 2.4—2.5. Table 1 gives the distribution of tin species and Table 2 the concentrations of other metals. Sample 6 is the one used for identification of the tin species. Total tin varies from <0.1 ng ml^{-1} to 142.5 ng ml^{-1}. The sample with the lowest tin content (not detectable) is the only one delivered in a glass bottle and without any food additives. Sample 2 is a synthetic product mainly made of citric acid (only addition of lemon juice) and therefore contains very little pectin material; so 100%

TABLE 1

Distribution of tin in different lemon juices

Sample no.	Total Sn ($ng\ ml^{-1}$)	Soluble Sn		Insoluble Sn		Organotins ($ng\ ml^{-1}$ as Sn)	
		($ng\ ml^{-1}$)	(%)	($ng\ ml^{-1}$)	(%)	Soluble	Insoluble
1	15.4	9.4	61	6.0	39	—	—
2	3.1	3.1	100	—	—	—	—
3	<0.1	—	—	—	—	—	—
4	4.7	2.1	45	2.6	55	—	—
5	133.4	83.4	62	50.0	38	15.8	5.9
6	142.5	82.7	58	59.8	42	—	—

TABLE 2

Concentrations of Mg, Ca, Fe, Zn and Cu in lemon juices

Sample no.	Mg ($\mu g\ ml^{-1}$)	Ca ($\mu g\ ml^{-1}$)	Fe ($ng\ ml^{-1}$)	Zn ($ng\ ml^{-1}$)	Cu ($ng\ ml^{-1}$)
1	6.08	8.28	555	38	193
2	0.83	5.24	5	1	22
3	5.94	11.28	56	27	225
4	6.21	6.31	486	533	308
5	5.90	9.40	226	254	376
6	6.13	8.75	274	305	97

of tin is soluble. All the other lemon juices contain 45—62% of soluble tin and the rest bound to pectin. Only in one sample were organotins detected; these are coordinated like inorganic tin and are a mixture of mono- and di-organotins, 30% of the organotins being bound to pectin and 70% to soluble citrates. Samples 1 and 5 are different samples from the same manufacturer. In spite of the difference in total tin (factor 10), the ratio of soluble/insoluble tin is the same. Thus this ratio seems to depend more on the origin and production of the sample rather than on total tin content. HPLC of the samples gave tin signals at the same retention times as for tin citrate. Also the signals for magnesium and iron did not change. For zinc, signals were obtained at 5.3 min from two juices (1 and 5), at 7.1 min from another two juices (3 and 6) and at both retention times from juice no. 4. As explained earlier, this seems to depend on matrix composition (ratio of metal to free citrate), but cannot be fully explained by the data presented here.

I thank Dr. M. Linscheid and Dr. E. H. Korte for cooperation with the mass and infrared spectrometry. This work was supported by the Ministerium für Wissenschaft und Forschung des Landes Nordrhein-Westfalen and by the Bundesministerium für Forschung und Technologie der Bundesrepublik Deutschland.

REFERENCES

1 M. Bernhard, F. E. Brinckman and P. J. Sadler (Eds.), The Importance of Chemical Speciation in Environmental Processes, Dahlem Konferenzen, Springer, Berlin, 1986.
2 K. Lee and F. M. Clydesdale, J. Food Sci., 44 (1979) 549.
3 G. Weber and G. Schwedt, Fresenius' Z. Anal. Chem., 316 (1983) 594.
4 F. Taleb, M. Carrier and J. J. Vallon, Ann. Falsif. Expert. Chim., 778 (1979) 441.
5 P. Hocquellet, Atom. Spectrosc., 6 (1985) 69.
6 G. Weber, Fresenius' Z. Anal. Chem., 321 (1985) 217.
7 S. G. Schäfer and U. Femfert, Reg. Toxicol. Pharmacol., 4 (1984) 57.
8 S. Kojima, K. Saito and M. Kiyozumi, Yakugaku Zasshi, 98 (1978) 495.
9 S. G. Schäfer and W. Forth, Ecotoxicol. Environ. Safety, 7 (1983) 87.
10 A. P. De Groot, Food Cosmetic Toxicol., 11 (1973) 955.
11 E. D. Katz and R. P. W. Scott, Analyst, 110 (1985) 253.
12 L. Brown, S. J. Haswell, M. M. Rhead, P. O'Neill and K. C. C. Bancroft, Analyst, 108 (1983) 1511.
13 D. Bushee, D. Young, I. S. Krull, R. N. Savage and S. B. Smith, J. Liquid Chromatogr., 5 (1982) 693.
14 K. Jinno, S. Nakanishi and T. Nagoshi, Chromatographia, 18 (1984) 437.
15 I. S. Krull, K. W. Panaro and L. L. Gershman, J. Chromatogr. Sci., 21 (1983) 460.
16 D. Kollotzek, D. Oechsle, G. Kaiser, P. Tschöpel and G. Tölg, Fresenius' Z. Anal. Chem., 318 (1984) 485.
17 H. Fritsche, W. Wegscheider, G. Knapp and H. M. Ortner, Talanta, 26 (1979) 219.
18 G. Weber, Fresenius' Z. Anal. Chem., 322 (1985) 311.
19 H. Berndt and W. Slavin, Appl. Atom. Absorp. Spectrom., 14 (1979) 1.
20 E. D. Coppola, Food Technol., 4 (1984) 88.
21 S. H. Ashoor and M. J. Knox, J. Chromatogr., 299 (1984) 288.
22 S. Capone, A. De Robertis, C. De Stefano and S. Sammartano, Talanta, 33 (1986) 763.
23 A. M. Gutierrez, C. Perez-Conde and M. P. Rebollar, Anal. Chim. Acta, 171 (1985) 381.
24 H.-D. Belitz, W. Grosch: Lehrbuch der Lebensmittelchemie, Springer-Verlag, Berlin, 1982.
25 M. P. Filippov, Zh. Anal. Khim., 39 (1984) 92.

Analytica Chimica Acta, 200 (1987) 89—100
Elsevier Science Publishers B.V., Amsterdam — Printed in The Netherlands

ANALYSIS FOR TRACE ELEMENTS WITH A SLOWPOKE REACTOR

D. E. RYAN*, A. CHATT and J. HOLZBECHER

Trace Analysis Research Centre, Department of Chemistry, Dalhousie University, Halifax, N.S. B3H 4J1 (Canada)

(Received 27th March 1987)

SUMMARY

The SLOWPOKE reactor is very useful for neutron activation analysis and has been in operation at Dalhousie University for ten years. Improvements to the reactor are outlined and flux evaluations after major changes are reported. Its use for the determination of trace elements in a broad variety of materials is described.

In the centenary issue of Analytica Chimica Acta [1], the performance of a small research reactor (SLOWPOKE) developed by the Atomic Energy of Canada Limited, was described. Details of the composition, homogeneity, and reproducibility of the flux, sensitivities for 78 elements by neutron activation, and direct analysis of several matrices were described.

The merits of neutron activation analysis (multi-element capability, high sensitivity, low matrix interference, minimal contamination) are well known. All elements present are activated concurrently according to their individual nuclear properties; the absence of any indication of a given element in a sample allows an upper limit to be placed on its concentration.

Developments in neutron sources, detectors, and computers have made neutron activation even more attractive for elemental determinations. Practical neutron activation analyses with short-lived nuclides and resulting fast turn-around times are possible for many elements.

The SLOWPOKE-2 reactors are licensed to operate without an operator in attendance; the reactor physics aspects have been described by Kay et al. [2]. Nuclear reactivity, defined in terms of the reactor neutron balance, is positive when k, the effective multiplication constant, is greater than 1.0. Inherent safety of the SLOWPOKE-2 reactor is guaranteed by a limited maximum excess reactivity ($k - 1$) of 0.0034 which, combined with its negative temperature coefficient, provides for self-regulating characteristic behaviour.

During reactor operation, uranium-235 is consumed and fission products build up. The resulting slow reduction in reactivity is compensated by the periodic addition of beryllium shim plates to the top of the core reflector. The useful thickness of this top reflector is approximately 10 cm. The Dal-

0003-2670/87/$03.50

house SLOWPOKE-2 reactor was initially loaded with fuel until k = 0.995 and about 1.7 cm of beryllium shim plates were then added to provide the initial excess reactivity of 3.4 mk. Shim additions from 1.7 to 10 cm, to compensate for fuel burn-up, permitted ten trouble-free calendar years of operation.

The core lifetime of the reactor can be extended [3] by a simple modification to the beryllium reflector which allows for extra reactivity to be added to the critical assembly. This provides for a relatively inexpensive alternative to a complete core replacement, and a big shim addition was successfully done for the first time in December 1986 to the Dalhousie SLOWPOKE. The modification is expected to extend the core lifetime by 8 to 10 years.

EXPERIMENTAL AND RESULTS

Counting equipment

Several γ-ray spectrometry systems were used for analyzing various matrices. The four systems consisted of the following parts: (1) an Aptec hyperpure Ge detector (full width at half maximum (f.w.h.m.) of 2.08 keV at the 1332-keV photopeak of ^{60}Co) in conjunction with a high throughput pulse processor coupled to a Nuclear Data multichannel analyzer (either ND-6700 or ND-66); (2) an Aptec low-energy photon detector (f.w.h.m. of 560 eV at the 122-keV peak of ^{57}Co) connected to a Canberra Jupiter multichannel analyzer; (3) a Canberra Ge(Li) detector (f.w.h.m. of 1.88 keV at the 1332-keV peak) connected to a Tracor Northern TN-11 multichannel analyzer; and (4) a Princeton Gamma-Tech Ge(Li) detector (f.w.h.m. of 2.02 keV at the 1332-keV peak) in conjunction with a TN-1700 multichannel analyzer. The efficiency of the detectors (relative to a standard NaI(Tl) detector) varied between 3 and 10% and peak-to-Compton ratios ranged from 20:1 to 35:1.

The cadmium-shielded site

The activity of many nuclides is greatly reduced by use of shielding materials for thermal neutrons; the activity of nuclides primarily produced by absorption of epithermal neutrons is decreased to a much smaller extent. The installation of a permanent cadmium-shielded site in the core of the SLOWPOKE reactor provides for simple epithermal neutron activation analysis (n.a.a.); shielding takes place in the reactor core and the disadvantage of handling shielding materials is avoided. The Cd-shielded site makes possible direct instrumental analysis for a number of important elements in complex matrices. An evaluation of the site has been described recently; cadmium ratios and sensitivities are given for nuclides most likely to be encountered in epithermal n.a.a. [4].

The big shim

As mentioned above, the core lifetime of the reactor has been extended

for a projected 8—10 years by a modification of the beryllium reflector. Experiments to determine the effect of such an innovation are described below.

The thermal neutron flux was determined with cobalt wires and the fast flux was measured by using $^{32}S(n,p)^{32}P$ and $^{54}Fe(n,p)^{54}Mn$ reactions; Fisher primary standard ammonium sulphate and ammonium dihydrogenphosphate (Baker and Adamson, >98% pure) were used as comparator standards. The cadmium ratio for gold was determined by irradiation of gold/aluminium wire under a 1-mm thick cadmium shield. Different sites were compared by irradiation of Au/Al wires held in well-defined positions by polyethylene holders. Flux gradients were measured by counting sections of these wires. Reactor Experiments (0.112% Au/Al) and Alfa (Co, Fe) flux wires were used.

The Dalhousie University SLOWPOKE-2 Reactor (DUSR) facility has five inner pneumatic sites located in the side beryllium reflector and three outer sites in the water surrounding this reflector; Fig. 1 shows the critical assembly. Each inner site can hold up to two irradiation vials of 7-ml capacity while vials of 25-ml capacity are needed for the outer sites. The

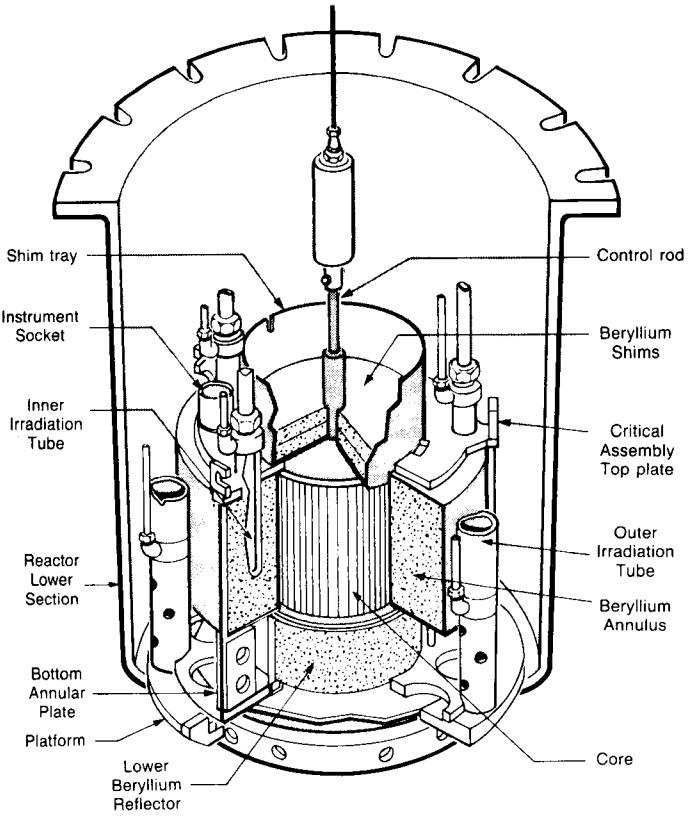

Fig. 1. Schematic diagram of the SLOWPOKE critical assembly (courtesy of Atomic Energy of Canada Limited — Research Company).

50% reduction of flux in the outer site can, therefore, be more than compensated by increasing the sample size whenever needed and possible. The outer site can also be advantageously used for irradiation of chunks of material such as rocks. One of the outer sites (no. 9) is shielded with 0.8-mm thick cadmium for epithermal instrumental n.a.a. The rapid pneumatic transfer system is located at inner site no. 1 for cyclic instrumental n.a.a.

Table 1 shows the composition and homogeneity of the neutron flux prior to and after the big shim addition. The thermal, epithermal (as estimated by means of the cadmium ratio for gold) and fast flux in inner sites are essentially the same as before the addition. The thermal flux in the outer sites is also the same as before and the small differences in fast flux and cadmium ratio are well within experimental errors.

Table 2 shows that neither the big shim addition nor the recent instal-

TABLE 1

Composition and homogeneity of the DUSR neutron flux

Parameters	Inner site		Outer site	
	1977[a]	1987[b]	1977[a]	1987[b]
Maximum thermal flux (n cm^{-2} s^{-1})	1.1×10^{12}	1.1×10^{12}	5.4×10^{11}	5.4×10^{11}
Maximum fast flux (n cm^{-2} s^{-1})	2.4×10^{11}	2.4×10^{11}	2.0×10^{10}	2.4×10^{10}
Fast-to-thermal flux ratio	0.22	0.22	0.037	0.044
Cadmium ratio for Au	2.2	2.2	5.3	4.3
Variation in vertical homogeneity (% cm^{-1})	< 1	~0.5	< 1	~0.5
Variation in radial homogeneity (% cm^{-1})	< 1	~0.5	~5	6

[a]Prior to Cd-site and big Be shim installations. [b]After Cd-site and big Be shim installations.

TABLE 2

Reproducibility of the DUSR neutron flux

Site	Counts ($\times 10^{-4}$) per mg of 0.1% Au flux wires		
	1977[a]	1982[b]	1987[c]
(A) Inner site			
1	1.01	1.00	1.01
2	0.977	0.987	1.00
3	1.01	0.998	1.01
4	1.01	0.992	1.00
5	1.01	0.982	0.997
(B) Outer site			
8	0.347	0.347	0.363
9	0.386	0.080	0.083
10	—	0.365	0.380

[a]Prior to the Cd-site installation. [b]After the installation of Cd-site 9. [c]After the installation of big Be shim.

lation of a cadmium-shielded site in position 9 had any appreciable effect on the flux. The big shim addition also did not result in any significant change in the flux gradients. Differences between counts per mg for data reported here and those given earlier [1] result from different irradiation and counting conditions [1, 4].

Analysis of different matrices

Tables 3—7 show data for a broad variety of materials analyzed by neutron activation with the SLOWPOKE reactor. A brief commentary for each matrix is given below.

Atmospheric wet precipitation. Detection, identification and measurement of trace elements in atmospheric wet precipitation (air, acid rain, snow, fog) are of considerable interest in studying long-range transport of pollutants. Both instrumental n.a.a. and n.a.a. after preconcentration are being extensively used in this laboratory for multi-element determinations in the above matrices [5, 6]. Samples of atmospheric particulate matter are collected by using both high-volume and 5-stage Anderson samplers based on mass median diameter fractionations while Sangamo Type A, automatic, wet-only collectors are used for wet deposition. The latter samples are separated into particulate matter and soluble fractions through Nuclepore membranes. As shown in Table 3, concentrations of up to 35 elements can be measured conveniently in atmospheric particulate matter and particulate fraction of wet deposition by instrumental n.a.a. Although instrumental n.a.a. can be used for determining several elements in the soluble fraction, preconcentration is necessary because of the very low levels of several elements of interest; post-irradiation radiochemical separation methods cannot be used for short-lived nuclides. A preconcentration method based on Chelex-100 ion-exchange resin has been used here for measuring up to 15 elements by direct irradiation of the resin after separation. Concentration correlation coefficients show that Cu, Hg, Se and Zn are highly enriched (enrichment factor 100) and significantly correlated ($r > 0.8$ at $p = 99.9$), suggesting common anthropogenic sources of emission. Mathematical modelling of data gives an estimate of the long-range transport of these and other pollutants.

Reliability of results at low levels of trace elements often necessitates procedures which concentrate the analyte and/or separate it from macro quantities of matrix components. For example, in seawater, sodium, chloride and bromide are serious interferences in n.a.a. and one can either remove the interference, mask it, or preconcentrate; enrichment permits detection limits to be substantially lowered. Nanograms per gram and less of Ag, As, Co, Cr, Cu, Fe, Hg, La—Lu, Mn, Mo, Sb, Se, Sm, Ti, U, V and Zn have been successfully determined in seawater by n.a.a. with SLOWPOKE after preconcentration [7, 8].

House dust. House dust is an environmental material to which humans are almost inevitably exposed; knowledge of the levels of materials in the

TABLE 3

Multi-element content of atmospheric materials by instrumental n.a.a. and n.a.a. after preconcentration

Element	Atmospheric particulate matter[a]	Wet deposition particulate matter[b]	Wet deposition soluble fraction[b]	House dust[d]
Al	860	100	4.9	2.4×10^4
As	2.2	38.2[c]	0.17	15.8
Au	0.002	3.5[c]	6.4[c]	0.42
Ba	15	0.87	3.98[e]	—
Br	31	190[c]	45.4	37.1
Ca	250	11.6	490	1.5×10^4
Ce	4.7	0.40	0.33	23.6
Cl	280	6.72	7.3	4006
Co	0.32	—	—	8.59
Cr	2.2	1.1	0.38[e]	103
Cs	0.07	—	—	—
Cu	410	1.7	14.3[e]	230
Dy	2.3	—	—	—
Eu	0.04	—	—	—
Fe	460	67.5	—	1.0×10^4
Hf	0.06	—	—	2.12
Hg	0.08	0.14	0.17[e]	—
I	0.57	—	—	<8
In	0.01	—	—	—
K	270	40.8	86	1.3×10^4
La	1.5	0.06	0.05[e]	11.9
Lu	0.02	—	—	—
Mg	220	45.2	10.8	5.9×10^3
Mn	3.3	1.02	5.6	207
Na	880	6.75	45.4	1.2×10^4
Rb	1.8	—	—	—
Sb	0.03	0.05	0.32	10.0
Sc	0.08	18.5	1.55[e,c]	2.9
Se	1.2	0.17	0.09[e]	—
Sm	0.12	41[c]	6.28[e]	1.22
Sr	3.2	—	—	—
Th	—	—	—	3.4
Ti	26	25.3	—	2.0×10^3
V	28	0.85	0.14[e]	30
Zn	11	16.8	3.8	845

[a—d]Mean of 11 samples: [a]In ng m^{-3}; [b]In $\mu g\ l^{-1}$; [c]In ng l^{-1}; [d]In $\mu g\ g^{-1}$. [e]By n.a.a. after preconcentration.

dust is a guide to any possible hazard. House dust in 10—12 houses in each of six areas in Christchurch, New Zealand was randomly selected for sampling; three or four samples were taken from each house. The dust was collected with a small diaphragm vacuum pump onto a Gelman Type A glass filter; street dust and soil were collected from the same six areas. Samples were weighed into polyethylene envelopes and analyzed by instrumental n.a.a.; overall errors are uncertain but comparison of results obtained for international standards with published data suggest an error of 10—15% for most elements (Table 3). Unsurprisingly, soil is the major contributor to both street (87%) and house (45—50%) dusts. Some contributions (2—3%) come from tire wear, cement and car emissions, 1% comes from salt, and the remainder is organic. The elemental composition of house dust throughout the city is relatively uniform except for pollution elements such as lead [9].

Soil. A soil sample (Tibet 83-401) was prepared as a possible reference material by the Institute of Environmental Chemistry, Chinese Academy of Sciences, from soil obtained from a 7000-m high mountain in Tibet; samples were sent here for analysis. The material had been ground (200-mesh) in an aluminium oxide ball mill and the homogeneity of the sample with respect to half-a-dozen elements had been established by x-ray fluorescence in China; four additional elements were examined for their homogeneity here by neutron activation and shown to be also homogeneously distributed. The results of instrumental n.a.a. of the reference material are shown in Table 4; IAEA soil 5, NBS 1646 sediment and several USGS rock standards were analyzed for comparison, with excellent results. The high value for aluminium in the Chinese soil sample is probably due to contamination from the grinding process.

Meteorite. The meteorite analyses were part of a study of three New Zealand chondrites [10]. The Morven meteorite in the Otago Museum, Dunedin, New Zealand consists of a large stone and a small fragment which were believed to originate from the same parent body. Analyses done by x-ray fluorescence, inductively-coupled plasma emission and instrumental n.a.a. showed that the two stones have different compositions; the smaller fragment is an LL-type chondrite while the larger is an H4/5 meteorite. The results of instrumental n.a.a. of the smaller fragment are given in Table 4.

Glasses. The long-term safety of the possible storage of high-level radioactive wastes in crystalline rock formations and sub-seabeds is being evaluated in this laboratory. Sodium borosilicate glasses are particularly suitable as host matrices for immobilized wastes. In an accident situation, radionuclides can be leached from the waste by groundwater. In an attempt to develop a mechanism of leaching, simulated vitrified high-level wastes and their leachates are being analyzed by a combination of instrumental n.a.a. and epithermal instrumental n.a.a. The elemental content of a typical sample of sodium borosilicate glass is shown in Table 5. Boron was measured by using an indirect instrumental n.a.a. method by irradiating glass samples with and without a 10-μg ml^{-1} vanadium spike solution.

TABLE 4

Elemental content of geological materials by instrumental n.a.a. and epithermal instrumental n.a.a.[a]

Element	NRCC sediment RM MESS-1		GME deep-sea sediment	New Zealand meteorite	Chinese soil standard, Tibet 83-40
	This work	NRCC value			
Al (%)	5.98±0.11	5.84±0.20	2.40±0.08	—	7.41±0.0
As	11.0±0.3	10.6±1.2	3.55±0.52	2.28±0.20	3.50±0.3
Au	—	—	—	193±18[b]	—
Ba	263±22	—	288±60	—	456±11
Br	150±15	—	165±1	4.2±0.1	1.18±0.3
Ca (%)	0.429±0.050	0.482±0.046	24.2±0.9	—	2.6±0.2
Ce	80.2±4.8	—	3.90±3.0	—	—
Cl (%)	0.84±0.03	0.82±0.07	2.21±0.20	—	—
Co	11.6±0.71	10.8±1.9	11.4±0.8	444±3	12.4±0.5
Cr	70.9±5.3	71±11	38.3±1.6	0.289±0.016[c]	61.8±3.1
Cs	4.15±0.16	(4)	1.21±0.27	—	7.2±0.12
Eu	1.46±0.023	—	0.991±0.030	—	1.21±0.0
Fe (%)	3.07±0.13	3.05±0.17	3.53±0.23	18±1	3.28±0.0
Hf	18.5±1.5	—	2.12±0.18	—	6.80±0.2
I	68.0±2.7	—	4.04±0.44	—	—
In	57.2±11.7	—	—	—	—
Ir	—	—	—	320±12[b]	—
K (%)	2.05±0.59	2.24±0.04	0.678±0.148	—	2.26±0.1
La	45.9±4.94	—	13.9±0.6	—	39.6±1.3
Lu	1.74±1.14	—	0.541±0.184	—	0.41±0.0
Mg (%)	1.66±0.21	1.74±0.11	2.05±0.02	—	1.85±0.0
Mn	514±21	513±25	878±59	—	—
Na (%)	1.89±0.06	1.85±0.11	1.55±0.10	1.84±0.02	1.61±0.0
Nd	45.6±5.7	—	16.4±3.8	—	42±3
Ni	—	29.5±2.7	4.28±0.52	0.76±0.01[c]	—
Os	—	—	—	623±71[b]	—
Rb	78.0±5.8	—	13.6±1.8	—	142±5
Sb	0.818±0.092	0.73±0.08	0.258±0.055	245±7[b]	0.41±0.0
Sc	11.7±1.1	—	12.7±1.8	6.79±0.18	10.3±0.4
Si (%)	40.3±0.8	42.1±1.2	4.95±0.83	—	32.3±0.9
Sm	6.42±0.81	—	2.59±0.41	—	6.80±0.2
Sr	100±5.3	(89)	1220±128	—	152±16
Ta	1.57±0.04	—	1.14±0.07	—	1.10±0.0
Tb	2.63±0.72	—	2.95±0.01	—	0.71±0.0
Th	14.7±1.2	—	3.41±0.21	—	17.8±0.04
Ti (%)	0.540±0.037	0.543±0.017	0.38±0.034	—	0.36±0.0
Tm	1.40±0.58	—	0.463±0.170	—	—
U	3.54±0.54	—	0.338±0.145	—	3.90±0.4
V	68.9±2.1	72.4±5.3	51.4±3.5	—	82±3
Yb	3.93±0.31	—	4.15±0.79	—	3.50±0.2
Zn	187±10	191±17	112±12	—	—
Zr	—	—	86.6±20	—	—

[a]All values are in $\mu g\ g^{-1}$ unless otherwise noted. [b]In $ng\ g^{-1}$. [c]In percent.

TABLE 5

Elemental content of glass, silica and aluminium by instrumental n.a.a. and epithermal instrumental n.a.a.[a]

Element	Glass	Biogenic silica	Aluminium
Al	22900 ± 1600	170—7610	—
As	—	0.80—10.0	28—32[b]
Au	—	<10—160[b]	—
Ba	2770 ± 160	—	—
Br	<3	<0.3—1800	10—20[b]
Ca	<4074	<50—630	—
Ce	6220 ± 280	—	200—870[b]
Cl	<7	<5—175	11—12
Co	1.18 ± 0.36	<5—10.1	—
Cr	919 ± 68	<10—30	—
Cs	<0.133	—	—
Cu	—	<15—350	—
Dy	—	—	50—100[b]
Eu	7.72 ± 0.81	—	—
Fe	26100 ± 1500	—	—
Ga	—	—	<10—260[b]
Hf	204 ± 9	—	—
I	—	<0.6—51	—
La	3140 ± 200	<0.1—0.6	90—210[b]
Mg	42800 ± 3000	<150—1010	—
Mn	<50	<1—45	40—120[b]
Mo	10400 ± 1500	<150—18000	—
Na	108000 ± 11100	40—4500	—
Nd	6620 ± 763	—	—
Ni	29200 ± 2800	—	—
Pt	—	<5—150	—
Sb	—	<0.2—7.4	30—90[b]
Sc	0.0760 ± 0.0095	<0.5—5.2	100—130[b]
Si	243000 ± 62200	—	—
Sm	10700 ± 2600	—	10—30[b]
Ta	0.180 ± 0.021	—	—
Th	22.9 ± 1.8	<1.0—2.8	40—80[b]
Ti	—	110—400	—
U	8.82 ± 0.68	<0.4—7.5	60—110[b]
V	—	<0.1—1.6	—
W	—	<0.2—30	—
Yb	38.8 ± 7.1	—	—
Zn	517 ± 47	<150—3840	—
Zr	7700 ± 670	—	—

[a]All values are in $\mu g\ g^{-1}$ unless otherwise noted; ranges are given for silica and aluminium.
[b]In $ng\ g^{-1}$.

Deep-sea sediments. Sediments and pore water collected from potential repository sites are being characterized for major, minor and trace constituents as part of a global study to evaluate the suitability of the sub-seabed disposal option. Typical levels in samples collected from the Great Meteor East (GME) site are shown in Table 4. To evaluate the accuracy of the methods, several certified reference materials were also analyzed. Results for the National Research Council of Canada (NRCC) sediment reference material (RM-MESS-1) are given in Table 4. The values generally agree well with those certified by NRCC.

Aluminium. Aluminium slugs used as electrodes in fundamental studies of electroluminescence [11] were analyzed for their trace-element content (Table 5); trace elements can markedly affect light emission at electrode surfaces and knowledge of their presence and levels is critical. The samples were irradiated for 7 h at a flux of 5×10^{11} n cm^{-2} s^{-1} and allowed to decay for 3 days before counting; ^{24}Na is formed by the reaction of fast neutrons with aluminium but multi-element determination of ng g^{-1} levels of long-lived nuclides is readily done after the 3-day waiting period.

Animal tissues. Analysis of biogenic silica obtained from the cell walls of marine diatoms is of interest in studying the morphological development of

TABLE 6

Elemental content of animal tissues by instrumental n.a.a. and radiochemical n.a.a.

Element	Type of tissue[a]			NBS Bovine Liver (SRM-1577)[b]	
	Kidneys	Livers	Lungs	This work	NBS values
Al	11.2±3.2	13.4±13.5	18.3±4.3	—	—
As	30±10[c]	40±11[c]	370±170[c]	0.054±0.002	0.055±0.005
Br	20.0±9.3	18.5±11.1	33.7±7.6	9.2±0.2	—
Ca	148±75	150±60	200±85	120±20	124±6
Cl	3260±1060	3420±1150	4670±900	2640±200	(2700)
Co	500±140[c]	350±175[c]	290±50[c]	0.19±0.03	(0.18)
Cu	14.6±3.5	10.9±1.9	12.5±2.7	201±8	193±10
Fe	400±54	688±410	480±50	275±19	268±8
Hg	—	152±72[c]	—	0.015±0.002	0.016±0.002
K	6940±2180	7780±1820	9750±1470	9500±600	9700±600
Mg	522±117	580±103	730±40	609±25	640±9
Mn	2.06±0.50	2.13±0.77	2.19±0.47	9.8±1.0	10.3±1.0
Mo	1.18±0.77	2.33±1.21	1.27±0.85	3.5±0.4	(3.4)
Na	2410±700	2630±890	3340±490	2360±160	2430±130
Rb	17.2±4.0	18.4±5.2	23.6±2.2	18.4±1.2	18.3±1.0
Se	3.85±1.12	2.55±0.48	2.31±0.16	0.96±0.06	1.1±0.1
V	<0.20	170±30[c]	<0.1	—	—
Zn	70.6±23	85.5±12.6	82.1±14.7	123±15	130±13

[a] Average of 4 samples from mice with tumors, in $\mu g\ g^{-1}$. [b] In $\mu g\ g^{-1}$. [c] In ng g^{-1}.

TABLE 7

Elemental determination through short-lived nuclides by cyclic instrumental n.a.a.

Element	Nuclide	Half-life (s)	γ-ray (keV)	Sensitivity[a] (counts μg^{-1})	Content ($\mu g\ g^{-1}$)
Ag	^{110}Ag	24.0	658	5.1×10^2	0.80 ± 0.05[b]
Au	^{197m}Au	7.2	279	1.6×10^0	—
Br	^{79m}Br	4.8	208	3.9×10^1	9.3 ± 0.5[c]
Cl	^{38m}Cl	0.72	671	3.7×10^1	0.25 ± 0.02[c,d]
Dy	^{165m}Dy	78	108	4.7×10^3	0.06 ± 0.01[b]
Er	^{167m}Er	2.3	208	1.6×10^5	—
F	^{20}F	11.2	1633	4.8×10^0	62 ± 8[e]
Ge	^{75m}Ge	47.7	160	2.2×10^1	2.5 ± 0.4[f]
Hf	$^{179m1}Hf$	18.7	214	1.5×10^3	4.1 ± 0.3[g]
In	$^{116m2}In$	2.16	164	5.8×10^4	1.05 ± 0.08[g]
Pb	^{207m}Pb	0.81	570	4.6×10^{-1}	7500 ± 1500[g]
Pd	^{107m}Pd	21.3	188	7.9×10^1	—
Rb	^{86m}Rb	62.4	556	1.8×10^3	5.1 ± 0.4[b]
Sc	^{46m}Sc	18.7	142	1.1×10^4	0.060 ± 0.007[b]
Se	^{77m}Se	17.4	162	1.1×10^3	0.99 ± 0.01[c]
W	^{183m}W	5.3	108	7.5×10^1	0.29 ± 0.04[h]
Y	^{89m}Y	16.1	909	6.4×10^0	0.13 ± 0.02[f]

[a]Flux of 1.1×10^{12} n cm^{-2} s^{-1}; irradiation time = counting time = 3 s; ten cycles. [b]NBS Oyster Tissue (SRM-1566). [c]NBS Bovine Liver (SRM-1577). [d]In percent. [e]ICES Fish Flour. [f]Coal sample. [g]NBS Urban Particulate Matter (SRM-1648). [h]In ng m^{-3} for an aerosol sample.

such diatoms [12]. Several such silica samples were analyzed and the ranges of the results obtained are shown in Table 5.

The analysis of biological materials is illustrated by a study of the relationship between neoplasia and the concentrations of trace elements, in which a combination of instrumental n.a.a. and radiochemical n.a.a. was used. Hepatoma H6 spontaneous solid tumors were developed in the livers of experimental mice of the A/J strain, and samples of several tissues were analyzed. The radiochemical method involved distillation and ion-exchange separation [13, 14]. The trace element contents of a few tissue samples are shown in Table 6. Also presented are results for the NBS Bovine Liver standard reference material (SRM); the values agree well with the certified ones. Biological materials such as blood serum and urine can be advantageously analyzed for elements such as uranium [15], bromine and iodine [16] by epithermal n.a.a.

Table 7 shows some results obtained by using cyclic instrumental n.a.a. and short-lived nuclides; the use of short-lived nuclides not only reduces total experimental time but also provides superior precision and detection limits for several elements. In this technique, a sample is irradiated for a

short time (1—30 s) and rapidly transferred (within 600 ms), by using a specially designed automated cyclic system, to a detector for counting; the entire process is repeated for an optimum number of cycles [17, 18]; a method has been developed to correct for coincidence losses [19]. To illustrate the use of this technique of instrumental n.a.a. in practical samples, elemental levels in a variety of matrices are listed in Table 7.

This work was supported by the Natural Sciences and Engineering Research Council of Canada. It is a pleasure to acknowledge our indebtedness to G. Burbidge, J. Hilborn, M. Spender and B. Townes of Atomic Energy of Canada Limited.

REFERENCES

1 D. E. Ryan, D. C. Stuart and A. Chattopadhyay, Anal. Chim. Acta, 100 (1978) 87.
2 R. E. Kay, P. D. Steves-Guille, J. W. Hilborn and R. E. Jervis, Int. J. Appl. Radiat. Isotop., 24 (1973) 509.
3 J. W. Hilborn and B. M. Townes, J. Radioanal. Nucl. Chem., 110 (1987) 385.
4 J. Holzbecher, A. Chatt and D. E. Ryan, Can. J. Spectrosc., 30 (1985) 67.
5 E. P. Hamilton and A. Chatt, J. Radioanal. Chem., 71 (1982) 29.
6 J. E. Milley and A. Chatt, J. Radioanal. Nucl. Chem., 110 (1987) 345.
7 R. S. Murthy, J. Holzbecher and D. E. Ryan, Rev. Anal. Chem., 1 (1982) 113.
8 R. S. Murthy and D. E. Ryan, Anal. Chem., 55 (1983) 1682.
9 J. E. Fergusson, E. A. Forbes, R. J. Schroeder and D. E. Ryan, Sci. Total Environ., 50 (1986) 217.
10 P. P. Sipiera, R. R. Brooks, J. H. Johnston, P. L. Hoek, J. Holzbecher, D. E. Ryan, V. E. Neal and R. D. Reeves, Chem. Geol., 54 (1986) 17.
11 J. J. Kankare, University of Turku, Finland, personal communication.
12 A. Rogerson, A. S. W. DeFreitas and A. G. McInnes, Trans. Am. Microsc. Soc., 105 (1986) 59.
13 A. Chatt and C.-S. Tse., Trans. Am. Nucl. Soc., 44 (1983) 24.
14 C.-S. Tse, Ph.D. Thesis, Dalhousie University, 1980.
15 J. Holzbecher and D. E. Ryan, Anal. Chim. Acta, 119 (1980) 405.
16 J. Holzbecher and D. E. Ryan, Clin. Biochem., 13 (1980) 277.
17 K. N. DeSilva, Ph.D. Thesis, Dalhousie University, 1981.
18 R. E. Tout and A. Chatt, Anal. Chim. Acta, 133 (1981) 404.
19 K. N. DeSilva and A. Chatt, Proc. Ann. Conf. Can. Nucl. Soc., (1981) 328.

Analytica Chimica Acta, 200 (1987) 101—114
Elsevier Science Publishers B.V., Amsterdam — Printed in The Netherlands

VOLTAMMETRIC/AMPEROMETRIC DETECTION FOR LIQUID CHROMATOGRAPHY

CRAIG E. LUNTE[a], JOHN F. WHEELER and WILLIAM R. HEINEMAN*
Department of Chemistry, University of Cincinnati, Cincinnati, OH 45221 (U.S.A.)
(Received 7th April 1987)

SUMMARY

A voltammetric/amperometric detector based on a dual-electrode electrochemical detector is described for liquid chromatography. The detector combines the advantages of both voltammetric and amperometric detection. A three-dimensional data array of current response as a function of both time (chromatographic domain) and potential (electrochemical domain) is obtained. From the chromatographic point of view, this allows post-experimental choice of the optimal detection potential. Different detection potentials can even be chosen for each chromatographic peak. Having the voltammetric data as well as the chromatographic data provides ready identification of chromatographically unresolved compounds and the ability to resolve such co-eluting compounds voltammetrically. The voltammetric data also provide a second method of peak identification for greater certainty in peak assignments. Voltammetric detection limits of less than 10 pmol of material injected on the column were achieved with this detection method. From the electrochemical perspective, voltammetric/amperometric detection provides a technique for obtaining hydrodynamic voltammograms with small amounts or small volumes of sample. Voltammograms can also be obtained for the individual components of complex mixtures without the need for isolation steps.

To date, most reports on electrochemical detection for liquid chromatography have dealt with amperometry [1]. This has been because of the ease of operation of such detectors and the extremely low detection limits which can readily be achieved. Interest in voltammetric detectors, however, is increasing because they provide improved resolving power by obtaining data in both the potential (electrochemical) and time (chromatographic) domains.

---

*William R. Heineman received his B.S. degree from Texas Tech University in 1964 and his Ph.D. from the University of North Carolina at Chapel Hill in 1968. He was a research chemist at the Hercules Research Center from 1968 to 1970 before becoming a research associate with Professor Ted Kuwana at Case Western Reserve University and The Ohio State University. He joined the faculty at the University of Cincinnati in 1972 where he is Professor and Chairman of the Analytical Division. Heineman's research interests include thin-layer spectroelectrochemistry, EXAFS spectroelectrochemistry, electrochemical immunoassay, polymer modified electrodes, stripping voltammetry and the analytical chemistry of technetium radiopharmaceuticals.

[a]Current address: Department of Chemistry, The University of Kansas, Lawrence, KS 66045, U.S.A.

0003-2670/87/$03.50

Development of acceptable voltammetric detectors has been hindered by the much higher detection limits that can be achieved with these detectors because of the large charging currents associated with scanning the applied potential.

To overcome this charging-current problem, several techniques have been reported. Pulse techniques are the most commonly used methods to diminish charging-current contributions. With these techniques the charging current is allowed to decay before the faradaic current is sampled. Several pulse waveforms have been used, including staircase [2], differential pulse [3], normal pulse [4], and squarewave [5–9]. In addition to pulse techniques, alternating current (AC) voltammetric techniques have been used to discriminate against the charging current [10]. Recently, microelectrodes have been used with electrochemical detectors to alleviate charging-current problems [11, 12]. Coulostatic detectors have also been designed to obtain voltammetric information [13, 14]. Even with these advanced techniques, the detection limits achieved with voltammetric detection are several orders of magnitude higher than for amperometric detectors.

In recent work from this laboratory, a voltammetric detector was described for flow-injection systems [15, 16]. A series-configuration dual-electrode thin-layer flow cell is used in which the potential at the upstream electrode is scanned while the potential of the downstream electrode is held constant. A similar approach has been described by Trubey and Nieman [17], using a coulostatic technique to achieve the potential sweep. The downstream electrode is used to monitor either the formation of product or depletion of reactant at the upstream electrode. If products are detected, the technique is termed collection mode, while if depletion of reactant is determined the technique is termed shielding mode. In this way, the current response at the downstream electrode reflects the voltammetric behavior of the analyte at the upstream electrode without the charging current associated with scanning the potential. These processes are illustrated in Fig. 1 along with the upstream excitation waveform and a typical downstream response. A detection limit of 10^{-7} M was achieved by flow injection analysis during the initial characterization of this detection technique. In this report, the detection technique, termed voltammetric/amperometric detection, is extended to application to liquid chromatography. Instrumental improvements are described and data analysis techniques are demonstrated. Sample analysis is illustrated by the detection of oxidizable compounds in a beer extract.

EXPERIMENTAL

Reagents and instrumentation

Caffeic acid, *p*-coumaric acid, gentisic acid, and vanillic acid were obtained from Sigma Chemical Co. Ferulic acid and sinapic acid were purchased from Aldrich Chemical Co. All chemicals were used as received. Standard solutions

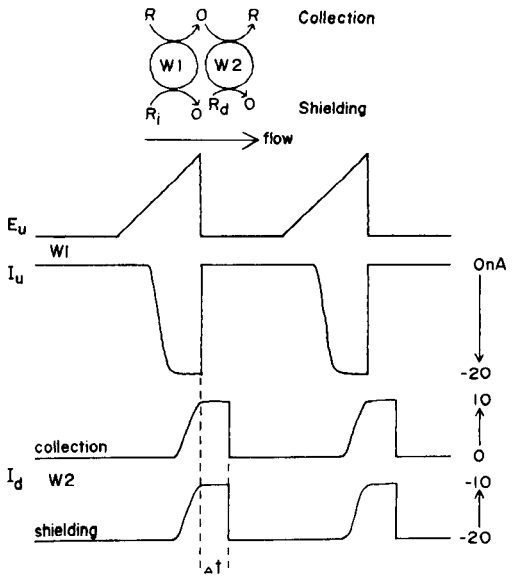

Fig. 1. Timing diagram for dual-electrode voltammetric/amperometric detection in the collection and shielding modes. W1, upstream electrode; W2, downstream electrode; E_u upstream (W1) potential; I_u, upstream (W1) current; I_d, downstream (W2) current; Δt, time delay between electrodes.

were prepared in 0.1 M ammonium phosphate buffer, pH 4. Stock solutions were prepared fresh weekly and standards were prepared daily from the stock solutions.

The chromatographic system was a Bianalytical Systems (West Lafayette, IN) LC-400 liquid chromatograph. A 200-μl sample loop was used for all experiments. A Brownlee RP-18 ODS, 5 μm (4.6 mm $\times$ 10 cm) column was used. The mobile phase was 0.1 M ammonium phosphate buffer, pH 4 with 15% (v/v) methanol. A flow rate of 1 ml min^{-1} was used unless otherwise noted. A BAS dual-electrode thin-layer cell with glassy-carbon working electrodes was used. The reference electrode was Ag/AgCl for all experiments and potentials were reported versus this reference.

Waveform generation and data acquisition and analysis were controlled by a Zenith 158 personal computer (Franklin Park, IL) with 640 kbyte of memory and 20-Mbyte hard disk. The computer was interfaced with an ADALAB-PC interface card (Interactive Microware, State College, PA) equipped with a 12-bit fast analog-to-digital converter (A/D), a 12-bit integrating A/D, two 12-bit digital-to-analog converters (D/A), and four 16-bit timers. The D/As had output ranges of -2.5 to $+2.5$ V. The integrating A/D had a range of -1.0 to $+1.0$ V while the fast A/D had a range of -10 to $+10$ V. The rate of data acquisition and waveform output during an

individual potential scan was controlled by one of the timers. The ADALAB-PC interface card was connected to a Pine Instrument RDE-3 bipotentiostat (Grove City, PA) through its external potential inputs and current jacks. The bipotentiostat provided the reference and current-to-voltage converter circuitry but was not used to generate the waveform. Software for data acquisition and instrument timing was written in assembly language while software for data analysis and processing was written in both BASIC and assembly language. Data was stored in memory during the chromatography and could be transferred for permanent storage to a disk (either hard or floppy) after data collection was complete. Real-time display of the current at a user-defined potential was used to monitor the chromatogram.

The waveform consists of 100 equally spaced steps from the initial potential to the final potential. After the final step, the potential is returned to its initial value until the next scan is initiated. The initial potential, final potential, and scan rate are user-defined parameters which set the step height and step width. The scan frequency is user-defined with the limitation that there be sufficient delay between initiation of each scan for the scan to occur plus approximately 450 ms of overhead time for data to be transferred to high memory. In general, a scan rate of 2.0 V s^{-1} over a 1.0-V range at a frequency of 1 scan s^{-1} provides good voltammetric information while maintaining good density in the chromatographic data. Because of memory limitations of the personal computer system, a maximum of 1600 scans can be acquired for any chromatographic run.

Sample preparation

The beer sample (1 ml) was acidified to pH 2 with acetic acid. The acidified sample was then applied to a C-18 Sep-Pak cartridge (Waters Associates). The Sep-Pak was rinsed with 10 ml of water and the phenolic acids then eluted with 2 ml of 0.5 M ammonia solution. The basic extract was acidified with acetic acid and injected onto the analytical column.

RESULTS AND DISCUSSION

Background subtraction

In the ideal case, voltammetric/amperometric detection would exhibit no charging-current response at the downstream amperometric electrode. However, the two working electrodes in the dual-electrode cell are not completely independent and a small current is observed at the downstream electrode when a large current is present at the upstream electrode. This nonfaradaic current at the amperometric electrode is termed cross-talk and arises from small changes in the interfacial potential at the amperometric electrode caused by the iR drop of the scanned potential electrode. The absolute cross-talk current is scan-rate dependent but the relative cross-talk is independent of scan rate and is approximately 0.1% of the upstream charging current for the electrochemical cell used in these experiments.

Even in the presence of the cross-talk background current, voltammetric/amperometric detection provides lower detection limits than direct voltammetric detection because the background is 3—4 orders of magnitude smaller. In addition, because this background is now on the same order of magnitude as the signal (nA), subtraction of the background signal is possible to lower the detection limit further. Similar background subtraction techniques have previously been used with direct voltammetric detection [2, 11]. In these experiments, background voltammograms are collected prior to sample injection until a steady background is achieved. This steady background voltammogram is stored in memory and can be subtracted from subsequent chromatographic voltammograms to lower the detection limit. Figure 2 shows the raw and background-subtracted voltammograms for a chromatographic injection of 85 pmol of caffeic acid. All subsequent voltammograms shown are background-subtracted.

Flow characterization

Under the hydrodynamic conditions of the series dual-electrode thin-layer flow cell, there is a finite time delay between when any given segment of solution flows over the upstream electrode and when it reaches the downstream electrode. This time delay must be known in order to correlate the downstream current response to the upstream potential. This time delay is dependent upon the flow rate and cell geometry. Because the cell geometry is constant for all experiments reported here, only the flow-rate dependence need be determined. The flow-rate dependence was found as previously described [16]. A plot of the inverse of delay time (s^{-1}) versus flow rate ($\mu l\ s^{-1}$) gave a straight line of slope 1.03 μl^{-1} with an intercept of $-1.11\ s^{-1}$ and a correlation coefficient (r^2) of 0.9991. This relationship is incorporated into the software to correlate the current to the potential.

The shape of the voltammetric wave is also dependent on flow rate. The voltammograms of chromatographic peaks exhibited maxima followed by a plateau region at higher potential. This behavior cannot be ascribed to a change in the concentration of the analyte during the course of the voltammetry because peaking is observed in voltammograms from both the leading and tailing edge of the chromatographic peak. The degree of "peaking" was found to increase as the flow rate increased (Fig. 3). This is in contrast to the results of White et al. [11] who observed an inverse relationship between "peaking" and flow rate for a fiber microelectrode thin-layer cell. For the present flow-injection system, this inverse relationship has also been observed, but only at low flow rates (<0.5 ml min^{-1}). At the flow rates used here, well-defined hydrodynamic voltammograms were observed when the usual flow-injection configuration was used to introduce the sample. While this result does not detract from the utility of voltammetric/amperometric detection with this cell, work is currently under way to attempt to explain these anomalous results.

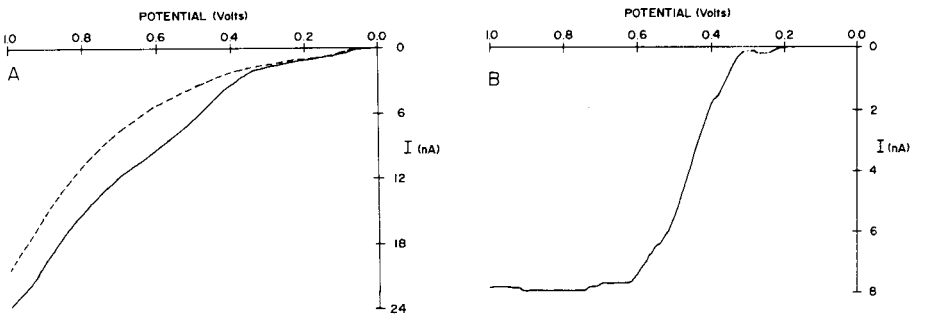

Fig. 2. Background current subtraction. (A) Background current (----) and raw voltammogram for 85 pmol of caffeic acid injected (——). (B) Background-subtracted voltammogram. The scan rate was 2.0 V s^{-1} and the retention time for caffeic acid was 4.5 min.

Effect of scan rate

Because the resistance of the thin-layer flow cell is high, *iR* drop considerations are important. With the flow cell used in these experiments, scan rates up to 2.0 V s^{-1} could be used with little apparent *iR* drop. At scan rates of greater than 5.0 V s^{-1}, the *iR* drop is apparent as a skewing of the voltammetric curve (Fig. 4). A scan rate of 2.0 V s^{-1} is sufficient for chromatographic detection. This allows a large potential window to be scanned while maintaining good density in the chromatographic data. For example, a typical experiment would be to scan a 1.0-V potential window at a frequency of 1 scan s^{-1}.

The scan rate also affects the degree of "peaking" of the voltammograms as described previously. The slower the scan rate, the more peaked the voltammograms, while the plateau current is independent of scan rate. This behavior is also contrary to that observed in flow injection analysis and reported by White et al. [11] for a carbon fiber microelectrode. Because of this scan rate dependence of the peak current, quantitation at the peak potential will be more sensitive but dependent on scan rate. However, quantitation at a potential on the current plateau will be slightly less sensitive but the current response will be independent of scan rate. While the results shown for the previous sections have been for collection-mode detection, the results are the same when the shielding mode is used.

Chromatographic detection

Collection mode. The collection mode is achieved by operating the downstream electrode at a potential to reverse the reaction occurring at the upstream electrode. In other words, this detection mode involves redox cycling of the analyte and is amenable only to chemically reversible compounds. The chemical reversibility of a compound determines its collection efficiency. The collection efficiency is defined as the ratio of downstream response to upstream response when both responses are on their respective mass transport-limited plateaus. In this application, the collection efficiency can be

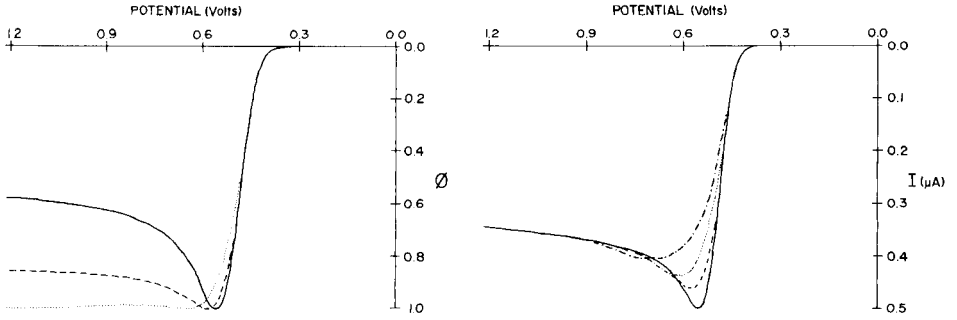

Fig. 3. Effect of flow rate on collection mode voltammetry. Caffeic acid (5 nmol) injected with a scan rate of 2.0 V s^{-1}; ϕ is the normalized current response. Flow rate: (...) 1 ml min^{-1}; (----) 2 ml min^{-1}; (——) 3 ml min^{-1}.

Fig. 4. Effect of scan rate on collection mode voltammetry. Caffeic acid (5 nmol) injected at a flow rate of 3 ml min^{-1}. Scan rate: (——) 0.5 V s^{-1}, (- - - -) 1.0 V s^{-1}; (···) 2.0 V s^{-1}; (—·—) 5.0 V s^{-1}.

considered as a response factor for a given compound. The collection efficiencies of the phenolic acids used in this study are listed in Table 1. In addition to depending upon the compound, the collection efficiency is a function of the cell geometry. For the cell used in these studies, a collection efficiency of 0.3 corresponds to a chemically reversible compound.

Voltammetric/amperometric detection results in a three-dimensional data array of current response versus both time and applied potential. A chromatovoltammogram for a mixture of phenolic acids is shown in Fig. 5. The optimal detection potential depends on the compound and experimental conditions. An advantage of voltammetric/amperometric detection is that all of the information needed to make the choice of the optimal detection potential is generated at the time of the experiment. Voltammograms of the eluting peaks can be obtained by looking at a potential scan at the chromatographic peak. Figure 6 shows the voltammograms of the peaks from the chromatovoltammogram of Fig. 5. From these voltammograms, the proper choice of potential for chromatographic detection can be made from the actual data instead of relying on predetermined values.

For example, to determine all of the phenolic acids in the sample, a potential of 1.2 V is required as shown in Fig. 7A. If it is preferred not to detect the phenolic acids which are difficult to oxidize, a potential of 0.9 V can be chosen as shown in Fig. 7B. At this potential, gentisic acid, caffeic acid, and sinapic acid are still on their mass-transport limited plateau, whereas vanillic acid, *p*-coumaric acid, and ferulic acid give very little response at 0.9 V. If these hard-to-oxidize compounds are of interest and the other compounds are interferences, a difference mode approach can be used

TABLE 1

Collection and shielding efficiencies for phenolic acids

Compound	Collection efficiency	Shielding efficiency	Compound	Collection efficiency	Shielding efficiency
Gentisic acid	0.30	0.68	*p*-Coumaric acid	0.07	0.68
Vanillic acid	0.24	0.68	Ferulic acid	0.23	0.69
Caffeic acid	0.30	0.69	Sinapic acid	0.13	0.70

as previously described [11, 16]. A difference chromatogram of i(1.2 V) − i(0.9 V) is shown in Fig. 7C. All the chromatograms in Fig. 7 are from a single chromatographic run. Voltammetric/amperometric detection allows choice of optimal detection method with little pre-experimental planning. Because all of the voltammetric and chromatographic data are stored in memory, several presentation techniques can be evaluated for optimal information retrieval.

By using a flow rate of 1.0 ml min^{-1} and a scan rate of 2.0 V s^{-1} with a scan frequency of 1 scan s^{-1}, current response was linear over at least four orders of magnitude (320 nmol—32 pmol gentisic acid injected, slope = 0.095 nA $pmol^{-1}$, intercept = −0.74 nA, r^2 = 0.9998) using either the peak or the plateau currents. A voltammetric detection limit of 7.4 pmol of gentisic acid (retention time, 1.5 min) and 32 pmol of caffeic acid (retention

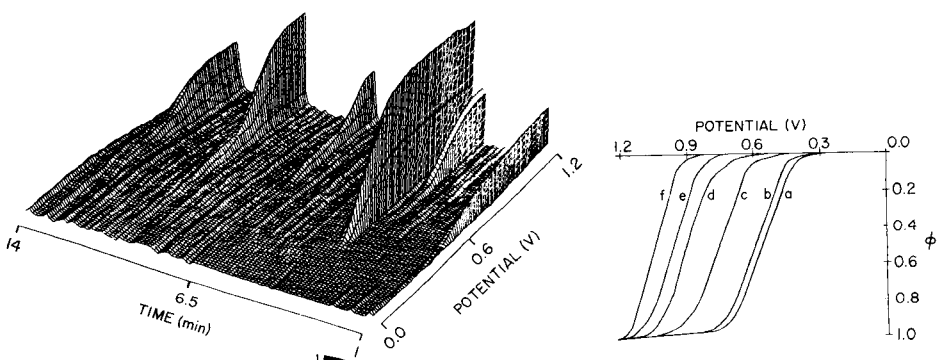

Fig. 5. Chromatovoltammogram of phenolic acid mixture obtained in the collection mode. Scan rate 2.0 V s^{-1}, flow rate 1.0 ml min^{-1}, downstream (amperometric) detection at −0.2 V. Injection of 80 pmol of gentisic acid, 130 pmol of vanillic acid, 220 pmol of caffeic acid, 520 pmol of *p*-coumaric acid, 410 pmol of ferulic acid, and 580 pmol of sinapic acid.

Fig. 6. Voltammograms of the chromatographic peaks extracted from the chromatovoltammogram of Fig. 5. Compounds: (a) caffeic acid; (b) gentisic acid; (c) sinapic acid; (d) ferulic acid; (e) vanillic acid; (f) *p*-coumaric acid. ϕ is the normalized current response.

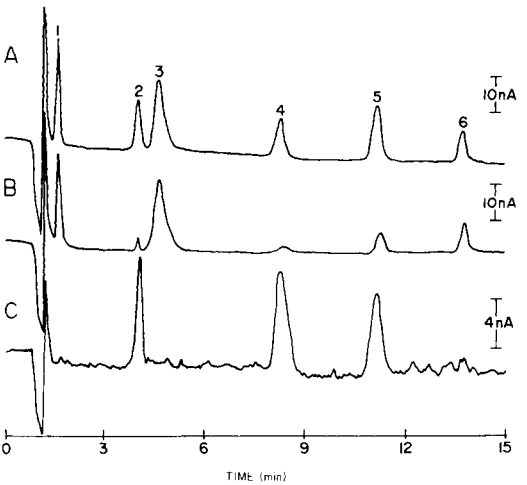

Fig. 7. Individual chromatograms extracted from the chromatovoltammogram of Fig. 5: (A) single-potential chromatogram at 1.2 V; (B) single-potential chromatogram at 0.9 V; (C) difference chromatogram of i(1.2 V) − i(0.9 V). Peak identities: (1) gentisic acid; (2) vanillic acid; (3) caffeic acid; (4) *p*-coumaric acid; (5) ferulic acid; (6) sinapic acid.

time, 4.5 min) injected on column was achieved with acceptable voltammetric response (Fig. 8). The detection limit is obviously dependent on the retention time of the compound with later eluting compounds having higher detection limits because of dilution during the chromatographic separation. However, voltammetric detection of 10 to 100 pmol injected is readily achieved. As can be seen from Fig. 8, the detection limit is determined by the resolution of the analog-to-digital converter and not by the noise of the system. Because the background is subtracted after data collection, at low analyte concentrations the background signal limits the gain that can be used without saturating the output. This gain and the resolution of the A/D converter then determine the smallest current changes that can be differentiated. This digitization is readily apparent in Fig. 8. In order to achieve reasonable voltammetric curves at least a 10—20 bit change is necessary. With the system used for these experiments, the digitization limited the ability to obtain good voltammetric curves rather than the noise in the voltammetry. The use of an A/D converter with greater resolution should lower the detection limits.

Shielding mode. The shielding mode is achieved by operating the downstream electrode at a potential on the mass transport-limited plateau for the reaction occurring at the upstream electrode. The upstream voltammetry will then cause a decrease in the response at the downstream electrode. Shielding-mode detection is characterized by the shielding efficiency which is analogous to the collection efficiency. The shielding efficiency, as shown

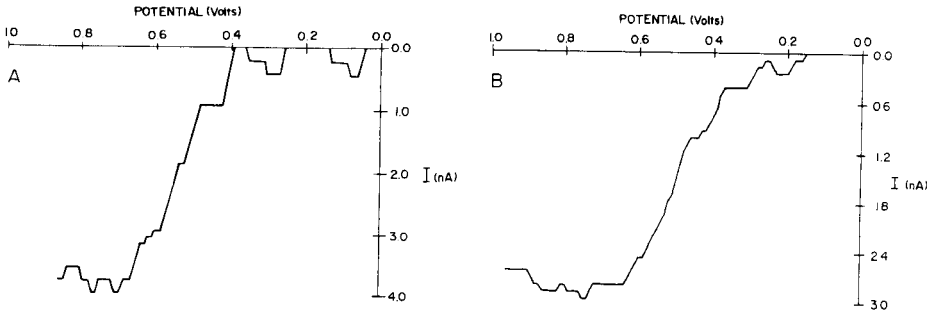

Fig. 8. Voltammograms from the injection of 7.4 pmol of gentisic acid (A) and 32 pmol of caffeic acid (B).

in Table 1, is independent of the electrochemistry of a given compound and is dependent only on the cell geometry. Because the shielding mode makes use of mass-transport phenomena while the collection mode makes use of electrochemical phenomena, these are complementary techniques. The collection mode offers greater selectivity while the shielding mode is more universal. As the hardware and software requirements are identical, both methods can be applied to the same sample on alternative chromatographic runs to establish the most useful method for a given sample.

Figure 9 shows the chromatovoltammogram obtained in the shielding mode for the same phenolic acid mixture used previously with the collection mode. As can be seen, the response is markedly different when the shielding mode is used. The maximum chromatographic response is obtained at the smallest upstream potential because all material passes to the downstream

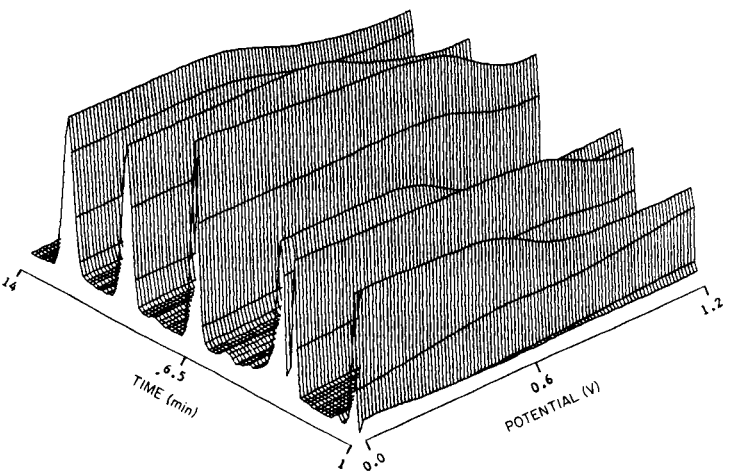

Fig. 9. Chromatovoltammogram of phenolic acid mixture obtained in the shielding mode. Scan rate 2.0 V s^{-1}, flow rate 1.0 ml min^{-1}, downstream detection (amperometric) at +1.2 V. The mixture was the same as for Fig. 5.

electrode to be detected. As the potential of the upstream electrode reaches values sufficient to oxidize the eluting material, the downstream response decreases because the amount of material in the reduced form reaching the downstream electrode is decreased. While the three-dimensional presentation may appear confusing, the same information is obtained with this experimental arrangement as with the collection mode. Voltammograms can be obtained by taking the "spine" of a chromatographic peak and are identical to those obtained in the collection mode. The same types of chromatographic presentations can be done with the shielding-mode data as with collection-mode data. However, in the case of shielding mode, the most sensitive response is at the lowest upstream potential (Fig. 10A and B). Difference-mode presentation can also be used to detect hard-to-oxidize compounds selectively in the presence of easily oxidized compounds, as shown in Fig. 10C.

The shielding-mode response was linear over four orders of magnitude (320 nmol or 16 pmol of gentisic acid injected, slope = 0.093 nA $pmol^{-1}$, intercept = —0.19 nA, r^2 = 0.9999). The detection limit for the shielding mode is slightly lower than for the collection mode with this detector configuration. While it would seem that the detection limit should be lower for the collection mode because the downstream potential is more optimal for amperometric detection, in practice the downstream noise is lower in the shielding mode. This is because the major source of noise in the voltammetric signal arises from the cross-talk interference which is somewhat lower in the shielding mode for the cell and potentiostat design of these

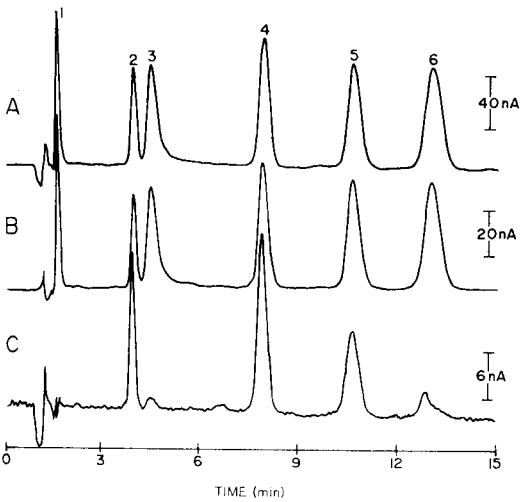

Fig. 10 Individual chromatograms extracted from the chromatovoltammogram of Fig. 9: (A) single-potential chromatogram at 0.1 V, (B) single-potential chromatogram at 1.2 V; (C) difference chromatogram of $i(1.2\ V) - i(0.9\ V)$. Peak identities as in Fig. 7.

experiments. A voltammetric detection limit of 3.7 pmol of gentisic acid and 16 pmol of caffeic acid injected on column was achieved.

Test sample. To test the utility of this detector, a sample of extracted beer was injected onto the chromatographic column. The potential was scanned from 0.0 V to 1.2 V at 2.0 V s^{-1} at a frequency of 1 scan s^{-1}. The three-dimensional chromatogram is shown in Fig. 11. A chromatogram extracted from the three-dimensional data is shown in Fig. 12A. Chromatographic peaks B, C, E, F and G elute at the same time as standards of vanillic acid, caffeic acid, *p*-coumaric acid, ferulic acid and sinapic acid, respectively. The voltammetric responses of these peaks are also the same as for the standard compounds (Fig. 6). Combining both chromatographic and voltammetric comparisons provides a high degree of certainty for these assignments of peak identity.

The voltammetry can also provide information about unidentified peaks. For example, examination of the voltammetry of chromatographic peak A (Fig. 13) indicates that there are actually two unresolved components. This can be seen by comparing voltammograms from the front, peak and tail and noting how the voltammetry changes across the peak. While chromatographically unresolved, the two components can be resolved voltammetrically. This can be done either by using the extracted voltammogram or by using the difference-mode chromatographic presentation as shown in Fig. 12B. A more complete evaluation of the utility of voltammetric deconvolution of chromatographically unresolved peaks is currently underway.

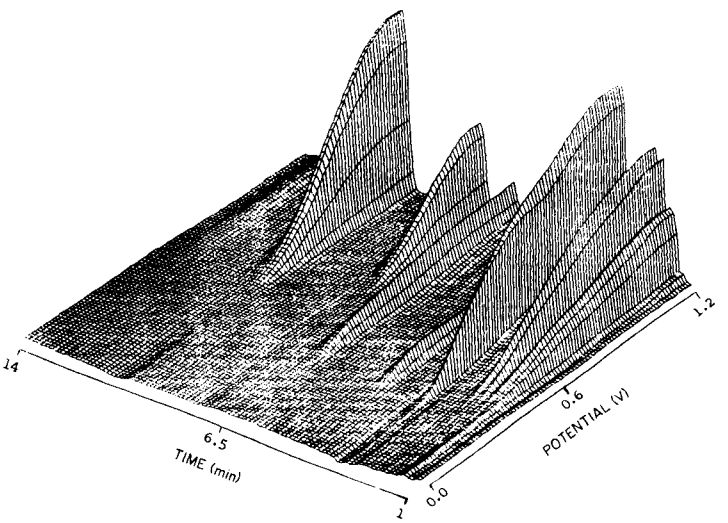

Fig. 11. Chromatovoltammogram of beer extract.

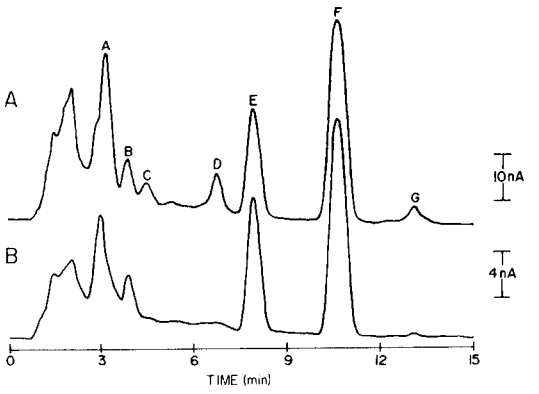

Fig. 12. Individual chromatograms extracted from the chromatovoltammogram of Fig. 11: (A) single-potential chromatogram at 1.2 V; (B) difference chromatogram of i(1.2 V) — i(0.9 V).

Conclusions

Voltammetric/amperometric detection provides advantages relative to either amperometric or direct voltammetric detection individually. The voltammetric data generated during the chromatographic analysis can be used for confirmation of peak identity or classification. Having the entire chromatovoltammogram allows post-experimental choice of the optimal detection potential, including the use of different potentials for each chromatographic peak. Adding voltammetric resolution to the chromatographic resolution permits identification of coeluting compounds and the ability to resolve them voltammetrically.

Voltammetric/amperometric detection realizes these advantages while achieving detection limits lower than direct voltammetric techniques and approaching amperometric detection. Improvements in the computer inter-

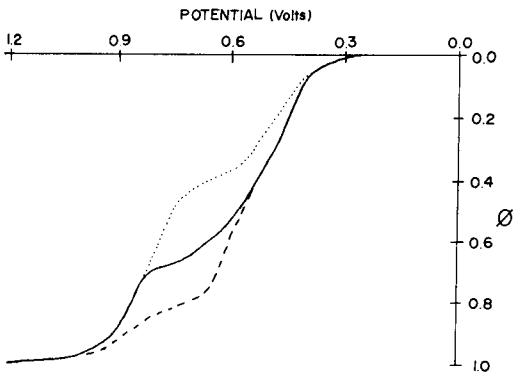

Fig. 13. Voltammograms of the front (···), peak (——) and tail (---) of peak A.

face and the flow cell should lower the detection limits even further. From an electrochemical point of view, voltammetric/amperometric detection provides a method of obtaining voltammograms with small amounts or small volumes of sample. Voltammograms of the individual components of a complicated mixture can also be obtained without the need for isolation. This last capability should find great use in bioelectrochemical investigations.

REFERENCES

1 R. E. Shoup, Ed., Bibliography of Recent Reports of Electrochemical Detection, BAS Press, West Lafayette, IN, 1982.
2 W. L. Caudill, A. G. Ewing, S. Jones and R. M. Wightman, Anal. Chem., 55 (1983) 1877.
3 W. A. MacCrehan, Anal. Chem., 53 (1981) 74.
4 M. Stastny, R. Volf, H. Benadikova and I. Vit, J. Chromatogr. Sci., 21 (1983) 18.
5 R. Samuelson, J. O'Dea and J. G. Osteryoung, Anal. Chem., 52 (1980) 2215.
6 J. Wang, E. Ouziel and C. H. Yarnitzky, Anal. Chim. Acta, 102 (1978) 99.
7 J. J. Scanlon, P. A. Flaquer, G. W. O'Brien and P. E. Sturrock, Anal. Chim. Acta, 158 (1984) 169.
8 P. A. Reardon, G. E. O'Brien and P. E. Sturrock, Anal. Chim. Acta, 162 (1984) 175.
9 M. B. Thomas, H. Msimanga and P. E. Sturrock, Anal. Chim. Acta, 174 (1985) 287.
10 R. E. Panzer and P. J. Elving, Electrochim. Acta, 20 (1975) 635.
11 J. G. White, R. L. St.Claire III and J. W. Jorgenson, Anal. Chem., 58 (1986) 293.
12 J. G. White and J. W. Jorgenson, Anal. Chem., 58 (1986) 2992.
13 T. A. Last, Anal. Chim. Acta, 155 (1983) 287.
14 T. A. Last, Anal. Chem., 55 (1983) 1509.
15 C. E. Lunte, S.-W. Wong, K. W. Chan, T. H. Ridgway and W. R. Heineman, Anal. Chim. Acta, 188 (1986) 263.
16 C. E. Lunte and W. R. Heineman, Anal. Chem., 59 (1987) 761.
17 R. K. Trubey and T. A. Nieman, Anal. Chem., 58 (1986) 2549.

Analytica Chimica Acta, 200 (1987) 115—129
Elsevier Science Publishers B.V., Amsterdam — Printed in The Netherlands

DETERMINATION OF INORGANIC SULFUR SPECIES IN HIGHLY ALKALINE SOLUTIONS BY LIQUID CHROMATOGRAPHY WITH POLAROGRAPHIC DETECTION

ZAMIR UDDIN[a], RICHARD MARKUSZEWSKI and DENNIS C. JOHNSON*
Department of Chemistry, Iowa State University, Ames, IA 50011 (U.S.A.)
(Received 16th January 1987)

SUMMARY

Indirect anodic detection of sulfide, polysulfide, sulfite and thiosulfate can be achieved at a dropping mercury electrode based on the anodic oxidation of mercury to produce stable products of Hg(II). Results for sulfide (S^{2-}) and polysulfide (S_x^{2-}) ions in alkaline media are emphasized. The maximum value of x in S_x^{2-} was found to be 5, which is in agreement with the literature. Values of diffusion coefficients for the various species of S_x^{2-} (D_x; x = 1—5) were found to decrease dramatically as x is increased, e.g., $D_1/D_2 = 3.6$ and $D_1/D_5 = 32.4$. Mixing solutions of S_5^{2-} with S^{2-} is not followed by rapid re-equilibration to produce a polysulfide with average $x < 5$. It is concluded that polarography alone is not sufficient for quantifying S^{2-} and S_x^{2-} in their mixtures. High-performance anion-chromatography with polarographic detection was examined for separation of alkaline mixtures of inorganic sulfur compounds. Separations were achieved within ca. 12 min. Polysulfide (S_x^{2-}) is concluded to undergo dissociation to S^{2-} and S^0 on the anion-exchange column and no cathodic detection peak is obtained which is characteristic of the polarographic reduction of S_x^{2-}. A negative peak in the cathodic baseline current for reduction of dissolved oxygen at $E < 0.0$ V just prior to the peak for $S_2O_3^{2-}$ is attributed to the effect of eluted S^0. The retention time of the S^0 peak is independent of the concentration of nitrate in the mobile phase, which is consistent with a non-ionic interaction between S^0 and the anion-exchange separator. The technique does not detect sulfate.

The simultaneous determination of inorganic sulfur species in mixtures is made difficult especially because of their reactivity toward the oxygen present in aqueous solutions. Most inorganic sulfur compounds are unstable

---

*Dennis C. Johnson is Professor of Chemistry at Iowa State University, Ames, IA. He received a B.A. degree from Bethel College, St. Paul, MN, in 1963 and a Ph.D. from the University of Minnesota in 1967. He joined the faculty at Iowa State University in 1968. His research interests include the electrocatalysis of anodic oxygen-transfer reactions at noble metal, oxide, and mixed metal oxide electrodes, application of pulsed potential amperometric and coulometric detection for organic compounds, and applications of flow-through electrochemical detectors in flow injection and liquid chromatographic analysis.

[a]Present address: Department of Chemistry, Manatee Community College, Venice, FL 34284, U.S.A.

0003/2670/87/$03.50

thermodynamically in the presence of oxygen, with the exception of sulfate, of course. The fact that it is virtually impossible completely to eliminate dissolved oxygen adds further to the complexity of the problem; hence, it is highly desirable to have a method for the rapid and simultaneous determination of as many forms of inorganic sulfur as possible under the ambient conditions of temperature, solution composition, pH and dissolved oxygen. Numerous classical methods for determination of inorganic sulfur species have appeared [1—3]; by far the most efficient method for the simultaneous determination appears to be that of Story [4]. However, the method described is still complicated and requires prior chemical treatment for the conversion of all sulfur species to sulfate which is eventually quantified spectrophotometrically after chelation with Fe(III). Sulfide, sulfite, thiosulfate and polysulfide can be detected anodically at a dropping mercury electrode [5—9]; however, it is not clear that the conventional application of polarography for a complex mixture in highly alkaline samples is useful. Liquid chromatography (LC) and electrochemical (EC) detection are compatible technologies which can offer important advantages of selectivity, sensitivity and economy for complex mixtures [10]. Voltammetric detection in LC has been demonstrated by many (see, e.g. [11—15]) and the subject has been reviewed [16, 17].

Here, polarographic studies of several inorganic sulfur species, especially S^{2-} and S_x^{2-}, are described and results are presented from the application of LC/EC with polarographic detection to mixtures of S^{2-}, S_x^{2-}, SO_3^{2-} and $S_2O_3^{2-}$ in alkaline solutions which are typical of samples expected from the molten caustic desulfurization of coal [18, 19].

EXPERIMENTAL

Reagents

Analytical reagent-grade chemicals were used without further purification. A stock solution of sodium sulfide was prepared using triply distilled and deoxygenated water, and the solution was stored under nitrogen. To minimize air oxidation of sulfide, small aliquots of the concentrated stock solution were transferred by a microsyringe to a known volume of aqueous supporting electrolyte solution previously deoxygenated with high-purity (99.99%) nitrogen. Stock solutions of Na_2S_x with a maximum value of x were prepared by adding excess of elemental sulfur in aqueous solutions of sodium sulfide under nitrogen and stirring the solution continuously under nitrogen for 3—4 days until the solution turned an orange-red color of constant hue and intensity. Small aliquots of the concentrated stock solution were transferred directly to the polarographic cell containing the deoxygenated electrolyte solution.

Solutions of tetraalkylammonium hydroxide (R = methyl, ethyl and t-butyl) were prepared by passing the corresponding aqueous solutions of R_4NBr through an anion-exchange column in the hydroxide form. The

solutions of R_4NOH thus obtained were then standardized by titration with primary standard potassium hydrogen phthalate.

The solution of antioxidant buffer was prepared by dissolving 250 g of sodium acetate, 65 g of ascorbic acid and 85 g of sodium hydroxide in 600 ml of distilled water and then diluting to 1.0 l. This solution was diluted 1:1 with distilled water for use as a supporting electrolyte.

Sulfide solutions were standardized iodometrically with oxidation to sulfate by potassium iodate in alkaline solution [20]. Polysulfide solutions were also standardized by using this iodometric method; however, only the ionic sulfur (not S^0) was determined [21].

Samples

Alkaline samples of the inorganic sulfur species were prepared to be representative of samples produced by the caustic desulfurization of coal [18, 19]. In the typical desulfurization procedure, a 50-g sample of powdered coal is mixed with 500 g of an 80:20 (wt.%) mixture of solid sodium hydroxide and potassium hydroxide and then is heated to 375°C for 1 h in a crucible. The solid coal is separated from the molten caustic solution by filtration in a stainless-steel wire basket. The spent caustic in the crucible is dissolved in 1--2 l of water to produce a solution called "Process Stream No. 1 (PS-1)". The treated solid coal carries with it about twice its weight of sodium hydroxide and is washed with 1—2 l of water to produce an alkaline solution called "Process Stream No. 2 (PS-2)". Concentrations of sodium hydroxide in PS-1 and PS-2 are typically ca. 4.5 M and 1.3 M, respectively.

Apparatus

Polarograms were obtained using a PAR Model 174A Polarographic Analyzer (EG&G Princeton Applied Research, Princeton, NJ) and a PAR Model K23 dropping mercury electrode (DME) with a PAR Model 1747 mechanical drop timer. All potentials are reported relative to the saturated calomel electrode (SCE).

The flow-through electrochemical detector was a conventional DME under the control of a PAR Model 174/707 mechanical drop timer, fitted with a PAR Model H165 flow cell, under potentiostatic control by a PAR Model 174A Polarographic Analyzer. Sampled-DC polarographic (DCP) detection was applied with a drop time of 1.0 s.

The LC system consisted of a Model 2020i Advanced Chromatography Module with a HPIC-AS3 or AS6 anion separator column (Dionex Corp., Sunnyvale, CA). A post-column mixer for addition of buffer to the effluent stream was constructed from an Altex three-way teflon connector followed by a 2.5-in. length of Altex tubing (0.8-mm i.d.) filled with glass beads (0.5 mm; B. Braun Melsungen AG, Germany). A Minipuls-2 peristaltic pump (Gilson Medical Electronics, Middleton, WI) was used for pumping the buffer reagent.

RESULTS AND DISCUSSION

Sulfide

Sulfide is detected at a DME [5, 6] on the basis of the anodic current from the reaction:

$$Hg + S^{2-} \rightarrow HgS(s) + 2e^- \quad (1)$$

Detections of sulfite and thiosulfate are based on analogous anodic reactions. The current/voltage curve for 0.1 mM sulfide in 0.1 M sodium hydroxide obtained by sampled-DC polarography is shown in Fig. 1 for a positive potential sweep. The half-wave potential is —0.78 V, which agrees well with the literature. As the concentration of sulfide was increased beyond 0.2 mM, a distortion was observed in the rising portion of the wave with the consequence of producing a two-step wave. The product of the anodic electrode reaction, HgS, is insoluble and forms a protective film around the mercury drop. Charge transfer at the electrode/solution interface is restricted by the film and is responsible for the distortion. As the potential is scanned further in the positive direction, the inhibited electron-transfer reaction is again able to proceed at a transport-limited rate because of the additional energy applied at the larger positive potentials.

Polysulfide

The sampled-DC response for 0.14 mM Na_2S_5 in 0.1 M sodium hydroxide is shown in Fig. 2 (curve b). Anodic and cathodic waves are obtained resulting from the following reactions:

$$S_x^{2-} + Hg \rightarrow HgS_x + 2e^- \text{ (anodic process; } -0.77 \text{ to } -0.2 \text{ V)} \quad (2)$$

$$S_x^{2-} + 2(x-1)e^- \rightarrow xS^{2-} \text{ (cathodic process; } -1.8 \text{ to } -0.77 \text{ V)} \quad (3)$$

A limiting cathodic current plateau for reduction of S_x^{2-} is not obtained in the potential region more negative than —0.8 V. Sulfide, the product of the cathodic reaction, is a surface-active anion [6] and adsorbs at the electrode surface. The adsorbed anionic sulfide electrostatically repels the anionic polysulfide, thereby restricting the approach of the latter to the reaction plane in the double-layer region. As a result, the current passes through a minimum instead of the expected plateau. At a very low polysulfide concentration, insufficient S^{2-} is produced to saturate the surface of the electrode. Hence, the electron-transfer reaction is expected to proceed at a moderate rate. This was confirmed for a very small S_x^{2-} concentration. Zhadanov and Kiseley [7] obtained similar polarographic curves for the reduction of sulfur in ethanolic solution containing lithium perchlorate and proposed the following reaction sequence:

$$Hg + S^0 \rightarrow HgS \quad (4)$$

$$HgS + 2e^- \rightarrow Hg + S^{2-} \quad (5)$$

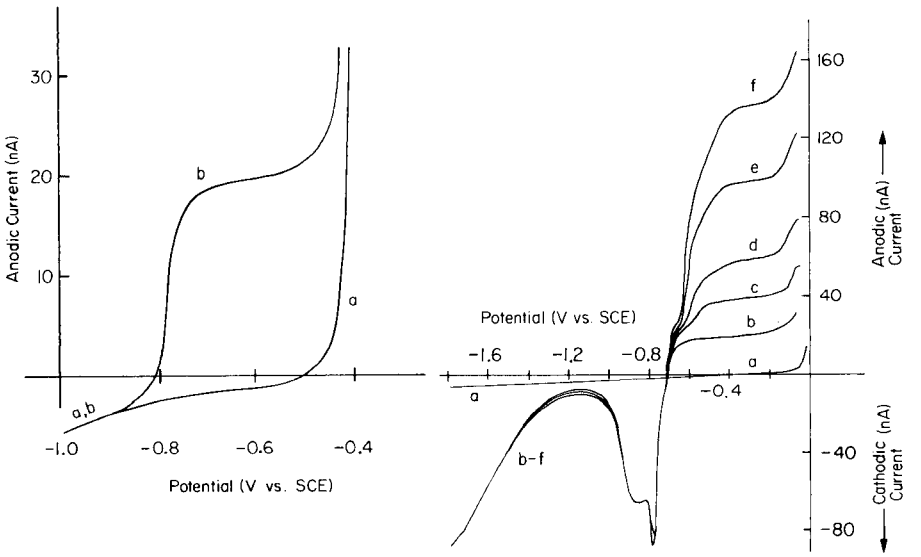

Fig. 1. Polarographic *i/E* curve for sulfide. Conditions 1.0-s drop time, +5 mV s^{-1} scan rate, sampled DC polarography; 0.10 M NaOH as supporting electrolyte. Curves: (a) residual; (b) 0.10 mM Na_2S.

Fig. 2. Polarographic *i/E* curves for S_5^{2-} as a function of added sulfide. Conditions as in Fig. 1 but with 0.14 mM Na_2S_5 in 0.10 M NaOH. Curve (a) is residual. Na_2S added (mM): (b) 0.00, (c) 0.10, (d) 0.20, (e) 0.40, (f) 0.60.

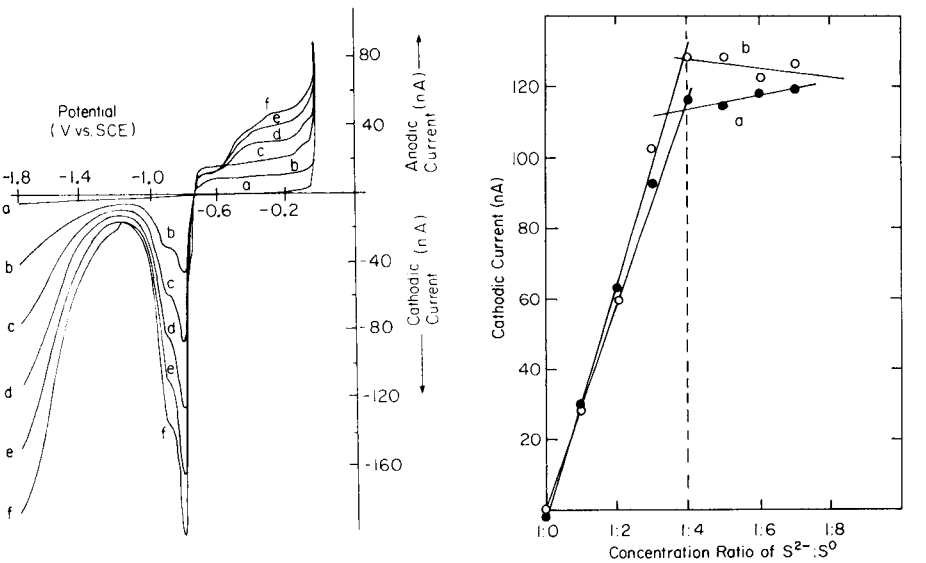

Fig. 3. Polarographic *i/E* curves for S_5^{2-} as a function of concentration. Conditions as in Fig. 1; 0.10 m NaOH supporting electrolyte. Na_2S_5 added (mM): (a) 0.0, (b) 0.097, (c) 0.193, (d) 0.290, (e) 0.386, (f) 0.482.

Fig. 4. Plots of cathodic current for S_x^{2-} as a function of S^{2-}/S^0. Original *i/E* curves obtained as in Figs. 1 and 2, 0.10 mM S^{2-} with added S^0 in 0.10 M NaOH. Cathodic current measured at (a) —0.90 V, (b) —1.75 V.

$$S^0 + S^{2-} \rightarrow S_2^{2-} \quad (6)$$

$$S_2^{2-} + 2e^- \rightarrow 2S^{2-} \quad (7)$$

$$\text{Net: } S^0 + 2e^- \rightarrow S^{2-} \quad (8)$$

They attributed the minimum in the cathodic wave to inhibition of the reduction of S_2^{2-} by the negative charge on the electrode and observed that the minimum deepened after addition of S^{2-}, which they concluded to correspond to a shift to the right of the equilibrium in Eqn. 6. A significant further suppression of the cathodic current by addition of S^{2-} to a solution of S_5^{2-} was not observed in this research, as is demonstrated in Fig. 2 (curves b—f).

Several *i/E* curves are shown in Fig. 3 for solutions with successively increasing concentrations of S_5^{2-}. Multiple anodic waves were observed for concentrations above ca. 0.3 mM. This is attributed to formation of multiple layers of the insoluble product of the anodic reaction. Standard additions of S^{2-} to a solution of S_x^{2-} produced an anodic response equivalent to the sum of the anodic signals for the respective pure solutions. It is concluded, tentatively, that mixtures of S^{2-} and S_x^{2-} ($x > 2$) do not undergo re-equilibration to produce a polysulfide ion having an intermediate value of x. This conclusion is considered more rigorously in a later section.

Determination of the maximum x *in* S_x^{2-}. Polysulfide is reduced to sulfide according to Eqn. 3 in the potential range —1.8 to —0.8 V. The number of electrons involved in the cathodic process is a direct function of the number of sulfur atoms present in the S_x^{2-} ion, i.e., $n = 2x - 2$. Solutions of S_x^{2-} corresponding to mole ratios of S^{2-}:S^0 = 1:1, 1:2, 1:3, 1:4, 1:5, 1:6 and 1:7 were prepared by stirring elemental S^0 in oxygen-free Na_2S solutions under nitrogen. After ca. 48 h, the elemental sulfur completely dissolved in the flasks with S^{2-}/S^0 up to 1:4, whereas some sulfur remained undissolved in the remaining flasks. This observation is consistent with a maximum value of $x = 5$. The polarographic response for diluted solutions of each mixture was obtained and values of cathodic current were presented in Fig. 4 as a function of S^{2-}/S^0. The cathodic current values are observed to level off at $S^{2-}/S^0 \geqslant 1{:}4$ indicating a maximum value of $x = 5$ for S_x^{2-}. Based on the absorption spectrum of S_x^{2-} in the visible region, the absorbance of S_x^{2-} solutions was measured at 365 nm and plotted as a function of S^{2-}/S^0. All of these results were consistent with a maximum value of $x = 5$. This value is in agreement with a previous conclusion by Pringle [22].

Diffusion coefficients of S_x^{2-} *species*. It is observed in Fig. 2b that the *i/E* curve for a S_x^{2-} solution consists of an anodic and a cathodic wave. From the ratio of limiting anodic and cathodic currents, the number of electrons for the cathodic reaction of the polysulfide anions can be calculated, assuming $n_a = 2$ for the anodic reactions, from

$$n_{c,x} = 2(i_{l,c}/i_{l,a}) \quad (9)$$

The experimental results are presented in Table 1 in comparison to the expected values for solutions of S_x^{2-} with assumed integral values of x. The agreement between experimental and expected results is good, especially for large x.

Values of the limiting anodic current ($i_{1,a}$) for x = 1--5 and the estimated limiting cathodic current ($i_{1,c}$) for x = 2--5 were linear functions of the concentration of S_x^{2-}. The relative values of the diffusion coefficients, D, for the polysulfide species were calculated from the ratio of limiting anodic currents of S^{2-} and S_x^{2-}, by means of the equation

$$D_{S^{2-}}/D_{S_x^{2-}} = [(i_{1,a,S^{2-}}/C^b_{S^{2-}})/(i_{1,a,S_x^{2-}}/C^b_{S_x^{2-}})]^2 \quad (10)$$

where C^b is the bulk concentration. The results are given in Table 2. The ratio of diffusion coefficients was calculated also from the limiting anodic current for S^{2-} and the estimated limiting cathodic current for S_x^{2-}, by means of the equation

$$D_{S^{2-}}/D_{S_x^{2-}} = [(i_{1,a,S^{2-}}/C^b_{S^{2-}})/(i_{1,c,S_x^{2-}}/C^b_{S^0})]^2 \quad (11)$$

The results are included in Table 2. Obviously, from the results in Table 2, the values of diffusion coefficients decrease drastically as x increases from 2 to 5. The agreement between the values in Table 2 evaluated by the two methods is considered satisfactory in view of the use of cathodic currents which are only estimates of the limiting values.

Re-equilibration of mixtures of S^{2-} and S_x^{2-}. Mixtures of S^{2-} and S_x^{2-} ($x > 2$) are predicted from thermodynamics [23] to react spontaneously to produce polysulfide with an intermediate average value of x. It was observed that the total anodic current obtained for solutions containing S^{2-} and S_x^{2-} was the algebraic sum of the individual currents for solutions of S^{2-} and S_x^{2-}, as stated earlier for Fig. 2. This observation can be explained only if re-equilibration to form a species of intermediate x value does not occur. A strenuous test of this conclusion comes from a consideration of the cathodic

TABLE 1

Calculation of the number of electrons involved in cathodic reaction of S_x^{2-} species

S_x^{2-}	i_c/C^b (mM)[a]	i_a/C^b (mM)[a]	i_c/i_a	$n_{c,x}$ (experimental)	$n_{c,x}$ (expected)
S^{2-}	—	155.56	—	—	0
S_2^{2-}	64.71	83.33	0.78	1.6	2
S_3^{2-}	75.00	40.91	1.83	3.7	4
S_4^{2-}	86.67	28.57	3.03	6.1	6
S_5^{2-}	105.26	26.92	3.91	7.8	8

[a] C^b is the bulk concentration.

TABLE 2

Relative diffusion coefficients of various S_x^{2-} species using the anodic and cathodic current data

Calculation based on	D_1/D_2	D_1/D_3	D_1/D_4	D_1/D_5
Eqn. 10	3.6	14.7	30.8	32.4
Eqn. 11	5.8	19.1	29.3	36.7

wave for S_5^{2-} in Fig. 2 as a function of added S^{2-}. The reaction of S^{2-} with S_5^{2-} to produce S_2^{2-} is thermodynamically spontaneous [23].

$$3S^{2-} + S_5^{2-} \rightleftharpoons 4S_2^{2-} \quad (12)$$

If S^{2-} reacts with S_5^{2-} to form S_2^{2-}, a large increase in the limiting cathodic current would be observed because of the large difference in the diffusion coefficients of S_2^{2-} and S_5^{2-}. However, no change in the cathodic current was obtained with addition of S^{2-} and it can be concluded that $S_x^{2-}(x < 5)$ is not produced on the time-scale of these experiments (1—2 h).

Cathodic current plateau for S_x^{2-}. For an electroactive species, it is customary to expect a current plateau that corresponds to the diffusion-limited transport of electroactive species to the electrode surface. The convenience of a plateau for quantitative purposes is obvious. Because a cathodic-current plateau was not obtained for S_5^{2-} when sodium hydroxide served as the supporting electrolyte, an attempt was made to establish whether such a plateau can be obtained.

The *i/E* curve of an S_5^{2-} solution, using tetramethylammonium hydroxide instead of sodium hydroxide as the supporting electrolyte, is shown in Fig. 5. A well-defined cathodic current plateau is observed. Tetramethylammonium ions (Me_4N^+) are adsorbed at Hg and are expected to decrease the extent of S^{2-} adsorption. Hence, the adsorbed cationic Me_4N^+ substantially decreases the repulsive effect between adsorbed S^{2-} and S_x^{2-}, thereby promoting the cathodic reaction. A decrease in the plateau current is observed as the size of the alkyl group (R) in R_4NOH is increased. The trend is reasonable because the extent of adsorption should increase with the increasing hydrophobic character of the more bulky R_4N^+ cations leaving fewer reaction sites for S_x^{2-} on the electrode surface. The cathodic currents on the plateau were observed to vary linearly with the concentration of S_5^{2-} in 0.1 M Me_4NOH.

Effect of surface-active buffers

Noel [24] reported the use of a sulfur antioxidant buffer consisting of an alkaline solution of EDTA and ascorbic acid, to keep the solution free of dissolved oxygen. Stephenson [25] used a buffer consisting of an alkaline solution containing salicylate and ascorbic acid to achieve the same purpose.

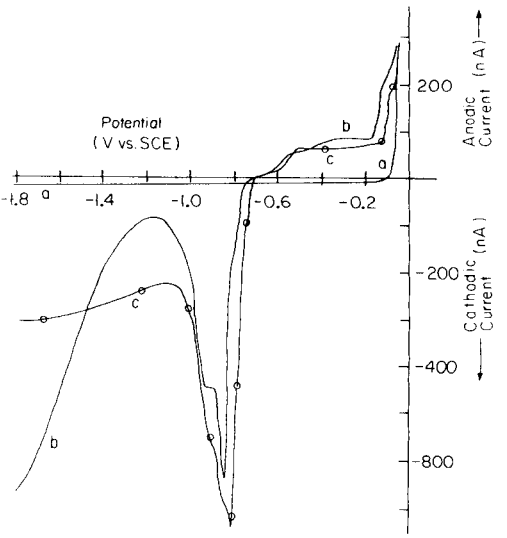

Fig. 5. Comparison of polarographic *i/E* curves for S_5^{2-} obtained in NaOH and Me_4NOH. Conditions: 1.0-s drop time, 5 mV s^{-1} scan rate, sampled DC polarography. Curves: (a) residual curve in 0.10 M NaOH; (b) 0.40 mM Na_2S_5 in 0.10 M NaOH; (c) 0.40 mM Na_2S_5 in 0.10 M Me_4NOH.

Both buffer solutions were tested and that of Stephenson was found to produce a wider possible potential range for polarographic work. The *i/E* curve for S_5^{2-} in this buffer solution is presented in Fig. 6. A well-defined cathodic-current plateau was obtained for S_5^{2-} in comparison to the case of sodium hydroxide alone. The buffer apparently has a similar effect on the surface of electrode as the tetraalkylammonium hydroxide. In this case, the salicylate, being a bulky species, is expected to adsorb preferentially at the electrode surface minimizing the adsorption of S^{2-}, while the ascorbate is responsible for reducing the dissolved oxygen. A series of *i/E* curves for different concentrations of S_5^{2-}, using the antioxidant buffer as the supporting electrolyte, yielded a linear plot of cathodic current vs. concentration.

It was observed for the positive potential scan that the cathodic wave in the presence of this buffer passes through a peak at ca. —0.94 V before the current changes sign. The peak was found to decrease in height by addition of Triton X-100. This is evidence that the peak is a current maximum of the sort frequently observed in polarographic work. The peak has been observed also for alcoholic solutions of elemental sulfur [26] and organic sulfide solutions [27]. According to Werner and Konopik [28], the cathodic peak is observed because of inhibition of the part of the reaction which is caused by S_x^{2-} ions when the charge on the electrode surface changes sign from positive to a negative value; this was termed the "anionic effect". The electrocapillary maximum (ECM) in 0.1 M sodium hydroxide was found at ca. —0.55 V and any relationship of the ECM to the peak maximum at —0.94 V was not obvious.

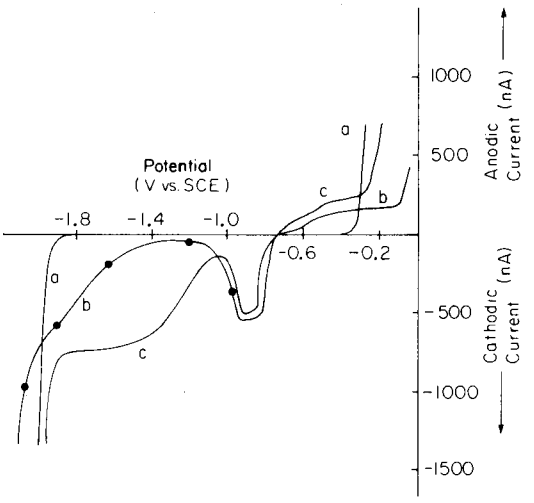

Fig. 6. Comparison of polarographic *i/E* curves for S_5^{2-} obtained in NaOH and the antioxidant buffer. Conditions as in Fig. 5. Curves: (a) residual curve in 0.1 M NaOH; (b) 5.0 mM Na_2S_5 in 0.10 M NaOH; (c) 5.0 mM Na_2S_5 in 0.10 M antioxidant buffer.

Liquid chromatographic separations

The half-wave potentials of four inorganic sulfur compounds, as determined by sampled DCP in 0.2 M potassium nitrate, are ($E_{1/2}$ vs. SCE): −0.78 V for S^{2-}, −0.12 V for $S_2O_3^{2-}$, +0.01 V for SO_3^{2-} and +0.22 V for $S_2O_4^{2-}$. Polarographic resolution of mixtures appears possible; however, it is necessary to note that hydrogen sulfide is volatile under neutral conditions ($pK_{a,1} \approx 7$) and pH ⩾ ca. 10 is necessary to minimize loss of S^{2-} from samples. For alkaline solutions, however, the anodic wave for hydroxide at the DME ($E_{1/2} \approx +0.1$ V vs. SCE) eclipses the anodic waves for $S_2O_3^{2-}$, SO_3^{2-} and $S_2O_4^{2-}$.

Liquid chromatography with electrochemical detection was tested for solutions of inorganic sulfur compounds with chromatographic separation on anion-exchange columns using an alkaline mobile phase followed by post-column neutralization of the effluent stream just prior to detection at the DME. A phosphate buffer at pH 7.6 was chosen which consisted of 0.020 M each of NaH_2PO_4 and Na_2HPO_4. A typical chromatogram for an alkaline sample of S^{2-}, SO_3^{2-} and $S_2O_3^{2-}$ is shown in Fig. 7A; a Dionex HPIC-AS6 column was used with a mobile phase of 0.050 M KNO_3/0.010 M NaOH. Separation was achieved in ca. 25 min. A peak for hydroxide was obtained at 1.4 min because the capacity of the phosphate buffer was insufficient to neutralize the excess of sodium hydroxide in the sample. A typical chromatogram for a solution of lower sodium hydroxide concentration obtained with a column of a lower capacity (Dionex HPIC-AS3) is shown in Fig. 7B. The separation was complete in less than 6 min, and there was no peak for hydroxide.

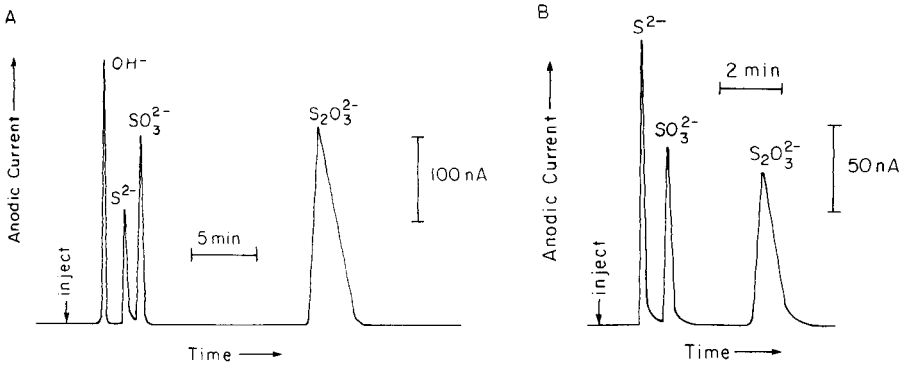

Fig. 7. Chromatographic separation with polarographic detection of S^{2-}, SO_3^{2-} and $S_2O_3^{2-}$ in an alkaline sample. Column: (A) Dionex HPIC-AS6; (B) Dionex HPIC-AS3. Mobile phase: 0.010 M NaOH/0.050 M KNO_3 at 1.1 ml min^{-1}. Buffer: 0.020 M NaH_2PO_4/ 0.020 M Na_2HPO_4 at pH 7.6. Detection: sampled DCP, +0.08 V vs. SCE, 1.0-s drop time.

Chromatograms obtained for injections of S_x^{2-} with detection at 0.08 V always contained two anodic peaks with t_R values identical for S^{2-} and $S_2O_3^{2-}$. Oxidation of S_x^{2-} by dissolved oxygen in alkaline media is moderately fast and the height of the $S_2O_3^{2-}$ peak increased with increasing time of exposure of the S_x^{2-} sample to the laboratory atmosphere prior to injection.

For $E < 0.0$ V, the net baseline current was cathodic, as shown in Fig. 8, because of reduction of oxygen dissolved in the buffered effluent stream. Superimposed on the cathodic baseline was a small "anodic" peak (t_R = ca. 8 min in Fig. 8) for injections of S_x^{2-}. The value of t_R for the "anodic" peak for injections of S_x^{2-} was independent of x. The peaks for S^{2-} obtained following each injection of S_x^{2-} are not shown in Fig. 8. It is concluded that S_x^{2-} dissociates in the anion-exchange column to yield S^{2-} and S^0, and the anodic peak does not represent oxidation but results from the depression of the cathodic oxygen current caused by adsorption of the eluted S^0 at the DME. No cathodic peak could be obtained for large negative values of potential, as would be expected for S_x^{2-} (see Figs. 1—3). The height of the "anodic" peak for S^0 was found to be a function of the concentration of atomic S^0 in S_x^{2-} samples; however, the sensitivity was very low and quantitative application is not recommended. For $E = -0.2$ V, separate peaks were observed for both S^0 and $S_2O_3^{2-}$ (see Fig. 8).

The retention times for S^{2-}, SO_3^{2-}, $S_2O_3^{2-}$ and S^0 are shown in Fig. 9 as a function of the concentration of nitrate in the mobile phase. Retention of S^{2-}, SO_3^{2-} and $S_2O_3^{2-}$ decreased with increasing nitrate concentration, as expected for the anion-exchange mechanism. The value of t_R for the peak believed to correspond to S^0 was independent of nitrate concentration, which is supporting evidence for the assignment of neutrality for the charge on the eluting sulfur species.

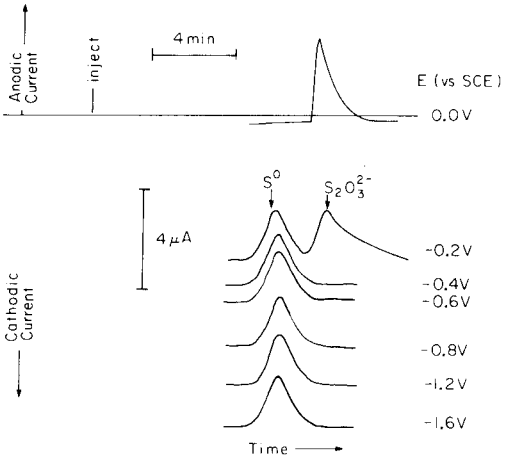

Fig. 8. Chromatographic response for S_5^{2-} with polarographic detection as a function of potential. Dionex HPIC-AS3 column; other conditions as in Fig. 7.

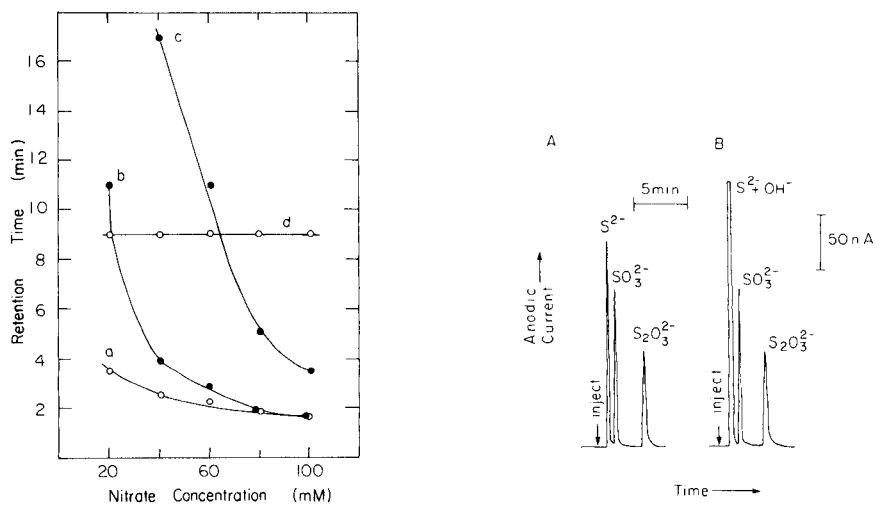

Fig. 9. Retention times for S^{2-}, SO_3^{2-}, $S_2O_3^{2-}$ and S^0 as a function of nitrate concentration. Curves: (a) S^{2-}, (b) SO_3^{2-}, (c) $S_2O_3^{2-}$, (d) S_x^{2-}. Dionex HPIC-AS3; other conditions as in Fig. 7.

Fig. 10. Chromatographic interference by high levels of hydroxide in samples. Curves: (A) 0.2 mM S^{2-}, 0.1 mM SO_3^{2-} and 0.5 mM $S_2O_3^{2-}$ in 5.0 mM hydroxide; (B) 0.2 mM S^{2-}, 0.1 mM SO_3^{2-} and 0.5 mM $S_2O_3^{2-}$ in 0.50 M hydroxide. Dionex HPIC-AS3; other conditions as in Fig. 7.

Samples from caustic desulfurization of coal are highly alkaline Chromatograms are compared in Fig. 10 for mixtures of S^{2-}, SO_3^{2-} and $S_2O_3^{2-}$ in 5.0 and 500 mM NaOH. The large hydroxide peak for the most highly alkaline sample was not resolved from the S^{2-} peak for the HPIC-AS3 column at flow rates exceeding 1.1 ml min^{-1}. Neutralization of sodium hydroxide in samples prior to injection is not practical because any local excess of added acid will cause loss of S^{2-} as hydrogen sulfide. Furthermore, it appeared impractical to increase indefinitely the capacity of the phosphate buffer to handle all eventualities. A useful separation of hydroxide and S^{2-} was achieved by using a slow flow rate for the mobile phase of ca. 1.0 ml min^{-1} (see Fig. 11). Following elution of hydroxide and S^{2-} at a flow rate of about 1.0 ml min^{-1}, the flow rate was increased to 3.0 ml min^{-1} to achieve rapid elution of SO_3^{2-} and $S_2O_3^{2-}$. Peak heights for S^{2-}, SO_3^{2-} and $S_2O_3^{2-}$ were found to be linear functions of concentration and standard-addition methods were used for quantitation.

No S_x^{2-} was found in samples of PS-1 and PS-2 for the caustic desulfurization of Illinois No. 6 coal. Typical values of S^{2-}, SO_3^{2-} and $S_2O_3^{2-}$ (reported as %S by weight) were 0.88, 0.56, and 0.54, respectively, for PS-1; and 0.30 0.42 and 0.38, respectively, for PS-2. Confirmation of the accuracy of these values using standard methods was not attempted.

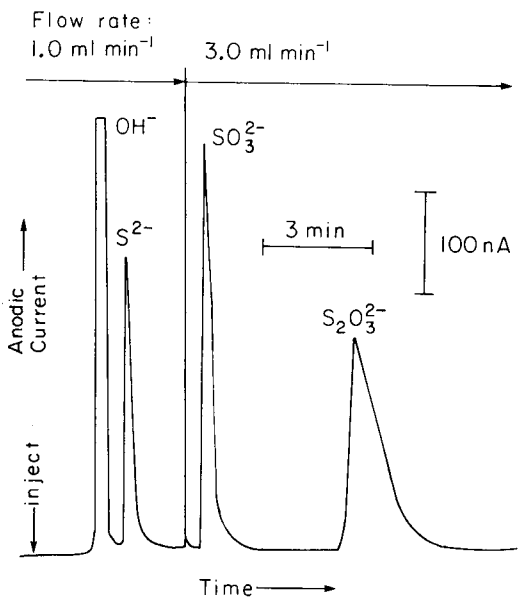

Fig. 11. Chromatographic response for highly alkaline sample by using a flow-rate program. Sample: 0.9 mM S^{2-}, 0.3 mM SO_3^{2-}, 0.5 mM $S_2O_3^{2-}$ in 0.1 M OH^-. Dionex HPIC-AS3 column; 0.20 M KNO_3/5.0 mM M NaOH as mobile phase; other conditions as in Fig. 7.

Conclusions

The diffusion coefficients of the various sulfide species S_x^{2-} (x = 1—5) decrease sharply as x is increased. Hence, the quantitative characterization of a solution of S^{2-} and S_x^{2-} requires determination of three parameters. (i) x, the number of S atoms in S_x^{2-}; (ii) the bulk concentration of S^{2-}; and (iii) the bulk concentration of S_x^{2-}. From the i/E curve, one can obtain only two useful parameters for the mixture, i.e., the values of $i_{1,a}$ and $i_{1,c}$. However, three variables are needed for solving the three simultaneous equations describing this situation. Consequently, x must be determined by an independent method or the mixture must be separated prior to polarographic detection of the different species. Hence, it is concluded that the polarographic method alone cannot provide the necessary data for the quantitative description of an unknown mixture of S^{2-} and S_x^{2-}.

The quantitative separation of S^{2-} and S_x^{2-} by high-performance anion-exchange chromatography with polarographic detection was found to be unsatisfactory also because of dissociation of S_x^{2-} in the column, apparently to S^{2-} and S^0. Because LC/EC with polarographic detection does not detect sulfate, its application for alkaline samples produced by the caustic desulfurization of coal is recommended at this time only for testing for completeness of oxidation of soluble sulphur species.

This investigation was supported by the Fossil Energy Program of Ames Laboratory operated for the U.S. Department of Energy by Iowa State University, Ames, IA, under contract no. W-7405 ENG-82. The authors also acknowledge with gratitude the preparation of samples from the caustic desulfurization of coal by D. R. Mroch.

REFERENCES

1 J. N. Chakrabarti, in C. Karr, Jr., Ed., Analytical Methods for Coal and Coal Products, Academic Press, New York, 1978, Vol. 1, Chap. 9.
2 F. P. Treadwell and W. T. Hall, Analytical Chemistry, 9th edn., Vol. 2, Wiley, New York, 1942, p. 617.
3 M. Tamale and L. Ryland, Ind. Eng. Chem. Anal. Ed., 8 (1936) 16.
4 J. N. Story, J. Chem. Sci., 21 (1983) 272.
5 I. M. Kolthoff and C. S. Miller, J. Am. Chem. Soc., 63 (1942) 1405.
6 A. J. Bard (Ed.), Encyclopedia of Electrochemistry of the Elements, Dekker, New York, 1975, Vol. IV, p. 279.
7 S. I. Zhadanov and B. A. Kiseley, Collect. Czech. Chem. Commun., 31 (1966) 788.
8 D. R. Canterford and A. S. Buchanan, J. Electroanal. Chem., 45 (1973) 193.
9 E. Werner and N. Konopik, Monatsh. Chem., 83 (1952) 599.
10 P. T. Kissinger, Anal. Chem., 49 (1977) 447A.
11 J. G. Koen, J. F. K. Huber, H. Oppe and G. den Boef, J. Chromatogr. Sci., 8 (1970) 192.
12 L. Michel and A. Zatka, Anal. Chim. Acta, 105 (1979) 109.
13 H. D. Hanekamp, P. Bos and R. W. Frei, J. Chromatogr., 186 (1979) 489.
14 H. B. Hanekamp, W. H. Voogt, P. Bos and R. W. Frei, J. Liq. Chromatogr., 3 (1980) 1205.

15 W. Kutner, J. Debowski and W. Kemula, J. Chromatogr., 191 (1980) 47.
16 H. B. Hanekamp, P. Bos and R. W. Frei, Trends Anal. Chem., (1982) 135.
17 D. C. Johnson, S. G. Weber, A. M. Bond, R. M. Wightman, R. E. Shoup and I. S. Krull, Anal. Chim. Acta, 180 (1986) 187.
18 C. D. Chriswell, D. R. Mroch and R. Markuszewski, Anal. Chem., 58 (1986) 319.
19 R. Markuszewski, D. R. Mroch, G. A. Norton and W. E. Strazheim, in R. Markuszewski and B. D. Blaustein (Eds.), Fossil Fuels Utilization: Environmental Concerns, American Chemical Society, Washington, DC, 1986, Chap. 4.
20 I. M. Kolthoff and R. Belcher, Volumetric Analysis, Vol. 3, Interscience, New York, 1957, p. 292.
21 G. Nickless (Ed.), Inorganic Sulfur Chemistry, Elsevier, New York, 1968, p. 215.
22 D. L. Pringle, Ph.D. Dissertation, Department of Chemistry, Iowa State University, Ames, IA, 1967.
23 D. D. Wagman, Selected Values of Chemical Thermodynamic Properties, N.B.S. Technical Note 270-3, U.S. Government Printing Office, Washington, 1968, p. 43.
24 D. L. Noel, Tappi, 61 (1978) 73.
25 M. D. Stephenson, M.Sc. Thesis, Department of Chemical Engineering, Iowa State University, Ames, IA, 1982.
26 R. F. Bergstrom, D. R. Kay and J. G. Wagner, Life Sci., 27 (1980) 189.
27 M. E. Hall, Anal. Chem., 25 (1953) 556.
28 E. Werner and N. Konopik, Monatsh. Chem., 83 (1952) 1187.

Analytica Chimica Acta, 200 (1987) 131—141
Elsevier Science Publishers B.V., Amsterdam — Printed in The Netherlands

QUENCHED PEROXYOXALATE CHEMILUMINESCENCE DETECTION IN AQUEOUS LIQUID CHROMATOGRAPHIC SEPARATIONS

P. VAN ZOONEN[a], H. BOCK, C. GOOIJER*, N. H. VELTHORST** and R. W. FREI***

Department of General and Analytical Chemistry, Free University, De Boelelaan 1083, 1081 HV Amsterdam (The Netherlands)

(Received 14th March 1987)

SUMMARY

Several analytes, such as bromide, iodide, sulphite, nitrite, substituted anilines and organosulphur compounds cause quenching of peroxyoxalate chemiluminescence. This phenomenon, quenched peroxyoxalate chemiluminescence, can be used as a method of detection for liquid chromatography. The potential of quenched chemiluminescence is discussed, with special attention given to its compatibility with aqueous separation systems. An immobilized fluorophore, 3-aminofluoranthene on controlled pore glass, is packed in the detector cell. Liquid-state studies show that the influence of both the nature and concentration of the fluorophore is small, which indicates a more complicated mechanism of the chemiluminescence reaction than previously assumed. It is shown that bis(2-nitrophenyl)oxalate is a more suitable oxalate for quenched chemiluminescence detection than bis(2,4,6-trichlorophenyl)oxalate. This is demonstrated for ion-chromatography of bromide and iodide and the aqueous reversed-phase separation of organosulphur compounds. Detection limits in the low nanogram and sub-nanogram region are reported for the above compounds. When an electronic inverter was used, calibration curves were linear over a concentration range of 2—3 decades. The method is quite selective and can be applied to relatively complex matrices without sample pretreatment.

---

*Cees Gooijer received a Ph.D. in physical chemistry (magnetic resonance spectroscopy) at the Free University of Amsterdam in 1974. He is now an assistant professor in general and analytical chemistry with current research interests in the combination of applied spectroscopy and physical separation methods.

**Nel H. Velthorst received a Ph.D. in physical chemistry at the Free University of Amsterdam. She is now a professor of general chemistry. Her research interests are in molecular emission spectroscopy for detection in chromatography and in environmental, pharmaceutical and bioanalyses.

***Roland W. Frei received a diploma in chemistry in Berne, Switzerland and a Ph.D. in analytical chemistry at the University of Hawaii. After a postdoctoral fellowship and a teaching appointment with Doug Ryan at Dalhousie University, Nova Scotia, he became head of analytical research at Sandoz Ltd. in Basel. He is now a professor of analytical chemistry at the Free University. His research interests are in the physical separation sciences, spectroscopy, and electrochemistry for trace analysis of organic pollutants and pharmaceutically active compounds.

[a]Present address: Laboratory for Organic Analytical Chemistry, National Institute of Public Health and Environmental Hygiene, P.O. Box 1, 3720 BA Bilthoven, The Netherlands.

0003-2670/87/$03.50

Peroxyoxalate chemiluminescence is well known as a means of detecting various fluorophores [1–3] and hydrogen peroxide [4–6]. In a preliminary study [7], the detection of quenchers by peroxyoxalate chemiluminescence was additionally reported. The latter method, denoted as quenched chemiluminescence, has potential for the detection of easily oxidizable compounds such as anilines, organosulphur compounds and certain inorganic ions (nitrite, sulfite, iodide and bromide). In the previous paper [7], a simple model for the quenching mechanism was proposed. It was assumed that peroxyoxalate chemiluminescence reaction occurs via a chemically induced electron-exchange luminescence mechanism [8, 9] described schematically as

$$X + F \rightarrow [F^{\cdot+} \cdots X^{\cdot-}] \rightarrow F^* + \text{products}$$

where F is the fluorophore and X a highly energetic intermediate. The crucial step in quenching the luminescence was assumed to be the reaction of the quenching analyte Q with the intermediate X, to give non-chemiluminescent products, in competition with the reaction of the fluorophore F with X. The effect of the quencher on the chemiluminescence intensity can then be described by a Stern-Volmer type relationship:

$$I_0/I = 1 + k_Q\,[Q] \qquad (1)$$

where I_0 is the chemiluminescence intensity in the absence of a quencher, I the intensity in the presence of the quencher and k_Q the quenching constant. Experimentally [7] it was shown that $1/I$ indeed depends linearly on [Q]. On the basis of the proposed model, one can expect that both the nature and the concentration of the fluorophore influence k_Q, so that a more suitable fluorophore might be found for analyses based on quenched peroxyoxalate chemiluminescence.

In the present study, this hypothesis and the practical applicability of the quenched detection technique are studied. Especially, its potential for detection in ion-chromatography is considered because improvement of detection techniques in this area is still of major concern. Special attention is paid to the compatibility of the chemiluminescence reaction system with aqueous phases typically used in reversed-phase and ion-chromatography. Additionally, it will be shown that the proposed quenching mechanism is probably too simple, which seems to be in line with a recent kinetic study [10].

EXPERIMENTAL

Chemicals

Bis(2,4,6-trichlorophenyl) oxalate (TCPO) was prepared as described by Mohan and Turro [11] and bis(2-nitrophenyl)oxalate (2-NPO) as described by Honda et al. [12]. Acetonitrile (HPLC gradient grade; Baker, Deventer, The Netherlands) was purified as described previously [6]. 3-Aminofluoranthene was immobilized on controlled-pore glass (CPG-10, 77Å; Serva, Heidelberg) as described earlier [13]; CPG was pretreated with 5% (v/v) nitric

acid and dried. The air was removed from the pores by placing the CPG in a vacuum and it was then treated with 3-glycidoxytrimethoxysilane in either water, dry toluene or water-saturated toluene. The resulting intermediate was then coupled to 3-aminofluoranthene.

Apparatus

Basically the chemiluminescence detector is the packed flow cell described in several previous papers [6, 7, 13]. It was used either in the two-layer mode (TCPO and immobilized fluorophore) [6] or packed with only 3-aminofluoranthene. Several experimental arrangements were used in this study.

Flow-injection system for tests of the fluorophore (liquid state). Figure 1A shows a block diagram of a simple flow-injection system for screening fluorophores. The pump was a Kontron 410 (Zürich, Switzerland); a Rheodyne valve equipped with a 3-ml loop was used for the injections of sample plugs containing the different fluorophores; the sample plugs differed from the carrier stream only with respect to the fluorophore. TCPO was added from a solid-state reactor as described previously [5]. The chemiluminescence signal was monitored by a Kratos FS-970 (Ramsay, NJ) fluorescence detector equipped with a 5-μl flow cell.

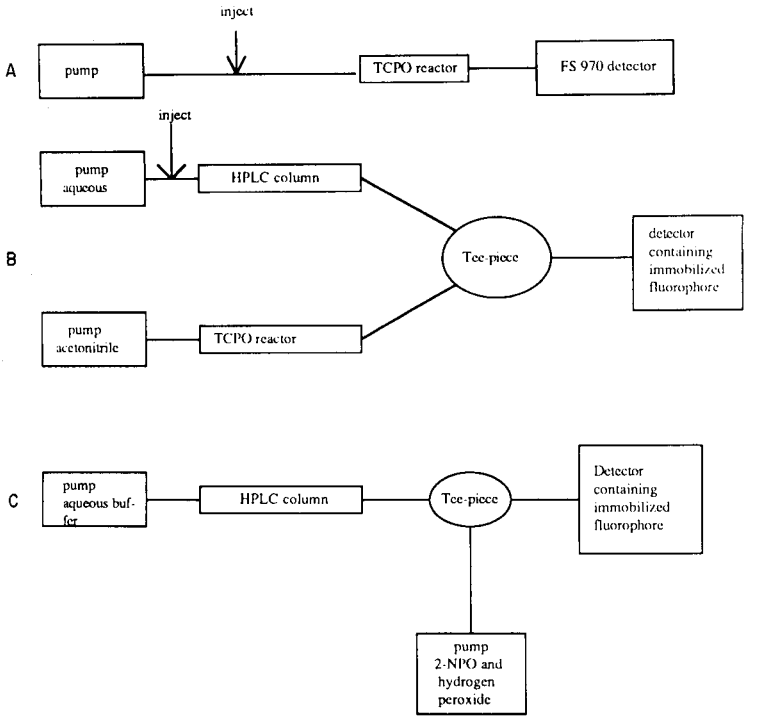

Fig. 1. Block diagrams of the experimental set-ups. See text for details.

Chromatographic system with off-line solid-state addition of TCPO. Figure 1B is a block diagram of the detection system with off-line solid-state addition of TCPO. The flows were delivered by one or two Kratos SF-400 dual-head HPLC pumps equipped with home-made membrane pulse dampers. The chromatographic column was either a PRP-X-100 (100 × 4.6 mm) strong anion-exchanger (Hamilton, Bonaduz, Switzerland), a Spherisorb RP-18 (250 × 4.6 mm) (Merck) or a 150 × 3 mm column packed with 5-μm spherical carbon particles type PCG which were a gift from J. H. Knox (Edinburgh). The T-piece was a vortex type mixing tee as supplied by Kratos (part 2500-0322). Detection took place in a reactor cell packed with immobilized 3-aminofluoranthene as described previously [6].

System for inorganic ions and sulphur compounds with 2-NPO. A block diagram of this set-up is given in Fig. 1C. The hardware employed here was basically the same as used in B.

Chromatographic conditions

The experiments were done under various chromatographic conditions denoted as **a**, **b** and **c**. In **a** (inorganic ions), the PRP-X-100 column was used and the mobile phase was aqueous ammonium benzoate (10 mM, pH 5) at a flow rate of 0.8 ml min^{-1}. In **b** (anilines), the spherical carbon (type PCG) column was used with a mobile phase of 85% acetonitrile/aqueous ammonium benzoate (10 mM, pH 5) at a flow rate of 1 ml min^{-1}. In **c** (sulphur compounds), the RP-18 column was used in combination with the same mobile phase as in **a**. The reagent flow, 0.05 M H_2O_2/8 mM 2-NPO in acetonitrile, was kept at 1.2 ml min^{-1}.

RESULTS AND DISCUSSION

First, the choice of the fluorophore is discussed, because the simple quenching model proposed indicates that 3-aminofluoranthene, as applied in the previous work, is not the most appropriate one for detection by quenched chemiluminescence. Secondly, the choice of oxalate is considered, because it must be compatible with the mobile-phase composition required for the separation of analytes. Thirdly, various applications are discussed and finally the implications of the experimental results for the mechanism of the chemiluminescence reaction are treated briefly.

Choice of fluorophore

In the simple model for quenching, the quencher and the fluorophore denoted as Q and F, compete for reaction with the intermediate X. Hence, it is to be expected that a less efficient F and/or a lower concentration of F implies a more efficient quenching and thus a higher k_Q and a higher sensitivity for quenched chemiluminescence (see Eqn. 1). To verify this statement, the performance of a number of F's in the liquid state was tested by means of flow-injection experiments using a 3-ml injection loop. Table 1 reflects the

TABLE 1

Values of k_Q and I_0 for several fluorophores in the liquid state with methimazole (5.2×10^{-5} M) as quencher

Fluorophore[a]	I_0 (relative units)	k_Q (10^3 M^{-1})
Fluorene	8	28
Anthracene	790	42
Fluoranthene	3000	26
Diphenylanthracene	5100	44
Perylene	40 500	44
3-Aminofluoranthene	45 000	37

[a]Concentration, 4×10^{-5} M.

TABLE 2

Effect of the concentration of the fluorophore (perylene) on the quenching constant measured with methimazole (5.2×10^{-5} M)

Concentration (M)	4×10^{-5}	4×10^{-6}	4×10^{-7}
I_0 (relative units)	40 500	10 000	1200
k_Q (10^3 M^{-1})	44	48	42

influence of the nature of F on k_Q; in Table 2 the role of the concentration of F for perylene as a model fluorophore is given. As expected, both the nature and concentration of F influence I_0, the chemiluminescence intensity in the absence of quencher, very strongly. In comparison, their influence on k_Q is only marginal; I_0 varies over 4 decades, whereas the dispersion of k_Q values for the same set of experiments is only over a factor of two. From these data, for the liquid state, it is clear that the choice of F in terms of concentration and nature is not as important for optimization of k_Q as expected from the previous study [7].

It should be realized, however, that detection by quenched chemiluminescence is based on a decrease in the signal. Hence the noise of this luminescence signal should be reduced as much as possible to achieve a favourable signal-to-noise ratio for quenched chemiluminescence. This can be reached most easily at high I_0, because a greater dynamic range is then obtainable. From these considerations, it can be concluded that 3-aminofluoranthene, suitable for hydrogen peroxide detection by peroxyoxalate chemiluminescence [6, 13], is also appropriate for the quenched chemiluminescence mode. This fluorophore is also advantageous because it can easily be immobilized on glass beads and thus offers a simpler experimental set-up than liquid-phase addition.

Once immobilized fluorophores have been chosen, it is relevant to examine the interrelationship between quenching constant and chemiluminescence intensity for various batches. The results for immobilized 3-aminofluoranthene

TABLE 3

Chemiluminescence intensities and k'_Q values of different batches of immobilized 3-aminofluoranthene, measured with methimazole; effect of dilution with underivatized glass beads

Batch	Immobilization procedure[a]	Dilution (w/w)	I_0 (rel. units)	k'_Q (10^3 M^{-1})
I	A	–	32	6
		1:2	13	6
		1:8	6	6
II	A	–	15	14
III	B	–	52	12
		1:3.5	10	24
IV	B	–	29	30
		1:2	9	47
V	C	–	40	21
VI	D	–	69	14
VII	B	–	60	20
VIII	D	–	180	2
		1:15	18	8

[a]A, silanization in water; B, silanization in dry toluene; C, silanization without solvent; D, silanization in water-saturated toluene.

are summarized in Table 3. The quenching constants are given as k'_Q, because they were measured in a flow-injection system utilizing a 20-μl injection loop instead of the 3-ml loop used for the experiments in Tables 1 and 2. Hence dispersion influences the results so that the actual k_Q is greater than k'_Q because the concentration of quencher observed at the top of the peak will be lower than the actual concentration injected. For comparison purposes, however, these data suffice; k'_Q is proportional to k_Q. The main difference between the batches is the solvent used in the silanization step of the preparation procedure. It is known from the literature [14–16] that in dry toluene a monolayer of the silane is formed; the amount of water present during the silanization step determines the degree of polymerization at the surface of the carrier. From the data presented in Table 3 it can be seen that immobilized fluorophores yield much larger variations in k_Q than expected from the liquid phase experiments (Tables 1 and 2). This is why optimization of k_Q by means of manipulation of the fluorophore was attempted. The effect of "dilution" of the batches with underivatized glassbeads was studied. Interpretation of the results presented in Table 3 is rather difficult. The reproducibility between batches for the synthesis of immobilized fluorophore with respect to the quenching constants is rather poor. As a general trend it might be concluded that silanization in dry toluene is the most suitable for quenched chemiluminescence, because it yields the highest quenching constants at intermediate chemiluminescence intensities.

Mobile-phase compatibility

Both ion-chromatography and the separation of organosulphur compounds generally require aqueous mobile phases, whereas peroxyoxalate

chemiluminescence needs a high acetonitrile content. Unfortunately, the most frequently used oxalate, TCPO, is poorly soluble in aqueous solvents so that clogging of the flow system by precipitation upon post-column addition of the reagent is a major constraint in applying TCPO. A similar problem is encountered if detection by peroxyoxalate chemiluminescence is coupled to enzymatic reactors producing hydrogen peroxide.

The coupling can be done by adding TCPO from a solid reagent bed placed in the effluent stream [6, 13]. A disadvantage of this set-up is that, because of consumption of TCPO, the life-time of the solid-state addition tube is only about 4 h. After this time, an increase of band-broadening and noise caused by voids in the reactor is encountered. This makes the method less suitable for liquid chromatographic procedures requiring prolonged measuring times. Addition of TCPO from a larger bed outside the path of the column effluent has also been shown to be possible for separation systems with relatively high modifier contents [17, 18]. However, with aqueous mobile phases, complications arise, as observed above. Acetonitrile contents higher than 40% through the TCPO bed cause precipitation of TCPO on post-column mixing with aqueous mobile phases, so that the maximum acetonitrile content in the actual chemiluminescence reaction mixture can be at most 20%. Under these conditions the efficiency of the chemiluminescence reaction is too low so that addition of TCPO from the solid state was abandoned for this particular application. It should be stressed, however, that the bad solubility properties of TCPO make it extremely useful for solid-state addition in a number of other applications [5, 6, 17–19]. Alternatively, liquid-phase addition of TCPO in acetonitrile was tried. In this way, precipitation can be prevented but the TCPO concentration that can be applied is very low and so the I_0 values observed in such a set-up are unfavourable.

For the above reasons, another oxalate, bis(2-nitrophenyl)oxalate (2-NPO), was studied. 2-NPO is known to have better solubility characteristics in polar solvents with a stability comparable to that of TCPO [12]. The solubility of 2-NPO in acetonitrile was reported to be six-fold better than that of TCPO. A mixture of 2-NPO and 0.1 M hydrogen peroxide in acetonitrile was found to be stable for at least six hours. This allows these reagents to be premixed so that in combination with an immobilized fluorophore a fairly simple post-column reaction system can be constructed utilizing only one reagent pump (see Fig. 1C). An additional advantage of the 2-NPO system is its greater sensitivity in quenched chemiluminescence. Peak heights are about ten times higher compared to the TCPO system, as shown by the chromatograms in Fig. 2. A simple explanation of this effect is difficult because buffer, pH, flow characteristics and the oxalate are changed simultaneously within this comparison.

Applications

With 2-NPO as the oxalate, it is possible to combine quenched chemiluminescence with virtually every possible acetonitrile/water ratio for the

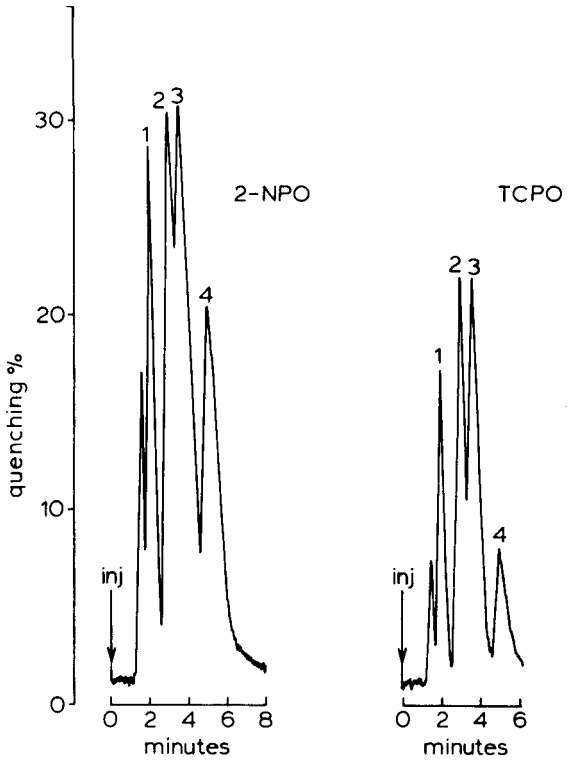

Fig. 2. Chromatograms of a mixture of anilines; comparison of solid-state addition of TCPO and liquid-state addition of 2-NPO. Peaks and amounts injected(ng) for the 2-NPO method (the amounts for the TCPO method are given in parentheses): (1) *p*-isopropylaniline, 25 ng (100); (2) *N,N*-dimethylaniline, 8 ng (32); (3) *N*-ethyl-*m*-toluidine, 17 ng (68); (4) *N,N*-dipropylaniline, 25 ng (100). Chromatographic conditions: for 2-NPO, see under Experimental (method b); for TCPO, 1.2 ml min^{-1} 90% acetonitrile through a 50 × 4.6 mm TCPO bed reactor as reagent flow.

separation system. This was demonstrated with the reversed-phase separation of several organosulphur compounds and their detection in urine, and furthermore with the ion-exchange separation of iodide and bromide. In Fig. 3, a chromatogram is shown for the separation of iodide and bromide based on quenched chemiluminescence detection.

In Table 4, the limits of detection (S/N = 3) for several analytes under chromatographic conditions are presented. When an electronic signal inverter was used, the linear dynamic range of the quenched chemiluminescence method was 2–3 decades; a typical calibration curve for methimazole (N = 8) yields a correlation coefficient of 0.9989. The reproducibility of the method was measured by a five-fold injection of 80 ng of methimazole and calculated to be 4.3% (r.s.d.). The selectivity of the method proves to be quite satisfactory as can be seen from Fig. 4, which shows a chromatogram of spiked

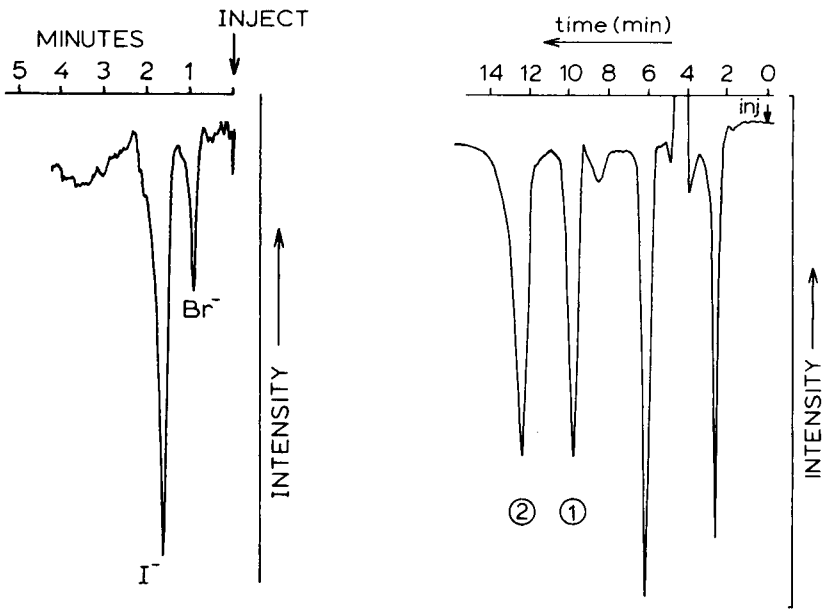

Fig. 3. Chromatogram of 15 ng of bromide and 10 ng of iodide (20-μl injection); conditions as in method a (see Experimental).

Fig. 4. Chromatogram of a urine sample spiked with 100 ng of *N*-allylthiourea (peak 1) and 25 ng of methimazole (peak 2); injection volume 20 μl; chromatographic conditions as in method c (see Experimental).

TABLE 4

Detection limits (S/N = 3) under various chromatographic conditions

Analyte	Detection limit (ng)	Chromatographic conditions[a]	Analyte	Detection limit (ng)	Chromatographic conditions[a]
Bromide	1.5	a	*N*-Ethyl-m-toluidine	1.0	b
Iodide	0.3	a	*N,N*-Dipropylaniline	8.0	b
Sulphite	1.1	a	Thiourea	1.0	c
Nitrite	0.3	a	*N*-Allylthiourea	1.6	c
p-Isopropylaniline	1.4	b	Ethynylthiourea	2.0	c
N,N-Dimethylaniline	0.6	b	Methimazole	0.4	c

[a]For details, see Experimental.

urine; no pretreatment or dilution of the sample was necessary to detect methimazole and *N*-allylthiourea in this matrix.

Mechanistic aspects

From the above results, it must be concluded that the previously assumed model for the quenching mechanism is too simple. In the liquid state, the

nature and concentration of the fluorophore hardly affects k_Q which rules out the kinetic competition of F and Q for the same intermediate, as suggested in the introductory paragraphs. Furthermore, for 2-NPO in the liquid state, no effect of the oxalate concentration on k_Q could be found so that it is improbable that quenching can be connected to the reaction between the oxalate and hydrogen peroxide. This is supported by the earlier results showing that k_Q does not depend on the hydrogen peroxide concentration [7]. Thus the small influence of [oxalate], [H_2O_2] and [F] on k_Q indicates that the quenching step takes place after the reaction between the oxalate and peroxide producing the intermediate X and also after the first encounter of the fluorophore and the intermediate.

For immobilized 3-aminofluoranthene, the results are even more complicated because the immobilization procedure significantly affects k_Q; this indicates that the quenching takes place at the surface of the glass beads carrying the immobilized fluorophore. A reaction taking place at the surface is the charge-transfer chemi-excitation step. Hence it can be speculated that the quencher causes radiationless deactivation of the charge transfer complex $F^{\cdot+}X^{\cdot-}$.

Conclusions

The potential of the quenched peroxyoxalate chemiluminescence method as a detection technique in liquid chromatography has clearly been shown. It is compatible with aqueous separation systems if post-column liquid-state addition of 2-NPO in acetonitrile containing hydrogen peroxide is utilized. Therefore it can be applied to ion-chromatography and other aqueous separation systems when analytes with poor ultraviolet absorbance properties need to be quantified, provided that these analytes have high chemiluminescence quenching rate constants.

The chromatograms obtained for spiked urine samples illustrate the selectivity of quenched chemiluminescence. In the examples studied, no sample pretreatment was required; apparently, only a small number of urine constituents induce efficient chemiluminescence quenching. Detection limits for efficient quenchers are in the low to sub-nanogram range, and the linear dynamic range is two to three decades. From these points of view, quenched chemiluminescence is comparable to the quenched phosphorescence detection technique [20]. However, in quenched chemiluminescence, no deoxygenation of the eluent is required and the detection device is less expensive. Further, this detection system is more selective than quenched phosphorescence detection, in which more quenching mechanisms are operative. This feature of course limits the applicability of quenched chemiluminescence because a smaller number of analytes can be detected.

Finally it is emphasized that, although it may be rather unexpected, the most appropriate fluorophore at this moment is 3-aminofluoranthene immobilized on glass beads. This implies that the same detector can be used for detection of hydrogen peroxide and for quenched chemiluminescence.

This work was financed by the Dutch Society for the Technical Sciences under Grant no. VCh 11/0137. The loan of equipment from Kratos Inc. is gratefully acknowledged. J. H. Knox is thanked for the gift of the carbon packing material.

REFERENCES

1 S. Kobayashi and K. Imai, Anal. Chem., 52 (1980) 424.
2 S. Kobayashi, J. Sekino and K. Imai, Anal. Biochem., 112 (1981) 432.
3 K. W. Sigvardson, J. M. Kennish and J. W. Birks, Anal. Chem., 56 (1984) 1096.
4 G. Scott, W. R. Seitz and J. Ambrose, Anal. Chim. Acta, 115 (1980) 221.
5 P. van Zoonen, D. A. Kamminga, C. Gooijer, N. H. Velthorst and R. W. Frei, Anal. Chim. Acta, 167 (1985) 246.
6 P. van Zoonen, D. A. Kamminga, C. Gooijer, N. H. Velthorst, R. W. Frei and G. Gübitz, Anal. Chim. Acta, 174 (1985) 151.
7 P. van Zoonen, D. A. Kamminga, C. Gooijer, N. H. Velthorst and R. W. Frei, Anal. Chem., 58 (1986) 1245.
8 G. B. Schuster, Acc. Chem. Res., 12 (1979) 366.
9 G. B. Schuster and S. P. Schmidt, Adv. Phys. Org. Chem., 18 (1982) 187.
10 F. J. Alvarez, N. J. Parekh, B. Matuszenski, R. G. Givens, T. Higuchi and R. L. Schowen, J. Am. Chem. Soc., 108 (1986) 6435.
11 A. G. Mohan and N. J. Turro, J. Chem. Educ., 51 (1976) 528.
12 K. Honda, K. Miyaguchi and K. Imai, Anal. Chim. Acta, 177 (1985) 103.
13 G. Gübitz, P. van Zoonen, C. Gooijer, N. H. Velthorst and R. W. Frei, Anal. Chem., 57 (1985) 2071.
14 C. R. Hastings, W. A. Aue and J. M. Augl, J. Chromatogr., 53 (1970) 487.
15 P. P. Herman, C. R. Field and S. Abbot, J. Chromatogr. Sci., 19 (1981) 470.
16 R. E. Majors and M. J. Hopper, J. Chromatogr. Sci., 12 (1974) 767.
17 J. R. Poulsen, J. W. Birks, P. van Zoonen, C. Gooijer, N. H. Velthorst and R. W. Frei, Chromatographia, 21 (1986) 587.
18 P. van Zoonen, D. A. Kamminga, C. Gooijer, N. H. Velthorst and R. W. Frei, J. Liq. Chromatogr., 10 (1987) 819.
19 P. van Zoonen, I. de Herder, C. Gooijer, N. H. Velthorst, R. W. Frei, E. Küntzberg and G. Gübitz, Anal. Lett., 19 (1986) 1943.
20 J. J. Donkerbroek, A. C. Veltkamp, C. Gooijer, N. H. Velthorst and R. W. Frei, Anal. Chem., 55 (1983) 1886.

Analytica Chimica Acta, 200 (1987) 143—150
Elsevier Science Publishers B.V., Amsterdam — Printed in The Netherlands

EXAMINATION OF COVALENTLY BOUND POLYMERIC STATIONARY PHASES BY LUMINESCENCE SPECTROSCOPY

C. H. LOCHMÜLLER* and M. T. KERSEY

P. M. Gross Chemical Laboratory, Duke University, Durham, NC 27706 (U.S.A.)

(Received 3rd March 1987)

SUMMARY

Luminescence spectroscopy is used to probe silica-gel surfaces derivatized with [3-(3-pyrenyl)propyl]methyldichlorosilane. Evidence of solution pre-polymerization and subsequent derivatization to accessible surface silanols is presented. Conformational changes of the bound ligands in polar and non-polar solvents indicate a dynamic surface which minimizes its surface area in hostile solvents.

Reversed-phase bonded stationary phases for liquid chromatography are generally classified into two categories, brush and polymeric. They are produced by reacting monofunctional or polyfunctional silanes, respectively, to accessible surface silanols of silica gel [1—5]. Early chromatographic experiments predominantly used brush-phase columns because of the greater reproducibility in the bonded-phase derivatization and higher column efficiencies. Recently, polymeric stationary phases were shown to provide a more selective separation of polycyclic aromatic hydrocarbons with similar efficiencies when compared to brush phases [2, 6, 7]. Verzele and Mussche [3] argued that, chromatographically, there are no differences between brush and polymeric phases; however, Sander and Wise [2] have demonstrated selectivity changes of polycyclic aromatic hydrocarbons for the two bonded-phase types. More information is required to characterize these chemically modified polymeric surfaces.

Several spectroscopic methods have been developed to probe the physicochemical micro-environment of these complex surfaces. Nuclear magnetic resonance and infrared spectroscopy have been used to characterize the shape and solvent-dependent conformations of chemically bound silanes [8—11]. Lochmüller et al. [12—15] introduced steady-state and time-dependent luminescence spectroscopy to examine the micro-environment of the bound

*Charles H. Lochmüller is Professor of Chemistry and Biochemical Engineering at Duke University. His roughly 100 publications include work on robotics, proton-induced x-ray emission and n.m.r. but his main thrust has been in fundamental studies of separation mechanisms. He received the Pioneer Award for his work in robotics in 1985 and is the recipient of the 1987 Chromatography Award of the American Chemical Society.

0003-2670/87/$03.50

silanes. These techniques were used to examine the distribution of surface silanols, the conformational changes of chemically modified brush phases in common liquid-chromatographic solvents and the surface polarity of end-capped bonded phases [12—15].

In the present work, [3-(3-pyrenyl)propyl] methyldichlorosilane-bonded phases were examined by using luminescence spectroscopy. The data reported indicate solution pre-polymerization of the silane oligomer. Data from mass spectral and supercritical fluid chromatographic analyses suggest formation of low-molecular-weight polymers. Luminescence data indicate a structural rearrangement of these low-molecular-weight polymeric phases in polar and non-polar solvents.

EXPERIMENTAL

Materials

Whatman Partisil-10 silica gel (BET, N_2 surface area 323 $m^2\ g^{-1}$, mean pore diameter 93 Å, and mean particle size 10 μm) was used as the support. Synthesis of the pyrene silane and subsequent hydrosilylation reactions were done in this laboratory under conditions previously described [12]. Methyldichlorosilane (Petrarch Systems) was used without further purification in the synthesis of the difunctional pyrene silane. Spectral-grade hexane and methanol (Mallinckrodt) were used as contact solvents.

Fluorescence studies

Steady-state studies. All steady-state fluorescence spectra were obtained by using a Perkin-Elmer Model MPF-66 spectrophotometer. Emission spectra were collected from 360 to 530 nm at an excitation wavelength of 315 nm. Excitation spectra were collected from 270 to 370 nm at emission wavelengths of 390 nm (monomer) and 480 nm (excimer). All spectra were measured at 22°C. Carbon and hydrogen determinations (M. H. W. Lab., Phoenix, Arizona) were run on all bonded phases and these were diluted with underivatized silica to avoid inner-filter effects. Derivatized silica samples were prepared for data acquisition by adding approximately 20 mg of the derivatized silica to 2 ml of solvent. The solvent/silica slurry was freeze/pump/thawed a total of three times to avoid oxygen quenching of the fluorescence signal. After the final thaw, the cell was inverted and the silica settled into the quartz tube. The cell was then placed into a specially designed holder which fits into both spectrometers. The cell and holder were designed in this laboratory and are illustrated in Fig. 1.

Time-dependent studies. Instrumentation, data collection, and numerical analysis have been discussed [13]. Data were acquired at an excitation wavelength of 315 nm and an emission wavelength of 390 nm. An average instrument response of 4.3 ns (FWHM) was recorded when 0.5 atm of nitrogen (National Specialty Gases) was used in the flashlamp.

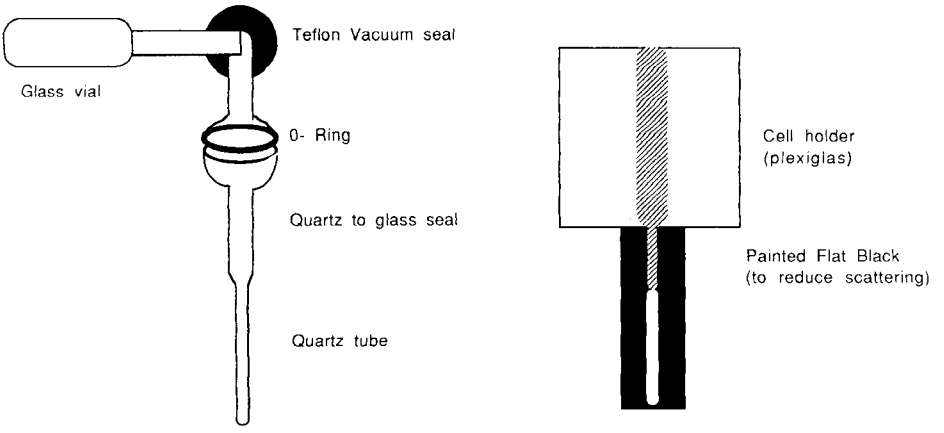

Fig. 1. Freeze/pump/thaw cell and holder. The quartz tube is inserted through the shaded area of the holder.

Solution polymerization

[3-(3-Pyrenyl)propyl] methyldichlorosilane was polymerized by using the same bonded-phase reaction conditions (without silica) previously described [15]. Polymerization was terminated by adding an excess of trimethylchlorosilane (Petrarch Systems). Samples of the mixture were removed, solvent was evaporated by bubbling dry nitrogen through the mixture and the pale-green, viscous liquid was examined by mass spectrometry and supercritical fluid chromatography. The latter data were acquired on a Hewlett-Packard model 1082B liquid chromatograph modified for the purpose. Aliquots of the polymerized solution were diluted in chloroform to concentrations between 10^{-3} and 5×10^{-7} M in monomer. Allylpyrene solutions, within the same concentrations, were used to compare the polymeric solutions with a non-aggregating model compound.

RESULTS AND DISCUSSION

Difunctional silanes were used in this work because of the inherently less complex polymeric structures, compared to trifunctional silanes, formed during polymerization. Polymers synthesized with trifunctional silanes exhibit cross-linking; however, difunctional silane polymers only form linear or cyclic structures. Further, only linear structures bind to accessible surface silanols and the unreactive cyclic polymers are washed from the silica surface. Possible cyclic and linear structures formed by the condensation of three difunctional silane monomers are shown below (R = 3-propylpyrene).

The photophysics of pyrene is well documented [16—19]. Pyrene forms excited-state dimers (excimers) in a collisional quenching process involving an excited-state pyrene molecule and one in the ground state. Excimer formation decreases the quantum yield of the monomer emission (378 nm) and

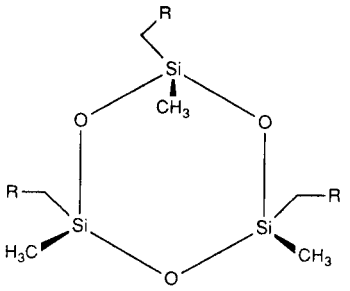

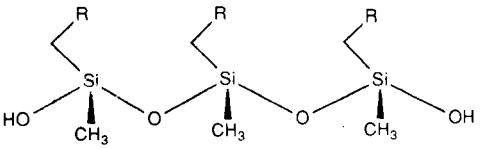

gives rise to a broad, structureless emission (λ_{max} = 470 nm). Figure 2 illustrates the loss in intensity of the monomer emission with a corresponding rise in the excimer emission for two covalently bound polymeric phases in contact with methanol. Similar spectra have been observed for pyrene in solution [16].

Steady-state fluorescence measurements of polymer solutions

The aggregation of difunctional pyrenesilanes in solution was observed by using steady-state fluorescence spectroscopy. The association of difunctional silane monomers was monitored by measuring the excimer/monomer ratio of the polymer solutions and comparing that to measurements made with allylpyrene solutions. Figure 3 compares the excimer/monomer ratio for polymerized [3-(3-pyrenyl)propyl] methyldichlorosilane and allylpyrene solutions. A plot of the excimer/monomer ratio vs. allylpyrene concentration in solution approaches zero as the concentration of allylpyrene decreases. However, compared with the allylpyrene solutions, the polymerized difunctional silane solutions exhibit increased excimer formation. The greater excimer intensity observed for the difunctional silane solutions is indicative of silane polymerization because, upon dilution, the difunctional silane oligomers maintain the

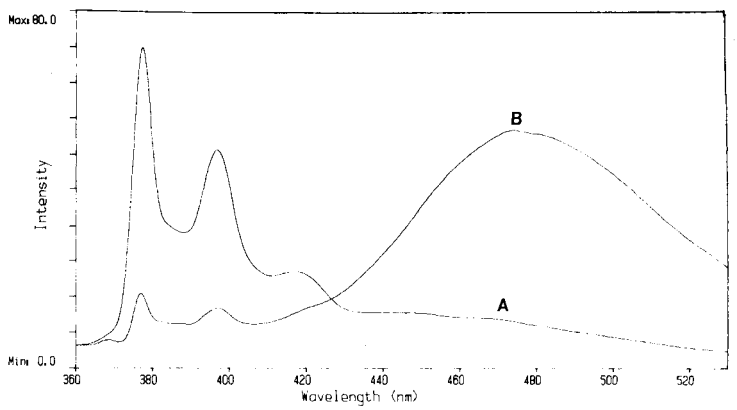

Fig. 2. Steady-state fluorescence spectra: (A) 1.36% carbon diluted 1/20 in methanol; (B) 7.24% carbon diluted 1/1000 in methanol.

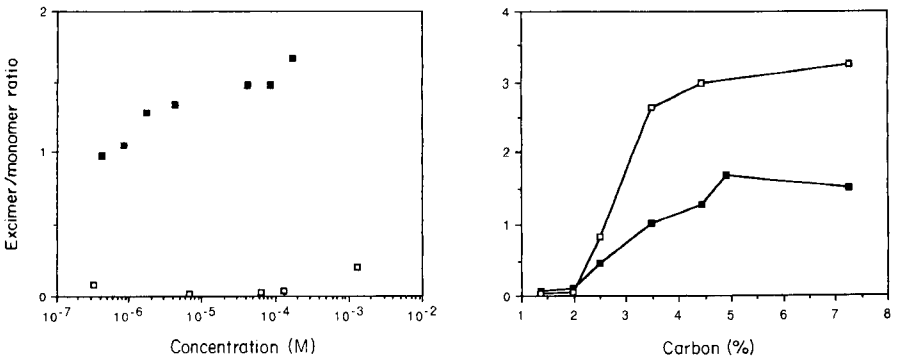

Fig. 3. Steady-state fluorescence excimer/monomer intensity ratios vs. concentration of polymerized difunctional pyrenesilanes (■) and allylpyrene (□) in chloroform.

Fig. 4. Steady-state fluorescence excimer/monomer intensity ratios vs. percent carbon for difunctional propylpyrene bonded phases in hexane (■) and methanol (□).

critical interaction distance for excimer formation. Consequently, a percentage of the polyfunctional silane must be covalently bound to one another. The results of supercritical fluid chromatography and mass spectral analyses indicate, in addition to individual difunctional silanes, the presence of dimers and trimers. Evidence of larger-molecular-weight polymers was not observed.

Steady-state fluorescence measurements of polymeric bonded phases

Steady-state spectra of polymeric bonded phase samples ranging from 1.36% to 7.24% carbon were collected in contact with hexane and methanol. Surface coverages (μmol m^{-2}) of these polymeric bonded phases cannot be determined because an average molecular weight of the bound polymer is unknown. Figure 4 illustrates the changes observed in the excimer/monomer ratio for polymeric phases in the two solvents. The ratio increases with increasing percent carbon. This trend has also been observed for both pyrene in solution [16] and for monofunctional pyrenesilanes bound to silica gel [13].

Differences in the excimer/monomer ratios for methanol and hexane are observed above 2% carbon and increase with increasing pyrenesilane surface coverage. The larger excimer/monomer values in methanol are attributed to the collapse of the bound ligands which, at higher percent carbon, have a greater probability of coming within the critical interaction distance to form excimers. The greater degree of excimer emission observed in methanol for similar carbon loadings compared with hexane has also been demonstrated for brush phases [12, 13]. Changes observed for the excimer/monomer ratio in methanol and hexane may be explained by solvent-induced conformational changes in the bonded phase caused by "solvophobic" interactions between the bound ligands and solvent [20]. This experiment demonstrates that

polymeric bonded phases, like their monofunctional silane counterparts, appear to reduce the total surface area of the bound ligand moieties in hostile solvents. These results support a dynamic model for polymeric phases which suggests that the ligands swell in good solvents and shrink in hostile solvents.

Time-dependent measurements of polymeric bonded phases

Values of the pre-exponential factors (A_i), lifetimes (τ_i) and percent carbon in hexane and methanol are listed in Table 1. The validity of the numerical analysis and model based upon the pre-exponential factors has been defended [13]. When the "component incrementation" of Isenberg et al. [21] was used, it was concluded that difunctional pyrene bonded phases fit to a sum of three exponentials.

Figure 5(a) illustrates the pre-exponential factors for the series of difunctional bonded phases, 1.36% to 7.24% carbon, in methanol. One observes that the population of bound pyrene molecules which form excimers is approximately 80% and increases from 80 to about 95% between 5 and 7.24% carbon. The data appear to indicate that up to 5% carbon, the degree of eximer formation for difunctional propylpyrene bonded phases is independent of carbon loading. Increased pre-exponential factors for carbon loadings

TABLE 1

Normalized pre-exponential factors (A_i) and lifetimes[a] (τ_i) as a function of solvent and percent carbon

Carbon (%)	1.36	1.99	2.51	3.48	4.43	4.91	5.11	7.24
coverage[b] (μmol m^{-2})	0.19	0.28	0.35	0.50	0.64	0.71	0.74	1.10
Hexane								
A_1	0.736	0.637	0.451	0.468	0.835	0.904	0.801	0
A_2	0.062	0.083	0.368	0.390	0.154	0.086	0.097	0
A_3	0.176	0.280	0.173	0.143	0.011	0.009	0.102	0
τ_1	4.7	2.7	20.2	14.9	12.8	9.3	3.4	7
τ_2	100.3	60.5	53.5	45.1	40.3	32.3	42.8	33
τ_3	157.5	138.2	97.0	101.2	135.8	119.9	123.3	123
Methanol								
A_1	0.846	0.837	0.709	0.739	0.941	—	0.843	0
A_2	0.143	0.064	0.171	0.213	0.049	—	0.086	0
A_3	0.011	0.099	0.120	0.048	0.011	—	0.071	0
τ_1	0.5	0.8	4.4	10.2	5.7	—	1.3	6
τ_2	164.8	132.4	45.2	45.1	33.4	—	33.5	30
τ_3	220.5	183.7	119.8	124.7	93.2	—	106.3	117

[a]Lifetimes are in ns. [b]These values are based on calculations which assume that the predominant surface oligomer is monomeric (and as if monomeric chemistry was used); it is not the intent of this calculation to suggest that this is the case here and the values are presented solely for comparison to other published work where "monomeric" chemistry indeed was used.

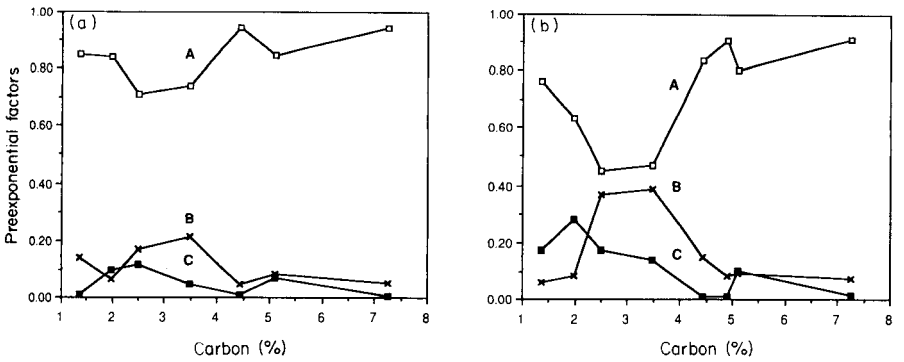

Fig. 5. Plots of the pre-exponential factors vs. percent carbon for difunctional propylpyrene bonded phases in methanol (a) and in hexane (b): (A) A_1, (B) A_2, (C) A_3.

greater than 5% indicates the interaction of oligomeric units on the more densely packed surface. Polymeric phases may exhibit large excimer-forming populations at low percent carbon because either linear polymers form in solution and then bind to accessible surface silanols and/or, as Sander and Wise [2] suggest, the polymeric network is initiated on the surface and "grows out" into solution.

The large excimer-forming population at low percent carbon is attributed to solution pre-polymerization and subsequent reaction of the polymerized silane to surface silanols. The extent of silane-surface initiated polymerization at low carbon coverages would be less than the competitive process of silane reaction to the more accessible surface silanols for two reasons: first, the probability of a pyrenesilane ligand in solution encountering an accessible surface silanol is greater than one reacting with a bound silane; and second, the interaction of a bound silane and one in solution is more hindered and less favorable than the competitive process of binding to a more accessible surface silanol. The model of polymer formation with polyfunctional silanes suggested by Sander and Wise may be more applicable to higher carbon loadings because there are fewer surface silanols to compete with the residual silane silanols.

Figure 5(b) illustrates the pre-exponential factors for the polymeric bonded phases in hexane. At low percent carbon, a greater degree of excimer formation than expected from brush-phase results [13] is observed. However, the excimer population decreases up to 3% carbon and then increases. This anomalous behavior may indicate the difficulty in reproducibly synthesizing polymeric phases.

Examination of the lifetimes, τ_2 and τ_3, listed in Table 1 indicate a concentration-quenching kinetic model of the pyrene monomer emission up to 3% carbon [16]. The constant lifetimes, within experimental error, for greater than 3% carbon is a departure from true, diffusion-controlled behavior. This might be expected in constrained systems where the ligands are bound to the surface.

Comparison of the lifetimes in hexane and methanol supports a dynamic stationary-phase model for polymeric bonded phases. The lifetimes, τ_2 and τ_3, are longer in methanol than those in hexane below 2.5% carbon. The shorter lifetimes observed in hexane correspond with increased solvation of the alkyl chains. This solvation gives the silane a greater degree of motion which, on average, decreases the relaxation time of the pyrene molecule. Conversely, methanol, a Θ-solvent, restricts the ligand motion increasing the average relaxation time of the hydrophobic pyrene ligands. Pyrene crystal quantum yields and lifetimes have been observed to increase with decreasing temperature [17]. Above approximately 3% carbon, there are no significant differences in the lifetimes, τ_2 and τ_3, between the two contact solvents, which indicates that the ligands are motionally constrained to the same degree.

The differences between τ_1 in hexane and methanol can be attributed to the degree of solvation of the pyrene ligands. Silanes solvated by hexane take longer, on average, to form excimers than in methanol because of the increased mobility of the propyl chain and the larger separation between pyrene molecules. The shorter lifetimes observed in methanol may be indicative of the collapsed state of the ligands which put the pyrene molecules within the critical interaction distance for excimer formation.

We gratefully thank L. Mink for the supercritical fluid chromatographic data. This project was supported by the National Science Foundation, Grant CHE85-00658 (to C.H.L.)

REFERENCES

1 R. E. Majors, J. Chromatogr., 180 (1980) 488.
2 L. C. Sander and S. A. Wise, Anal. Chem., 56 (1984) 504.
3 M. Verzele and P. Mussche, J. Chromatogr., 254 (1983) 117.
4 H. Hemetsberger, M. Kellermann and H. Ricken, Chromatographia, 10 (1977) 726.
5 H. Colin and G. Guiochon, J. Chromatogr., 141 (1977) 289.
6 S. A. Wise and W. E. May, Anal. Chem., 55 (1983) 1479.
7 S. A. Wise and L. C. Sander, J. High Resolut. Chromatogr. Chromatogr. Commun., 8 (1985) 248.
8 R. K. Gilpin, J. Chromatogr. Sci., 22 (1984) 371.
9 C. H. Lochmüller, D. B. Marshall and D. R. Wilder, Anal. Chem., 52 (1980) 19.
10 L. C. Sander, J. B. Callis and L. R. Field, Anal. Chem., 55 (1983) 1068.
11 J. D. Miller and H. Ishida, Anal. Chem., 57 (1985) 283.
12 C. H. Lochmüller, A. S. Colborn and M. L. Hunnicutt, Anal. Chem., 55 (1983) 1344.
13 C. H. Lochmüller, A. S. Colborn, M. L. Hunnicutt and J. M. Harris, J. Am. Chem. Soc., 106 (1984) 4077.
14 C. H. Lochmüller, D. B. Marshall and D. R. Wilder, Anal. Chim. Acta, 130 (1981) 31.
15 C. H. Lochmüller, M. T. Kersey and M. L. Hunnicutt, Anal. Chim. Acta, 175 (1985) 267.
16 J. B. Birks, Photophysics of Aromatic Molecules, Wiley-Interscience, New York, 1970, p. 302.
17 J. B. Birks, Rep. Prog. Phys., 38 (1975) 903.
18 G. Marconi and P. R. Salvi, Chem. Phys. Lett., 123 (1986) 254.
19 T. Azumi, A. T. Armstrong and S. P. McGlynn, J. Chem. Phys., 41 (1964) 3839.
20 C. Horvath and W. J. Melander, Chromatogr. Sci., 15 (1977) 393.
21 I. Isenberg, R. D. Dyson and R. Hanson, Biophys. J., 13 (1973) 1090.

Analytica Chimica Acta, 200 (1987) 151—169
Elsevier Science Publishers B.V., Amsterdam — Printed in The Netherlands

THERMALLY STABLE, HIGHLY FLUORINATED STATIONARY PHASES FOR GAS CHROMATOGRAPHY

RENA M. POMAVILLE and COLIN F. POOLE*
Department of Chemistry, Wayne State University, Detroit, MI 48202 (U.S.A.)
(Received 30th March 1987)

SUMMARY

The chromatographic properties of three highly fluorinated stationary phases namely Fomblin YR [a poly(perfluoroalkyl) ether], PPF-20 [a poly(perfluorphenylene) ether], and Fluorad FC-430 [a fluoroalkyl ester], are compared with those of conventional phases. The importance of phase structure, coating solvent, and the surface chemistry of the support for the preparation of efficient and stable column packings is outlined. The retention of solutes of different structures is shown to occur by a combination of gas-liquid partitioning and interfacial adsorption. The relative importance of partitioning compared to adsorption is influenced by the degree of fluorination and the measurement temperature. From accurately determined gas-liquid partition coefficients, corrected McReynolds phase constants and partial molar free energies of solution for a methylene group (ΔG) were determined for the highly fluorinated phases. In the case of Fomblin YR, the very low value for $\Delta G(CH_2)$ compared to conventional phases provides a quantitative indication of the weak intermolecular forces operating in the chromatographic system. Higher values for PPF-20 indicate stronger dispersive interactions for the perfluoroaromatic phase compared to the perfluoroalkyl phases.

The introduction of fluorine into an organic molecule has a dramatic influence on its chemical and physical properties [1—3]. A high degree of fluorination results in properties that may no longer resemble those of the parent hydrocarbon compound. These changes result from the unique properties of fluorine, in particular, its small size and large electronegativity. Manifestations of these properties are the strong carbon-fluorine bonds that are resistant to attack by most chemical reagents and the very weak inter-

*Colin F. Poole is an Associate Professor of Analytical Chemistry at Wayne State University, Detroit, Michigan. He received his Ph.D from the University of Keele (1975), M.S. from the University of Bristol (1972), and B.Sc. from the University of Leeds (1971), all in Great Britain. Following postdoctoral appointments with Professor M. Verzele at the University of Ghent, Belgium, and with Professor A. Zlatkis at the University of Houston, Texas, he joined the faculty at Wayne State University in 1980. His main research interests are the application of gas, liquid, and thin-layer chromatographic techniques to problems of environmental and biomedical nature, mass spectrometry, and the solvent properties of liquid organic salts and highly fluorinated polymers. In 1985 he was awarded the Tswett Chromatography Medal.

0003-2670/87/$03.50

molecular forces existing in perfluorocarbon solvents. Perfluorocarbon solvents possess the following unusual properties: (a) relatively low boiling points which belie their true molecular weights (perfluorocarbon compounds boil at only slightly higher temperatures than the noble gases of similar molecular weight); (b) extremely low surface tension (believed to include the lowest values recorded); (c) refractive indices lower than those of any other liquids; (d) low critical temperatures and pressures; and (e) high liquid densities and coefficients of expansion.

On account of the above combination of physical and chemical properties, perfluorocarbon compounds have found many industrial applications [4, 5]. The same combination of high chemical stability and very weak intermolecular forces is attractive for certain chromatographic applications provided that these properties can be wedded to the requirements of modern column technology.

Sporadic accounts of the use of perfluorocarbon compounds and highly fluorinated stationary phases have appeared almost from the inception of gas-liquid chromatography. The applications of these phases are summarized in Table 1 [6—26]. Perfluorocarbon phases have been used to separate substances of high chemical reactivity such as metal fluorides, halogens, interhalogen compounds, and the halide compounds of hydrogen, sulfur, and phosphorus. These compounds generally destroy conventional stationary phases and can only be separated on chemically inert perfluorocarbon phases, which in turn, are usually coated on teflon-type supports. Another common application of highly fluorinated phases is the separation of perfluroocarbon compounds and freons that are difficult to resolve on conventional phases. Isomeric perfluorocarbon compounds have very similar boiling points, usually much closer than their hydrocarbon analogs, and require selective phases for their separation. In regard to physical forces, the origin of this selectivity for highly fluorinated phases remains obscure; however it should be noted that the solubility of perfluorocarbon compounds in highly fluorinated solvents frequently exceeds that in analogous hydrocarbon solvents. The solubility differences may be very great; in some instances, a perfluorocarbon compound may be virtually insoluble in a hydrocarbon-type solvent while miscible in all proportions with its highly fluorinated analog. Highly fluorinated phases have also been exploited as a method of separating thermally labile substances at lower column temperatures than is possible for conventional phases and as a means of extending the range of molecular weights of substances that can be separated by gas chromatography [18, 19, 21]. Here, the weak dispersive interactions between perfluorocarbon phases and hydrocarbon compounds are responsible for the separation characteristics observed.

Those very same properties that result in the unique separation properties of highly fluorinated phases also account for the considerable technical difficulties encountered in preparing efficient columns with these phases. Weak interactions with support surfaces coupled with a high temperature

TABLE 1

Highly fluorinated stationary phases and their gas chromatographic applications

Stationary phase	Abbreviation or trade name	Chromatographic application	Ref.
1 Perfluoroalkanes		(a) Perfluoroalkanes and perfluoroalkenes	6—8
		(b) Freons, UF_6, ClF_3, HF BrF_3, BrF_5, ClF, ClO_2F	9
2 Poly(chlorotrifluoroethylene) $Cl(CF_2CFCl)_nCF_3$	Kel-F	(a) Perfluorinated alkanes, alkenes and aromatics, and freons	6—8, 10—13
		(b) As for 1(b)	
		(c) Freons, Cl_2, ClF, ClF_3, Br_2, BrF_5, HF, UF_6	10
		(d) SF_4, SF_6, S_2F_{10}, SF_5Cl, SO_2F_2	11
		(e) PCl_3, $PSCl_3$, $POCl_3$	14
		(f) ClF_3, ReF_6, WF_6, OsF_6, SF_6, SeF_6, TeF_6, VF_5, NbF_5, TaF_5, SbF_5, MoF_4, AsF_3, $ReOF_5$, WOF_4, $MoOF_4$, VOF_3	15, 16
$Cl(CF_2CFCl)_3CF_2COOR$ (R = H or C_2H_5)	Fluorolube	(a) As for 2(a)	12
	Kel-F acid or ester	(a) As for 1(a)	6, 7
		(b) Freons, HF, F_2, ClF_3, SF_4, SF_6, NF_3	17
3 Poly(perfluoroalkyl)ether $-(O-\underset{\displaystyle CF_3}{\underset{\vert}{CF}}-CF_2)_m-(OCF_2)_n-\underset{\displaystyle CF_3}{\underset{\vert}{CF}}-$	Fomblin	(a) Alkanes, alkenes, petroleum distillates, freons, perfluoroalkanes	18, 19
$F-(\underset{\displaystyle CF_3}{\underset{\vert}{CF}}-CF_2O)_n-CF_2CF_3$	Krytox	(a) As for 2(a)	12
		(b) Freons, HF, HCl	20
4 Fluorocarbon surfactants	FC-430	(a) Acids, aldehydes, haloalkanes, alcohols, esters, ketones, amines	21
	FC-431	(b) As for 4(a)	22, 23
5 Miscellaneous			
Di-ωH-octafluoropentyl ester of tetranitrodiphenic acid	FTND	(a) As for 4(a), also cyanoalkanes, aromatics, and nitroalkanes	24
Tetrameric bis(1,1,9-trihydrohexadecafluorononyl)phosphonitrilate	FPN	(b) As for 5(a)	24
α-Perfluoroalkenyl-ω-methoxypoly(oxyethylene)	Fluortensid	(c) As for 1(a)	8
Perfluorotributylamine		(d) As for 1(a)	6
Fluoroalkyl tosylate $H(CF_2)_4CH_2OSO_2C_6H_4CH_3$		(e) As for 2(b)	17
Fluoroalkyl esters of pyromellitic and camphoric acids	Zonyl E-7 and E-91	(f) As for 2(b)	17, 25
$CH_2=CHCO_2CH_2(CF_2CF_2)_3H$		(g) Perfluoroalkanes	26

coefficient of viscous flow tend to result in unstable films of the stationary phase that are easily disrupted by temperature changes. Column packings, therefore, are often characterized by poor efficiency and narrow ranges of operating temperature. Some representative chromatographic properties of highly fluorinated phases are summarized in Table 2.

The problems discussed in the previous paragraph have tended to diminish interest in the use of highly-fluorinated phases for general gas chromatographic applications. The purpose of this paper is to establish those properties most desirable in new highly fluorinated phases for gas chromatography by augmenting and unifying results available in the literature. In particular, the interrelationship between phase structure and support characteristics resulting in acceptable film-forming properties are discussed. Also, the principal solute-solvent interaction mechanisms are identified for the phases studied and used to interpret the retention properties of the highly fluorinated phases. From these results, it is possible to predict those properties required of a highly fluorinated stationary phase for high temperature operation in gas chromatography.

EXPERIMENTAL

Materials

Fluorad FC-430 was obtained from the 3M Co. (St. Paul, MN), Fomblin YR from Montedison (New York, NY), Santovac (PPE-5) from Monsanto (St. Louis, MO), and PPE-20 from Supelco (Bellefonte, PA). Pentafluorophenol and 1,1,2-trichlorofluoroethane (Freon-113) were obtained from Aldrich Chemical Co. (Milwaukee, WI). Chromosorb W-AW (100—120 mesh), Chromosorb P-AW (100—120 mesh), Gas-Chrom Q (100—120 mesh), Silyl-8, and test solutes in the form of Theta Kits were obtained from Anspec Co. (Ann Arbor, MI). Carbopack B (60—80 mesh) was obtained from Supelco (Bellefonte, PA). Other chemicals and solvents were general laboratory grade in the highest purity available.

A sample of high-molecular-weight poly(perfluorophenylene ether), PPF-20 was prepared by modification of the method described by Pummer and Wall [27]. Pentafluorophenol (ca. 4.0 g) and a half molar-equivalent weight of solid potassium hydroxide were sealed in a teflon-lined bomb of 23-ml volume (Model 4749; Parr Instrument Co., Moline, IL). The stainless-steel bomb has a maximum operating temperature of 250°C and a pressure limit of 1800 psi. The bomb was heated at 210°C for 72 h and allowed to cool to room temperature, and the products were extracted with tetrahydrofuran. The residue from the tetrahydrofuran extract was triturated several times with methanol and the methanol extract was discarded. The poly(perfluorophenylene ether) was obtained as a methanol-insoluble brown gum, that flowed on warming, in about 70% yield. The molecular weight was estimated from size-exclusion chromatography to be approximately 3700, corresponding to a polymer with about 20 perfluorophenyl

TABLE 2

Column-operating characteristics for highly fluorinated stationary phases

Stationary phase	Maximum column temperature (°C)	McReynolds constants[a]					Average column efficiency[b]
		X'	Y'	Z'	U'	S'	
Perfluoroalkane (largely $C_{22}F_{44}$)	100	−38	−56	−41	38	27	200—1000
Kel-F (wax)	200	55	67	114	143	116	400—1200
Fluortensid	120	219	430	357	508	451	
Krytox		20	50	101	118	99	300—600
Fluorad FC 430	250	178	466	381	462	460	1300—1500
Fluorad FC 431	200	281	423	297	509	360	
Fomblin YR	255	−15	138	88	141	51	2000—2500
Zonyl E-91		223	359	468	549	465	

[a]Phase constants may have been measured at different temperatures. The normal temperature is 120°C; for Fomblin YR, measurements were made at 45°C [19]. X' benzene; Y', butanol; Z', 2-pentanone; U', nitropropane; S' pyridine. [b]Expressed as N m^{-1} where N is the number of plates. Column efficiency varies with phase loading, coating efficiency, and test solute. Perfluorocarbon solutes may give higher values than hydrocarbon solutes [12].

rings. Infrared and ^{1}H-, ^{13}C- and ^{19}F-NMR spectra were consistent with the following structure (with $n = 18$)

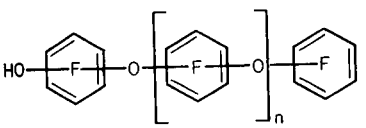

in which all protons are phenolic and coupling of the rings is not stereospecific.

Density measurements as a function of temperature were made by using a modified Lipkin bicapillary pycnometer. Procedural and calibration details are given elsewhere [28]. Density relationships were fitted to the equation

$$\rho_T = A - BT \quad (1)$$

where ρ_T is the density of the stationary phase at temperature T (°C) and A and B are constants.

The coefficients for the different phases are given in Table 3. The very high viscosity of the poly(phenylene ether), PPE-20, prevented normal filling and operation of the pycnometer. Its density was estimated from values measured for mixtures of PPE-5 and PPE-20.

TABLE 3

Coefficients for determining the density of liquid phases

Stationary phase	Abbreviation	Temperature of measurement (°C)	Coefficients	
			A	B
Fomblin YR		70—160	1.9696	2.0215×10^{-3}
Fluorad FC-430		70—130	1.2180	1.0205×10^{-3}
Poly(perfluorophenylene ether)	PFF-20	70—160	1.8944	1.7843×10^{-3}
Poly(phenylene ether)	PPE-5	100—160	1.2212	0.8553×10^{-3}
	PPE-20	150	$\rho = 1.2945$	

Column packings and evaluation

Column packings containing 5—20% (w/w) of liquid phase were prepared by using the rotary evaporator technique. Freon-113 was used as the slurry solvent for the perfluorocarbon phases except as noted in the text. Tetrahydrofuran was used for the other liquid phases. After coating, the packings were dried in a fluidized-bed drier and sieved to remove fines prior to packing them into glass columns (1—3.5 m long, 2 mm i.d.) with the aid of suction and gentle vibration. Soxhlet extraction for 20—30 h with the coating solvent was used for accurate determination of individual phase loadings [29]. Prior to use, some packings were conditioned by on-column silanization. Approximately 50 μl of Silyl-8 column conditioner was injected slowly into the column held at about 100°C. Afterwards, the column was conditioned at the same temperature for several hours until a stable baseline was obtained. The above treatment was repeated as many times as necessary to obtain maximum column efficiency and minimum peak tailing. For Chromosorb-P supports, several sequential treatments over one to two days were usually required.

For column evaluation, a Varian 3700 temperature-programable gas chromatograph (Varian, Palo Alto, CA) with heated on-column injectors and a flame-ionization detector was used. The carrier gas was nitrogen, adjusted to a known flow rate of ca. 20 ml min^{-1}. Data were recorded on a Spectra-Physics SP4100 computing integrator (Spectra-Physics, Santa Clara, CA) and calculations were performed off-line by an IBM-PC using programs written in BASIC and described elsewhere [30].

In general terms, the several contributions to retention in gas-liquid chromatography can be represented [31, 32] by

$$V_N = K_L V_L + K_{LS} A_{LS} + K_{GS} A_{GS} \quad (2)$$

where V_N is the net retention volume per gram of support, V_L is the volume of liquid phase per gram of support, K_L is the gas-liquid partition coefficient, K_{LS} is the coefficient for adsorption at the gas-liquid interface, K_{GS} is the coefficient for adsorption at the gas-support interface, A_{LS} is the

surface area of the liquid phase, and A_{GS} is the available surface area of the support surface.

The net retention volume was determined by using the equation

$$V_N = \tfrac{3}{2}\ ((P^2 - 1)/(P^3 - 1))(t_R - t_m)\ F_a(T_c/T_a)\ (1 - P_W/P_a) \quad (3)$$

where P is P_i/P_a, P_i is the column inlet pressure, P_a is the column outlet pressure, t_R is the retention time, t_m is the dead time (assumed to be equal to the retention time of methane at T_c), F_a is the column flow rate measured at atmospheric pressure, T_c is the column operating temperature, T_a is the ambient temperature, and P_W is the vapor pressure of water at T_a. Column flow rates were measured with a soap-film bubble meter. Corrections for gas-phase imperfections were not made.

The gas-liquid partition coefficient, K_L, can be evaluated from Eqn. 2 after rearrangement to

$$V_N/V_L = K_L + (A_{LS}K_{LS} + A_{GL}K_{GS})/V_L \quad (4)$$

The gas-liquid partition coefficient is obtained as the intercept on the V_N/V_L axis from a plot of V_N/V_L vs. $1/V_L$. Equation 4 is valid when the solute is either at infinite dilution or zero coverage with respect to all possible retention mechanisms or at constant concentration independent of V_L.

From the gas-liquid partition coefficients, the corrected retention indices for McReynolds test probes were calculated [31] from

$$I^C_{PH}(P) = 100z + 100[(\log K^P_L - \log K^z_L)/(\log K^{z+1}_L - \log K^z_L)] \quad (5)$$

where $I^C_{PH}(P)$ is the retention index for probe P corrected for interfacial adsorption on phase PH, K^P_L the gas-liquid partition coefficient for probe P, K^z_L the gas-liquid partition coefficient for an n-alkane with z carbon atoms eluting immediately before probe P, and K^{z+1}_L the gas-liquid partition coefficient for an n-alkane with $z + 1$ carbon atoms eluting immediately after probe P.

The partial molar Gibbs free energy of solution for a methylene group was determined by the method of Golovnya and Misharina [33] from

$$\Delta G(CH_2) = -2.303\ RT_c b \quad (6)$$

where $\Delta G(CH_2)$ is the partial molar free energy of solution for a methylene group, R the universal gas constant, T_c the column temperature, and b the slope of a plot of log K_L vs. carbon number for a homologous series of n-alkanes, fatty acid methyl esters, n-bromoalkanes, etc.

RESULTS AND DISCUSSION

Systematic studies of the chromatographic properties of highly fluorinated stationary phases are lacking. It is generally recognized that perfluorocarbon phases, particularly perfluoroalkanes, are difficult to coat efficiently on all supports. The temperature tolerance of these phases is frequently

governed by film instability rather than by vapor-pressure considerations. The retention mechanism of organic solutes on highly fluorinated phases has never been established. The contributions made by adsorption mechanisms to retention remain unknown, which compromises the correct interpretation of available data. From the correct evaluation of retention data, it should be possible to establish in a clear and unambiguous manner the strength of dispersive interactions in highly fluorinated and analogous hydrocarbon phases. The present research was undertaken to address these questions.

Preparation of efficient column packings with highly fluorinated phases

Several methods were evaluated for the preparation of efficient column packings with the three highly fluorinated phases selected for study. The results obtained were dependent on the structures of the stationary phases, the solvent used for coating, and the nature of the support and its chemical treatment. These properties are interrelated and are not readily considered in isolation. However, certain general features can be deduced.

The selection of the coating solvent is very important. Because Fomblin YR is only soluble in Freon-type solvents, these solvents were used in this work. These solvents are also appropriate for the PPF-20 and Fluorad FC-430 phases. These phases are reasonably soluble in a wide range of solvents but consistently produce less efficient packings when coated from solutions of non-fluorinated solvents. The effect of the coating solvent was most marked for PPF-20 where differences of 2—5 fold in the efficiency of column packings were noted.

The four chromatographic supports evaluated were Chromosorb W-AW, Chromosorb P-AW, Gas-Chrom Q, and Carbopack B. For all three phases, the worst results were obtained on Gas-Chrom Q where typical column efficiencies averaged 150—350 plates per meter. Also noticeable on Gas-Chrom Q was that symmetrical peaks could be obtained for the separation of test mixtures at 40°C, but after heating briefly to 100—150°C, and returning the column to 40°C for re-evaluation, asymmetric peaks with diminished retention were obtained. This suggests that the stationary-phase films formed on Gas-Chrom Q are unstable and redistributed themselves unevenly on the support surface at higher temperature.

A striking difference was found between the coating characteristics of Fluorad FC-430 and Fomblin YR and PPF-20 phases on Chromosorb W-AW and P-AW. Both of these supports gave stable efficient packings with Fluorad FC-430. Column efficiencies similar to those obtained for conventional phases coated on the same batch of support were obtained. Fomblin YR and PPF-20, by contrast, did not provide efficient packings when coated onto Chromosorb W-AW. The difference in efficiency between packings prepared with Chromosorb W-AW and Chromosorb P-AW is about 2-fold. A further increase in efficiency was obtained by on-column silanization of the coated packings. Partial or exhaustive silanization prior to coating was not an effective method of film stabilization.

The influence of on-column silanization can be gleaned from the representative results for PPF-20 at a 7% (w/w) phase loading on Chromosorb P-AW (Table 4). On-column silanization causes deactivation of the support with a reduction in peak tailing for polar probes and an increase in film homogeneity and stability. Neither PPF-20 nor Fomblin YR shows strong support deactivation, as can be seen from the large reduction in retention of hexanol, 1,4-dioxane, and to a lesser extent nitrobenzene, on the silanized compared to the unsilanized support. The efficiency of all probes, including those for which adsorption is not the dominant retention mechanism, is improved markedly after silanization, attesting to the improved film-forming properties. The importance of solute-support interactions is also seen in Fig. 1. The change in slope of the dipolar and hydrogen-bonding probes on the silanized and unsilanized surfaces is noteworthy. Support interactions play a significant role in the retention mechanism on the unsilanized support.

The film-forming properties of the three highly fluorinated phases on Chromosorb P-AW can also be judged by their temperature tolerance. The maximum allowable column-operating temperature for Fluorad FC-430 (250°C) corresponds to the vapor-pressure limit or thermal stability of the phase. For Fomblin YR, the vapor-pressure limit corresponds to 275°C, although the column-operating limit is lower, at 255°C. Heating Fomblin YR packings above 255°C results in a loss of efficiency caused by breakdown of the stationary-phase film. For PPF-20, thermal decomposition commences slowly at 250°C but again the column-operating limit is lower at 210°C because of disruption of the stationary-phase film at higher temperatures.

Some experiments were done with PPF-20 and Carbopack B as support. Carbopack B, with a surface area of ca. 100 m^2 g^{-1}, should provide a more energetic surface for film building. However, as demonstrated in Fig. 2, the

TABLE 4

Influence of on-column silanization of the chromatographic properties of a 7% (w/w) phase loading of PPF-20 on chromosorb P-AW at 100°C

Solute	Unsilanized packing		On-Column silanized packing	
	Retention time (min)	Column efficiency (N m^{-1})	Retention time (min)	Column efficiency (N m^{-1})
Dodecane	2.25	700	2.93	1000
Hexanol	2.17	850	0.77	—
1,4-Dioxane	2.21	—	0.42	—
Iodobenzene	3.21	1200	3.65	1300
Nitrobenzene	10.64	1000	9.35	1500
o-Dichlorobenzene	3.17	1450	3.62	1900

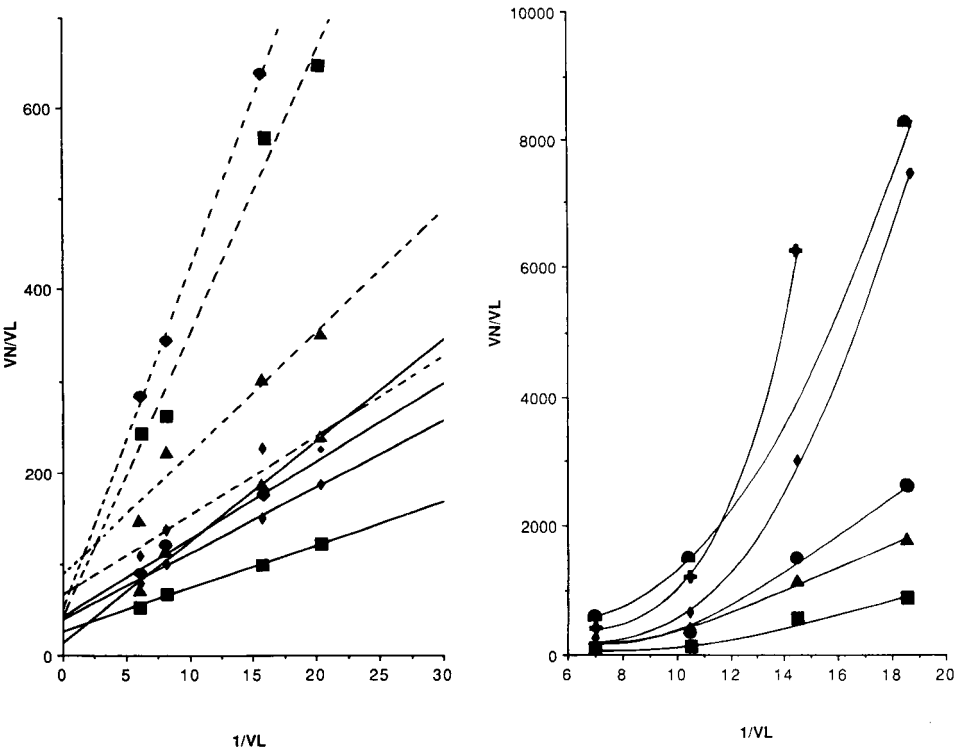

Fig. 1. Plots of V_N/V_L vs. $1/V_L$ for a series of test probes on PPF-20. The support was Chromosorb P-AW: (—) silanized on-column; (- - -) unsilanized. Probe identification: (▲) decane; (●) hexanol; (■) 1,4-dioxane; (◆) nitropropane.

Fig. 2. Plots of V_N/V_L vs. $1/V_L$ for a series of test probes on PPF-20 coated onto Carbopack B at 120°C. Probe identification: (▲) nonane; (●) iodobutane; (■) butanol; (◆) 2-octyne; (+) xylene; (▲) 2-pentanone.

retention properties of the packings were dominated by support-solute interactions. The liquid-phase acted as a modifier by reducing retention at high phase loading. Because our interests were in the solvent properties of the highly fluorinated phases, no further studies were done with Carbopack B.

The column efficiency and temperature tolerance of the highly fluorinated polymers studied here is much greater than that generally noted for other such phases in the literature. This is clearly related to the structure of the polymers. Similar column-preparation procedures for perfluorohydrocarbon phases, for example, provided poor quality packings as judged against the above results. The fluorocarbon groups in these phases may contribute to the good wetting characteristics of the phases but cannot be expected to make a significant contribution to film stability because of their weak interactions with the support surface. The polar functional groups present in the polymers must be responsible for this property. For Fomblin YR and

PPF-20, the "anchor groups" for film stabilization are the ether oxygens that are present in each monomer unit of the polymer. The structure of Fluorad FC-430 is proprietary information. Its ^{1}H-, ^{19}F-, and ^{13}C-NMR spectra and infrared spectra, however, indicate that it is a fluoroalkyl ester with isolated CH_2 and CF_2 groups in an unknown ratio. There is also evidence for the presence of a hydroxyl group. It is probably the presence of the ester and hydroxyl groups that contribute to the favorable film-stabilizing and support-deactivating properties of this phase.

Relationship between phase structure and retention mechanism

Any fundamental understanding of the retention properties of a stationary phase presupposes a knowledge of all possible mechanisms involved in retention. No such studies are available for highly fluorinated phases so that any conclusions drawn from earlier studies concerning the solution behavior of organic solutes are highly speculative. One important unresolved question is whether the highly fluorinated phases behave as solvents at all, or whether their low retention of solutes can be explained by weak gas-liquid adsorption interactions.

Fluorad FC-430 shows nearly ideal behavior for a partitioning system (Fig. 3). The phase is a good support-deactivating agent and there is little evidence for significant adsorption by the support or for adsorption at the liquid surface for most solutes. The gas-liquid partition coefficients and McReynolds phase constants, after correction for interfacial adsorption, calculated from Eqn. 5 are given in Table 5.

In the case of Fomblin YR, insufficient retention of the McReynolds probes at 100 or 120°C prevented the accurate measurement of phase constants. Reducing the temperature to 45°C provided reasonable retention values but because of significant adsorption interactions (Fig. 4A) and a greater than desirable scatter in the experimental data, accurate partition coefficients were unobtainable. For comparison purposes, a second set of less volatile probes and a higher temperature were used. In this instance (Fig. 4B) more homogeneous data were obtained and reliable values for the gas-liquid partition coefficients are given in Table 6. One striking feature of these data is the much smaller partition coefficients for the solutes on Fomblin YR compared to PPF-20 and PPE-5. This difference exceeds an order of magnitude in some instances. The difference in partition coefficients between PPF-20 and PPF-5 is smaller, being about a factor of two or less for the fluorinated phase.

Data for the retention of test solutes on PPF-20 are presented in Fig. 5A. Interfacial adsorption makes a substantial contribution to the retention of most organic solutes. The gas-liquid partition coefficients, calculated from Eqn. 5, and corrected McReynolds phase constants for PPF-20 are given in Table 7. For comparison purposes, similar data are presented in Table 7 for PPE-5. Most test probes show substantial adsorption on PPE-5 (Fig. 5B) although the contribution made by interfacial adsorption to retention is less

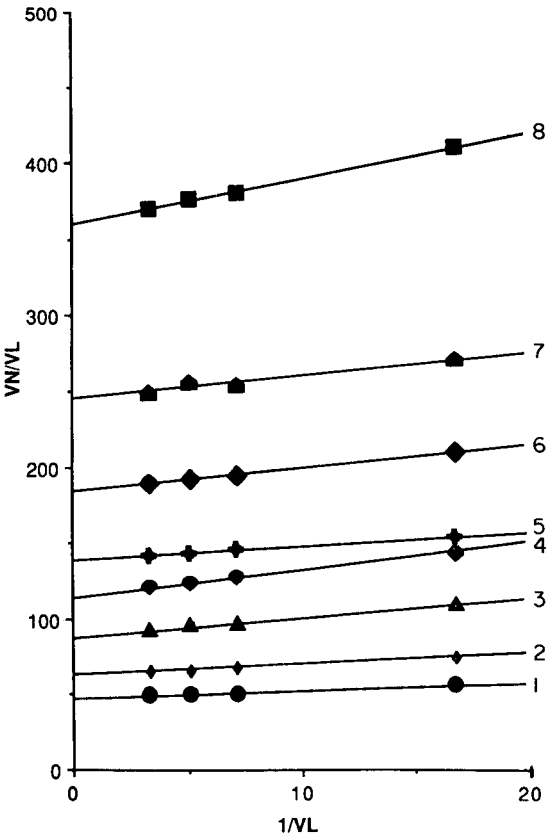

Fig. 3. Plots of V_N/V_L vs. $1/V_L$ for a series of test probes on Fluorad FC-430 at 100°C. Probe identification: (1) benzene; (2) 2-pentanone; (3) 1,4-dioxane; (5) 2-octyne; (6) nitropropane; (7) chlorobenzene; (8) undecane.

TABLE 5

Gas-liquid partition coefficients and corrected McReynolds phase constants for fluorad FC-430 at 100°C

Test solute	Partition coefficient	Phase constants	Test solute	Partition coefficient	Phase constants
Benzene	47.2	158	2-Octyne	138.8	123
n-Butanol	114.3	355	1,4-Dioxane	88.0	251
2-Pentanone	63.5	229	Octane	41.7	—
1-Nitropropane	184.1	353	Nonane	91.2	—
2-Methyl-2-pentanol	116.3	252	Decane	183.5	—
			Undecane	360.4	—
Iodobutane	130.8	137	Dodecane	688.0	—

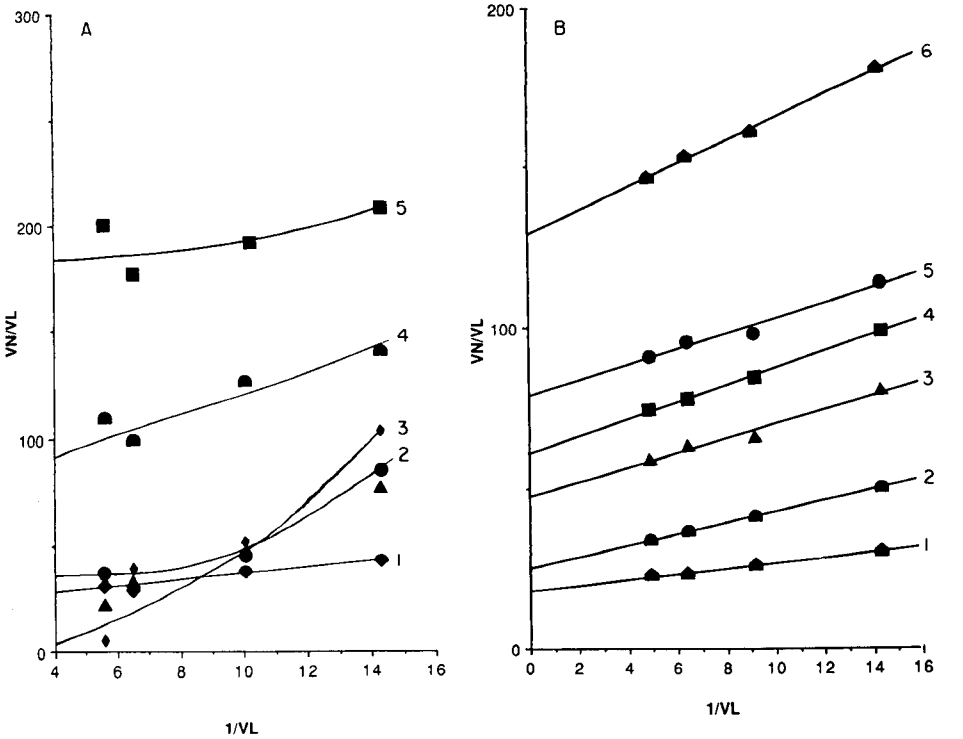

Fig. 4. Plots of V_N/V_L vs. $1/V_L$ for a series of test probes on Fomblin YR at 45°C (A) and at 100°C (B). Probe identification in A: (1) toluene; (▲) 2-pentanone; (2) nitropropane; (3) n-butanol; (4) nonane; (5) iodobenzene. Probe identification in B: (1) tridecane; (2) benzaldehyde; (3) acetophenone; (4) n-octanol; (5) naphthalene; (6) anisole.

TABLE 6

Gas-liquid partition coefficients at 100°C for test solutes on Fomblin YR, PPF-20, and PPE-5

Test solute	Partition coefficient			Test solute	Partition coefficient		
	Fomblin YR	PPF-20	PPE-5		Fomblin YR	PPF-20	PPE-5
Nitrobenzene	62.5	1346	2293	n-Octanol	60.8	284	799
Dodecane	70.3	309	654	Acetophenone	47.4	1397	1865
Tridecane	93.0	604	1289	Benzaldehyde	25.3	570	869
Naphthalene	78.8	3091	3392	Anisole	18.2	312	436

than was found for PPF-20. In terms of the selectivity of the two phases, PPF-20 shows a large increase in proton-donor interactions (perhaps because of the presence of a phenol group in its structure) and a more modest increase in proton acceptor and orientation interactions. These enhancements in selective interactions are accompanied by smaller phase constants for benzene and 2-octyne, indicating a reduction in the strength of dispersive (or charge-transfer) interactions for PPF-20 compared to PPE-5.

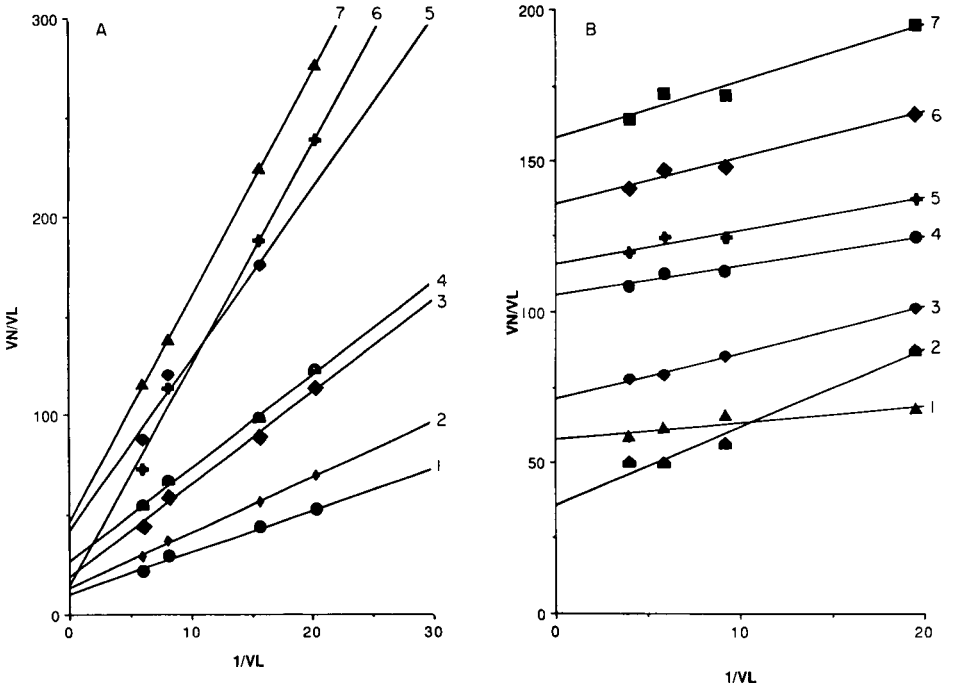

Fig. 5. Plots of V_N/V_L vs. $1/V_L$ for a series of test probes on PPF-20 (A) and on PPE-5 (B) at 100°C. Probe identification in A: (1) n-butanol; (2) 2-octyne; (3) benzene; (4) 1,4-dioxane; (5) hexanol; (6) decane; (7) ethylbenzene. Probe identification in B: (1) benzene; (2) octane; (3) 2-methyl-2-pentanol; (4) 1,4-dioxane; (5) toluene; (6) nitropropane; (7) 2-octyne.

TABLE 7

Gas-liquid partition coefficients and corrected McReynolds phase constants for PPF-20 and PPE-5 at 100°C

Test solute	Partition coefficient		Phase constant	
	PPF-20	PPE-5	PPF-20	PPE-5
Benzene	21.2	57.5	123	208
Butanol	13.2	47.1	299	244
2-Pentanone	37.3	65.2	460	251
Nitropropane	64.6	118.4	396	308
2-Methyl-2-pentanol	30.3	71.1	308	200
Iodobutane	21.7	106.7	80	128
2-Octyne	34.7	157.9	8	158
1,4-Dioxane	45.6	105.6	321	290
Octane	—	35.7		
Nonane	11.5	78.5		
Decane	37.6	161.1		
Undecane	39.0	331.2		
Dodecane	76.4	669.3		

Relationship between phase structure and dispersive contributions to retention

Of particular interest to this study is the notion that dispersive interactions in highly fluorinated phases are substantially lower than those in conventional phases. The change in relative strength of dispersive interactions is unlikely to be accurately reflected in the values for the McReynolds phase constants because of a degree of compensation created by using a relative retention scale determined by the chromatographic properties of the hydrocarbons. A more accurate measurement of dispersive interactions can be obtained from the partial molar free energy of solution for a methylene group, calculated from Eqn. 6 for a series of homologous compounds such as the n-alkanes, 2-alkanones, 1-bromoalkanes, or saturated fatty acid methyl esters (Table 8). For the three highly fluorinated phases, at 100°C the partial molar free energy per methylene group for Fomblin YR is substantially lower than for the other phases, PPF-20 is intermediate in value, and Fluorad FC-430 and PPE-5 have similar values. At 150°C, the partial molar free energy per methylene group for PPE-20 and PPF-20 are similar in value. These data allow several interpretations of which the following points are probably the most important. The weakest dispersive interactions occur with Fomblin YR which is the only phase with completely perfluorinated alkyl groups. Fluorad FC-430 contains partially fluorinated alkyl groups (although its exact structure and ratio of CF_2 to CH_2 group are unknown) and exhibits dispersive interactions which are close to those of the unfluorinated phase

TABLE 8

Partial molar free energy per methylene group for different phases

Stationary phase	Temp. (°C)	Homologous series	Range	Correlation coefficient	Slope[b]	Free energy per CH_2 group (cal mol^{-1})
Fomblin YR	100	n-Alkanes	C_{13}—C_{17}	0.9998	0.181	—309
PPF-20	100	n-Alkanes	C_7—C_{12}	0.9990	0.272	—463
Fluorad FC-430	100	n-Alkanes	C_8—C_{12}	0.9996	0.302	—515
PPE-5	100	n-Alkanes	C_8—C_{12}	0.9997	0.318	—542
PPE-20	150	n-Alkanes	C_{13}—C_{17}	0.9998	0.190	
	150	1-Bromoalkanes	C_7—C_{11}	0.9997	0.203	
	150	2-Alkanones	C_6—C_9	0.9998	0.205	Average
	150	FAME	C_7—C_{10}	0.8922	0.199	—385
PPF-20	150	n-Alkanes	C_{13}—C_{17}	0.9999	0.222	
	150	1-Bromoalkanes	C_7—C_{11}	0.9991	0.224	
	150	2-Alkanones	C_6—C_9	0.9977	0.218	Average
	150	FAME	C_7—C_{11}	0.9974	0.195	—415

[a]FAME, saturated fatty acid methyl esters. [b]Obtained from a plot of log K_L vs. carbon number; b term in Eqn. 7.

PPE-5. Thus, perfluorination of the alkyl chains seems to be important in reducing dispersive interactions to low values. The PPE-20 and PPF-20 phases have a similar number of rings and a similar free energy. In this case, the reduction in dispersive interactions must be offset by the large increase in molecular weight for the PPF-20 phase. Alternatively, it is known that strong interactions exist between hydrocarbon and perfluoroaromatic compounds, caused either by charge-transfer interactions or by increased dispersive interactions attributed to the greater polarizability of fluorinated aromatic compounds [34, 35]. From a totally pragmatic point of view, without any attempt to argue a weak case based on inadequate supporting physical data, there seems to be little significant lowering of dispersive interactions in the perfluoroaromatic systems indicated by the experimental data in Table 8. The candidacy, therefore, of perfluoroaromatic stationary phases seems to be not as well founded as that of the perfluoroalkyl-containing phases.

Possible design aspects of new highly fluorinated stationary phases

None of the phases studied so far is ideal for preparing open tubular columns. In most instances, the problem is one of limited film stabilizing properties of the highly-fluorinated phases at elevated temperatures and not limited thermal stability of the phases themselves (except for PPF-20 which decomposes at 250°C). Thus, there remains a need for highly fluorinated phases that can be used at high temperatures to enable very high-molecular-weight compounds (by gas chromatographic standards) to be separated without compromising column efficiency.

The last few years have witnessed several major advances in open tubular column technology that have a direct bearing on the desirable properties of new stationary phases [36]. Ease of handling combined with a high degree of chromatographic inertness, unmatched by other glasses, quickly led to the widespread acceptance of fused silica columns. However, most liquid phases show poor film-fixation properties on fused silica which resulted in the development of new surface-preparation procedures and new phases specifically for fused silica column preparation. New high-viscosity gum phases were introduced for the preparation of thermally stable films. Gum phases show superior film-fixation properties that resist droplet formation at high temperatures. Immobilized phases were also developed around the same time as the gum phases. Immobilized phases are prepared by bonding some functional group of the liquid phase to the column wall, or by cross-linking the stationary phase in situ to form a nonextractable rubber, or a combination of both techniques. Stationary-phase immoblization has been achieved by two different mechanisms. In early studies, columns were coated with α,ω-hydroxypolysiloxane prepolymers and then polymerized in situ by thermosetting in the presence of ammonia or some similar catalyst. An alternative approach involves free-radical cross-linking of long polymer chains by using peroxides, azo compounds, γ-radiation, etc., as free-radical

catalysts. In this case, cross-linking, which is deliberately kept low (0.1—1.0%), occurs through the formation of Si—C—C—Si bonds. This approach has proven successful for only polysiloxane and poly(ethylene oxide) phases; the former are generally purposefully synthesized to incorporate easily cross-linked functional groups such as vinyl, octyl, or tolyl groups in their structure. The first question worthy of consideration is whether these aspects of modern column technology can be adapted to the synthesis of highly-fluorinated stationary phases.

Among the varied possibilities, perfluorocarbon-siloxanes with fluorine attached to α- or β-carbon atoms have low thermal stability [37, 38]. Hybrid poly(fluorocarbonsiloxanes), e.g., structure I, are thermally stable and easily

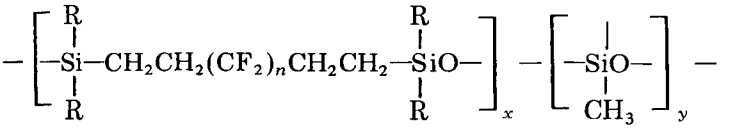

($R = CH_3$ or $C_5H_4F_7$, $n = 1—10$, y is a few % of x)

synthesized gum materials that can be cross-linked in the same way as other siloxanes [39—41]. In polymers of this kind, the concentration of perfluorocarbon groups is comparatively low and may not have sufficient impact on the properties of the phase to produce materials significantly different from conventional phases in terms of the strength of dispersive interactions.

The poly(perfluoroalkyl ethers) such as Fomblin YR show remarkable thermo-oxidative stability and chemical inertness [42]. The same lack of chemical reactivity that imparts these properties to the polymers, however, also precludes their cross-linking to elastomer gums by free radical initiation. One possible solution to the problem would be to synthesize poly(perfluoroalkyl ethers) containing substituents that might easily be cross-linked. Copolymerization of hexafluoropropene oxide with 4-bromoheptafluoro-1,2-epoxybutane could be used to provide a perfluorinated polymer that could be cross-linked through the pendant bromine group using free-radical cross-linking reagents [43]. On the debit side, the difficult synthesis of the prepolymers has not been successfully optimized so far.

The poly(perfluoroalkyl ethers) are prepared by the anionic polymerization of hexafluoropropylene oxide or the symmetrical diadduct of hexafluoropropylene oxide with oxalyl fluoride [44—47]. Polymers prepared in this way are monofunctional materials. To overcome this limitation the prepolymers, which contain reactive acyl fluoride end groups, could be derivatized by suitable reagents to introduce cross-linking or chain-extension sites. Some possibilities include reaction with ammonia to form perfluoroether dinitrile monomers that can be thermally set to polytriazine polymers (gum-like materials) thermally stable to over 400°C [47, 48] or by copolymerization of the acyl fluoride prepolymer with tricyanobenzene in the presence of *N,N'*-terphthalonitrile dioxide using thermal setting at 150—

200°C [46—49]. This latter reaction could, presumably, be achieved on the column wall during column preparation, as is normally practiced in conventional crosslinking of polysiloxanes.

Conclusions

In spite of a great deal of industrial and academic interest in the chemistry and physical properties of highly fluorinated compounds, their use as stationary phases in gas chromatography has yet to reach maturity. For the separation of chemically reactive substances and as a route to extending the molecular-weight range accessible by gas chromatography, they are indispensible and have no substitutes. These reasons alone are sufficient to maintain interest in the development of new highly fluorinated stationary phases synthesized specially for gas chromatography. These phases are likely to be gum materials, of high molecular weight, capable of elastomer modification by a free radical or similar cross-linking mechanism. They will also most likely contain functional groups to promote interactions between the phase and its support and perhaps also to interact with each other to reduce the temperature coefficient of viscous flow to aid film building by thermal setting, etc. Most of their structures will contain primarily perfluoroalkyl chains to impart the desired solvent properties and chemical inertness to the new phases. These materials may not be easy to synthesize, but when completed these phases should provide most of the virtues sought in the highly fluorinated phases without many of the vices of presently available materials.

REFERENCES

1 O. R. Pierce, Kirk-Othmer Encyclopedia of Chemical Technology, Vol. 10, Wiley, New York, 1980, p. 830.
2 T. M. Reed, in J. H. Simons (Ed.), Fluorine Chemistry, Academic, New York, 1964, p. 133.
3 R. D. Chambers, Fluorine in Organic Chemistry, Wiley, New York, 1973.
4 R. E. Banks (Ed.), Preparation, Properties, and Industrial Applications of Organofluorine Compounds, Wiley, New York, 1982.
5 R. E. Banks (Ed.), Organofluorine Chemicals and Their Industrial Applications, Wiley, New York, 1979.
6 T. M. Reed, Anal. Chem., 30 (1958) 221.
7 R. D. Dresdner, T. M. Reed, R. E. Taylor and J. A. Young, J. Org. Chem., 25 (1960) 1464.
8 U. Muller, P. Dietrich and D. Prescher, J. Chromatogr., 259 (1983) 243.
9 W. S. Pappas and J. G. Million, Anal. Chem., 40 (1968) 2176.
10 J. F. Ellis, C. W. Forrest and P. L. Allen, Anal. Chim. Acta, 22 (1960) 27.
11 R. H. Campbell and B. J. Gudzinowicz, Anal. Chem., 33 (1961) 842.
12 F. Vernon and G. T. Edwards, J. Chromatogr., 110 (1975) 73.
13 H. Pscheidl, E. Oberdorfer, E. Moller and D. Haberland, J. Chromatogr., 365 (1986) 383.
14 S. H. Shipotafsky and H. C. Moser, Anal. Chem., 33 (1961) 521.
15 R. S. Juvet and R. L. Fisher, Anal. Chem., 37 (1965) 1752.
16 R. S. Juvet and R. L. Fisher, Anal. Chem., 38 (1966) 1860.
17 I. Lysyj and P. R. Newton, Anal. Chem., 35 (1963) 90.

18 S. C. Dhanesar and C. F. Poole, J. Chromatogr., 267 (1983) 388.
19 S. C. Dhanesar and C. F. Poole, Anal. Chem., 55 (1983) 1462.
20 J. L. Glajch and W. G. Schindel, LC-GC Mag., 4 (1986) 574.
21 S. C. Dhanesar and C. F. Poole, Anal. Chem., 55 (1983) 2148.
22 W. W. Blaser and W. R. Kracht, J. Chromatogr. Sci., 16 (1978) 111.
23 H. J. Neu and F. J. Heeg, J. High Resolut. Chromatogr. Chromatogr. Commun., 3 (1980) 537.
24 I. Brown, I. L. Chapman and G. J. Nicholson, Aust. J. Chem., 21 (1968) 1125.
25 G. E. Baiulescu and V. A. Ilie, Stationary Phases in Gas Chromatography, Pergamon Oxford, 1975, p. 195.
26 S. A. Greene and F. M. Wachi, Anal. Chem., 35 (1963) 928.
27 W. J. Pummer and L. A. Wall, J. Res. Natl. Bur. Stand., Sect. A, 68 (1964) 277.
28 K. G. Furton and C. F. Poole, J. Chromatogr., 399 (1987) 47.
29 E. F. Sanchez, J. A. G. Dominguez, J. G. Munoz and M. J. Molera, J. Chromatogr., 299 (1984) 151.
30 K. G. Furton and C. F. Poole, Anal. Chem., 59 (1987) 1170.
31 B. R. Kersten and C. F. Poole, J. Chromatogr., 399 (1987) 1.
32 J. R. Conder and C. L. Young, Physicochemical Measurements by Gas Chromatography, Wiley, New York, 1979, p. 459.
33 R. V. Golovnya and T. A. Misharina, J. High Resolut. Chromatogr. Chromatogr. Commun., 3 (1980) 51.
34 C. R. Patrick, in R. E. Banks (Ed.), Preparation, Properties, and Industrial Applications of Organofluorine Compounds, Horwood, Chichester, 1982, p. 232.
35 F. W. Swinton, Chemical Thermodynamics, Royal Society of Chemistry Specialists Periodical Report, Vol. 2, Royal Chemical Society, London, 1978, p. 147.
36 C. F. Poole and S. A. Schuette, Contemporary Practice of Chromatography, Elsevier, Amsterdam, 1984, p. 79.
37 W. W. Wright, in R. T. Conley (Ed.), Thermal Stability of Polymers, Vol. 1, M. Dekker, New York, 1970, p. 287.
38 E. D. Morgan and C. F. Poole, J. Chromatogr., 89 (1974) 225.
39 O. R. Pierce and Y. R. Kim, J. Elastoplast., 3 (1971) 82.
40 O. R. Pierce, G. W. Holbrook, O. K. Johanson, J. C. Saylor and E. Brown, Ind. Eng. Chem., 52 (1960) 783.
41 Y. K. Kim, O. R. Pierce, A. G. Smith and W. X. Bajzer, Polym. Prepr. Am. Chem. Soc., Div. Polym. Chem., 12 (1971) 489.
42 P. R. Resnik, Kirk-Othmer Encyclopedia of Chemical Technology, Vol. 10, Wiley, New York, 1980, p. 956.
43 K. L. Paclorek, T. I. Ito, J. H. Nakahara and R. H. Kratzer, Ind. Eng. Chem., Prod. Res. Dev., 22 (1983) 5.
44 J. T. Hill, J. Macromol. Sci., A8 (1974) 499.
45 H. S. Eleuterio, J. Macromol. Sci., Chem., 6 (1972) 1027.
46 E. J. Soloski, M. C. Tamborski and T. Psarras, J. Fluorine Chem., 11 (1978) 601.
47 W. S. Rosser, J. A. Parker, R. J. DePasquale and E. C. Stump, in E. J. Vandenberg (Ed.), Polyethers, American Chemical Society Symposium Series, No. 6, Washington, DC, 1975, p. 185.
48 C. Wakselman and J. Leroy, J. Fluorine Chem., 12 (1978) 101.
49 R. E. Cochoy, J. Appl. Polym. Sci., 20 (1976) 1035.

Analytica Chimica Acta, 200 (1987) 171—179
Elsevier Science Publishers B.V., Amsterdam — Printed in The Netherlands

SEPARATION AND DETERMINATION OF TRACES OF HEAVY METALS COMPLEXED WITH HUMIC SUBSTANCES IN RIVER WATERS BY SORPTION ON INDIUM-TREATED AMBERLITE XAD-2 RESIN

MASATAKA HIRAIDE, YOSHIO ARIMA and ATSUSHI MIZUIKE*
Faculty of Engineering, Nagoya University, Chikusa-ku, Nagoya 464 (Japan)
(Received 29th January 1987)

SUMMARY

A nonionic macroreticular styrene/divinylbenzene copolymer, Amberlite XAD-2, resin is pulverized to 1—10 μm and treated with indium ions to saturate traces of cation exchange sites for the quantitative separation of humic complexes from cations. A 100-ml filtered sample is passed through an indium-treated XAD-2 column (16-mm diameter, 5 mm tall) at pH 5 at a flow rate of 2 ml min^{-1} to sorb heavy metals complexed with humic and fulvic acids. Inorganic cations and anions, EDTA complexes and colloidal hydrated iron(III) oxide are not retained on the column at all. The heavy metals sorbed on the column are then ultrasonically desorbed with 0.5 M nitric acid and determined by graphite-furnace atomic absorption spectrometry. The results for two river water samples obtained are in good agreement with those obtained when the macroreticular weak-base anion-exchanger DEAE-Sephadex A-25 is used.

Traces of heavy metals may exist in river waters in a variety of physicochemical forms, which will exhibit different geochemical behavior and biological effects. Among them, humic complexes are important because humic and fulvic acids are generally present in river waters. For the determination of humic complexes, it is necessary to separate them from co-existing metal species and to increase their concentrations.

The separation of humic complexes by sorption on a macroreticular weak-base anion-exchanger, DEAE-Sephadex A-25 (cross-linked dextran gel with diethylaminoethyl groups), column was proposed recently [1]. Negatively charged humic complexes were quantitatively sorbed on the column over a

*Atsushi Mizuike obtained the degrees of B. Eng. in Industrial Chemistry in 1947 and Dr. Eng. in 1961, both at the University of Tokyo. After some industrial experience with the Nippon Electric Company, he became Assistant, then Associate, Professor of Chemistry at the University of Tokyo and moved to Nagoya University as Professor of Chemistry in 1965. He was a Fulbright Research Scholar at Cornell University (1963—64) and received the Japan Society for Analytical Chemistry Award in 1974. He has served as Vice-president of the Japan Society for Analytical Chemistry, and on the Analytical Chemistry Division Committee of IUPAC. He is the author or coauthor of ca. 180 research papers, some 50 review articles and five books in the areas of micro and trace analysis.

0003-2670/87/$03.50

wide pH range, whereas cations and positively charged colloids were not retained at all. If anionic metal species other than humic complexes are present, however, they will be sorbed and cause a positive error.

Low-energy physical sorption [2, 3] on the nonionic macroreticular styrene/divinylbenzene copolymer, Amberlite XAD-2 resin, has been used for the concentration of humic substances from natural waters [4–6] and of organic species of trace metals from sea water [7]. The present authors tried to apply this technique to the separation of humic complexes in river waters, but significant amounts of simple metal cations were also sorbed on the resin. Mackey [8, 9] reported similar results and speculated that this phenomenon could be caused by polar impurities, i.e., oxidized products having cation-exchange capacity (e.g., carboxyl groups). Methylation of the resin in an attempt to reduce the cation sorption was not very effective [9].

In the present work, the XAD-2 resin is pulverized to 1–10-μm particles to achieve effective sorption and then treated with indium ions to saturate its cation-exchange sites. This highly selective separation method is successfully applied to the determination of traces of heavy metals complexed with humic substances in river waters by graphite-furnace atomic absorption spectrometry.

EXPERIMENTAL

Apparatus

The resin was pulverized in a Retsch model MM vibrating pulverizer (an 18-mm i.d. × 50-mm tall agate grinding vial with two agate balls of 12-mm diameter). A Branson model B-52H ultrasonic cleaning apparatus (47 kHz, 120 W) was used for purification of the resin as well as desorption of metals from the resin. Heavy metals were determined on a Nippon Jarrell-Ash AA-1 Mark II atomic absorption spectrometer with an FLA-10 graphite-furnace atomizer under the following conditions: wavelengths (in nm) Cd 228.8, Cr 357.9, Cu 324.8, Fe 248.3, In 304.0, Mn 279.5 and Pb 217.0; drying at 160°C for 15 s; decomposition at 400°C for 20 s; atomization at 1500°C (Cd), 2000°C (Mn, Pb) and 2500°C (Cr, Cu, Fe, In) for 10 s. A Shimadzu UV-180 spectrophotometer with 5-cm cells was used for the absorbance measurement at 400 nm to determine humic substances. All separation procedures were conducted in a Hitachi ECV-843 BY clean bench (class 100 cleanliness).

Reagents

A humic acid solution (0.45 mg ml^{-1}) was prepared by dissolving humic acid powder (Aldrich and Nakarai) in 0.1 *M* potassium hydroxide and filtering through 0.4-μm Nuclepore polycarbonate filters. A fulvic acid solution (1 mg ml^{-1}) was prepared by dissolving fulvic acid powder [10] in water. An indium solution (10 mg In ml^{-1}) was prepared by dissolving 1.0 g of

indium metal (99.9999% purity) in 4 ml of 14 M nitric acid and diluting to 100 ml with water. A portion of the solution was diluted to 10 μg In ml^{-1} and adjusted to pH 5 with water and potassium hydroxide. Standard metal solutions (1 mg ml^{-1} metal) were prepared from high-purity metals and potassium dichromate and were diluted to appropriate concentrations with 0.5 M nitric acid immediately before use. A synthetic fresh water (pH 7) was prepared to contain 9.8 mg Na, 1.2 mg Mg, 1.0 mg Ca, 9.2 mg Cl, 6.4 mg CO_3 and 4.8 mg SO_4 per liter [11]. The DEAE-Sephadex A-25 (0.05–0.1-mm diameter; Pharmacia) was washed ultrasonically in 0.1 M hydrochloric acid for 1 min and stored in water [1].

Preparation of the indium-treated XAD-2 column. A portion (1.5 g) of the Amberlite XAD-2 resin (0.2–0.8-mm diameter; Rohm and Haas) was pulverized to 1–10 μm, and ultrasonically washed in methanol, 2 M nitric acid and then water for 3 min each; the solutions were removed by centrifugation at 3000 rpm for 3 min. The resin was then immersed in 30 ml of indium solution (10 μg ml^{-1}, pH 5) overnight to saturate the cation-exchange sites and packed into a column as shown in Fig. 1. The Nuclepore filter was used to prevent the sintered-glass disk from becoming clogged with the resin. The dimensions of the treated XAD-2 column were 16-mm diameter, 5-mm tall, unless otherwise stated.

Recommended procedure

A water sample was filtered through a 0.4-μm Nuclepore filter (47-mm diameter, previously immersed in 1 M nitric acid and rinsed with water). A 100-ml aliquot of the filtrate, after adjustment of the pH to 5 with 0.1 M hydrochloric acid, was passed through the indium-treated XAD-2 column at a flow rate of 2 ml min^{-1} to sorb the humic complexes. The effluent was

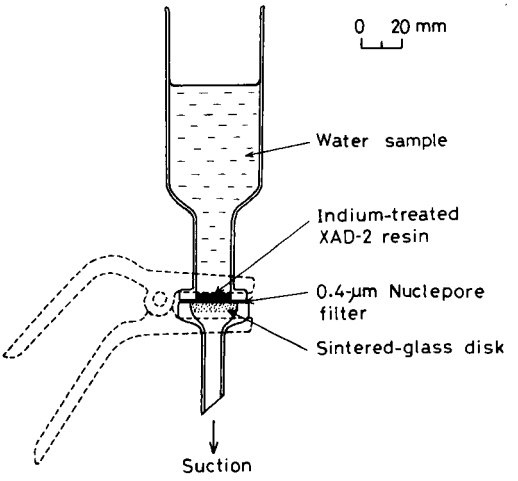

Fig. 1. Separation system.

reserved. The apparatus was disassembled to transfer the resin to a 10-ml beaker with 3 ml of 0.5 M nitric acid. The heavy metals were desorbed from the resin by ultrasonic irradiation for 1 min, and the resin was filtered off on a 0.4-μm Nuclepore filter (25-mm diameter) and washed with 2 ml of 0.5 M nitric acid. The combined filtrate was evaporated to dryness and the residue was dissolved in 1 ml of 0.5 M nitric acid. A 50-μl aliquot of the solution (after dilution, if necessary) was transferred to the graphite tube for the determination of heavy metals by atomic absorption spectrometry.

Calibration graphs, prepared with standard metal solutions in 0.5 M nitric acid, were linear up to at least 0.25 ng for cadmium and 5.0 ng for copper and lead, with maximum deviations of 0.005 ng for cadmium, 0.05 ng for copper and 0.10 ng for lead.

Other procedures

The A-25 method [1]. A 100-ml filtered sample was passed through a DEAE-Sephadex A-25 column (16-mm diameter × 5 mm) at a flow rate of 20 ml min^{-1}. The effluent was reserved. The A-25 was transferred to a 10-ml beaker with 3 ml of 4 M nitric acid and the heavy metals were desorbed by ultrasonic irradiation for 1 min. The A-25 was filtered off on a 0.4-μm filter and washed with 2 ml of 4 M nitric acid. The combined filtrate was evaporated to dryness and the residue was dissolved in 1 ml of 0.5 M nitric acid for graphite-furnace atomic absorption spectrometry.

Analysis of the column effluent for heavy metals. For synthetic freshwater samples, heavy metals in the effluent were directly determined by graphite-furnace atomic absorption spectrometry. For river-water samples, cations and other metal species in the effluent were determined after coprecipitation, extraction and evaporation as described below.

Determination of total dissolved species of heavy metals [12, 13]. To a 100-ml filtered sample was added 2 ml of indium solution (10 mg In ml^{-1}) and the pH was adjusted to 9.5 to precipitate indium hydroxide. The precipitates were centrifuged and dissolved in 1.8 ml of 8.5 M hydrobromic acid. After dilution of the solution to 3 ml (acidity 5 M) with water, the indium was extracted into 3 ml of diisopropyl ether by shaking for 2 min. The organic phase was discarded and the extraction was repeated twice more with 3 ml each of fresh diisopropyl ether. A 1-ml aliquot of the aqueous phase was evaporated to dryness and the residue was dissolved in 1 ml of 0.5 M nitric acid for graphite-furnace atomic absorption spectrometry.

Determination of humic substances. Because humic substances sorbed on the XAD-2 or the A-25 were not desorbed quantitatively even with alkaline solutions, the humic concentration was estimated separately. A 200-ml filtered river-water sample was evaporated to dryness and humic substances were extracted with 10 ml of 1 M potassium hydroxide on a water bath for 30 min. The solution was filtered through a 0.4-μm Nuclepore filter and its absorbance at 400 nm was compared with the Aldrich humic acid solution. Iron(III) was determined by graphite-furnace atomic absorption spectrometry and its contribution to the absorbance at 400 nm was corrected.

RESULTS AND DISCUSSION

Indium treatment of the XAD-2 resin

To eliminate the sorption of cations on the XAD-2 resin, pretreatment with indium ions was selected from the following reasons: (i) trivalent indium ions are sorbed more strongly on the cation-exchange sites than univalent and bivalent ions; (ii) indium would not be involved in the trace elements of interest in water analysis; (iii) indium does not interfere with the later determination step; (iv) high-purity indium metal (e.g., 99.9999% purity) is commercially available. The effectiveness of the indium treatment is shown in Table 1.

Metal anions such as chromium(VI), EDTA complexes of cadmium, copper(II) and lead and colloidal hydrated iron(III) oxide were not retained on the column at all. The amount of indium desorbed from the resin with 0.5 M nitric acid was 40–50 μg in the recommended procedure.

Sorption of humic substances on the indium-treated XAD-2 column

Metal humic complexes are expected to behave similarly to humic and fulvic acids in sorption. Therefore, 500 μg of humic or fulvic acid in 100 ml of synthetic fresh water was sorbed on the column (16-mm diameter × 5 mm) at different pH values at a flow rate of 2 ml min^{-1} and the recoveries were determined from the decrease in the absorbance at 400 nm of the effluent. As shown in Fig. 2, the sorption is quantitative between pH 3 and 5 for humic acid and at pH 3 for fulvic acid, but the recoveries are lower at higher pH values, where the dissociation of metal humic complexes is minimized. Consequently, pH 5 was selected for the sorption. When the flow rate

TABLE 1

Sorption of heavy metal cations in synthetic fresh-water samples (100 ml) on XAD-2 resin

Metal added	Amount added (μg l^{-1})		Recovery in effluent (%)	Metal added	Amount added (μg l^{-1})		Recovery in effluent (%)
Indium-treated resin				*Untreated resin*			
Cd	5.0		97, 101	Cd	5.0		84
	10		92	Cu(II)	30		37
Cu(II)	25		97, 105	Pb	30		58
	30		96	Cu(II)	50	Cu	73
	50		98	+Pb	50	Pb	74
Pb	25		96				
Cd	10	Cd	99				
+Cu(II)	50	Cu	94				
+Pb	50	Pb	95				
+Mn(II)	50	Mn	99				

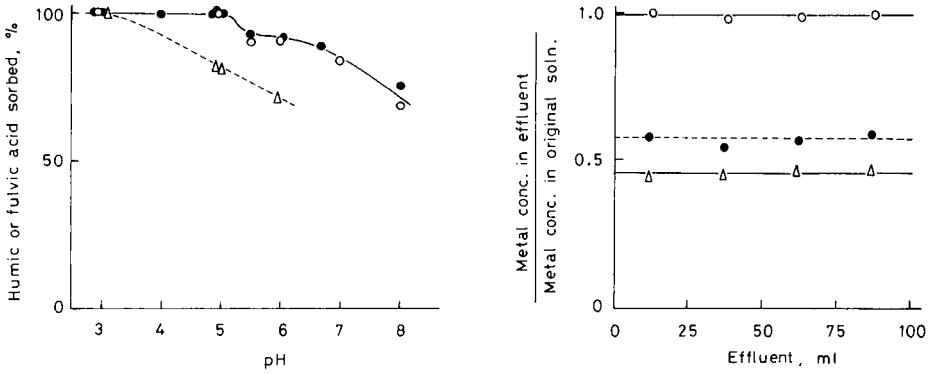

Fig. 2. Effect of pH on sorption of humic and fulvic acids: (•) Aldrich humic acid; (○) Nakarai humic acid; (△) fulvic acid.

Fig. 3. Metal recoveries in column effluent: (○) Cd; (△) Cu(II); (•) Pb. Synthetic fresh water to which 5.0 $\mu g\ l^{-1}$ Cd, 30 $\mu g\ l^{-1}$ Cu(II), 30 $\mu g\ l^{-1}$ Pb and 5000 $\mu g\ l^{-1}$ humic acid had been added was passed and 25-ml portions of effluent were analyzed.

was increased to 3 ml min^{-1}, the humic acid recovery decreased to 93% at pH 5. Without pulverization of the resin, a longer column (10 mm diameter × 100 mm) was required to obtain recoveries better than 92% at pH 5.

The specific surface area of the resin, measured by the BET method, remained unchanged before and after pulverization (306 and 294 $m^2\ g^{-1}$, respectively), which suggests that nitrogen molecules (used in the BET method) penetrate into the interstitial space of the macroreticular resin, whereas humic substances do not.

Separation of humic complexes from cations

Synthetic fresh water to which heavy metals and humic acid (Aldrich) had been added was passed through the column and the metal concentrations in effluent fractions were measured at intervals. They may change if an equilibrium shift occurs during the separation. Nearly constant recoveries were obtained as shown in Fig. 3. Because the A-25 sorption offers a reliable separation of humic complexes from cations [1], the heavy metal concentrations in the effluents from A-25 and indium-treated XAD-2 columns were compared with each other. Table 2 shows a good agreement between the two; no dissociation of humic complexes seems to occur at pH 5.

Synthetic fresh water (pH 7) to which humic acid (Aldrich) and traces of heavy metals had been added was analyzed by the recommended procedure, with the results shown in Table 3. The humic and fulvic acids sorbed on the column were not desorbed with 0.5 M nitric acid at all.

Analysis of river waters

Organic species other than humic complexes can also be sorbed on the indium-treated XAD-2 resin, depending on the aromaticity and size of the

TABLE 2

Sorption of heavy metal cations added with humic acid to synthetic fresh-water samples (100 ml) on indium-treated XAD-2 and A-25 columns

Sample	Substance added	Amount ($\mu g\ l^{-1}$)	Found in effluent (%)		
			Indium-treated XAD-2[a]	A-25[a]	A-25[b]
1	Cd	5.0	Cd 99	99	100
	+Cu(II)	30	Cu 45	48	48
	+Pb	30	Pb 57	62	60
	+humic acid	5000	HA 0	0	0
2	Cd	5.0	Cd 91	96	95
	+Cu(II)	30	Cu 36	39	37
	+humic acid	5000	HA 0	0	0
3	Cu(II)	30	Cu 38	36	35
	+humic acid	5000	HA 0	0	0

[a]pH 5, [b]pH 7, [c]HA = humic acid.

TABLE 3

Separation and determination of humic complexes and cations in synthetic fresh-water samples (100 ml)

Sample	Added	Amount added ($\mu g\ l^{-1}$)	Found ($\mu g\ l^{-1}$)		
			Humic complexes (A)	Cations[a] (B)	Total (A + B)
1	Cd	5.0	Cd 0.0	5.0	5.0
	+Cu(II)	30	Cu 14	17	31
	+Pb	30	Pb 11	18	29
	+humic acid	5000	HA —	—	—
2	Cd	5.0	Cd 0.0	5.0	5.0
	+Cu(II)	30	Cu 10	18	28
	+Pb	30	Pb 10	20	30
	+humic acid	5000	HA —	—	—
3	Cu(II)	30	Cu 21	9	30
	+humic acid	5000	HA —	—	—

[a]In effluents from the column, [b]HA = humic acid.

hydrophobic groups. Although high affinity of sodium dodecylbenzenesulfonate and sodium anthraquinonesulfonate for the XAD-2 has been reported [2], it may not be important from the viewpoint of complex formation with heavy metals as well as occurrence in uncontaminated river waters. The indium-treated XAD-2 method may cause a negative error because of incomplete sorption of fulvic acid complexes, however. In contrast, the A-25

TABLE 4

Analysis of river waters (concentrations in $\mu g\ l^{-1}$ metal)

Sample		Humic complexes		Cations etc.[a] (B)	Total dissolved species	
		Indium-treated XAD-2 method (A)	A-25 method		Calculated (A + B)	Determined
Kiso River[b]	Cd	0.00, 0.01	0.01, 0.01	0.08, 0.08	0.08, 0.09	0.09, 0.09
	Cu	0.9, 1.0	1.0, 1.1	0.6, 0.5	1.5, 1.5	1.6, 1.4
	Pb	0.2, 0.2	0.3, 0.2	0.8, 0.9	1.0, 1.1	1.1, 1.2
Shonai River[c]	Cd	0.02, 0.01	0.03, 0.05	0.09	0.11	0.11
	Cu	0.9, 0.8	1.0, 0.9	0.6	1.5	1.5
	Pb	0.2, 0.2	0.3, 0.2	0.5	0.7	0.7

[a]In effluents from the indium-treated XAD-2 column. [b]Humic substances 0.4 mg l^{-1}, Fe 29 $\mu g\ l^{-1}$. [c]Humic substances 0.5 mg l^{-1}, Fe 18 $\mu g\ l^{-1}$.

method can produce a positive error because of sorption of anionic metal species other than humic complexes.

Table 4 shows the results obtained for two river water samples, which were stored at 4°C for as short a time as possible before the analysis to minimize the change of physicochemical forms of heavy metals [14]. The blank values (μg metal l^{-1} of water) were <0.003 for cadmium and <0.06 for copper and lead for all the determinations. The results for humic complexes obtained by the two methods are in good agreement with each other, which means that the errors described above should be negligible for these samples. Also the sum of the heavy metals sorbed on the indium-treated XAD-2 column and in the effluent agreed with the independently determined concentrations of total dissolved species of the heavy metals.

The recommended procedure required ca. 2.5 h.

We are grateful to Dr. Yoshitaka Kuwahara of the Government Industrial Research Institute, Nagoya, for the measurement of the specific surface area of the resin. We also thank Profs. Shigemitsu Arai and Kyoichi Kumada of Nagoya University for providing fulvic acid.

REFERENCES

1 M. Hiraide, S. P. Tillekeratne, K. Otsuka and A. Mizuike, Anal. Chim. Acta, 172 (1985) 215.
2 R. L. Gustafson and J. Paleos, in S. J. Faust and J. V. Hunter (Eds.), Organic Compounds in Aquatic Environments, M. Dekker, New York, 1971, p. 213.
3 S. Boggs, D. G. Livermore and M. G. Seitz, J. Macromol. Sci., Rev. Macromol. Chem., 25 (1985) 599.
4 R. F. C. Mantoura and J. P. Riley, Anal. Chim. Acta, 76 (1975) 97.
5 K. L. Cheng, Mikrochim. Acta, Part II, (1977) 389.

6 J. A. Leenheer, in R. A. Minear and L. H. Keith (Eds.), Water Analysis, Vol. III, Academic, Orlando, FL, 1984, p. 83.
7 Y. Sugimura, Y. Suzuki and Y. Miyake, J. Oceanogr. Soc. Jpn., 34 (1978) 93.
8 D. J. Mackey, Mar. Chem., 11 (1982) 169.
9 D. J. Mackey, J. Chromatogr., 236 (1982) 81.
10 S. Arai and K. Kumada, Soil Sci. Plant Nutr. (Tokyo), 29 (1983) 543.
11 D. P. H. Laxen, Water Res., 19 (1985) 1229.
12 M. Hiraide, J. Mizutani and A. Mizuike, J. Chem. Soc. Jpn., (1981) 161.
13 A. Mizuike, M. Hiraide and K. Mizuno, Anal. Chim. Acta, 148 (1983) 305.
14 T. M. Florence, Talanta, 29 (1982) 345.

Analytica Chimica Acta, 200 (1987) 181—189
Elsevier Science Publishers B.V., Amsterdam — Printed in The Netherlands

INVESTIGATIONS OF THE EXTRACTION OF ADENOSINE PHOSPHATES WITH *N,N'*-DIOCTADECYL-1,4-DIAZABICYCLO-[2.2.2]OCTANE AND *N,N,N',N'*-TETRAMETHYL-*N,N'*-DIOCTADECYL-DIAMMONIUM ALKANES

YUKIO FUJII
Faculty of Engineering, Gifu University, Gifu City (Japan)
GILBERT E. PACEY*
Department of Chemistry, Miami University, Oxford, OH 45056 (U.S.A.)
(Received 2nd April 1987)

SUMMARY

The extraction of adenosine phosphates with hydrophobic cyclic diammonium or alkyl diammonium salts is described. The selectivity of these compounds is governed by two factors, the length of the spacer arm between the two ammonium nitrogens and the pH of the system. The cyclic compound exhibits less selectivity than the similar noncyclic alkyl compounds. It is shown that several of the compounds are fairly selective for adenosine 5'-triphosphate (ATP). The best of these, *N,N,N',N'*-tetramethyl-*N,N'*-dioctadecyldiammoniumethane, is tested for assay of ATP in spiked urines.

Research and development in analytical organic reagents has been heavily directed toward organic ligands for cations. Recently, Lehn and co-workers have investigated di(quaternary ammonium) ligands and macrocyclic polyamines [1—5]. Nakai and Glinsmann [6] have investigated the interaction between nucleotides and the naturally occurring polyamines putrescine, spermidine and spermine. Kimura et al. [7, 8] have also investigated a series of macrocyclic polyamines. The work of both Dietrich et al. [4, 5] and Kimura et al. [7, 8] indicates that the macrocyclic polyamines are receptors not only for inorganic anions but also for the organic phosphates, such as adenosine, mono-, di- and tri-phosphates (AMP, ADP and ATP).

Both ADP and ATP are used in clinical assays in one of several reactions between the analyte of interest and a measurable species. Commonly, neither ATP nor ADP is the species measured, because of the lack of reagent selectivity and matrix problems. However, the measurement of ATP or ADP, if possible, would eliminate the need for additional reactions in many clinical tests. Thus, there is a need for the development of selective reagents for ADP and ATP. This need has intensified the search for a reagent that is selective for ATP or ADP. Tabushi et al. [9—11] have reported the liquid-liquid extraction and transport of anions with ammonium salts such as *N,N'*-dioctadecyl-1,4-diaza-bicyclo[2.2.2]octane dichloride. This particular

0003-2670/87/$03.50

salt is a fairly effective receptor and carrier for anions of the diphosphate type. However, Tabushi et al. gave neither an explanation of the mechanism nor an optimization of the extraction when these compounds were used.

There were also some unanswered questions with respect to the need for a molecule of the bicyclic type to achieve the desired adenosine phosphate extraction. Therefore, several *N,N,N′,N′*-tetramethyl-*N,N′*-dioctadecyldiammonium alkanes were synthesized. The bicyclic and alkane diammonium compounds were studied to establish their extraction properties. This paper describes the results of the study.

EXPERIMENTAL

Reagents

1,4-Diaza-bicyclo[2.2.2]octane, 1-bromooctadecane, and *N,N,N′,N′*-tetraalkylamines were purchased from Aldrich Chemical Co. Adenosine 5′-monophosphate (AMP), 5′-diphosphate (ADP) and 5′-triphosphate (ATP) were from Sigma Chemical Co. The chloroform was spectrophotometric-grade solvent (Aldrich). All water was deionized/double glass-distilled in a Barnstead Nanopure system. All other chemicals were of analytical grade and were used without further purification.

Synthesis of diammonium salts

The bicyclic diammonium salt was synthesized as follows. A mixture of 1,4-diaza-bicyclo[2.2.2]octane (10 mmol), 1-bromooctadecane (20 mmol) and 100 ml of dimethylformamide (DMF) was stirred in a round-bottomed flask at 70°C for 2 days. After cooling, the white precipitate was separated by filtration and recrystallized from DMF. These crystals were purified further by careful recrystallization from ethanol (99.5% v/v) and dried under vacuum at 60°C.

The bromide counter-ion was converted to phosphate via the hydroxide by using silver oxide. The purity of the salt was 99.4 ± 0.5% as determined by spectrophotometric measurement after ion-pair extraction with picrate ion.

The synthesis of the *N,N,N′,N′*-tetramethyl-*N,N′*-dioctadecylammonium salts was the same as for the bicyclic compound except that the corresponding *N,N,N′,N′*-tetraalkylamine was used. The alkyl spacer between the ammonium nitrogens was varied from one CH_2 group to four groups.

Figure 1 presents the compounds investigated, and Table 1 shows the melting points, percentage yields, and NMR data for all five compounds

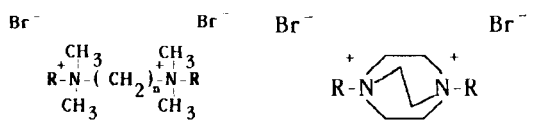

Fig. 1. Structures of the compounds used. Compounds with n = 1—4 are numbered 1—4 in Table 1. Compound 5 is the bicyclic compound.

TABLE 1

Characteristics for the diammonium salts

Diammonium salt[a]	Crystal form	Melting point (°C)	Yield (%)	NMR data, $CDCl_3$, chemical shifts (δ)
1	White granules	110—112	40	0.86 (6H CCH_3), 1.27 (6OH CH_2), 1.80 (4H $NCCH_2$), 3.50 (4H NCH_2 and 12H NCH_3).
2	Needles	185—187	85	0.90 (6H CCH_3), 1.30 (6OH CCH_2), 1.85 (4H $NCCH_2$), 3.50 (4H NCH_2 and 12H NCH_3), 4.78 (4H NCH_2CH_2N).
3	White granules	185—188	81	0.90 (6H, CCH_3), 1.29 (6OH CCH_2), 1.83 (4H, $NCCH_2$), 3.50 (4H, NCH_2 and 12H NCH_3), 3.80 (2H $NCCH_2CN$), 2.83 (4H NCH_2CCH_2N).
4	White granules	184—186	88	0.90 (6H CCH_3), 1.29 (6OH CCH_2), 1.85 (4H $NCCH_2$), 3.50 (4H NCH_2 and 12 H NCH_3), 2.80 (4H $NCCH_2CH_2CN$), 3.82 (4H NCH_2CCCH_2N).
5	Thin plates	103—104	85	0.87 (6H CCH_3), 1.30 (6OH CCH_2), 1.80 (4H, $NCCH_2$), 3.50 (4H NCH_2), 3.90 (12H NCH_2CH_2N).

[a]See Fig. 1.

synthesized. Elemental analysis was done on the bromide salts. The data obtained were as follows. For compound 1: found, 63.5% C, 11.5% H, 3.3% N; calculated for $C_{41}H_{88}N_2Br_2$, 64.0% C, 11.5% H, 3.6% N. For compound 2: found, 64.2% C, 11.75% H, 3.4% N; calculated for $C_{42}H_{90}N_2Br_2$, 64.4% C, 11.6% H, 3.6% N. For compound 3: found, 64.3% C, 11.3% H, 3.5% N; calculated for $C_{43}H_{92}N_2Br_2$, 64.8% C, 11.6% H, 3.5% N. For compound 4: found, 64.5% C, 11.4% H, 3.35% N; calculated for $C_{44}H_{94}N_2Br_2$, 65.2% C, 11.7% H, 3.45% N. For compound 5: found, 63.9% C, 10.8% H, 3.5% N; calculated for $C_{42}H_{86}N_2Br_2$, 64.8% C, 11.1% H, 3.6% N.

Extraction of nucleotides

A chloroform solution (10 ml) containing the diammonium salt and a 10-ml aliquot of aqueous solution containing the nucleotide were introduced into a 50-ml stoppered centrifuge tube. The tube was shaken for 1 h in a water bath thermostatted at 25.0 ± 0.2°C. This shaking time was found to be sufficient for complete equilibration. After centrifugation, an aliquot of the

aqueous and/or organic phases was taken and the absorbance was measured on a Hewlett-Packard 8450A (U.S.A.) or Jasco UVIDEC 430 (Japan) ultraviolet-visible spectrophotometer. The molar absorptivity of adenosine phosphates was calculated to be 1.45×10^4 (λ_{max} = 260 nm) in aqueous solution and 1.40×10^4 (λ_{max} = 262 nm) in chloroform. The pH of the aqueous solution was measured by using an Orion Research Microprocessor Ionalyzer 901.

The ionic strength, μ of the aqueous phase was kept constant at 0.03 M with sodium hydrogen phosphate. The solution of nucleotides and diammonium salt was freshly prepared, just before each experiment in order to minimize the slow hydrolysis that might occur at pH values higher than 7. A fresh solution was considered necessary because some hydrolysis had been noted (hydrolysis products less than 3%) after 4 h in a solution at pH 7.5 [12].

Extraction studies were done at pH values varying from 12.9 to 10.8 in the initial studies and at pH 8 and 3 for specific studies. In the monohydrogenphosphate buffer system (μ = 0.03, pH = 8), the equilibrium pH was adjusted to 8.00 ± 0.01 by adding a small amount of 0.1 M NaH_2PO_4 or 0.1 M NaOH solution when necessary. This addition did not significantly affect the total ionic concentration or the volume of the aqueous phase. For the pH 3 studies, a sodium dihydrogen phosphate buffer with an ionic strength of 0.03 was used. The equilibrium pH was adjusted to 3.0 ± 0.01 by adding a small amount of Na_2HPO_4 or H_3PO_4 to the solution.

RESULTS AND DISCUSSION

It was expected that the overall extraction equilibria and mechanisms would be affected by the presence of certain cations and anions in the aqueous phase. In order to evaluate this effect, competitive extractions were done by extracting an aliquot that contained both the diammonium salt and the anion or cation in question. The extractions that were done at or above pH 8 have AMP^{2-}, ADP^{3-}, and ATP^{4-} as the primary aqueous adenosine nucleotide species [13—16].

Initially, the extraction of AMP, ADP, and ATP was observed for solutions with different sodium hydroxide concentrations. The data in Table 2 show that the extraction order in most cases is AMP < ADP < ATP. The data also indicate that the extraction is not significantly influenced by the presence of sodium hydroxide in concentrations lower than 2.5×10^{-3} M. All extraction values (%) were identical within experimental error in the pH range 8—10.9. This pH range was chosen as the optimum condition because hydrolysis was slow and extraction efficiency high.

The bicyclic compound (compound 5) was the most efficient extraction reagent for all adenosine phosphate species. The diammonium ethane compound (2) which does not contain the cyclic structure but has about the same spacing between ammonium nitrogens, is an efficient extractor of ATP, but is less efficient for ADP and much less efficient for AMP.

TABLE 2

Effect of sodium hydroxide concentration on the extraction[a] of adenosine phosphates

Compound[b]	C_{NaOH} (M)	Extracted (%)		
		AMP	ADP	ATP
1	0.00063	14.5 ± 0.7	9.6 ± 0.7	25.4 ± 0.7
	0.0025	10.0 ± 0.7	7.4 ± 0.7	25.4 ± 0.7
	0.01	6.5 ± 0.7	7.1 ± 0.7	24.6 ± 0.7
	0.08	1.7 ± 0.7	0.5 ± 0.7	21.1 ± 0.7
2	0.00063	11.9 ± 0.6	66.0 ± 0.6	99.8 ± 0.5
	0.0025	4.1 ± 0.6	62.3 ± 0.6	97.8 ± 0.5
	0.01	0.7 ± 0.6	57.4 ± 0.6	97.8 ± 0.5
	0.08	0.1 ± 0.6	43.4 ± 0.6	88.2 ± 0.5
3	0.00063	2.7 ± 0.5	65.0 ± 0.6	99.8 ± 0.5
	0.0025	2.7 ± 0.5	61.9 ± 0.6	99.3 ± 0.5
	0.01	0.0 ± 0.5	51.3 ± 0.6	99.0 ± 0.5
	0.08	0.0 ± 0.5	33.9 ± 0.6	95.9 ± 0.5
4	0.00063	3.7 ± 0.5	66.4 ± 0.6	99.3 ± 0.5
	0.0025	2.4 ± 0.5	57.9 ± 0.6	98.8 ± 0.5
	0.01	1.7 ± 0.5	50.8 ± 0.6	98.0 ± 0.5
	0.08	0.4 ± 0.5	42.3 ± 0.6	94.5 ± 0.5
5	0.00063	39.6 ± 0.8	78.4 ± 0.6	99.9 ± 0.5
	0.0025	34.6 ± 0.8	76.5 ± 0.6	99.7 ± 0.5
	0.01	33.7 ± 0.8	77.4 ± 0.6	99.8 ± 0.5
	0.08	27.8 ± 0.8	60.0 ± 0.6	97.8 ± 0.5

[a]Extracting agent: diammonium bromide concentration 2×10^{-4} M; initial concentration of nucleotide in the aqueous phase, 5×10^{-5} M; equal volumes of aqueous and organic phases. The ± values denote the relative error after blank correction. [b]See Fig. 1.

The equilibria for the chemical species that appeared possible in extraction at pH 8 into the organic phase by the diammonium salt (DAX) can be written as

$$[ATP^{4-}] + 2[DAX]_o \overset{K_{ex}}{\rightleftharpoons} [(DA)_2ATP]_o + 2X^{2-}$$

$$2[ADP^{3-}] + 3[DAX]_o \overset{K_{ex}}{\rightleftharpoons} [(DA)_3(ADP)_2]_o + 3X^{2-}$$

$$[AMP^{2-}] + [DAX]_o \overset{K_{ex}}{\rightleftharpoons} [DAAMP]_o + X^{2-}$$

where X^{2-} is HPO_4^{2-}. The subscript 'o' denotes the organic phase; all other species are in the aqueous phase. The extraction constants are given by

$$K_{ex}(ATP) = [(DA)_2ATP]_o[X^{2-}]/[ATP^{4-}][DAX]_o^2$$

$$K_{ex}(ADP) = [(DA)_3(ADP)_2]_o[X^{2-}]^3/[ADP^{3-}]^2[DAX]_o^3$$

$$K_{ex}(AMP) = [DAAMP]_o[X^{2-}]/[AMP^{2-}][DAX]_o$$

When the aqueous and organic phases have the same volumes, the distribution ratios D are given by

$$D_{ATP} = [ATP]_o/[ATP] = (C_TATP - [ATP])/[ATP]$$

$$D_{ADP} = [ADP]_o/[ADP] = (C_TADP - [ADP])/[ADP]$$

$$D_{AMP} = [AMP]_o/[AMP] = (C_TAMP - [AMP])/[AMP]$$

where C_TATP, C_TADP and C_TAMP denote the initial aqueous phase concentrations of ATP, ADP, and AMP, respectively. The concentrations in square brackets represent the equilibrium concentrations. The distribution ratios for the adenosine phosphate species can also be represented by

$$D_{ATP} = [(DA)_2ATP]_o/[ATP^{4-}]$$

$$D_{ADP} = 2[(DA)_3(ADP)_2]_o/[ADP^{3-}]$$

$$D_{AMP} = [DAAMP]/[AMP^{2-}]$$

These equations can be combined with the K_{ex} expressions to arrive at the following equations:

$$D_{ATP} = K_{ex}ATP([DAX]_o^2/[X^{2-}]^2)$$

$$D_{ADP} = K_{ex}ADP([ADP^{3-}][DAX]_o^3/[X^{2-}]^3)$$

$$D_{AMP} = K_{ex}AMP([DAX]_o/[X^{2-}])$$

Therefore, a plot of log D_{ANP} vs. log$[DAX]_o$, where ANP is a general designation for the adenosine phosphates, should give a straight line with slope b which can be related to the stoichiometry.

The experimental data for ATP were fitted to a linear model by the method of least squares. The observed slope was 2.0, which implies that the extracted species is $(DA)_2ATP$. The slope for AMP was 1.0 which indicates that the extracted AMP species is AMPDA. For the ADP system, an assumption must be made about the stoichiometry of the complex. Given the ATP and AMP cases, the most logical assumption is that the complexed species is $(DA)_3(ADP)_2$. Therefore, a plot of log $D_{ADP}[ADP^{3-}]^{-1}$ vs. log $[DAX]_o$ should produce a line with slope equal to 3; the slope actually obtained was 3.0, which suggests that the species, $(DA)_3(ADP)_2$, is correct. Plots based on other DA/ANP stoichiometries did not yield slopes consistent with the model used.

The stoichiometry of these complexes was the same for all five diammonium compounds at pH 8. The only uncertainty was in the AMP cases, for which the extraction was poor (compounds 3 and 4). When the stoichiometry of the complex species had been determined, the extraction constants were evaluated; the values are shown in Table 3.

TABLE 3

Extraction constants for diammonium cations/adenosine complexes at pH 8

Compound[a]	log K_{ex}(ATP)	log K_{ex}(ADP)
2	5.24 ± 0.09	10.35 ± 0.11
3	5.08 ± 0.09	9.14 ± 0.10
4	4.87 ± 0.09	8.88 ± 0.10
5	6.05 ± 0.11	10.82 ± 0.11

[a]See Fig. 1.

Extracted species

In contrast to the poor extraction of AMP^{2-}, the extraction of ADP^{3-} and ATP^{4-} with the diammonium salt is efficient. This fact requires that some consideration be given to the species responsible for the extraction. The possible bindings between the cation and nucleotide at pH 8 are depicted in Fig. 2. The value of $K_{ex}(AMP^{2-})$ is regarded as a measure of the contribution of adenosine moiety to the extraction of geminal dianion $^{-}O—P—O^{-}$ (see species DAX and AMPDA in Fig. 2). The low value indicates that the introduction of adenosine group at the dianion $^{-}O—P—O^{-}$ results in a slight effect on the exchange extraction. Thus, the diammonium cation recognizes AMP^{2-} more favorably (by a factor of 5) than it does HPO_4^{2-}.

In order to interpret the efficiency of extraction for anions of the diphosphate type, an attempt was made to use the additivity of free energy which permits the expression of the extraction constant, K_{ex}, as the product of contributing terms $K_{ex}(1)$, $K_{ex}(2)$,..., where each of the terms is expected to contribute independently to the extraction constant. Our data give the constants, log $K_{ex}(PO^{-}) = -1.3$, log $K_{ex}(^{-}OPO^{-}) = 0$, log $K_{ex}(^{-}OPOPO^{-}) = 6.4$ and log $C = 0.7$, where C denotes the contribution of adenosine moiety to

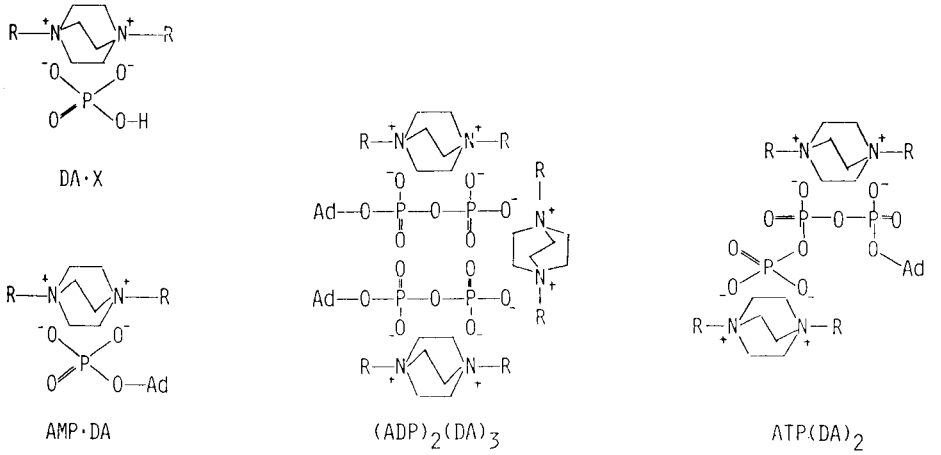

Fig. 2. Proposed binding modes of diammonium phosphates. R, $C_{18}H_{37}$; Ad, adenosine.

the extraction constant. These results show that the relative contribution of the anionic fragments on the nucleotide extraction follow in the order: $^-O—P—O—P—O^- \gg {}^-O—P—O^- > P—O^-$. The diammonium cation recognizes and extracts the vicinal anion, $^-OPOPO^-$, more selectively than the geminal anion $^-OPO^-$ by a factor $10^{6.4}$. It is therefore concluded that it is the extremely high selectivity of the cation for the diphosphate type nucleotide that leads to the efficient extraction of ATP and ADP.

From the extraction data at pH 8 and the elucidated structures of the complexes, it became obvious that the use of a lower pH in which the adenosine phosphates would be protonated should lead to a more selective extraction. When extracting from an acidic solution at pH 3, AMP, ADP, and ATP form the protonated species, H_2AMP, H_2ADP^- and H_2ATP^{2-}. Consequently, by using this pH, only H_2ATP^{2-} will be appreciably extracted from solution (Table 4). The complexation stoichiometry, based on data from mole-ratio experiments, suggests that the stoichiometry of the complex is $DA(HADP)_2$ and DAH_2ATP. These results clearly show that the selective extraction of ATP over ADP can be accomplished at pH 3 and in the presence of the diammonium ethane (compound 2). The bicyclic compound (compound 5) was not as selective for ATP under these conditions.

Interferences

Interference by other common ions was studied at pH 8 and pH 3. The relative inhibitions by foreign anions on the extraction of ATP at pH 8 are in the order $ClO_4^- > SCN^- > Br^- > Cl^- > HPO_4^{2-} > H_2PO_4^- > OH^- > CH_3CO_2^- > F^-$. A similar order was observed by Tabushi and co-workers [11]. The use of high concentrations ($>5 \times 10^{-2}$ M) of alkali metal ions such as Li^+ or Na^+ will also inhibit nucleotide extraction. The interferences of alkali metal ions are apparently due to the formation of ion-pair complexes between the alkali metal ion and the nucleotides in the aqueous phase [17]. The onset of interference by perchlorate and thiocyanate began at an ATP/interfering

TABLE 4

Extraction data for the diammonium ethane (2)[a] cation/adenosine phosphate complexes at pH 3

Concentration (M)	Extraction (%)[b]		
	AMP	ADP	ATP
1.32×10^{-4}	0.0	1.5 ± 0.5	87.5 ± 0.5
8.7×10^{-5}	0.0	3.3 ± 0.7	80.2 ± 0.5
5.7×10^{-5}	0.0	3.4 ± 0.7	66.3 ± 0.5
3.8×10^{-5}	0.0	3.3 ± 0.7	49.3 ± 0.5
2.5×10^{-5}	0.0	3.5 ± 0.7	35.4 ± 0.5
1.6×10^{-5}	0.0	3.4 ± 0.7	25.8 ± 0.6
1.1×10^{-5}	0.0	3.4 ± 0.7	19.4 ± 0.7

[a]Diammonium ethane, see Fig. 1, [b]Mean and standard deviation for 5 runs.

anion ratio of 1:2; complete elimination of ATP extraction occurred at a ratio of 1:20. For bromide, the interference began at 1:2.3 and completely eliminated ATP extraction at 1:1000. All the other ions tested began to interfere at ratios near 1:500. The potential interference by organic anions was not tested. The only ions of concern are other diphosphonates. However, most of those compounds do not have the same structural features as the adenosine phosphates and at pH 3 will not possess the same ionic charge. At pH 3 the interferences by inorganic anions were less than at pH 8. However, perchlorate and thiocyanate ions were still the major interferents.

Because the eventual goal of this research is to design ATP- and ADP-specific reagents which possess their own analytical tag, the methodology was applied to urine samples which had been spiked with ATP and ADP. The pH 3 system with the diammonium ethane (compound 2) was used in an automated flow-injection extraction system [18]. Recoveries from the spiked urine samples were in the range of 96—99% with a relative standard deviation of 2%. However, as expected, the blank was significant. This clearly suggests that the selective ATP compound should be tagged with a fluorescent molecule that emits light above 600 nm, thereby eliminating the effects of potential ultraviolet-visible interferences in the biological matrix. By eliminating the background, improved sensitivity and precision should be possible.

REFERENCES

1 J. M. Lehn, Pure Appl. Chem., 50 (1978) 871.
2 J. M. Lehn, Pure Appl. Chem., 52 (1980) 2441.
3 B. Dietrich, J. Guihem, J. M. Lehn, C. Pascard and V. E. Sonveau, Helv. Chim. Acta, 67 (1984) 91.
4 B. Dietrich, M. W. Hosseini, J. M. Lehn and R. B. Sessions, J. Am. Chem. Soc., 103 (1981) 1283.
5 B. Dietrich, M. W. Hosseini, J. M. Lehn and R. S. Sessions, Helv. Chim. Acta, 66 (1983) 1962.
6 C. Nakai and W. Glinsmann, Biochemistry, 16 (1977) 5636.
7 E. Kimura, A. Watanabe and M. Kodama, J. Am. Chem. Soc., 105 (1983) 2063.
8 E. Kimura, M. Kodama and T. Yatsunami, J. Am. Chem. Soc., 104 (1982) 3182.
9 I. Tabushi, J. Imuta, N. Seko and Y. Kobuke, J. Am. Chem. Soc., 100 (1978) 6287.
10 I. Tabushi, Y. Kobuke and J. Imuta, J. Am. Chem. Soc., 102 (1980) 1794.
11 I. Tabushi, T. Kobuke and J. Imuta, J. Am. Chem. Soc., 103 (1981) 6152.
12 M. W. Hosseini, J. M. Lehn and M. P. Mertes, Helv. Chim. Acta, 66 (1983) 2454.
13 E. R. Tucci, E. Doody and N. C. Li, J. Phys. Chem., 65 (1961) 1570.
14 G. Weitzel and T. Spoor, Z. Physiol. Chem., 47 (1958) 1701.
15 M. M. Taqui Khan and A. E. Martell, J. Am. Chem. Soc., 88 (1966) 668.
16 N. C. Melchior, J. Biol. Chem., 205 (1954) 615.
17 J. Botts, A. Chashin and H. L. Young, Biochemistry, 4 (1965) 1788.
18 B. Karlberg and S. Thelander, Anal. Chim. Acta, 98 (1978) 1.

Analytica Chimica Acta, 200 (1987) 191—211
Elsevier Science Publishers B.V., Amsterdam — Printed in The Netherlands

APPLICATION OF AMALGAM ELECTRODES IN STUDIES OF HEAVY METALS UNDER NATURAL WATER CONDITIONS

J.-P. BERNHARD, J. BUFFLE* and N. PARTHASARTHY

Department of Inorganic, Analytical and Applied Chemistry, University of Geneva, Geneva (Switzerland)

(Received 31st March 1987)

SUMMARY

The application of amalgam electrodes for measuring the degree of complexation of metal ions is described with respect to natural water conditions. The amalgam electrodes are compared with the corresponding capabilities of ion-selective electrodes. A special cell is described for preparing the amalgam and for filling a hanging amalgam drop electrode. Factors affecting the reproducibility of the standard potentials and slopes, the response time and the detection limits are discussed. Complexation measurements are described with lead and zinc amalgam electrodes. Triethylenetetramine, carbonate and nitrolotriacetic acid are used as ligands, to test the ability of these electrodes to measure correctly the degree of complexation even at low total-metal concentrations (down to ca. 10^{-7} M) and at very low concentrations of free metal ion (10^{-15} M). Results obtained with well-characterized fulvic compounds and an algal culture medium (AAP) are also reported. The observed results are in complete accordance with theoretical predictions (based on Nernstian behaviour), even at the lowest concentrations of total and free metal ion used. An important limitation is that any oxidant in the solution can interfere by oxidizing the amalgam. Solutions must be carefully degassed to eliminate oxygen. It is shown that the interfering action of oxidants can be corrected for by means of equations which are theoretically sound, even when the nature of the oxidant is unknown, provided that its content is not too high. Compared to ion-selective electrodes, amalgam electrodes are more reproducible, inexpensive and readily prepared for various metal ions which cannot be measured with ion-selective electrodes.

The importance of knowing the degree of complexation of metals for making predictions on their environmental behaviour is now well established [1—3]. It has been shown, in particular for adsorption on suspended particles, complexation by dissolved ligands or uptake by organisms, that in

*J. Buffle graduated in chemistry and biochemistry at the University of Geneva, and obtained his Ph.D. in 1969. He did post-doctoral work at the Heyrovsky Institute and at Texas A&M University. He has been Maitre d'enseignement et de recherche at the University of Geneva since 1972 and invited professor at the University of Quebec since 1982. His main interests are in environmental sciences and in the application of the methods and concepts of analytical chemistry to environmental problems. He is particularly interested in the characterization of natural aquatic colloidal and macromolecular compounds, their interactions with trace elements, and the resulting impact on the biogeochemistry of aquatic systems.

0003-2670/87/$03.50

many cases the free metal-ion concentration (or preferably its activity) is the master variable which governs the extent of the reaction. Free metal-ion activity can be measured by several methods [3], but most of these are indirect measurements based on assumptions, the validity of which often decreases with increasing complexity of the mixture of the complexes studied. The direct determination of the free metal-ion activity is the only means to circumvent the limitations introduced by making these assumptions. Unfortunately, very few methods are available for such measurements. As the total concentrations of metal ions of interest are most often below 10^{-5}—10^{-6} M [3, 4], the only usable methods reported up to now are ion-selective electrodes (ISE) (see e.g. [1, 3, 5]) and membrane ultrafiltration [6, 7]. The latter, however, cannot be applied to systems containing ligands smaller than the pore size of the membrane, and copper(II) and possibly lead(II) ISE's are the only ones suitable for application to complexation measurements in natural conditions. Although cadmium(II) and thallium(I) ISE's have been described, they are not usable below 10^{-5} M.

Besides the dearth of usable electrodes, four problems limit their application to determinations of free metal-ion concentrations in natural waters [3]. The problems can be understood from Fig. 1. At constant ionic strength, the potential E of an ISE sensitive to a given metal ion M is given [8] by

$$E = E_0 + S \log [M] \quad (1)$$

where [M] is the free metal ion concentration. In non-complexing medium, $[M] = [M]_t$, whereas in complexing medium, $[M] = [M]_t/\alpha$. Here, $[M]_t$ is the total metal concentration, α is the degree of complexation ($\alpha > 1$), and E_0 is a constant depending on the whole potentiometric assembly, the activity coefficient of M and a constant which depends on the nature of the reaction between M and the membrane. For Nernstian behaviour, the theoretical value of S is $2.303\ RT/zF$, where z is the charge of M. In practice, both E_0 and S are measured experimentally from the calibration curve.

The four problems mentioned above are as follows. First, the precision and reproducibility of E and E_0 are often inadequate [3, 9]: an error of 1 mV in E or E_0 corresponds to an error of 8% in [M]. This implies that, to obtain precise [M] data, the precision in the potential reading should be 0.1 mV and therefore the reading must be taken when the potential drift is less than 0.02 mV s^{-1}. Such a condition is not easily fulfilled with many ISE. Still worse is the fact that the reproducibility of E_0 from one calibration to another is often not better than 2—3 mV. Secondly, the lower limit (LL, Fig. 1) of the usable total metal concentration [3] is generally not lower than $[M]_t = 10^{-6}$ M. This is caused by contamination of the test solution by the membrane itself by processes (solubilization or adsorption/desorption) which are not easy to avoid or control. Further decrease of the LL below 10^{-6} M, i.e., extension of the $[M]_t$ range in the domain of aquatic conditions, seems difficult to achieve with such electrodes. The third problem is the limit of Nernstian behaviour in complexing medium, at $[M]_t$

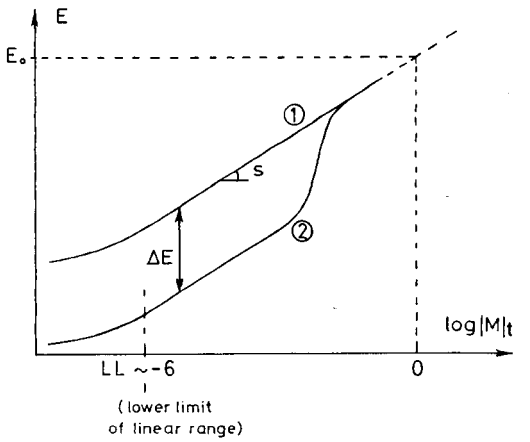

Fig. 1. Schematic representation of limits of application of potentiometric electrodes to complexation measurements. (1) Calibration curve ($\alpha = [M]_t/[M] = 1$); (2) curve obtained in complexing solution ($\alpha > 1$). S, slope of the calibration curve; LL, lower limit of the linear range. The jump in curve 2 corresponds to saturation of the ligand.

> LL. In complexing medium, [M] is computed from the experimentally measured value of E and by using E_0 and S values obtained from the calibration curve, assuming Eqn. 1 to be valid. This implies that thermodynamic equilibrium (i.e., very fast exchange of M) exists between the membrane and the solution [3]. In some cases, it has been shown [8] that this exchange is indeed fast, so that Nernstian behaviour is observed down to very low free M concentrations (e.g., $<10^{-15}$ M for silver ions). However, the exchange-rate constants are often not very large and not well defined. Thus, the limit of applicability of Eqn. 1 in complexing medium is often either unknown or rather limited. The fourth problem is adsorption of compounds at the electrode surface. With a solid non-renewable electrode, the electrode surface (and so the values of E_0 and S, and the exchange rates) may be modified by transference from the pure calibration solution to the complex test medium, owing to adsorption of surface-active compounds. Regenerating the surface to give correct values of E_0, S and response time is often not easy.

Owing to these limitations, the use of amalgam electrodes instead of ISE seems to be attractive. Amalgams are formed by many metals including Pb, Tl, Cd and Zn which are of environmental importance and for which good ISE are not available. The charge-transfer rate constants between the amalgamated metal and its ion are well-known and often large [3] so that stable E_0 values and Nernstian behaviour down to very low activities can be obtained. In principle, renewable electrode surfaces can be obtained by using the hanging mercury drop electrode (HMDE) commonly used in stripping voltammetry. This enables problems related to the previous "history" of the electrode, e.g., adsorption, to be avoided. A further advantage is that the

detection limit can be expected to be governed by the oxidation of the amalgam by the oxidants in solution, their influence being predictable and only slightly dependent on the amalgam composition.

The aim of this work was to test some of these points by using lead and zinc amalgams. These two metals were chosen because of their environmental importance and the large differences in their reduction properties and charge-transfer rate constants (0.8 and 0.05 cm s^{-1} in 1 M KNO_3 and 0.1 M $NaNO_3$, respectively [10]). It was expected, therefore, that the results obtained with these electrodes would enable the behaviour of Tl or Cd ones to be predicted. Amalgam electrodes for measuring complexation reactions are not new; they have been used for studying lead(II) hydrolysis by Carell and Olin [11] and Schorch and Ingri [12], for determining the stability constants of zinc acetate complexes by Bottari and Janosionowska [13], and for studying the complexes of cadmium(II) with pyridine and chloride by Gutz and Almeida Neves [14]. However, all the measurements reported so far with amalgam electrodes have been made in synthetic solutions at high $[M]_t$ values. In the present work, amalgam electrodes were tested specifically to assess their ability to measure correct complexation data under environmental conditions, i.e., with an electrode device easy to operate, at low $[M]_t$ values and at very low [M] values, and in the presence of natural, adsorbable, complexing agents.

EXPERIMENTAL

Reagents, samples and solutions

Unless otherwise stated, all chemicals were Merck analytical-reagent grade. All measurements were made in 0.1 M $NaClO_4$ electrolyte solution. All solutions were prepared with Milli-Q or twice-distilled water. The stock 1 M sodium perchlorate solution was prepared by mixing equimolar amounts of Suprapur sodium hydroxide and perchloric acid. Lead(II) and Zn(II) stock solutions were obtained by dissolving lead carbonate or zinc oxide in perchloric acid. The pH of all the stock solutions was 3—4. Triethylenetetramine (trien; Fluka "purum") was used as received; the exact trien concentrations were determined by acid/base titration.

The fulvic compounds were pedogenetic refractory organic matter (for definitions, see [15]), originating from the pond Mare aux Evees in the Fontainebleau forest (France). The water sample was treated as described earlier [16]: preconcentration was done by freezing concentration, and cascade filtration through Schleicher and Schuell (0.45-μm pore size) Amicon XM300 and PM10 filters. The PM10 filtrate was used as the stock solution for fulvic compounds, the characteristics of which have been described [16, 17]. The dissolved organic carbon (DOC) of this stock solution was 87 mg l^{-1} and its iron content was 4×10^{-6} M. The Ca and Mg contents were 3.6×10^{-4} and 1.2×10^{-4} M, respectively. Other metals were undetectable.

The initial hydrogencarbonate content was 1.1×10^{-3} M, but it was eliminated by acidifying with perchloric acid, degassing with nitrogen, and adjusting to the desired pH with sodium hydroxide.

The composition of the medium used for algal culture (AAP medium) was as given by Payne [18]; it contains nine metals and seven inorganic anions plus 8×10^{-7} M EDTA, the ionic strength and pH being 1 mM and 7.0, respectively. It was used to grow a green algae, *Chlamydomonas variabilis*. Complexation measurements were made by sampling the culture medium before introducing algae and during the exponential phase of growth (the number of cells was 2×10^5 cells/ml). In both the cases, the ionic strength was adjusted to 0.01 M with sodium perchlorate, but in the second case, samples were filtered through 3.0-μm pore-size filters to eliminate the algal cells. No other change was made before complexation measurements.

Oxygen must be eliminated very carefully from the solutions, as it is the main oxidant of the amalgams and, therefore the main factor governing LL (Fig. 1). Solutions were degassed with nitrogen supplied by Carbagaz (Geneva). To attain LL $\approx 10^{-6}$ M, a gas with purity 99.995% was used (symbol $N_2(45)$, $O_2 < 10$ ppm). To attain LL $\approx 3 \times 10^{-7}$ M, a gas with purity 99.9990% had to be used (symbol $N_2(50)$, $O_2 < 1$ ppm). To reach minimal oxygen content in the test solution ($<5 \times 10^{-8}$ M), a flow rate of 6—10 l h^{-1} was needed. The gas was pre-equilibrated with the aqueous phase by bubbling N_2 through the electrolyte solution before passing into the measuring cell. The N_2 outlet of the cell was connected to a wash-bottle containing the same electrolyte solution in order to prevent air penetration into the cell. Nylon tubing with low gas permeability was used for passing N_2 and all the electrodes as well as the gas inlet and outlet fittings were sealed in the cell cover by means of air-tight stoppers combined with rubber O-rings specially designed in this laboratory [19] to prevent air penetration. The measuring cell was a Metrohm EA-880-VT polarographic cell, modified to improve the air tightness between the plastic cover and the glass cell [19].

Instrumentation

The solution in the cell was stirred by means of a magnetic bar and a synchronous motor (Metrohm EA504). The pH was measured with a Metrohm EA682 pH meter, and potentials were measured by means of a Tacussel ARIES-20000 potentiometer and a W+W-1100 recorder. A Tacussel BIPAD apparatus was used as galvanostat for the determination of amalgam concentrations. A Perkin-Elmer flameless atomic absorption spectrometer (model 2280) with a HGA-500 furnace was used for the same purpose. The HMDE device was a Metrohm "microdoseur" EA290; this device, filled with amalgam, will hereafter be referred to as the hanging amalgam drop electrode (HADE). All potentials were measured against a double-junction Ag/AgCl/1 M NaCl/electrolyte, reference electrode (where the electrolyte is a predegassed solution of the same electrolyte as in the measuring solution). The measuring cell was thermostatted at 25 ± 0.1°C.

Preparation of the HADE

Figure 2 shows the cell specially designed to prepare the amalgam and fill it into the HADE device under a nitrogen atmosphere to avoid oxidation of the amalgam during the transfer. This is important because, as will be seen, it is often useful to work with dilute amalgams which are easily oxidized. The preparation modes were very similar for the lead and zinc amalgams. A mercury pool (3 ml) was placed into cell C1, with 20 ml of 0.01—0.1 M Pb(II) or Zn(II) acetate solutions at pH 4, the piston being in the "upper" position (as illustrated in Fig. 2), and the HMDE body was placed in compartment C2. The solution in C1, the compartment C2 and the salt bridge solution were degassed with nitrogen for 45 min. Electrolysis was then done at constant current (typically 3 mA) for a fixed duration (typically 15 min). During the electrolysis, the solution was only stirred by passing a stream of nitrogen, as preliminary tests showed that more efficient stirring was not necessary. At the end of electrolysis, the piston was lowered to let part of the amalgam enter compartment C2, and the HADE was filled by aspiration under vacuum, as recommended in the Metrohm procedure for the HMDE. When the amalgam is in the HADE, it can be stored therein without oxidation for at least 2 weeks. The stock amalgam may also be stored in the preparative cell for a long period provided that cell C1 is very air-tight.

The theoretical concentrations of metal M in the amalgam, C_M, can be computed from Faraday's law and the volume of mercury pool. It was found

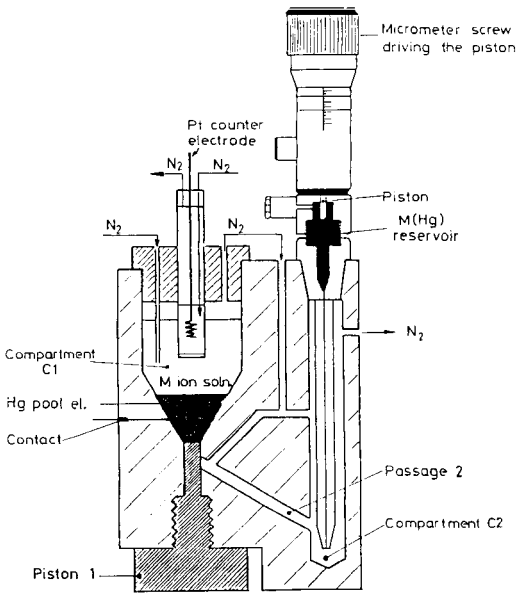

Fig. 2. Apparatus used for the preparation of amalgam electrodes. C1, amalgam preparation compartment; C2, microdoseur filling compartment. Passage 2 is closed by piston 1 during electrolysis. The piston is then lowered to fill compartment C2. The cell body is made of plexiglas [19].

to be 4.5×10^{-3} M under the above conditions. Most experiments were done with $3 \times 10^{-4} < C_M < 4 \times 10^{-3}$ M. Depending on the conditions, the yield of electrolysis varied between 80 and 100%, for reasons which are not studied in detail. One of the major causes is re-oxidation of the amalgam by oxygen produced at the anode and diffusing through the salt bridge. It is therefore essential to degas the salt-bridge solution during the electrolysis. In any case, as the value of C_M must be known very accurately for complexation measurements (see below), it was determined for each new HADE.

Determination of C_M

The concentration of lead or zinc in the amalgam (C_M) can be measured directly in the HADE by chronopotentiometry or electrothermal atomic absorption spectrometry.

Chronopotentiometry. The HADE, a Pt auxiliary electrode and a reference electrode are placed in a cell similar to that used for complexation measurements, containing 50 ml of sodium perchlorate (0.1 M) and Pb(II) or Zn(II) (10^{-3}—10^{-2} M). This solution is carefully degassed with nitrogen and an amalgam drop of known radius r is formed at the HADE. (The drop size was precalibrated with pure mercury; typically $r = 0.0335$ cm corresponds to two small divisions of the micrometer screw). A constant positive current is then applied to oxidize the metal in the drop and the resulting potential/time curve is recorded under stirred conditions. A big potential jump (e.g., 750 mV for lead) is obtained at the transition time, τ, corresponding to the time at which metal concentration becomes zero on the amalgam side of the drop/solution interface. It has been shown that τ is related to the flux ϕ_i, of the oxidized metal at the interface by [20]

$$\tau = (C_M\, r/3\,\phi_i) - (2r^2/30D_R) \qquad (2)$$

where D_R is the diffusion coefficient of M in mercury. If the flux of M is controlled by the current, i, one has $\phi_i = i/nFA$, where n is the number of electrons exchanged ($n = 2$ for Pb and Zn), F is the Faraday constant, and $A = 4\pi r^2$ is the surface area of the drop. Time τ was measured for various values of i, typically in the range 0.5—2.5 μA, by using successive drops; τ values ranging from 30 to 160 s were obtained under the above conditions, for $c_M \approx 3 \times 10^{-3}$ M. By plotting τ vs. $1/i$, perfect straight lines were obtained, allowing C_M to be computed with a standard deviation of ca. 2%. This error increases with decrease in C_M, because of the resulting small τ values. Furthermore, a systematic error in C_M may be caused by the presence of traces of oxygen; because oxygen oxidizes M, it increases its global flux which then includes a "chemical" component, ϕ_{ch}:

$$\phi = \phi_i + \phi_{ch}$$

ϕ_{ch} is proportional to the flux of oxygen diffusing towards the electrode [20] and may be estimated to be: $\phi_{ch} = D_{O_2}C_{O_2}/m\delta$ where D_{O_2} and C_{O_2} are the diffustion coefficient and concentration of oxygen, δ is the thickness

of the diffusion layer on the solution side of the electrode surface ($\delta \approx 10$—20 μm in stirred solutions) and m is the ratio of the number of electrons exchanged for the oxidation of M (n) and the reduction of oxygen (n_{O_2}); $m = 2$ for Zn and Pb amalgams if oxygen is reduced to O(—II). From the above expressions for ϕ_i and ϕ_{ch}, one can estimate the minimum current usable for the chronopotentiometric analysis, in order to make negligible the systematic error caused by $\phi_{ch} : \phi_i \gg \phi_{ch}$, or $i \gg n_{O_2} FS D_{O_2} C_{O_2}/\delta$. For instance, with $n_{O_2} = 4$, $\delta = 10$ μm, $D_{O_2} = 2.4 \times 10^{-5}$ cm^2 s^{-1}, $C_{O_2} = 5 \times 10^{-8}$ M and $r = 0.0335$ cm, ϕ_{ch} will produce an error of 7% on C_M if $i = 0.1$ μA.

Electrothermal atomic absorption spectrometry. A known number (100) of drops from the HADE placed in a 100-ml volumetric flask were dissolved in 10 ml of 10% (v/v) nitric acid by vigorous shaking, and the solution was diluted to the mark with the same acid. This solution was used directly for atomic absorption spectrometry. Internal standards were used for calibration. Results for both lead and zinc agreed with the chronopotentiometric results, within 2% errors. Nonetheless, the chronopotentiometric method was preferred for routine use because fewer drops ($\approx$10) were required; a maximum of 300 drops with $r = 0.0335$ cm can be formed from a completely filled HADE.

CALIBRATION CURVES AND SENSITIVITY LIMITS

For reversible systems, $M^{n+}/M(Hg)$, the Nernst equation is obeyed, so that at constant ionic strength the measured potential can be written as

$$E = E_0' + S \log ([M^{n+}]/C_M) \quad (3)$$

where $S = 2.303\ RT/nF$ and E_0' is the apparent standard potential of the oxidation/reduction couple, expressed vs. the reference electrode used and incorporating the activity coefficients as well as the junction potential of the reference electrode salt bridge. In a non-complexing medium, the free M ion concentration $[M^{n+}]$ is equal to the corresponding total concentration $[M]_t$. Therefore, at constant C_M, E depends linearly on $\log [M]_t$:

$$E = E_0'' + S \log [M]_t \quad (4)$$

Reproducibility of E_0' *and* S *values*

Calibration curves were obtained experimentally by adding to a predegassed solution of electrolyte (0.1 M $NaClO_4$), small increments of concentrated degassed lead(II) or zinc(II) stock solutions at pH 4.5. The resulting E vs. $[M]_t$ plots (Fig. 3) show that Eqn. 4 is fulfilled for both the metals down to 10^{-6} M; S was found to be 29.4 and 29.2 mV for Pb(II) and Zn(II), respectively. A systematic comparison of 14 calibration curves recorded with different lead amalgam electrodes, over a period of eight months showed that the variations in slopes were 0.35 mV, the average slope value being

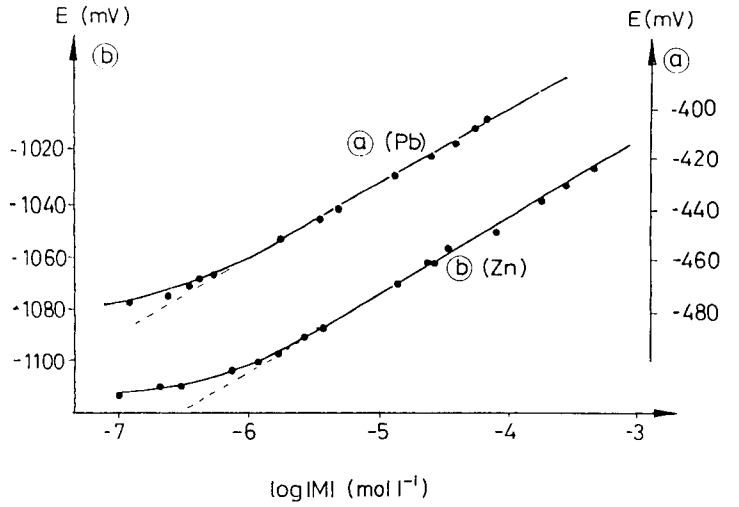

Fig. 3. Calibration plots for the HADE at T = 25° C, I = 0.1 M and Ag/AgCl/1 M NaCl/ 0.1 M $NaClO_4$ reference electrode: (a) Pb-HADE, $C_M = 3.45 \times 10^{-4}$ M; (b) Zn-HADE, $C_M = 1.8 \times 10^{-3}$ M.

29.4 mV (theoretical value, 29.5 mV). The corresponding average E_0' value was −383.3 ± 1.7 mV. (Under similar conditions, a theoretical value of −371.0 mV was computed using the standard potential of the Pb^{2+}/Pb(Hg) couple reported in the literature [21]. The difference between these two values of E_0' might partly be due to the junction potential of the double salt bridge of the reference electrode). But the most important feature is the very small drift in E_0' value observed over eight months during which time many refilled HADE were used. This is in contrast to the behaviour of many ISE for which the observed drift in E_0 may be up to tens of mV over a period of several months. The zinc amalgam electrode showed similar behaviour. Its E_0' value was found to be −1009.0 mV which is also close to the theoretical value.

Response time of the electrode

When a new amalgam drop is formed at the HADE, in a Pb(II) or Zn(II) solution, a potential drift is observed, as shown in Fig. 4. The drift is directly related to the processes which limit the sensitivity of the electrode (see below). For practical use of the electrode, the following points must be noted. Under normal conditions (sufficiently large C_M and low $[O_2]$), E quickly tends to vary linearly with time. This linear drift is observed almost instantaneously for $[M]_t > 5 \times 10^{-6}$ M (Fig. 4a), while a long transition period may be required at lower concentrations (Fig. 4b). The exact cause of the initial potential maximum at low $[M]_t$ (Fig. 4b) is not known, but it is probably related to the charging of the double layer around the drop after its formation. This seems to be confirmed by the fact that an instantaneous correct response is obtained when a potential step is produced by addition of

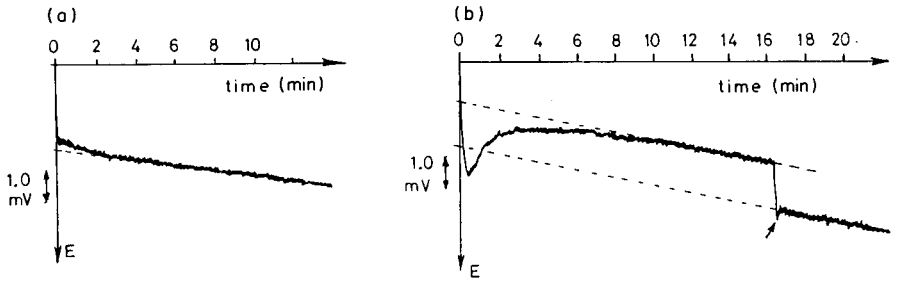

Fig. 4. Examples of potential drifts of the Pb-HADE. Zero time corresponds to the formation of a new drop. Curves: (a) obtained for $[M]_t > 10^{-6}$ M; (b) obtained for $[M]_t < 10^{-6}$ M. The arrow on curve (b) indicates an addition of Pb^{2+} to the solution without a change of the amalgam drop.

Pb(II) without changing the drop (Fig. 4b). A detailed study [22] of the cause of the linear part of the drift of E with time showed that it is due to the slow decrease of C_M inside the drop, resulting from the oxidation of M by traces of oxidants (particularly oxygen) present in the solution. Consequently, to measure correct values of E, the linear part of the potential shift must be extrapolated to $t = 0$; the calibration curves of Fig. 3 were obtained in that way. It can be shown that the change of E with time, dE/dt, is inversely proportional to C_M, and that almost stable E values are obtained for $C_M > 3 \times 10^{-3}$ M in normally degassed solutions. In fact, dE/dt is a useful parameter for extending the application range to HADE to lower $[M]_t$ values (see below).

Sensitivity limit of HADE

Below ca. 10^{-6} M, E is no longer proportional to the logarithm of added $[M]_t$ and tends to level off when the added $[M]_t$ is small (Fig. 3). For each value of E in the curved part of the calibration plots, a value of ΔC can be computed from $\Delta C = [M]_{t,2} - [M]_{t,1}$ (for definitions, see Fig. 5b). For both the lead and zinc amalgam electrodes, ΔC was found to vary from one calibration plot to another, but it was found to be independent of $[M]_t$ in the curved part of a given calibration plot. For example, ΔC was found to be $(1.12 \pm 0.09) \times 10^{-7}$ M and $(3.6 \pm 0.6) \times 10^{-7}$ M for lead and zinc, respectively, in Fig. 3. This suggests that a constant M concentration is introduced into the solution from a source other than the standard used for addition. Two possible sources are: (i) contaminations by the glassware and reagents, which introduce initially, in the bulk of the solution, a constant concentration of total M ion (denoted below by ΔC_c), independent of the additions made, and (ii) oxidation of the amalgam (producing ΔC_{ox}) by traces of oxidants present in solution (particularly oxygen). Thus

$$\Delta C = \Delta C_c + \Delta C_{ox} \tag{5}$$

For instance, in the case of the lead plot in Fig. 3 (where $\Delta C = 1.12 \times$

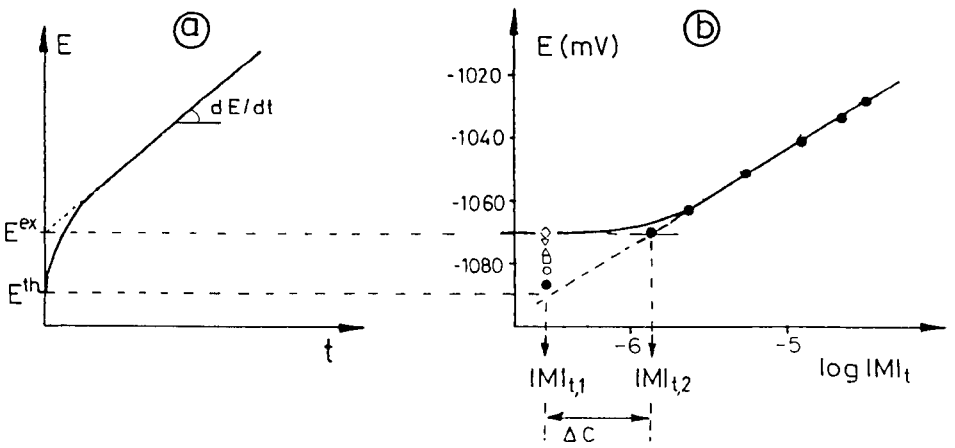

Fig. 5. Role of oxygen in the HADE response (after [3]). (a) The solid line shows the $E = f(t)$ variation caused by oxidation of M by oxygen with $[O_2] = 2.9 \times 10^{-6}$ M; E^{ex} is the value of E extrapolated to $t = 0$ and corresponding to point ◇ in (b); E^{th} is the theoretical value which would be obtained in the absence of O_2 and of contamination. (b) Calibration curve for the Zn-HADE at $T = 25°C$, $I = 0.1$ M, pH 5.2 and $C_M = 1.8 \times 10^{-3}$ M. $[O_2]$: • $< 10^{-8}$ M, i.e., maximum possible deoxygenation with pure N_2 in the conditions used; (○) 0.7×10^{-6} M; (□) 1.3×10^{-6} M; (△) 1.8×10^{-6} M; (▽) 2.0×10^{-6} M; (◇) 2.9×10^{-6} M. $[M]_{t,1}$ is the total metal ion concentration added to the solution by the standard; $[M]_{t,2}$ is the effective total metal ion concentration at the electrode surface ($=[M]_{t,1} + \Delta C$).

10^{-7} M), direct measurement of ΔC_c was made by anodic stripping voltammetry in the electrolyte solution prepared for the lead(II) calibration plot, inside the potentiometric cell, prior to the first addition of standard lead(II) solution. A value of $\Delta C_c = 3 \times 10^{-8}$ M was found, indicating that $\Delta C_{ox} \approx 8.2 \times 10^{-8}$ M. The amount of lead(II) produced in the bulk solution by the complete oxidation of 20 drops can be estimated to be 2×10^{-8} M in the conditions of the lead plot of Fig. 3 ($C_M = 3.4 \times 10^{-4}$ M and $r = 0.0335$ cm). It therefore cannot account for the observed value of ΔC_{ox}. In fact, detailed studies [3, 22] have shown that ΔC_{ox} primarily reflects the fact that the oxidation of M produces a value of M ion concentration at the electrode surface, $[M]_0$, larger than $[M]_t$ (Fig. 6). Because the solution is stirred, δ is constant and therefore $\Delta C_{ox} = [M]_0 - [M]_t$ is independent of $[M]_t$ and time. Like dE/dt, ΔC_{ox} is proportional to the oxidant concentration present in the bulk solution, and its value can be computed theoretically from the shift in E with time [3, 22] : $\Delta C_{ox} = \text{const.}\,(dE/dt)$. This relationship was tested experimentally and found to be fulfilled. The constant depends on the stirring mode, the radius of the drop, the diffusion coefficient of M^{n+}, and the value of C_M but not on the nature or concentration of the oxidant [3, 22] ; it can therefore be obtained by measuring simultaneously ΔC_{ox} and dE/dt at various oxidant concentrations. This calibration procedure is valid even if the nature of this oxidant is unknown, which

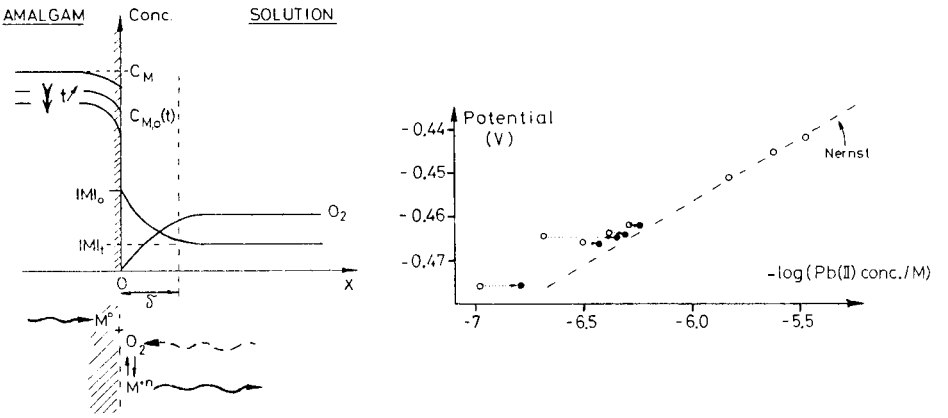

Fig. 6. Schematic representation of concentration gradients at the interface: C_M is the initial M concentration in the amalgam; δ is the diffusion layer thickness in solution.

Fig. 7. Application of the correction procedure for the effect of oxidation of the amalgam, at low $[M]_t$ values. Pb-HADE: lower part of a calibration curve; $C_M = 3.45 \times 10^{-4}$ M, 25°C, I = 0.1 M, pH 4.5; $[O_2]$ content varies from point to point. (○) Measured potential plotted as a function of added Pb(II) ($[Pb]_t$); (•) measured potential plotted as a function of corrected Pb concentration ($[Pb]_0 = [Pb]_t + \Delta C_{ox}$).

is most often the case in natural media. The value of the constant can then be used to compute the true total concentration of M ions at the electrode surface [3] by

$$[M]_0 = [M]_t + \Delta C_{ox}$$

This procedure makes it possible to use the curved portion of the calibration curve for complexation measurements, allowing extension of the usable range to lower $[M]_t$ values. The above correction procedure was tested for the oxidation of lead amalgam by oxygen and the specified fulvic compounds, and for the oxidation of zinc amalgam by oxygen and hydrogen ions [19, 22].

An example of the usefulness of such a correction is shown in Fig. 7 for the lead HADE. Measurements were made in solution containing only Pb(II) and the electrolyte, but during the addition of Pb(II), oxygen was not eliminated regularly, so that the content of traces of O_2 in solution (therefore ΔC_{ox}) varied during the titration, resulting in a large dispersion of the points for $[M]_t < 10^{-6}$ M. However, for each of these points, $[M]_0$ can be computed from the corresponding value of dE/dt, and it is seen that the plot E vs. log $[M]_0$ is close to Nernstian behaviour even at these low concentrations (the remaining difference is probably due to the uncorrected ΔC_c).

To summarize, the salient points for using the HADE correctly at $[M]_t \leqslant 10^{-6}$ M are as follows. The potential readings to be introduced into Eqn. 1 are obtained by extrapolating the linear portion of the E vs. time curves to $t = 0$. Only the relationship E vs. log $[M]_0$ yields a linear plot. In normal

operating conditions, $[M]_0 \approx [M]_t$ for $[M]_t > 10^{-6}$ M. At low $[M]_t$ values, one must bear in mind that $[M]_0 = [M]_t + \Delta C_{ox} + \Delta C_c$. The value of ΔC_c can be minimized only by purifying reagents and cleaning glassware as thoroughly as possible. The value of ΔC_{ox} can be minimized by eliminating as much as possible any trace oxidant (particularly O_2) present in the test solution.

Theoretical considerations as well as experimental tests [3, 22] show that

$$\Delta C_{ox} = (n/n_{O_2})\,[O_2]\,(D_{O_2}/D_M)^{1/2} \tag{6}$$

where D_M is the diffusion coefficient of M ions in solution. By using $n_{O_2} = 4$ (see above), $D_{O_2} = 2.4 \times 10^{-5}$ cm^2 s^{-1} and $D_M = 8 \times 10^{-6}$ cm^2 s^{-1}, one gets $\Delta C_{ox} = 3.5\,[O_2]$, which shows that even traces of oxygen may produce large differences between $[M]_0$ and $[M]_t$. If ΔC_{ox} cannot be completely eliminated, then it may be corrected for by using the specified procedure.

APPLICATION TO COMPLEXATION MEASUREMENTS

Two sets of complexation experiments were done. In the first set, the use of Pb and Zn HADE for the determination of complexation constants was tested with well-characterized ligands under conditions where both free and total metal concentrations were low. In the second set, the HADE were tested for studying complexation reactions of environmental significance. In all cases, the values of $[M]_t$ were converted to $[M]_0$ as discussed above, for interpreting the complexation data.

Complexation of Pb(II) and Zn(II) by strong synthetic ligands

Lead(II)/trien system. This system was first studied by titrating a constant concentration of trien ($[L]_t = 9.2 \times 10^{-5}$ M) with Pb(II), at constant pH (9.55), temperature (25°C) and ionic strength (0.1 M $NaClO_4$) (Fig. 8a). In a second experiment (Fig. 8b), a very low constant concentration of Pb(II) ($[Pb]_t = 3 \times 10^{-7}$ M) was mixed with trien ($[L]_t = 7.5 \times 10^{-4}$ M) and its pH was varied between 7.64 and 10.5 to change the free ligand concentration. In these two experiments, the free Pb^{2+} concentrations varied between 10^{-3} and 10^{-13} M. The terms α and δ_{OH} in Fig. 8(b) are given by

$$\alpha = [Pb]_t/[Pb^{2+}] = 1 + \delta_{OH} + \delta_L \tag{7}$$

where $\delta_{OH} = ([PbOH] + [Pb(OH)_2] + [Pb(OH)_3] + 3[Pb_3(OH)_4])/[Pb^{2+}]$ and $\delta_L = ([PbL] + [Pb(HL)] + [PbLOH])/[Pb^{2+}]$. The last two complexes in parentheses were reported by McBryde and Powell [24] and Park and Lee [25]. (Charges of complexes are omitted.)

The value of α is obtained experimentally from the difference in potential readings, ΔE, in complexing and non-complexing media, at constant $[Pb]_0$; δ_{OH} was computed from the pH used and the stability constants of the Pb(II) hydroxo complexes [23]; can be converted to

$$\delta_L = \beta_L\,[L] + \beta_{1,H}\beta_{LH}\,[H^+]\,[L] + \beta_{LOH}\,[OH^-]\,[L] \tag{8}$$

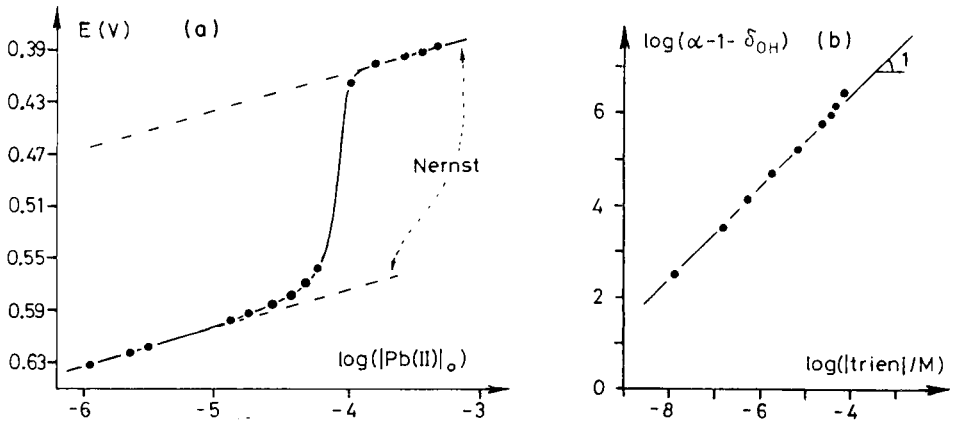

Fig. 8. Complexation of Pb(II) by triethylenetetramine (trien) at I = 0.1 M and 25°C. (a) $[trien]_t$ = 9.5 × 10^{-5} M, pH 9.5, variable $[Pb(II)]_t$, C_M = 7.4 × 10^{-4} M; (b) $[trien]_t$ = 7.5 × 10^{-4} M, $[Pb(II)]_t$ = 3 × 10^{-7} M, pH variable from 7.6 to 10.5 resulting in the variable free trien concentration given on the ordinate, C_M = 5 × 10^{-4} M.

where $\beta_L = [PbL]/[Pb^{2+}]\,[L]$, $\beta_{LH} = [Pb(HL)]/[Pb^{2+}]\,[HL]$ and $\beta_{LOH} = [PbLOH]/[L]\,[OH]\,[Pb^{2+}]$. In Fig. 8(b), [L] was computed from $[L]_t$, pH values, and the acid/base constants for LH ($\beta_{1,H}$), LH_2 ($\beta_{2,H}$), LH_3 ($\beta_{3,H}$), and LH_4 ($\beta_{4,H}$), the logarithmic values of which are, respectively, 9.74, 18.82, 25.38 and 28.64 [23]. The fact that the plot of $\log \delta_L$ vs. log [L] gives a straight line of slope 1 (Fig. 8b) indicates that, under these conditions, only the 1:1 PbL complex is formed. The β_L values obtained from the two experiments (Table 1) are in good agreement with the literature values, despite the low free and total metal concentrations used for their determination.

The Zn(II)/NTA and Zn(II)/trien systems. The Zn(II)/trien complexes were studied, as described above, by conducting two experiments. In the first, $[Zn]_t$ was varied over the range 10^{-6}—10^{-3} M, whereas $[L]_t$ (9.7 × 10^{-5} M) and pH (9.55) were kept constant. In the second, $[Zn]_t$ (9.1 × 10^{-7} M) and $[L]_t$ (9.7 × 10^{-5} M) were kept constant and pH was varied between 4.4 and 10. Other conditions are given in Table 1. For the analysis of the data, Eqns. 7 and 8 were used [Pb(II) was replaced by Zn(II)] except that only the 1:1 ZnL complex was considered, because evidence is available only for this species in the literature [23, 24]. In the present case, however, none of the experiments could be interpreted solely in terms of 1:1 complexes. In view of the high pH used in these experiments, the second set of data was evaluated by using the first and third terms in Eqn. 8 written for Zn(II) (Fig. 9). The straight line thus obtained suggests that ZnLOH could be formed. The values of log β_L and log β_{LOH} obtained from this graph are 11.1 and 17.05, respectively. It must be noted, however, that the same data could equally well be interpreted in terms of ZnL and ZnL_2 complexes, with

TABLE 1

Examples of complexation measurements with the HADE for Pb^{2+} and Zn^{2+}
(25°C, I = 0.1 M; concentrations in mol l^{-1}; 1:1 complexation constants in l mol^{-1})

System		$-\log [M]_t$[b]	$-\log [L]_t$[b]	pH[b]	$-\log [M]_0$[c]	Complexation constants[d]			
M^{2+}[a]	Ligand						This work	Literature values	
Pb^{2+} (7.4×10^{-4})	Trien	6.0—3.3	4.02	9.55	11.7	β_L	10.31 ± 0.05	10.4	[23]
Pb^{2+} (5×10^{-4})		6.52	3.12	7.6—10.5	12.9	β_L	10.40 ± 0.1	10.4	[23]
Pb^{2+} (3.8×10^{-4})	CO_3^{2-}	6.3—6.0	3.05—0.46	7.0—8.75	11.3	β_L	6.3 ± 0.1	6.1—6.4	[26—29]
						β_{2L}	9.6 ± 0.2	9.1—9.8	
Zn^{2+} (9.4×10^{-4})	NTA	5.7—3.5	5.3	5.5	10.5	β_L	10.4 ± 0.1	10.4	[23]
Zn^{2+} (2.8×10^{-3})	Trien	6.0—3.3	4.01	7.4—10.0	14.8	β_L	11.4 ± 0.4	12.03	[23]
						β_{2L}	17.2 ± 0.1		

[a]The concentration of metal in the amalgam, C_M, in mol l^{-1}, is given in parentheses. [b]Value or range of variation of this parameter during the experiment. [c]Minimum free metal concentration measured at the electrode surface during the experiment. [d]β_L and β_{2L} are the complexation constants for synthetic ligand; logarithmic values are given.

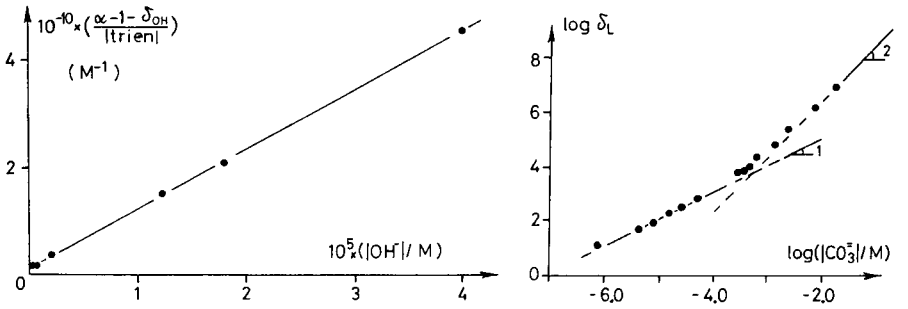

Fig. 9. Complexation of Zn(II) by trien (25°C, I = 0.1 M). $[Zn]_t = 9.1 \times 10^{-7}$ M, $[trien]_t = 9.7 \times 10^{-5}$ M, $C_M = 1.8 \times 10^{-3}$ M; pH variable between 7.38 and 10.02, resulting in the variable free trien concentration given.

Fig. 10. Complexation of Pb(II) by carbonate. (25°C, $C_M = 3.8 \times 10^{-4}$ M). The graph includes three sets of data: (i) $[Pb]_t = 1 \times 10^{-6}$ M, pH 7.0, $[HCO_3^-]$ variable from 9.0×10^{-4} to 0.052 M; (ii) $[Pb]_t = 5 \times 10^{-7}$ M, $[HCO_3^-] = 0.054$ M, pH variable from 8.05 to 8.51; (iii) $[Pb]_t = 5 \times 10^{-7}$ M, $[HCO_3^-] = 0.35$ M, pH variable from 7.25 to 8.75.

log β_L = 11.4 and log β_{2L} = 17.2. For the first set of data, the first interpretation does not hold; indeed, because they were obtained at constant pH, if only ZnL and ZnLOH were formed, a straight line should be obtained by plotting $(\alpha - 1 - \delta_{OH})$ vs. [L], the slope corresponding to an apparent equilibrium constant, β_L^*, equal to $\beta_L + \beta_{LOH}$ [OH]. Because such a fitting was not possible, the second interpretation (ZnL + ZnL_2 complexes) is more likely. At any rate, these results show that the value of 12.0 reported for log β_L in the literature [23] is too high; it may have been positively biased by the fact that ZnL_2 was not considered. A lower value of β_L for Zn(II) seems the more realistic as even the corresponding value for PbL is lower.

The zinc HADE was also tested by titrating NTA ($[L]_t = 5 \times 10^{-6}$ M) with Zn(II) at pH 5.5 and 0.1 M $NaClO_4$ (other conditions are given in Table 1). Under these conditions, Zn(II) is only weakly complexed. These data gave a value for the Zn/NTA complexation constant which agrees fairly well with the literature value (Table 1).

These results exemplify the usefulness of the lead and zinc HADE for studying complex formation, and show that Nernstian behaviour is exhibited even at very low free metal ion concentrations (down to 10^{-15} M in the second experiment; Table 1) and total metal concentrations ($<10^{-6}$ M).

Complexation measurements with compounds of environmental significance

Carbonato complexes of Pb(II). In natural waters, the formation of $PbCO_3$ was first measured in sea water by anodic stripping voltammetry (ASV) by Zirino and Yamamoto [26], and then by Ernst et al. [27] in freshwater conditions by differential pulse polarography (DPP) and anodic stripping differential-pulse voltammetry (DPASV). In both cases, the data

were interpreted in terms of only 1:1 complexes. Some authors have postulated the formation of 1:2 bicarbonato complexes, but Bilinski et al. [28], using ASV, showed that their data can be well interpreted in terms of the formation of 1:1 and 1:2 Pb-CO_3^{2-} complexes (Table 1). This was confirmed by Nürnberg et al. [29], by stripping voltammetry, in seawater conditions (Table 1). All these studies were done with voltammetric techniques. The present purpose was to check the above results by means of a potentiometric method, at low $[Pb]_t$ values.

Three sets of experiments were done. In all of these, $[Pb]_t$ was maintained constant at 10^{-6} or 5×10^{-7} M. Free CO_3^{2-} concentration was varied in the range 10^{-6}–2×10^{-2} M by varying either the pH or the total carbonate concentrations, $[CO_3]_t$. In most cases, the ionic strength was close to 0.1 M, but in some cases it had to be raised to 0.45 M. This ionic-strength variation was corrected for by computing activity coefficients from the Davies equation (see, e.g. [2]). The data are plotted in Fig. 10; δ_L, α and δ_{OH} are related by Eqn. 7. In this case, provided that only 1:1 and 1:2 complexes are formed, the theoretical expression of δ_L ($L = CO_3^{2-}$) is given by

$$\delta_L = \beta_L [CO_3^{2-}] + \beta_{2L} [CO_3^{2-}]^2 \quad (9)$$

where β_L and β_{2L} are the cumulative stability constants.

Figure 10 shows that two straight lines can be drawn through the points, with slopes of 1 and 2 for the ranges of low and large $[CO_3^{2-}]$ values, respectively. This result confirms the formation of 1:1 and 1:2 complexes. The values of $\log \beta_L$ and $\log \beta_{2L}$ are, respectively, 7.1 ± 0.1 and 10.4 ± 0.4 at zero ionic strength, and 6.26 ± 0.1 and 9.56 ± 0.2 at 0.1 M ionic strength. These results are in good agreement with those of Nürnberg et al. [29] and Bilinski et al. [28] (Table 1). In these experiments, the free lead ion concentrations were also low (down to 5×10^{-12} M).

Complexation of lead(II) by fulvic compounds. Most complexation studies of fulvic substances by ion-selective electrodes (ISE) have been made at unrealistic concentrations of the fulvic substances, because of the poor sensitivity of ISE, particularly the lead-ISE. The purpose of this experiment was to test the applicability of the HADE to the study of the complexation of Pb(II) by fulvic compounds (see Experimental) in normal aquatic concentrations (5.5 and 15.4 mg l^{-1} organic matter corresponding to 2.5 and 6.2 mg l^{-1} DOC), and to evaluate the effects of adsorption of the fulvic compounds on the amalgam drop, because this effect has been shown severely to affect voltammetric measurements on mercury electrodes [3]. Two series of experiments were done at constant pH (6.0), ionic strength (0.1 M) and concentration of fulvic compounds, by titration with lead(II).

Adsorption did not affect the shape of the E vs. time curves (Fig. 11, insert). Their slopes, however, were found to increase with DOC (Fig. 11), implying that these fulvic compounds may oxidize lead metal. Quinonic groups or Fe(III) impurities might play a role in this process, but the exact reason is not known. However, for all the measured E values, $[M]_0$ was

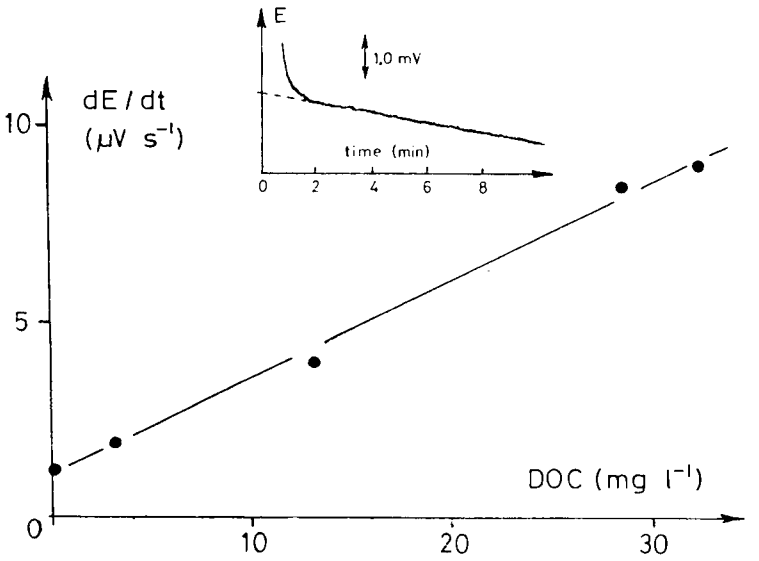

Fig. 11. Influence of the fulvic compounds on the lead amalgam electrode: the change in potential drift, dE/dt, with concentration of fulvic compounds expressed as dissolved organic carbon (DOC) at pH = 6.0. Insert is an example of response time.

computed from $[M]_t$ and dE/dt as described above (see section on sensitivity limit). This indicates that such corrections are possible not only for pure well-known oxidants (like oxygen in the previous experiments), but also for unknown compounds like the fulvic substances. Plots of E vs. log $[Pb]_0$ obtained in this manner are shown in Fig. 12. It can be seen that the complexation effect is small under the conditions used. Nevertheless, analysis of the data in terms of average complexation parameters [17] enables values to be computed for the average stability constant ($\log \beta_1 = 5.2$) of the Pb/fulvic substances complex and for the average equivalent weight ($M_{eq} = 1780$). These results are in excellent agreement with those obtained with the same sample of fulvic substances, with the lead ISE, but at higher concentrations [17].

The effect of pH on complexation was also studied in unbuffered solution, by keeping constant both the concentrations of the fulvic compounds (14.4 mg l^{-1} DOC) and $[Pb]_t$ (10^{-6} M). The pH was modified by adding sodium hydroxide solution to an initially acidic solution of the fulvic compounds. By plotting log δ_L (where L indicates fulvic substances and δ_L is defined as for Eqn. 7) as a function of pH, two straight-line segments were obtained, intersecting at pH 8 [19]. The slopes were 0.52 and 1.04 below and above pH 8, respectively. These values correspond to the average numbers of protons liberated during the complexation reaction [5, 17] and agree well with those obtained for copper(II) [30]. All these findings show that the HADE gives correct complexation data even at a low degree of complexation and in the presence of adsorbable fulvic substances which may oxidize

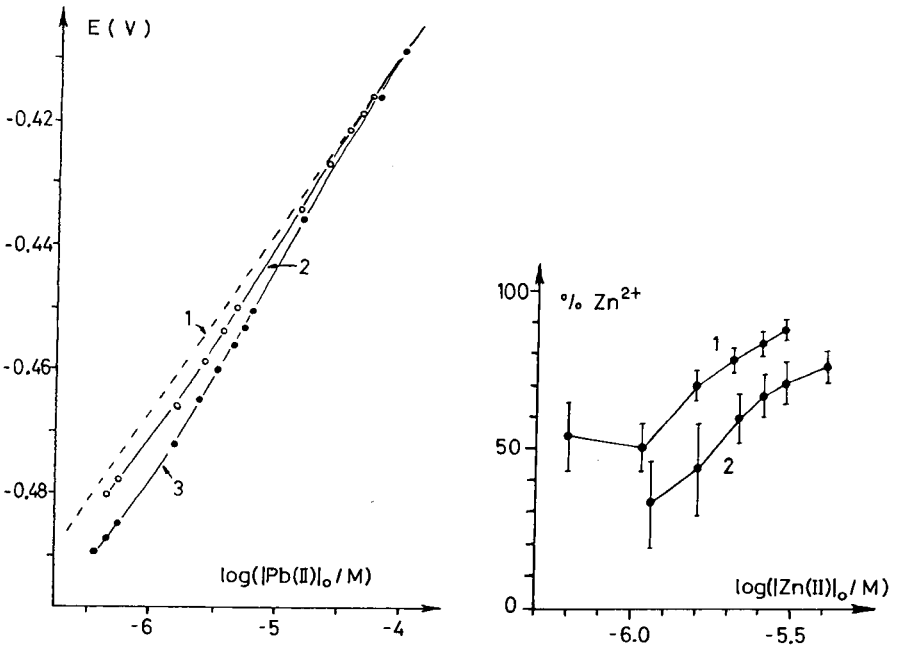

Fig. 12. Complexation of Pb(II) by the specified fulvic compounds (I = 0.1 M, 25°C, pH 6.0, C_M = 4.2 × 10^{-4} M). Calibration curves: (1) DOC = 0; (2) DOC = 2.8 mg l^{-1}; (3) DOC = 7.7 mg l^{-1}.

Fig. 13. Complexation of Zn(II) by algal culture medium before (1) and after (2) the culture. pH 7.00, I = 0.01 M, C_M = 1.8 × 10^{-3} M, 25°C.

the amalgam. Table 2 gives a comparison of the data obtained for the same sample of pedogenetic refractory organic material by different methods.

Complexation of zinc in algal culture media. Studies of uptake of metals by unicellular organisms are generally made in culture media, the complexation strength of which must be known and controlled, because it strongly affects the metal uptake (see, e.g. [31]). Some of these culture media, such as that used below (AAP) are sufficiently well defined and dilute enough to allow calculation of the degrees of metal complexation by models based on thermodynamic considerations. The validity of such calculations is, however, limited by the possible slow kinetics of complex formation/dissociation. More important is the fact that, during the culture, organisms release organic compounds, the exact nature and complexation properties of which are unknown, and which therefore cannot be introduced into model calculations. In this respect, the possibility of measuring experimentally the degree of complexation in such media is very important and the availability of a zinc-sensitive electrode is particularly useful because no other zinc-selective electrode exists and zinc is an important metal which has both vital and toxic roles. This was tested by measuring Zn(II) complexation in

TABLE 2

Comparison of complexation properties of lead(II) with the specified fulvic compounds, measured by three different methods (I = 0.1 M, pH 6.0, 25°C)

Parameter	Method		
	Voltammetry	ISE	HADE
M_{eq}[a], g/Pb(II)	2000	2100	1800
log (β_1/M^{-1})	5.4	5.6	5.2
dlog β_1/dpH			0.52

[a]"Equivalent" complexing weight is defined as the average weight of organic matter corresponding to the complexation of 1 mol of Pb(II). This M_{eq} cannot be measured by voltammetric methods and is then taken as the average of the two values obtained by ISE and HADE.

AAP medium, before and after culture of a green algae *Chlamydomonas variabilis*.

The ionic strength of AAP medium was adjusted to 0.01 M with sodium perchlorate, pH was maintained at 7.03 using a nitrogen/CO_2 mixture and the solution was titrated with a zinc ion solution. This procedure was repeated in AAP medium before culture and during the exponential growth phase of the algae (the number of cells in the medium was 2×10^5 ml^{-1}). Figure 13 shows the variation of free zinc ions as a function of $[Zn]_0$ (i.e., $[Zn]_t$ corrected for ΔC_{ox}) in the medium, before and during the culture. Because of the low concentrations and degrees of complexation, the errors in $[Zn^{2+}]$ are rather large. Nevertheless, it can be seen that the AAP medium is more complexing after than before the culture. Although the observed difference is relatively small, it is significant. The amount of organic matter released by the algae during the culture was measured and found to correspond to 2.0 mg l^{-1} DOC. It is therefore probable that the increase in the degree of complexation before and after culture is caused by these organic compounds released by the algae.

Conclusion

The results presented above show that amalgam electrodes are potentially very useful to measure complexation properties, not only of synthetic ligands in pure and concentrated solutions, but also of complexing agents of environmental significance in rather dilute solutions. The amalgams are easy to prepare, store and use. The factors governing the sensitivity limit are identical for all amalgam electrodes, namely, the contaminants from reagents and glassware and the oxidation of the amalgam by traces of oxidants present in solution. The oxidation process can be monitored and corrected for. Because of this, and in contrast to ISE, the curved part of the E vs. log $[M]_t$ plot can be used for complexation measurements. Furthermore, owing to the large charge-transfer rate constants of many of

the amalgams of interest, Nernstian behaviour is observed even at extremely low concentrations of free ion, so that even very strong complexation reactions can be studied. Other amalgam electrodes should prove satisfactory for ions for which there is no good ISE, e.g., Tl(I), Bi(III) or Cd(II).

C. Bernard and F. Bujard are gratefully acknowledged for designing the cell for preparation of amalgams and filling of the HADE, and for the adaptations of the measuring assembly to avoid contaminations by oxygen. This work was supported by Swiss National Foundation (project no. 2.674.080).

REFERENCES

1 C. J. M. Kramer and J. C. Duinker (Eds.), Complexation of Trace Metals in Natural Waters, Martinus Nijhoff, The Hague, 1984.
2 W. Stumm and J. J. Morgan, Aquatic Chemistry, 2nd edn., Wiley, New York, 1981.
3 J. Buffle, Complexation Reactions in Aquatic Media, Horwood, Chichester, 1987.
4 A. M. Mota, J. Buffle, M. L. Goncalves and S. P. Kounaves, Anal. Chim. Acta, 172 (1985) 13.
5 J. Buffle, P. Deladoey, F. L. Greter and W. Haerdi, Anal. Chim. Acta, 116 (1980) 255.
6 J. Buffle and C. Staub, Anal. Chem., 56 (1984) 2837.
7 J. Tuschall, Jr. and P. L. Brezonik, Anal. Chim. Acta, 149 (1983) 47.
8 K. Cammann, Working with Ion-selective Electrodes, Springer, Berlin, 1979.
9 J. Buffle, in H. W. Nurnberg, F. Pellerin and T. West (Eds.), Methods for the Determination of Trace Metals in Natural Waters, Pergamon, Oxford, 1987.
10 J. Heyrovsky and J. Kuta, Principles of Polarography, Academic, London, 1966.
11 B. Carell and A. Olin, Acta Chem. Scand., 14 (1960) 1999.
12 G. Schorch and N. Ingri, Acta Chem. Scand., 21 (1967) 2727.
13 E. Bottari and R. Janosionowska, Ann. Chim., 69 (1979) 153.
14 I. G. R. Gutz and E. Almeida Neves, J. Electroanal. Chem., 183 (1985) 123.
15 J. Buffle, in H. Sigel (Ed.), Metal Ions in Biological Systems, Vol. 18, M. Dekker, New York, 1984, Chap. 6.
16 J. Buffle, P. Deladoey, J. Zumstein and W. Haerdi, Schweiz. Z. Hydrol., 44 (1982) 325.
17 J. Buffle, F.-L. Greter and W. Haerdi, Anal. Chem., 49 (1977) 216..
18 A. G. Payne, Water Res., 9 (1975) 437.
19 J. P. Bernhard, Ph.D. Thesis, 2054, University of Geneva, 1982.
20 J. Buffle, M. Pelletier and D. Monnier, J. Electroanal. Chem., 43 (1973) 185.
21 A. J. Bard, R. Parsons and J. Jordan (Eds.), Standard Potentials in Aqueous Solution, M. Dekker, New York, 1985.
22 J. Buffle and J. P. Bernhard, J. Electroanal. Chem., in press.
23 R. M. Smith and A. E. Martell, Critical Stability Constants, Vols. 2 and 4, Plenum, New York, 1976.
24 W. A. E. McBryde and H. K. J. Powell, Can. J. Chem., 57 (1979) 1785.
25 Y. K. Park and C. H. Lee, Taehan Hwahakhoe Chi, 24 (1980) 129.
26 A. Zirino and S. Yamamoto, Limnol. Oceanogr., 17 (1972) 661.
27 R. Ernst, H. E. Allen and K. H. Mancy, Water Res., 9 (1975) 969.
28 H. Bilinski, R. Huston and W. Stumm, Anal. Chim. Acta, 84 (1976) 157.
29 H. W. Nürnberg, P. Valenta, L. Mart, B. Raspor and L. Sipos, Fresenius' Z. Anal. Chem., 282 (1976) 357.
30 J. Buffle, Anal. Chim. Acta, 118 (1980) 29.
31 S. Bates, A. Tessier, P. G. C. Campbell, M. Bisson and J. Buffle, J. Phycol., 18 (1982) 521.

Analytica Chimica Acta, 200 (1987) 213—225
Elsevier Science Publishers B.V., Amsterdam — Printed in The Netherlands

CONTINUOUS MONITORING OF COPPER AND CADMIUM IN ZINC PLANT ELECTROLYTE USING A MICROPROCESSOR-BASED BATTERY-OPERATED DATA ACQUISITION SYSTEM, MULTIPLE ION-SELECTIVE ELECTRODES AND REDUNDANCY PRINCIPLES

A. M. BOND*, H. A. HUDSON, D. L. LUSCOMBE, K. L. TIMMS and F. L. WALTER

Division of Chemical and Physical Sciences, Deakin University, Waurn Ponds, Victoria 3217 (Australia)

(Received 1st April 1987)

SUMMARY

Monitoring of both copper and cadmium is essential in the electrolytic production of zinc because these elements must be removed in order to improve the efficiency of the zinc electro-refining process. A new high-volume flow-through cell with an assembly of four ion-selective electrodes (four copper, four cadmium or two copper and two cadmium electrodes), reference electrode and temperature probe coupled with microprocessor-based instrumentation can be used for this purpose. Determinations can be done continuously for 72-h periods without maintenance in an on-line mode when multiple electrode determinations and redundancy principles are implemented. A microcomputer system incorporating low-power CMOS technology with multichannel and multiplexing capabilities is used for data acquisition. The use of the battery-powered data acquisition system provides excellent signal-to-noise ratios, meets the special demands of the harsh industrial environment, and is preferable to conventional mains-powered monitoring systems based on ion-selective electrodes.

In principle, ion-selective electrodes (ISEs) should be ideal for continuous monitoring in industrial plant liquors [1—7]. They are compact, inexpensive devices which are easily interfaced to computers; all of these features are desirable characteristics for on-line applications. Unfortunately, ISEs are not always sufficiently selective in the chemical sense, being prone to interferences of both physical and chemical kinds. In addition, they may not have sufficient long-term stability. Consequently, their use has not been as widespread as was once anticipated. However, an array of ISEs sensing the same parameter as an alternative to a single sensing element could enhance the notion

*A. M. Bond is Foundation Professor of Chemistry at Deakin University. He received his Ph.D. (1971) and D.Sc. (1977) degrees from the University of Melbourne, where he held teaching and research positions. His major research interests involve the development and application of modern electroanalytical techniques, and he is the author or co-author of over 200 papers on this subject. He is a recipient of a Fulbright Scholarship (1972), the Rennie Medal (1975) of the Royal Australian Chemical Institute, and the David Syme Prize (1977). He is a member of the Royal Australian Chemical Institute, the American Chemical Society and the Electrochemical Society.

0003-2670/87/$03.50

of an ISE as a reliable sensor. Construction of an instrument which can systematically examine the data from all the probes as they accumulate should enable failed probes to be identified. Subsequently, suitable action can be taken to discard any further data from that probe until it is removed from the sensing unit. This procedure would maximize efficiency and reliability, and minimize operating expenses, thereby providing the prospect of long-term monitoring. Stetter [8, 9] has described this kind of concept with an array of electrochemical sensors for the collection of data during the detection of hazardous gases and airborne chemicals.

Frequently, industrial liquors provide harsh environments both physically and chemically, thus producing a challenge for long-term on-line monitoring with ISEs. In the particular case of zinc plant electrolyte, which is being addressed in this paper, the monitoring program has to be implemented under conditions of very high ionic strength, high temperature, variable acidity and severe instrument operating conditions such as large electrical fields and corrosive conditions. All of these factors mitigate against implementation of conventional instrumentation for ion-selective electrodes.

The monitoring of trace metals in zinc electrolyte occupies a key role in process plant control and operation management. For example, the concentrations of Cd, Sb, Ni, Co and Cu all need to be carefully determined and their levels controlled if acceptable current efficiency in the zinc deposition stage is to be achieved [10, 11]. Traditionally, on-site sample collection followed by off-line analysis in a conventional laboratory has been used for industrial plant management. The off-line analytical methods which have generally been applied are atomic absorption spectrometry [12—14], voltammetry [15—17] or spectrophotometry [18].

In the cementation stage of the zinc electrolyte purification, the copper and cadmium levels are monitored in order to control the dosage levels of zinc dust required for their removal from the circuit electrolyte. In order to use ISEs to monitor the copper and cadmium, concentrations need to be greater than about 10^{-5} M. At lower concentrations, the response times of the ISEs are very slow and the limit of detection is being approached. Consequently, applications will be restricted to the purification plant and not to the cell-room solutions. Figure 1 is a generalized flow diagram of a zinc extraction process showing the location in which a copper or cadmium ISE system can be applied. De Bellefroid [19] mentioned the use of "a selective copper electrode" to control coarse zinc dust addition at the Balen plant, Vieille-Montague, Belgium. Geissler and Kunze [20] have recently examined the use of a copper ISE for determining copper in zinc plant electrolyte. Whilst their method was off-line and conventional analog instrumentation was used, their work highlights the difficulties which exist. They discussed the problems of long-term reproducibility, the need for periodic cleaning of the electrode surface and difficulties with the reference electrode in the high ionic strength environment.

Martin and Freiser [21] reported an example of multiprobe instrumenta-

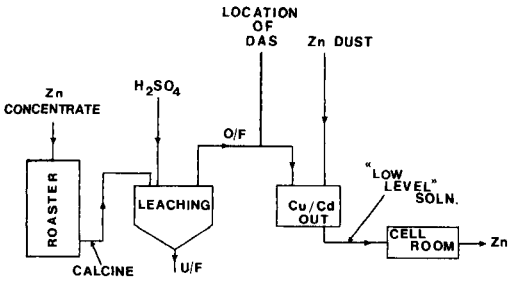

Fig. 1. Schematic flow diagram of an electrolytic zinc extraction plant showing the location in which the data acquisition system (DAS) can be used. O/F and U/F refer to the "overflow" and "underflow", respectively, in the leaching operation.

tion in which a mains-powered microcomputer was used to collect and treat data. Other examples of this approach are also available [1, 6, 7]. In the present work, battery-operated microprocessor-based instrumentation based on complementary metal-oxide semiconductor (CMOS) circuitry, with multichannel multiplexing capabilities was used with copper and cadmium ISEs. The battery-operated system was designed to be portable, and easily shielded from the harsh electronic and chemical environment. The multiplexing facility coupled with a newly designed cell enabled four identical electrodes or a range of different electrodes to be used. The installing of a number of identical electrodes has three advantages: (i) the signal can be amplified; (ii) deliberate application can be made of a redundancy philosopy; and (iii) long-term continuous operation can be provided with minimal operator intervention. The equipment design therefore incorporates the maximum of flexibility, ranging in application from a multiprobe unit completely dedicated to the determination of one variable and involving the redundancy principle, to a multivariable instrument. This instrumentation, when combined with a standard mains-powered computer-controlled liquor supply line, is applied to zinc electrolyte from the Electrolytic Zinc Company refinery at Risdon, Tasmania.

EXPERIMENTAL

Electrodes

The ion-selective electrodes used were Orion Model 94-48 cadmium ISEs and Model 94-29 copper ISEs. Prior to initial use or when departures from Nernstian behaviour were observed, the sensing membrane was polished by rubbing with an alumina strip for 30 s in the presence of a drop of water as described in the Orion Manual maintenance instructions. The sensing surface of the probe was then conditioned by immersion in a 10^{-5} M solution of the metal ion for 5 min.

An Orion Ag/AgCl (saturated KCl) double-junction reference electrode (Model 90-02) was used. The outer chamber contained either 2 M sulphuric acid or a zinc sulphate solution matching the plant liquor. The latter gave greater stability. A $Hg/Hg_2SO_4/H_2SO_4$ system provides a convenient single-junction reference electrode as described by Geissler and Kunze [20] and can also be used successfully.

Reagents

Zinc plant electrolyte was provided by the Electrolytic Zinc Company (Australasia), Risdon, Tasmania. All other chemicals were of analytical-reagent grade.

Standard solutions were prepared from "low-level" zinc plant electrolyte, which is obtained after the copper purification stage. The background levels of both cadmium and copper in this "low-level" standard solution from the plant were known to be less than 10^{-7} M. Because the detection limit of interest is greater than or equal to 10^{-5} M, the residual cadmium and copper levels in the standard solutions do not cause any measurable errors. These standards provide an excellent matrix-match to the zinc electrolyte being monitored by the ISE, because the major constituents are also present in the standard solutions. The pH values for all plant electrolyte after cooling to 25°C were found to be constant in the range 5.1 ± 0.1. No pH adjustment was undertaken. Furthermore, because of the high ionic strength of the zinc electrolyte, there was no need to use any ionic strength adjustor.

Multichannel instrumentation for monitoring

Figure 2 illustrates the completely integrated relationship between the data acquisition system (DAS) and the plant circuit solutions in the copper purification stage. The microcomputer data acquisition system uses CMOS integrated circuitry exclusively and is based on a multiplexed address then data bus. The unit is based on a field data acquisition system described earlier [22]. In the development of this instrument, the following design objectives were achieved: (a) use of low-power CMOS technology to provide a battery-operated, self-contained, portable, low-noise device that can operate

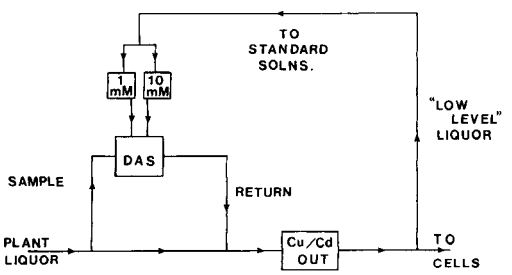

Fig. 2. Relationship between the DAS and the plant circuit solution at the cementation stage of the zinc extraction process.

in a harsh environment; (b) six input channels, four for ISEs, one for the reference electrode and a separate one for the temperature sensor; (c) use of a sealed metal box to protect the instrument from the hostile chemical and physical environment of an industrial plant; (d) a monitoring program which prompts the operator regarding the state of the instrument and condition of the batteries; (e) an RS232 interface to a mains-powered printer, plant computer, microcomputer or control room. Concentrations were calculated with these mains-powered devices in the conventional manner.

Figure 3 is a schematic diagram of the operating system in which the DAS is used for the determination of copper and cadmium in zinc refinery electrolyte. An important feature of this instrument is the multiplexing capability which enables redundancy principles to be included in the analytical scheme. Eight-channel multiplexing is used to enable selection of the multivariable input modules under software control so that a number of similar electrodes can be used to ensure continuous operation without interruption to the monitoring process.

Figure 4 illustrates a simple circuit diagram showing the use of the multiplexer within the DAS. The analog-to-digital (AD) input is connected to the output of the multiplexer switches. Each DAS input module is connected to the input side of the relevant multiplexer switch. Channel selection is provided by the binary 1 of 8 decoder section of the multiplexer. At the required time, as determined by the software, the microprocessor outputs a binary value, say 000, to the channel-select lines A0, A1 and A2. In this manner, the required input channel is selected, e.g., the temperature monitor. After a short delay of about 1 s, which allows the multiplexer to settle, the AD converter is issued with a start conversion signal. The analog signal switched through the multiplexer is thus converted to a 12-bit digital signal which is manipulated and stored under program control. This sequence of starting the AD converter and collecting the resultant digital data is repeated the

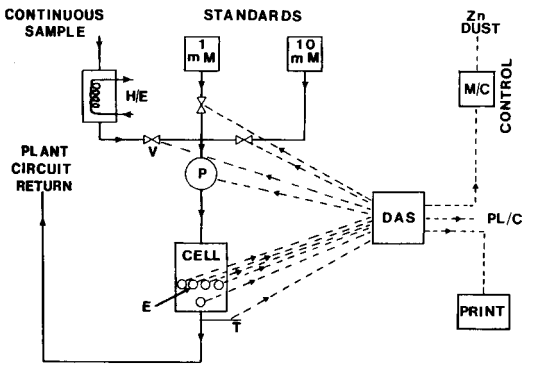

Fig. 3. Schematic diagram of the operating system with the DAS for the determination of copper and cadmium in zinc refinery electrolyte. E, Electrodes; H/E, a heat exchanger for cooling the plant liquor sample; P, centrifugal pump; M/C, microcomputer for local process plant control; PL/C, major plant computer; T, temperature probe; V, control valves.

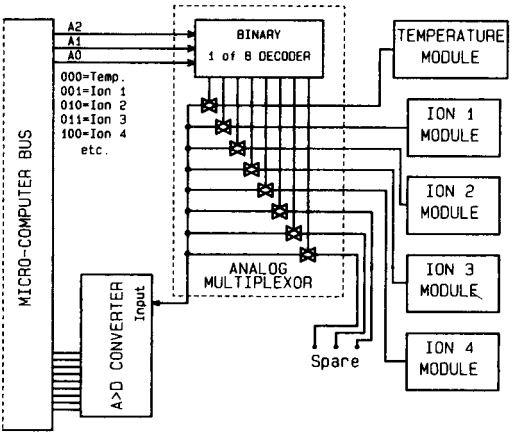

Fig. 4. Simple circuit diagram of the multiplexing unit (for description see text).

prescribed number of times, and the resultant data are added and averaged for a final result. The next channel for attention can then be selected and the process repeated. Although only a simple device, the multiplexer increases the flexibility and breadth of applications for which the DAS can be used, particularly when multi-electrode determinations and/or redundancy principles are being applied.

Preliminary measurements were undertaken with an Orion Research expandable Ionalyzer EA940.

The flow-through electrochemical cell

A modified form of an earlier design of flow-through electrochemical cell [5] was used. Because the absence from the electrolyte of any interference to the ISE has been verified (see later), the cell requires no chemical dosing capability, in contrast to the use of a Δ-shaped cell [23] with which an interference can be chemically annulled. Figure 5 is a schematic diagram of the new design. In the present study, large volumes of plant circuit electrolyte are available for sampling and the output from the cell can conveniently be returned to the circuit stream, so that the use of a large flow cell with high throughput, multisensing capacity and operating on a single-pass flow is a viable proposition.

The potentiometric measurement technique requires the existence of turbulence to produce a stable response; the turbulence also ensures that the sensing surfaces of the electrodes are continually exposed to fresh electrolyte and kept as clean as possible. The capacity of the 10-cm wide cell is 300 ml, and a typical flow rate is 1500 ml min^{-1}. The sensing electrodes are orientated in the same plane at right angles to the direction of flow. This plane is situated at the turn of the 90° elbow of the cell. The transverse alignment of the electrodes permits all probes to sense the solution simultaneously. The

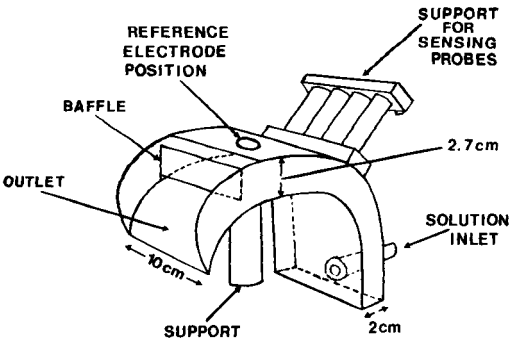

Fig. 5. Schematic diagram of the flow-through electrochemical cell. Height 14 cm, length 15 cm.

electrodes are immersed to a depth of 6 mm in the electrolyte. The reference electrode is placed downstream of the sensing electrodes, thus avoiding any contamination or physical interference to the stream flow patterns. Experimentally, it was shown that the reference electrode can be a considerable distance away from the sensing probes.

In addition to incorporating the ion-sensing electrodes and the reference electrode in the cell design, temperature can be continuously monitored by using an alumel/chromel IDA Type K thermocouple (S.I.R.S. Sales, Geelong, Australia). The temperature of the plant circuit liquor is about 80°C. In order to ensure reproducibility of results, the analytical procedure includes cooling of the electrolyte as a preliminary step to measurement in the cell. The temperature of the solution can be controlled by varying the flow rate or solution path length and by introducing a stainless-steel cooling coil before the electrolyte enters the electrochemical cell as shown in Fig. 3. In this work, the monitoring temperature was typically 25°C and standards were matched to the actual measured temperature.

The cell was built of poly(vinyl chloride) with conventional PVC glue used in the joints. This plastic, as the material of construction, is preferable to glass, being not only easier and cheaper to machine, but far more robust and capable of withstanding the severe operating conditions in industry. The carbon content in grey PVC discharges any stray currents which might otherwise accumulate on the cell. In contrast, if the cell is built of perspex, spurious results occur.

Instrument configuration

For operation in a zinc refinery, use is made of a two-stage handling process consisting of a battery-powered ISE data acquisition system for monitoring copper and cadmium coupled with a conventional mains-powered liquor delivery unit. The battery-powered DAS is used to minimize noise problems in the data measurement by avoiding the impact of extraneous currents which are common in any industrial electrolytic process.

RESULTS AND DISCUSSION

Copper electrode response in plant electrolyte

In "synthetic $ZnSO_4$ solution" made from analytical reagent-grade zinc sulphate in distilled water over the concentration range 100—150 g Zn l^{-1} (1.53—2.29 M zinc solution), plots of potential against log concentration of copper were linear with a Nernstian slope of 29 ± 1 mV at 25°C over the copper concentration range 10^{-4}—10^{-2} M, which is the range of interest in this work.

When "low-level" plant liquor (see Experimental) was used, Nernstian responses over the same copper concentration range as above were observed. Because this liquor is an excellent match for the matrix of the plant solution to be monitored, this liquor is recommended for calibration purposes, rather than the synthetic solutions of zinc sulphate. An additional advantage in using this plant solution is that a ready supply is at hand and can be removed from the process circuit downstream of the zinc dust cementation stage. In addition, the waste from the flow-through cell can be returned to the process stream.

Geissler and Kunze [20] reported the formation of surface layers on the copper-sensing surface when the electrode was left standing in zinc sulphate solutions. We have also observed that after a period of time a dark grey layer forms on the surface of the electrodes used here. With time and the appearance of the grey surface layer, the slope of a plot of potential against log of the copper concentration decreases. For example, in the high-volume flow-through cell, the Nernstian slope (±2 mV) could be maintained for three days. With longer times the slope decreased, but could be restored to Nernstian behaviour by polishing as described under Experimental. As a diagnostic criterion, the electrode should not be used unless it exhibits the expected Nernstian value ±2 mV. This diagnostic test forms part of the automation routine. The solution flow rate is also important in determining the period for which the electrode exhibits Nernstian behaviour. The Orion CuS/Ag_2S electrodes and the cell used in this work apparently have longer-term stability than the Cu_2Se/Ag_2Se electrode and conventional cell used in the study by Geissler and Kunze [20]. The different origins of the zinc sulphate in the two studies could also contribute to the difference in long-term stability. To achieve any long-term stability, Geissler and Kunze introduced regular polishing with a vibrator and brush. Hirata [24] has recently reviewed different automatic polishing methods for renewing the surfaces of ISEs. Here, it proved possible to avoid this extra complication in the final ISE cell design.

Cadmium electrode response in plant electrolyte

The cadmium-selective electrode responded in a similar fashion to the copper-selective electrode. In both "synthetic $ZnSO_4$ solution" and "low-level" plant electrolyte, a slope of 25 ± 2 mV could be maintained for a three-day period for cadmium concentrations in the range 10^{-4}—10^{-2} M at

25°C. The slightly lower than Nernstian slope was reproducible. Over extended periods, the performance deteriorated in the same way as for the copper-selective electrode. The near-Nernstian response was restored by polishing.

Calibration

Standardization was achieved with two copper or cadmium solutions, 10^{-3} M and 10^{-2} M. These concentrations cover the normal range of interest. Furthermore, the Nernstian relationship applies a decade above and below these concentration levels so that reliable data can be ensured over the concentration range 10^{-4}—10^{-1} M. The instrument layout diagram (Fig. 3) illustrates the relationship between the plant liquor flow path and that of the calibrating solutions.

According to the manufacturer, these ISEs can be operated at temperatures up to 80° C. Experiments undertaken in the range of 60—70° C did not provide adequate reproducibility. Cooling the plant solution to 25 ± 5°C prior to the measurements is therefore recommended. The exact temperature of the solution at the cell is monitored with every reading. To ensure similar conditions of measurement for the process sample and the standards, all solution paths pass through a similar heat exchanger to that of the continuous sample stream (H/E) in Fig. 3. The frequency of calibration and all operations can be varied by changes in the software. Typically, calibration was undertaken every eight hours.

Validation of the method

The use of the proposed calibration procedure based on the "low-level" plant electrolyte produced results in good agreement with those from the off-line laboratory methods, which involved determination of cadmium by polarography and copper by atomic absorption spectrometry (AAS); relative errors were better than or equal to ±10% for the copper concentration range 1.9×10^{-3}—6.8×10^{-3} M (120—435 mg l^{-1} Cu) and the cadmium concentration range 8.9×10^{-4}—2.7×10^{-3} M (100—300 mg l^{-1} Cd). Typical comparative values for copper determinations are listed in Table 1.

Because high precision is not required for this process control of copper, the rather poor precision of the ISE method is acceptable. The relative precision of the measurements is similar to the off-line measurements of Geissler and Kunze [20].

Optimization of the on-line computer-controlled monitoring system

The features incorporated into the monitoring system include simple calibration procedures, long-term reliability (minimum of three days maintenance-free operation), automatic reporting of a malfunction, and convenient reporting procedures to enable plant control operations to be activated.

The systems described below incorporate features relevant to all of the above concepts.

TABLE 1

Comparison between nominal copper(II) concentrations and values determined by the ISE and AAS methods

Nominal Cu(II) concentration		ISE determination (mM)	AAS determination (mM)
(mg l^{-})	(mM)		
120	1.9	1.9 ± 0.2[a]	1.9
210	3.3	3.3 ± 0.3	3.5
220	3.5	3.4 ± 0.3	—
300	4.7	4.7 ± 0.5	5.0
320	5.0	4.7 ± 0.5	—
410	6.4	6.5 ± 0.6	6.8
435	6.8	6.4 ± 0.6	—

[a]Standard deviation for continuous measurements over 30 min.

Operation with four multiplexed copper electrodes. The recommended operating mode involves the simultaneous use of four copper electrodes with multiplexed instrumentation. The computer takes readings with respect to the reference electrode in the following sequence. First, the potential of copper electrode no. 1 is sampled thirty times over a time interval of approximately 3 ms. The arithmetic mean value of the readings is computed and stored in memory. Although there is a time interval of only 720 ns between input channel selection and start of measurement [25], a stabilization period of approximately 1 s was allowed between readings from one electrode to the next, i.e., a 1-s delay was allowed between the next channel selection and commencement of the measurement. This time interval avoids any unwanted perturbations and gives the reference electrode and the selected ISE time to equilibrate. Secondly, this process is repeated sequentially for copper electrodes no. 2, 3 and 4. Thirdly, on completion of this cycle, the stored data for the electrodes are transferred to a local visual display unit for data examination and concentration evaluation. Further data treatment can be done by a down-line computer (PL/C, Fig. 3) if required.

The apparent concentration is evaluated from data obtained at each electrode. If all four concentration values are within 10% of the average, the average value is accepted. If one value is erratic and clearly different from the other three, then this response is discarded. If on three consecutive occasions the same probe provides apparently anomalous data, then it is declared non-operational and the results from it are ignored during the evaluation sequence. The malfunction of this electrode is further verified if it gives non-Nernstian responses from the two-point calibration procedure specified above. Typically, this means a very low slope. From this evidence, a warning is issued that this electrode requires attention. However, the application of the redundancy concept still enables the measuring system to continue. If another electrode malfunctions prior to the routine maintenance every three days, the measuring system reverts to a two-electrode system.

In general, if all four copper electrodes suddenly produce erratic responses, then the computer assumes that the reference electrode is faulty and a warning signal is issued to the effect that the reference electrode needs replacement. Measurements are terminated under these conditions.

If the upper acceptable limit of copper is apparently exceeded, for example 10^{-2} M copper, a re-calibration is immediately introduced into the measurement procedure and the copper concentration is determined again. If the upper acceptable limit is still exceeded, then it is assumed the plant needs attention. At the end of each three days of operation, routine maintenance incorporates polishing all electrodes, refilling the reference electrode and after an inspection, cleaning the cell and calibration. In the above mode, the system proved to be very reliable for three-day periods, which is not true for a single-electrode system. The effect of deliberately building redundancy into the system combined with the cell design ensures much longer-term stability and reliability than is normally associated with ion-selective electrodes.

Operation with four cadmium electrodes. Essentially, the operation of the cadmium monitoring program follows the same pattern as for copper and need not be discussed in any detail. However, instead of the Nernstian slope for a plot of potential against log cadmium concentration, slightly lower slopes were observed reproducibly, e.g., 26 mV/pCd at 25°C instead of the theoretically expected 29 mV.

All operational and calibration procedures are the same for cadmium as for copper with a maintenance-free three-day operational period being attainable.

Operation with two copper and two cadmium probes. The obvious advantage of using two copper and the two cadmium electrodes is that two elements can be determined with a single piece of equipment. The disadvantage is the loss in cross-correlation between electrodes during the course of routine operation. Because malfunctioning electrodes are usually apparent only at the calibration stage under this mode of operation, an increase in the frequency of calibration is recommended. The standard solutions can contain both copper and cadmium.

Redundancy principle. Statistical arguments indicate that the advantages of two electrodes over a single electrode are not immense. However, four electrodes represent a distinct advantage. To achieve maintenance-free reliability over three days with any confidence using individual or even two sensing elements is very difficult. From the present studies, it can be concluded that the advantages of deliberate introduction of redundancy with the four electrodes offset the higher capital cost of the instrument package.

Redundancy was not built into the reference electrode because, in principle, reference electrodes are much more reliable, particularly with a regular three-day maintenance schedule. In addition, during multiplexing, a single reference electrode ensures that exactly the same reference potential is being continually used.

Interferences

Ion-selective electrodes are seldom specific so that interferences can arise. Kivalo et al. [26] reported that copper interferes with cadmium detection in pure aqueous solutions. Similarly, iron(III) has been reported to interfere with determinations of cadmium [27] and copper [5, 28—30]. None of the species at their known concentrations present in this plant electrolyte caused interference.

In contrast to the observations of Kivalo et al. [26] for pure aqueous solutions, no interference with the copper response by the presence of cadmium, or vice versa, was observed during determinations in a concentrated zinc sulphate electrolyte. No change in millivolt reading of the copper electrode was registered when 200 mg l^{-1} aliquots up to 1000 mg l^{-1} cadmium were added to a 500 mg l^{-1} Cu(II) standard solution containing 150 g l^{-1} zinc at pH 5.00. Similarly, on addition of comparable levels of copper during the determination of cadmium, no interference occurred in the same matrix.

Conclusion

By applying redundancy principles to the use of ion-selective electrodes in the determination of copper and cadmium in a zinc refinery plant electrolyte, continuous monitoring with a high volume flow-through cell is possible for a three-day period. A battery-operated data acquisition system is recommended for operation in a harsh plant environment.

Finance for the development of the CMOS-based data acquisition system was generously provided by the Deakin University Research and Consultancy Company Ltd. The authors express their gratitude to the Electrolytic Zinc Company of Australasia, Risdon, Tasmania for their support in enabling this project to be undertaken using their plant liquors.

REFERENCES

1 J. Koryta, Anal. Chim. Acta, 61 (1972) 329; 91 (1977) 1; 111 (1979) 1; 139 (1982) 1; 159 (1984) 1.
2 E. H. Hansen, A. K. Ghose and J. Růžička, Analyst, 102 (1977) 705.
3 A. Hulanicki, T. Krawczynski vel Krawczyk and M. Trojanowicz, Chem. Anal. (Warsaw), 24 (1979) 435.
4 K. Tóth, G. Nagy, Z. Fehér, G. Horvai and E. Pungor, Anal. Chim. Acta, 114 (1980) 45.
5 A. M. Bond, H. A. Hudson, P. A. van den Bosch, F. L. Walter and H. R. A. Exelby, Anal. Chim. Acta, 136 (1982) 51.
6 M. A. Arnold and M. E. Meyerhoff, Anal. Chem., 56 (1984) 20R.
7 M. A. Arnold and R. L. Solsky, Anal. Chem., 58 (1986) 84R.
8 J. R. Stetter, in D. Schuetzle and R. Hammerle (Eds), ACS Symposium Series No. 309, Fundamentals and Applications of Chemical Sensors, 1986, p. 299.
9 J. R. Stetter, P. C. Jurs and S. L. Rose, Anal. Chem., 58 (1986) 860.
10 E. S. Pilkington, C. Weeks and A. M. Bond, Anal. Chem., 48 (1976) 1665.
11 Y. M. Wang, T. J. O'Keefe and W. J. James, J. Electrochem. Soc., Electrochem. Sci. Technol., 127 (1980) 2589.

12 J. Ramirez-Muñoz, Atomic Absorption Spectroscopy, Elsevier, Amsterdam, 1968.
13 G. Horlick, Anal. Chem., 56 (1984) 278R.
14 J. A. Holcombe and T. M. Rettberg, Anal. Chem., 58 (1986) 124R.
15 A. M. Bond, Modern Polarographic Methods in Analytical Chemistry, Marcel Dekker, New York, 1980.
16 P. T. Kissinger and W. R. Heineman (Eds.), Laboratory Techniques in Electroanalytical Chemistry, Marcel Dekker, New York, 1984.
17 J. Wang, H. D. Dewald and B. Greene, Anal. Chim. Acta, 146 (1983) 45.
18 J. A. Howell and L. G. Hargis, Anal. Chem., 58 (1986) 108R.
19 Y. de Bellefroid, in K. Tozawa (Ed.), Zinc '85, Proc. Int. Symp. on Extractive Metallurgy of Zinc, October, 1985, Tokyo, Japan, p. 383.
20 M. Geissler and R. Kunze, Fresenius' Z. Anal. Chem., 318 (1984) 15.
21 C. R. Martin and H. Freiser, Anal. Chem., 51 (1979) 803.
22 A. M. Bond, H. A. Hudson and F. L. Walter, Anal. Chim. Acta, 180 (1986) 327.
23 A. M. Bond, H. A. Hudson, P. A. van den Bosch, F. L. Walter and H. R. A. Exelby, Anal. Chem., 55 (1983) 2071.
24 H. Hirata, PPM-PPMMDV, 15 (1984) 37 (Chem. Abstr., 102 (1985) 208869x).
25 Motorola — CMOS Integrated Circuits, Series C-1, Motorola Inc., 1978, p. 166.
26 P. Kivalo, R. Virtanen, K. Wickström, M. Wilson, E. Pungor, K. Tóth and G. Sundholm, Anal. Chim. Acta, 87 (1976) 387.
27 S. Sakura and R. Virtanen, Bull. Chem. Soc. Jpn., 54 (1981) 1360.
28 M. J. Smith and S. E. Manahan, Anal. Chem., 45 (1973) 836.
29 Y. S. Fung and K. W. Fung, Analyst, 103 (1978) 149.
30 J. Vesely, D. Weiss and K. Stulik, Analysis with Ion-Selective Electrodes, Horwood, Chichester, 1978, pp. 194—199.

Analytica Chimica Acta, 200 (1987) 227—235
Elsevier Science Publishers B.V., Amsterdam — Printed in The Netherlands

EFFECT OF APPLIED CURRENT ON COPPER SULPHIDE-BASED ION-SELECTIVE ELECTRODES

E. G. HARSÁNYI, K. TÓTH and E. PUNGOR*

Institute for General and Analytical Chemistry, Technical University of Budapest, Gellért tér 4, 1111-Budapest (Hungary)

M. SOMA

National Institute for Environmental Studies, Yatabe, Tsukuba, Ibaraki 305 (Japan)

Y. UMEZAWA

Department of Chemistry, Faculty of Science, Hokkaido University, Sapporo 060 (Japan)

(Received 19th November 1986)

SUMMARY

The properties of precipitate-based copper sulphide electrodes are investigated. Solid-phase studies were done by x-ray photoelectron spectroscopy and solution-phase studies by combined potentiometric and atomic absorption spectrometric techniques. The predominant valence state of copper in the copper sulphide samples is shown to be Cu(I), but Cu(II) can also be identified at the surfaces. The oxidation of the membrane surface results in dissolution of copper ion and a decrease in the Cu/S ratio in the solid phase; reduction of the surface causes sulphide dissolution and an increase in the Cu/S ratio. Application of anodic or cathodic currents was used to study the redox behaviour of the copper sulphide membrane.

Among the various ion-selective electrodes based on sulphide precipitates, the copper sulphide electrode seems to be the most complicated. Different explanations for its functioning have been offered. The copper sulphide electrode can be used for the measurement of both Cu(II) and Cu(I) ions. Some workers have suggested that the potentiometric function of the electrode is due to Cu(I) ions and that the response to Cu(II) ions takes place through a Cu(I) $\rightleftharpoons$ Cu(II) equilibrium [1, 2]. It has been shown that oxidizing agents with a redox potential higher than +0.8 V react with the surface of the copper sulphide electrode and block its surface by producing sulphur compounds of higher charge. If such a surface is treated with strong reducing agents or complexing agents, the normal functioning of the electrode membrane can be restored [3].

The redox behaviour of sulphide minerals has been studied by several authors [4–7]. The electrodes investigated were made from natural minerals. For investigating copper sulphide electrodes, current-flow conditions have also been applied, mainly with cyclic voltammetry [8, 9]. From the *i/E* curve, it was assumed that the copper dissolves from the electrode material on anodic polarization, while sulphur is formed at the surface. Ghali and

0003-2670/87/$03.50

Lewenstam [10] reached the same conclusions by investigating the CuS ion-selective membrane in chloride medium. The effect of reducing treatments has also been studied. Smith and Manahan [11] established that the reduction of copper(II) sulphide disturbs the electrode function. In another paper [12], it was shown that the slope of the calibration curve could be increased after treatment of the electrode in reducing solution.

With regard to the nature of the copper sulphide material, investigations done with x-ray photoelectron spectroscopy [13—15] made it clear that the precipitate corresponding to CuS overall stoichiometry, as well as natural minerals, contain copper in the copper(I) state. Sulphur exists in the CuS crystal structure in different valence forms, such as S^{2-} and S_2^{2-}. Crystallographic studies on natural copper-sulphide minerals [16] also support the previous results.

To obtain a clearer picture of the behaviour of the copper sulphide (given by the composition of CuS), the present investigations were designed to cover different points of view, and both the solid phase and the solution phase at the interface were studied. The surface-measurement techniques indicated that Cu(I) prevails at the surface of the CuS membrane but sometimes Cu(II) is also present. The effects of surface oxidation and reduction on the functioning of precipitate-based CuS ion-selective electrodes are reported below. Polarization was used to investigate the redox processes at the copper sulphide surface. Changes in the composition of the solid surface during polarization were followed by x-ray photoelectron spectroscopy (XPS).

EXPERIMENTAL

Electrodes and calibration

The electrodes used for the measurements were home-made precipitate-based copper sulphide membranes. The precipitate was prepared as described earlier [3]. Calibration curves were prepared for the concentration range 10^{-6}–10^{-2} mol l^{-1} copper(II) ion. The solutions were prepared by serial dilution from a 1 mol l^{-1} copper(II) nitrate stock solution. The ionic strength was adjusted in all cases with 0.1 mol l^{-1} potassium nitrate. In the calibration measurements, both conventional solution volumes (50 ml) and small volumes (300 μl) were used. In the latter case, the solutions were used for combined potentiometric and atomic-absorption measurements, i.e., the actual copper concentration in the 300-μl solutions was also measured by atomic absorption spectrometry. This combined method has already been used in earlier work [12, 17, 18]. The measuring period of the electrode potential in the large volumes was 2 min in stirred solution, whereas in the microcell, the potential was followed for 10 min without stirring. The measurements were made at 25 ± 0.5°C.

Potential measurements under current flow

The copper sulphide electrode was polarized in a simple galvanostatic system with three electrodes. A schematic diagram of the circuit is given in Fig. 1.

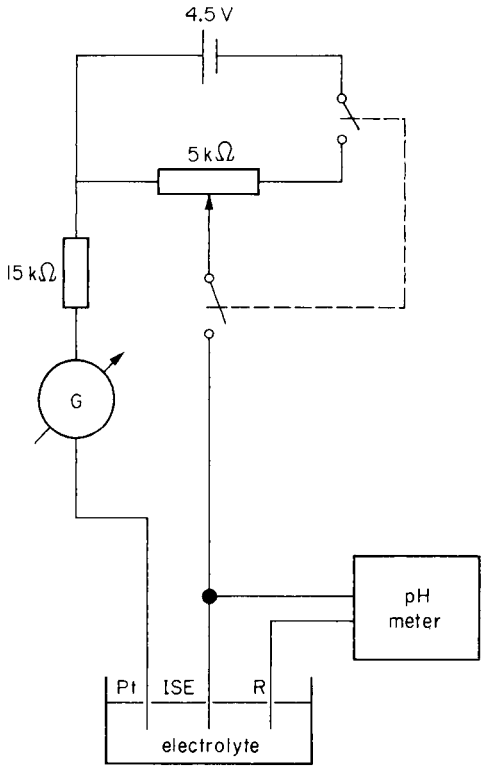

Fig. 1. Circuit used for the polarization experiments.

Surface measurements

X-ray photoelectron spectra (XPS or ESCA) were recorded on a vacuum generator (ESCA Lab. 5) equipped with a Nicolet 1070 signal averager. The copper sulphide pellets of 1-cm diameter were mounted on stainless-steel holders with a silver paste to guarantee correct contact. The precision of measurement of the spectral intensities was 5%.

The electrochemical treatment preceding the study by XPS was done with a Yanagimoto voltammetric analyzer in the controlled-potential mode.

A LABTEST ICP spectrometer was used for the simultaneous determination of copper and sulphur dissolved from a copper sulphide membrane electrode under current loading. The background emission from 0.1 M KNO_3 was corrected for.

RESULTS AND DISCUSSION

Copper(I) and copper(II) on the solid surface

Copper(II) exhibits a characteristic shake-up peak (Cu 2*p*), which is the best criterion of valence discrimination between mono- and di-valent copper:

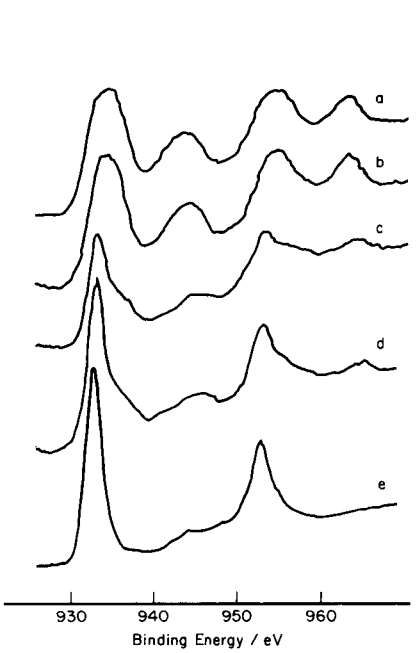

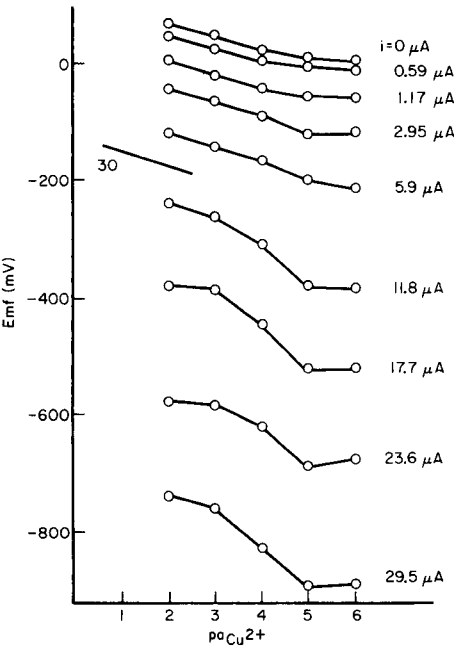

Fig. 2. Copper 2*p* signals in x-ray photoelectron spectra of different CuS-based membranes: (a) CuS powder (home-made); (b) CuS/Ag_2S mixed (1:1) powder (home-made); (c) CuS/Ag_2S coprecipitated (1:1) powder (home-made); (d) CuS powder (from Wako Chemical Company, Tokyo); (e) CuS pellet (made from home-made powder).

Fig. 3. Copper calibration curves obtained with different cathodic currents at pH 3.3. Sample volume, 50 ml. The line marked 30 shows the theoretical slope for the response.

only copper(II) gives this shake-up peak. XPS was used to examine several kinds of copper sulphide (pure CuS, coprecipitated Ag_2S/CuS and mechanically mixed Ag_2S/CuS) in both powder and pellet forms. Figure 2(a—d) shows the copper 2*p* signals from four different types of copper sulphide-based powder. Although the magnitude of the shake-up peaks differs to some extent depending on the species, all show shake-up peaks which are characteristic of copper(II) ions. Coprecipitated Ag_2S/CuS gives the smallest shake-up peak, i.e., the least copper(II) at the surface. Unlike the powder samples, well-polished copper sulphide pellets give very small or almost no shake-up peaks (Fig. 2e). These results clearly suggest that in the bulk and well-polished surface of the copper sulphide and related crystals, copper exists as Cu(I) in terms of the definition in XPS. It was also found that residual shake-up peaks for the copper sulphide pellet samples were further eliminated by treatment with chelating agents like EDTA, which also supports the assumption that the copper(II) exists only at the surface rather than in the bulk of the micro crystals. The presence of copper(I) in copper sulphide samples is also supported by electron spin resonance measurements [19]. It

was found that bands corresponding to copper(II) are negligibly small or absent in the spectra for the samples studied. The XPS results described above are consistent with those of Nakai et al. [13], i.e., the different copper sulphide samples contain copper as Cu(I). If Cu(II) is present at the surface, it could be due to oxidation. From these surface measurements, it can be concluded that the surface of the copper sulphide membrane slowly oxidizes. Therefore, it was of interest to study the redox behaviour of the membrane by using anodic and cathodic polarization.

Behaviour of the copper sulphide electrode under current-flow conditions

Dissolution of the membrane material with polarization. The concentration of copper dissolved from the copper sulphide electrode was measured in 300 μl of 0.1 M potassium nitrate during polarization. The data are summarized in Table 1. It is obvious that the concentration of copper dissolved from the electrode material decreases when a cathodic current is applied and increases when an anodic current is applied, compared to the dissolution without current. In a separate experiment, the presence of an excess of sulphide at the interface during cathodic polarization was proved by simultaneous measurements of copper and sulphur dissolved from the copper sulphide membrane at various applied currents (Table 2). These measurements were obtained by means of inductively-coupled plasma/atomic emission spectrometry (ICP/AES).

Surface change of the copper sulphide membrane after polarization. The change in the composition of the surface layer of the solid phase was examined by XPS after anodic or cathodic polarization. The relative intensity data obtained are listed in Table 3. The results show that copper becomes deficient relative to sulphur at the solid surface upon anodic treatment. Cathodic treatment results in a slight increase in the Cu/S ratio. The results are consistent with the data shown in Tables 1 and 2. Anodic treatment causes copper dissolution from the membrane whereas cathodic treatment decreases the copper dissolution and increases the sulphur dissolution. The surface oxidation and reduction processes may be described by the following reactions [6].

TABLE 1

Concentration of dissolved copper in 300 μl of 0.1 M potassium nitrate

Current (μA)		Cu conc. (mol l^{-1})	E.m.f.[a] (mV)	Current (μA)		Cu conc. (mol l^{-1})	E.m.f.[a] (mV)
None		1.6×10^{-5}	58	Anodic	1.18	2.8×10^{-5}	68
Cathodic	11.8	5.4×10^{-6}	−170		5.9	6.0×10^{-5}	299
	14.75	1.5×10^{-6}	−210		11.8	1.04×10^{-4}	1187
	17.7	4.6×10^{-7}	−247				
	20.65	3.3×10^{-7}	−287				
	23.6	$<3 \times 10^{-7}$	−313				

[a]Vs. Ag/AgCl.

TABLE 2

Simultaneous ICP/AES determinations of copper and sulphur dissolved from the copper sulphide membrane with cathodic current loading[a]

Cathodic current (μA)	Copper (mol l^{-1})	RSD (%)	Sulphur (mol l^{-1})	RSD (%)
11.8	2.04×10^{-6}	4.0	1.13×10^{-5}	3.7
23.6	1.5×10^{-6}	5.5	1.5×10^{-5}	9.5
47.2	1.05×10^{-6}	8.0	3.6×10^{-5}	4.0
118	7.3×10^{-7}	25	6.2×10^{-5}	2.6

[a]The solution volume was 2 ml. The CuS electrode applied here was different from that used for Table 1, but was of the same type. The polarization time with each current was 15 min. The relative standard deviations are for 3 tests.

TABLE 3

Corrected intensity ratios of XPS peaks[a] (CuS membrane)

Peak	Anodic[b] polarization	Cathodic[c] polarization	Polished and rinsed surface
Cu $2p^{3/2}$	4.512	8.902	7.813
S $2p(-2)$	1	1	1
Cu Auger	5.299	8.038	7.004
Cu $2p^{1/2}$	4.826	8.837	7.983

[a]All values are normalized to the S $2p$ intensity. [b]Anodic treatment in 0.1 M $NaNO_3$ at +0.5 V (vs. SCE) for 5 min, and at +1.00 V (vs. SCE) for another 5 min. [c]Cathodic treatment in 0.1 M $NaNO_3$ at −0.5 V (vs. SCE) for 10 min.

For the anodic process,

$$CuS \rightarrow Cu^{2+} + S + 2e^-$$

and for cathodic processes,

$$2\,CuS + 2e^- \rightarrow Cu_2S + S^{2-}; \quad Cu_2S + 2e^- \rightarrow 2\,Cu + S^{2-}$$

These reactions are written on the basis of the overall stoichiometry of the bulk of the membranes.

Calibrations for copper ion with polarized electrodes. The calibration curves obtained with different applied cathodic currents (Fig. 3) for 50 ml of solutions show that when the cathodic current is increased, the E^0 value decreases significantly and the slope of the calibration curve increases. For comparison, the calibration curve obtained without applied current is also given in the figure. The increase in the slope of the copper calibration might originate from the change of the solid phase during polarization or it might be the consequence of changes on the solution side of the interface.

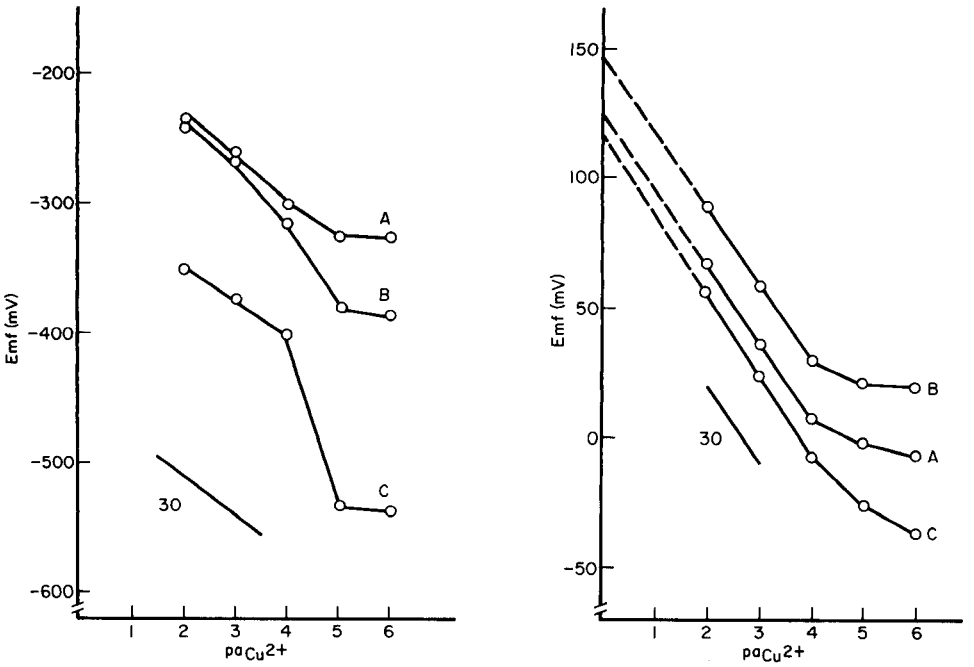

Fig. 4. Copper calibration curves obtained with a cathodic current of 11.8 μA at three pH values: (A) 2.1; (B) 3.3; (C) 6.4.

Fig. 5. Comparison of the copper calibration curves obtained after application of current. Sample volume, 50 ml. (A) Untreated membrane; (B) anodic polarization treatment; (C) cathodic polarization treatment. The line marked 30 shows the theoretical slope for the response.

To find an explanation for the behaviour of the electrode during cathodic polarization, further experiments were conducted. At a given cathodic current (11.8 μA) the calibration was repeated at three different pH values (Fig. 4), i.e., 2.1, 3.3, and 6.4. At pH 2.1, the calibration shows the normal slope. Above this pH, the increase in the slope is obvious. During cathodic polarization, sulphide ions are produced at the interface (see above). Because sulphide ions remain in the solution only at higher pH values, the increase in pH results in excess of sulphide at the interface. In this case, when copper ions are added in increasing concentrations, the excess of sulphide should be gradually titrated at the surface to give an S-shaped curve with a slope of >30 mV at pH 6.4 (Fig. 4). This kind of curve has also been observed with Ag_2S membranes in studies of the sulphide response [20]. The processes at the surface of the CuS membrane can be complicated by other reactions which also depend on the pH. At higher pH values, $CuOH^+$ species could also be formed at the interface and the electrode would respond to this species with an increased slope.

It should be mentioned that with applied anodic current, calibration curves

could not be obtained because the potential values changed rapidly, indicating rapid oxidation and parallel dissolution.

Calibration curves were also taken at zero applied current after anodic or cathodic polarization, i.e., the polarization was used only for pretreatment of the electrode. The values for these calibrations were obtained from 50-ml stirred solutions. These curves are given in Fig. 5. Shifts in the E^0 value can be observed compared with the calibration curve for the untreated membrane. These shifts indicate changes in the electrode composition during the polarization. On anodic pretreatment, excess of copper ion appears at the interface, and therefore the actual copper ion concentration at the surface is higher than the nominal value. Because of this, the calibration curve is bent more at low copper ion concentrations. After cathodic pretreatment, the excess of copper ion at the surface decreases owing to sulphide production. Therefore, at the lower concentration range of the calibration curve, the electrode shows better performance than without pretreatment (Fig. 5C). The E^0 value of metal sulphide electrodes depends on the composition, i.e., the metal-to-sulphur ratio of the solid surface. If the metal-to-sulphur ratio increases, the E^0 value decreases, and if the metal-to-sulphur ratio decreases, the E^0 value increases [7].

The potentiometric behaviour of the polarized copper sulphide electrode, the solid-phase XPS studies, and the copper and sulphur determinations by ICP/AES and atomic absorption spectrometry in the solutions contacting the electrode, all indicate the same trend. With anodic polarization, the membrane loses copper ions from the solid phase and when a cathodic current is applied, sulphide ions pass into the solution contacting the electrode. The processes at the interface can be complicated further by other reactions at the surface.

The authors thank L. Bezur for making ICP measurements, and the Hungarian Academy of Sciences and the Japan Society for Promotion of Sciences for supporting the research work. Y. U. is grateful for a Visiting Fellowship of the National Institute for Environmental Studies during the term 1983—1987.

REFERENCES

1 A. Hulanicki, M. Trojanowicz and M. Cichy, Talanta, 23 (1976) 47.
2 M. Neshkova and H. Sheytanov, Talanta, 32 (1985) 654.
3 E. Pungor, K. Tóth, M. K. Pápay, L. Pólos, H. Malissa, M. Grasserbauer, E. Hoke, M. F. Ebel and K. Persey, Anal. Chim. Acta, 109 (1979) 279.
4 W. Noddack, K. Wrabetz and W. Herbst, Z. Electrochem., 59 (1955) 752.
5 K. Werbetz, Z. Electrochem., 60 (1956) 722.
6 M. Sato, Econ. Geol., 55 (1960) 1202.
7 D. F. A. Koch, in J. O'M. Bockris and B. E. Conway (Eds.), Modern aspects of electrochemistry, No. 10, Plenum, New York, 1975.
8 I. D. Klein and R. T. Shuey, Geophysics, 43 (1978) 1222.
9 E. Hillrichs, Anodische Auflösung von Kupfersulfiden, Dissertation, Technische Universität, Braunschweig, 1981.

10 E. Ghali and A. Lewenstam, in E. Pungor (Ed.), Ion-selective Electrodes 3: Mátrafüred 1980, Akadémiai Kiadó, Budapest, 1980.
11 M. I. Smith and S. E. Manahan, Anal. Chem., 45 (1973) 836.
12 E. G. Harsányi, K. Tóth and E. Pungor, Anal. Chim. Acta, 152 (1983) 163.
13 I. Nakai, Y. Sugitani and K. Nagashima, J. Inorg. Nucl. Chem., 40 (1978) 789.
14 L. D. Partain, R. A. Schneider, L. F. Donaghey and P. S. McLeod, J. Appl. Phys., 57 (1985) 5056.
15 J. C. W. Folmer and F. Jellinek, J. Less-Common Met., 76 (1980) 153.
16 R. T. Shuey, Semiconductor Ore Minerals, Elsevier, Amsterdam, 1975.
17 E. G. Harsányi, K. Tóth, L. Pólos and E. Pungor, Anal. Chem., 54 (1982) 109.
18 E. G. Harsányi, K. Tóth, E. Pungor, Y. Umezawa and S. Fujiwara, Talanta, 31 (1984) 579.
19 T. Watanabe and Y. Umezawa, unpublished results.
20 E. G. Harsányi, K. Tóth and E. Pungor, Anal. Chim. Acta, 161 (1984) 333.

Analytica Chimica Acta, 200 (1987) 237—244
Elsevier Science Publishers B.V., Amsterdam — Printed in The Netherlands

ELECTROCHEMICAL BIOSENSORS FOR DETERMINATION OF NYSTATIN ACTIVITY

MARCO MASCINI*

Istituto di Chimica Analitica, Universita' di Firenze, Via G. Capponi 9, 50121 Firenze (Italy)

ADRIANA MEMOLI and FEDERICO OLANA

Istituto di Chimica Farmaceutica, I Universita' di Roma, La Sapienza, Rome (Italy)

(Received 18th March 1987)

SUMMARY

Nystatin is determined by recording the current of an oxygen-based biosensor or the potential of carbon dioxide-based biosensor. The yeast strain *Saccharomyces cerevisiae* is immobilized on an acetylcellulose filter and fixed to the surface of the electrochemical sensor. Both biosensors monitor the death of the strain after the addition of nystatin. Both the lag time, defined as the time elapsed between the addition of the antifungal solution and a measurable change of the current (or potential), and the slope of the recording at the midpoint of the sigmoidal curve can be related to the nystatin activity. The carbon dioxide-based biosensor provides a larger response range (100—500 U ml^{-1} nystatin) but the oxygen-based sensor is more sensitive (25—100 U ml^{-1} nystatin). All analyses are done at pH 4.5 where the response times of the electrochemical sensors are similar.

Various microbial sensors have been developed in recent years for the determination of metabolites essential to living organisms [1—8]. The death of bacteria has also been exploited for quantifying some antibiotic compounds; when the electrochemical response depends on the number of cells, the cell death can be monitored by the sensor, and the concentration of antibiotic can then be deduced from the data. Several such applications have been described [9—15]. The present paper is concerned with an extension of previous work in which nystatin was determined with an oxygen electrode [12]. A potentiometric sensor for carbon dioxide can be assembled for monitoring the respiration rate of microbial cells [1] and so also for monitoring their death when nystatin is present.

---

*Marco Mascini was recently (1986) appointed as Professor of Qualitative Analysis at the University of Firenze, after 23 years of scientific activity at the University of Rome. His main contributions have been in the area of preparation and characterization of ion-selective electrodes and gas probes. Most recently, his interest has lain in development of biosensors with immobilized enzymes, bacteria and whole tissues for electrochemical monitoring of substances of clinical, biochemical or pharmaceutical importance. Over 70 papers have been published on such topics.

0003-2670/87/$03.50

Antibiotics such as nystatin are believed to bind with the sterol present in biological membranes, leading to the formation of pores from which leakage of cellular material kills the microbial cells. The application of this principle provides a rapid and quantitative measurement of antifungal activity and the method can easily replace the microbiological assays which are often dependent of several factors. It can be used for quick screening of new products with presumed antifungal activity and for quality control of pharmaceutical preparations. *Saccharomyces cerevisiae*, a very common strain, is used. This yeast strain is immobilized on an acetylcellulose membrane held on the surface of an oxygen or carbon dioxide sensor. This coupling gives a biosensor which is easily assembled and rapid in response. This strain can be used without any expertise in microbiological culture techniques, because it is available in any grocery store. The addition of a certain amount of nystatin leads to the death of the cells and the shape of the electrochemical response is related to the concentration of nystatin.

EXPERIMENTAL

Apparatus and reagents

An Orion Research oxygen electrode (model 97-08) was used, with an Orion pH meter (model 701A) attached to an Omniscribe recorder (Houston Instruments). The gas-permeable membranes were polypropylene and the internal solution was 0.1 mol l^{-1} potassium chloride. For calibration of the oxygen sensor, the meter reading was set to 10.0 (in the pH scale) with the sensor in aerated buffer without living cells; in this way, a decrease of 1.0 in the pH scale on the meter corresponds to a decrease of 10% of the saturation level. The carbon dioxide sensor was obtained from Radiometer (model pCO_2 E-5036-0) and the gas-permeable membranes were teflon (D-602): the internal solution was 0.01 mol l^{-1} sodium hydrogencarbonate/0.1 mol l^{-1} potassium chloride. Measurements were made in a cell thermostated at 30 ± 0.2°C. All chemicals used were of reagent grade. Solutions were prepared with distilled/deionized water.

Culture and immobilization of the micro-organisms

The yeast strains were obtained from bakeries or from the American Testing Culture Collection (ATCC 2814). The strain was cultured as described previously [1], i.e., under aerobic conditions in Sabourand dextrose/agar at 27°C for 48 h. The cells were then washed with water until the oxygen content of a 0.25% (w/v) suspension was stable; this confirmed the removal of all nutrients. Such a suspension diluted tenfold had an absorbance of 0.35 at 526 nm. A portion (0.5 ml) of the diluted suspension was placed dropwise, under moderate vacuum, on a porous acetylcellulose membrane (7-mm diameter, 0.45-μm pore size, Metricel; Gelman, Ann Arbor, MI) and used without further delay.

The use of a different type of acetylcellulose filter caused sluggish responses of the sensors and less reproducible results.

The amount of suction applied to fix the micro-organisms in the pores of the membrane is important, because cells packed in different ways will metabolize glucose to different extents, so that the steady state reached will vary. Accordingly, the vacuum pressure used should be constant and carefully controlled.

Experiments done with bakery yeast and with a defined ATCC strain gave similar results, thus most of the experiments reported below were done with the fresh bakery strain.

Assembly and testing of the microbial sensors

The immobilized micro-organism was coupled with the electrode by fixing the porous membrane against the gas-permeable membrane by means of a polypropylene net (80 mesh) and a rubber ring. The treated side of the porous membrane faced the gas-permeable membrane.

For testing the probes, 20 ml of a phthalate buffer (0.1 mol l^{-1}, pH 4.5) was placed in a thermostated cell at 30°C under constant and moderate magnetic stirring, and aliquots of a standard solution of glucose were added. The phthalate buffer solution was saturated with air before testing was started. The choice of pH 4.5 was based on previous experience [1].

The membranes were prepared daily. When the membrane did not provide stable signals (equivalent to 10% of saturation level for the oxygen sensor or 10^{-3} mol l^{-1} hydrogencarbonate for the carbon dioxide sensor; see below), it was necessary to change the yeast. This happened every 3–4 weeks.

Assay procedures

Method for nystatin. A probe, once tested, was immersed in 20 ml of a 0.05 mol l^{-1} phthalate buffer pH 4.5, containing 2 g l^{-1} glucose (unless specified otherwise). After a few (usually 5–6) minutes, the probe reached a stable signal. In the case of the oxygen sensor, the stable current recorded was near zero (about 10% of the saturation level); in the case of the carbon dioxide sensor, the potential obtained was reproducible at about ± 5 mV and corresponded to a hydrogencarbonate concentration of 10^{-3} mol l^{-1}.

Nystatin was dissolved in dimethylformamide (DMF) and added to the phthalate buffer where the sensor was immersed. The concentration of DMF in the sample solution was kept below 0.66% (v/v). The electrode signal of both sensors was displayed continuously on a recorder and the rate of current increase or of electrode potential decrease was calculated from the linear portion of the response curve. The lag time was measured as the time between the introduction of DMF and the beginning of the signal increase or decrease (see Fig. 3). The criterion was a shift of 0.1 mg l^{-1} with the oxygen probe or of 1 mV for the carbon dioxide probe.

Method for pharmaceutical preparations. A tablet was weighed and finely powdered in a mortar, and a weighed amount (200 mg) was dissolved in a suitable amount of DMF to give a concentration of about 3 mg ml^{-1} nystatin, by stirring for 3–4 h. The solution was then filtered and was tested as described above.

For ointments, a sample of 200 mg was weighed and then extracted with several small aliquots of DMF by mixing intimately in a porcelain mortar. Then the DMF was collected and diluted to a final standard volume to provide a concentration of about 3 mg ml^{-1} nystatin.

In both cases, the yellow color of nystatin disappeared from the residue, which appeared translucent (ointment) or white (tablet). The DMF solution was yellow.

RESULTS AND DISCUSSION

Response of the biosensor to the number of cells

Figure 1 shows how the two sensors, based on oxygen or carbon dioxide measurements, follow the respiration rate of the micro-organisms; if sufficient nutrients are present in the solution, the current of the oxygen sensor, or the potential of the carbon dioxide sensor, depends on the number of cells. It can be seen from Fig. 1(a) that increasing the number of the cells decreases the oxygen current linearly almost to zero, whereas with the carbon dioxide sensor, the response to carbon dioxide production is linear over a much wider range under anaerobic conditions (the potential is linear with the logarithm of the cell numbers, Fig. 1b). Above a certain number of cells, the production of carbon dioxide is hindered because of the packing of the cells and the limiting concentration of the glucose.

Figure 2 shows the calibration curves for glucose with both sensors assembled with a fixed amount of cells. With the oxygen-based sensor, the current is in a linear relationship with the glucose concentration; with the CO_2-based sensor, the potential (mV) is related linearly to the logarithm of the glucose concentration over a higher range.

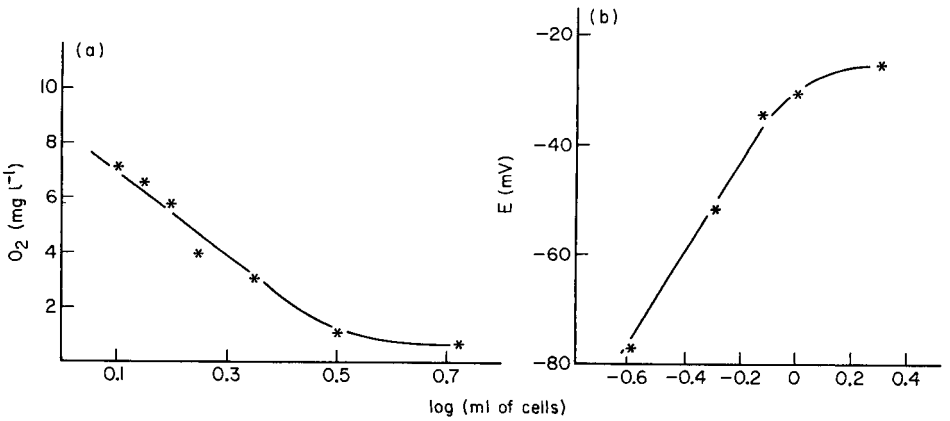

Fig. 1. Steady-state current of oxygen sensor (a) and potential of carbon dioxide sensor (b) as a function of the number of yeast cells immobilized. The abscissa relates to ml (or log ml) of diluted suspension (as described in the Procedure) filtered through the acetylcellulose filter (7-mm diameter).

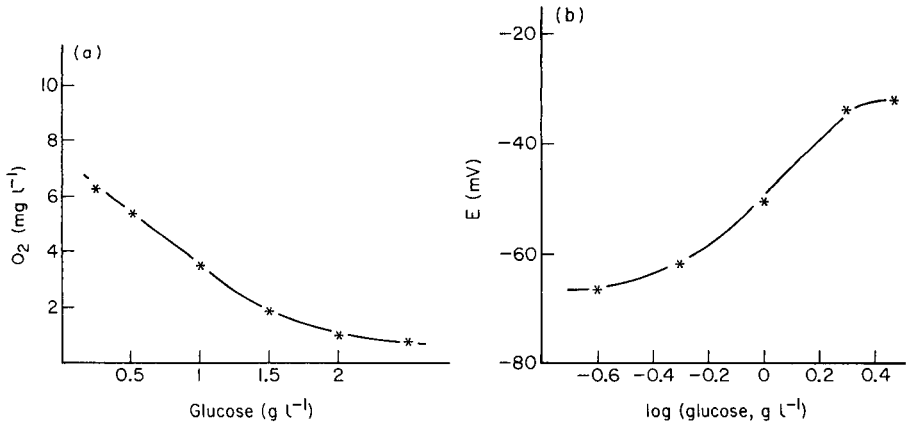

Fig. 2. Calibration curve for the oxygen-based (a) and carbon dioxide-based (b) biosensors as a function of glucose concentration.

Obviously, the glucose concentration and the number of cells are the two important parameters governing the output of the sensors. The third vital parameter is the pH, as described previously [1].

Response to nystatin

Figure 3 shows the response of both sensors to added nystatin. When the antifungal solution is added to the buffered glucose solution, after a certain lag time both sensors monitor the death of the micro-organisms by indicating

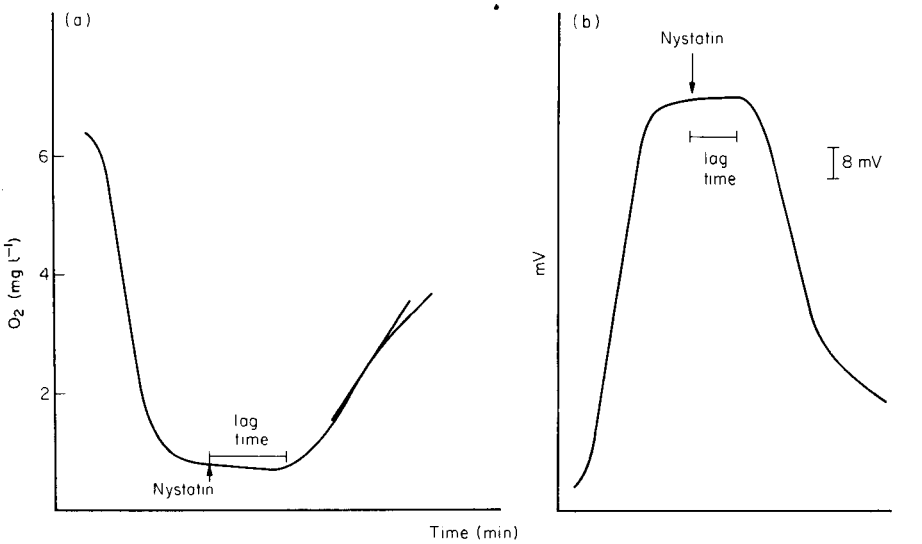

Fig. 3. Effect of nystatin on the oxygen-based (a) and carbon dioxide-based (b) biosensors. Conditions: 2 g l^{-1} glucose, 0.5 ml of immobilized cells, 50 U ml^{-1} nystatin.

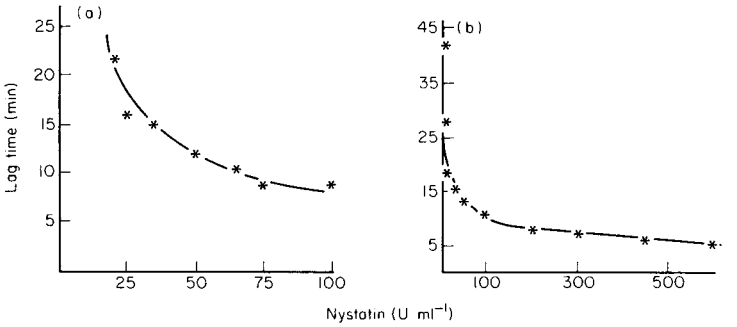

Fig. 4. Calibration curves based on lag times vs. nystatin concentration with the oxygen-based (a) and carbon dioxide-based (b) biosensors. Conditions: 2 g l^{-1} glucose, 0.5 ml of immobilized cells. The equation of the continuous line is $y = ax^b$ with $a = 130$, $b = -0.606$, $r = 0.98$ for the oxygen-based biosensor (a) and $a = 54.7$, $b = -0.371$, $r = 0.98$ for the carbon dioxide-based biosensor (b). The standard deviation for all measurements was ≤ 1 min.

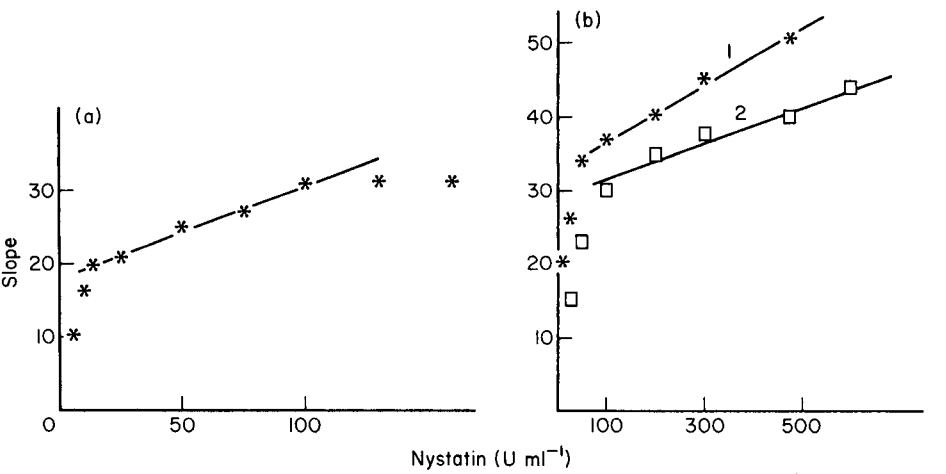

Fig. 5. Calibration curves based on slopes vs. nystatin concentration with the oxygen-based (a) and carbon dioxide-based (b) biosensors. The slopes are given in arbitrary units. Conditions: 2 g l^{-1} glucose; 0.5 ml of immobilized cells for (a) and for curve 2 in (b), but 1.5 ml of immobilized cells for curve 1 in (b). The equations of the continuous lines are: (a) $y = 0.126x + 18$ with $r = 0.989$; (b) for curve 1, $y = 0.04x + 32$ with $r = 0.998$, and for curve 2, $y = 0.026x + 29$ with $r = 0.98$.

an increase in the oxygen content (increase of current) and a decrease in the carbon dioxide concentration (decrease of potential). The lag time and the slope at the mid-point of the sigmoidal curve were taken as the analytical parameters (see Fig. 3); in Figs. 4 and 5, calibration curves for nystatin are presented with the oxygen-based and carbon dioxide-based biosensors.

The lag time (y) vs. nystatin concentration (x) plot can be described by the

TABLE 1

Determination of nystatin in a pharmaceutical preparation (Mycostatin tablets and ointment from Squibb).
(The nystatin was extracted as described in the procedure and the DMF solution was added in three different aliquots to give the nominal values. Each value is the average of 3 determinations. The results were calculated from the lag time via the equation $y = ax^b$ (Fig. 4) and from the slopes via the equations given in Fig. 5 within the linear range.)

Nystatin content (U ml^{-1})				
Nominal	Oxygen-based		Carbon dioxide-based	
	Lag time	Slope	Lag time	Slope
Tablet				
25	20 ± 5	50 ± 10	—	—
50	40 ± 5	80 ± 10	70 ± 10	30 ± 10
100	—	—	110 ± 20	125 ± 20
Ointment				
25	25 ± 5	0	—	—
50	80 ± 10	100 ± 20	50 ± 10	60 ± 10
100	—	—	110 ± 10	150 ± 30

equation $y = ax^b$; the coefficients and the correlation coefficient are reported in the legend of Fig. 4. These curves were applied in the analysis of the unknowns listed in Table 1. The carbon dioxide-based sensor has a wider useful range for nystatin (25–200 U ml^{-1}) than the oxygen-based sensor. This is more evident from Fig. 5; with the oxygen-based biosensor, a linear relationship is evident between the slope of the response and the nystatin concentration in the range 25—100 U ml^{-1} whereas with the carbon dioxide-based biosensor, the linear range is 100—500 U ml^{-1}. In both cases, the behaviour is strictly experimental and theoretical justification is not yet available, but all these calibration curves are useful for unknown samples.

Table 1 reports the results obtained for a common pharmaceutical preparation, available as tablets and ointment, with the oxygen-based and carbon dioxide-based sensors with the help of the slope and the lag-time calibration curves. The results obtained from lag times are more accurate than those obtained from slopes. The oxygen-based sensor can be used in the low range whereas carbon dioxide-based sensor can be used in the higher range. Unfortunately, no other samples were commercially available, but from these results, the method is considered to have adequate precision and accuracy for the control of bacteriological activity.

Conclusion

The coupling of an amperometric oxygen probe or a potentiometric carbon dioxide probe with *Saccharomyces cerevisiae* strain gives biosensors which can be exploited for assaying nystatin-based pharmaceutical preparations or for comparing the antifungal activity of new formulations.

The wide availability of *Saccharomyces cerevisiae* makes the method of interest because culture equipment and expertise are not required. The yeast cells are destroyed by nystatin and a new yeast membrane is needed for each analysis, but the preparation and replacement of a membrane is a simple matter provided that the bacteria can be obtained fresh from bakeries or groceries. Membranes are easily prepared and tested for efficiency.

Both lag times and slopes can be used as the analytical parameters to correlate the signals with the activity of the antifungal preparation.

REFERENCES

1 M. Mascini and A. Memoli, Anal. Chim. Acta, 182 (1986) 113.
2 I. Karube and S. Suzuki, Ion Select. Electr. Rev., 1 (1985) 3.
3 C. L. Dipaoloantonio and G. A. Rechnitz, Anal. Chim. Acta, 141 (1982) 1.
4 A. P. F. Turner, W. J. Aston, I. J. Higgins, J. M. Bell, J. Colby, G. Davis and H. A. O. Hill, Anal. Chim. Acta, 163 (1984) 161.
5 R. K. Kobos, D. J. Rice and D. S. Flournoy, Anal. Chem., 51 (1979) 1122.
6 S. R. Grobler, N. Basson and C. W. Van Wyk, Talanta, 29 (1982) 49.
7 P. M. Kovach and M. E. Meyerhoff, Anal. Chem., 54 (1982) 217.
8 R. R. Walters, B. E. Moriarty and R. P. Buck, Anal. Chem., 52 (1980) 1680.
9 D. L. Simpson and R. K. Kobos, Anal. Lett., 15 (1982) 1345.
10 D. L. Simpson and R. K. Kobos, Anal. Chem., 55 (1983) 1974.
11 D. L. Simpson and R. K. Kobos, Anal. Chim. Acta, 164 (1984) 273.
12 I. Karube, T. Matsunaga and S. Suzuki, Anal. Chim. Acta, 109 (1979) 39.
13 K. Matsumoto, H. Seijo, T. Watanabe, I. Karube, I. Satoh and S. Suzuki, Anal. Chim. Acta, 105 (1979) 429.
14 I. Karube, T. Matsunaga, T. Nakahara and S. Suzuki, Anal. Chem., 53 (1981) 1024.
15 I. Karube, T. Nakahara, T. Matsunaga and S. Suzuki, Anal. Chem., 54 (1982) 1725.

Analytica Chimica Acta, 200 (1987) 245—260
Elsevier Science Publishers B.V., Amsterdam — Printed in The Netherlands

DETERMINATION OF pH VALUES OVER THE TEMPERATURE RANGE 5—60°C FOR SOME OPERATIONAL REFERENCE STANDARD SOLUTIONS AND VALUES OF THE CONVENTIONAL RESIDUAL LIQUID-JUNCTION POTENTIALS

A. K. COVINGTON* and M. J. F. REBELO[a]

Department of Physical Chemistry, University of Newcastle upon Tyne, Newcastle upon Tyne NE1 7RU (Great Britain)

(Received 23rd March 1987)

SUMMARY

Direct measurements of the pH of six new operational standard solutions for the British Standard pH scale are reported from measurements with hydrogen gas electrodes in cells with liquid junctions reproducibly formed in vertical capillary tubes (1 mm internal diameter). Comparison with assigned pH values from cells without liquid junction enables values of the conventional residual liquid-junction potential to be calculated.

The British Standard (BS) "Specification for pH Scale" [1a] was published in 1950 following initiatives established by the Royal Society. Unlike the National Bureau of Standards (NBS) multistandard scale [2–4], the British scale is based on assigned values to a single primary-reference standard of aqueous 0.05 mol kg^{-1} potassium hydrogenphthalate [1]. Also listed [1a] were values for secondary standards determined with reference to the primary standard in the operational pH cell [3, 4] with liquid junction. A revision of BS1647 was published in 1961 [1b], which took into account the agreement for a convention (Bates-Guggenheim convention [5]) for assigning values to the single ion activity coefficient of the chloride ion and recently published measurements extending the scale(s) from 60–95°C [6]. Thus it became possible to express pH values of certain solutions to three decimal places [7], but the necessary measurements for the secondary standards of the British Scale determined by the operational cell with liquid junctions reproducibly formed within capillary tubes [8] were not available. Such work

*Arthur K. Covington is Professor of Electroanalytical Chemistry at the University of Newcastle upon Tyne. He is a graduate of the University of Reading where he studied with the late E. A. Guggenheim and J. E. Prue. He received the 1986 Royal Society of Chemistry Award and Medal for Electroanalytical Chemistry for his contributions to the development of reference standards and electrode systems in analytical potentiometry relating to chemical and biomedical applications.

[a]Permanent address: CECUL, Faculdade de Ciencias, Rua da Escola Politecnica, Lisboa, Portugal.

0003-2670/87/$03.50

was commenced in 1960 at what is now City University, London, and was published in 1967 [9]. A further revision of BS1647 was published in 1984 [1c] which incorporated these results and new measurements made at Newcastle University, which are here reported in detail. The description of such standards as operational standards (OS) rather than secondary standards is now preferred [10]. The respective merits of the BS and NBS approaches to pH scale specification have been discussed [10, 11]. Associated work on redetermination of pH values of the primary standard (PS) [12] and a method of estimating the purity of samples of potassium hydrogenphthalate have been reported [13].

The cell design used by Alner et al. [9, 14] was initially used in the present work but an improvement in cell design was effected which allowed direct measurement of the operational cell involving two liquid junctions, as described below.

EXPERIMENTAL

The operational cell

Two measurements of the e.m.f. of the cells

$$Hg|Hg_2Cl_2|\text{sat. KCl}|PS \text{ or } OS|H_2|Pt$$

or one measurement, effectively of the cell

$$Pt|H_2|PS|\text{sat. KCl}|OS|H_2|Pt \qquad (I)$$

lead to values of the pH of the operational standards, pH(OS), given by

$$pH(OS) = pH(PS) - \Delta E/k + \Delta E_J/k \qquad (1)$$

where $k = RT(\ln 10)/F$ and $\Delta E_J = E_{J(OS)} - E_{J(PS)}$ is the liquid-junction potential contribution to the cell e.m.f. (ΔE) arising from the junction between the test solution and saturated KCl, $E_{J(OS)}$, and the standard solution and sat. KCl, $E_{J(PS)}$. The last term in Eqn. 1 is known as the residual liquid-junction potential and assumed to be zero when calculating pH(OS) [10].

Design of cell vessel

The cell vessel used by Alner et al. [9] consisted of two electrode compartments, one for the hydrogen gas electrode and the other for the reference electrode, linked by a 1-mm internal diameter capillary tube, within which the liquid junction is formed. They used saturated calomel electrodes over the temperature range 0–50°C and silver/silver chloride electrodes at 60°C, as reference electrodes. On account of the tendency of calomel electrodes to have a variable potential, they used at least six electrodes in the reference half-cell compartment and periodically checked bias potentials, discarding electrodes differing by more than 10 μV.

In order to assign pH values to the secondary standards, Alner et al. [9] set up a pair of cells, one for the primary standard solution, and the other

for the secondary standard. Then pH(OS) was calculated from the difference in e.m.f. of these two cells, which corresponds to that of cell I.

It seemed better to measure directly the e.m.f. of cell I, so that the number of operations necessary was halved, and the use of calomel electrodes was avoided. At first, it was thought possible to use an inverted U-tube filled with saturated potassium chloride to interconnect the two reference compartments of two cell vessels. However, it seemed advantageous to attempt to set up cell I in one cell vessel, consisting essentially of two compartments (A, A′) for the two hydrogen electrodes, one for the primary standard and one for the operational standard. An essential feature is to keep the two liquid junctions within their respective capillary tubes. In order to provide an easy way of filling the cell with the required amount of bridge solution, a third compartment (B) for saturated potassium chloride is required, which also houses a commercial reference electrode as a check on the stability of the individual hydrogen electrodes and liquid junctions.

After a number of trials and modifications, the final design shown in Fig. 1 was evolved. The bridge solution is confined to the lower halves of the capillary tubes (G, G′), the 6-mm internal diameter tubing that connects them to the three-way tap (E), and the annular film formed in the tap. The three-way

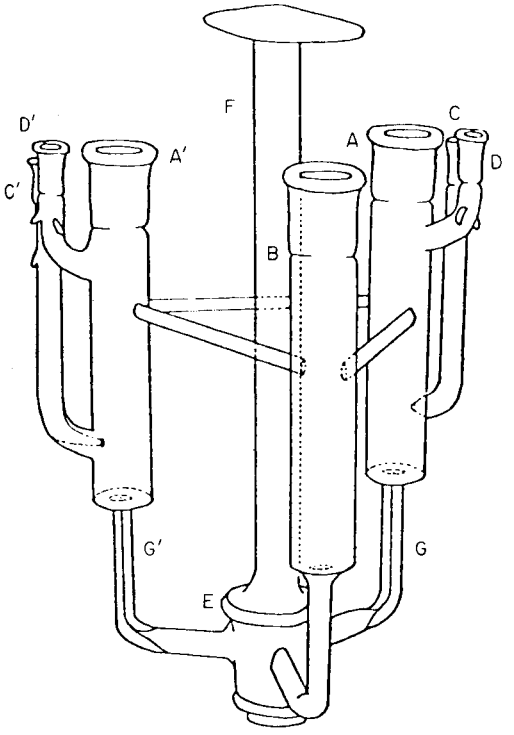

Fig. 1. Cell vessel for double liquid-junction cell (I). For A—G, see text.

tap is greased only at the top and bottom so that, when closed (with F), it leaves a central conducting path of bridge solution.

To form the liquid junction, the cell is used in the following manner. The bridge solution contained in B is allowed, by tilting the vessel and turning the tap to the appropriate position, to flow halfway up the capillary of one of the electrode compartments, and the tap is closed. The cell vessel is tilted so that the other electrode compartment is in the upper position, the tap is turned to connect to it and the same procedure is followed. The standard reference solutions are introduced into the capillary tubes with a syringe having a long hypodermic needle, which is also used to remove any air bubble trapped between the bridge solution and the standard solutions. More of the solution is then added to each electrode compartment to bring the liquid level to a predetermined mark. This mark, and a similar one on the bridge compartment, are positioned to give equal hydrostatic heads in all three compartments to minimise any tendency for flow through the incompletely greased tap to lead to the liquid junction moving out of the capillary tubes.

After the measuring compartments (A, A′) have been filled, the palladized platinum electrode (for the primary standard, PS) and the platinized electrode (for the operational standard, OS) are rinsed with the corresponding solutions and the hydrogen flow is started at a rate of two bubbles per second. The hydrogen is passed through a presaturator containing some of the same solution, and enters the cell through C and C′, escaping from it through D and D′. To equalize the hydrogen gas pressure in the two electrode compartments, D and D′ are led to a polythene Y tube and a common exit [10]. The hydrogen electrodes are allowed to reach equilibrium and the e.m.f. ΔE of the cell is read on a Hewlett-Packard 3455A digital voltmeter. After equilibrium has been reached at a set temperature, the temperature is changed and the same procedure followed. Some of the saturated potassium chloride crystallizes at low temperatures but this does not seem to affect the results.

The stability of the liquid junction was followed for about 3 h. It was found that after about 70 min it was constant to within 0.02 mV. The stability was further checked on the bench at room temperature. Tetrachlorotetrabromofluorescein was added to saturated potassium chloride to colour it red, and the cell was filled as described previously. The diffusion of the salt was followed visually into 1:1 phosphate. Both the e.m.f. measurements (Table 1) and visual observation confirmed junction stability, which was to be expected because the gradients of concentrations and electrical potential are throughout parallel to the tube axis and the liquid junction has cylindrical symmetry [8].

CHOICE OF STANDARD REFERENCE MATERIALS

The ideal properties of pH standard reference substances are [15]: (1) good buffer capacity; (2) good crystallization conditions, i.e., on crystallization from an aqueous solution, which contains an excess of acidic or alkaline com-

TABLE 1

Variation of e.m.f. of the cell $Pt|H_2|0.025$ mol kg^{-1} KH_2PO_4 — 0.025 mol kg^{-1} $NaHPO_4|$ sat. $KCl|PS|H_2|Pd$ with time at room temperature

E.m.f. (V)	Time (min)	E.m.f. (V)	Time (min)	E.m.f. (V)	Time (min)	E.m.f. (V)	Time (min)
0.1663	20	0.1676	145	0.1676_5	258	0.1677	340
0.1665	35	0.1676	160	0.1676_5	280	0.1677	355
0.1669	55	0.1675_5	175	0.1677_5	295	0.1677_5	370
0.1671	68	0.1675_5	215	0.1677	310	0.1677_5	385
0.1673	85	0.1676_5	240	0.1678	330	0.1677_5	400
0.1675	130						

ponents, crystals of the proper composition must be formed; (3) moderate solubility at room temperature so that easy purification of the salt can be achieved by recrystallization; (4) the pH in solution must show only slight dependence on concentration; (5) the pH in the solution must show only slight dependence on temperature. To these, NBS workers add the requirement of low residual liquid junction potential [3].

Substances proposed as operational standards for the British Standard and which are not included by the NBS are: sodium hydrogendiglycolate, piperazine phosphate, 4-aminopyridine and sodium sesquicarbonate. The pH of these operational standards, and others common to the NBS scale, and certain additional substances, was evaluated as described below.

Determination of pH(OS) for some operational standards

The pH(OS) for 0.05 mol kg^{-1} sodium hydrogendiglycolate; 0.02 mol kg^{-1} and 0.05 mol kg^{-1} piperazine phosphate; disodium hydrogenphosphate and potassium hydrogenphosphate at mole ratios of 3.5:1 and 4:1; 0.01667 mol kg^{-1} Tris + 0.0500 mol kg^{-1} Tris HCl; 0.02 mol kg^{-1} 4-aminopyridine + 0.02 mol kg^{-1} 4-aminopyridine HCl; 0.025 mol kg^{-1} sodium sesquicarbonate were determined by using the operational cell (I).

Sodium hydrogendiglycolate. The advantages of using sodium hydrogendiglycolate as an alkalimetric primary standard and as a reference buffer for pH standardization were pointed out by Keyworth and Hahn [16, 17]. Its solutions are close in pH to those of potassium hydrogenphthalate, so it could be used as an alternative to this standard. The other characteristics that make it a good reference buffer are as follows. It can be prepared by the half-neutralization of inexpensive, commercially available diglycolic acid. Two recrystallizations from water give a very pure salt which assays at 100.00 ± 0.05%. Sodium hydrogendiglycolate has a high molecular weight, is soluble in water, and is very stable in air. It is easily dried in 2 h at 120°C. It contains negligible impurities. It is non-hygroscopic and it has high buffer capacity. Covington and Cairns [18] have determined paH (= $-\log a_{H^+}$) over the temperature range 5—65°C from cells without liquid junction.

Piperazine phosphate [15, 19]. Piperazine phosphate, which fulfils the first four conditions described earlier, was originally proposed as a pH standard by Grove-Rasmussen [15], but rejected by Bates [3] on account of the high residual liquid-junction potential. It is commercially available but it can also be prepared by crystallization from an aqueous solution of a equimolar mixture of piperazine and phosphoric acid. The buffer capacity of a 0.05 mol kg^{-1} solution was found to be 0.037 (for the same molarity, that for potassium hydrogenphthalate is 0.023). No measurable change in pH was found for a dilution of a 0.05 mol kg^{-1} solution with an equal volume of water.

(3.5:1) Phosphate [2] and (4:1) phosphate [20]. These molar proportions (see above) are used because the pH is within the physiological range. The (4:1) phosphate has the further advantage of having an ionic strength (0.13) close to that obtained in physiological media (ca. 0.16). It has keeping qualities as good as the (1:1) primary standard, and its other buffer properties are claimed [20] to be adequate.

Tris(hydroxymethyl)aminomethane [2-amino-2(hydroxymethyl)-propane-1,3-diol; Tris]. The buffer solution formed by Tris (0.01667 mol kg^{-1}) and its hydrochloride (0.0500 mol kg^{-1}) was proposed by Durst and Staples [21] as a pH secondary standard for the physiological pH range. The advantage over the phosphate buffers used in this range is that Tris is more compatible with biological fluids than phosphate which, for example, precipitates many multicharged cations and inhibits some enzymatic processes. Its temperature coefficient of pH approximates more closely to that of whole blood and plasma than that of the phosphate buffers. Its high liquid-junction potential led Durst [22] to warn that it should not be used for the calibration of pH instrumentation.

4-Aminopyridine. 4-Aminopyridine is a solid at room temperature, melting at 161°C. It can easily be purified by recrystallization from toluene or benzene, or by sublimation. Bates and Hetzer [23] determined the dissociation constant of the 4-aminopyridinium ion and suggested the use of the compound to provide a pH buffer solution in the pH region 8.5–9.5, where undesirable side-reactions of borate buffers (such as the formation of stable complexes with many hydroxyl compounds) often preclude the use of borate.

Sodium sesquicarbonate. The advantage of using sodium sesquicarbonate instead of the carbonate/hydrogencarbonate standard is that only one substance is necessary to prepare the solution. It is a by-product of the ammonia/soda process and could be made available commercially as the dihydrate.

Preparation of the standard buffers

Details of the solution preparation are given in Table 2. Other details are given below.

Sodium hydrogendiglycolate (0.05 mol kg^{-1}). This was made from a sample prepared by Covington and Cairns [18] from Fluka puriss. grade (ca. 99%) with melting range 143–145°C.

TABLE 2

Compositions of the operational standard solutions

Substance	Concentration (mol kg^{-1})	Weight of substance (g)	Volume of HCl	Amount of H_2O
Potassium hydrogenphthalate	0.05	5.0685	—	To give 500 ml
Sodium hydrogendiglycolate	0.05	1.95086	—	250 g
Piperazine phosphate	0.05	2.52685	—	250 g
Piperazine phosphate	0.02	1.01074	—	250 g
Disodium hydrogenphosphate	0.025	3.533	—	To give 1 l
Potassium dihydrogenphosphate	0.025	3.387	—	
Disodium hydrogenphosphate	0.03043	4.302	—	To give 1 l
Potassium dihydrogenphosphate	0.008695	1.179	—	
Disodium hydrogenphosphate	0.04	1.41977	—	250 g
Potassium dihydrogenphosphate	0.01	0.34022	—	
Tris	0.01667	4.0382	25 ml HCl[a]	To give 504.95 g
Tris-HCl	0.500			
4-Aminopyridine	0.02	0.37648	2 ml HCl[a]	To give 100.45 g
4-Aminopyridinium chloride	0.02			
Sodium sesquicarbonate	0.025	0.56508	—	100 g

[a] 1 mol dm^{-3} HCl.

Piperazine phosphate. A Pfaltz and Bauer sample was recrystallized twice from water and dried at 40°C to constant weight. A comparison of this recrystallized sample with a sample used as received at the same concentration did not show any difference in pH. This comparison was done by measuring the e.m.f. of the comparator cell [24]:

$$Pt|H_2|L: R|H_2|Pt \qquad (II)$$

where L was 0.02 mol kg^{-1} piperazine phosphate (as received) and R was 0.02 mol kg^{-1} piperazine phosphate (twice recrystallized) at 25°C. The steady value of the e.m.f. was 0.02 mV.

Phosphate. Disodium hydrogenphosphate (BDH AnalaR) was recrystallized from water (the temperature should be between 50 and 95°C [25]) and dried at room temperature in a desiccator for several days over phosphorus pentoxide. This is done because the disodium salt separates from cold solutions as the dodecahydrate and cannot be dried directly to the anhydrous salt because it dissolves in its own water of crystallization at ca. 35°C and dries to form a hard cake of the heptahydrate. When the gross composition corresponds approximately to the heptahydrate, it is recommended that the drying be completed at 110°C. In this work, after drying, the solid was divided in two parts. Both were dried in a vacuum oven at 60°C, and one was further dried at 110°C to study the effect of temperature of drying on the stability of the compound. Differential thermal analysis and thermogravimetry of the salt indicated a slight feature at 70°C.

Three 0.025 mol kg^{-1} solutions of disodium hydrogen phosphate were prepared in carbon dioxide-free distilled water from (i) the salt dried at 60°C; (ii) that dried at 110°C; and (iii) AnalaR material without further purification dried at 60°C. The two recrystallized samples were compared with the other in the comparator cell. The e.m.f. of the cell II, with L = 0.025 mol kg^{-1} Na_2HPO_4 (not recrystallized) and R = 0.025 mol kg^{-1} Na_2HPO_4 (recrystallized, dried at 60°C) was 0.09 mV at 25.00°C. That with L = 0.025 mol kg^{-1} Na_2HPO_4 (recrystallized, dried at 110°C) and R = 0.025 mol kg^{-1} Na_2HPO_4 (not recrystallized) was 0.08 mV at 25.00°C.

Potassium dihydrogenphosphate (BDH AnalaR) was recrystallized from water and dried at 120°C to constant weight. The 0.025 mol kg^{-1} buffer was prepared with this salt and disodium hydrogenphosphate recrystallized and dried at 110–120°C, and compared with the solutions prepared from BDH AnalaR salts (i) without further purification, (ii) dried at 110–120°C, and (iii) with NBS SRM 186 dried at 110–120°C. The e.m.f. of the comparator cell (II) at 25°C in these circumstances was −0.08 mV for 0.025 mol kg^{-1} Na_2HPO_4/0.025 mol kg^{-1} KH_2PO_4, when L was the recrystallized salt and R was the BDH salt, not recrystallized. It was concluded that drying of Na_2HPO_4 at 60°C compared to 110°C did not make a noticeable difference.

All the differences in e.m.f. observed were within the experimental error of preparation of solutions (each cell involved four weighings and two solutions). No special precautions were taken with atmospheric carbon dioxide while recrystallizing Na_2HPO_4. Although its saturated solution at 25°C has a pH of 9.3, Manov [25] found that the pH values at 25°C for two solutions, prepared from differently dried salts, having a buffer ratio of Na_2HPO_4/KH_2PO_4 = 2, agreed to within 0.002 in pH. For one solution, the sodium salt used had been recrystallized and dried for 6 weeks before final drying in an oven at 130°C. For the other, this sodium salt had been recrystallized in an atmosphere of nitrogen gas and dried in a vacuum oven.

4-Aminopyridine. 4-Aminopyridine (Matheson, Coleman and Bell, melting range 158–160°C), was purified by sublimation at 100°C under reduced pressure (ca. 10 mm Hg).

Sodium sesquicarbonate. The solution (0.025 mol kg^{-1}) was prepared from a sample obtained from ICI Mond Division (Winnington, Cheshire) and dried at 40°C, because differential thermal analysis and thermogravimetry indicated that it started losing weight at 60°C.

Saturated (at 20°C) potassium chloride. Potassium chloride (74.55 g; BDH AnalaR) was dissolved in warm carbon dioxide-free distilled water, transferred to a 250-ml volumetric flask and allowed to cool to room temperature, and water was added to give 250 ml.

RESULTS AND DISCUSSION

The e.m.f. values measured (ΔE) and the corresponding values of pH and pH(OS) (based on the work of Butikofer and Covington [12]) are summarized

in Table 3. For 1:1 phosphate, Table 3 shows that the present results are in good agreement with those of Alner et al. [9]. The agreement for sodium sesquicarbonate and the carbonate/hydrogencarbonate buffer is within 0.01 pH.

Variation of pH(OS) with temperature

In order to analyze the variation of pH with temperature, the pH values were fitted to the equation:

$$\mathrm{pH} = A + B(T - 298.15) + C(T - 298.15)^2 + D(T - 298.15)^3 \qquad (2)$$

by polynomial linear regression analysis based on a MIDAS program for the IBM 370 computer.

Table 4 shows the coefficients of Eqn. 2 and the corresponding squared multiple correlation coefficients (r^2) for the eight operational standards studied and for sodium sesquicarbonate. The smoothed pH values, which agree to within ±0.002 with the raw data, are presented in Table 5. Table 6 gives the pH temperature coefficients at 25°C and 37°C. The amine buffers show a stronger dependence on temperature than the others. This dependence decreases with increase in temperature. For completeness, Table 7 shows the coefficients for fitting Eqn. 2 calculated by Butikofer from the results of Alner et al. [9] for ten operational standards.

Comparison of pH(OS) with paH

Values of the operational pH can be compared with $p_aH = -\log a_{H^+}$ obtained for cells without liquid junction as used in the NBS multistandard pH scale [2–4]. Values for 0.1 and 0.01 mol dm^{-3} acetic acid/sodium acetate buffers were calculated from data provided by Bates [26], converted to absolute millivolts. The required values of E^0 were calculated from an equation [27] used to fit data of Harned and Ehlers [28]. With these values for E^0 and the observed e.m.f., $p_aH = -\log a_{H^+}$ was calculated by the usual method [2–4]. These data were fitted by a polynomial linear regression analysis based on a MIDAS program for the IBM 370 to Eqn. 2 with $D = 0$. The equations are for 0.1 mol dm^{-3} acetate:

$$\mathrm{pH} = 4.6539 - 0.15035 \times 10^{-3}\,(T - 298.15) + 0.40341 \times 10^{-4}\,(T - 298.15)^2$$

(with $r^2 = 0.0994$)

and for 0.001 mol dm^{-3} acetate:

$$\mathrm{pH} = 4.7202 + 0.17749 \times 10^{-3}\,(T - 298.15) + 0.33291 \times 10^{-4}\,(T - 298.15)^2$$

(with $r^2 = 0.939886$)

The corresponding smoothed values for 0–50°C are shown in Table 8.

Differences between paH and pH(OS) are an estimate of the error caused by the residual liquid-junction potential. They are designated [10] as conventional residual liquid-junction potentials because their evaluation is based on the adoption of the Bates-Guggenheim convention which led to the NBS

TABLE 3

ΔE Measurements of operational standards and calculated pH(OS) values

Solution		Temperature (°C)										
		0	5	10	15	20	25	30	37	40	50	60
0.05 mol kg^{-1}	ΔE/mV	—	29.38	29.60	—	30.15	30.20	30.53	31.16	30.90	31.60	32.02
Sodium hydrogen-	ΔpH	—	0.5323	0.5269	—	0.5184	0.5105	0.5076	0.5064	0.4973	0.4928	0.4846
diglycolate	pH(OS)	—	3.4657	3.4701	—	3.4816	3.4945	3.5034	3.5156	3.530	3.557	3.595
0.02 mol kg^{-1}	ΔE/mV	—	136.82	136.12	—	134.30	133.36	132.26	130.58	129.78	126.95	123.78
						134.28	133.32	132.24				
piperazine							133.32					
phosphate	ΔpH	—	2.479	2.423	—	2.309	2.254	2.199	2.122	2.089	1.980	1.872
						2.309	2.254	2.198				
							2.254					
	pH(OS)	—	6.477	6.420	—	6.310	6.259	6.210	6.144	6.116	6.030	5.952
						6.310		6.209				
0.05 mol kg^{-1}	ΔE/mV	—	137.12	136.32	—	134.32	133.44	132.15	130.26	129.45	126.66	123.66
						134.38	133.38	132.13	130.21	129.35	126.71	123.72
piperazine							133.35					
phosphate	ΔpH	—	2.484	2.426	—	2.309	2.256	2.197	2.117	2.083	1.975	1.871
						2.310	2.255	2.197	2.116	2.082	1.976	1.872
							2.254					
	pH(OS)	—	6.482	6.423	—	6.310	6.261	6.208	6.139	6.110	6.025	5.951
						6.311	6.260		6.138	6.109	6.026	5.952
							6.259					
0.025 mol kg^{-1}	ΔE/mV	160.85	162.23	163.78	165.34	166.91	168.50	170.34	172.92	173.81	177.32	181.00
			162.17	163.72		166.69	168.51		172.80			
phosphate				163.68		166.86	168.52					
	ΔpH	2.968	2.939	2.915	2.8919	2.8696	2.8483	2.8320	2.810	2.797	2.766	2.7382
			2.938	2.914		2.8658	2.8485		2.808			
				2.913		2.8687	2.8487					
	pH(OS)	6.967	6.937	6.912	6.889	6.870	6.853	6.543	6.832	6.824	6.816	6.818
			6.936	6.911		6.866	6.854		6.830			
				6.910		6.869	6.854					

3.5:1 phosphate	ΔE/mV	190.10	191.92 192.28 192.43	194.82 194.43 194.58	197.06	199.21 198.80 198.95	201.32 201.20 201.26	203.18 203.25	205.95	—	—	—
	ΔpH	3.508	3.477 3.484 3.487	3.468 3.461 3.463	3.447	3.425 3.418 3.420	3.403 3.401 3.402	3.378 3.379	3.347	—	—	—
	pH(OS)	7.508	7.475 7.482 7.485	7.465 7.458 7.460	7.445	7.425 7.418 7.420	7.408 7.406 7.407	7.389 7.390	7.369			
4:1 phosphate	ΔE/mV	—	193.93	196.11	—	200.40 200.30	202.60 202.66 202.35	204.64	208.14	—	—	—
	ΔpH	—	3.514	3.491	—	3.445 3.444	3.425 3.426 3.420	3.402	3.382	—	—	—
	pH(OS)	—	7.512	7.488	—	7.446 7.445	7.430 7.429 7.425	7.413	7.404	—	—	—
0.01667 mol kg^{-1} Tris	ΔE/mV	238.44	233.95 234.14	229.50 229.60	224.92	220.15 220.31	215.56 215.61	210.71	203.93 203.82	200.42	190.20	179.50
0.0500 mol kg^{-1} Tris HCl	ΔpH	4.399	4.239 4.242	4.085 4.086	3.9340	3.785 3.788	3.644 3.645	3.503	3.314 3.312	3.226	2.966	2.715
	pH(OS)	8.399	8.237 8.240	8.082 8.083	7.932	7.785 7.788	7.649 7.650	7.514	7.336 7.334	7.234	7.016	6.795
0.02 mol kg^{-1} 4-amino-pyridine	ΔE/V	—	311.75	—	305.95	—	299.70	296.42	291.58	289.32	281.55	—
	ΔpH	—	5.6488	—	5.3513	—	5.0662	4.9281	4.7382	4.6565	4.3911	—
0.02 mol kg^{-1} 4-amino-pyridine HCl	pH(OS)	—	9.646	—	9.345	—	9.071	8.939	8.760	8.683	8.441	—
0.025 mol kg^{-1} sodium sesqui-carbonate	ΔE/V	—	343.63	—	349.03	—	354.68	357.62	361.74	363.58	369.53	—
	ΔpH	—	6.2262	—	6.1048	—	5.9956	5.9456	5.8783	5.8516	5.7633	—
	pH(OS)	—	10.224	—	10.103	—	10.001	9.957	9.900	9.879	9.813	—

TABLE 4

Coefficients of the equation pH(OS) = $A + B(T - 298.15) + C(T - 298.15)^2 + D(T - 298.15)^3$ and corresponding regression coefficients for operational standards

Buffer solution	Temperature range (°C)	A	$B \times 10^2$	$C \times 10^4$	$D \times 10^6$	r^2
0.05 mol kg^{-1} sodium hydrogendiglycolate	5—60	3.4924	+0.18871	0.27983	0.04838	0.99787
0.02 mol kg^{-1} piperazine phosphate	5—60	6.2589	—1.0099	0.39601	—0.04977	0.99999
0.05 mol kg^{-1} piperazine phosphate	5—60	6.2587	—1.0503	0.37764	0.3306	0.99994
0.025 mol kg^{-1} phosphate (1:1)	0—60	6.8542	—0.27466	0.61299	—0.3730	0.99896
(3.5:1) phosphate	0—60	7.4060	—0.32435	0.17178	—0.5439	0.99411
(4:1) phosphate	5—37	7.4277	—0.31767	0.80661	1.4713	0.99836
0.01667 mol kg^{-1} Tris, 0.0500 mol kg^{-1} Tris HCl	0—60	7.6484	—2.747	0.9619	—0.2493	0.99998
0.02 mol kg^{-1} 4-aminopyridine, 0.02 mol kg^{-1} 4-aminopyridine HCl	5—50	9.0715	—2.6906	0.81630	—0.5658	1.00000
0.025 mol kg^{-1} sodium sesquicarbonate	5—50	10.001	—0.93047	0.83855	—0.4684	1.00000

assigned values. The conventional residual liquid-junction potentials at 25°C are plotted in Fig. 2. Included are the values for 0.05 mol kg^{-1} piperazine phosphate which are given in Table 9. From Fig. 2 it is evident that, in the intermediate pH range, buffers that are not of the amine-type show very low conventional residual liquid-junction potentials. This is in agreement with the fact that ionic mobilities are rather uniform. With similar ionic mobilities, and when ionic strengths of test and reference solutions are not greatly different, and when the hydrogen and hydroxyl ions account for only a small fraction of the ionic strength of the solution, only small residual liquid junctions are to be expected. This is seen to be the case with tartrate, acetate, phosphate and 0.01 mol kg^{-1} borate. Also shown in Fig. 2 are the values obtained by Paabo and Bates [29] which are in good agreement with those of Maas [30]. The results in Fig. 2 are not in agreement with a recent study in which glass combination electrodes were used; Wu et al. [31] found that for the 1:1 phosphate, tartrate, phthalate, borate and carbonate buffers the values did not exceed ±0.002 pH. Variations in the conventional residual liquid-junction potentials are a combination of the assumption of the Bates-Guggenheim convention [5] and a residual liquid junction itself. A variation from 1.5 to 2.0 in the ionic size parameter (at 0.1 mol kg^{-1} ionic strength) in the expression for the calculation of the activity coefficient of chloride causes a change of 0.01.

Larger conventional residual liquid-junction potentials are found for amine-type buffers, especially piperazine phosphate [19]. The inadequacy of the Debye-Hückel equation for amine-type buffers where the cation is of the form BH^+ was pointed out by Bates and Pinching [32] on the basis of the improbably small, often zero, and sometimes negative, values for the ion-size parameter to fit activity coefficient terms of the form $\gamma_{BH^+}\gamma_{Cl^-}/\gamma_B$. Consequently, it would be wrong to attribute the observed high conventional residual liquid-junction potentials for amine-type buffers to high residual

TABLE 5

pH(OS) values of some operational standard solutions at temperatures of 0–60°C. (Values in brackets are from smoothing equations in Table 4 [9])

Temp. (°C)	Solutions								
	0.05 mol kg^{-1} sodium hydrogen-diglycolate	0.02 mol kg^{-1} piperazine phosphate	0.05 mol kg^{-1} piperazine phosphate	0.025 mol kg^{-1} phosphate (1:1)	3.5:1 phosphate	4:1 phosphate	0.01667 mol kg^{-1} Tris 0.0500 mol kg^{-1} Tris HCl	0.02 mol kg^{-1} 4-amino-pyridine 0.02 mol kg^{-1} 4-amino-pyridine-HCl	0.025 mol kg^{-1} sodium sesqui-carbonate
0	—	—	—	6.967 (6.961)		—	8.399	—	— (10.273)
5	3.465	6.477	6.481	6.937 (6.935)	7.482	7.512	8.238	9.647	10.224 (10.212)
10	3.470	6.420	6.424	6.911 (6.912)	7.460	7.489	8.083	9.435	10.161 (10.134)
15	3.476	6.364	6.368	6.888 (6.891)	7.441	7.466	7.933	9.349	10.103 (10.098)
20	3.484	6.310	6.312	6.870 (6.872)	7.423	7.445	7.788	9.208	10.049 (10.045)
25	3.492	6.259	6.259	6.854 (6.856)	7.406	7.428	7.648	9.072	10.001 (9.995)
30	3.503	6.209	6.207	6.842 (6.843)	7.390	7.414	7.513	8.939	9.956 (9.948)
37	3.519	6.143	6.139	6.830 (6.828)	7.369	7.404	7.332	8.759	9.900 (9.889)
40	3.527	6.116	6.111	6.826 (6.823)	—	—	7.257	8.684	9.879 (9.866)
50	3.558	6.030	6.025	6.818 (6.814)	—	—	7.018	8.684	9.813 (9.800)
60	3.595	5.952	5.952	6.817 (6.817)	—	—	6.794	—	— (9.754)

TABLE 6

Temperature coefficients, $\partial pH/\partial T$, of operational standards at 25 and 37°C

Operational standard	$(\partial pH/\partial T)$ (K)	
	25°C	37°C
0.05 mol kg^{-1} sodium hydrogendiglycolate	1.88×10^{-3}	2.58×10^{-3}
0.02 mol kg^{-1} piperazine phosphate	-1.00×10^{-2}	-9.17×10^{-3}
0.05 mol kg^{-1} piperazine phosphate	-1.05×10^{-2}	-9.45×10^{-3}
0.025 mol kg^{-1} phosphate (1:1)	-2.75×10^{-3}	-1.44×10^{-3}
(3.5:1) phosphate	-3.24×10^{-3}	-3.06×10^{-3}
(4:1) phosphate	-3.18×10^{-3}	-6.05×10^{-4}
0.01667 mol kg^{-1} Tris, 0.0500 mol kg^{-1} Tris HCl	-2.75×10^{-2}	-2.53×10^{-2}
0.02 mol kg^{-1} 4-aminopyridine 0.02 mol kg^{-1} 4-aminopyridine HCl	-2.69×10^{-2}	-2.52×10^{-2}
0.025 mol kg^{-1} sodium sesquicarbonate	-9.30×10^{-3}	-7.49×10^{-3}

TABLE 7

Values of the constants of Eqn. 2 for the ten operational standard solutions (recalculated from [9])

Buffer	Conc. (mol kg^{-1})	A	$B \times 10^4$	$C \times 10^6$	$D \times 10^7$
Tetroxalate	0.1	1.4787 ±0.0015	8.7078 ±0.0003	7.756	−1.266
Tetroxalate	0.05	1.6462 ±0.0014	3.1845 ±0.0001	−8.733	3.136
Tartrate	Sat.[a]	3.5555 ±0.0001	−14.7515 ±0.0000	40.281	−0.0301
Acetic acid/ sodium acetate	0.02	4.7130 ±0.0005	2.9095 ±0.0000	37.174	−0.1575
Acetic acid/ sodium acetate	0.2	4.6435 ±0.0008	−0.7529 ±0.0001	31.991	0.9828
Phosphate	0.025	6.8567 ±0.0008	−29.7767 ±0.0001	49.338	0.8568
Borate	0.05	9.1818 ±0.0012	−98.9233 ±0.0001	75.587	0.9281
Borate	0.01	9.1793 ±0.0018	−87.0216 ±0.0002	81.179	−2.189
Carbonate	0.025	9.9947 ±0.0016	−96.7029 ±0.0001	67.187	3.571
Calcium hydroxide	Sat.[b]	12.4305 ±0.0011	−334.8801 ±0.0001	141.778	−2.037

[a]Saturated at 25°C. [b]Saturated at 20°C.

TABLE 8

Smoothed p*a*H and pH(OS) values for 0.1 and 0.01 mol dm^{-3} acetate for 0—50°C

Temperature (°C)	0.1 mol dm^{-3} acetate		0.01 mol dm^{-3} acetate	
	p*a*H	pH(OS)	p*a*H	pH(OS)
0	4.683	4.664	4.737	4.729
10	4.665	4.652	4.725	4.717
20	4.656	4.645	4.720	4.713
25	4.654	4.644	4.720	4.713
30	4.654	4.644	4.722	4.715
37	4.658	4.647	4.727	4.722
40	4.661	4.650	4.730	4.726
50	4.675	4.663	4.745	4.743

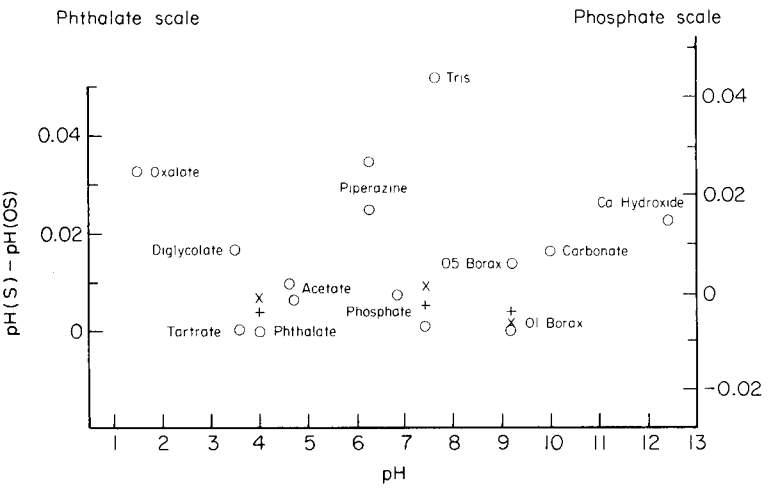

Fig. 2. Plot of conventional liquid-junction potential expressed in terms of pH for some buffer solutions at 25°C: (⊙) this work (relative to phthalate); (+) Paabo and Bates (relative to 1:1 phosphate [29]); (×) Maas (relative to 1:1 phosphate [30]).

TABLE 9

pH(OS), p*a*H and ΔpH of 0.05 mol kg^{-1} piperazine phosphate for 5—50°C

Temperature (°C)	5	10	20	25	30	37	40	50
pH(OS)[a]	6.481	6.424	6.312	6.249	6.207	6.139	6.111	6.026
p*a*H[b]	6.525	6.463	6.348	6.294	6.243	6.176	6.149	6.066
p*a*H − pH(OS)	0.044	0.039	0.036	0.035	0.036	0.038	0.038	0.040

[a]Present work. [b]From [19].

liquid-junction potentials. The large difference between 0.02 and 0.05 mol kg^{-1} piperazine phosphate is also attributable to the inapplicability of the Bates—Guggenheim convention used by Hetzer et al. [19] for these solutions. They argued that the symmetrical arrangement of the activity coefficients indicates that the change in p*a*H value with concentration should be small. At 25°C, the p*a*H values for 0.02 mol kg^{-1} piperazine phosphate are 6.284 and 6.294, respectively, i.e., a difference of 0.01. The pH(OS) values from the present work are 6.2589 and 6.2587 respectively. This difference of 0.030 ± 0.005 is consistent with some pH measurements [15, 19]. The data given by Hetzer et al. [19] for the p*a*H of piperazine phosphate should be re-examined in terms of a better equation for the activity coefficients than that given by the Debye-Hückel theory with the Bates-Guggenheim convention for the ionic size parameter.

REFERENCES

1 British Standard Institution, Specification for pH Scale, BS 1647: (a) 1950, (b) 1961, (c) Part I and Part II, 1984.
2 R. A. Durst, Standard Reference Materials, Standardization of pH Measurements, NBS Special Publication, 260-53, 1975.
3 R. G. Bates, Electrometric pH Determinations, Wiley, New York, 1964.
4 R. G. Bates, Determination of pH, Theory and Practice, 2nd edn., Wiley, New York, 1973.
5 R. G. Bates and E. A. Guggenheim, Pure Appl. Chem., 1 (1960) 163.
6 V. E. Bower and R. G. Bates, J. Res. Natl. Bur. Stand., 59 (1957) 261.
7 R. G. Bates, J. Res. Natl. Bur. Stand., Sect. A, 66 (1966) 179.
8 E. A. Guggenheim, J. Am. Chem. Soc., 52 (1930) 1315.
9 D. J. Alner, J. J. Greczek and A. B. Smeeth, J. Chem. Soc. A, (1967) 1205.
10 A. K. Covington, Anal. Chim. Acta, 127 (1981) 1.
11 R. G. Bates, Crit. Rev. Anal. Chem., 10 (1981) 247.
12 H. P. Butikofer and A. K. Covington, Anal. Chim. Acta, 108 (1979) 179.
13 A. K. Covington and A. J. Utting, Analyst, 105 (1980) 470.
14 D. J. Alner and J. J. Greczek, Lab. Pract., 14 (1965) 721.
15 K. V. Grove-Rasmussen, Acta Chem. Scand., 7 (1953) 231.
16 D. A. Keyworth and R. B. Hahn, Anal. Chem., 30 (1958) 1343.
17 D. A. Keyworth and R. B. Hahn, Talanta, 1 (1958) 41.
18 A. K. Covington and J. Cairns, J. Solution Chem., 9 (1980) 517.
19 H. B. Hetzer, R. A. Robinson and R. G. Bates, Anal. Chem., 40 (1968) 634.
20 S. J. G. Semple, G. Mattock and R. Uncles, J. Biol. Chem., 237 (1962) 963.
21 R. A. Durst and B. R. Staples, Clin. Chem., 18 (1972) 206.
22 R. A. Durst, Clin. Chem., 23 (1977) 292.
23 R. G. Bates and H. B. Hetzer, J. Res. Natl. Bur. Stand., Sect. A, 64 (1960) 427.
24 F. G. K. Baucke, Chem. Eng. Tech., 49 (1977) 739.
25 G. G. Manov, J. Assoc. Off. Anal. Chem., 30 (1947) 500.
26 R. G. Bates, private communication.
27 H. P. Butikofer, A. K. Covington and D. A. Evans, Electrochim. Acta, 24 (1979) 1071.
28 H. S. Harned and R. W. Ehlers, J. Am. Chem. Soc., 1350 (1932) 2179.
29 M. Paabo and R. G. Bates, unpublished work, quoted in ref. 4.
30 A. H. J. Maas, Clin. Chim. Acta, 28 (1970) 373.
31 Y. C. Wu, W. F. Koch and G. Marinenko, J. Res. Natl. Bur. Stand., 89 (1984) 395.
32 R. G. Bates and G. D. Pinching, J. Res. Natl. Bur. Stand., 42 (1949) 419.

Analytica Chimica Acta, 200 (1987) 261—268
Elsevier Science Publishers B.V., Amsterdam — Printed in The Netherlands

THE INFLUENCE OF FLUORIDE AND SULPHATE ON BUFFERS USED FOR THE DETERMINATION OF THE pH AND SPECIATION OF PROTOLYTES IN SEAWATER

DAVID DYRSSEN and MARGARETA WEDBORG*

Department of Analytical and Marine Chemistry, Chalmers University of Technology and University of Göteborg, S-412 96 Göteborg (Sweden)

(Received 1st May 1987)

SUMMARY

Various aspects of the measurement of pH in seawater are described. The assumptions underlying the assignment of a pH to a buffer are discussed, as well as the links to the alkalinity titration and calculations of carbonate speciation. Although the correction for fluoride is small, the correction for sulphate (0.129) can be significant.

The work of Bates at the National Bureau of Standards (NBS) resulted in recommendations on how pH should be measured potentiometrically with a glass and a reference electrode (see, e.g. [1]). It proved to be difficult to estimate the true hydrogen ion activity with pure water as a standard state from calibration of the cell in buffers of low salinity. Therefore, Bates suggested that the pH should be operationally defined, so that it depends on the practical procedure of measurement as well as on the choice of standard state.

Today, Bates' recommendations and the NBS buffers are widely accepted. Unfortunately, the operational pH is affected by the irreproducible change in the liquid-junction potential of the reference electrode when it is transferred from the buffer to the sample. This effect increases as the difference in composition between the buffer and the sample becomes greater. Because seawater with an ionic strength of 0.7 M is quite different from the low-salinity NBS buffers with an ionic strength of less than 0.1 M, and because it is desirable to make very precise pH measurements, this problem has been much debated by marine chemists over the last decades (see, e.g., Hansson [2]; Johnson et al. [3]; Bates [4]; Hansson et al. [5]; Bates and Culberson [6]; UNESCO [7, 8]). The problem is, however, far more general because many media used in practical work are different from the low-salinity aqueous buffers.

Essentially two ways have been tried to avoid the irreproducibility problem. One way is to make one's own buffer, which is similar to seawater in ionic composition [2, 6, 9]. Another way is to try to make the measurements in such a way that the irreproducible changes cancel out, and to improve the

0003-2670/87/$03.50

construction of the reference electrode [10, 11]. The carbon dioxide subgroup of the Joint Panel on Oceanographic Tables and Standards (JPOTS) has recently recommended the first-mentioned way [8]. Still, efforts to improve the reliability of the liquid junction are important, especially for measurements in estuarine and other waters of low salinity [11—13].

The purpose of this paper is to discuss some of the links between theory and practice in the determination of pH in seawater.

MEASUREMENT OF pH IN SEAWATER

The application of various standard states for the hydrogen ion in seawater and in estuarine waters has been discussed by many workers [7, 8, 13—15]. In practical work, one must be aware of the assumptions on which the measurements are based and of the limitations relevant to the reliability of the results obtained. Bates [1] outlined a practical procedure for the estimation of pH:

$E_s = E_{ks} - a\ \mathrm{pH(S)}$ (standard buffer with known pH)

$E_x = E_{kx} - a\ \mathrm{pH(X)}$ (unknown solution)

where E_s and E_x are the measured e.m.f.'s, $a = RT \ln 10/F$ and E_{ks} and E_{kx} are the intercepts which depend on the electrodes and on the standard state chosen for the standard buffer. Generally, it is assumed that $E_{ks} = E_{kx}$. If, however, a buffer of low salinity with a pH assigned on the infinite dilution scale is used for a measurement in a solution of high salinity such as seawater, this is not true. Then E_{ks} and E_{kx} will differ by ΔE_j, the difference in liquid-junction potential. This displacement of the operational pH will depend on the equipment used. Even if the same electrodes are used, the displacement will change with time. Thus the use of correction terms for ΔE_j is a dubious practice.

It has been suggested that the problem of the liquid-junction potential can be overcome if apparent constants are determined experimentally with the same equipment as is used for the pH measurement [3, 8]. From the above discussion, it is evident that such a consistency is very difficult to achieve. The simplest way to avoid the problem is to make a buffer which is similar in composition to the unknown solution. With such buffers, the ionic medium is defined as the standard state, not only for acids and bases, but also for the hydrogen ion. Buffers of this kind are not commercially available at present, but they can be assigned pH values by the experimental procedure of Hansson [2] which will be discussed in the next section.

The theoretical basis for the ionic medium scale (which is, in fact, an infinite number of scales, one for each composition) is really an extension of the infinite dilution scale. Thus, in both cases, free hydrogen ions and those which are interacting with the medium are taken as the activity. With pure water as the standard state, the activity is defined as the sum of all hydrated hydrogen ions (so-called free hydrogen ions). If the reference medium contains

dissolved salts, the activity is defined as the sum of all the hydrated hydrogen ions and all the hydrogen ions which interact with the ions present in the medium. What is included in the activity does not depend on the response mechanism of the ion-selective electrode used, which is generally considered to respond to the free hydrogen ions, but on the standardization procedure.

It is important to remember this, because three slightly different compositions have been suggested for the seawater standard buffers: (1) as seawater, but without sulphate and fluoride [4, 6]; (2) as seawater, but without fluoride [2, 16]; (3) as seawater [8, 15]. From a practical point of view, any one of these media could be selected, because all of them are sufficiently close to seawater to make ΔE_j negligible. Hansson [2] did not add fluoride to his media, because its effect is only around one hundredth of a logarithmic unit, and because he wished to restrict the number of protolytes that would interfere with his measurements of the carbonate system. Bates [4] suggested chloride media of the same ionic strength as seawater, which would give the hydrogen ion activity on the free ionic medium scale. In contrast to the infinite dilution scale, conversion between any two of the three activity scales above is quite straightforward and essentially free from experimental irreproducibilities.

How the activity scales are related

This treatment of the activity scales is in accord with recommendations made by the UNESCO panel [8]. The scales are summarized in Table 1. It should be noted that they differ not only in the choice of reference state but also in the concentration units used. For the NBS scale, $k_H a_H(\text{NBS}) = 10^{-pH(NBS)}$, where k_H describes the effect of changes in the liquid-junction potential when the electrodes are transferred from buffers to seawater; $a_H(\text{NBS}) \approx m_H \gamma_H$, where γ_H is the activity coefficient of the hydrogen ion on the NBS scale.

In the total hydrogen-ion concentration scale,

$$m_H(\text{SWS}) = m_H(1 + K_{HSO4}\,[SO_4^{2-}]_T + K_{HF}\,[F^-]_T)$$

where $[SO_4^{2-}]_T$ and $[F^-]_T$ are the total concentrations and K_{HSO4} and K_{HF} are the conditional stability constants for HSO_4^- and HF. In this scale,

$$[H]_{SWS} = m_H(\text{SWS})/(1 - 10^{-3}\,S)$$

where S is the salinity and thus $10^{-3}\,S$ is equal to the weight (kg) of salt in 1 kg of solution.

In the Hansson scale,

$$[H]_H = m_H(1 + K_{HSO4}\,[SO_4^{2-}]_T)/(1 - 10^{-3}\,S)$$

ASSIGNMENT OF pH AND CALIBRATION IN BUFFERS

Hansson [2] selected 2-amino-2(hydroxymethyl)-propane-1,3-diol [Tris; tris(hydroxymethyl)aminomethane] as the buffer substance because its log

TABLE 1

Scales and symbols

The NBS pH scale	a_H(NBS)	pH(NBS)
The "free" hydrogen ion concentration scale (mol kg^{-1} of H_2O)[a]	m_H	pm_H
The Hansson scale (mol kg^{-1} of solution)[b]	$[H]_H$	pH(H)
The "total" hydrogen-ion concentration scale		
(mol kg^{-1} of H_2O)[c]	m_H(SWS)	pm_H(SWS)
(mol kg^{-1} of solution)[c]	$[H]_{SWS}$	pH(SWS)

[a] As seawater but without sulphate and fluoride. [b] As seawater but without fluoride. [c] As seawater.

K_1 ($[HB^+]/[H^+][B]$) value is close to the pH of surface seawater. It was desirable to keep the total concentration of Tris as low as possible in order not to affect the medium composition, but high enough to give an acceptable buffer capacity. Hansson decided on 10 mM, which is still used for the preparation of the Hansson buffers. Almgren et al. [16] gave an equation for the calculation of the pH(H) of Hansson's buffers, which was obtained from a least-squares fit to his experimental results.

The procedure used for the assignment of pH to a buffer is simple. First, the buffer is titrated with hydrochloric acid and the equivalence point is estimated from a Gran function applied to the region where excess of acid is present. Then E_{ks} is calculated in each titration point for $v > v_{eq}$, with the assumption that the hydrogen ion activity is equal to the analytical excess of hydrochloric acid. Finally, the mean value of E_{ks} is used, together with the e.m.f. for $v = 0$, to calculate the pH of the buffer. This procedure will always give a pH which is based on the composition of the buffer solution as the reference state, because all hydrogen ions, except those consumed in the main reaction $H^+ + B \rightarrow HB^+$ are included in the activity. It should be noted that the most important part of the procedure is the calculation of E_{ks} in the titration of the buffer. This is where the presence of sulphate and fluoride really affects the concentration of free hydrogen ions and thus the e.m.f. measured. When the buffer has its maximum buffer capacity, however, addition of fluoride and sulphate up to the seawater concentrations cannot measurably affect the quotient $[HB^+]/[B]$, which then regulates $[H]_{free}$. This is seen very clearly from comparison of two calculations on the titration with the HALTAFALL program [17]. Curve A in Fig. 1 was obtained when sulphate and fluoride were excluded from the calculation, and curve B for $[SO_4^{2-}]_T = 0.0289$ M, $[F^-]_T = 0.00007$ M, $K_{HSO4} = 11.8$ and $K_{HF} = 398$. Log K_1 for $TrisH^+$ was taken from Hansson [2] and adjusted to the $[H]_{free}$ scale. The values obtained for log $[H]_{free}$ in the two buffers before the titration was started were the same to at least the fifth decimal. In the region of excess of acid, however, the difference corresponds to log ($[H^+] + [HSO_4^-] + [HF]$).

It has been pointed out [8, 15] that for media containing weak acid/base pairs such as HSO_4^-/SO_4^{2-} and HF/F^-, one should in principle make a correction

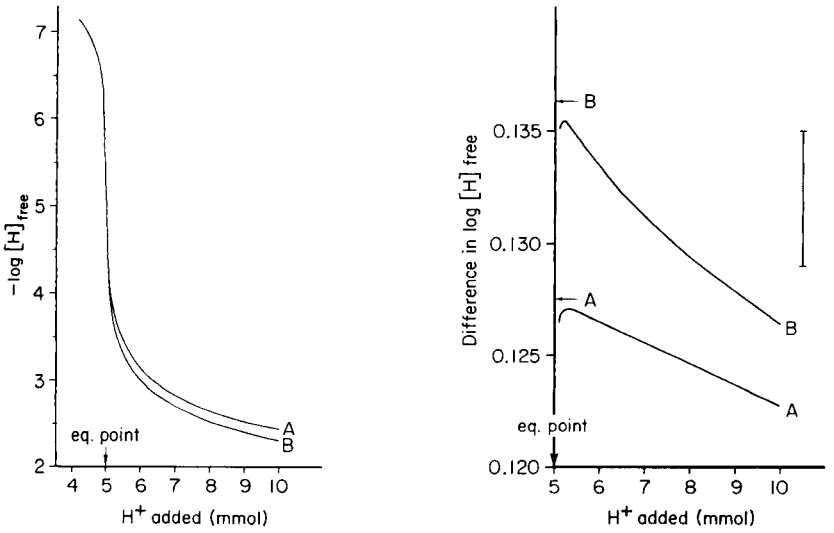

Fig. 1. Theoretical titration curves for the titration of 0.005 M Tris + 0.005 M TrisH$^+$ with strong acid. The volume in the titration vessel is set constant, the salinity is 35 and the temperature 25°C. Curves: (A) chloride medium; (B) chloride medium with $[SO_4^{2-}]_T$ = 0.0289 M and $[F^-]_T$ = 0.00007 M.

Fig. 2. Calculated difference in log $[H]_{free}$ from comparison between titration in a chloride medium and in media to which sulphate and fluoride have been added. Curves: (A) log $[H]_{free}$(chloride) − log $[H]_{free}$(sulphate); (B) log $[H]_{free}$(chloride) − log $[H]_{free}$ (sulphate, fluoride). The bar indicates an error of ±0.003 pH in the measurement, which corresponds to 0.18 mV at 25°C. The arrows marked A and B indicate the values of $\log(1 + K_{HSO_4}[SO_4^{2-}]_T + K_{HF}[F^-]_T)$ for the two cases.

for the fact that the free concentrations of sulphate and fluoride (i.e., the conditional free concentrations, which include the weak medium interactions) decrease slightly as a result of the formation of HSO_4^- and HF in the part of the titration curve where E_{ks} is estimated. For a buffer containing sulphate and fluoride, this can be done as follows:

$$[H](\text{excess}) = (v - v_{eq})t/(v_0 + v) = [H]_{free}(1 + K_{HSO_4}[SO_4^{2-}] + K_{HF}[F^-])$$

(where t is the titre of the acid and v_0 is the initial volume) is combined with

$$[SO_4^{2-}]_T = [SO_4^{2-}](1 + K_{HSO_4}[H]_{free}) \text{ and } [F^-]_T = [F^-](1 + K_{HF}[H]_{free})$$

and solved for $[H]_{free}$. Then

$$[H]_{SWS} = [H]_{free}(1 + K_{HSO_4}[SO_4^{2-}]_T + K_{HF}[F^-]_T)$$

is estimated.

The effect of the increased formation of HSO_4^- and HF is illustrated in Fig. 2. Curve A shows the difference between log $[H]_{free}$ in a chloride medium

and one that contains sulphate, and curve B shows the difference between a chloride medium and one that contains sulphate and fluoride. The arrows marked A and B indicate the values that correspond to the $[H]_{SWS}$ scale. The bar is included in order to relate these effects to a measurement error of ±0.003 pH units (±0.18 mV). Figure 3 shows how much log [H](excess) deviates from log $[H]_{SWS}$ as a function of log $[H]_{SWS}$. If titration points down to pH(SWS) = 3 are used for the calculation of E_{ks}, the deviation has a maximum of 0.001 pH unit for the case with sulphate added (curve A) and 0.003 pH units for the case with sulphate and fluoride (curve B).

THE NEED FOR CONSISTENCY IN ALKALINITY TITRATION AND CALCULATIONS OF CARBONATE SPECIATION

Although the pH(SWS) scale is accepted for seawater, it should not necessarily be used for all kinds of calculations. On the contrary, there are good reasons not to do so at some stages in the evaluation of the alkalinity titration. For the potentiometric titration, transformation of the titration curve to linear Gran functions has been discussed by Hansson and Jagner [18] and Bradshaw et al. [19], and non-linear curve-fitting by Dickson [20] and Johansson and Wedborg [14]. A complete treatment of the exact procedures used by the various workers is not possible, because this would require exact knowledge of the various computer programs used, some of which are no longer available. It is, however, quite possible from the published reports to

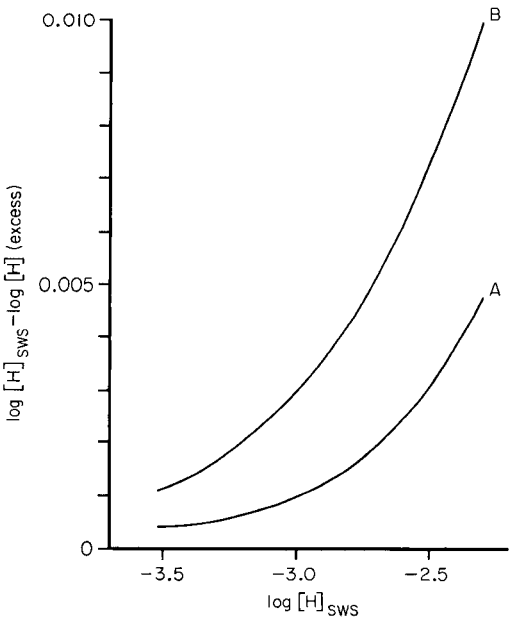

Fig. 3. The difference [log $[H]_{SWS}$ − log [H](excess)] versus log $[H]_{SWS}$. Curves: (A) sulphate included in the calculation; (B) sulphate and fluoride included in the calculation.

make some remarks as to the differences. Hansson and Jagner [18] and Dickson [20] did purely theoretical tests of their procedures, but the Hansson-Jagner program was later adapted to practical work [16]. Bradshaw et al. [19] and Johansson and Wedborg [14] tested their procedures on experimental as well as theoretical titration curves.

Hansson and Jagner [18] actually used two different pH scales in their program and the procedure of Bradshaw et al. [19] seems to have been similar in this respect. For the Gran functions, the $[H]_{free}$ scale was applied, which is the best way to account for the increased importance of hydrogensulphate and hydrogen fluoride in the region of excess of acid. For the calculation of the intercept in the Nernstian equation, E_k, the pH(SWS) scale was automatically obtained, however, because the analytical excess of acid was defined as the hydrogen ion activity. It is then required that the equilibrium constants used for the calculations be expressed on the same scale. Thus neither the equations of Almgren et al. [16] nor those of the UNESCO panel [8] give the correct values for the carbonate and borate constants to be used in the Gran functions. In the first-mentioned case these constants must be recalculated by the factor $(1 + K_{HSO4}[SO_4^{2-}]_T)$ and in the second case by $(1 + K_{HSO4}[SO_4^{2-}]_T + K_{HF}[F^-]_T)$.

Dickson [20] applied the pH(SWS) scale in a consistent way. He thus omitted hydrogensulphate and hydrogen fluoride from his equation, and consequently his value for E_k from the curve-fitting was defined on the pH(SWS) scale. One drawback of his procedure is that it will give systematic errors if titration points in the region of excess of acid are included in the curve-fitting. Johansson and Wedborg [14] applied the pH(free) scale in a consistent way. All of their equilibrium constants, including those for the minor species were recalculated to that scale and therefore E_k from the curve-fitting was obtained on that same scale. Also, their procedure worked in the region of excess of acid.

For subsequent speciation calculations, the pH scale of E_k must be known, because the pH obtained for the sample will depend on that. The best practice would probably be to use the pH(SWS) scale for such calculations, but then care must be taken to convert the equilibrium constants to that scale in order to achieve consistency. Most measurements of the equilibrium constants of interest were made in media which contained sulphate but not fluoride. As pointed out above, the correction for fluoride is rather small, 0.009 logarithmic units for a salinity of 35, compared to the correction for sulphate, 0.127 logarithmic units. If the experimental methods are further improved, such small corrections as the one for fluoride may become important.

REFERENCES

1 R. G. Bates, Determination of pH. Theory and Practice, 2nd edn., Wiley-Interscience, New York, 1973.
2 I. Hansson, Deep-Sea Res., 20 (1973) 479.
3 K. S. Johnson, R. Voll, C. A. Curtis and R. M. Pytkowicz, Deep-Sea Res., 24 (1977) 915.

4 R. G. Bates, in E. D. Goldberg (Ed.), The Nature of Seawater, Dahlem Konferenzen, Berlin, 1975, pp. 313—338.
5 I. Hansson, S. Ahrland, R. G. Bates, G. Biedermann, D. Dyrssen, E. Högfeldt, A. E. Martell, J. J. Morgan, P. W. Schindler, T. B. Warner and M. Whitfield, Conventions for seawater equilibria, in E. D. Goldberg (Ed.), The Nature of Seawater, Dahlem Konferenzen, Berlin, 1975, pp. 263—280.
6 R. G. Bates and C. H. Culberson, in N. R. Anderson and A. Malahoff (Eds.), The Fate of Fossil Fuel CO_2 in the Oceans, Plenum, 1977, pp. 45—61.
7 UNESCO, Report from the carbon dioxide sub-group of the Joint Panel on Oceanographic Tables and Standards, Miami, FL, September 1981, UNESCO Technical Papers in Marine Sciences, No. 42, 1983.
8 UNESCO, Report from the carbon dioxide sub-group of the Joint Panel on Oceanographic Tables and Standards, La Jolla, CA, December 1984, UNESCO Technical Papers in Marine Sciences, No. 00, 1987.
9 K. H. Khoo, R. W. Ramette, C. H. Culberson and R. G. Bates, Anal. Chem., 49 (1977) 29.
10 R. M. Pytkowicz, S. E. Ingle and C. Mehrbach, Limnol. Oceanogr., 19 (1974) 665.
11 C. H. Culberson, in M. Whitfield and D. Jagner (Eds.), Marine Electrochemistry, Wiley, New York, 1981, pp. 187—261.
12 R. A. Butler, A. K. Covington and M. Whitfield, Oceanol. Acta, 8 (1985) 433.
13 M. Whitfield, R. A. Butler and A. K. Covington, Oceanol. Acta, 8 (1985) 423.
14 O. Johansson and M. Wedborg, Oceanol. Acta, 5 (1982) 209.
15 A. G. Dickson, Geochim. Cosmochim. Acta, 48 (1984) 2299.
16 T. Almgren, D. Dyrssen and M. Strandberg, Deep-Sea Res., 24 (1975) 345.
17 N. Ingri, W. Kakolowicz, L. G. Sillén and B. Warnquist, Talanta, 14 (1967) 1261; 15 (1968) xi (erratum).
18 I. Hansson and D. Jagner, Anal. Chim. Acta, 65 (1973) 363.
19 A. L. Bradshaw, P. G. Brewer, D. K. Shafer and R. T. Williams, Earth Planet. Sci. Lett., 55 (1981) 99.
20 A. G. Dickson, Deep-Sea Res., Part A, 28 (1981) 609.

Analytica Chimica Acta, 200 (1987) 269—279
Elsevier Science Publishers B.V., Amsterdam — Printed in The Netherlands

POLAROGRAPHIC STUDIES OF IRON COMPLEXES AS POTENTIAL CONTRAST AGENTS IN MAGNETIC RESONANCE IMAGING

A. JACOBSEN and W. LUND*
Department of Chemistry, University of Oslo, Box 1033, 0315 Oslo (Norway)
E. JACOBSEN**
Department of Pharmacy, University of Oslo, Box 1068, 0316 Oslo (Norway)
(Received 6th April 1987)

SUMMARY

Iron(III) complexes of polyaminopolycarboxylic acids of potential use as contrast agents in magnetic resonance imaging were investigated by differential pulse polarography. The complexes with diethylenetrinitrilopentaacetic acid, *trans*-1,2-cyclohexylenedinitrilotetraacetic acid and triethylenetetranitrilohexaacetic acid (TTHA) were found to decompose slowly at pH 7.2. With TTHA, a mixture of 1:1 and 2:1 complexes was obtained, and the transformation between the two complexes was slow. Ethylenediiminobis[(2-hydroxyphenyl)acetic acid] (EHPG) was found to be the most suitable ligand. The complex formation is kinetically slow, and a special procedure for the preparation of the complex is required; the complex is then stable for one week at pH 7.2. The polarographic measurements are preferably made at pH 9.2, where a well-defined reduction peak is obtained. The complex is stable for 2 days at pH 9.2. At pH values below 9, a double peak is obtained, except for low concentrations of the complex. Both Fe(III)EHPG and Fe(II)EHPG adsorb at the mercury electrode. The polarographic determination can be done in the presence of 10% of urine or serum without interference. The detection limit is in the low μM range.

The recent successful use of magnetic resonance imaging (MRI) in diagnostic medicine has resulted in an intensive search for effective contrast agents for nuclear magnetic resonance (NMR). Attention has been focused especially on the paramagnetic gadolinium(III), iron(III) and manganese(II) ions [1, 2]. To minimize the toxic effect of the free metal ions, these are normally administered as stable metal-ion complexes. Gadolinium(III) complexes appear to be the most potent, but the biological effects of this metal are of some concern. In contrast, the biological effects of iron are well known so that iron(III) complexes are of particular interest as NMR contrast agents.

In order to be a useful agent, the complex should have a very high formatin constant, or rather a high conditional constant, at the biological pH

**E. Jacobsen and W. Lund graduated and obtained their doctoral degrees from the University of Oslo. E. Jacobsen is Professor of Analytical Chemistry. His research field is polarography of pharmaceuticals. W. Lund is Senior Lecturer. His field is electroanalytical and spectroscopic methods for trace metal analysis.

0003-2670/87/$03.50

value. An excess of ligand must usually be avoided, because the free ligand may react with essential elements in the body. To be a useful agent, the complex should also show some organ-selective distribution in the body, and its excretion should be sufficiently fast and complete. Among the ligands that have received special attention in MRI are those of the polyaminopolycarboxylic acid type, which form strong polydentate chelates with gadolinium and iron ions. In particular, gadolinium diethylenetrinitrilopentaacetate has frequently been utilized in MRI studies [1, 3–6], but the iron complex with ethylenediimino-bis[(2-hydroxyphenyl)acetic acid] also shows promise for such studies [7].

In this work we have investigated the iron(III) complexes of DTPA, CDTA, TTHA and EHPG (see below for definitions). The complexes were studied by differential pulse polarography. This technique is particularly well suited to such studies, because of its ability to discriminate between the free metal ion, the metal complex and the free ligand.

EXPERIMENTAL

Apparatus

A polarographic analyzer model 174A and a static mercury drop electrode model 303, both from Princeton Applied Research Corporation, were used. A conventional dropping mercury electrode was used in a few experiments. An Ag/AgCl/sat.KCl system and a platinum wire served as reference and counter electrodes, respectively. Dissolved oxygen was removed by passing purified nitrogen through the solution for 4 min, except for samples containing serum, in which case 10% (w/v) 1 M sodium sulphite was added to the solution, in order to avoid excessive foam formation. The following instrument settings were normally used: scan rate 2 mV s^{-1}, modulation amplitude 25 mV, drop time 1 s, medium drop size. All potentials given in this work refer to the above-specified Ag/AgCl reference electrode.

Controlled potential electrolysis was done with a home-made potentiostat. A platinum gauze served as the working electrode, and the anode and cathode compartments were separated by a glass sinter. Nitrogen was passed through the solution during electrolysis.

Reagents

The ligands studied were all of analytical-reagent grade: diethylenetrinitrilopentaacetic acid (DTPA; Fluka), *trans*-1,2-cyclohexylenedinitrilotetraacetic acid (CDTA; Fluka), triethylenetetranitrilohexaacetic acid (TTHA; Sigma), and ethylenediiminobis[(2-hydroxyphenyl)acetic acid] [ethylene-*N*,*N*′-bis(2-hydroxyphenylglycine); EHPG; Fluka].

The reagents were dissolved in 1 M sodium hydroxide and then neutralized to pH 7 with hydrochloric acid. The iron(III) stock solution was prepared by dissolving the pure metal in sulphuric acid, followed by oxidation with nitric acid; excess of nitric acid was removed by boiling. Acetate,

phosphate and ammonia buffers (0.1 M) were used as pH buffers. For final adjustment of pH to 7.2 and 9.2, 0.1 M sodium hydroxide was added dropwise to the solutions. The mercury used was of high purity (triply distilled), and the serum was a commercial standard (Seronorm, NYCOMED, Norway).

RESULTS AND DISCUSSION

Polarographic investigations of metal ion complexes are normally done in the presence of an excess of the ligand. For the determination of the metal ion, as well as for the evaluation of the composition and formation constant of the metal complex, such an excess of the ligand is usually essential. However, in magnetic resonance imaging (MRI), an excess of the ligand is normally unacceptable because of the possible toxic effects of the free ligand. Further, MIR studies require that particular attention be given to the results obtained at the biological pH value, i.e., pH 7.

Very few reports in the literature deal specifically with the polarography of metal complexes when the metal ion and the ligand are present in equivalent amounts.

Diethylenetrinitrilopentaacetic acid

DTPA forms a colourless 1:1 complex with iron(III), with a formation constant of ca. 1×10^{28} (literature values, 2×10^{27}—5×10^{28} [8]). The complex is reduced reversibly in a one-electron process, and the half-wave potential is constant in the pH range 5.5—9 [9], when DTPA is present in excess. In the present work, solutions were prepared with equivalent amounts of iron(III) and DTPA (100 μM each), in a phosphate buffer at pH 7.2. The differential pulse polarogram exhibited a symmetric peak; the peak potential (E_p) was —0.15 V, and the peak half-width ($w_{1/2}$) was 90 mV, which indicates a reversible one-electron reduction. However, the complex was found to decompose with time, as signalled by a decrease in the peak height (i_p) and an increase in $w_{1/2}$. At the same time, a new peak appeared at a potential of ca. +0.03 V. The rate of decomposition was ca. 7% per 24 h in the pure buffer, and 3—4% in the presence of 10% (v/v) urine and serum, for concentrations of 0.01—0.1 mM of the complex.

The appearance of the peak at +0.03 V in the polarogram signals the release of DTPA. The peak is due to the oxidation of mercury to a HgDTPA complex. Thus, the decomposition was probably brought about by the slow precipitation of hydrated iron(III) oxide as a result of insufficient stability of the Fe(III)DTPA complex.

Trans-*1,2-Cyclohexylenedinitrilotetraacetic acid*

CDTA forms a colourless 1:1 complex with iron(III), and the formation constant is ca. 1×10^{30} (literature values, 10^{27}—10^{30} [8]). The differential pulse polarogram at pH 7.2 showed a symmetric peak with E_p = —0.14 V and $w_{1/2}$ = 90 mV, which indicates a reversible one-electron reduction. The

complex was found to decompose at a rate of ca. 7% per 24 h at pH 7.2, and was thus quite similar to the Fe(III)DTPA complex, although the formation constant appears to be somewhat higher for the CDTA complex.

Triethylenetetranitrilohexaacetic acid

Because TTHA is a relatively large molecule, it has a more pronounced tendency to form binuclear complexes than most of the other polyaminopolycarboxylic acids. The formation constant of the 1:1 complex is reported to be 6×10^{26} [8, 10], but the value of 3×10^{29} has also been given [11]. Jacobsen et al. [12] found that the 1:1 complex predominated when TTHA was in excess, whereas only the binuclear complex was observed in a 2:1 mixture of iron and TTHA. The 1:1 complex was reduced reversibly in a one-electron diffusion-controlled process, and the peak potential was constant in the pH range 4—10. The 2:1 complex was reduced in a two-electron process, and the peak potential varied with pH in the pH range 3—10. The reduction product was strongly adsorbed at the mercury electrode.

A differential pulse polarogram recorded for a 0.1 mM 1:1 mixture of iron(III) and TTHA at pH 7.2 exhibited one peak at ca 0.0 V, and a double peak with E_p values at ca. —0.20 V and —0.28 V. The heights of the peaks were found to depend on the time between the preparation of the complex and the recording of the polarogram.

A polarogram recorded for 0.1 mM iron(III) in a 2:1 mixture with TTHA exhibited only a single peak, with E_p = —0.28 V. This peak height also changed with time; after 4 days it had decreased by ca. 10%. At the same time, $w_{1/2}$ decreased from 85 to 60 mV.

These results indicate that the peak at —0.28 V is due to a two-electron reduction of the binuclear $Fe(III)_2TTHA$ complex. The peak observed at —0.20 V for the 1:1 mixture is probably due to a one-electron reduction of the mononuclear Fe(III)TTHA complex, whereas the peak at ca. 0.0 V is caused by the presence of the free ligand, which forms a strong complex with mercury.

In the polarogram recorded from the 1:1 mixture, the peak at —0.28 V increased with time, at the expense of the peak at —0.20 V, indicating a transformation from the mononuclear to the binuclear complex. For a more dilute 1:1 mixture, containing 0.01 mM concentrations of the reactants, only a single peak corresponding to the binuclear complex was observed. The peak increased by 50% over the course of 4 days, again illustrating the predominance of the binuclear complex over the mononuclear species.

The insufficient stability of the 1:1 complex, and the transformation to the 2:1 complex, makes TTHA an unattractive ligand for complexation of iron in MRI studies.

Ethylenediiminobis[(2-hydroxyphenyl)acetic acid]

EHPG is a tetraprotic acid and a hexadentate ligand, which forms a red

1:1 chelate with iron(III) in the pH range 3—11 [13]. The chelate has a very high formation constant of 8×10^{33} [8, 14, 15]. The use of iron(III)EHPG in MIR has recently been investigated by Lauffer et al. [7]. It was found that the chelate was an effective hepatobiliary MR contrast agent, which possessed sufficient paramagnetism and biliary excretion to alter the relaxation times of normal liver tissue and to enhance image intensity.

Unlike the other ligands studied, EHPG reacts slowly with iron(III). Therefore it is recommended to wait for between 30 min [7] and 1 day [14] after mixing the solution, to ensure complete complexation. However, when an iron(III) solution is mixed with an alkaline EHPG solution and the pH adjusted to 7, there is a risk that some hydrated iron oxide will precipitate before the complexation is complete, leaving some unreacted ligand in solution. That such a reaction can actually take place is indicated by the need in some cases for filtering the chelate solution [7]. Therefore, the procedure used for preparing the chelate was studied in some detail.

Preparation of the complex. In the procedure tested 0.1 mM iron and EHPG solutions were mixed at pH 3.5, and the pH was finally adjusted to 7.2 with a phosphate buffer. The pH when mixing the reagents should be below 4, to avoid the risk of precipitation of hydrated iron oxide, and above 3, in order to assure complete complexation. The following procedures were tested: (1) mixing and immediate pH adjustment to 7.2; (2) mixing and waiting for 30 min before pH adjustment to 7.2; (3) mixing and waiting for 24 h before pH adjustment to 7.2; (4) mixing, heating to 100°C and subsequent cooling before pH adjustment to 7.2.

For all procedures, a polarogram with a double peak was obtained, as shown in Fig. 1A. Procedure 1 gave the lowest peaks, and procedure 4 gave the highest peaks, indicating that heating to 100°C is necessary in order to ensure complete complex formation. During these experiments, it was further noticed that the highest peaks were observed only when the ligand solution had been freshly prepared, indicating that the pure reagent decomposed with time. The decomposition rate was of the order of some percent per day.

From the above experiments, the following requirements were established for the preparation of the Fe(III)EHPG complex: (1) the reagent solution must be freshly prepared; (2) the Fe(III) and EHPG must be mixed at pH 3—4; and (3) the solution must be heated to 100°C and then cooled before the final adjustment of pH. When this procedure was followed, the Fe(III)EHPG complex was found to be completely stable for 7 days.

Effect of pH. The effect of pH was studied by recording polarograms of 0.10 mM Fe(III)EHPG at various pH values in the range 3—11. A double peak was observed for all pH values between 3 and 8.5. The splitting of the peak increased with increasing pH up to pH 8. At the same time, E_p values for both peaks were shifted ca. 100 mV per pH towards more negative values, which indicates that two protons are consumed in the reduction of Fe(III)EHPG, in this pH region. The reaction is probably

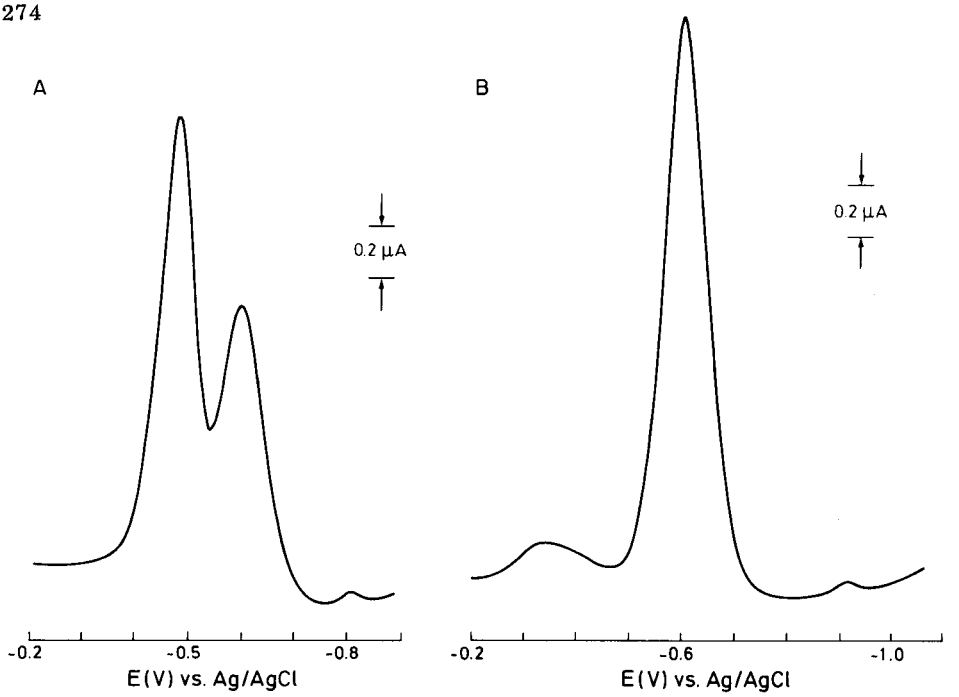

Fig. 1. Differential pulse polarograms of 0.10 mM Fe(III)EHPG: (A) at pH 7.2; (B) at pH 9.2.

$$Fe(III)EHPG + 2H^+ + e^- \rightarrow Fe(II)H_2EHPG$$

At pH values above 8.5 the two peaks merged to a single peak. The E_p value of this peak was independent of pH, indicating that protons were not consumed in the reduction process in this pH region. A polarogram recorded from a solution at pH 9.2 is shown in Fig. 1B. The symmetric peak has E_p = —0.62 V and $w_{1/2}$ = 90 mV, which indicates a reversible one-electron reduction. No decrease in the peak current was observed after two days, indicating a very stable complex.

The single peak obtained at pH 9.2 is particularly attractive for quantitative work. However, at concentrations of the complex below 0.01 mM a single peak is obtained also at pH 7.2.

Electrode reactions

The above results indicate that the polarographic reduction of the Fe(III)-EHPG complex is not a simple process. Therefore, the electrode reaction was studied in some detail also by d.c. polarography and cyclic voltammetry.

D.c. polarograms were recorded from 0.10 mM Fe(III)EHPG at pH 9.2 at different heights of the mercury column. It was found that the limiting current was proportional neither to $h^{1/2}$ nor to h, where h is the height of the mercury column after correction for the "back-pressure". This indicates that the electrode reaction is influenced by both diffusion and adsorption processes [16].

Electrocapillary curves were obtained for the complex, the ligand and the ammonia buffer by measuring the drop time as a function of the potential [16]. The curves shown in Fig. 2 indicate a marked adsorption of the complex, and a weaker adsorption of the ligand, with a desorption potential at ca. —1.1 V.

Cyclic voltammograms were recorded at different scan rates and different concentrations of the complex at pH 9.2 and 7.2. A voltammogram of 0.10 mM Fe(III)EHPG at pH 9.2, recorded at a scan rate of 5 mV s^{-1} is shown in Fig. 3A. It can be seen that the complex is reversibly reduced; the peak potentials of the complex are —0.66 and —0.59 V for the cathodic and anodic processes, respectively. In addition, a prewave is observed at ca. —0.40 V, and a small irreversible wave at —0.90 V. A similar voltammogram was obtained at higher scan rates, but the waves at —0.40 and —0.90 V were then less pronounced. In Fig. 3B a voltammogram of 0.010 mM complex at pH 9.2 and a scan rate of 100 mV s^{-1} is shown. The prewave has disappeared, and the complex peak is more symmetric than expected for a diffusion-controlled process.

At pH 7.2, a double peak was observed on the cyclic voltammograms at high scan rates, for a 0.10 mM solution of the complex. The first part of the double peak changed to a prewave at slower scan rates. The symmetric shape of the peaks increased with increasing scan rate. No prewave or double peak was observed on voltammograms recorded from solutions with con-

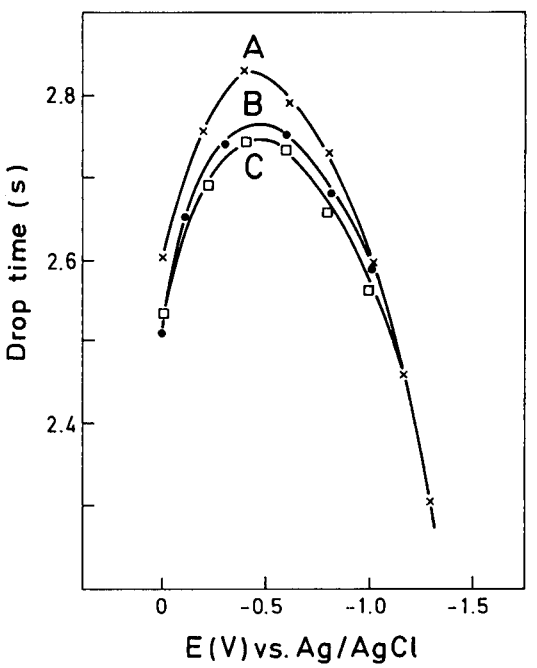

Fig. 2. Electrocapillary curves at pH 9.2: (A) ammonia buffer; (B) 0.10 mM EHPG; (C) 0.10 mM Fe(III)EHPG.

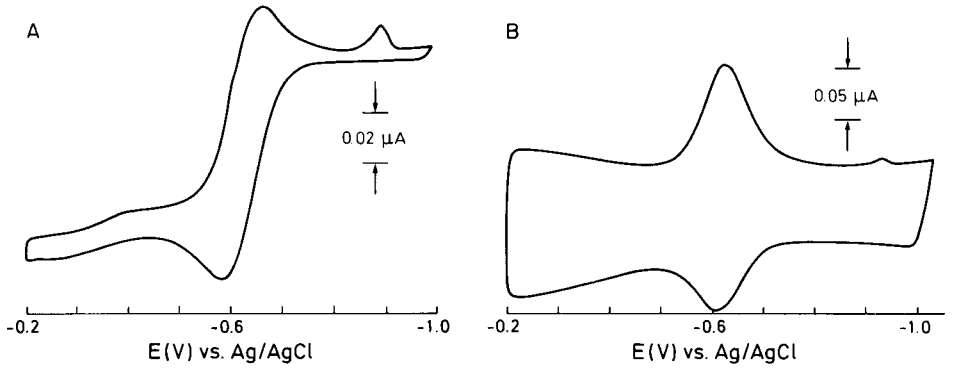

Fig. 3. Cyclic voltammograms for different concentrations of Fe(III)EHPG at pH 9.2 and different scan rates: (A) 0.10 mM Fe(III)EHPG at 5 mV s^{-1}; (B) 0.010 mM Fe(III)EHPG at 100 mV s^{-1}.

centrations of the complex less than 0.01 mM.

The presence of the prewave, which was observed at high concentrations and slow scan rates, indicates strong adsorption of the reduction product (Fe(II)EHPG [17]. The increased symmetry of the cathodic peak, which was observed at low concentrations and high scan rates, indicates adsorption of the reactant [17].

The cyclic voltammetric measurements are summarized in Table 1. From the table it can be seen that the current function $i_c C^{-1}\ v^{-1/2}$ increases slightly when the scan rate is increased from 20 to 500 mV s^{-1}, which indicates adsorption [17]. In the current function, i_c represents the height of the cathodic peak, C the concentration of the complex and v the scan rate. However, $i_c C^{-1}\ v^{-1}$ is not constant, so apparently also other electrode processes are involved. The $i_a i_c^{-1}$ ratio is in most cases larger than 1, indicating adsorption of the reduction product, but the ratio decreases with increasing scan rate, which implies adsorption of the reactant Fe(III)EHPG. From Table 1 it can be seen that the current function increases with dilution. This effect should also indicate adsorption.

Although the results in Table 1 do not present a clear picture, the following conclusions seem justified. First, the reduction product adsorbs strongly at the mercury electrode:

$$\text{Fe(III)EHPG} + e^- \rightarrow \text{Fe(II)EHPG(ads)}$$

The adsorption is more pronounced at pH 7.2 than at pH 9.2, hence a double peak is observed at the lower pH and high concentrations. Secondly, the reactant adsorbs weakly:

$$\text{Fe(III)EHPG} \rightarrow \text{Fe(III)EHPG(ads)} + e^- \rightarrow \text{Fe(II)EHPG(ads)}$$

Reduction of EHPG

The electrochemical behaviour of the EHPG reagent was also of interest. A differential pulse polarogram of a freshly prepared 0.1 mM EHPG solution

TABLE 1

Cyclic voltammetric measurements of the Fe(III)EHPG complex

C (mM)	pH	v (mV s^{-1})	i_c (μA)	i_a (μA)	$i_a i_c^{-1}$	$i_c C^{-1} v^{-1/2}$ (μA mM^{-1} $mV^{-1/2}$ $s^{1/2}$)	$i_c C^{-1} v^{-1}$ (μA mM^{-1} mV^{-1} s)
0.1	9.2	5	0.078	0.082	1.05	0.35	0.16
		10	0.103	0.113	1.10	0.32	0.10
		20	0.150	0.165	1.10	0.34	0.08
		50	0.250	0.275	1.10	0.35	0.05
		100	0.390	0.430	1.10	0.39	0.04
		200	0.640	0.660	1.03	0.45	0.03
		500	1.20	1.13	0.94	0.54	0.02
0.01	9.2	5	0.013	0.010	0.77	0.6	0.26
		10	0.021	0.016	0.79	0.7	0.21
		20	0.029	0.025	0.86	0.6	0.15
		50	0.053	0.043	0.81	0.7	0.11
		100	0.096	0.080	0.83	1.0	0.10
		200	0.132	0.097	0.74	0.9	0.07
		500	0.240	0.175	0.73	1.1	0.05
0.1	7.2	5	0.078	—		0.35	0.16
		10	0.083	—		0.26	0.08
		20	0.075	0.088	1.17	0.17	0.04
		50	0.135	0.150	1.11	0.19	0.03
		100	0.225	0.225	1.00	0.23	0.02
		500	0.750	0.625	0.83	0.33	0.02
0.01	7.2	5	0.011	0.013	1.18	0.5	0.23
		10	0.018	0.022	1.22	0.6	0.18
		20	0.025	0.035	1.40	0.6	0.13
		50	0.043	0.061	1.42	0.6	0.09
		100	0.068	0.093	1.37	0.7	0.07
		200	0.133	0.150	1.13	0.9	0.07

at pH 9.2 is shown in Fig. 4 (curve A). The polarogram is rather complicated, with pronounced peaks at −0.24, −0.93 and −1.44 V. A cyclic voltammogram at a hanging mercury drop was simpler, with mainly one pronounced cathodic peak at −0.99 V; no corresponding anodic peak was observed. The symmetry of the peak indicated adsorption. When the solution was electrolyzed at −0.12 V for 5 min at the mercury drop electrode before recording the voltammogram, the peak at −0.99 V increased many fold, and in addition new peaks appeared, which were barely noticeable on the first voltammogram. This result indicates that the observed peaks are not tensammetric peaks but are due to the reduction of EHPG via adsorption processes.

When polarograms and voltammograms were recorded from old solutions of the reagent, and for the complex prepared from an old reagent solution, new peaks were observed (Fig. 4, curve B), indicating decomposition of the reagent with time.

In addition to the direct reduction of EHPG at the mercury electrode,

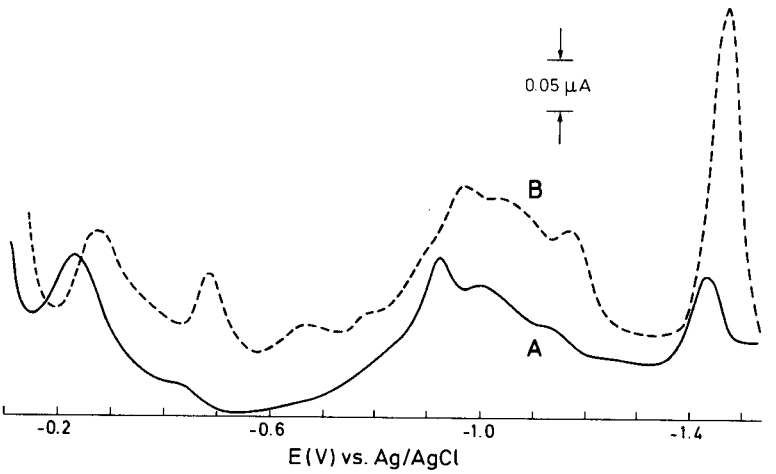

Fig. 4. Differential pulse polarograms of 0.10 mM EHPG at pH 9.2: (A) from stock solution (1 mM) freshly prepared; (B) from stock solution 5 weeks old.

there was also the possibility that the reagent might be reduced by the Fe(II)EPHG formed at the electrode surface. To study this effect, controlled-potential electrolysis was used to study a solution containing 0.10 mM Fe(III)EHPG at pH 9.2; a platinum gauze served as the working electrode, and the reduction potential was —1.0 V. Samples were taken from the solution at regular intervals, and examined by polarography and cyclic voltammetry.

From the differential pulse polarogram, it could be seen that the complex peak decreased as a function of the electrolysis time, and the same was true for the reagent peak observed at ca. —0.90 V. However, the reagent peak at ca. —1.45 V increased with time. From the cyclic voltammograms no build-up of Fe(II)EHPG could be detected. Instead, both the cathodic and anodic complex peaks decreased to the same extent as a function of the electrolysis time.

Because no build-up of Fe(II)EHPG was observed, Fe(II)EHPG must be oxidized by the ligand, which is in turn reduced during the process. The following reaction may therefore be postulated:

$$\text{Fe(II)EHPG} + \text{EHPG} \rightarrow \text{Fe(III)EHPG} + \text{EHPG}^*$$

where EHPG* represents the reduced species. In addition, EHPG is reduced directly at the working electrode.

The curves obtained after prolonged electrolysis were similar to those obtained for solutions that had been stored for weeks, indicating that the same processes take place during electrolysis and storage.

The above results agree with those of Frost et al. [13], who also observed a rapid oxidation of iron(II) in the presence of the ligand. However, Schrøder [18] claimed that a kinetically stable Fe(II)EHPG complex is produced upon electrochemical reduction of Fe(III)EHPG. His results could not be confirmed in this work.

Analysis of biological materials

Polarograms were recorded, and standard curves obtained for the Fe(III)-EHPG complex at pH 9.2, in the presence of 10% (v/v) urine and 10% (v/v) serum, respectively. In the serum samples, oxygen was removed by the addition of sodium sulphite instead of bubbling with nitrogen, to avoid excessive foam formation. A well-defined complex peak at ca. −0.63 V was obtained in both urine and serum. The standard curves, which passed through the origin, were linear for concentrations below 50 μM, with a slope of 25 μA mM^{-1} for urine and 20 μA mM^{-1} for serum. At higher concentrations, a slight curvature was observed, probably because of the strong adsorption of the complex. The detection limit was 1 μM for 10% urine and 5 μM for 10% serum, with the instrumental settings used in this work.

When biological materials are analyzed by differential pulse polarography, the presence of proteins may interfere with the measurements, owing to strong adsorption of the proteins at the mercury electrode. In this work, the adsorption of the Fe(III)EHPG complex at the electrode minimizes this interference.

We thank Dr. Jo Klaveness, NYCOMED A.S., for valuable discussions.

REFERENCES

1 D. H. Carr, Physiol. Chem. Phys., 16 (1984) 137.
2 J. A. Koutcher, C. T. Burt, R. B. Lauffer and T. J. Brady, J. Nucl. Med., 25 (1984) 506.
3 D. H. Carr, J. Brown, A. W.-L. Leung and J. M. Pennock, J. Comput. Assist. Tomogr., 8 (1984) 385.
4 D. H. Carr, J. Brown, G. M. Bydder, H.-J. Weinmann, U. Speck, D. J. Thomas and I. R. Young, Lancet, (1984) 484.
5 H.-J. Weinmann, R. C. Brasch, W.-R. Press and G. E. Wesbey, Am. J. Roentgenol., 142 (1984) 619.
6 G. L. Wolf, E. S. Fobben, Invest. Radiol., 19 (1984) 324.
7 R. B. Lauffer, W. L. Greif, D. D. Stark, A. C. Vincent, S. Saini, V. J. Wedeen and T. J. Brady, J. Comput. Assist. Tomogr., 9 (1985) 431.
8 A. E. Martell and R. M. Smith, Critical Stability Constants, Vol. 1, Plenum, New York, 1974.
9 G. Kalland and E. Jacobsen, Acta Chem. Scand., 17 (1963) 2385.
10 L. Harju, Anal. Chim. Acta, 50 (1970) 475.
11 K. H. Schrøder, Acta Chem. Scand., 19 (1965) 1797.
12 E. Jacobsen, W. Lund and T. Rojahn, Anal. Chim. Acta, 63 (1973) 147.
13 A. E. Frost, H. H. Freedman, S. J. Westerback and A. E. Martell, J. Am. Chem. Soc., 80 (1958) 530.
14 G. Anderegg and F. L'Eplattenier, Helv. Chim. Acta, 47 (1964) 1067.
15 K. H. Schrøder, Nature 202 (1964) 898.
16 L. Meites, Polarographic Techniques, 2nd edn., Interscience, New York, 1965.
17 R. H. Wopschall and I. Schain, Anal. Chem., 39 (1967) 1514.
18 K. H. Schrøder, Acta Chem. Scand., 18 (1964) 596.

Analytica Chimica Acta, 200 (1987) 281—290
Elsevier Science Publishers B.V., Amsterdam — Printed in The Netherlands

A STUDY OF THE POLAROGRAPHIC REDUCTION OF METHAQUALONE

LESLIE G. CHATTEN, RICHARD E. MOSKALYK and ANDY CHIN

Faculty of Pharmacy and Pharmaceutical Sciences, University of Alberta, Edmonton, Alberta T6G 2N8 (Canada)

PETR ZUMAN*

Department of Chemistry, Clarkson University, Potsdam, NY, 13676 (U.S.A.)

(Received 4th May 1987)

SUMMARY

Methaqualone [2-methyl-3-*o*-tolyl-4(3H)-quinazolinone] is reduced at pH 1.5—5 in a single two-electron step. At pH 1.5—3, wave i_1 appears and is gradually replaced by wave i_2 which predominates in the solution between pH 4.5 and 6.5. At pH > 5, the height of wave i_2 decreases in the shape of a dissociation curve with increasing pH. For both waves, the diprotonated form of methaqualone (I_a) is reduced to 1,2-dihydromethaqualone as the final product. In wave i_1, the monoprotonated form I_b is further protonated at the electrode surface before it accepts the first electron; in wave i_2, the free base form I accepts two protons at the electrode surface before the first electron uptake. Polarographic curves are complicated by the presence of three waves of catalytic hydrogen evolution. Wave $i_{1,cata}$ appears at pH < 5, waves $i_{2,cata}$ at —1.5 V and $i_{3,cata}$ at —1.7 V at pH > 5. Citrate buffers pH 1.5—3 or Britton-Robinson buffers at pH 2.6—3.6 are most suitable for quantitative work with either d.c. polarography or differential pulse polarography.

In order to be able to use polarographic methods for the determination of organic medicinal agents in pharmaceutical preparations as well as in biological fluids, it is essential to understand the nature of the processes occurring at the dropping mercury electrode (DME). In view of its widespread usage, both licit and illicit, the possibility of determining methaqualone [2-methyl-3-*o*-tolyl-4(3H)-quinazolinone; I] by electrochemical reduction attracted the early attention of Japanese [1] and German [2] pharmaceutical chemists as a means of analyzing commercial preparations. Pflegel and Wagner [2] also

*Petr Zuman, born in Prague (Czechoslovakia), was associated for 18 years with Professor J. Heyrovský, spent three and a half years at the University of Birmingham, Gt. Britain, and, since 1970, has been a Professor of Chemistry at Clarkson University at Potsdam, New York. His research interests are organic polarography, substituent effects, use of polarography, voltammetry and spectral methods in the study of mechanisms of organic reactions, often of analytically important reactions, and practical applications of polarography, mostly in pharmaceutical analysis.

0003-2670/87/$03.50

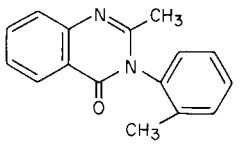

I

made some preliminary studies on the electroreduction of methaqualone and several other quinazolinones.

The character and pH-dependence of d.c. polarographic waves reported by Pflegel and Wagner [2] showed some significant differences when compared to those obtained in a later study of the determination of methaqualone in pharmaceutical products on the Canadian market [3]. In the present investigation, processes occurring during electroreduction of substance I were examined by using d.c. and differential pulse polarography (d.p.p.) as well as by controlled potential electrolysis.

In 1975, Patel et al. [4] presented a useful summary of the physicochemical properties of methaqualone, but this publication did not include any reference to the electrochemical characteristics of substance.

EXPERIMENTAL

Apparatus

A PAR polarographic analyzer, Model 174, was fitted with a drop-timer, Model 172A, and used in conjunction with a Houston Omnigraphic recorder, Model 2000. The PAR electrolytic cell, Model 9301, maintained at 25 ± 1.0°C was fitted with a three-electrode combination which consisted of a saturated calomel electrode, a dropping mercury electrode and a platinum wire as the auxiliary electrode. Unless stated otherwise, the drop time (t) was 2 s, the mercury flow rate (m) was 1.15 mg s^{-1}, the height of the mercury column (h) was 70 cm, and the scan rate was 2 mV s^{-1}.

A Wenking potentiostat (Model 61RM) was connected to a PAR Model 379 digital coulometer. A mercury pool formed the working electrode, the reference electrode was saturated calomel, and the auxiliary electrode which was made of platinum gauze was in a compartment separated from the electrolyzed solution by a fritted glass of medium porosity.

Reagents and solutions

Methaqualone (99.4%) and methaqualone hydrochloride (99.7%) were obtained respectively from William H. Rorer (Bramalea, Ontario) and Merck Frosst (Montreal). The purity was confirmed by means of the BP procedure [5]. Stock solutions (0.01 M) were prepared in 96% ethanol from both the free base and the hydrochloride. Working solutions were prepared by diluting a stock solution with the appropriate buffer of desired pH.

The buffers used were Sorensen's citrate buffers from pH 1.2 to pH 5.0,

Sorensen's phosphate buffers from pH 5.0 to pH 8.0 and Britton-Robinson (B-R) buffers for pH 2.6—8.0. All buffers were prepared at intervals of 0.4—0.5 pH with distilled, deionized water.

All reagents for the preparation of buffers and all solvents were of analytical grade. Ultraviolet indicating silica gel DF-5 (Camag, Switzerland) was utilized for thin-layer chromatography (TLC).

Preparation of dihydromethaqualone

Methaqualone (1 g; 0.004 mol) was dissolved in 10 ml of methanol, 0.06 g of platinum(IV) oxide monohydrate was added and the sample was hydrogenated in a standard apparatus. At the completion of hydrogenation, the catalyst was removed by filtration and the methanol was removed by distillation at reduced pressure. The resulting product was recrystallized from an ethyl acetate/hexane (2:1) mixture. The m.p. was 192—3°C (lit. [6], 192—3°C). Authenticity of the dihydromethaqualone was confirmed by infrared, NMR and ultraviolet spectroscopy.

Procedures

In a typical polarographic experiment, 1 ml of the ethanolic stock 0.01 M solution of methaqualone (I) was added to 19 ml of the supporting electrolyte, so that the final concentration was 5×10^{-4} M in I and 4.8% in ethanol. The sample was purged for 10 min with oxygen-free nitrogen and then the current/voltage curve was recorded.

For the controlled-potential electrolysis, 38 ml of buffer, either pH 2.6 or 3.6, was placed in the coulometric cell and purged for 10 min with nitrogen. The supporting electrolyte was then purified by electrolysis for 1 h at the chosen potential. Any remaining residual current was compensated by applying a counter-current. A portion (2 ml) of the ethanolic stock 0.01 M solution of I was then added, purged for another 10 min, and electrolyzed for 40 min. The applied potential corresponded to the limiting current of I but was always considerably more positive than that which corresponds to the reduction of hydrogen ions or to that of other constituents in the supporting electrolyte.

The products of controlled-potential electrolysis were separated by TLC and solvents were removed from the samples by distillation under reduced pressure at about 50°C. The residue was dissolved in 25 ml of methanol, the solution was filtered and the methanol was distilled off at reduced pressure; the procedure was then repeated. Finally, the residue was dissolved in 10 ml of methanol and filtered, so that the final concentration of the electrolysis product of methaqualone was approximately 1×10^{-3} M. Separation was done on silica gel-coated TLC plates with an ethyl acetate/benzene (4:1) solvent system. The plates were examined under UV lamps at both long and short wavelengths.

RESULTS AND DISCUSSION

Methaqualone (I) is reduced in two-electron waves: i_1 predominates between pH 1.5 and 3, and i_2 is the predominating wave between pH 4.5 and 6.5. The number of electrons transferred in these two processes was confirmed by comparisons with the heights of waves produced by equimolar solutions of benzophenone, 1,4-naphthoquinone, cinnamaldehyde and nitrobenzene in Britton-Robinson buffers at pH 2.6 and 3.6 (Table 1). Wave i_1 is optimally developed in citrate buffers (Fig. 1) and its height decreases with increasing pH in the shape of a dissociation curve with an inflection point at pH 4.2 (Fig. 2, Table 2). The sum of waves i_1 and i_2 was followed in Britton-Robinson buffers, with which the separation of waves i_1 and i_2 is poor and replacement of wave i_1 by wave i_2 is shown only by two linear segments on the plot of potential (E) as a function of $\log[i/(i_d - i)]$. The presence of two waves is also indicated by the drawn-out character of the waves (i_1 and i_2) between pH 3.2 and 5.2. The total current remains diffusion-controlled and practically constant up to a pH value of ca. 5 (Table 2). At higher pH, the current decreases and the plot assumes the shape of a dissociation curve with a slope which is twice that observed for a monobasic acid and an inflection point at a pH about 5.7 (Fig. 3). The presence of two waves is further confirmed by the change in the slope of the $E_{1/2}$ vs. pH plots (Fig. 4) which show a slope of 55 mV/pH for wave i_1 and 102 mV/pH for wave i_2.

The number of electrons transferred in the polarographic reduction of methaqualone at pH < 5 at the DME was further confirmed by using controlled-potential coulometry at a mercury pool electrode at an applied potential corresponding to the polarographic limiting current. Eight determinations in Britton-Robinson buffers pH 2.6 and 3.6 gave n-values ranging from 1.95 to 2.06 with a mean value of 2.03. Similar experiments in Sorensen's citrate buffer pH 2.6 gave an average n-value of 2.2, indicating some contribution of the catalytic hydrogen evolution (see later).

TABLE 1

Peak potentials and limiting currents for equimolar solutions of methaqualone and other substances[a]

Compound	$E_{1/2}$ (V)		i_d (μA)			
	$E_{1/2}$ (1)	$E_{1/2}$ (2)	i_d (1)	i_d (2)	I (1)[b]	I (2)[b]
Benzophenone	−0.963	−1.205	1.0	1.06	1.54	1.59
Cinnamaldehyde	−0.80	−1.246	1.28	1.28	1.86	1.86
Naphthoquinone	+0.01	—	2.1	—	3.16	—
Nitrobenzene	−0.36	−0.928	4.6	2.06	6.95	3.10
Methaqualone	−1.27	—	1.99	—	2.99	—

[a]All samples were 5×10^{-4} M in Britton-Robinson buffer at pH 3.60. The solvent system was 1 ml of ethanol and 19 ml of B-R buffer. [b]Diffusion current constant.

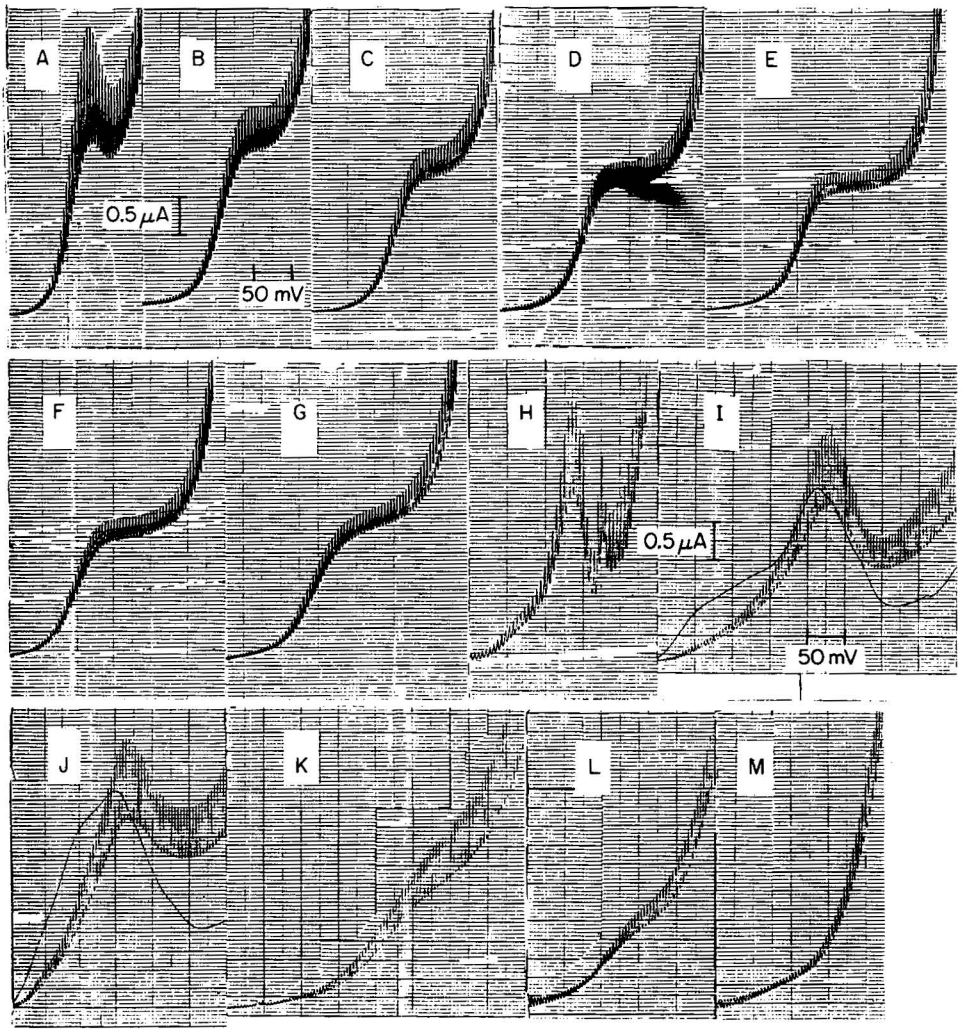

Fig. 1. Influence of pH on the d.c. polarographic waves of 2×10^{-4} M methaqualone. Citrate buffers: A, pH 0.7; B, pH 1; C, pH 1.2; D, pH 1.8; E, pH 2.6; F, pH 3.0; G, pH 4.0; H, pH 5.0. Phosphate buffers: I, pH 5.6; J, pH 6.0; K, pH 6.6; L, pH 7.4; M, pH 8.0. Curves A—C start at —0.6 V, D—F at —0.8 V, and G—M at —1.0 V.

The product of the preparative controlled-potential electrolysis of methaqualone at the mercury pool electrode was analyzed by TLC using a long-wavelength ultraviolet lamp for detection. The only product detected had an R_f value of 0.69 and was identified by using an authentic sample of 1,2-dihydromethaqualone (II). It was clearly separated from the starting material which had an R_f value of 0.57. Formation of 1,2-dihydromethaqualone by polarographic reduction at the DME was further confirmed by the absence of reduction waves at pH 2.5 in a solution of compound II. The

TABLE 2

Dependence of d.c. polarographic currents of methaqualone (I) on pH at 25°C

A. Sorensen's citrate buffers, 5×10^{-4} M methaqualone							
pH	1.3	1.6	1.8	2.0	2.4	2.6	2.8
i_1 (μA)	2.85	2.45	2.37	2.42	2.33	3.35	2.47
$E_{1/2}$ (V vs. SCE)	−1.16	−1.17	−1.18	−1.19	-1.20_5	−1.22	-1.23_5
pH	3.0	3.2	3.4	3.6	3.8	4.0	5.0
i_1 (μA)	2.33	2.22	2.11	2.06	1.86	1.58	0.2
$E_{1/2}$ (V vs. SCE)	-1.24_7	−1.25	-1.26_5	−1.28	−1.29	−1.30	−1.35

B. Britton-Robinson buffers, 2×10^{-4} methaqualone									
pH	2.65	2.99	3.52	3.90	4.48	5.01	5.41	6.00	6.4
i_1 (μA)	1.48	1.54	1.67						
$i_1 + i_2$ (μA)				1.48	1.50				
i_2 (μA)						1.50	1.21_5	0.5	0.1
$E_{1/2}$ (V vs. SCE)	−1.21	-1.22_5	−1.25	-1.26_5[a]	-1.31_5[a]	−1.36	-1.39_5	−1.46	

[a]Two overlapping waves.

polarographic inactivity of metolazone [7-chloro-1,2,3,4-tetrahydro-2-methyl-4-oxo-3-*o*-tolyl-6-quinazoline sulphonamide; III] and of quinethazone [7-chloro-2-ethyl-1,2,3,4-tetrahydro-4-oxo-6-quinazoline sulphonamide; IV]

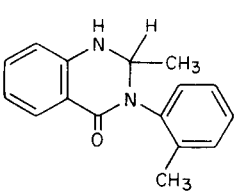

II

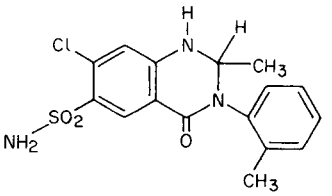

III

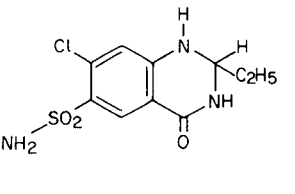

IV

indicates that for the reducibility of compound I, the presence of the 1,2-double bond in the heterocyclic ring is essential.

Studies of the polarographic reduction of methaqualone are complicated by the presence of three catalytic waves corresponding to hydrogen evolution. The first ($i_{1,\mathrm{cata}}$) is observed in a solution of methaqualone at pH <1.5, where this wave is superimposed on wave i_1. This catalytic process causes the increase of current i_1 at pH 1.3 (Fig. 2). In 0.45 M sulphuric acid (pH 0.7), the current reading of 7.2 μA is outside the range shown in Fig. 2.

At pH >5.5, two more catalytic waves ($i_{2,\mathrm{cata}}$ and $i_{3,\mathrm{cata}}$) are observed at −1.5 and −1.7 V, respectively. The heights of these waves increase characteristically with decreasing pH (Fig. 5), the shape of the increase depending on the composition of the buffer and the concentration of methaqualone. These waves at pH 6 are almost one order of magnitude higher than the wave i_2 at pH 4. In some buffers, the waves show characteristic round maxima with little sensitivity to surfactants. Waves $i_{2,\mathrm{cata}}$ and $i_{3,\mathrm{cata}}$ may be superimposed

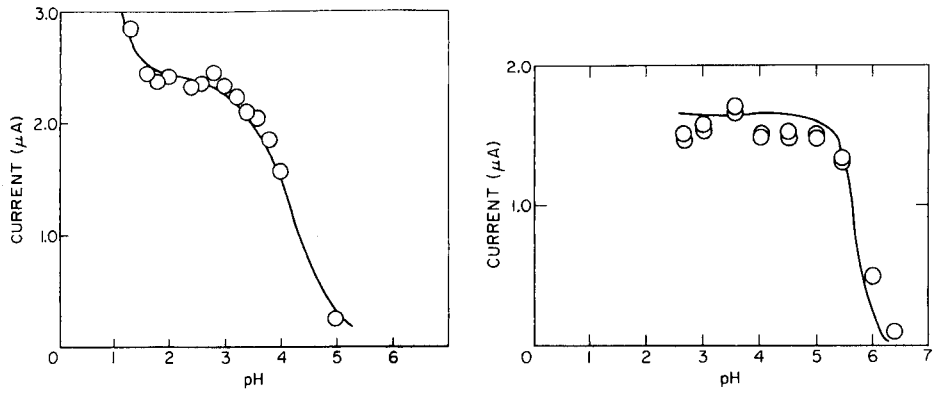

Fig. 2. Dependence of the limiting current of wave i_1 for 5×10^{-4} M methaqualone on pH in citrate buffers. (○) Experimental points; (—) theoretical curve for the dissociation of a monobasic acid.

Fig. 3. Dependence of the total limiting current ($i_1 + i_2$) for 2×10^{-4} M methaqualone on pH in Britton-Robinson buffers. (○) Experimental points from parallel experiments; (—) theoretical curve for the dissociation of a dibasic acid.

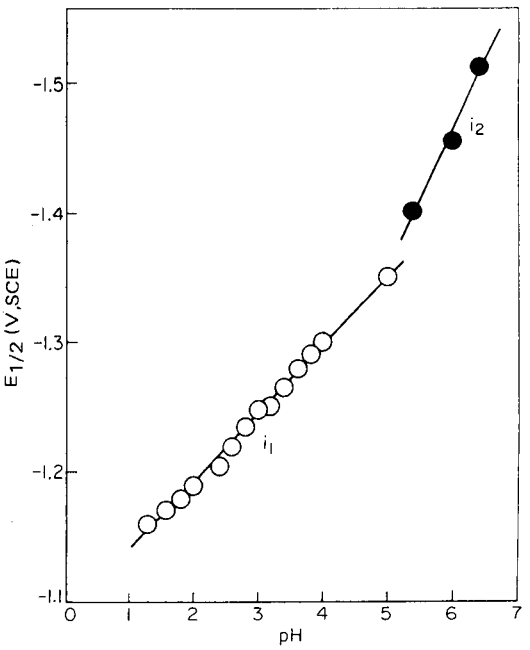

Fig. 4. Dependence on pH of the half-wave potentials of wave i_1 (○) and i_2 (●) of methaqualone in citrate and Britton-Robinson buffers.

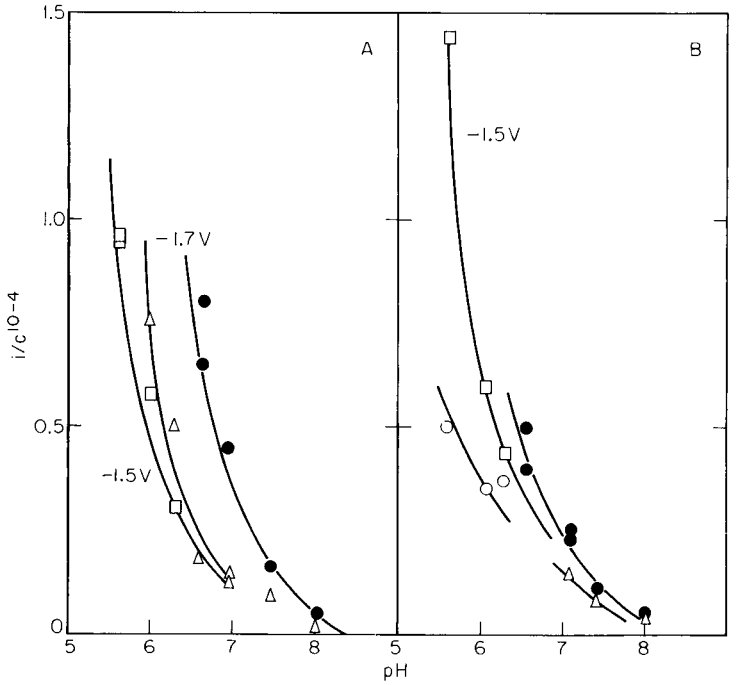

Fig. 5. Dependence on pH of the catalytic waves $i_{2,cata}$ and $i_{3,cata}$ expressed as i/c, in phosphate (A) and Britton-Robinson (B) buffers. Waves: (○) $i_{2,cata}$ at −1.5 V, 2×10^{-4} M methaqualone; (●) $i_{3,cata}$ at −1.7 V, 2×10^{-4} M methaqualone; (□) $i_{2,cata}$ at −1.5 V, 5×10^{-4} M methaqualone; (△) $i_{3,cata}$ at −1.7 V, 5×10^{-4} M methaqualone.

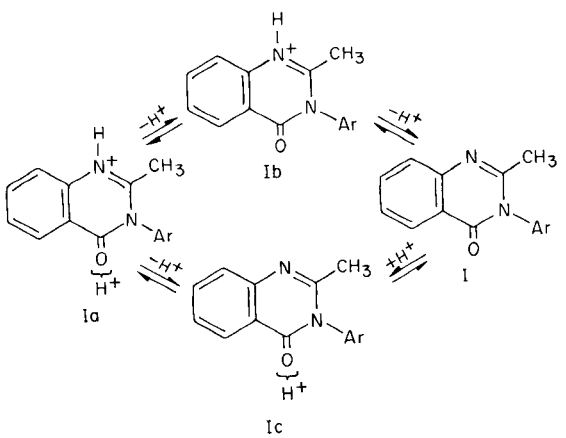

on the reduction wave of the conjugate base of methaqualone. Hence, it cannot be decided whether the oxidized or the reduced form of methaqualone participates in the catalytic process. The mutual positions of the i_{cata} vs. pH plots (Fig. 5) indicate that the species involved in the reduction of hydrogen ions in wave $i_{2,cata}$ is a stronger acid by about one pK unit than that governing the process corresponding to wave $i_{3,cata}$.

The shifts of half-wave potentials of wave i_1 (Fig. 4) indicate that at pH

<4, the reducible species bears one more hydrogen ion than does the species predominating in the bulk of the solution. The acid—base equilibria in solutions of methaqualone can be described by the following scheme (where Ar = *o*-tolyl):

Wave i_1 corresponds to a two-electron reduction of the form I_b preceded by a proton transfer at the electrode surface, so that I_a is actually the reduced species. Absence of a change in the shape of the $E_{1/2}$ vs. pH plot at pH 2.5, which corresponds to the pK_a (measured) of the equilibrium between the monoprotonated and diprotonated forms, indicates that the contribution of the equilibria $I_a \rightleftharpoons I_c \rightleftharpoons I$ in the bulk of the solution is not negligible. Consequently, the value of pK_a (measured) = 2.5 [4] does not correspond to the equilibrium $I_a \rightleftharpoons I_b + H^+$, but rather to a system $H^+ + I_c \rightleftharpoons I_a \rightleftharpoons I_b + H^+$. For reduction in wave i_1, it is thus possible to propose the sequence:

$$I + H^+ \rightleftharpoons I_b \qquad (1)$$

$$I_b + H^+ \underset{\text{surface}}{\rightleftharpoons} I_a \qquad (2)$$

$$I_a + 2e^- \rightarrow II \qquad (3)$$

As long as the protonation in reaction 1 is fast (up to pH 3) and can convert all the conjugate base I to the protonated form, a two-electron diffusion-controlled wave is observed. With pH increasing above 3, the rate of protonation in reaction 1 decreases and this results in the gradual decrease of wave i_1 (Fig. 2).

Reduction in wave i_2 occurs in a pH range where the free base I predominates in the bulk of the solution and in the solution in the vicinity of the electrode, but is biprotonated at the surface of the electrode, as is indicated by the −102 mV/pH shift of the half-wave potentials of wave i_2. At pH >5, these protonation reactions are no longer fast enough to convert I to I_a and the height of wave i_2 decreases (Fig. 3). The steep dissociation curve observed corresponds to a dibasic acid.

For the region between pH 1.5 and 3 in citrate buffers and 2.6 and 4 in Britton-Robinson buffers, the waves of methaqualone are well-developed and the diffusion-controlled total limiting current ($i_1 + i_2$) can be measured accurately and used for analytical purposes. With d.c. polarography, the waves are suitable for quantitative purposes from 1×10^{-4} to 5×10^{-4} M, whereas the limits for d.p.p. range from 1×10^{-5} to 5×10^{-4} M. At pH values above 4 in Britton-Robinson buffers, recording of the peaks by d.p.p is not recommended, even when the total current remains diffusion-controlled and the height is pH-independent (Fig. 3). The presence of two ill-resolved waves at pH >4 results in broad, ill-defined d.p.p. peaks which are lower than those obtained at pH <4.

REFERENCES

1 Y. Nagase, Y. Kanaya and H. Hoshida, Tokyo Yakka Diagaku Kenkyu, 12 (1963) 117; from Chem. Abstr. 59 (1963) 6199c.
2 P. Pflegel and G. Wagner, Pharmazie, 22 (1967) 643.
3 L. G. Chatten, R. E. Moskalyk, R. A. Locock and F. J. Schaefer, Analyst, 103 (1978) 837.
4 D. M. Patel, A. J. Visalli, J. J. Zalipsky and N. H. Reavey-Cantwell, in K. Florey, (Ed.), Analytical Profiles of Drug Substances, Vol. 4, Academic, New York, 1975, p. 245.
5 British Pharmacopoeia 1973, HMSO, London, 1973, p. 296.
6 K. H. Boltze, H. D. Dell, H. Lewald, D. Lorenz and M. Ruberg-Schweer, Arzneim. Forsch., 13 (1963) 688.

Analytica Chimica Acta, 200 (1987) 291—303
Elsevier Science Publishers B.V., Amsterdam — Printed in The Netherlands

THE DETERMINATION OF PURINES IN FRESH AND SEA WATER BY CATHODIC STRIPPING VOLTAMMETRY AFTER COMPLEXATION WITH COPPER(I)

B. C. HOUSEHAM, C. M. G. VAN DEN BERG* and J. P. RILEY

Department of Oceanography, University of Liverpool, Liverpool L69 3BX (Great Britain)

(Received 29th April 1987)

SUMMARY

Nanomolar levels of the purines, guanine, hypoxanthine, xanthine and adenine, in aqueous solution can be determined by cathodic stripping voltammetry (CSV). After the sample has been brought to pH 8.5 and made 150 nM with respect to copper(II), the Cu(I) complex of the purine is adsorbed on a hanging mercury drop electrode. After deposition for 60 s, the complex is stripped from the electrode and the peak current corresponding with the reduction of Cu(I) to Cu(0) is measured. The limits of detection are 0.2 nM for guanine, 0.3 nM for hypoxanthine and adenine, and 1.0 nM for xanthine; these can be lowered further by extending the adsorption time prior to the scan.

A program to quantify the different forms (organic and inorganic) of dissolved nitrogen in coastal and estuarine waters is under way in this laboratory. In recent studies it was observed that, in periods of the year when break-down processes were predominant, a large fraction of the nitrogen occurred as unidentified organic nitrogenous material, which was not composed of amino acids. To investigate the possibility that this material is composed of purines, an electrochemical method has been developed to determine low levels of purines in seawater.

Most of the conventional electrochemical methods for the determination of dissolved organic molecules have been based on polarographic techniques with a dropping mercury electrode but these generally have only poor sensitivity. Recently, stationary electrodes have been used to determine lower levels of organic compounds by including a preconcentration step at a fixed potential, prior to a potential scan in a negative direction [1—9]. This technique is called cathodic stripping voltammetry (CSV), as the reduction current of the collected material is measured. The reaction mechanism of the accumulation of organic molecules on the hanging mercury drop electrode (HMDE) can involve either the formation of sparingly soluble compounds with mercury [3, 6, 10] or adsorption [1, 2, 4, 8, 11, 12]. Interaction of certain active groups of the organic molecule with the mercury are considered to be an important prerequisite for the accumulation step; examples

0003-2670/87/$03.50

are thiol [1, 12], or amino [6] groups. Recent experiments with metal complexes have indicated that a chemical bond with the mercury is not always required for adsorptive accumulation [11, 13, 14].

The present investigation into techniques suitable for the determination of low concentrations of purines has indicated that they can be measured by CSV preceded by adsorptive collection of their complexes with copper(I) on the HMDE. The procedure gives limits of detection between 0.1 and 1.0 nM, which is below previously reported values. Experiments based on tensammetry indicate that adsorption only occurs in the presence of copper(I) generated from copper(II) in the solution immediately surrounding the electrode. The use of a copper-amalgam electrode [11] is not essential. Forsman [15] has reported very sensitive determinations of various penicillins based on their accumulation on the HMDE in solutions containing copper(II) with formation of the copper(I) complexes at the electrode.

EXPERIMENTAL

Equipment

Voltammograms were recorded by using a PAR 174A polarograph in conjunction with a PAR 303 HMDE, a PAR model 305 magnetic stirrer, and a 10-ml teflon cell with a teflon-coated magnetic follower. The reference electrode was Ag/AgCl, sat. KCl and the surface area of the mercury drop was 0.0294 cm^2. For voltammetric experiments with pH monitoring, a 60-ml glass cell was used with a Radiometer combined pH electrode (GK-2401C) and a Radiometer pHM-64 research pH meter, standardized with a pH 4 potassium hydrogenphthalate buffer. Tensammetric experiments were done with a Metrohm polarograph, model E506, and a Metrohm model 663-VA HMDE.

Reagents

All chemicals were supplied by BDH. Stock solutions of organic compounds were stored at room temperature in 25-ml polycarbonate tubes washed in methanol and 0.1 M nitric acid. Distilled water was prepared by a silica double-distillation unit. Seawater (salinity 32) was collected from the Menai Straits and stored in 50-l plastic containers. Contaminating trace metals were removed by equilibrating the seawater with manganese dioxide followed by filtration through a 0.45-μm (Oxoid) filter [14]. Organic material was removed by ultraviolet irradiation for 3 h with a 1-kW mercury lamp.

Stock solutions of adenine, hypoxanthine, xanthine, guanine, uric acid and allantoin, were prepared by dissolving 1 mg of the purine in 3 ml of 0.5 M sodium hydroxide and then diluting to 20 ml with distilled water. Stock solutions were found to be stable for several weeks.

Stock solutions of Cu(II), Pb(II), Cd(II), V(V), Zn(II), Fe(III), Mn(II),

U(VI) and Ni(II), were prepared by dilution of atomic absorption standard (Spectrosol) solutions. Two pH buffer solutions were prepared, one containing 1 M boric acid/0.4 M NaOH, and one with 1 M 4-(2-hydroxyethyl)-1-piperazineethane sulphonic acid (HEPES)/0.4 M NaOH, to give, respectively, pH 8.6 and 7.6 in seawater at 100-fold dilution. A stock solution of 0.1 M disodium-EDTA was prepared and adjusted to pH 8 by addition of sodium hydroxide solution. All solutions of amino acids (except tyrosine and cysteine) and sugars, cyclic adenosine monophosphate (AMP), adenosine triphosphate (ATP), creatinine, creatine, pimelic and oxalic acids, were freshly prepared by dissolving 1 mg in 20 ml of distilled water. Tyrosine, cystine, and adenosine were prepared as for purines.

Procedure

A 10-ml aliquot of ultraviolet-irradiated seawater was pipetted into a polarographic cell and 100 μl of buffer was added. The magnetic stirrer was started, and the solution was purged with argon to remove oxygen. The potentiostat was switched on at the required accumulation potential (E_{acc}), usually —0.15 V. A new drop was extruded and the adsorption time (t_{ads}), usually 60 s, was measured from this point. At the end of this time, the stirrer was switched off and, after a 10-s quiescence period, a negative potential scan was made from —0.15 to —0.7 V. The polarographic parameters were: scan rate 10 mV s^{-1}, differential pulse (DP) modulation with a pulse amplitude of 25 mV, and pulse time 0.1 s. The procedure was repeated after the addition of copper(II) nitrate (usually 150 nM), and again after a standard addition of the purine. This stepwise addition enabled the adsorption profiles of the organic, copper/organic and copper/purine species present to be monitored.

Preliminary experiments showed that the CSV peak height diminishes with time as a result of adsorption of copper and purine onto the cell wall. It is therefore recommended that the cell should be conditioned by soaking in a solution of similar composition to the analyte containing added copper. Between experiments, the cell should be rinsed with distilled water only.

RESULTS AND DISCUSSION

The structures of the purines tested are shown in Fig. 1. Analytically useful reduction peaks were obtained by DPCSV in the presence of 150 nM copper for adenine, guanine, hypoxanthine and xanthine; a peak for uric acid was obtained only at a high concentration of uric acid (75 nM) and no peak was obtained for allantoin. The DPCSV scans for the first four compounds were characterized by the presence of two peaks: one for free copper (not complexed by a purine) at —0.2 V, and one for a copper complex of each purine at potentials between —0.3 and —0.5 V. A third peak was apparent at intermediate concentrations of adenine (15—200 nM). Examples of measurements of adenine, guanine, hypoxanthine and xanthine added to

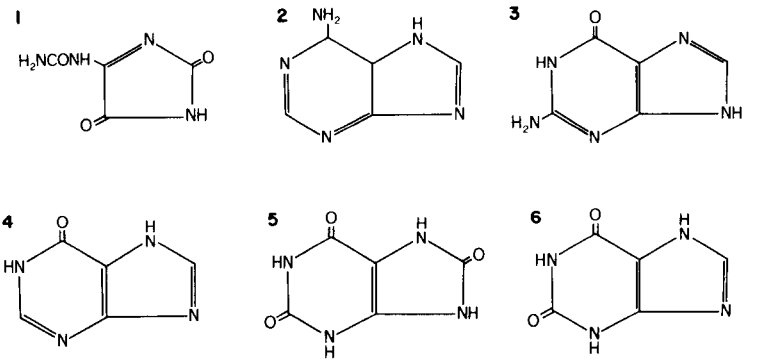

Fig. 1. Molecular structures studied: (1) allantoin; (2) adenine; (3) guanine; (4) hypoxanthine; (5) uric acid; (6) xanthine.

seawater are shown in Fig. 2. The peak height and peak potential of each purine complex were found to depend on the purine as well as on the copper concentration, the solution pH, the collection potential and the collection period. These parameters were therefore investigated to optimize the analytical conditions.

Cyclic voltammetry was used to study the reversibility and mechanism of the electrode process, and tensammetry to establish the potential range over which adsorption took place.

Cyclic voltammetry of adenine, guanine, hypoxanthine and xanthine

Cyclic voltammetry was applied at various scan rates, and was preceded by 60 s adsorption at −0.15 V. A second scan was made on the same mercury drop immediately after the first scan without further collection. A single cathodic peak was apparent for guanine and hypoxanthine. The anodic peak potential was 0.12 V more positive than that of the cathodic peak for guanine, and 0.11 V more positive for hypoxanthine, probably as a result of diffusion of reduced copper into the mercury drop and diffusion of the uncomplexed purine away from the electrode. The same effect caused the cathodic peak of the second scan to be smaller and shifted in a positive direction. The scans for hypoxanthine, which are shown in Fig. 3, were very similar to those for guanine.

Adenine and xanthine showed a more complicated behaviour. A second cathodic adenine peak became apparent in the second cyclic scan, and the main cathodic peak contained a shoulder in both scans (Fig. 3). Xanthine produced three cathodic peaks more clearly, but only one anodic peak (Fig. 4). The fourth cathodic peak, which appeared at −0.2 V in the second cyclic scan, was due to free Cu(I) which had been released from the complexes after the first scan. All the peaks produced by xanthine (and by adenine, guanine and hypoxanthine) were related to reduction of complexed copper, as no peaks were apparent in the absence of added copper. The

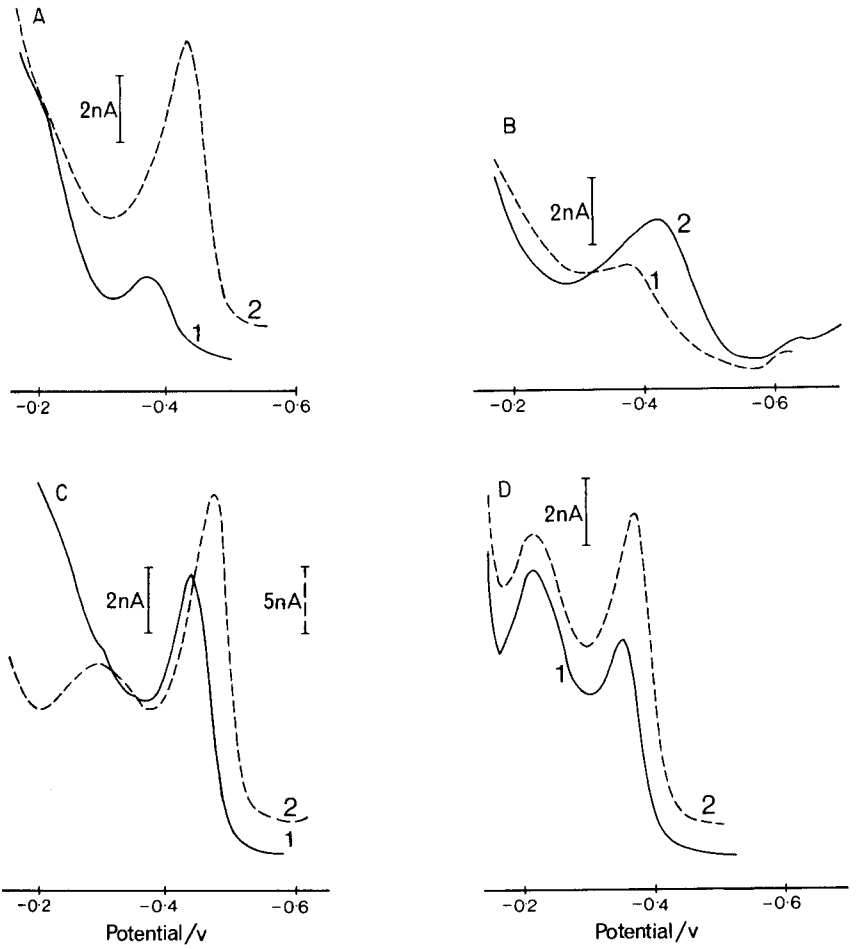

Fig. 2. DPCSV scans of purines in seawater. All at pH 8.5, except hypoxanthine which was at pH 7.7. Scans: (A) guanine at 2.3 nM and 17.7 nM (150 nM Cu); (B) xanthine at 8 nM and 13 nM (75 nM Cu); (C) adenine at 6.6 nM and 45 nM (150 nM Cu); (D) hypoxanthine at 4.5 nM and 9.0 nM (200 nM Cu).

multiple peaks therefore seem to correspond to different adsorbed complexes of the purines with copper.

When the scan rate was increased in steps from 20 to 500 mV s^{-1}, it was found that the cathodic peak height for adenine increased linearly, whereas the peak potential shifted from —0.6 to —0.76 V. The linear increase is to be expected for the reduction of adsorbed material [16]. The increase was non-linear at scan rates >200 mV s^{-1} for xanthine and guanine, and for scan rates >50 mV s^{-1} for hypoxanthine. This non-linear increase suggests that kinetic factors limit the peak height for these compounds. The peak potentials for xanthine, guanine and hypoxanthine shifted 0.1 V in a negative

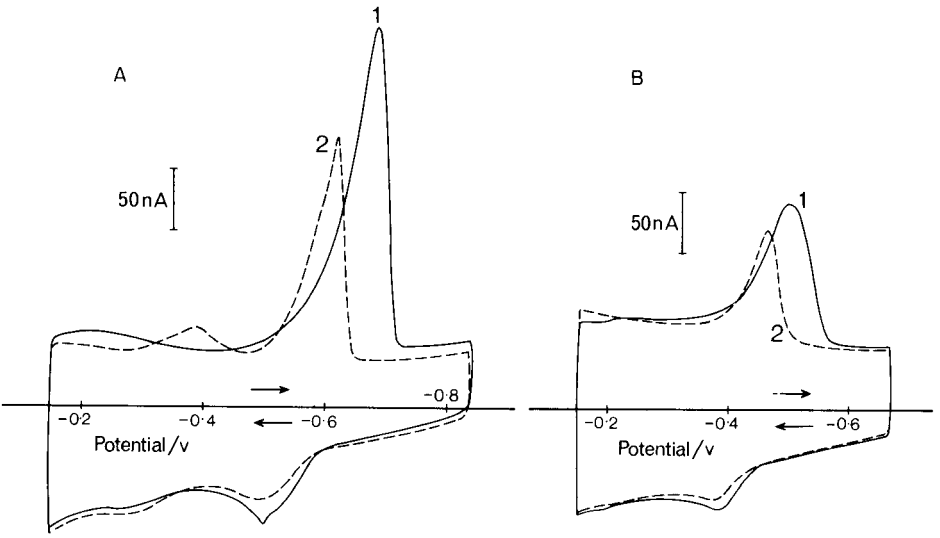

Fig. 3. Cyclic voltammetry of adenine (A) and hypoxanthine (B) in seawater. Scan 1 preceded by 60-s adsorption at —0.15 V; scan 2 immediately followed scan 1 on the same mercury drop. Conditions: 350 nM adenine or 100 nM hypoxanthine; 400 nM Cu; scan rate 50 mV s^{-1}.

direction when the scan rate was increased from 20 to 500 mV s^{-1}, presumably as a result of slow kinetics of the dissociation of the complex.

Tensammetry

Adsorption of all six purines tested onto the mercury electrode was investigated by using tensammetry in the presence and absence of copper, and after adsorption at various potentials. The current was sampled at 90° out of phase with the a.c. waveform. The results for adenine (Fig. 5) are similar to those for guanine, xanthine and hypoxanthine. Upon addition of adenine (1 μM) to the electrolyte solution (seawater at pH 8.5), the capacitance was suppressed to a small extent. However, this suppression was much greater when copper (1.5 μM) was added to the solution. At —0.65 V the capacitance current rose again sharply, at the potential where the main reduction wave for copper/adenine complex was situated; no capacitance suppression occurred at lower potentials, suggesting that only the copper complexes adsorbed, whereas the free ligands desorbed from the electrode. Most of the capacitance suppression was eliminated similarly by adsorbing at —0.7 V prior to the scan from —0.2 V, which confirmed that only the complexed purines adsorbed.

The results for guanine, hypoxanthine and xanthine were analogous to those for adenine. No adsorption was apparent from allantoin (400 nM), and only a relatively small capacitance suppression was caused by uric acid

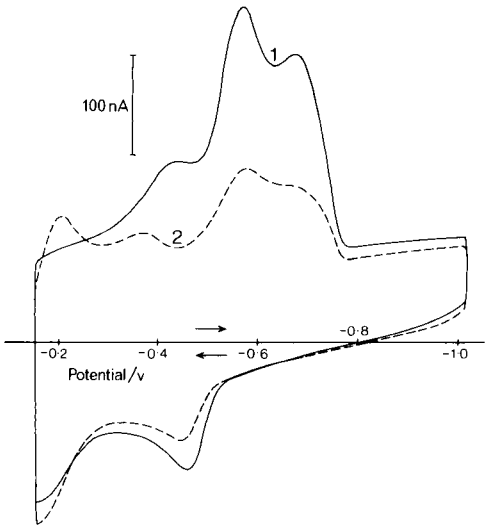

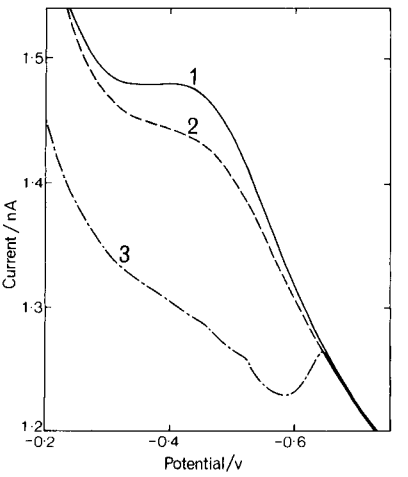

Fig. 4. Cyclic voltammetry of 700 nM xanthine in seawater, at pH 8.5 and with 1 μM Cu. Scan 1 after 60-s adsorption at —0.15 V, immediately followed by scan 2. Scan rate 50 mV s^{-1}.

Fig. 5. Tensammetry of adenine in seawater. Each scan preceded by 60-s adsorption at —0.2 V. Scans: (1) seawater with borate buffer, (2) 1 μM adenine; (3) 1 μM adenine with 1.5 μM Cu.

(415 nM) in the presence of copper (1.5 μM). These results agree with the finding that no copper-complex peak is formed with allantoin, and with uric acid only at a high concentration of uric acid.

The effect of varying the copper concentration

The copper concentration was varied between 10 nM and 300 nM in the presence of 5—15 nM purine in order to optimize the analytical conditions. The reduction peaks for the copper complexes of adenine, hypoxanthine, xanthine and guanine increased strongly with the copper concentration until approximately 100 nM copper(II), above which the rate of increase diminished (Fig. 6); the peak height then became limited by the purine concentration.

The peak for free copper increased in height with the added copper concentration most strongly when the increase for the purine complex levelled off. Separate measurements of the copper peak, with and without an adsorption period prior to the scan, and in the absence of added purines, showed that the peak current of free copper was approximately doubled by adsorption of presumably Cu(I) chloride complexes when the scan was preceded by a collection period. Adsorption of Cu(I) chloride complexes on the mercury electrode has previously been observed by Nelson [17].

At a higher purine concentration, the purine reduction peak could be

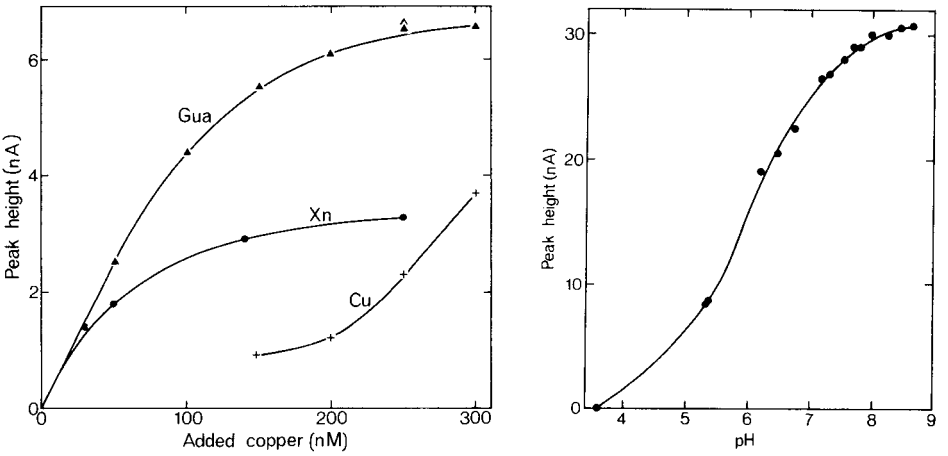

Fig. 6. The effect of varying the copper concentration on the peak height obtained using DPCSV for 11 nM guanine (Gua) and 8 nM xanthine (Xn). The solution (seawater) contained 0.01 M borate pH buffer, the collection time was 60 s at —0.15 V. The height of the free Cu(I) peak is indicated by Cu.

Fig. 7. The effect of the pH on the peak height obtained for 32 nM adenine in seawater in the presence of 90 nM Cu. The collection period was 60 s at —0.15 V.

increased further by increasing the copper concentration, indicating that excess of copper was required for optimal analytical conditions. However, at high copper and low purine levels, the free copper peak sometimes interfered with the measurement of the purine peak. A concentration of 150 nM copper was therefore selected as being optimal for the determination of low levels of purines.

Effect of varying the pH

The solution pH affects the stability of the purine/copper complex and therefore the peak potential as well as the peak height. This is shown in Fig. 7 in which the peak height of adenine is plotted as a function of the pH. No adsorption of the copper complex was apparent at pH 3.5, but the peak then increased with increasing pH as a result of diminished protonation of the purine. A pH of 8.6, produced with borate buffer, was selected as the optimum for analytical purposes, as precipitation of magnesium hydroxide occurs in seawater at higher values.

The sensitivities for the other purines by CSV were examined at several pH values with other buffers (sodium acetate at pH 4.5, HEPES at pH 7.7) and the responses were found to be similar to that for adenine. There are two further advantages of using borate (pH 8.6) pH buffer rather than HEPES at pH 7.7: (1) the peak potentials of the purine/copper complexes are more negative, which positions the peaks at potentials at which the baseline is flatter and further removed from the free copper peak; and (2) con-

taminating organic material can be removed from the borate buffer by ultraviolet irradiation, which would destroy the HEPES solution.

Effect of varying the collection potential

The DPCSV peak height for the purines decreased when the collection potential was lowered from —0.15 V (Fig. 8). As would be expected, no purine peaks were produced when the collection potentials were more negative than the reduction potentials of the purine complexes. The formation of the complexes of the purines with the added copper apparently requires the production of Cu(I) at the electrode surface during the collection period, and this Cu(I) is produced increasingly less efficiently at potentials further below —0.2 V at which the free Cu(I) reduction peak is located. The Cu(I) which is produced from amalgamated copper upon switching of the potential to —0.15 V prior to initiating the scan, is not sufficient to complex the purines to a significant extent, indicating that the purines do not adsorb well in the absence of Cu(I) (the Cu(I) involvement will be discussed further below).

Effect of extending the collection time

Generally the purine complex adsorption, and therefore the CSV peak height increased with the collection time, but there were some differences in response between the purines. The peak height for 8 nM adenine increased linearly with the collection time up to 1.5 min, and to 2 min for 0.45 nM

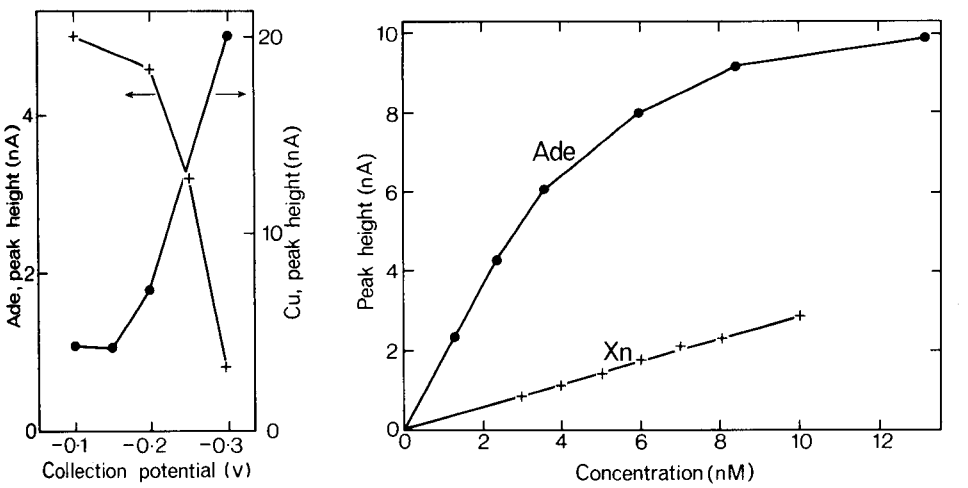

Fig. 8. Effect of varying the collection potential on the DPCSV peak height for 9 nM adenine in the presence of 200 nM copper in seawater, containing 0.01 M HEPES.

Fig. 9. The peak height as a function of the concentration of adenine (Ade) and xanthine (Xn) in seawater at pH 8.6. Adenine with 100 nM Cu, and xanthine with 50 nM Cu.

adenine, after which time the increase levelled off. With collection times greater than 3 min for 8 nM adenine, a second, smaller peak was formed which was ca. 0.1 V more positive. This was probably due to the adsorption of a different copper complex. The response for guanine increased linearly up to 2 min, for hypoxanthine up to 5 min, and for xanthine up to 7 min; the free Cu(I) peak always diminshed as the purine peaks increased. The levelling off of the increase in the purine peak height with longer collection times was not due to drop saturation as the peak height could be increased further by adding more copper and purine.

Electrode mechanism

The copper complexes of the purines tested were evidently formed with Cu(I) rather than with Cu(II) as the complexes of the latter are very weak: for example, the stability constant (log K) for the Cu(II) complex of adenine is ca. 1.7 at pH 8.5 [18]; this means that the Cu(II) concentration would have to be greater than 0.01 M for there to be significant complexation of adenine. Copper(I) is stabilized in chloride medium as a result of the formation of complexes of the type $CuCl_2$. The reduction potential for Cu(I)/Cu(0) is therefore shifted in a negative direction to about —0.2 V, whereas the Cu(II)/Cu(I) reduction wave is masked by that of mercury [14, 17, 19]. Copper(I) is therefore generated at the electrode surface when the potential is held at a potential $>$—0.2 V in seawater. This Cu(I) is then available for complex formation with the purines prior to the adsorption of the formed complexes.

Values for the stability constants of the Cu(I)/purine complexes were estimated from their reduction potentials (obtained with DPCSV and in the presence of 150 nM Cu) after correction for chloride complexation of Cu^+ using the constants given by Smith and Martell [20], and are given in Table 1. In making the calculations it was assumed that either 1:1 or 1:2 (Cu:L) complexes could have formed. Because it is possible that the complexes are stabilized by adsorption, the calculated values for the stability constants have probably been overestimated. The stability constants in Table 1 are very high, similar to those (log K' = 18.5 and log $\beta'_{1,2}$ = 24.9) for

TABLE 1

Values for the conditional stability constants for complexation of four purines with Cu(I) in seawater, calculated from the peak shift

Ligand	Log K'	log $\beta_{1,2}$	pH
Adenine	16.8	23.4	8.5
Guanine	16.4	23.6	8.5
Hypoxanthine	15.6	23.7	7.7
Xanthine	18.3	26.6	8.5

complexes of Cu^+ with cysteine [21, 22]. The active Cu(I)-binding groups are probably the azine-N groups, perhaps combined with an amine group; examples of powerful Cu(I)-binding diazines are the phenanthrolines such as 2,9-dimethyl-1,10-phenanthroline with a log $\beta_{1,2}$ of 19.1 [18].

Analytical aspects: linear range and limit of detection

The relationship between the DPCSV peak height and the purine concentration was found to be linear over a limited concentration range, which depended on the excess copper concentration. For instance, the DPCSV peak height for adenine increased linearly between 0.3 and 2 nM adenine in the presence of 100 nM copper, after which the increase became non-linear (Fig. 9). Similar responses were apparent for xanthine, hypoxanthine and guanine. Though a high copper concentration was useful in extending the linear range, it interfered with the measurement of low purine levels because of the large size of the free copper peak. A level of 100—200 nM Cu is therefore optimal for low and sub-nanomolar levels of purines.

The limits of detection were calculated from 3× the noise of the determination of a low level of each purine. For a collection period of 60 s, the values were: 0.3 nM hypoxanthine, 0.2 nM guanine, 0.3 nM adenine and 1.0 nM xanthine. The detection limits for xanthine, hypoxanthine and guanine could be lowered by a factor of 5 by extending the collection period to 5 min. These limits of detection are well below those reported previously [11], which suffered from chloride ion interference. The relative standard deviation for the determination of 4 nM of these purines was ca. 3%.

Interferences

Other organic molecules could interfere with the determination of the purines tested, if they adsorb on the mercury drop electrode and produce a complex with Cu(I) or Cu(II), or if they are electroactive themselves with a reduction potential close to that of the purines. Several amino acids including those with thiol or π-orbital electrons were added (up to 100 nM) to seawater to test their possible DPCSV response in the presence and absence of added copper, and at pH 8.6. No peaks were obtained with alanine, hydroxyproline, phenylalanine, glutamic acid, methionine, ethionine and tyrosine. Reduction peaks were obtained with cystine and cysteine which behaved similarly to the purines [22]; however, their reduction potentials were more negative than those for the purines and they did not interfere. No interference was produced by the sugars ribose and galactose, or by oxalic acid, pimelic acid, cyclic AMP, ATP or adenosine. An organic chelating agent without adsorptive or electroactive properties could interfere if present at a sufficiently high concentration to mask the added copper. Addition of 10^{-4} M EDTA, for instance, caused the peak height for guanine to diminish by 81%, and the peak disappeared altogether when 10^{-3} M EDTA was added. Such an interference, though improbable in samples of natural water could be overcome by adding more copper.

Catechol was added to the solution as an example of a compound which is known to form electroactive complexes with Cu(II) which adsorb onto the electrode [14]. With 10^{-4} M catechol and in the presence of 150 nM copper(II) and 15 nM guanine, two reduction peaks were formed, one for the two-electron reduction of the copper complex with catechol at −0.31 V, the second for the one-electron reduction of the Cu(I) complex with guanine at −0.45 V. The sensitivity for guanine decreased by 80% under these conditions, but interestingly the linear range was much extended to 135 nM guanine and the peak height continued to increase non-linearly to >500 nM guanine. The drop surface was saturated under these conditions with copper/catechol complexes, which caused the guanine peak height to diminish when the adsorption time was increased.

Non-electroactive surface-active material could interfere by inhibiting adsorption of the metal-purine complexes. Triton X-100 was added to the solution as a model surfactant: the sensitivity for adenine was diminished by 21% and 60%, respectively, in the presence of 0.1 and 0.5 mg l^{-1} of this Triton. Interference as a result of diminished sensitivity caused by the presence of surface-active material, or by the adsorption of other copper complexes, can be overcome to some extent by means of standard additions of the purines.

High concentrations of metals other than copper were added in order to test for their possible interference. No peaks for hypoxanthine, adenine, allantoin or uric acid were obtained (and so no interference was caused) when 10^{-7} M Pb(II), V(V), Cd(II), Zn(II), Fe(III), Mn(IV), U(VI) or Ni(II) was added.

Conclusions

Very low levels of purines can be detected by using DPCSV in the presence of copper ions. However, the similarity of the peak potentials precludes the practical determination of these purines individually in complex mixtures. Experiments are presently under way to investigate the possibility of using HPLC with CSV detection to determine low levels of purines in environmental samples.

B.C.H. was supported by a research studentship from NERC. The manuscript was typed by Mrs V. Hughes.

REFERENCES

1 T. M. Florence, J. Electroanal. Chem., 97 (1979) 219.
2 J. Wang and B. A. Freiha, Bioelectrochem. Bioenerg., 12 (1984) 235.
3 R. A. Grier and R. W. Andrews, Anal. Chim. Acta, 124 (1981) 333.
4 R. Kalvoda, Anal. Chim. Acta, 162 (1982) 197.
5 H. Klukanova, M. Studnickova and J. Kovar, Bioelectrochem. Bioenerg., 12 (1984) 279.

6 E. Palecek, J. Osteryoung and R. A. Osteryoung, Anal. Chem., 54 (1982) 1389.
7 Y. Vaneesorn and W. F. Smyth, Anal. Chim. Acta, 117 (1980) 183.
8 J. Wang, D.-B. Luo, P. A. M. Farias and J. S. Mahmoud, Anal. Chem., 57 (1985) 158.
9 A. Webber and J. Osteryoung, Anal. Chim. Acta, 157 (1984) 17.
10 E. Palecek, Anal. Biochem., 198 (1980) 129.
11 S. Glodowski, R. Bilewicz and Z. Kublik, Anal. Chim. Acta, 186 (1986) 39.
12 R. Parsons and P. C. Symons, Trans. Faraday Soc., 64 (1968) 1077.
13 B. Pihlar, P. Valenta and H. W. Nürnberg, Fresenius' Z. Anal. Chem., 307 (1981) 337.
14 C. M. G. van den Berg, Anal. Chim. Acta, 164 (1984) 195.
15 U. Forsman, Anal. Chim. Acta, 146 (1983) 71.
16 A. J. Bard and L. R. Faulkner, Electrochemical Methods, Wiley, New York, 1980.
17 A. Nelson, Anal. Chim. Acta, 169 (1984) 273.
18 R. M. Smith and A. E. Martell, Critical Stability Constants, Vol. 2, Plenum, New York, 1975.
19 M. Odier and V. Plichon, Anal. Chim. Acta, 55 (1971) 209.
20 R. M. Smith and A. E. Martell, Critical Stability Constants, Vol. 4, Plenum, New York, 1976.
21 I. M. Kolthoff and W. Stricks, J. Am. Chem. Soc., 173 (1951) 1728.
22 C. M. G. van den Berg, B. C. Household and J. P. Riley, J. Electroanal. Chem., in press.

Analytica Chimica Acta, 200 (1987) 305—312
Elsevier Science Publishers B.V., Amsterdam — Printed in The Netherlands

ANODIC STRIPPING VOLTAMMETRY WITH MEDIUM EXCHANGE IN TRACE ELEMENT SPECIATION

T. M. FLORENCE* and K. J. MANN
CSIRO Division of Energy Chemistry, Private Mail Bag 7, Menai, NSW 2234 (Australia)
(Received 25th March 1987)

SUMMARY

The application of medium exchange in anodic stripping voltammetry (ASV) was investigated by determining the fractions of ASV-labile copper, lead, cadmium and zinc in the presence of a variety of natural and synthetic ligands in a soft water. Pristine and polluted samples of river water were also tested. Medium exchange, where the test solution is replaced after electrodeposition by a simple electrolyte such as acetate buffer, before the oxidation (stripping) of the deposited metals, can ensure that the ASV-labile metal fraction depends only on the parameters of the electrodeposition step. Significant differences were found for ASV-labile fractions when medium exchange was used for the two river water samples, and for several metal/ligand combinations such as copper/chloride, copper/humic acid, and zinc/tannic acid. It is recommended that medium exchange be used routinely for ASV-labile determinations.

Anodic stripping voltammetry (ASV) is now widely used to determine trace element speciation [1]. Knowledge of the speciation (i.e., the different physicochemical forms) of an element in a water sample is essential to an understanding of the likely toxicity of a water. Reasonable correlations between ASV-labile copper and toxicity towards some test organisms have been found, especially when the water contained only natural ligands [1, 2].

Anodic stripping voltammetry consists of two discrete processes: deposition of trace elements from solution into an electrode (usually mercury), then electrochemical oxidation (stripping) of the deposited element into the solution and measurement of the resulting current peaks. The fraction of a metal in solution that is ASV-labile (i.e., reactive at the electrode) depends on the kinetics of metal complex dissociation during the deposition step, the concentration of excess of ligand, and the diffusion-layer thickness [1]. The ratio i_k/i_d, where i_k is the kinetic current flowing during the deposition step as a result of dissociation of a metal complex, and i_d is the diffusion current that would be observed for the same concentration of metal in the absence of complexing ligand, is an index of the lability of the complex. At a hanging mercury drop electrode (HMDE), i_k/i_d is given [3] by

$$i_k/i_d = [r_0(r_0 + \delta)^{-1} + \sigma r_0(r_0\ \eta \coth \eta + \delta)^{-1}]^{-1} \quad (1)$$

where $\sigma = k_f\ [L]/k_d$, k_f and k_d being the formation and dissociation rate

0003-2670/87/$03.50

constants, respectively, for dissociation of the metal complex, ML, at the electrode; $\eta = \delta D^{-1/2} (k_d + k_f[L])^{1/2}$; δ is the diffusion layer thickness (cm), D the diffusion coefficient of the metal ion in solution ($cm^2\ s^{-1}$), and r_0 the radius of the HMDE (cm).

Thickness δ at an HMDE in a stirred solution can be evaluated [4] by measuring the d.c. diffusion current, i_d:

$$i_d = nFADC/\delta \qquad (2)$$

where n is the number of electrons involved in the metal ion reduction, F is the faraday, A the electrode area, and C the metal concentration. A typical value for δ in a solution stirred magnetically is 2×10^{-3} cm.

Both molecular metal/ligand complexes and reducible metal ions adsorbed on colloidal particles (e.g., humic acid) can yield kinetic currents and ASV-labile metal [1, 5, 6]. The preceding discussion assumes that only the deposition step affects the relative magnitudes of the stripping peaks for labile and total metal in the sample and hence the calculated percentage of labile metal. Ideally, this should be the case, so that labile metal is determined solely by the fraction of metal accumulated in the electrode during the deposition step. However, under certain circumstances the kinetics of the stripping process (electro-oxidation), especially when pulse techniques are used, may have a significant effect on the peak heights obtained by the stripping. This can occur if a complexing agent or surface-active substance present in the sample solution, but not in the standard solution used to measure i_d, affects the stripping chemistry or kinetics [3, 7]. This situation could arise from a number of causes. If a ligand in the sample solution stabilizes an intermediate valency state of the metal, leading to a smaller number of electrons being involved in the electrochemical oxidation, lower stripping peaks will result. This has been observed for the ASV determination of copper in the presence of chloride and some other ligands [8–11]. In the case of chloride, the problem could be overcome by adding the same concentration of chloride to the standard as is present in the sample.

The presence of complexing agents or surface-active substances in the sample may be important in the stripping process because of the large surface excess of the oxidized metal ion (compared with the bulk solution) that is present during the initial stages of stripping [7, 12]. This excess can cause the precipitation of metal compounds on the electrode which may then affect the stripping current.

A method of minimizing any effects of interfering substances during stripping is to use the technique of medium exchange. With medium exchange, deposition is done from the sample solution but, before the stripping process begins, the sample solution is exchanged for a reference medium, such as acetate buffer, in which the calibration measurements for i_d have previously been made [13, 14]. The deposited metals are then stripped into this reference solution and the peaks heights are measured. In this way, the percentage of ASV-labile metal should depend only on the parameter of the deposition process.

This paper describes the application of medium exchange to the determination of ASV-labile Cu, Pb, Cd and Zn in synthetic soft water containing a variety of ligands, and in a pristine and a polluted river water.

EXPERIMENTAL

Apparatus

An E.G. and G. Princeton Applied Research Model 384 polarographic analyzer, with a Model 303 static mercury drop electrode (SMDE) assembly and a Model 305 magnetic stirrer was used for all ASV measurements. The ASV conditions were, unless otherwise stated: deposition potential, −1.25 V; deposition time, 300 s; differential pulse amplitude, 25 mV; scan rate, 5 mV s^{-1}; drop size, small; magnetic stirrer rate, fast; deaeration (nitrogen) time, 300 s. Electrode potentials refer to the silver/silver chloride reference. The diffusion layer thickness at the SMDE was calculated [1] to be 2.5×10^{-3} cm.

Analytical measurements were made in a class-100 clean room at 25 ± 0.5°C.

Reagents and samples

Fulvic acid was soil-derived by pyrophosphate extraction [6, 15]. The tannic acid, humic acid and iron(III)/humic acid colloidal solutions were prepared as described previously [16]. All ligand solutions were analyzed for Cu, Pb, Cd and Zn. The acetate buffer, pH 4.7, was prepared from Merck Suprapur sodium acetate and nitric acid. The water used was reverse-osmosis Milli-Q water.

Synthetic soft water (SSW). The SSW contained in mg l^{-1}: $NaHCO_3$, 48; $CaSO_4 \cdot 2H_2O$, 30; $MgSO_4$, 30; KCl, 2.0. It was filtered (0.45 μm) and adjusted to pH 7.4.

River water. Two samples of South Creek water were taken near St Marys,

TABLE 1

South Creek water quality data

	South Creek 1	South Creek 2[a]
pH	7.5	7.6
DOC, mg l^{-1}	14	11
Iron, mg l^{-1}	0.20	0.10
Fulvic/humic acid, mg l^{-1}	24	19
Conductivity, μS cm^{-1}	945	840
Total hardness, g $CaCO_3$ l^{-1}	136	117
Copper complexing capacity, 10^{-7} M[b]	3.0	5.0
Total copper, 10^{-8} M	4.1	8.3
Total lead, 10^{-8} M	0.11	1.6
Total cadmium, 10^{-9} M	1.0	1.0
Total zinc, 10^{-7} M	0.28	2.7

[a]After passing through industrial area and water-treatment plant. [b]ASV titration in acetate buffer, pH 4.7.

Sydney [16]. The first sample (South Creek 1) was collected near farmland, and was essentially pristine. The creek passes through the St Marys industrial area and then a water-treatment plant. A second sample was taken (South Creek 2) a few km after the creek left the treatment plant. Both water samples were filtered through 0.45-μm filters and stored at 4°C. Analysis of the waters is shown in Table 1.

Medium-exchange procedure

A conventional type of medium-exchange cell [13, 14] was constructed by modifying a standard PAR Model 384 cell (Fig. 1). The cell fitted into its normal position in the 384 voltammeter assembly, and the tube from the reservoir holding the exchange solution entered the cell block through the top hole normally used for standard addition. A 10-ml sample volume was used.

The SSW was made 0.03 M in acetate buffer pH 4.7. The blank concentrations of ASV-labile Cu, Pb, Cd and Zn in this mixture were, respectively, ($\times 10^{-8}$ M): 1.8, 0.29, <0.01, 3.1. Standard additions of 4×10^{-8} M Cu, Pb, Cd and Zn were made to this solution plus the ligand for ASV-lability measurements. The percent ASV-labile metal, calculated from peak-height ratios in the presence and absence of ligand, was evaluated after correction for metal concentrations in the ligand stock solutions [6, 16].

Medium exchange was done after a 300-s deposition time; then "HOLD" was applied at the "EQUILIBRATE" stage while 5 ml of the sample solution was run from the cell. The deaerated exchange solution (50 ml of 0.03 M acetate buffer pH 4.7 in SSW) was then run into the cell while the remaining sample solution was simultaneously drained out through the bottom tap. This procedure takes about 50 s. Care must be taken not to break contact with the mercury drop or the auxiliary electrode, otherwise deposited metal will be lost instantly from the mercury drop electrode, even though there is a

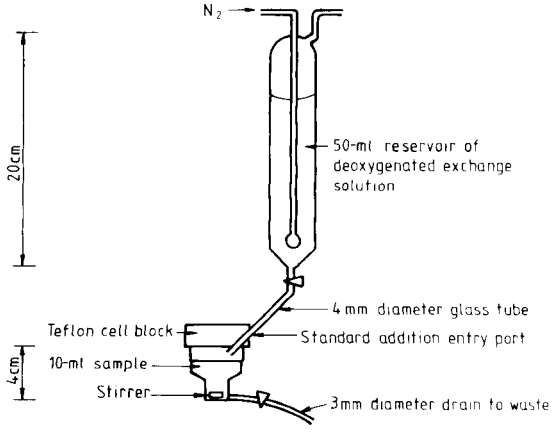

Fig. 1. Medium-exchange apparatus for use with the PAR Model 303 static mercury drop electrode assembly.

nitrogen blanket in the cell. Use of a small mercury drop and relatively slow exchange of the solution ensures that the drop does not fall off.

While the settings are in the "HOLD/EQUILIBRATE" position, the mercury electrode is held at the deposition potential (−1.25 V). However, the solution is not stirred during this period, and tests showed that additional deposition during medium exchange was negligible.

After 50 ml of exchange solution had passed through the cell, and the 10-ml cell solution was now 0.03 M acetate buffer, the CONTINUE button was pushed, and the stripping program allowed to proceed.

RESULTS

Efficiency of exchange

The efficiency of removal of the test solution by the medium-exchange solution was measured by using ferroin indicator. A solution of the indicator was prepared so that the absorbance (1-cm cell) at 410 nm was close to 1.0. This solution (10 ml) was used as sample in the voltammeter cell, and then exchanged in the normal manner with 50 ml of water. The absorbance of the new cell solution was then measured at 410 nm and the per cent exchange calculated. Four replicate measurements gave exchange values of 99.8, 99.2, 99.7 and 99.7%. Medium exchange is, therefore, essentially complete.

Effect of medium exchange on ASV-lability of metal complexes

When the 0.03 M acetate buffer pH 4.7 in SSW was used as the medium-exchange solution, and the same mixture plus 4×10^{-8} M Cu, Pb, Cd, Zn

TABLE 2

Effect of medium exchange (MX) on ASV-labile metal in a synthetic soft water

Ligand	Conc.	ASV-labile metal, % of total[a]							
		Zn		Cd		Pb		Cu	
		−	MX	−	MX	−	MX	−	MX
Chloride	0.5 M	80	91	109	108	118	116	61	87
Fulvic acid	5 mg l^{-1}	68	66	100	100	82	75	17	28
Humic acid	5 mg l^{-1}	100	114	100	100	100	100	17	44
Iron/humic acid	—[b]	90	90	87	86	79	65	15	31
Tannic acid	2 mg l^{-1}	51	71	100	100	122	122	100	100
Nitrilotriacetic acid	1×10^{-6} M	59	71	100	100	81	86	100	100
LAS[c]	0.5 mg l^{-1}	87	100	79	73	82	74	88	90
Triton X-100	1 mg l^{-1}	7	9	26	38	40	54	50	50
Gelatine	50 mg l^{-1}	5	6	42	44	100	100	30	39
South Creek No. 1	—	69	100	57	100	<7	42	17	27
South Creek No. 2	—	<7	12	38	100	<7	<7	10	22

[a]All solutions were in synthetic soft water (see text) with 0.03 M acetate buffer, pH 4.7, added. [b]0.8 mg l^{-1} Fe + 5 mg l^{-1} humic acid. [c]Linear alkylbenzene sulphonate.

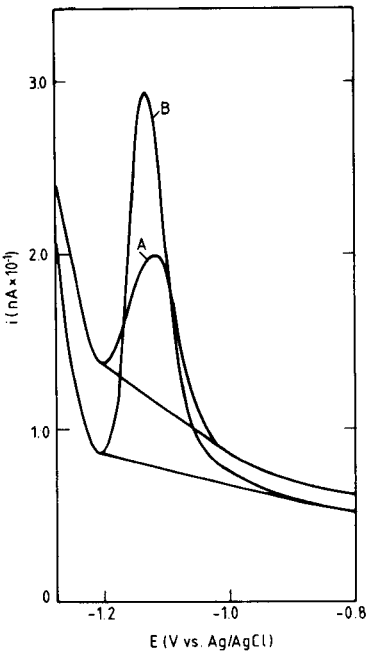

Fig. 2. Zinc in South Creek 2 water: (A) without medium exchange; (B) with medium exchange.

(each) as test solution, the ASV peak heights in the presence and absence of medium exchange were not significantly different (<5%).

Results obtained in the presence of various ligands are shown in Table 2. Medium exchange led to a considerable increase in ASV-labile metal in several cases, especially for the South Creek waters (Fig. 2). Medium exchange eliminated the depression of the cadmium peaks in both waters, and of the zinc peak in the South Creek 1 sample.

Retention of adsorbed film on mercury electrode during medium exchange

Although it was shown that the standard medium-exchange procedure ensured complete removal of the test solution, it is possible that an adsorbed film of surface-active ligand remains on the mercury drop after medium exchange. This possibility was tested by using a surface-active detergent, Triton X-100, and fulvic acid, which would not be expected to form a film as strongly adherent as Triton X-100. The presence of a film of Triton X-100 on the mercury drop was tested by using three separate ASV measurements: (a) SSW in acetate buffer with addition of 4×10^{-8} M Cu, Pb, Cd and Zn (each) and 1 mg l^{-1} Triton X-100, 5 min deposition; (b) test solution as for (a) but without Triton X-100, 5 min deposition; (c) test solution as for (a) in the cell but, with the deposition time set at 10 min, deposition was actually done for 5 min, then, without interrupting deposition, the cell solution was

TABLE 3

Carry-over of ligand film on mercury electrode during medium exchange[a]

Ligand	Conc. (mg l^{-1})	Peak current ratio[b], c/(a + b)			
		Zn	Cd	Pb	Cu
Triton X-100	1	0.71	0.82	0.81	0.99
Fulvic acid	5	0.87	0.90	0.85	1.00

[a]Synthetic soft water (SSW) with 0.03 M acetate buffer, pH 4.7, added. [b]Solution (a): SSW, acetate buffer pH 4.7/ligand/4 × 10^{-8} M Cu, Pb, Cd, Zn with 5 min electrodeposition, no medium exchange. Solution (b): as for (a) but without ligand. Solution (c): as for (a), but with 10 min electrodeposition; after 5 min deposition, medium exchange was done with the SSW/acetate buffer pH 4.7/4 × 10^{-8} M Cu, Pb, Cd, Zn mixture while electrodeposition was still proceeding.

replaced with solution (b) as indicated above for medium exchange and the deposition was continued for the remaining 5 min. It was necessary to stop the stirrer during the exchange to avoid loss of deposited metal. The stripping peak currents resulting from measurements (a), (b) and (c) were compared. If no film of Triton X-100 remained after medium exchange in (c), then current (c) = (a) + (b), but if a film was carried over, then (c) < (a) + (b) (Table 3). The same experiment was repeated except that 5 mg l^{-1} fulvic acid solution was used instead of Triton X-100; these results are also shown in Table 3.

Comparison of ASV-labile copper and the toxic fraction

The ASV-labile fractions of copper in the presence of 5 mg l^{-1} fulvic acid in SSW were (Table 2) 17% without medium exchange, and 28% with medium exchange. The toxic fraction of copper in SSW with 5 mg l^{-1} fulvic acid added was determined by algal assay based on the green alga *Chlorella pyrenoidosa* [17, 18] and was found to be 35 ± 5%.

DISCUSSION

It is evident from Table 2 that, for several metal/ligand combinations, considerably smaller depressions of the ASV metal peaks are measured when medium exchange is used. These results show that the stripping process often has an influence on ASV-labile metal, even though it is usually assumed that lability is controlled solely by the parameters of the deposition step [1]. Particularly large increases in labile metal were found when medium exchange was used for the combinations of copper/chloride, copper/humic acid and zinc/tannic acid, and for zinc, cadmium and lead in South Creek sample 1, and zinc and cadmium in South Creek sample 2 (Fig. 2). The increases in ASV-labile metal in the South Creek waters were greater than for any of the metal/ligand mixtures (Table 2), which suggests that the natural waters had a

dominant ligand which was different from any of those tested. In the case of the Cu/fulvic acid combination, medium exchange gave an ASV-labile copper result which was much closer to the algal toxic fraction.

A possible complication in the medium-exchange technique is retention of a film of the ligand on the mercury drop after medium exchange, so that the kinetics of the metal oxidation (stripping) are affected by this film. The experiment conducted to detect the presence of a carry-over film showed that a film may persist in the case of Triton X-100, but not for fulvic acid (Table 3). Triton X-100 and fulvic acid exert their effects mainly on zinc and copper, respectively. Table 3 shows that there is no residual effect on copper by fulvic acid, but that the zinc peak is depressed by Triton X-100. These results provide no information as to whether or not a carry-over film affects the stripping process, although it is evident from Table 3 that such an effect would not be very large.

This study shows that for ASV-labile metal determinations, medium exchange should be routinely used. It is especially important for correlation studies between the ASV-labile and toxic fractions, where the electrodeposition process is used to model facilitated diffusion of a metal ion through a biomembrane [1]. A marked effect on labile metal by the stripping process would destroy the model. Medium exchange is simple to use, and adds little time to the analysis.

The authors are grateful to Dr G. E. Batley for constructing the medium-exchange cell and for helpful discussions.

REFERENCES

1 T. M. Florence, Analyst, 111 (1986) 489.
2 T. M. Florence, B. G. Lumsden and J. J. Fardy, Anal. Chim. Acta, 151 (1983) 281.
3 D. R. Turner and M. Whitfield, J. Electroanal. Chem., 103 (1979) 43.
4 W. Davison, J. Electroanal. Chem., 87 (1978) 395.
5 D. L. Olson and M. S. Shuman, Geochim. Cosmochim. Acta, 49 (1985) 1371.
6 K. J. Mann and T. M. Florence, Sci. Total Environ., 60 (1987) 67.
7 J. Buffle, J. Electroanal. Chem., 125 (1981) 273.
8 A. Nelson and R. F. Mantoura, J. Electroanal. Chem., 164 (1984) 237.
9 A. Nelson, Anal. Chim. Acta, 169 (1985) 273.
10 T. M. Florence and G. E. Batley, J. Electroanal. Chem., 75 (1977) 791.
11 G. E. Batley, Anal. Chim. Acta, 197 (1987) 327.
12 M. Reignier and C. Buess-Herman, Fresenius' Z. Anal. Chem., 317 (1984) 259.
13 M. Ariel, U. Eisner and S. Gottesfeld, J. Electroanal. Chem., 7 (1964) 307.
14 E. Desimoni, F. Palmisano and L. Sabbitini, Anal. Chem., 52 (1980) 1889.
15 J. E. Gregor and H. K. Powell, J. Soil Sci., 37 (1986) 577.
16 T. M. Florence, Anal. Chim. Acta, 141 (1982) 73.
17 J. L. Stauber and T. M. Florence, Mar. Biol., 94 (1987) 511.
18 Zhang Manping and T. M. Florence, Anal. Chim. Acta, 197 (1987) 136.

Analytica Chimica Acta, 200 (1987) 313—318
Elsevier Science Publishers B.V., Amsterdam — Printed in The Netherlands

DEOXYGENATION OF SUPPORTING ELECTROLYTES IN STRIPPING VOLTAMMETRY BY GLUCOSE AND CO-IMMOBILIZED GLUCOSE OXIDASE AND CATALASE IN A FLOW SYSTEM

LARS RISINGER, XIURONG YANG and GILLIS JOHANSSON*

Department of Analytical Chemistry, University of Lund, P.O. Box 124, S-221 00 Lund (Sweden)

(Received 5th May 1987)

SUMMARY

Carrier solutions for stripping voltammetry in flow systems are deoxygenated by reaction with glucose added to the carrier. The reaction was catalyzed by glucose oxidase and catalase co-immobilized in an enzyme reactor which was inserted before the injector. The oxygen was removed at least as efficiently as with nitrogen purging and the voltammetric behaviour of cadmium(II), lead(II) and zinc(II) was unaffected by the glucose/gluconic acid system. A particular advantage is the rapid start-up compared to the lengthy purging of carrier solution when nitrogen degassing is used. The enzyme reactor made from porous glass was effective for several months.

Dissolved oxygen interferes with most polarographic methods and it has therefore to be removed before any measurements can be made. This is normally done by purging the solutions with nitrogen or another inert gas. The lengthy, inconvenient nitrogen purging decreases the overall capacity of voltammetric methods.

Several alternatives have been described, particularly with applications in flow methods in mind. Trojanek and Holub [1] described the removal of oxygen by permeation through the walls of a silicone tubing into a surrounding nitrogen flow. Oxygen can be removed electrolytically [2], but hydrogen peroxide, which is formed in the reaction, will interfere seriously in many cases and it was recommended that the flowing solutions should be purged by inert gas to reduce the current and thus the peroxide interference. A more detailed discussion of these and other methods, including the classical sulphite reduction [3] has been given in a recent review [4].

In this paper, the use of an enzyme-catalyzed reaction to remove the dissolved oxygen is described. It is known from previous work in this laboratory [5, 6] that the oxidation of glucose by oxygen to gluconate and hydrogen peroxide works well even at very low concentrations of the reactants [5, 6]. The peroxide can be decomposed by co-immobilized catalase [7] so that the net reaction product becomes only gluconate.

0003-2670/87/$03.50

EXPERIMENTAL

Preparation of enzyme reactors

Glucose oxidase (E.C.1.1.3.4, Sigma Chemical Co.) and catalase (E.C.1.11.1.6, Boehringer Mannheim) were co-immobilized on two different supports. One support was glutaraldehyde-activated silica gel (Serva SP-500, pore size 40—80 nm, particle size 0.04—0.1 mm). Coupling, deactivation with glycine and reduction with sodium tetrahydroborate were done as recommended by the manufacturer. Glucose oxidase (26 mg) and catalase (2.5 mg) were mixed with 1 g of support and the coupling yield was 71%, as determined spectrophotometrically on the supernatant solution.

The enzymes were also immobilized on porous glass (CPG-10, pore size 50 nm, particle size 0.04—0.08 mm). Activation with n-propylaminosilane, glutaraldehyde and coupling was done as described earlier [5, 8]. The same amounts of enzymes were taken as above, which resulted in a coupling yield of 80%.

The immobilized enzymes were filled into thick-walled plexiglas tubes, i.d. 2.7 mm, to form enzyme reactors.

The voltammetric flow system

Voltammograms were recorded with a Princeton Applied Research potentiostat (model 174). The wall-jet glassy carbon mercury-film electrode was made as described earlier [9]. The flow-injection manifold (Fig. 1) consisted of two peristaltic pumps and a pneumatically operated valve (Cheminert, Kel-F, LDC/Milton Roy). The valve, the flow cell and the enzyme reactor were screwed together without connecting tubes.

The silica-bound enzyme reactor was found to leak zinc and a column of 8-quinolinol (250 μl) was therefore inserted between the enzyme reactor and the injector when zinc was determined. The immobilized chelating ion exchanger (Pierce Chemical Co.) removes most trace metals on-line, as described previously [9].

Hydrogen peroxide monitoring was done with a palladium/gold modified electrode [10] mounted in the flow-through cell instead of the mercury film

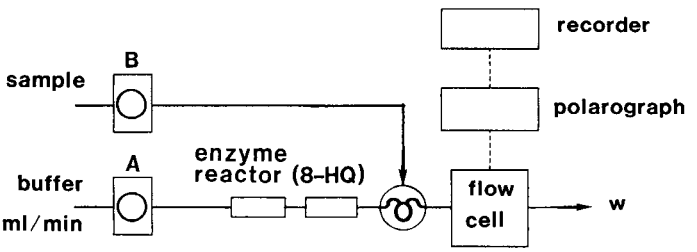

Fig. 1. Manifold for flow-injection determination of metal ions by differential-pulse anodic stripping voltammetry and deoxygenation by oxygen consumption in an enzyme reactor with co-immobilized glucose oxidase and catalase. The column with immobilized 8-quinolinol was only inserted when the enzymes were immobilized on a SP-500 support.

electrode. Oxygen was monitored with a Clark-type oxygen electrode (Beckman Monitor System 123303, with cell 39556) temporarily mounted in the same flow cell.

Comparisons were made with traditionally deoxygenated carrier solutions. Purified nitrogen, distributed with an all-stainless steel system, was bubbled through the carrier solution in a glass flask. The peristaltic pump was enclosed in a nitrogen-flushed housing and all external lines were protected by coaxial tubes flushed with nitrogen [9].

The carrier solution was 0.1 M sodium acetate/0.15 M sodium chloride, pH 6.0, containing 2.5 mM glucose unless otherwise specified. The buffer capacity of the carrier should be sufficient to level out the pH effect of the gluconic acid produced in the enzyme reactor. Standard solutions were prepared from the metal nitrate salts and the solutions were acidified with nitric acid (Suprapur). The sample volume was 1.0 ml unless otherwise stated.

RESULTS AND DISCUSSION

Enzyme reactors with co-immobilized glucose oxidase and catalase were mounted in the flow system of Fig. 1 and an amperometric oxygen sensor was inserted into the flow cell. A carrier solution which had not been purged from dissolved oxygen was pumped through the system continuously. Table 1 shows the oxygen electrode readings for eight different enzyme reactors, each tested with different glucose concentrations in the carrier solution. The reaction scheme

$$\beta\text{-D-glucose} + O_2 + H_2O \xrightarrow{\text{oxidase}} \text{gluconate} + H_2O_2 + H^+ \quad (1)$$

$$H_2O_2 \xrightarrow{\text{catalase}} 1/2\,O_2 + H_2O \quad (2)$$

TABLE 1

Concentration of dissolved oxygen (mg l^{-1}) at the outlet of enzyme reactors made with two different supports and with different volumes.
[Determination with a Clark oxygen electrode; the carrier solution consisted of 0.1 M sodium acetate, pH 6.0, with dissolved oxygen (about 8 mg l^{-1} as determined each day) and glucose as specified, at a flow rate of 1 ml min^{-1}]

Glucose concentration (mM)	SP-500 support volume (μl)			CPG-10 support volume (μl)				
	15	50	120	15	50	120	210	300
0.25	5.8	5.1	5.1	7.1	6.2	6.0	6.0	5.9
0.50	4.1	2.2	2.3	5.6	3.9	3.6	3.4	3.4
0.75	2.1	0	0	4.2	1.7	1.1	0.8	0.8
1.00	0.6	0	0	2.9	0	0	0	0
2.5	0.2	0	0	0.15	0	0	0	0
5.0	0.15	0	0	0.10	0	0	0	0
10.0	0.10	0	0	0.05	0	0	0	0

implies that two molecules of β-D-glucose will be required for each oxygen ultimately, after an infinite number of recyclings between Eqns. 1 and 2. Only the β-anomer, which constitutes 63.5% of the total glucose, will be enzymatically active. The glucose concentration should therefore be at least 3.2 times the oxygen concentration for an oxygen removal system, i.e., around 0.8 mM. The results confirm that about 1 mM glucose is necessary to reduce the oxygen meter reading to zero, provided that the enzyme reactors are sufficiently large.

It was not possible to remove oxygen completely with 15-μl reactors but the differences were small when the reactor volume was increased above 50 μl. The conditions selected for the following measurements were 120-μl reactors and a glucose concentration of 2.5 mM.

Enzyme immobilization is more convenient with the SP-500 support and the specific enzyme activity seems to be somewhat higher. This is partly offset by the shorter lifetime of SP-500-bound enzymes and by the leakage of metal ions. The lifetimes of the SP-500 reactors were only 2—3 weeks in contrast to the CPG-10 reactors which were so stable that no decrease in activity could be observed during this study. The good stability of the CPG-10 glucose oxidase/catalase reactors is in line with previous observations [7]. The effective lifetime is also a function of the specific activity and the reactor size as discussed earlier [11].

A separate test was made to ascertain that the catalase activity in the reactor was sufficient to remove all hydrogen peroxide. An amperometric peroxide electrode [10] was mounted in the cell and samples containing 2 mM hydrogen peroxide was injected. No hydrogen peroxide (<0.5 μM) was detected in the effluent. Injections of 4 mM hydrogen peroxide produced oxygen bubbles but no hydrogen peroxide response. The experiment thus demonstrates that the activity of the catalase is in excess over glucose oxidase, as it should be in a well-designed system. The pH-optimum for the enzymatic reaction was pH 6.0 with a fairly flat response from pH 5.5 to 6.5.

There was a more or less constant leakage of zinc(II) from the SP-500 support; it amounted to 4×10^{-8} M at a flow rate of 0.2 ml min^{-1}. The metal ions could be removed on-line with a column (250 μl) of 8-quinolinol immobilized on porous glass. The purification from metal ions was very effective and well suited for trace metal determinations as shown below. There was no leakage of zinc(II) or any other metal ions from the CPG-support, except during the first few hours after the preparation [12]. This material is therefore to be preferred in the present application, from the viewpoints of both lifetime and lack of contamination.

The voltammetric experiments were conducted with either the described deoxygenation system or traditional nitrogen purging (with no glucose in the carrier solution). Background curves recorded from −0.2 to −1.9 V vs. SCE, with DC polarography, showed almost identical background currents for the two methods. The backgrounds with differential-pulse polarography were equal at low potentials but increased more quickly with the nitrogen purging,

e.g., 83 nA with nitrogen purging and 40 nA with the enzyme reactor, measured at −1.6 V.

Calibration curves were prepared for the differential-pulse anodic stripping voltammetry (ASV) of Cd(II), Pb(II) and Zn(II), with the enzymatic method of oxygen removal (Fig. 2). The slopes will vary slightly with the way in which the flow cell is assembled and the differences between the series, which were prepared on different occasions, should therefore not be given too much significance. The conclusion to be drawn from these curves and from the fact that the detection limits (for 1.5-ml samples) became 0.1, 1 and 0.3 $\mu g\ l^{-1}$ for Cd(II), Pb(II) and Zn(II), respectively, is that the voltammetric behaviour is independent of the mode of deoxygenation.

Weak metal ion complexes have been reported to be formed with gluconate and with some sugars [13, 14]. No differences in peak positions for Cd(II), Pb(II) or Zn(II) could be observed polarographically under the present conditions, however, which indicates that the interactions are very weak indeed. The fact that glucose emerges close to the front in ligand-exchange chromatography of sugars on, for example, lead-saturated ion-exchangers points in the same direction, and indicates that glucose is to be preferred over many other sugars.

Conclusions

An enzyme reactor with co-immobilized glucose oxidase/catalase in a flow system can be used to remove dissolved oxygen from carrier solutions, provided that glucose is present in the solution. The start-up of the experiment

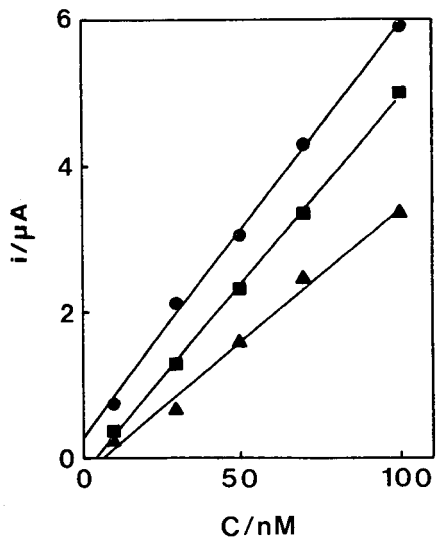

Fig. 2. Differential-pulse ASV calibration curves for Cd(II) (●), Pb(II) (■), and Zn(II) (▲) with the manifold shown in Fig. 1. Sample volumes, 1.0 ml.

is fast and the removal of oxygen seems to be at least as efficient as with nitrogen purging. The background current of the buffered carrier and the voltammetric properties of the metal ions seem to be unaffected by the presence of glucose and gluconate.

The samples were not deoxygenated but this is not necessary with differential-pulse ASV in a flow system because the oxygen-containing sample solution is dispelled from the cell prior to the stripping. Sample solutions should not be passed through the enzyme reactor because metal ions may be taken up and the enzyme may be inhibited. There will also be severe adsorption of metal ions on the support material. The method is therefore mainly suited for stripping analysis unless the samples are deoxygenated prior to injection.

The authors thank Dr. L. Gorton for gifts of palladium/gold sputtered peroxide electrodes. This work was supported by grants from the Swedish Natural Research Council.

REFERENCES

1 A. Trojanek and K. Holub, Anal. Chim. Acta, 121 (1980) 23.
2 H. B. Hanekamp, W. H. Voogt, P. Bos and R. W. Frei, Anal. Chim. Acta, 118 (1980) 81.
3 J. Heyrovsky and P. Zuman, Practical Polarography, Academic, London, 1968.
4 G. G. Wallace, Trends Anal. Chem., 4 (1985) 145.
5 L. Gorton and L. Ögren, Anal. Chim. Acta, 130 (1981) 45.
6 B. Olsson, L. Ögren and G. Johansson, Anal. Chim. Acta, 145 (1983) 101.
7 B. Olsson, B. Stålbom and G. Johansson, Anal. Chim. Acta, 179 (1986) 203.
8 H. H. Weetall and L. S. Hersch, Biochem. Biophys. Acta, 185 (1969) 464.
9 X. Yang, L. Risinger and G. Johansson, Anal. Chim. Acta, 192 (1987) 1.
10 L. Gorton, Anal. Chim. Acta, 178 (1985) 247.
11 G. Johansson, L. Ögren and B. Olsson, Anal. Chim. Acta, 145 (1983) 71.
12 L. Risinger, L. Ögren and G. Johansson, Anal. Chim. Acta, 154 (1983) 251.
13 M. Vicedomini, J. Coord. Chem., 12 (1983) 307.
14 S. J. Angyal, Pure Appl. Chem., 35 (1973) 131.

Analytica Chimica Acta, 200 (1987) 319—332
Elsevier Science Publishers B.V., Amsterdam — Printed in The Netherlands

THE LANGMUIR-BLODGETT MONOLAYER DIPOLE POTENTIAL: A SMEARED DIPOLE MODEL FOR A LIPID ARRAY, AND PULSING OF THE POTENTIAL BY DIRECT SUBPHASE INFUSION OF IMMUNOCHEMICAL AND LECTIN/POLYSACCHARIDE COMPLEXES

MICHAEL THOMPSON*, H. E. WONG and A. WALTER DORN

Department of Chemistry, University of Toronto, 80 St. George Street, Toronto, Ontario, M5S 1A1 (Canada)

(Received 22nd May 1987)

SUMMARY

An important contribution to the surface potential of lipid bilayers and monolayers comes from the intrinsic dipole moment of the lipid molecules. A theoretical model of the monolayer which involves a smeared dipole sheet approximation is introduced. This model is used to explore the nature and origins of the surface potential. In addition, the potential associated with phosphatidyl choline/cholesterol monolayers compressed on a Langmuir-Blodgett trough was measured with a non-contacting electrostatic voltmeter. A trough infusion configuration was fabricated to perform dynamic subphase experiments with compressed films in place. The potential/time response of monolayers to selective bimolecular systems such as antibody-antigen and concanavalin A-saccharide pairs was examined. These reactions induce spontaneous transients in dipole potential of magnitude 20—80 mV and duration of less than 1 s. The potential transients are attributed to local perturbation of lipid orientation and introduction of protein dipole fields caused by the formation of aggregates at the monolayer/water interface.

The structure of the bilayer lipid membrane (BLM) provides the foundation for an electrochemical sensing technique based on chemoreceptive control of transmembrane ion current [1—4]. Signal generation is intimately associated with perturbation of membrane properties such as fluidity and lipid molecular packing (the so-called steric factor) and electrostatics, by a selective bimolecular interaction between a stimulant (analyte) and membrane-imbedded receptor moiety [5]. An important element here is the magnitude of the transmembrane dipolar potential which originates from the anisotropic

*Michael Thompson received his B.Sc. (Chemistry) degree from the University College of Swansea, Wales, in 1966 and his Ph.D. degree in analytical chemistry from McMaster University, Hamilton, Canada in 1970. After working on ultraviolet photoelectron spectroscopy at the University College of Swansea, he became a lecturer at Loughborough University of Technology, where his research interests were in the field of ultraviolet and x-ray photoelectron spectroscopy and Auger spectroscopy. In 1976, he moved to the University of Toronto where he is now Professor of Analytical Chemistry. In recent years, his interests have been in electron spectroscopy, chemical and biosensor technology, lipid bilayer and Langmuir-Blodgett monolayer physical chemistry, and archaeological chemistry.

0003-2670/87/$03.50

alignment of polar lipid headgroups and unstirred water structure at each membrane/aqueous solution interface. Perturbation of this potential by lectin/polysaccharide complexation at the surface of BLM has been invoked to explain partially, transient changes in membrane conductance associated with this bimolecular interaction [6, 7].

Transient electrical phenomena are, of course, very well-established, if not completely understood, in the area of neurochemistry. However, interesting oscillations in electrical parameters have also been reported in a number of studies involving totally synthetic electrochemical cells [6—12]. Several years ago, del Castillo and coworkers [8, 9] observed changes in membrane conductance for BLM associated with antibody/antigen interaction and the term 'lipid membrane conductimetry' was coined to describe the technique. Recently, oscillations in electrical potential have been reported for measurements across membranes doped with trioleoylglyceride [10] and across oil layers of nitrobenzene containing picric acid [11]. In addition, the spontaneous pulsing of electrical potential observed across Langmuir-Blodgett (LB) films composed of dioleoyllecithin has been attributed to changes of permeability of Na^+ and K^+ caused by phase transitions in the film [12].

Langmuir-Blodgett film technology [13], which has undergone something of a renaissance in recent years, provides both a method for producing organized molecular assemblies on substrate surfaces by the dipping strategy and an analytical technique for the study of monolayer intermolecular association and dipolar potential [14, 15]. The relevance of such studies to the development of the BLM sensor has the premise that a monolayer represents half of the bilayer configuration and, therefore, LB film properties can be correlated with the physical chemistry of the bilayer. In the present paper, the electrostatic potential generated by a monolayer array of dipoles is discussed and the feasibility of direct subphase infusion for in situ study of compressed Langmuir-Blodgett films is demonstrated. With respect to the latter, monolayer area and dipole potential were monitored for the subphase injection of antigen/antibody and concanavalin A/polysaccharide pairs.

EXPERIMENTAL

Reagents

Lyophilized egg phosphatidyl choline was obtained from Avanti Polar Lipids (Birmingham, AL). Concanavalin A, dextran, glycogen, lyophilized salt-free rabbit immunoglobulin (IgG), lyophilized whole serum, whole molecule goat anti-rabbit IgG and human IgG were all obtained from Sigma Chemical Company. FAB fragment-specific antisera, goat anti-human IgG was provided by ICN Biochemicals (Cleveland, OH).

Equipment

The Langmuir-Blodgett apparatus consisted of a commercial Lauda film balance model 1974 (Sybron-Brinkmann, Toronto, Ontario) in which the

subphase volume was reduced from 1 l to 0.5 l by partitioning the trough with teflon barriers at points outside the surface enclosed by the two barriers. The water volume was further reduced to 350 ml by enclosing the well with a thin sheet of teflon. The arrangement for the infusion of various reagents underneath the surface of a monolayer at the air/water interface is shown in Fig. 1 [16]. The assembly consists of an external circulating pump which withdraws the subphase from the trough by means of a perforated tube and returns it to the water volume by a second similar tube. The pipes are mounted into the teflon surface with pressure-sensitive tape. Samples can be injected by syringe directly into the flowing stream through a Luer-lock connection in the flow line.

Surface potential measurements were made with an electrostatic millivoltmeter (Isoprobe 162, Monroe Electronics, Lyndonville, NY.) with a non-contacting electrode (Model 1015A type probe, Monroe Electronics). The probe is based on a field-chopping technique with a fixed sensitive electrode and a small specially designed tuning fork with tines which open and close an aperture, alternately exposing and shielding the electrode from the electrostatic field associated with the surface under measurement. The 1.6-mm diameter aperture is located at the bottom of the probe and makes possible non-contacting surface potential measurements on spots as small as 2.3 mm in diameter. The probe is purged with filtered ambient air. Probe purging improves the instrument performance with regard to zero stability, noise and height sensitivity. The purge kit (Monroe Electronics) maintains an even air flow, reduces temperature variations and filters dust and other particles. The gas-purged probe is equipped with fittings to permit a flow of clean air to be propelled through the probe housing and exhausted through the sensing aperture. The kit is complete with an air pump, filter/flow equalizer, and tygon tubing. No effects of the gas flow on potential measurements were observed at any time during the experiments.

The gas-purged probe is mounted directly onto the guide rails of a modified micromanipulator designed to position the electrode in proximity to the aqueous surface in a monolayer film trough [17].

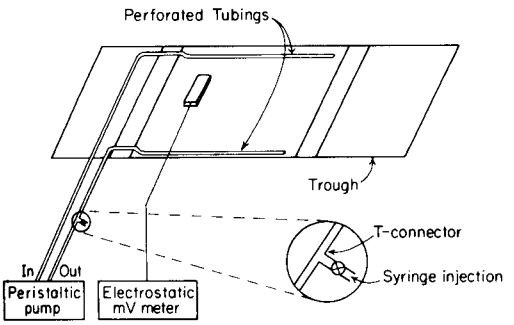

Fig. 1. Schematic representation of trough assembly for subphase circulation and infusion of reagents underneath a monolayer film. Surface potentials are measured by a non-contacting electrostatic voltmeter.

Procedures

The adjustment to provide insensitivity to the surface-to-electrostatic probe spacing was done with the micromanipulator device and grounded plate. The electrode was calibrated against an electrically grounded metal foil which provided a zero potential reference. A zero adjustment was done for a spacing range of 1—2 mm. After the initial adjustment to ensure height insensitivity in the electrostatic potential measurement, the non-contacting electrostatic probe electrode was positioned over the surface area available for lipid monolayer formation. The non-contacting electrode was lowered to a position 1—2 mm above the air/water interface. The electrostatic potential of the aqueous subphase is typically in excess of —600 mV. An adjustment was made to give the clean surface a zero reading.

To form monolayers, 0.1 ml of a solution of phosphatidyl choline (2 mg) and cholesterol (2 mg) dissolved in 5 ml of n-hexane was spread slowly into a subphase of 0.1 M KCl. After about 10 min, the film was compressed to a constant pressure of 0.032 N m^{-1}. The pump was then turned on and the electrostatic potential and surface area were monitored for introduction of various reagents into the subphase. For work with the lectin system, the final concentrations of species in the subphase were 10^{-7}—10^{-9} M concanavalin A, 10^{-4} M Mn^{2+} and Ca^{2+} and 10^{-5}—10^{-6} M dextran and glycogen. Analogously, the concentrations for the immunochemical systems were 0.7 mg l^{-1} for rabbit IgG, 4.0 mg l^{-1} for human IgG, 6.0 mg l^{-1} for human antisera and 1:2000 dilution for the rabbit antisera.

The response time for the overall configuration used for surface potential measurement was acquired by directing the output from the probe electrode through an analog-to-digital converter to a microcomputer. Variable electrical fields were applied to a foil by a square-wave signal generator set to give frequencies in the range 0.1—10 Hz and amplitudes of 100—300 mV. The ability of the analog-to-digital converter and the electrode to distinguish the square-wave signal was determined via the microcomputer. The response time of the electrode was then monitored by a rapid-scan oscilloscope with its signal output adjusted to the fastest speed with minimum overshoot for a step response.

Finally, dual measurements of surface potential were made over different portions of a compressed film by the use of two independent probes separated by a distance of 7—8 cm.

RESULTS

Response time of electrostatic probe

The limitation of the overall configuration with respect to response time is governed by its ability to distinguish applied electrical fields with minimal loss in characteristics. The computer used could acquire data at a rate of 5 Hz. The probe can resolve square-wave characteristics at a rate of about 2 Hz and the analog-to-digital converter at about 1 Hz. Thus, transient changes of less than 0.2 s were not distinguished from background signals.

The immunochemical system

Typical measurements of potential and area at constant pressure for the single addition of rabbit IgG antibody (A) and antiserum (B) to the subphase are depicted in Fig. 2. The presence of free antibody did not influence the lipid dipolar potential or the integrity of the monolayer film. Significant physical disruption of the phosphatidyl choline/cholesterol film was observed when only the antiserum was present. The film collapsed 8—10 min after the addition of the antiserum. Evidently, proteins present in the antiserum cause solubilization of the monolayer species into the subphase by protein/lipid interaction. A slight increase in the dipolar potential is observed as the film is compressed to compensate for the loss of lipid from the air/water interface. Similar results were obtained for the analogous human proteins (not shown).

A representative time/response profile for the addition of the rabbit antibody/antiserum pair is shown in Fig. 3A. Transient changes in potential occurred after an induction period of several minutes following the infusion of the antibody and antiserum solutions. There was no apparent correlation between the frequency of the transients and the time required for complete addition of the reagents. The following specific trends could be discerned from a number of experiments: (1) the transient signal occurs over about 1 s; (2) the frequency of the peak is not periodic and ranges from one to twenty events per minute; and (3) the magnitude of the potential changes associated with the transients is in the range 20—80 mV (95% of all experiments).

Similar results were obtained for the human antibody/antiserum pair (Fig. 3B).

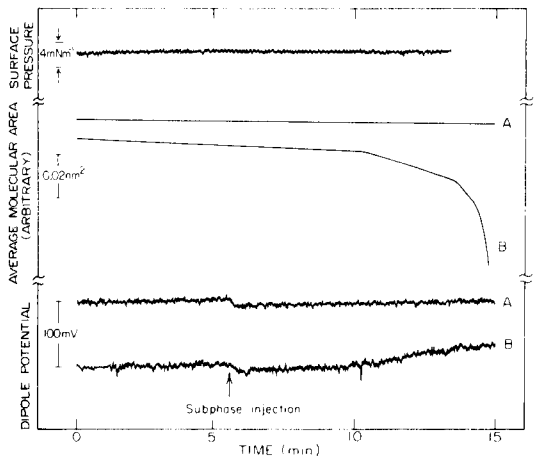

Fig. 2. Monolayer and potential/time profiles representative of: (A) rabbit IgG antibody; (B) rabbit IgG antiserum action on phosphatidyl choline/cholesterol monolayers under identical experimental conditions. The final concentration of rabbit IgG antibody introduced into a 0.1 M KCl subphase was 0.7 mg l^{-1}. The analogous rabbit IgG antiserum concentration was a 1:2000 dilution of a standard preparation in 0.1 M KCl. Time zero was the point at which the monolayer was compressed to a surface pressure of 0.032 N m^{-1}.

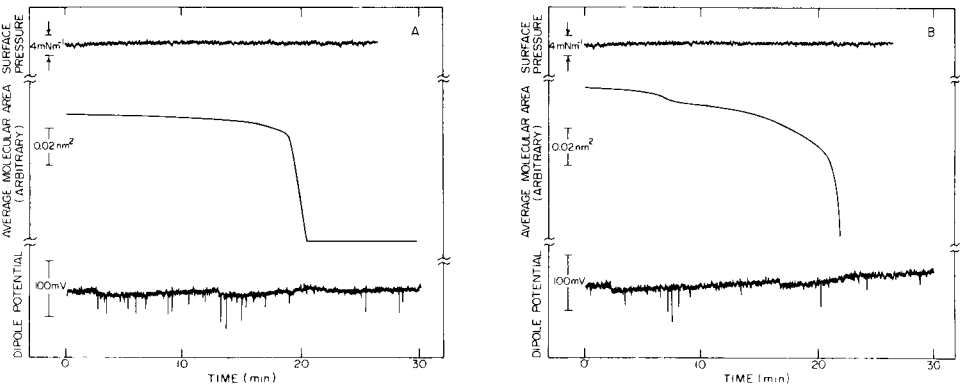

Fig. 3. Monolayer and potential/time profiles representative of the action of rabbit IgG antibody/antiserum (A) and human IgG antibody/antiserum (B) on phosphatidyl choline/cholesterol monolayers. For A, the final concentrations of reagents added were as in Fig. 2. For B, the final concentration of human IgG antibody and antiserum introduced into a 0.1 M KCl subphase were 4.0 mg l^{-1} and 6.0 mg l^{-1}, respectively. In both cases, the surface pressure was 0.032 N m^{-1}.

The concanavalin A/polysaccharide system

The introduction of the activating ions (Mn^{2+} and Ca^{2+}) alone did not perturb the potential or the physical properties of the lipid film. Gradual film loss from the air/water interface occurred with the individual infusion of concanavalin A, dextran or glycogen. This loss, which is reflected in area changes as with the antisera mentioned above, resulted in only minor alterations in potential which were likely to be caused by surface-pressure compensation in the film. Oscillations in potential similar to those described above were observed for the concanavalin A/polysaccharide system (Fig. 4). Considerable variation in the number of transients was often observed, however.

DISCUSSION

Theoretical aspects

In view of the results described above, it is necessary to examine the origin of the monolayer dipole potential associated with an array of zwitterionic headgroups from a closely packed assembly of phosphatidyl choline molecules. (The cholesterol used in the experiments acts as a modifier of this potential [18]). An examination of the literature indicated that, until recently, the dipolar nature of the monolayer or bilayer headgroup zone has received relatively little attention. During 1965—1985, according to a CAS Online Keyword Search, only about one hundred papers among >100 000 articles on membranes have mentioned this parameter. However, more recently, several studies have involved the effects of the dipole potential, on a qualitative basis, to explain membrane phenomena [19]. Accordingly, in the present work, new expressions are developed for the intrinsic mono-

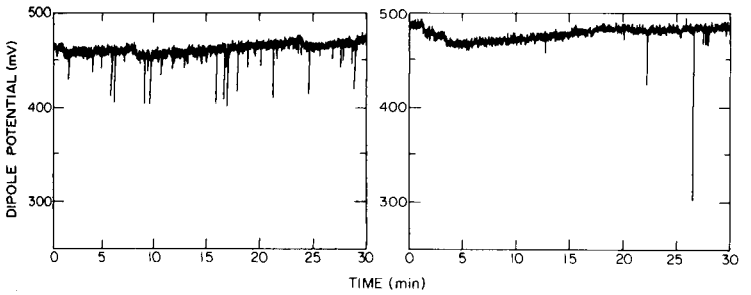

Fig. 4. Representative potential/time profiles for concanavalin A/polysaccharide action on phosphatidyl choline/cholesterol monolayers. Final reagent concentrations added were 10^{-4} M each of Mn^{2+} and Ca^{2+}, 10^{-8} M concanavalin A and 4×10^{-6} M dextran. The pressure was 0.032 N m^{-1}. Note the variation in frequency of the transient signals.

layer potential generated by a closely packed array of dipoles. The results can be compared with the previous work of Friedenberg et al. [20, 21] who assumed an array in which all the dipoles are directed towards a field point. The results are then discussed concisely in terms of the potential associated with the phosphatidyl choline headgroup.

The surface potential, ΔV, of a monolayer is defined as the change in the measured surface potential after the water surface has been covered with a monolayer of lipid. The gross assumption that the dipole layer behaves as a simple capacitor sitting in a dielectric medium of uniform permittivity, ϵ, leads to the Helmholtz equation [22]:

$$\Delta V = p/\epsilon A \tag{1}$$

where p is the dipole moment, and A is the area occupied by the lipid molecule. This derivation will only hold for a smeared dipole layer which extends to infinity in the plane of the layer. Furthermore, all the dipoles are assumed to be pointing vertically. In order to evaluate the effect of these assumptions, a more rigorous approach using a smeared dipole sheet model will now be considered.

To begin with, consider a dipole placed on the Z-axis of the coordinate system shown in Fig. 5, with its center at the origin. The potential, V, at a point P (r, ϕ, θ) in space can be obtained by adding the potentials produced by the two point charges [23]:

$$V = (qs \cos\theta / 4\pi\epsilon r^2)[1 + (s^2/8r^2)(5\cos^2\theta - 3) + \cdots\cdots] \tag{2}$$

where q is the charge and s is the dipole length. The potential is independent of ϕ, as one would expect from the symmetry around the Z-axis. The first term of the potential varies as the inverse square of r, while the second term involves the inverse fourth power of r. Thus, the first term represents the potential of an ideal point dipole (small ratio s/r). Such a parameter is the starting point for calculations involving dipole arrays.

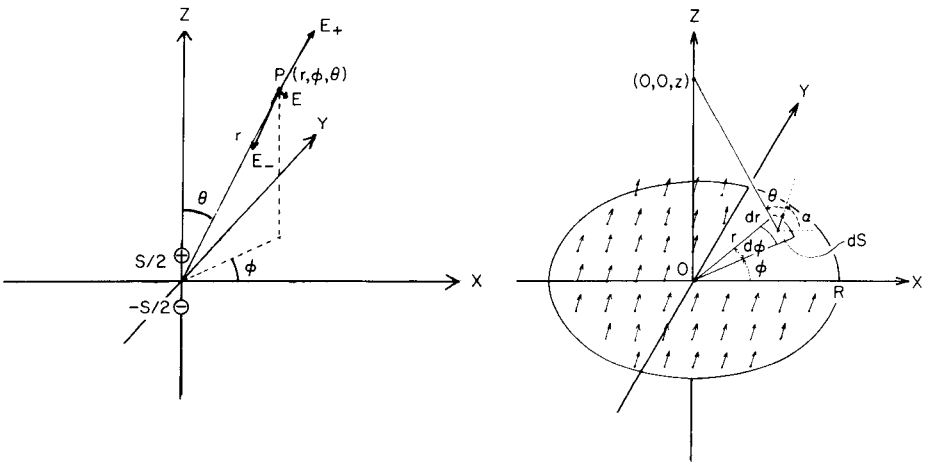

Fig. 5. The electric dipole with coordinates of the field point (P), electric field vectors ($\mathbf{E}_+$ and $\mathbf{E}_-$), and the net dipole field vector ($\mathbf{E}$).

Fig. 6. The smeared dipole disc of radius R with field point (0, 0, z). All dipoles make an angle, α, to the plane of the sheet (X—Y plane). Shown is the disc segment and coordinate system used for integration.

The potential at a point above a disc dipole region, S, in the X—Y plane is now described [23]. Each dipole makes an angle, α, with the X—Y plane as shown in Fig. 6. Assuming that the dipoles are "smeared out" over the region to be considered, the effective dipole moment per unit surface area is equal to that of the single dipole (p/A). The contribution of a differential element, dS, to the potential is

$$dV = [p \cos\theta / 4\pi A\epsilon(r^2 + z^2)]\, dS \tag{3}$$

An expression for $\cos\theta$ can be obtained by taking the product of two normalized direction vectors, that of the dipole vector and that of the vector joining the point dipole to the field point. The potential is measured at some point along the z axis (0, 0, z) so that

$$\cos\theta = (-x \cos\alpha + z \sin\alpha)/(x^2 + y^2 + z^2)^{1/2} \tag{4}$$

The total potential is obtained by integrating the potential, dV, over the region S. A disc region of radius R centered at the origin is chosen (Fig. 6). Converting to cylindrical polar coordinates (r, ϕ, z) and using the proper limits, the integral becomes

$$V = (p/4\pi\epsilon A) \int_0^R \int_0^{2\pi} [(-r \cos\phi \cos\alpha + z \sin\alpha)/(r^2 + z^2)^{3/2}]\, r\, dr\, d\phi \tag{5}$$

Integrating:

$$V = (p \sin\alpha / 2\epsilon A)[1 - z/(R^2 + z^2)^{1/2}] \tag{6}$$

TABLE 1

Electric potential, V, and the z-component of the electric field, E_z, for the single dipole and the sheet of smeared dipoles

Dipole	At angle α to horizontal	Pointed towards field point [20]
Single-dipole potential	$p \sin \alpha / 4\pi\epsilon z^2$	$p/4\pi\epsilon z^2$
Single-dipole field	$(2/4\pi\epsilon)p \sin \alpha / z^3$	$(2/4\pi\epsilon)p/z^3$
Smeared sheet of dipoles, potential	$(p \sin \alpha / 2\epsilon A)[1 - z/(R^2 + z^2)^{1/2}]$	$(p/4\epsilon A) \ln [(R^2/z^2) + 1]$
Smeared sheet of dipoles, field	$(p \sin \alpha / 2\epsilon A)[R^2/(R^2 + z^2)^{3/2}]$	$(p/2\epsilon A)[(1/z) - (z/(z^2 + R^2))]$

In the limit of $R/z \rightarrow \infty$ (infinite sheet), for a vertical set of dipoles, the potential reduces to $p/2\epsilon A$, which constitutes the Helmholtz expression for the potential difference between the two sides of the monolayer. In the limit of $R/z \rightarrow 0$ (small dipole region) the potential falls to zero, as one would expect. Finally, a summary of expressions for a single dipole, a smeared sheet and corresponding electrical fields (differentiation of V over z) are given in Table 1.

The potential generated by a monolayer of phosphatidyl choline molecules is now considered. Aside from the measurement dimensions (R and z), Eqn. 6 demands knowledge of the permittivity of the dielectric, the dipole moment, average area occupied by the lipid molecule and orientation of the headgroup, and associated dipole, with respect to the layer plane. Between the pH values of 4 and 9, phosphatidyl choline is known to be a neutral phospholipid. The dipole moment of the lipid can be estimated from the conformation found in crystals [24, 25]. An intramolecular P—N distance of about 0.4 nm is evident from crystal data on various derivatives of phosphatidyl choline. As a first approximation to the molecular dipole, the dipole moment is this distance multiplied by the electronic charge, yielding a value of 6.67×10^{-29} C m (20 D). As a check for this value, ab initio calculations were done [23] by using the program MONSTERGAUSS [26] which incorporates the integral, self-consistent field and gradient routines from Gaussian 80/82 [27]. A value of 17 D was found.

In crystals, the headgroups of lipids were found to be inclined at small angles to the planes of the layer [25]. With respect to the orientation of headgroups of monolayers and bilayers in contact with water, the picture is much less clear. Most studies have concluded that the orientation is parallel to the plane of a bilayer [28—30], while fewer have argued for a perpendicular arrangement [31—33]. Our study with CPK models revealed a very wide range of possible motion for the headgroup. The effect of this is to raise an obvious uncertainty as to the precise value of α to be used in Eqn. 6 for

compressed monolayers. However, this freedom of movement raises the distinct possibility of dipole reorientation caused by "external" processes. Indeed, it has been argued previously that such an effect will play an important role in controlling ion transport through bilayer membranes [2].

A value for the average area occupied by a lipid molecule can be obtained directly from the Langmuir-Blodgett experiment (in this case about 0.5 nm^2). Finally, because the potential experienced at a point in space is inversely proportional to the dielectric constant at that point in space [34, 35], the permittivity of free space (more rigorously, of air) must be used for the experimental measurement described in the present work. Accordingly, it becomes possible to use Eqn. 6 to predict values for the potential.

For the case of $\alpha = 20^\circ$ (an average angle) to the monolayer plane and electrostatic probe dimensions of $R = 1.0$ mm and $z = 1.5$ mm;

$$V = \frac{6.67 \times 10^{-29}(\text{C m}) \times 0.342}{2 \times 8.854 \times 10^{-12}(\text{C}^2/\text{J m}) \times 0.5 \times 10^{-18}(\text{m}^2)} \times \left\{ 1 - \left[\frac{1.5 \times 10^{-3}}{[(1.0 \times 10^{-3})^2 + (1.5 \times 10^{-3})^2]^{1/2}} \right] \right\}$$

from which $V = 0.44$ V

Similarly, for $\alpha = 45^\circ$, $V = 0.91$ V and for $\alpha = 90^\circ$, $V = 1.28$ V.

In summary, it appears that the theory discussed here is reasonably consistent with the experimentally measured potential of 0.5 V for compressed monolayers of phosphatidyl choline. Moreover, it is obvious that the two key controlling parameters are the dipole density (p/A) and average dipole angle to the plane of the layer.

Transients in dipole potential

In order to attempt at least a qualitative explanation of the potential transients after the above discussion of the origin of the monolayer dipole potential, a brief review of the common chemistry of the immunochemical and lectin/saccharide systems is required. Concanavalin A is a globulin capable of binding saccharides containing α-D-glucopyranosyl, α-D-mannopyranosyl and β-D-fructofuranosyl residues at non-reducing chain ends [36]. The binding activity of the protein exists in the pH range 5—8, and the conformation required for saccharide complexation is induced by the sequestering of Mn^{2+} and Ca^{2+}. Each protein tetramer can bind four saccharide residues and apparently a hydrophobic "pocket" is present which can bind non-specifically to membrane surfaces. An important feature of lectin/saccharide chemistry is that the polymerization and precipitation of the complex through polysaccharide cross-linking has often been compared to immunoprecipitation. In the latter, bivalent antibodies and multivalent antigenic species are involved in the formation of precipitates.

It is clear that the transient response must be associated with the lectin/saccharide and antibody-antigen chemistry at the monolayer headgroup-

to-water interface. Support for this statement comes from evidence that concanavalin A adsorbs to both hydrophobic and hydrophilic polymerized monolayers [37] and to membranes [38]. However, it should be emphasized that simple adsorption of species at the monolayer surface does not usually result in the type of potential transient described in this paper [39]. Accordingly, the formation of monolayer-bound aggregates produced by extensive cross-linking must be involved. In this respect, it is important to note that the formation of complexes of antibody-antigen pairs on Langmuir-Blodgett films has been successfully used to generate ordered crystals of such aggregate structures [40]. Furthermore, preliminary experiments involving fluorescence labelled lipid and the specified bimolecular systems in the Langmuir-Blodgett fluorescence microscope [41] have unequivocally demonstrated the presence of cross-linked aggregates at the monolayer surface [42]. However, the cause-effect relationship between aggregate formation at the monolayer surface and transients in potential is by no means obvious. Two possible schemes can be described: (1) a complete cycle of rapid realignment and relaxation of lipid dipoles induced by lipid-protein interaction that may involve a contribution of aggregate dipoles to the overall dipole field at the interface; and (2) the lateral tracking of lipid domains of the lower dipolar field (associated with aggregates) through a process of thermal or mechanical convection such that the potential response is caused by the transit time of such structures past the sensing zone of the probe.

Any model associated with these processes must take account of the magnitude of the reduction in surface potential as well as the transient nature of the response. Dealing with the magnitude of the signal first, it can be seen from Eqn. 6 that an angular reorientation of lipid dipoles towards the horizontal (net reduction of perpendicular dipole moment per molecule) can indeed yield a reduction in potential. As was shown above, for a lipid dipole moment of 20 D and molecular area of 0.50 nm^2, a reorientation of 90° to 0° for all lipid molecules over an area of about 4×10^4 μm^2 is required to elicit a measured change of 40 mV. If only lipid dipoles are considered, it is clear that such a perturbation would require an aggregate of sufficient size to distort the monolayer headgroup zone. In addition to lipid reorientation, the dipole contribution from monolayer-adsorbed aggregates must be included because the complex will contain a high density of "molecular" dipoles. The additive component of the electrostatic field from the complex presumably acts in opposition to the existing lipid surface potential. Such a contribution could significantly diminish the necessary area to be affected by the aggregate and/or the average perpendicular dipole moment per unit area.

Turning to the transient nature of the response, the kinetics of nucleation and growth of an interfacial aggregate at the monolayer/water interface must be considered. As discussed previously [6], the process may involve a nucleation rate governed by a critical supersaturation of the reactants in solution, followed by rapid heterogeneous, two-dimensional growth. A rapid growth of an aggregate could result in the instigation of the potential response,

but it is far from clear what is responsible for the return of the potential value to the baseline level. Possibly the aggregate, at a critical size, desorbs from the monolayer surface resulting in removal of the associated dipole field together with relaxation of lipid molecular reorientation.

A second possibility to explain the occurrence of transients in the potential is the convection of domains of aggregate-associated lipid past the fixed probe site. The shape of the signal caused by such an effect would clearly be related to the size and convective rate of the lipid domain in transit. If the aggregate size is significantly smaller than the measurement area of the probe, the results of this work would suggest a convective rate approaching 1 mm s^{-1}. Previous work has indicated rates of approximately 50 μm s^{-1} [41]. This discrepancy, taken together with the earlier observations of aggregate-induced transients in potential and conductance, which were completely motion- and site-independent, casts doubt on the concept of a convective mechanism [6—12].

An alternative concept to areas of reoriented lipid is the possibility of complex-induced "hole" formation between lipid domains. Dipole alteration through this mechanism would be equivalent to the lateral diffusion of vacancies between the lipid domains in the film structure. If such structures did exist, the corresponding average molecular area away from the hole region must be reduced to compensate for the increased local number density of dipoles. Calculation indicates that an area reduction of 10 to 20% must occur to be commensurate with the observed potential change. In a highly compressed film such as used in this work, such an explanation is extremely unlikely.

The results discussed above raise questions as to whether the monolayer areas affected by the polysaccharide or antibody-antigen complexes extend significantly beyond the probe measurement zone (about 1 mm^2) and whether propagation of an event occurs through the surface originating from a point elsewhere in the monolayer film. An attempt to establish the nature of the potential response was made by dual electrostatic potential measurements with the electrodes positioned at various locations over the lipid monolayer surface. The electrode probes were separated by 5—7 cm. The surface-potential/time profiles should provide an indication of the source of the perturbation. Identical potential response would imply surface perturbation extending at least over the entire monolayer film between the two electrodes.

Identical surface-potential/time profiles temporally displaced would be consistent with the propagation of signals over the distance of the separation. The similarity of response would then be limited by the range of the signal propagation. The lack of such an observation would not discount this possibility because the propagation of signals can be attenuated in the range of the probe separation. This additional consideration can give rise to a potentially complicated response of multiple propagating signals. Each probe can detect a temporally displaced and attenuated signal originating

from a position directly beneath the second electrode. The time dependence of the surface potential will appear to be random and will be difficult to assess.

Careful examination of dual potential/time profiles of the monolayer response to antibody-antigen addition revealed no obvious relationship between transients. Concurrent signals did not occur, indicating that the action of the complex pair on the monolayer did not cover at least the area bound by the two probes. Furthermore, statistical evaluation gave no indication of propagation of potential responses. Accordingly, the tentative view is expressed that the observations described here are the result of lipid angular realignment and the local surface modification induced by lipid-protein complex interaction.

Conclusions

Two aspects of the work described above are of relevance to the field of chemical sensor technology. First, the potential transients are apparently induced by highly selective bimolecular interactions at very low concentrations of reagents in the bulk phase. It is difficult to assess the precise concentration at the interface because the appropriate adsorption isotherm is not known and, in addition, there is a degree of adsorption on the overall trough surface. Secondly, the effects can be considered as primary digital signals instigated by analytical reactions. In recent years, there has been increasing attention paid to the possibility of avoiding the use of primary analog devices by introduction of concentration-"switchable" sensors [43]. Such sensors could alleviate difficulties associated with calibration and non-specific adsorption phenomena.

Finally, it is clear that further work is required to establish the true origin of the potential transients described above. Possibilities include radiolabelling techniques for concentration measurement and the use of electrostatic probes for increased time resolution [44] with reduced physical size.

We are indebted to the Natural Sciences and Engineering Research Council of Canada for the support of this work and for the provision of a Fellowship to H.E.W.

REFERENCES

1 M. Thompson and U. J. Krull, Anal. Chim. Acta, 117 (1980) 121.
2 M. Thompson and U. J. Krull, Anal. Chim. Acta, 147 (1983) 1.
3 U. J. Krull and M. Thompson, Trends Anal. Chem., 4 (1985) 90.
4 U. J. Krull, M. Thompson and H. E. Wong, in D. Schuetzle and R. Hammerle (Eds.), Fundamentals and Applications of Chemical Sensors, ACS Symposium Series 309, American Chemical Society, 1986, p. 351.
5 U. J. Krull and M. Thompson, IEEE Trans. Electron Devices, 32 (1985) 1180.
6 M. Thompson, U. J. Krull and L. I. Bendell-Young, Bioelectrochem. Bioenerg., 13 (1984) 255.
7 U. J. Krull and M. Thompson, Biochem. Biophys. Res. Commun., 141 (1986) 912.
8 E. Toro-Goyco, A. Rodriguez and J. del Castillo, Biochem. Biophys. Res. Commun., 23 (1986) 341.

9 J. del Castillo, A. Rodriguez, C. A. Romero and V. Sanchez, Science, 53 (1966) 185.
10 T. Ishii, Y. Kuroda, K. Yoshikawa, K. Sakabe, Y. Matsubaru and K. Iriyama, Biochem. Biophys. Res. Commun., 123 (1984) 792.
11 K. Yoshikawa and Y. Matsubara, J. Am. Chem. Soc., 106 (1984) 4423.
12 T. Ishii, Y. Kuroda, T. Omochi and K. Yoshikawa, Langmuir, 2 (1986) 319.
13 G. G. Roberts, Sens. Actuat., 4 (1983) 131.
14 U. J. Krull, M. Thompson and H. E. Wong, Analyst, 110 (1985) 1299.
15 U. J. Krull, M. Thompson and H. E. Wong, Bioelectrochem. Bioenerg., 15 (1986) 371.
16 M. A. McGregor and G. T. Barnes, J. Coll. Interface Sci., 60 (1977) 408.
17 A. Arya, U. J. Krull, M. Thompson and H. E. Wong, Anal. Chim. Acta, 173 (1985) 331.
18 U. J. Krull, M. Thompson, E. T. Vandenberg and H. E. Wong, Anal. Chim. Acta, 174 (1985) 83.
19 R. F. Flewelling and W. L. Hubell, Biophys. J., 49 (1986) 541.
20 R. Friedenberg, A. Blatt, V. Gallucci, J. F. Danielli and I. Shames, J. Theor. Biol., 11 (1966) 465.
21 R. Friedenberg, The Electrostatics of Biological Cell Membranes, North-Holland, Amsterdam, 1967.
22 G. L. Gaines, Insoluble Monolayers at Liquid-Gas Interfaces, Wiley-Interscience, New York, 1966.
23 W. H. Dorn, The Dipole Potential in Monolayers, Bilayers and Biological Membranes, M.Sc. Thesis, University of Toronto, 1985.
24 M. Sundaralingam, Ann. N.Y. Acad. Sci., 195 (1972) 324.
25 H. Hauser, I. Pascher, R. H. Pearson and S. Sundell, Biochim. Biophys. Acta, 650 (1981) 21.
26 M. R. Peterson and R. A. Poirier, MONSTERGAUSS program, Department of Chemistry, University of Toronto.
27 See W. C. Davidon, Mathematical Programming, 9 (1975) 1.
28 F. Vilallonga, Biochim. Biophys. Acta, 163 (1968) 290.
29 T. Seimiya, Y. Heki and H. Ochinata, Coll. Surf., 3 (1981) 37.
30 J. F. Yeagle, W. C. Hutton, C. Huang and R. B. Martin, Biochemistry, 15 (1976) 2121; 16 (1977) 4344.
31 H. Hauser, M. C. Phillips, B. A. Levine and R. J. P. Williams, Nature, 261 (1976) 390.
32 J. Seelig, H. U. Gally and R. Wohlgemuth, Biochim. Biophys. Acta, 467 (1977) 109.
33 G. Buldt, H. U. Gally, A. Seelig, J. Seelig and G. Zaccal, Nature, 271 (1978) 182.
34 P. Lorrain and D. Corson, Electromagnetic Fields and Waves, W. H. Freeman, San Francisco, 1970.
35 W. R. Smythe, Static and Dynamic Electricity, McGraw-Hill, New York, 1950.
36 B. B. L. Agrawal and I. J. Goldstein, Can. J. Biochem., 46 (1968) 1147.
37 H. Bader, R. Van Wagenen, J. D. Andrade and H. Ringsdorf, J. Coll. Interface Sci., 101 (1984) 246.
38 I. J. Goldstein, C. M. Reichert and A. Misaki, Ann. N.Y. Acad. Sci., 234 (1974) 283.
39 H. E. Wong, Ph.D. Thesis, University of Toronto, 1987.
40 E. E. Uzgiris and R. D. Kornberg, Nature, 301 (1983) 134.
41 W. M. Heckl, M. Losche, D. A. Cadenhead and H. Möhwald, Eur. Biophys. J., 14 (1986) 11.
42 H. Möhwald, W. M. Heckl and M. Thompson, unpublished work.
43 M. Thompson, W. H. Dorn, U. J. Krull, J. S. Tauskela, E. T. Vandenberg and H. E. Wong, Anal. Chim. Acta, 180 (1986) 251.
44 H. W. Trissl, Proc. Natl. Acad. Sci. U.S.A., 80 (1983) 7173.

Analytica Chimica Acta, 200 (1987) 333—345
Elsevier Science Publishers B.V., Amsterdam — Printed in The Netherlands

EXPERT SYSTEM FOR SOLVING PROBLEMS IN CARBON-13 NUCLEAR MAGNETIC RESONANCE SPECTROSCOPY

J. ZUPAN*, M. NOVIČ, S. BOHANEC and M. RAZINGER
Kemijski Inštitut "Boris Kidrič", Ljubljana (Yugoslavia)
L. LAH, M. TUŠAR and I. KOŠIR
Department of Chemistry, University of Ljubljana, Ljubljana (Yugoslavia)
(Received 8th April 1987)

SUMMARY

The expert system CARBON is built around a knowledge base consisting of spectra/structure correlations, tables of data, mathematical formulae and graph-theory procedures and on a data base of 2500 assigned ^{13}C-NMR spectra. The built-in knowledge enables the user to obtain suggestions for solutions to problems of different types arising in ^{13}C-NMR spectroscopy. Use of the system is facilitated by appropriate command files, large on-line help files, and user-friendly dialogue. The system can be used with spectrometries other than ^{13}C-NMR and in other fields concerned with correlations between chemical structures and properties.

New improved instrumentation linked with better computers requires better and more powerful software for instant and diverse use by spectroscopists. Simple search systems are no longer regarded as satisfactory and more problem-solving power is increasingly sought in the software packages applicable to different problems [1—4]. This means that better and more refined information is required rather than simple answers in the form of a retrieved structure or a spectrum, so that as much information as possible can be retrieved from available data. The case of ^{13}C-NMR spectroscopy is very illustrative. The user does not necessarily start the inquiry with a ^{13}C-

*Jure Zupan is the Professor of Chemometrics at the Chemistry Department of the University of Ljubljana. He graduated in 1966 and obtained his Ph.D. in 1972 in Chemistry at the University of Ljubljana. From 1966 to 1973 he worked on ceramic and quantum chemistry problems at Institute Josef Stefan. In 1974 he joined the Department for Structural Chemistry lead by Prof. D. Hadži at the Boris Kidrič Institute of Chemistry in order to form a group for research on applications of computers in chemistry. The group is presently involved in the development of different spectroscopies based on chemical expert systems. His research interests are algorithms and methods for hierarchical clustering, and feature extractions from complex data. He has worked at ETH Zürich and EPA, Washington, DC, and in 1982 was a visiting professor in the Department of Chemistry at Arizona State University in Tempe. He is the author and editor of several books in the field.

0003-2670/87/$03.50

NMR spectrum. The query could be any entity from the field of ^{13}C-NMR spectroscopy. Hence, an expert system in this field must accept spectra, subspectra, single chemical shifts, structures, substructures, sets of fragments, etc. as input data. Using input data of different types, the expert system should be able to handle various tasks from spectral and structural searches to simulation of spectra, prediction of structures and substructures, detection of structural locations where conformational isomerism can arise, pinpointing the positions for substituents, etc. The more such problems a system can handle, the more it deserves the term "expert".

Unfortunately, the present chemical expert systems are far from being able to solve really difficult problems. However, they can provide assistance with a number of valuable suggestions and hints deduced from the built-in knowledge, obtained by brute-force algorithms, or retrieved from data bases [5]. In the present paper, the CARBON system, which is designed for solving different problems raised in ^{13}C-NMR spectroscopy is described.

PHILOSOPHY OF THE CARBON SYSTEM

When the CARBON system is used, work is started on the problem by selecting one of the following seven routines: identification of entire and/or partial spectra, identification of structures and/or substructures, prediction of possible structural features, simulation of ^{13}C-NMR spectra, assignment of ^{13}C-NMR chemical shifts to selected carbon atoms, generation of all isomers from a given set of fragments, and various combinations of these options.

In addition to the manipulation of spectroscopic knowledge, handling and maintenance of intermediate results are also provided. The utility features are easy to deal with, hence even users having little experience with computers can work successfully.

At present, the data base contains 2536 ^{13}C-NMR spectra of various chemical compounds with about 30 000 assigned chemical shifts. All shifts in the data base are given with an accuracy of ±0.1 ppm, relative to TMS. The data base serves primarily as a source of spectra/structure correlations (needed for predictions of structural and spectral features) and shifts of different substituents (needed for assignments and spectra simulation), and secondarily, as a reference collection for different searches.

The quality of an expert system is determined by the quality of the knowledge built into it. In the CARBON system, knowledge is incorporated in the following four forms: (1) as a hierarchical tree of clusters of similar spectra, which serves for the prediction of structural fragments and structural types of queries, (2) as tables of chemical shifts of different substituents in different steric positions and conformation states, which can be used for simulation of ^{13}C-NMR spectra; (3) as mathematical formulae and statistical procedures on groups of data of different kinds and sizes; and (4) as graph-theory algorithms implemented in substructure search, assignments, and generation of constitutional isomers.

During the application of the system, it is possible to select any option offered and to use the intermediate results obtained in previous sessions as a new data base for further work. For example, the user can generate interactively a molecular graph and then choose one of the possible continuations: these can be either the simulation of a ^{13}C-NMR spectrum, a substructure search, or building a data base of structures by writing the generated structures on external file. In all cases, the results can be stored permanently or temporarily for further use. In another example, the user can begin the work with a single chemical shift, with a group of shifts, or with a whole ^{13}C-NMR spectrum. Having this type of input data, the user can select the search in the hierarchical tree, shift-by-shift search in the data base, or assignment of shifts. There are other features in the CARBON system which are valuable for spectroscopists and organic chemists, e.g., interactive generation of chemical structures and generation of all constitutional isomers from a given set of fragments.

The general idea was to link different programs together so that the CARBON system could be used for attacking many different problems, and partial results of one option could be taken as the input data for another option.

DESCRIPTION OF FEATURES OFFERED BY THE SYSTEM

Search by chemical shifts

This is the simplest and, for beginners, the most used part of the system. It enables those spectra having all the chemical shifts entered consecutively by the user to be retrieved from the data base of 2536 items. The default tolerance for each shift is ±0.5 ppm, but the user can alter this value provided that the number of retrieved spectra does not exceed 1000. The search procedure is shown in Fig. 1. The user can inspect or store the "good list" of structures at any point during the search. The possibility of selecting and storing permanently a small data base from which the work can be continued later is very useful. The number of data bases created in this manner is limited only by the external computer space available.

Shift-by-shift search is important for another reason. Selecting the answer "A" (for assignment) in the above search procedure (Fig. 1a) causes the system to check all retrieved spectra if the entered chemical shifts are assigned to carbon atoms linked together. The system acknowledges the connections between the carbon atoms even if they are separated by a number of consecutive heteroatoms. For example, two carbon atoms in a chain —C—O—C(=O)— having chemical shifts of 64.0 and 173.2 ppm respectively, are treated as connected. In the next step, the system searches for different fragments (up to the preselected size of the neighbourhood) having in the centre the carbon atom with the chemical shift given first. At present, the system displays the structures containing the selected fragments and writes their connection tables to a separate file for further use.

Search with complete spectrum

There are two reasons why the shift-by-shift search cannot satisfy all needs. First, an inherent problem in the shift-by-shift search, i.e., the very large number of retrieved references in certain regions of the ^{13}C-NMR spectrum, prevents fast, precise, and thus reliable, answers; secondly, very often a holistic approach to the retrieval of spectra is desired (i.e., the user is interested in the information about the type of structures that fit best the entire query spectrum not just an arbitrary part of it. In the case of a full spectrum search, the system starts with the preprocessing of the query spectrum into a 40-dimensional vector [6, 7] and inputs this representation at the root of the hierarchical tree (Fig. 2a). The choice of the path through the tree is based at each node on the comparison of three distances: two distances between both descending clusters and the query spectrum, and the third one between the descending clusters themselves. After the query traverses an assigned node, the assigned structural property is associated with the unknown structure. The reliability of the prediction is inversely

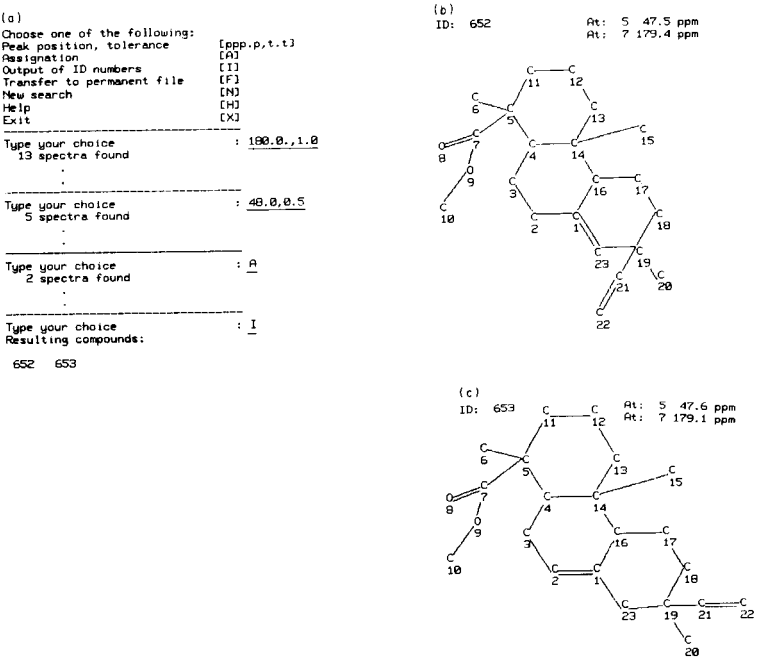

Fig. 1. Search procedure using single peaks. The default tolerance is ±0.5 ppm. The user can display the retrieved references at any point by typing "I", or save them on a permanent file using the "F" command. The command "A" prompts the system to check if the given chemical shifts belong to carbon atoms that are linked together in the reference structures. As seen in example (a), the resulting list of 5 compounds was reduced to only two compounds, (b) and (c), in which both shifts 180.0 ± 1.0 ppm and 48.0 ± 0.5 ppm belong to neighbouring atoms.

```
Chemical shifts:  1   213.6
                  2    36.7
                  3    22.0

Press [RETURN]    _
```

The path of the spectrum X through the tree

Node on the path	No. of spectra	Rejected node	D left	D right	D (%)	Fragments
1						
2	814	10	10.5	11.8	12.0	
3	751	4	10.0	14.4	44.0	
18	427	6	8.8	8.8	0.4	
33	421	546	8.7	13.3	52.4	
155	133	1715	7.7	7.8	0.6	
66	132	3800	7.7	16.0	107.4	
199	114	69	7.0	8.2	17.1	
209	110	231	6.6	8.7	32.9	
1425	69	710	5.6	8.1	43.8	
1551	64	1440	5.2	8.0	54.9	
1603	57	968	5.0	6.4	27.2	
1627	42	495	5.0	5.3	5.1	
904	27	1366	4.5	6.1	34.9	
1559	24	300	4.0	6.3	58.1	
1725	21	1264	3.6	5.0	37.4	
1763	17	303	3.1	5.3	69.9	
1544	8	808	2.7	3.7	34.7	4
235	7	2723	1.9	6.0	223.1	4 9
1636	6	2128	1.7	3.0	80.0	4 9
977	2	1634	0.0	2.5	-	4 9

```
Start at the root          [RETURN]
Start at the node          [number]
Exit                       [X]     : 977
Elapsed time:   0.7 seconds
```

Node No. 977 contains 2 compounds

Compounds to which the spectrum of X was linked:

No.	ID	Distance
1	908	0.00
2	1122	0.00

```
Press [RETURN]
```

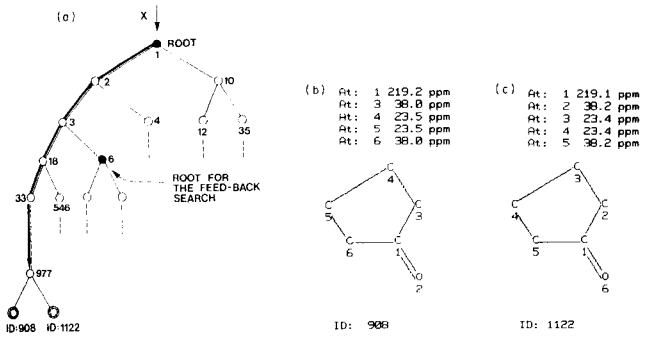

Fig. 2. Search in the hierarchical tree. First, the complete spectrum (213.6, 36.7, 22.0 ppm) is entered; secondly, the nodes on the main path are displayed together with the most interesting parameters (number of spectra in the node, omitted nodes, distances, the relative difference in distances in the percentage with the respect to the smallest one, and the identification number of predicted structural fragments). Thirdly, the ID numbers of the members of the final cluster to which the query spectrum was linked are shown (Nos. 908 and 1122 in this case). The omitted nodes at which the relative difference in the distances was small are potential candidates for the feed-back search (i.e., nodes 6 and 1715, 495, etc.). In node 1544, fragment no. 4 (—CH_2—) was predicted and in node 235 fragment no. 9 (—C(=O)—) was predicted. To clarify the procedure, a small part of the top of the decision tree is shown in detail in (a). Both compounds from cluster 977 are shown as (b) and (c). In fact, the query spectrum belonged to the same compound with spectra recorded under different conditions.

proportional to the distance measure between the query spectrum and the assigned node at which the prediction was made. The search can stop either at the end spectrum in the tree (at the leaf) or in the middle of the tree (at a cluster of spectra). The distance of the query spectrum to the leaf or to all members of the cluster at which the search stops, gives the user the information how similar the unknown structure and the reference structures are. A case in which the search stopped at node no. 977 is shown in Fig. 2(a). This node represents two identical compounds with very similar spectra. In the 40-dimensional representation, both spectra in node 977 are identical, not only with each other but also with the query. Both reference compounds found in node 977 are shown in Fig. 2(b and c). When the two spectra are compared with the chemical shifts in the query, the advantage of the method is evident: the differences in corresponding shifts (reference-to-query) are too large for a retrieval on the shift-by-shift basis to be successful. In fact, there are more than 1500 spectra in the data base for the peak 22.0 in the interval of ±0.5 ppm. Additionally, the mentioned interval does not even cover both reference spectra having 23.5 and 23.4 ppm shifts, respectively.

The assigned nodes (clusters of three or more spectra) in the hierarchical tree represent spectra of compounds having at least one structural feature in common. On the search path shown in Fig. 2, nodes 1544 and 235 are assigned to fragments 4 ($-CH_2-$) and 9 ($-C(=O)-$), respectively. The traverse of the query spectrum through the tree can, in principle, start at any node in the tree. The default start implemented in the first pass is at the root. After the first pass is complete, the user can redirect the next start of the query spectrum at any chosen node in the tree. The potential candidates for such feed-back searches [8] are the nodes at which the decision about the continuation was not a clear-cut one (i.e., the differences were approximately equal). In Fig. 2, nodes 4 and 1715 are the most appropriate candidates for the feed-back search.

Generation of molecular graphs

For many purposes (simulation of spectra, substructure search, update, etc.), the user must have a utility for simple and flexible generation of molecular graphs (i.e., connection tables). The set of commands for this purpose consists of the standard ones (for generation and linking of different structural parts together like RING, CHAIN, BRIDGE, ATOM, BOND, DELETE, OPEN, INSERT, etc.) and utility commands for making the generation and manipulation of structures more convenient (MENU, SAVE, DROP, TERMINAL, HELP, CT for connection table, etc.). With the option SAVE, for example, up to 20 user-defined structures can be saved for instant recall (with MENU, n command) when needed.

When a fragment is built, the atoms that could be connected to other fragments, substituents, or structures should be clearly marked as such. The atoms where a substituent could be attached are marked with an A, while the atoms where a substituent must be connected are marked with an X.

After a structure (or fragment) has been generated, it is written on a temporary file accessible from any option that uses connection tables as input (substructure search, assignment, simulation, update, etc.).

Substructure search

In the ^{13}C-NMR and other spectroscopies, structurally similar compounds are frequently studied. In the CARBON system, the substructure search is done in four steps: (1) generation of the query substructure; (2) fast pruning of the existing structural data base using the inverted files of atomic centred fragments; (3) atom-by-atom comparison of connection tables on the short remaining file with the connection table of the query fragment, and (4) search for all number-to-number correspondences between the numbering of atoms in the query and the numbering of atoms in the retrieved structures.

Because a reference structure can contain the query fragment in more than one structural position, more than one number-to-number correspondences can result. Because all carbon atoms in the data base are numbered and assigned to chemical shifts, the distribution of shifts at the equivalent positions is easily obtained. Figure 3 shows the query, the retrieved list of ID numbers of compounds containing the query fragment, the distribution of shifts for atom no. 4 in the query fragment, and two structures from the good-list.

Simulation of ^{13}C-NMR spectra

For any structure currently generated by the CARBON system, its ^{13}C-NMR spectrum can be simulated. The values of the chemical shifts associated with carbon atoms are calculated by adding partial contributions of neighbours to the standard chemical shift of each carbon atom. The partial contributions of substituents and standard shifts are taken from the literature [9, 10]. The system checks each atom, its α, β, γ and δ neighbours, and the substituents on these positions. The system identifies the type of the particular carbon atom (sp, sp^2, sp^3 hybridization, carbonyl-type, aromatic, pyridine ring, etc.), type and number of the substituents, and the position of the substituent with the respect to the central atom. Steric contributions (depending on whether the central atom is primary, secondary, tertiary or quaternary) to the chemical shifts are also considered. Additionally, the system detects the positions where isomerism can arise and asks for specification of the conformation (synperiplanar, synclinal, anticlinal, antiperiplanar, or free rotation). The corresponding contribution is then added to the total chemical shift.

If a contribution for a found substituent is not present in the tables, the system informs the user about the missing data. The user then inputs the appropriate value or just notes the insufficiency. A comparison between the simulated ^{13}C-NMR spectrum of a given structure and the experimental spectrum of the same compound found in the data base is given in Fig. 4.

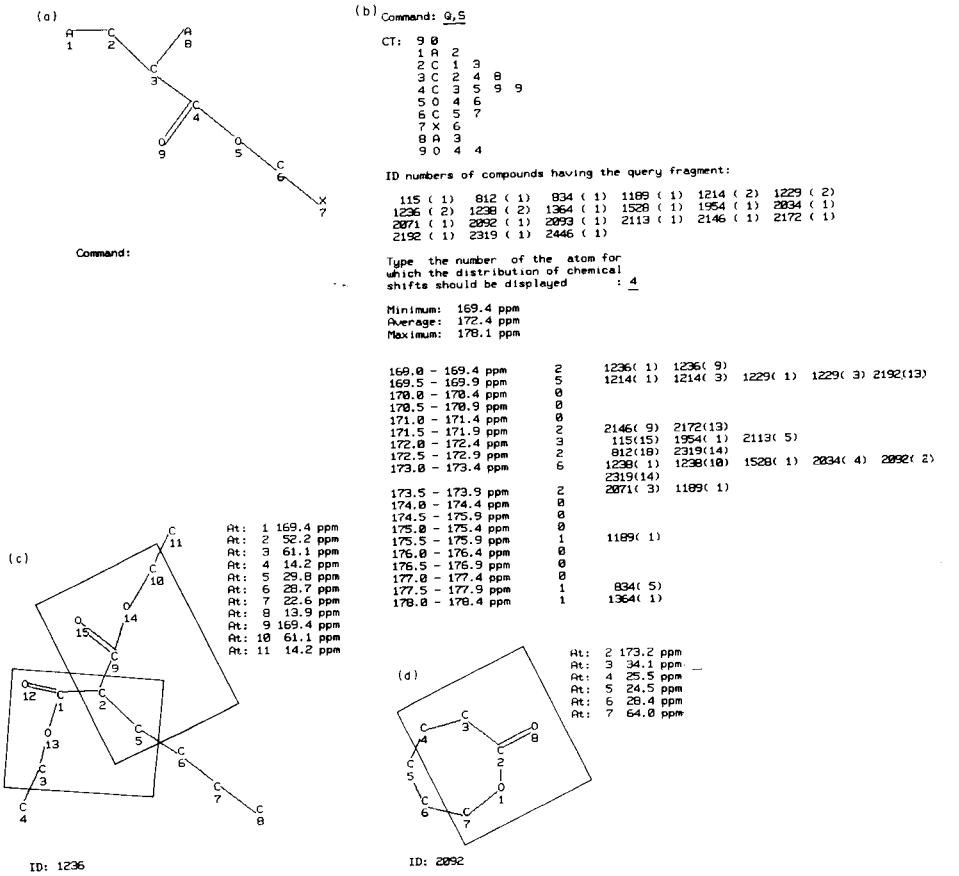

Fig. 3. The substructure search. In the query fragment (a), the sites where substitutions can take place are marked with A or X, depending whether the user wants a possible (A) or mandatory (X) substituent at a particular position. The substructure search starts with the command Q,S (for quit the structure generator and start searching). The list of retrieved compounds is accompanied by the number of times that the query fragment is encountered in each of them. After the resulting reference have been displayed, the user can inspect distributions of chemical shifts for any selected carbon atom in the query or look at the full reference (c and d). In all intervals of the distribution of chemical shifts, the ID numbers of the compounds together with the number of the particular carbon atom are shown. For example, compound 1236 (c) has 2 carbon atoms (1 and 9) that correspond to the atom 4 in the query structure. Both shifts (169.4 ppm) assigned to these 2 atoms are placed in the first interval of the distribution shown.

Generation of all constitutional isomers

A routine part of the structure elucidation process is assembling the structure from the set of fragments known to be present in the unknown compound. The list of possible fragments can be acquired and/or updated from various sources: the similarity search, the separate peak-position search, or from any other analytical method. Several isomer generators

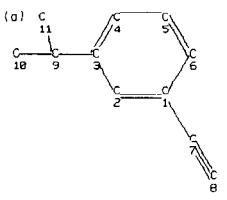

(b) Command:

```
Generation of new structure [G]
Exit                        [X]
Simulation                  [RETURN]
-------------------------------------

                            :

Enter corresponding answer for atoms
No.: 10 regarding atom No. :  2

Synperiplanar               [1]
Synclinal                   [2]
Anticlinal                  [3]
Antiperiplanar              [4]
Free rotation               [RETURN]
Not known                   [RETURN]
-------------------------------------

                            : _

Enter corresponding answer for atoms
No.: 11 regarding atom No. :  2

Synperiplanar               [1]
Synclinal                   [2]
Anticlinal                  [3]
Antiperiplanar              [4]
Free rotation               [RETURN]
Not known                   [RETURN]
-------------------------------------

                            : _
```

(c) Simulated spectrum

No	Atom	PPM	Status	Connected to
1	C	122.4	OK	6 - 2 = 7 -
2	C	130.3	OK	3 - 1 =
3	C	149.0	OK	2 - 4 = 9 -
4	C	126.3	OK	5 - 3 =
5	C	128.9	OK	4 - 6 =
6	C	129.8	OK	1 - 5 =
7	C	84.6	OK	1 - 8 #
8	C	78.3	OK	7 #
9	C	33.7	OK	3 - 10 - 11 -
10	C	24.4	OK	9 -
11	C	24.4	OK	9 -

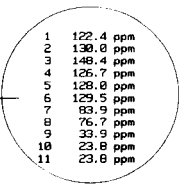

Fig. 4. Simulation of the ^{13}C-NMR spectrum. First, the structure is generated (a), then in an interactive dialogue between the system and the user, questions about the conformational positions are resolved (b), and the simulated spectrum is displayed. For comparison, the experimental spectrum of the same compound is also displayed (c). The OK entries in the fourth column of the simulated spectrum (labelled STATUS) refer to the fact that all partial contributions to all chemical shifts were found.

are implemented in different systems (e.g., DENDRAL [11] and CASE [12]). With the possibility of implementation of the designed system on personal computers, it was decided to try a new approach to the isomer generation problem.

The main difficulty of this problem lies in the fact that the isomer list has to be exhaustive but without redundancies. Because of this, each generated isomer has to be tested for possible graph isomorphism against all previously generated isomers. Because with a growing number of fragments (i.e., graph nodes) testing for isomorphism leads to a combinatorial explosion [13], it is obviously unsuitable for implementation on small computers or personal computers. In our solution, this slow testing for isomorphism is replaced by a quick comparison of each generated isomer (i.e., chemical graph) with all relevant entries in a special graph library. The graphs in the library are represented by their graphical partitions, i.e., sequences of valencies of all graph nodes. Because the input information has the same structure (set of fragments of known valency), the comparison can be done by simple matching and proceeds very quickly. The actual library contains graphs with 2—10 nodes.

At first glance, it would seem that such an approach is of very limited use because of the small number of nodes in a graph that can be precalculated

exhaustively and maintained efficiently later. But because the building blocks can also be larger fragments, rings, ring systems, etc., and not just single atoms, quite large molecules can be treated in this way. Compared with the brute-force approach, of course, the proposed scheme means that much of the work that could be done by the computer is left to the operator but it is still far better than to do everything by hand.

The generation of isomers is done in two steps. In the first step, the input distribution of fragments in a form of a set of numbers is checked in the files for the identical set. In the second step, the nodes of the matching graphs are substituted with all possible chemical fragments (Fig. 5). During this step (which can be more time-consuming), the user can discard some structural types on the basis of chemical knowledge about the problem.

Isomer generation can be of use in various fields of structure elucidation where information on the identity of fragments is gathered (infrared, mass spectrometry, etc.) and thus the option can be used by different specialists.

File manipulation

As has been shown, the user can start working on the system with queries of very different form, combine partial results from different options, save intermediate or final results on permanent files, change or update files, etc. In order to accomplish these tasks, the system must have a uniform and strict file organization; data files containing the same type of information (i.e., connection tables, ID numbers, set of shifts, etc.) should always be written in the same format regardless of the option in which they are created. Further, the file-manipulation capability must be flexible. The file-manipulation option is designed to help in these steps and to meet the condition of minimal user knowledge about computers. Because all options (program modules) are linked via the command files, the appropriate HELP information is included in these files and is thus always at hand if a wrong command is issued by the user. At present, there are about 100 kbytes of online help information available to assist users in different situations.

FUTURE DEVELOPMENT OF THE CARBON SYSTEM

Like any other expert system, the CARBON system can and will be further developed and improved in many areas. The following improvements are already in progress: (1) prediction of more structural features during the traverse of the hierarchical data base; (2) addition of chemical shifts of more substituents for simulation of ^{13}C-NMR spectra; (3) addition of new graph files for structure generator; and (4) automation of assignment of chemical shifts.

The prediction of structural features is improved by generating new trees (based on new representations of ^{13}C-NMR spectra such as Hadamard transforms [14]. For every node in the new tree, an analysis of structural features

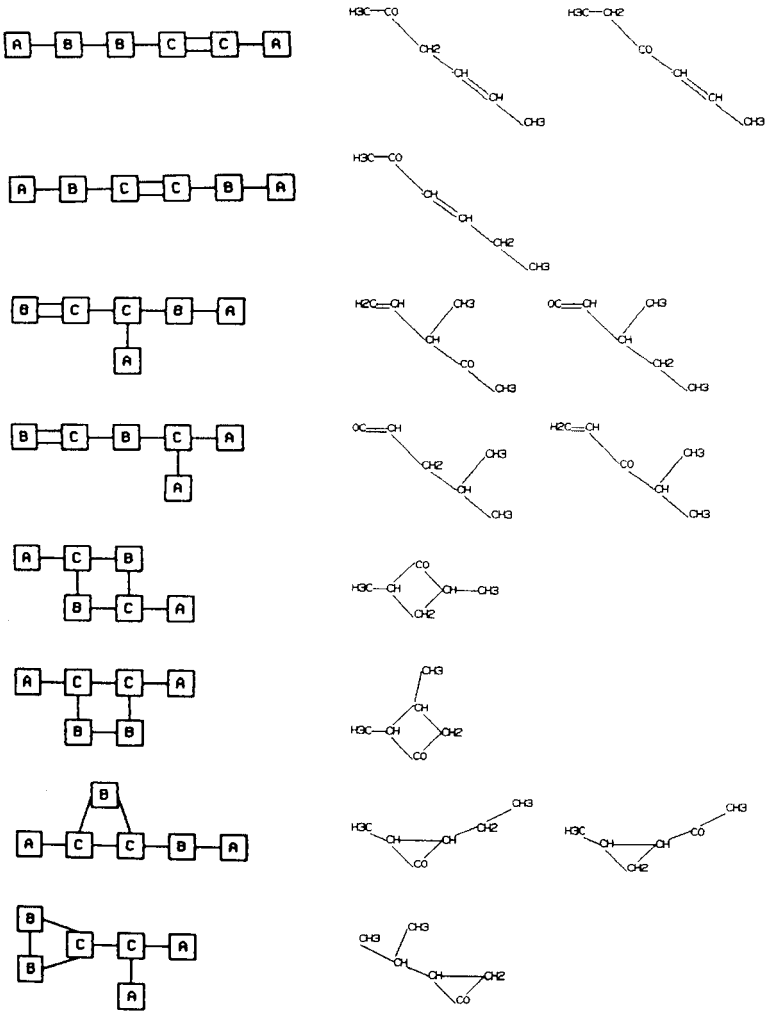

Fig. 5. The generation of constitutional isomers. The graphs on the left were retrieved from the graph library because they match the input parameters. The structures on the right were generated by the combination of these graphs and the input chemical fragments (six fragments, four of them different).

of linked compounds is made. After a tree with better prediction ability and with a larger assortment of predicted structural features has been found, it replaces the old one.

The problem of simulation of more complex compounds is tackled from two sides: first, by using the existing data base of assigned spectra in order to extract chemical shifts for substituents not found in the literature, and second, by introducing a set of skeletons with known chemical shifts. The latter approach is connected with the so-called super-structure search. Its purpose is to identify all members of a given set of structures (templates) that are substructures of a query structure; in contrast, a substructure search tests all structures from a data base if they contain the query structure as a substructure. Although the core algorithm for the comparison of structures is the same for both searches, the selection, exit conditions, and file organization for the super-structure search is quite different from that of the substructure search.

At present, the files of graphs for a given number of nodes (from 2 to 10) contain all acyclic, monocyclic and bicyclic graphs with single bonds and all acyclic graphs with double and triple bonds. The files of polycyclic graphs and cyclic graphs with multiple bonds are under development.

Assignment will be improved by the introduction of automatic assignment [4] and error detection. In the present version, the system shows structural fragments consisting of atoms assigned to a given set of chemical shifts and the user must choose the most appropriate fragment. In the next step, the user will input the set of shifts and the structure while the system will try to optimize the assignment.

A weak point in the system is the updating of new spectra and structures. The update is not intended for general public access because all the internal knowledge (hierarchical tree, assignments, structure prediction, etc.) is very sensitive to errors in the data base. Each addition of a new item changes many files and data on different levels (inverted files of shifts and structural fragments, hierarchical tree with assigned nodes, targets for assignments, etc.) and so the updated structures and spectra must be thoroughly checked. For these reasons, updating is done in blocks of 500 new entries at a time. Our main concern is to make the CARBON system a real expert system based on a good knowledge base rather than on a large data base. It is true that more knowledge can be extracted from a larger data base, but it is considered here to be more useful to make improvements on the basis of existing data and to add more features which will enable the CARBON system to interpret ^{13}C-NMR spectra intelligently, rather than to focus in adding new spectra to improve obvious tasks such as retrieval of similar spectra and structures.

Conclusion

The CARBON system was designed to help in solving problems related to ^{13}C-NMR spectroscopy. At present, it finds spectra similar or identical to

that of the query, predicts structural features on the basis of a single chemical shift, group of shifts, or entire ^{13}C-NMR spectrum, simulates ^{13}C-NMR spectra, helps in assignment problems, generates isomers from a given set of fragments, runs structure and substructure searches, and performs combinations of all these tasks. Additionally, the CARBON system can help in other fields besides ^{13}C-NMR and thus can be helpful to users interested in problems related to chemical structures. Substructure search and clustering of structures is applicable in many areas of structure elucidation while the isomer generator can be used successfully in mass spectrometry. The interactive structure generator can serve as a stand-alone program for input of connection tables if a chemical structure-oriented data base is required. Finally, the system can serve very well for educational purposes.

The system consists of approximately 20 command files governing about 60 programs written in either Fortran or Pascal and of about 20 different permanent data files. The entire system uses slightly less than 20 Mbyte of memory.

The authors thank many friends, co-workers and users who contributed programs, comments, ideas and criticism, helping to improve the performance of the system considerably. Among these, special thanks are due to Prof. Dušan Hadži, Prof. Morton E. Munk, Prof. Branko Stanovnik, Dr. Jurka Kidrič, Mr. Dušan Turk and Mr. Milan Hodošček. The financial support of Research Community of Slovenia is gratefully acknowledged.

REFERENCES

1 W. Bremser, L. Ernst, B. Franke, R. Gerhards and A. Hardt, Carbon-13 NMR Spectral Data, 3rd edn., Verlag Chemie, Weinheim, 1981.
2 J. Zupan, (Ed.), Computer-Supported Spectroscopic Data bases, Horwood, Chichester, 1986.
3 N. A. B. Gray, Prog. Nucl. Magn. Res. Spectrosc., 15 (1985) 201.
4 H. Kalchhauser and W. Robien, J. Chem. Inf. Comput. Sci., 25 (1985) 103.
5 R. Dessy, Anal. Chem., 56 (1984) 1200A, 1312A.
6 J. Zupan, Clustering of Large Data Sets, Research Studies Press, Wiley, Chichester, 1982.
7 M. Novič and J. Zupan, Anal. Chim. Acta, 177 (1985) 23.
8 J. Zupan and M. E. Munk, Anal. Chem., 58 (1986) 3219.
9 E. Pretsch, J. T. Clerc, J. Seibel and W. Simon, Tabellen zur Strukturaufklärung organischer Verbindungen mit spektroskopischen Methoden, Springer, Berlin, 1976.
10 D. W. Brown, A Short Set of Carbon-13 NMR Correlation Tables, J. Chem. Educ., 62(3) (1985) 209.
11 R. E. Carhart, D. H. Smith, N. A. B. Gray, J. G. Nourse and C. Djerassi, J. Org. Chem., 46 (1981) 1708.
12 C. A. Shelley and M. E. Munk, Anal. Chim. Acta, 133 (1981) 507.
13 R. C. Read, in B. Harris, Ed., Graph Theory Algorithms, Graph Theory and its Applications, Academic, New York, 1970, pp. 51—78.
14 R. Kaiser, J. Magn. Res., 15 (1974) 44.

Analytica Chimica Acta, 200 (1987) 347—361
Elsevier Science Publishers B.V., Amsterdam — Printed in The Netherlands

THE APPLICATION OF TWO-DIMENSIONAL NUCLEAR MAGNETIC RESONANCE SPECTROSCOPY IN COMPUTER-ASSISTED STRUCTURE ELUCIDATION

BRADLEY D. CHRISTIE and MORTON E. MUNK*

Department of Chemistry, Arizona State University, Tempe, AZ 85287 (U.S.A.)

(Received 8th April 1987)

SUMMARY

One of the most powerful tools for the determination of an unknown organic structure is two-dimensional NMR spectroscopy. In some cases, this information quickly leads to a unique structure, but in many cases there remains a large number of structural possibilities. A linked system of computer programs has been developed which uses several types of 2-D NMR data and generates all possible topological structures consistent with these data and user-input constraints. When symmetry is present, algorithms based on group theory limit the structures to those consistent with all the different symmetries that are possible. Applications of these programs to problems described in the literature, in which 2-D NMR was used to determine the structures of natural products, are described.

The use of spectroscopic data for the determination of the structure of an unknown organic molecule is a method common to many areas of organic chemistry. One of the most powerful spectroscopic techniques is two-dimensional NMR spectroscopy (2-D NMR). Because the result of 2-D NMR experiments is connectivity between NMR signals, with each signal corresponding to one or more nuclei, its role in determining the connectivity between the nuclei of an unknown structure is obvious.

As an ongoing project in this laboratory, a collection of programs has been developed for computer-assisted structure elucidation (CASE) [1]. The collective goal of these computer programs is to accept chemical and spectroscopic information about an organic compound of unknown structure and produce all compatible molecular structures. If the input information

*Morton E. Munk is a professor of chemistry at Arizona State University. He was born in 1928 and educated at Northwestern University (B.S., Chemistry, 1950) and Wayne State University (Ph.D., Organic Chemistry, 1955). His Ph.D. dissertation research on the chemistry of ketenimines was conducted under the direction of C. L. Stevens. After a year as a postdoctoral fellow in the laboratory of Charles Prevost at the Sorbonne in Paris, he accepted a position as research scientist at the pharmaceutical house, Parke Davis and Company. He joined the faculty in chemistry at Arizona State University in 1961. His field of interest is artificial intelligence in chemistry, with a major emphasis on computer-assisted structure elucidation.

0003-2670/87/$03.50

is sufficiently restrictive, this will result in a small number of structures, easily handled conceptually by the user. As part of the CASE system, a linked system of computer programs has been developed for the interpretation of selected 2-D NMR experiments followed by generation of all topological molecular structures consistent with both the interpretation and the user-entered information.

The aim is to produce tools that can be used to solve difficult problems in structure elucidation. The programs which will be described can accommodate most types of structural features and are therefore not limited to use with one or more specific classes of structures (e.g., steroids, alkaloids, ethers). Although the emphasis here is on NMR, it is expected that, just as in manual solution of a problem in structure elucidation, every resource commonly available in laboratories will be used. Besides the NMR data, the molecular formula is required by the programs described. If not evident from other data, it can be estimated by fast-atom-bombardment mass spectroscopy. It is also assumed here that there are no overlapping ^{13}C-NMR peaks. With the modern high-field instruments, this is generally the case.

Lindley et al. [2] have recently reported on the use of 2-D NMR-derived structural fragments for constrained structure generation. However, in this application the user is directly responsible for first reducing the 2-D NMR data to the atom-connectivity information (fragments) to be entered to the structure generator GENOA, and in the process, for taking into account the symmetry implications of these data. In our approach, the computer accepts signal-connectivity information, which the user reads directly from the 2-D NMR data. The computer then generates the fragments of structure compatible with these data and their symmetry implications.

DESCRIPTION OF THE PROGRAMS

The system of programs for the interpretation of 2-D NMR is outlined in Fig. 1. It can be divided into three separate sections: input, interpretation, and structure assembly.

Input

The program INPUT accepts data from 1-D and 2-D NMR experiments. These data are typed by the user at a standard terminal. The subroutine for 1-D NMR data accepts chemical shifts from ^{1}H- and ^{13}C-NMR, and integral and exchange information (for ^{1}H-NMR) or hydrogen multiplicities (for ^{13}C-NMR). All of this information, together with the molecular formula, is required for the subsequent interpretation. The 2-D NMR subroutine accepts data from three-bond proton—proton correlation (COSY), one-bond proton—carbon correlation, and one-bond carbon—carbon correlation (2-D INADEQUATE) [3]. The observed correlations are entered by the user as pairs of NMR shifts. At the present time, the 2-D programs do not use long-range coupling (greater than three-bond) obtained from the COSY

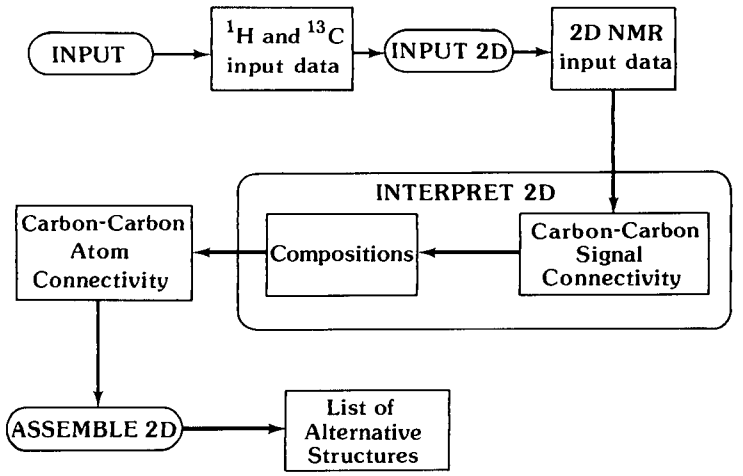

Fig. 1. Organization and information flow of the 2-D CASE programs.

data, and the user is warned not to enter any weak couplings that could be long-range. Any other data which give similar connectivity between NMR signals (such as proton–proton decoupling or the 1-D INADEQUATE experiment) can be used as well.

Interpretation

The program INTERPRET2D accepts the files of input data produced by INPUT and INPUT2D and creates a list containing every possible carbon atom substructure consistent with these data. In the first step, the input data are used to derive the connections between carbon signals. The INADEQUATE data give this carbon–carbon signal connectivity directly. The COSY and proton–carbon correlation data are used to derive carbon–carbon signal connectivity by identifying carbon signals that bear coupled vicinal protons.

In the next step, a specific number of carbon atoms is assigned to each carbon signal. That number may be greater than one for some signals only for molecules with symmetry. This step corresponds to the mathematical process of finding a composition, so that each possible specific assignment of carbon atoms to ^{13}C-NMR carbon signals will be referred to here as a composition. To allow for every possible interpretation, INTERPRET2D must consider every possible composition.

This concept is illustrated in Table 1 with data obtained from *o*-xylene (1). This compound displays four signals in its ^{13}C-NMR spectrum and has eight carbon atoms. Two compositions which are compatible with this information and the molecular formula are shown. However, of the two, only composition 1, with each carbon signal corresponding to two carbon atoms, gives rise to physically valid structures. One of the functions of INTERPRET2D is to eliminate physically impossible compositions.

TABLE 1

Possible compositions for *o*-xylene

Signal	*a*	*b*	*c*	*d*
Composition 1	2	2	2	2
Composition 2	1	3	2	2

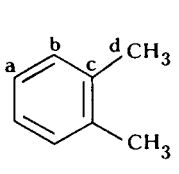

1

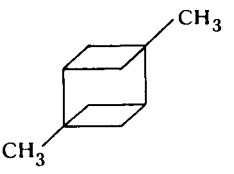

2

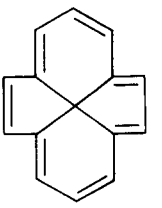

3

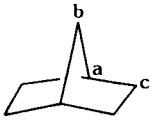

4

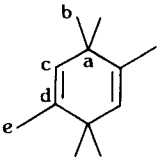

5

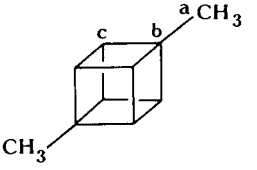

6

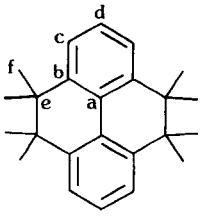

7

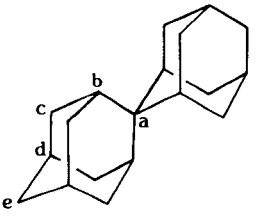

8

For this purpose, some elementary concepts from group theory are used. Symmetrical atoms in a molecule must define, through the operations which exchange the atoms, either the point group of the molecule or a subgroup of it. A subgroup defined in this manner is known as a site exchange group [4]. Using the molecule 2 (point group C_{2h}) as an illustration, the methyl groups are exchanged by the C_2 axis, and thus their site exchange group is C_2. The methylene groups are exchanged by both the C_2 axis and the plane, so their site exchange group is C_{2h}. It is important to note that the order of the site exchange group is equal to the number of atoms which define it.

Thus, the site exchange order for the methyl group is 2, and for the methylene groups, 4.

Point groups C_{nh}, D_n, D_{nd}, and D_{nh} each have a unique central location which may be occupied by a single atom with C_1 site exchange symmetry. An example is the hypothetical compound 3. The program will not allow more than one atom with C_1 site exchange symmetry when these point groups are used. The non-axial point groups T_d, O_h, and I_h are not used, because the corresponding compounds are generally trivial structure elucidation problems and the more complex relationships between the subgroups would greatly complicate the subsequent bonding algorithm.

Each point group has a limited number of subgroups, and therefore only a limited number of possible site exchange groups. In turn, this restricts the numbers of atoms that may be symmetric to each other (and share the same ^{13}C signal). The orders of the site exchange groups can be found by examining the unique symmetry environments of each point group. For example, the possible orders for C_{2v} are: (1) for points on the C_2 axis (atom *b* of structure 4); (2) for points in the plane (atoms *a* of 4); and (4) for points not lying in any symmetry element (atoms *c* of 4).

By means of this mental exercise with each axial point group, all of their possible site exchange orders have been determined. These are listed in Table 2. In a compound with no dynamic rotation, these site exchange orders will correspond directly with the composition numbers. Together, the composition numbers must be equal to, or a subset of, one of the sets of site exchange orders in Table 2. Any composition that does not match one of the sets of site exchange orders in Table 2 can therefore be eliminated from further consideration. Note that composition 2 of *o*-xylene (point group C_{2v}, $n = 2$) does not match any of these sets. Additional examples of valid compositions, for structures 4—8, are shown in Table 3.

Rotation within a molecule can make a set of atoms, which are not in the same site exchange group, symmetrical on the NMR time scale. Without explicit consideration of rotation, the exclusion of a valid connectivity (and ultimately a possibly correct molecular structure) might occur. To prevent this, possible two- and three-fold rotations are searched for as a composition is fitted to a point group. When a rotation is found, the symmetry of all atoms assigned to the rotation is reduced by a factor of 2 or 3, and another attempt is made to fit the composition to a point group. This overall process is illustrated for 7-*tert*-butylnorbornane (9) in Table 4.

Connectivity information from the 2-D NMR data is used to eliminate some rotations which are physically impossible. Without this step, structures could be produced on the basis of a rotation around a tetracoordinate carbon atom (going through a planar intermediate), or a rotation of one ring of naphthalene relative to the other ring, for example. Each rotation must have a limited number of hub atoms about which the other atoms rotate. To check that a possible rotation is valid, these hub atoms are searched for.

The first step in identifying a rotation is finding the rotating atoms. This is

TABLE 2

Axial point groups and their site exchange orders

Point groups	Possible site exchange orders
C_s C_n S_n	1, n
C_{nv}	1, n, $2n$
C_{nh} D_n	1 (unique), 2, n, $2n$
D_{nh} D_{nd}	1 (unique), 2, n, $2n$, $4n$

TABLE 3

Valid compositions for compounds **4**—**8**

	4	**5**	**6**	**7**	**8**
Point group:	C_{2v}	C_{2h}	D_{3v}	D_{2h}	D_{2d}
n (from Table 2):	2	2	3	2	2
Composition numbers					
a	2	2	2	2	1
b	1	4	2	4	4
c	4	2	6	4	8
d		2		2	4
e		2		4	2
f				8	

TABLE 4

Composition validation for 7-*tert*-butylnorbornane (**9**)

Signal	Invalid composition	÷	Rotation	=	Valid composition
a	3		3		1
b	1		1		1
c	1		1		1
d	2		1		2
e	2		1		2
f	2		1		2

a set of carbon atoms corresponding to a single ^{13}C signal whose composition number is divisible by 2 or 3 (e.g., signal *a* in compound **9**). Next, any atoms which are hubs of rotation must be identified. The composition number for these atoms must be equal to the composition numbers of the rotation atoms divided by the rotation number. In other words, they must possess the same symmetry as the rotating atoms, but without the rotation (signal *b* of **9**). Finally, any other connections of these centers of rotation are examined. These are the bonds around which the rotation occurs. There can be only one for each center of rotation. In compound **9**, this is the bond connecting signals *b* and *c*.

This process is repeated to find rotations upon rotations, as in the triphenylmethyl group of compound **10** (Table 5).

TABLE 5

Composition validation for 7-triphenylmethylnorbornane (10)

Signal	Invalid composition	÷ Rotation	= Invalid composition	÷ Rotation	= Valid composition
a	3	1	3	3	1
b	6	2	3	3	1
c	6	2	3	3	1
d	3	1	3	3	1
e	1	1	1	1	1
f	1	1	1	1	1
g	2	1	2	1	2
h	2	1	2	1	2
i	2	1	2	1	2

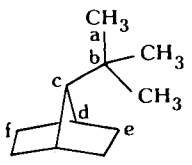

9

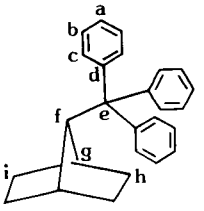

10

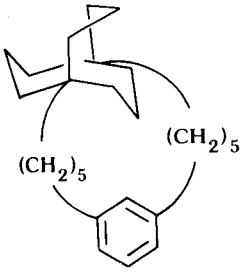

11

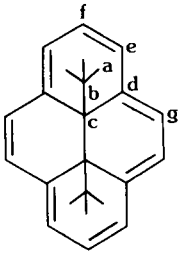

12

The algorithm does rule out a very small number of valid molecules, such as the metaphane, **11**. This occurs only when the rotating atoms cross one of

the symmetry elements of the point group (or, in mathematical terms, when the total symmetry group of the molecule is not equal to the direct product of the point group and the dynamic rotation groups) [5]. In our opinion, molecules of this type can be excluded from consideration with a negligible loss of the reliability of the system.

The di-*tert*-butyl-dihydropyrene compound (**12**) illustrates all the concepts used in the INTERPRET2D program. Both *cis* (C_{2v}) and *trans* (C_{2h}) **12** would show seven ^{13}C-NMR signals. The two compositions which pass the tests just described, plus simple rules for carbon atom valency, are shown in Table 6. Neither composition as shown fits any of the sets of site exchange orders in Table 2, but when the *tert*-butyl rotation is removed, and the methyl composition number reduced from 6 to 2, both compositions fit the second and third sets.

Once the composition has been validated, a spanning forest is built. A concept from graph theory, a spanning forest is a maximal subgraph which contains no cycles. Expressed in chemical terms, the spanning forest consists of all the carbon atom connections that can be formed without closing any rings. One at a time, each carbon signal connection is expanded to one or more carbon atom connections using the composition. This process is illustrated in Scheme 1. Ring closure bonds (which are the connections not used in the spanning forest) are placed in a separate list. With the earlier described restrictions on the composition numbers, connected carbon signals will usually have composition numbers of the form n and $n \times m$, where n and m are integers. In this case, every atom corresponding to the first carbon signal is connected to m atoms corresponding to the second signal. The only exception is the connection of carbon signals with composition numbers 2 and 3, possible with point groups C_{nh}, D_n, D_{nd}, and D_{nh} (Table 2). In this situation, every atom corresponding to the first signal is connected to every atom of the second signal. By using this algorithm, the composition (Table 6), together with the carbon signal connectivity, uniquely defines the spanning forest.

TABLE 6

Valid compositions for compound **12**

Signal	Composition 12a	Composition 12b	Connected signals
a	6	6	*b*
b	2	2	*a, c*
c	2	2	*b, d*
d	4	4	*c, e, g*
e	4	4	*d, f*
f	2	4	*e*
g	4	2	*d*

Beginning with signal *a* of composition **12a**, methyl groups are joined to quaternary carbon atoms (signal *b*) in the ratio of 3:1 (step 1 of Scheme 1). The carbon ratio of signal *b* to *c* is 1:1 , so one quaternary carbon atom is bonded to each carbon atom of signal *b* in constructing the spanning forest (step 2). Treating signals in the order listed in Table 6, the process continues until spanning forest **12c** is formed. The last step, expansion of the *e*—*f* signal connectivity is restricted. Although the *e*—*f* atom composition ratio of 1:2 requires each *e* carbon atom to join to two *f* carbon atoms, the second connection is not made (cycle formation). In a similar fashion, composition 12b gives rise to spanning forest **12d**.

In the final step of interpretation, ring closures consistent with signal connectivity are executed. Because of this last step, it is possible for a

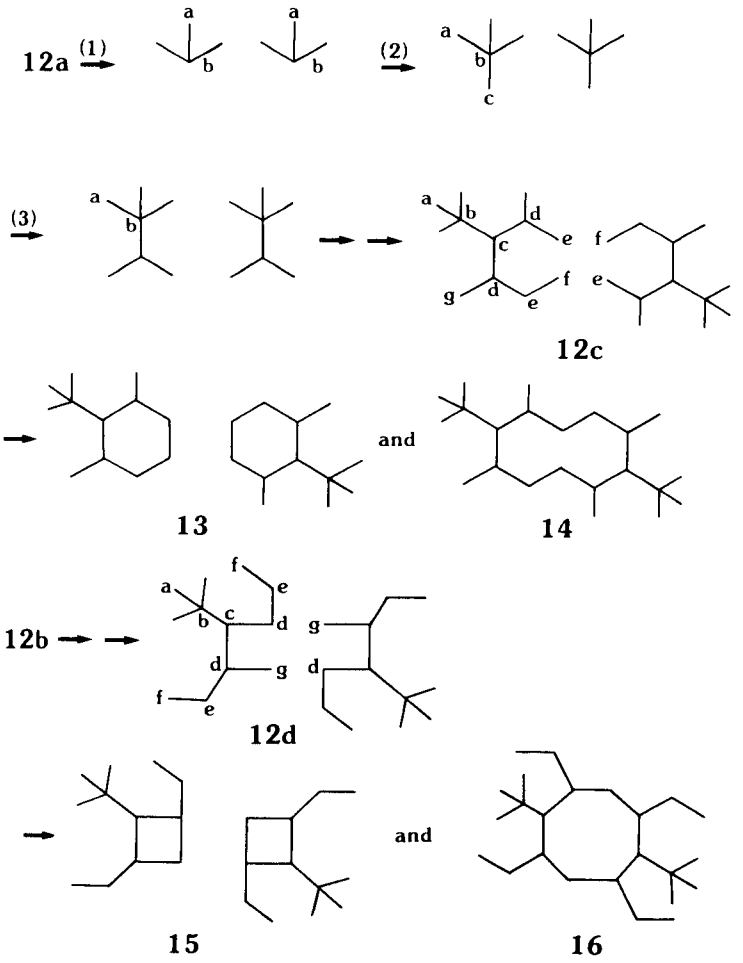

Scheme 1. Expansion of carbon signal compositions to carbon atom substructures.

spanning forest to give rise to more than one carbon atom substructure. These are produced by permuting any symmetrical ring closure bonds among the atoms corresponding to the carbon signal connectivity. Each possible carbon atom substructure is then tested for the correct symmetry and uniqueness against previous carbon atom substructures [6]. It should be noted that each substructure specifies carbon atom connectivity, but not the multiplicities of the bonds joining these atoms.

In the case of the di-*tert*-butyldihydropyrene example, each spanning forest has a pair of symmetrical ring closure bonds. The ring closure bonds for spanning forest 12c are a pair of *e*—*f* bonds. Permuting the ring closure bonds (which in this case is just an exchange) among the possible atoms gives two carbon atom substructures for each composition. Substructure 13 can be assembled to the dihydropyrene 12.

Assembly

To build molecular structures, the carbon atom substructures need to be connected and specific bond types (i.e., single, double, triple) must be assigned. The earlier program ASSEMBLE [7] was used together with a driver program (ASSEMBLE2D) to feed it each set of the carbon atom substructures and any user-input constraints as individual problems.

Briefly, ASSEMBLE accepts non-overlapping fragments of connected atoms, local constraints (atom tags) specifying the environment (number and type of neighboring atoms, α—β unsaturation, vicinal hydrogens, containment in a small ring, etc.) around a specific fragment atom, and global constraints that characterize the molecule as a whole, e.g., specific substructures that must be present (and may overlap the entered structural fragments) or absent [1]. The user is prompted for any desired atom tags or substructure constraints, and ASSEMBLE2D then combines this information with each carbon atom substructure set produced by INTERPRET2D and hands them to ASSEMBLE as separate problems.

ASSEMBLE does not include an atom tag that allows the specification of the hybridization of a particular carbon atom in a fragment. Since such assignments may be possible with ^{13}C-NMR chemical shift data, a new hybridization tag was added to ASSEMBLE. These tags (SP3, SP2, and SP12) are applied automatically by the interpretation program based on the ^{13}C chemical shifts, as listed in Table 7. These values are merely current estimates of the reasonable maximal ranges for each hybridization type.

To assist the user in the selection of global constraints, a list of "forbidden" substructures was written, which contains structural features that are often incompatible with the chemistry of a natural product. These are listed in Table 8. The user is queried as to the possible presence of any of these substructures which are consistent with the molecular formula. At the user's option, these substructures are passed to ASSEMBLE. The user also has the option of adding additional atom tags and constraints not listed in Tables 7 and 8.

TABLE 7

Hybridization atom tags used for input to ASSEMBLE

Carbon type	^{13}C-NMR shift		Tag	Carbon type	^{13}C-NMR shift		Tag
	Min.	Max.			Min.	Max.	
CH_2	—	90.0	⟨SP3⟩	C	—	60.0	⟨SP3⟩
	90.0	—	⟨SP2⟩		60.0	110.0	no tag
					110.0	140.0	⟨SP12⟩
CH	—	60.0	⟨SP3⟩		140.0	180.0	⟨SP2⟩
	60.0	110.0	no tag		180.0	200.0	⟨=O⟩
	110.0	170.0	⟨SP2⟩		200.0	—	⟨SP2⟩
	170.0	—	⟨=O⟩				

The output of ASSEMBLE is a file of structures, which can be displayed at a graphics terminal and drawn on a digital plotter.

EXAMPLES

To illustrate the use of the system of programs, some examples of structure elucidation with 2-D NMR data were simulated. The first is the structure of dihydrobinor-S (**22**), determined recently by Krishnamurthy et al. [8], using the INADEQUATE experiment. All of the carbon–carbon signal connectivity was obtained, but because of the symmetry of the molecule, several structures are consistent with this information. Owing to the lack of functionality, no constraints were necessary for this problem. The seven structures **17**—**23** were produced as output from the linked programs. The source of this compound [hydrogenation of binor-S (**24**)] effectively rules out all structures except **22**.

The second example chosen is velloziolide, a natural product for which the structure elucidation included a 2-D INADEQUATE experiment [9].

TABLE 8

Supplied substructure constraints

Substructure[a]	Name	Substructure[a]	Name	Substructure[a]	Name
C=C=C	allene	NCOH	hydroxyamine/ isoamide	1:C(=S)OC-1	α-thionolactone
OO	peroxide			1:C(=O)SC-1	α-thiolactone
OHCOH	*gem*-diol	N=C=O	isocyanate	1:C(=S)NC-1	α-thiolactam
1:C(=O)OC-1	α-lactone	NO	oxime	SCOH	α-hydroxysulfide/ thiono acid
C=C=O	ketene	1:C(=O)NC-1	α-lactam		
NN	hydrazine/ diimide	OS	—	XC=O	acid halide
		NS	—	XC=S	thiono acid halide
C=NH	imine	CH=S	thioaldehyde	NX	N-haloamine
N=C=N	carbodiimide	C=C=S	thioketene	OX	hypohalite
NC+N	cyanamide	1:C(=S)SC-1	α-dithiolactone	SX	—

[a]In ASSEMBLE format.

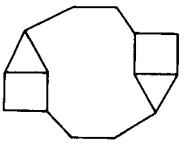

17

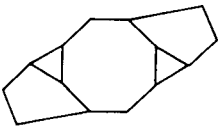

18

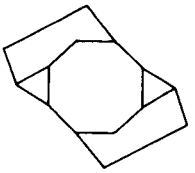

19

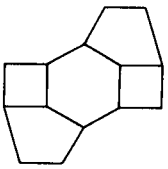

20

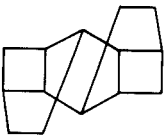

21

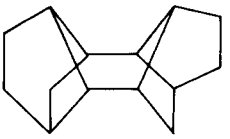

22

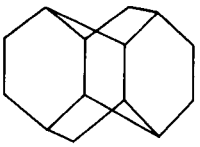

23

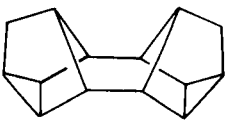

24

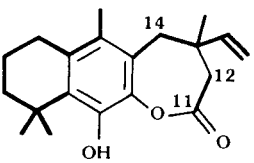

25

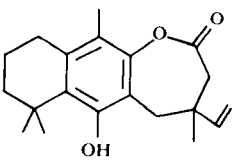

26

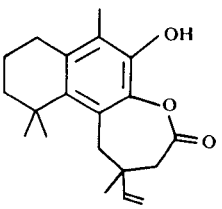

27

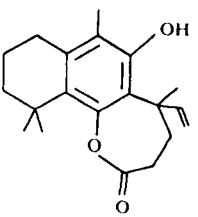

28

The heavy lines in structure 25 show the carbon—carbon connectivity that could be determined from the 2-D data. In this case, the connectivity obtained by 2-D NMR alone was not sufficiently restrictive to produce a small number of structures. By using available information that was derived from other sources, three atoms were constrained by atom tags: carbon-11 was specified as an ester carbon based on its ^{13}C chemical shift, and carbons-12 and -14 were required to have not more than one adjacent sp^2 atom and no adjacent oxygen atoms based on the ^{1}H-NMR shifts, and only geminal coupling. In addition, no N—N or N—O linkages or three-membered rings were allowed.

A total of 62 structures was produced, which could be divided into six phenols and 56 chemically unstable enols. The six phenols can be further

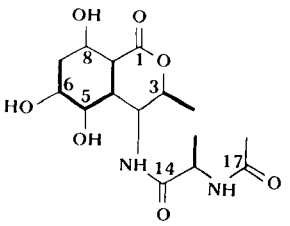

29

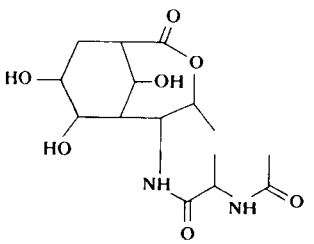

30

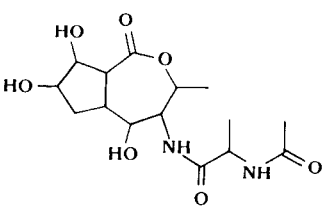

31

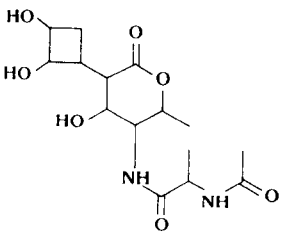

32

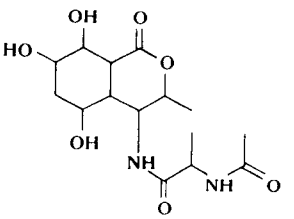

33

divided into two metacyclophanes and the four phenolic lactones **25**—**28**. In the original work, the correct structure was determined by an experiment based on the nuclear Overhauser effect using the phenylmethyl group and comparison of the ^{13}C-NMR of the aromatic carbon atoms to other *o*-dioxy substituted aromatic compounds.

The third example is a derivative of actinobolin, an antibiotic, the structure of which was determined manually in this laboratory several years ago without the benefit of 2-D NMR experiments [10]. The COSY and carbon—proton correlation spectra were obtained for *N*-acetyldihydroactinobolin (**29**). Because of overlapping signals and weak vicinal coupling in the proton-NMR, not all of the theoretically possible connectivities were observed. The heavy bonds in **29** show the carbon—carbon connectivity that the INTERPRET program produced from the input data.

Because a proportionally smaller amount of the molecule could be inferred from the 2-D NMR data, a larger number of constraints was necessary to limit the structures produced to a manageable number. Seven atom tags were used: from the ^{13}C-NMR, carbon-1 was identified as a lactone carbonyl, and carbons-14 and -17 as amide carbonyls. Carbons-5, -6, and -8 were shown to be bonded to the hydroxy groups based on couplings observed in the COSY spectrum (coupling to heteroatom-bound protons is not presently used by INTERPRET2D). Carbon-3, from its chemical shift, must be bonded to an oxygen.

From hydrolysis, the compound was known to contain an *N*-acetyl alanyl group. Because the compound was obtained by reduction of a β-keto lactone, it must contain a β-hydroxy lactone. The compound consumed exactly one equivalent of periodate, and therefore must have exactly one vicinal diol. Oxidation with permanganate produced threonine, which contains a N—C—C—CH_3 group. Because the *N*-acetyl alanyl group also contains this substructure, the constraint used specified that all structures must contain at least two of these groups.

As before, heteroatom—heteroatom linkages and three-membered rings were forbidden. Also forbidden were α-amino alkoxy compounds and β-lactones. Finally, the number of sp^3 carbon atoms was set at 12.

The output for this problem was the five structures **29**—**33**. The corresponding β-keto ester of structure **30** would form an anti-Bredt structure if it were to enolize, and because the β-keto ester is known to enolize easily, this structure can be ruled out of consideration. In the original work, the correct structure was determined by further degradation studies.

Experimental

All programs described were developed and run on a Prime 450 minicomputer and are written in FORTRAN 77 (the earlier program ASSEMBLE was written in FORTRAN IV). The interpretation program is about 600 lines of code. In all cases, interpretation of 2-D NMR data used less than five minutes of CPU time on the Prime 450.

Conclusions

This work was based on the idea that developing a system for automated structure elucidation using 2-D NMR can increase the productivity of chemists working on organic or natural products. Because of the complexity of current problems in structure elucidation, the 2-D NMR data alone are usually not sufficient to limit the possible structures to a small number. The system of programs developed can accept both the 2-D NMR data and a wide variety of user-specified information, and generate all structures consistent with both sets of information.

This system does have limitations. It produces only topological structures with no stereochemistry. At present, it does not use long-range or NOESY 2-D NMR data. Additional required substructures (as might be obtained from other spectroscopic methods) can be entered as constraints, but are used very inefficiently by ASSEMBLE. To solve some of these problems, the use of 2-D NMR data with a new structure reduction-based structure generator COCOA [11] is under investigation.

REFERENCES

1 M. E. Munk, C. Shelley, H. B. Woodruff and M. O. Trulson, Fresenius' Z. Anal. Chem., 313 (1982) 473.
2 M. R. Lindley, J. N. Shoolery, D. H. Smith and C. Djerassi, Org. Magn. Reson., 21 (1983) 405.
3 A. Bax, Two-dimensional Nuclear Magnetic Resonance Spectroscopy in Liquids, Delft, 1982.
4 (a) K. Mislow and J. Siegel, J. Am. Chem. Soc., 106 (1984) 3319.
(b) R. L. Flurry, Jr., Theor. Chim. Acta, 31 (1973) 221.
(c) S. L. Altmann, Rev. Mod. Phys., 35 (1963) 641.
5 S. L. Altmann, Proc. R. Soc. A, 298 (1967) 184.
6 C. A. Shelley, M. E. Munk and R. V. Roman, Anal. Chim. Acta, 103 (1978) 245.
7 C. A. Shelley, T. R. Hays and M. E. Munk, Anal. Chim. Acta, 103 (1978) 121.
8 V. V. Krishnamurthy, J. G. Shih and G. A. Olah, J. Org. Chem., 50 (1985) 3005.
9 A. C. Pinto, M. L. A. Gonalves, B. F. Raimundo, A. Neszmelyi and G. Lukacs, J. Chem. Soc., Chem. Commun., (1982) 293.
10 F. J. Antosz, D. B. Nelson, D. L. Herald, Jr. and M. E. Munk, J. Am. Chem. Soc., 92 (1970) 4933.
11 B. D. Christie and M. E. Munk, J. Chem. Inf. Comput. Sci., submitted.

Analytica Chimica Acta, 200 (1987) 363–377
Elsevier Science Publishers B.V., Amsterdam — Printed in The Netherlands

AUTOMATED RECOGNITION OF COMMON GEOMETRICAL PATTERNS AMONG A VARIETY OF THREE-DIMENSIONAL MOLECULAR STRUCTURES

YOSHIMASA TAKAHASHI, SHIGENORI MAEDA and SHIN-ICHI SASAKI*

Research Center for Chemometrics, Toyohashi University of Technology, Tempaku, Toyohashi 440 (Japan)

(Received 14th April 1987)

SUMMARY

A computer program, COMPASS, is described for searches for common geometrical pattern among a set of chemical compounds. The approach is based on a distance geometry method. The program allows the user to specify some search conditions which are defined with weighting atoms of different types and distance allowance. Information of charges on each atom in molecules can also be included. Examples are presented to illustrate the abilities of the program in relation to structure/activity problems.

There have been various important attempts to determine structural fragments which are common among a group of chemical compounds. In these studies, structural features of compounds having identical or similar properties are compared in order to identify common structural fragments which would be closely related to their properties. In the field of medicinal chemistry, in particular, investigations on structure/activity relationships are an active area of research. For groups of compounds which show identical or similar biological activities though they are different in chemical structure, it is assumed in these studies that the activities in question should be attributed to a partial structure which the compounds contain in common. Two major approaches have been used. One relies on statistics and pattern recognition based on model equations, while the other is to establish and recognize similarities and differences among the molecules in question by examining their structural features. For the latter, some methods have been

*Dr. Shin-ichi Sasaki is Vice-President of the Toyohashi University of Technology. He was born in 1925 and obtained his B.S. and D.Sc. degrees from Tohoku University. Honors include the 1974 Award of the Japan Society for Analytical Chemistry and the 1980 Dr. Niwa Memorial Medal of the Japan Information Center of Science and Technology. He is active in the Japan Society for Analytical Chemistry and is a Founder member of the Division of Chemical Information and Computer Science of the Chemical Society of Japan. He is on the editorial board of several journals concerned with applications of computers in chemistry. His prime current interests are automation in process control and structure/activity relationships.

0003-2670/87/$03.50

proposed which are aimed at recognizing and detecting, at a topological level, partial structures which are contained in all compounds of a group that show similar biological actions [1—4]. As previously reported [5, 6], a program system, MAXFIT, has been developed which examines chemical structural formulae in terms of chemical graphs to conduct, also at a topological level, searches for, and detection of, the maximal common substructure contained in two or more different chemical structures. Studies so far have been limited to establishing common substructures at a topological level. For biologically active compounds, however, structural factors which contribute to the development of pharmacological effects should be investigated not only topologically but also at a three-dimensional level in order to permit more detailed analysis of the relationships between structures and activities. Recently, computer graphics has become more widely used and techniques for utilizing it have progressed, making it possible to look through several structures that overlap each other [7—9]. One such technique is called the "retrieval of 3D-partial structure" [7]. A query structure is designated at a three-dimensional level, in a similar manner to the conventional substructure retrieval, and an operation is specified to establish if it exists simultaneously in two or more structures. Other attempts [8, 9] have also been made to examine structures overlapping each other and to compare the molecular shapes quantitatively.

In addition to investigations by mere structure-overlapping methods and retrieval of three-dimensional substructures, there have been studies focused on developing an automated operation for recognizing common substructures, which take into account the three-dimensional geometry of the molecules [10, 11]. This technique is greatly different from conventional ones in that designation of a query structure is not required. However, the operations reported so far seem to lack flexibility because of various restrictions. In particular, they generally require troublesome preliminary processing for which structural functionalities are taken into consideration, and other operations related to this processing such as conversion of three-dimensional geometrical distances into integer code numbers.

In the present report, a more general technique is proposed for automated recognition of three-dimensional common geometrical patterns, which is based on the "distance geometry method" developed by Crippen and coworkers [12, 13]. A new system on the basis of our algorithm will also be described.

METHOD

For the search of a three-dimensional common geometrical pattern in molecules, an algorithm is developed which meets the following prerequisites (1, 2) and requirements (3—5):

(1) the coordinates to represent the molecules are rigid;

(2) a molecule is treated as a set of points in three-dimensional rectangular coordinate space;

(3) it should be possible to weight these points to indicate the atomic species and electron charge characteristics;

(4) it should be possible to distinguish between geometries of enantiomers;

(5) simultaneous search of three or more molecules should be possible.

Outline of algorithm

An algorithm is described below which is designed to search for a pattern of common geometry in two molecules with different structures. First, three-dimensional coordinate data of each molecule are input. If all atoms are assumed to be equivalent, the structure of each molecule can be expressed by a set of points in the three-dimensional rectangular coordinate space. Then, it becomes possible to define the geometry of each molecule only by using a distance matrix corresponding to the set of points. Such distance matrices are easily developed from three-dimensional atomic coordinate data of the molecules. A distance matrix so produced is considered to represent an edge-weighted complete graph [14] which consists of the same number of nodes as that of constituent atoms in the molecule. Thus, the graph-theory approach can be applied to the search for a three-dimensional common geometrical pattern. The complete graphs for the two molecules are compared with each other according to the criteria of commonalities based on edge-weight, and then a new graph can be produced, which is a so-called docking graph [15]. The docking graph formed is either a connected or a disconnected graph, which contains information on the edges with the same weights (under prescribed conditions such as allowance of distance) as those given to the above-mentioned two complete graphs. Therefore, searching for some edge-weighted maximal common subgraph for the two complete graphs is equivalent to searching for a clique [14] in this docking graph. The set of nodes of each subgraph, which is a candidate for the clique, obtained in this search process corresponds to the set of constituent atoms of the desired common geometrical pattern. And the set of nodes consisting of the clique finally obtained is correlated with the constitution of the maximal common geometrical pattern and the set of their atoms.

Docking graph

For two graphs, G_1 and G_2, a docking graph, $\mathrm{Doc}(G_1, G_2)$ is defined as follows. It is assumed here that the weights on the distances between all nodes in each graph can be defined completely.

$$\mathrm{Doc}(G_1, G_2) = \langle \mathbf{V}, \mathbf{E} \rangle$$

where $V = \langle (\sigma,\mu) | \sigma \in G_1, \mu \in G_2 \rangle$

and $E = \langle [(\sigma_i,\mu_k), (\sigma_j,\mu_l)] \,||w_1(i,j) - w_2(k,l)| \leqslant \delta \rangle$

$w_1(i, j)$ is the weight on the edge between nodes i and j in graph G_1, and $w_2(k,l)$ is the weight on the edge between nodes k and l in graph G_2. Here,

V and E represent the sets of constituent nodes and edges in the docking graph $Doc(G_1, G_2)$, respectively, while σ and μ denote the nodes contained in graphs G_1 and G_2, respectively, and δ is the tolerance of weights which are considered to be equivalent at the time of forming the docking graph. In the present case, the weights correspond to the edge lengths, or the interatomic distances. When $\delta = 0.5$, for example, all edge weights that satisfy the following equation are assumed to be equivalent: $-0.5 \leqslant (w_1 - w_2) \leqslant 0.5$. The procedure for making the docking graph is described below, referring to an illustrative example shown in Fig. 1.

Two molecules, M_1 and M_2, are assumed (Fig. 1a). For these molecules, distance matrices in which all atoms are taken into account are developed, and edge-weighted complete graphs, G_1 and G_2, relevant to them are considered (Fig. 1b). It should be noted, however, that at this stage, only information on the relative configuration between the atoms is clear while the information on the absolute configuration is not known. If δ is assumed to be zero for simplification, the docking graph, $Doc(G_1, G_2)$, is obtained as shown in Fig. 1(c).

Clique search

To detect the clique, a tree search method is adopted which is essentially based on the back-track procedure proposed by Bron and Kerbosch [16].

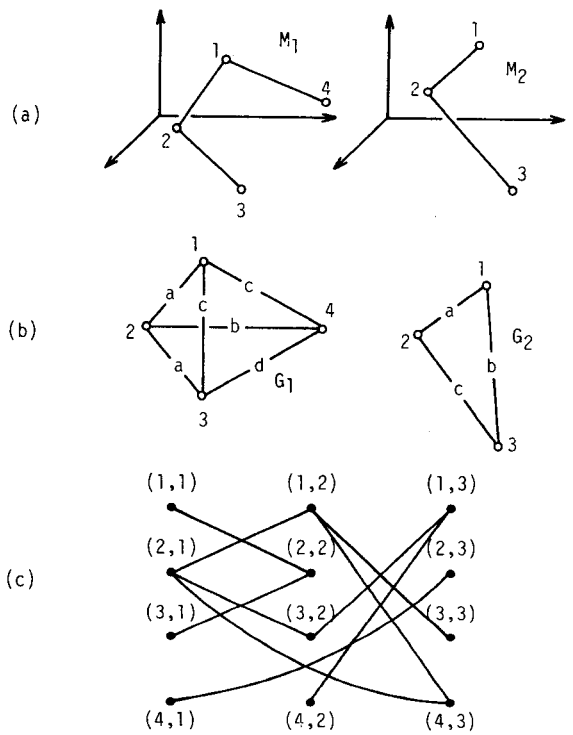

Fig. 1. Docking graph from graphs G_1 and G_2.

The procedure was improved to develop basic algorithms. First, an algorithm was worked out after setting up the following prepositions for graph $G(=\langle V,E\rangle)$:

$\langle P_l\rangle$: The set of constituent nodes in the complete partial subgraph at search level l

$\langle C_l\rangle$: the set of candidate nodes to be used for extending the complete partial graph at search level l

$\langle A(l,k)\rangle$: the set of all nodes adjacent to V_k, the kth element in $\langle C_l\rangle$

$\langle CSG\rangle$: the set of constituent nodes in the maximal complete subgraph at the stage in question

$N\langle S\rangle$: a function to be used for evaluating the number of elements in set S.

Then, the algorithms are

(1) $\langle P_0\rangle \leftarrow \langle\phi\rangle, \langle C_0\rangle \leftarrow \langle V\rangle$
for $i = 1$, $N(V)$ do $K(l) \leftarrow 0$
$l \leftarrow 0$, SIZE $\leftarrow 0$

(2) $K(l) \leftarrow K(l) + 1$
$l \leftarrow l + 1$
$\langle P_l\rangle \leftarrow \langle P_l\rangle \vee \langle v_{k(l)} | v_{k(l)} \in \langle C_{l-1}\rangle\rangle$
$\langle C_l\rangle \leftarrow \langle C_{l-1}\rangle \wedge \langle A(l-1), K(l)\rangle$
if $\langle C_l\rangle \neq \langle\phi\rangle$ then go to (2)
if $N(C_l) <$ SIZE then go to (3)
if $N(C_l) >$ SIZE then SIZE $\leftarrow l$
$\langle CSG\rangle \leftarrow \langle P_{SIZE}\rangle$

(3) $l \leftarrow l + 1$
if $l < 0$ then stop
if SIZE $\leqslant (l + N(C_l) - K(l))$ then go to (2)
$K(l) \leftarrow 0$
repeat (3)
end.

Figure 2 illustrates the process of clique search for $Doc(G_1, G_2)$ presented in Fig. 1(c). For convenience, sequential numbers are given to the nodes in this graph. The branching points in the search tree shown in Fig. 2 are represented by the above-mentioned $\langle P_l\rangle$ and $\langle C_l\rangle$. The left-hand portion of the tree expresses the set of constituent nodes in the complete subgraph at the relevant stage, while the right-hand portion represents the set of candidate nodes to be used for its extension. The superscript symbols indicate the labels given to the branching points. The search operation starts at the root point, denoted by a, of the search tree. At the starting point, the initial sets, $\langle P_0\rangle$ and $\langle C_0\rangle$, are defined by empty $\langle\phi\rangle$ and all constituent nodes in the given graphs, respectively. The search operation is conducted in the order of the node number, starting at the minimum. Where node 1 is the element of $\langle P_1\rangle$, 5 is the only element adjacent to it and therefore $\langle C_1\rangle = \langle 5\rangle$ (branch point b). Then, set $\langle P_2\rangle$ of $\langle 1,5\rangle$, which includes node 5, is considered (branch

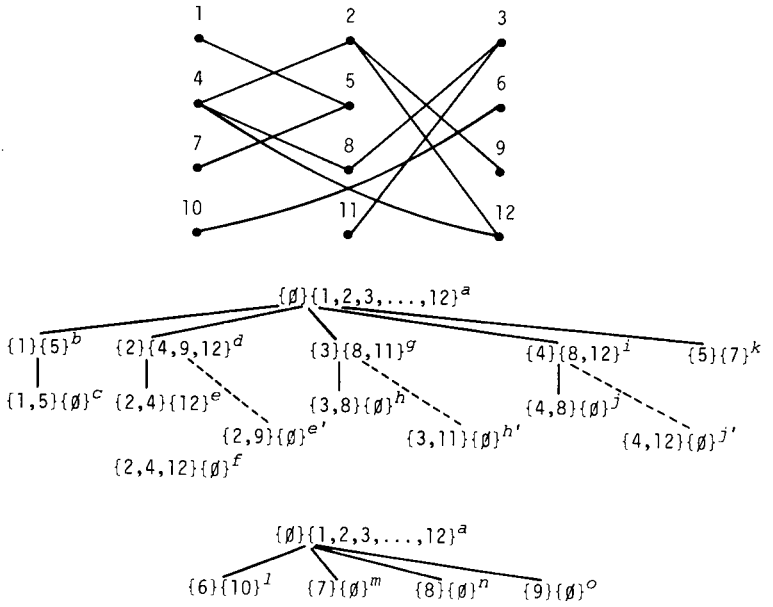

Fig. 2. A schematic tree for clique-finding procedure (ϕ is null set).

point c). In this case, $\langle C_2 \rangle = \langle \phi \rangle$, and the search operation which covers node 1 finishes. At this stage, ⟨1,5⟩ is adopted as a candidate clique. The position denoted by d is the branching point which is given when the search point is back-tracked from c to a with $\langle P_1 \rangle$ being assumed to be ⟨2⟩; $\langle C_1 \rangle$ becomes ⟨4, 9, 12⟩ in this case. When $\langle P_2 \rangle$ = ⟨2, 4⟩, node 12 is adjacent to both elements of $\langle P_2 \rangle$ and therefore node 12 is counted as a candidate node for extension. Thus $\langle C_2 \rangle$ = ⟨12⟩. Extension of $\langle P_2 \rangle$ by adding node 12 produces the relationships: $\langle P_3 \rangle$ = ⟨2, 4, 12⟩ and $\langle C_3 \rangle = \langle \phi \rangle$ (branch point f). Here, the previously detected candidate clique of ⟨1, 5⟩ is replaced by the new candidate of ⟨2, 4, 12⟩, which contains a greater number of constituent nodes. Besides, the other extension to e' should be examined after back-tracking to d. At this stage, however, only one element remains in the extended candidate-node set. If this one element is added to the number of clique candidate nodes detected before the extension, the sum total does not reach the maximum number of nodes of the clique candidate obtained so far. Thus, this search operation finishes because the nodes will not increase further. The next step is then conducted. Similar tree-search operations will be repeated according to the back-track procedure. For the example given in Fig. 2, the final clique is ⟨2, 4, 12⟩ with three constituent nodes to the set of nodes in the original docking graph, i.e., ⟨(1, 2), (2, 1), (4, 3)⟩. This indicates that the maximal common geometrical pattern of molecules M_1 and M_2 can be described by three atoms (i.e., ⟨1, 2, 4⟩ and ⟨2, 1, 3⟩) and their positions in the X, Y, Z coordinates.

Application to three or more molecules

Theoretically, it would be possible to apply the above algorithm directly to three or more molecular structures to establish the maximal common geometrical pattern among them. This is not practical, however, because the number of nodes in the docking graph to be produced increases exponentially with the number of molecular structures to be examined, requiring a huge computer capacity for the operation. For instance, 20^5, or 3,200,000, nodes would be required to establish a docking graph for five molecules consisting of 20 atoms each. In the proposed system the following procedure is used to avoid such exponential explosion. First, a "reference molecule" is selected from the group of molecules to be examined. In view of the nature of the algorithm it is desirable to adopt the molecule with the smallest number of constituent atoms. Then, another molecule which contains the next smallest number of atoms is selected and used in addition to the first molecule to develop a docking graph by the procedure described above, and the operation is repeated to search for candidate cliques. Each time a common geometrical pattern is detected during this clique search process, an examination is conducted to establish whether or not the pattern is also contained in the other molecules. This operation is equivalent to retrieval of three-dimensional substructures by using the 3-D geometry of the constituent atoms in a molecule as the query. Of the two geometrical patterns relevant to the clique in question, the one that originates from the geometrical pattern of the reference molecule should be used for the query structure in this case. A clique search procedure based on the formation of a docking graph can also serve for this purpose. Figure 3 diagramatically illustrates a scheme of searching for a common geometrical pattern simultaneously present in two or more molecules.

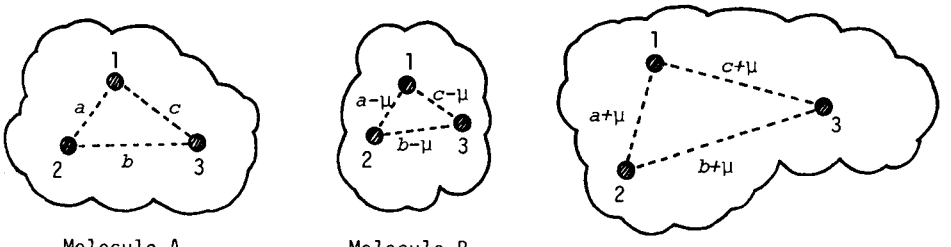

$P(A) = \{1,2,3 \mid all \in A\}$
$P(B) = \{1,2,3 \mid all \in B\}$
$P(C) = \{1,2,3 \mid all \in C\}$

$P(A)$ vs. $P(B)$: $|d^B_{12} - d^A_{12}| = |d^B_{13} - d^A_{13}| = |d^B_{23} - d^A_{23}| = \mu$

$P(A)$ vs. $P(C)$: $|d^C_{12} - d^A_{12}| = |d^C_{13} - d^A_{13}| = |d^C_{23} - d^A_{23}| = \mu$

$P(B)$ vs. $P(C)$: $|d^C_{12} - d^B_{12}| = |d^C_{13} - d^B_{13}| = |d^C_{23} - d^B_{23}| = 2\mu$

$\therefore P(A) = P(B), P(A) = P(C), P(B) \neq P(C)$ [with allowance μ].

Fig. 3. Distance commonality and allowance in the common geometrical pattern search for three or more molecules.

Thus, by establishing a reference molecule selected from three or more molecules and applying the three-dimensional substructure retrieval procedure, detection of a geometrical pattern which is contained commonly in three or more molecules can be done within the range of practical computer capacity. The following points should be noted. Common geometrical patterns which were obtained as a result of a pairwise search using a reference molecule-based query pattern are not always equal to each other within the prescribed tolerance. As an example, three molecules (A—C, Fig. 3) are considered. If molecule A is selected as the reference molecule, the geometric patterns of B⟨1, 2, 3⟩ and C⟨1, 2, 3⟩ are equal to A⟨1, 2, 3⟩ within the required tolerance when $\delta = \mu$. For the relations of B and C, however, the differences in distance between each set of nodes are all 2μ. But B⟨1, 2, 3⟩ $\neq$ C⟨1, 2, 3⟩, which indicates that these three geometrical patterns are not always equal when the tolerance is $\delta < 2\mu$. This also suggests that different results may be obtained from the same group of molecules depending on which one is selected as the reference molecule. A checking procedure for avoiding this is to compare the common pattern provided by the above procedure with a geometric pattern which originates from a molecule other than the reference. This operation is simple but rather time-consuming because of a large number of combinations. In view of this, the former approach still remains a useful approach. The program is designed to serve for either processing procedure by designating an appropriate option.

Identification of enantiomer geometry

A major problem with expressing a three-dimensional structure by a distance matrix is that the geometry of enantiomers cannot be distinguished. No information on enantiomer geometry is incorporated in the common geometric patterns which are obtained by the clique search method using a docking graph based on a distance matrix. For checking that geometry, three-dimensional coordinate data on the molecule are used in addition to the distance matrix in conducting the following operations: (1) combinations of four points ($_nC_4$, where n denotes the number of nodes) are produced from the set of nodes which are contained in the common geometric pattern recognized on the basis of a reference molecule; (2) three of the vertexes of each tetrahedron are selected arbitrarily to establish a reference plane, and the remaining one is taken as the probe point; (3) the reference plane is then looked at from such an angle that the constituent nodes with increasing code numbers are clockwise. The tetrahedral geometry is represented by $+1$ if the probe point is beyond the plane, by -1 in the contrary case, and by 0 if all four points are in the same plane or can be regarded as being in the plane in view of the tolerance (Fig. 4).

In this way, a spatial pattern vector is developed which can represent the configurations of all possible tetrahedral geometries resulting from the geometric pattern in question, by three values (i.e., 1, -1 and 0). Such a pattern vector for the geometric pattern based on the other molecule to be compared is generated with the reference plane corresponding to that

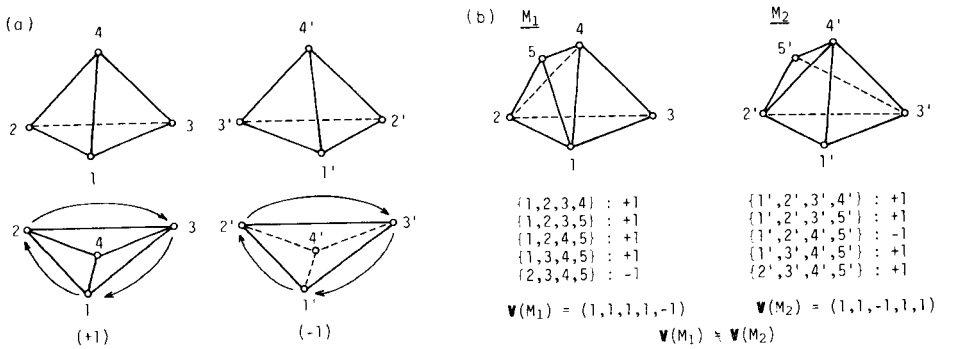

Fig. 4. Designation of configuration pattern vector in polyhedral geometry: (a) tetrahedral reference configurational pattern and the corresponding sample configurational pattern; (b) Generation and comparison of the configurational pattern vectors for two enantiomeric polyhedral geometric patterns.

of reference molecule. The enantiomer geometries of two distant-isomeric patterns can be distinguished from each other by comparing these two configurational pattern vectors.

RESULTS AND DISCUSSION

Based on the above algorithm, a system named COMPASS (COMmon geometric PAttern Search System) was developed, it serves to determine automatically common geometric patterns among three-dimensional molecular structures. Three-dimensional coordinate information on the molecules is used for the calculation. In addition, data such as the charge and connection table of each atom are also input when required. The latter data are utilized for weighting the atoms to express their atomic species, environmental conditions and other characteristic features. Parameters that can be used in COMPASS for weighting atoms are listed in Table 1. Charges of atoms can be assumed within a certain tolerance. By this processing operation, differences in atom type and electronic environment, as well as interatomic distances, can be reflected in the process for generating the docking graph to be used as the basis of the search for common geometric patterns. This operation, therefore, makes it possible to search for three-dimensional common geometric patterns which have distinctive chemical meanings (such

TABLE 1

Parameters useful for weighting in COMPASS

Atomic species	C, H, O, N, S, ...
Hybridization	sp^3, sp^2, sp
Valence type	e.g., nitrogen: —NH,>NH, =NH, —N(—)—, =N—, ≡N, :N(—)—, —N(+)(—)—, —N(+)=
Charge	Net charge on each atom (with allowance δ)

as those called pharmacophores). Furthermore, it is also possible to search for maximum common geometric patterns that contain some partial structures or geometric patterns specified by the user. Some examples of the application of the COMPASS are described below.

Example 1

As an example of the application of COMPASS, the maximal three-dimensional common geometric patterns between two molecules (haloperidide and milenperone) were sought. These molecules are known as dopamine antagonists. The coordinates were evaluated from data obtained by x-ray diffraction [17, 18]. The chemical structures of the molecules and results of the COMPASS operation are shown in the form of computer output in Fig. 5. For the search conditions, a distance tolerance of 0.5 Å was used and only the atomic species was used as weighting parameter. Four maximal common geometric patterns with 12 constituent atoms were obtained as given in Fig. 5, in which the numbers following the code numbers (F02, F10) indicate the numbers assigned to each atom in the structural formulae. In case

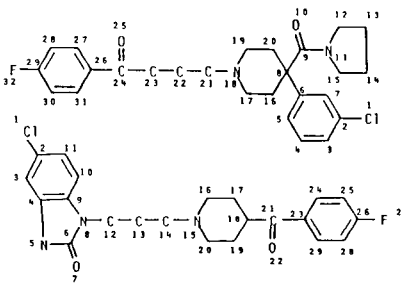

```
EXECUTION ========================
   INPUT-FILE :IN
   OUTPUT-FILE:OUT
   DATASET    :DATASET
-- SAMPLES --
     SAMPLE(1)= F02(Haloperidide)   (32)
     SAMPLE(2)= F10(Milenperone)    (29)
-- MATRIX SELECTION --
     DISTANCE MATRIX
      ALLOWANCE=  .50
-- MUTUAL CHECK --
     OFF
-- STEREO CHECK --
     OFF
-- NODE WEIGHT --
     ATOM TYPE=ON
     BOND TYPE=OFF
     CHARGE TYPE=OFF
-- NODE EXCLUSION --
       EXCLUSION     = NOT
-- FUNC. GROUP PRESERVATION --
       PRESERVATION = NOT
-- FUNC. GROUP COMPRESSION --
       COMPRESSION   = NOT
-- RESULT --
   ROTATION    1/   0
NO.  1
 (F02: 1)   2  3  4  5  6  7 20 21 23 29 31 32
 (F10: 1)   3  2 11 10  9  4 12 20 18 26 23 27
       2)   3  2 11 10  9  4 12 20 18 26 29 27
NO.  2
 (F02: 1)   2  3  4  5  6  7 20 23 29 30 31 32
 (F10: 1)   3  2 11 10  9  4 12 18 26 28 29 27
NO.  3
 (F02: 1)   2  6  7  8 17 18 19 20 21 22 26 30
 (F10: 1)  24 21 23 18 16 15 20 19 14 13 10  2
NO.  4
 (F02: 1)   2  6  8 16 17 18 19 20 21 22 26 30
 (F10: 1)  24 21 18 17 16 15 20 19 14 13 10  2

                NUMBER= 4
                SIZE  =12
```

Fig. 5. Maximal common geometric patterns found by COMPASS for haloperidide and milenperone. In weighting atoms, only different atomic species were considered for this search. The distance allowance is 0.5 A.

no. 1, two common geometric patterns for milenperone (F10) with one position occupied by a different constituent atom (23 or 29) are output, corresponding to a geometric pattern with 14 atoms, i.e., 2, 3, . . . , 32, which is contained in haloperidide (F20). This resulted from the use of distance tolerance only. The CPU time required was 30.9 s.

These results can easily be visualized by computer graphics for displaying superimposed structures. Structure superposition based on interatomic least-square fitting [19] was applied to the first pattern in case no. 1 in Fig. 5. The results obtained are illustrated in Fig. 6. The FITDISP program [20] was applied for the calculation of the structure superimposition and display of the structure.

Another search trial for the above two molecules was done by using additional information on the charges of the atoms in each molecule, "charge" in this case means the net charge (N) on each atom. The CNDO method [21] was used to calculate the point charge at the center of each atomic coordinate. Two modes of charge designation can be used in this system, in addition to the ordinary charge-tolerance designation. In one, a tolerance is designated in terms of the relative difference in charge between particular atoms to be compared (based on an idea similar to that for designation of distance tolerance); in the other, the weighting operation is done automatically according to range designation. Here, the latter mode is adopted and the atoms are weighted in three steps, i.e., $N \leqslant -0.100$, $-0.100 < N < 0.100$, and $0.100 \leqslant N$. Other search conditions including distance tolerance are the same as those used in the previous case. COMPASS finally provided eight maximal common geometric patterns, each composed of eleven constituent atoms. The CPU time required was 11.8 s. Of those obtained, the most interesting geometric pattern is illustrated in Fig. 7. The fluorine atom in the p-substituted benzoyl, the other benzene rings and carbonyl oxygen in the imido group in each molecule correspond consistently to their counterparts in the other molecule. Not only do the common portions of the two molecules displayed in Fig. 5 agree well with each other in terms of three-dimensional geometry, but also each atom in

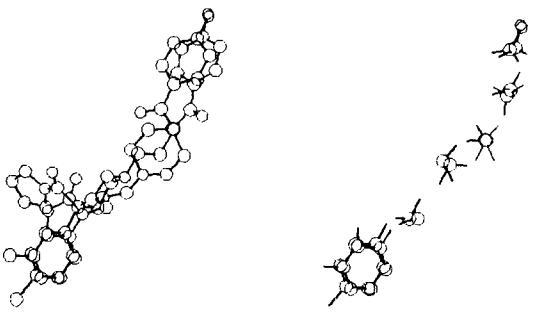

Fig. 6. Graphic representation for the first result in Fig. 5. The left-hand view shows the superimposition for the whole molecules, except for hydrogen atoms, and the right-hand view is for the relevant portions.

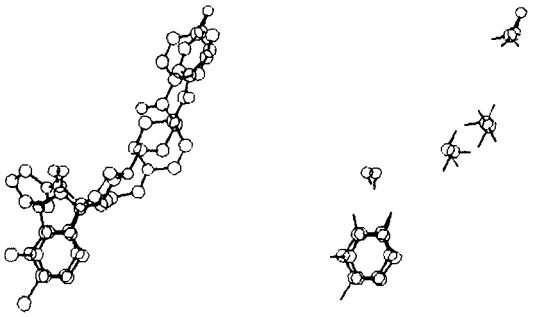

Fig. 7. The maximal common geometric pattern found by COMPASS. In weighting atoms, different atomic species and net atomic charges were considered in this search. The distance allowance is 0.5 Å.

one molecule, as expected from the search conditions, has a similar electronic environment to that of its counterpart in the other.

Example 2

In another example, COMPASS is applied to muscarine and related compounds. Muscarine acts as a neurotransmitter mainly for smooth muscles and secretory glands at postganglionic parasympathetic neuroeffector sites. With relatively rigid structures, muscarines are useful for investigations of structure/activity relationships, and various studies on them have been published. It is known that muscarine itself shows high stereoselectivity in the development of pharmacological effects. L(+)-muscarine has high activity whereas its enantiomer is almost inert [22].

Here, a search trial was done to provide maximal common geometric patterns among three molecules: L(+)-muscarine, 5-methylfurmethide and methacoline. The latter two compounds are structurally different from muscarine but all three compounds have similar biological activities. All three-dimensional coordinates used for expressing the molecular

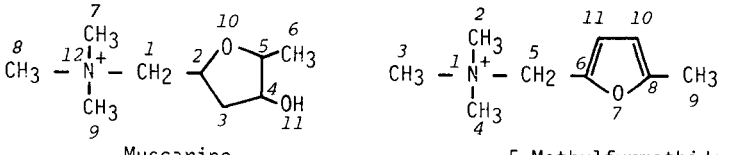

Muscarine

5-Methylfurmethide

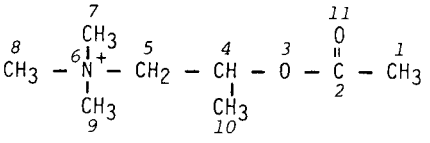

Methacholine

structures were based on data obtained by x-ray diffraction [23—25]. Some results of the search operation are listed in Fig. 8a. For the search conditions, the distance tolerance was 0.5 Å and the other weighting operation used in the case of Example 1 was also adopted. Further, the three methyls in the trimethylammonium group were not included in the set of atoms

(a)

```
EXECUTION ========================
   INPUT-FILE :IN_ATM
   OUTPUT-FILE:OUT_ATM
   DATASET    :DATASET
-- SAMPLES --
     SAMPLE(1)= A04(Methacholine)   ( 8)
     SAMPLE(2)= A10(5-Methylfurmeth( 8)
     SAMPLE(3)= A11(Muscarine)      ( 9)
-- MATRIX SELECTION --
     DISTANCE MATRIX
      ALLOWANCE=  .50
-- MUTUAL CHECK --
     ON
-- STEREO CHECK --
     OFF
-- NODE WEIGHT --
     ATOM TYPE=ON
     BOND TYPE=OFF
     CHARGE TYPE=OFF
-- NODE EXCLUSION --
       EXCLUSION     = DESIGNATE
             DATA 1 :  7  8  9
             DATA 2 :  2  3  4
             DATA 3 :  7  8  9
-- FUNC. GROUP PRESERVATION --
       PRESERVATION = NOT
-- FUNC. GROUP COMPRESSION --
       COMPRESSION  = NOT
  -- RESULT --
   ROTATION     1/   0
NO.   1
 (A04: 1)    1  2  3  4  5  6
 (A10: 1)    9  8  7  6  5  1
 (A11: 1)    6  5 10  2  1 12

              NUMBER= 1
              SIZE  = 6
```

(b)

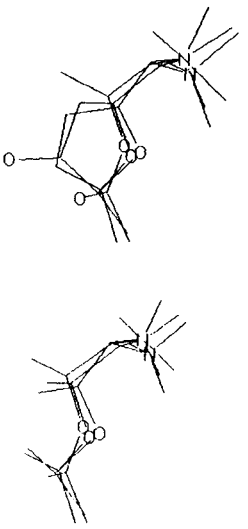

Fig. 8. Maximal common geometric patterns for the three compounds. (a) some results found by COMPASS; (b) graphic representation of the maximal common geometric pattern.

to be sought, in order to simplify the search operation. This was done by designating them as "excluded". The CPU time required was 1.4 s.

A maximal common geometric pattern composed of six constituent atoms was obtained, as indicated by the output results shown in Fig. 8a. The results are consistent with the classical five-atoms rule [26] for high muscarine-like activity; the five-atoms rule is based on empirical observations, irrespective of the detailed properties of the atoms contained in the molecule. It should be noted, however, that interatomic geometries in the molecules are included quantitatively in the present analysis for the search operation. Figure 8b illustrates the structural superimposition of the common portions given in Fig. 8a, while Table 2 shows the average interatomic distance matrix. The numbers for each row and column in the distance matrix in Table 2 correspond to the number assigned to each atom in muscarine. The net charges of the relevant atoms in muscarine, 5-methylfurmethide and methacoline are presented in the last three columns in Table 2 to compare the atomic functionalities. It can be seen that the correlation on the related portions is fairly good.

TABLE 2

Mean distance matrix and atomic net charge of the pharmacophore atoms obtained by COMPASS

	Distance matrix (A)						Atomic net charge (10^{-3})		
	6	5	10	2	1	12	A11	A10	A04
6[a]	C	1.511	2.462	3.721	4.727	5.388	−30	−46	−78
5		C	1.373	2.375	3.596	4.349	141	190	369
10			O	1.464	2.426	3.179	−254	−199	−213
2				C	1.469	2.522	134	75	158
1					C	1.535	69	85	82
12						N	88	77	61

[a]Each row or column number is referred to the number on the atom involved in muscarine (see text).

Various muscarine-related compounds have been synthesized [27]. Some studies on the structure/activity relationship for these compounds have posed questions about the importance of the ring oxygen in muscarine. Needless to say, such findings should be taken into account in conducting practical search operations for common patterns, though this matter is not discussed here because it is not the major aim of this paper.

In the above examples, only a few typical compounds were selected to illustrate the applicability of the COMPASS system to the determination of three-dimensional structure/activity relationships. To discuss three-dimensional structure/activity relationships in more detail from a strict pharmacological point of view, common pattern search trials should be conducted for a larger number of molecules which have similar activities and different structures. All data from x-ray diffraction were used as obtained, to give the coordinates of molecules in this study. To achieve more practical analysis of structure/activity relationships, however, the conformation of each molecule should be examined thoroughly prior to the operation of COMPASS, because possible conformations of a molecule under some assumption for actual interaction with a receptor do not always agree with those determined from x-ray diffraction. If there are several conformers which appear to be stable in terms of energy, each of them should be examined in conducting the analysis. Once reasonable three-dimensional molecular coordinates have been obtained during such a process, then COMPASS can perform automated search operation to provide candidate patterns which may be closely related to the biological activities of the molecules. For the COMPASS system, systematic handling of problems concerning the flexibility around a free-rotational bond axis is currently being studied.

In conclusion, the COMPASS system proposed in this paper can provide common patterns which are meaningful from the viewpoint of medicinal chemistry. The system can serve as a new tool for investigations of three-

dimensional structure/activity relationships and compares favourably with recent analytical techniques which rely on mere structural superimposition via computer graphics.

EXPERIMENTAL

The language used was FORTRAN-77 and the computer was an Eclipse-MV/6000 (Data General) comprising the AOS/VS operating system. A Yamaha YGT-100 graphic terminal was used for the display of some of the results obtained.

The authors thank the Computer Center, Institute for Molecular Science, for affording facilities for part of the computation in this work.

REFERENCES

1 J. E. Armitage, J. E. Crowe, P. N. Evans, M. F. Lynch and J. A. McGuirk, J. Chem. Doc., 7 (1967) 209.
2 M. M. Cone, R. Venkataraghavan and F. W. Mclafferty, J. Am. Chem. Soc., 99 (1977) 7668.
3 T. H. Varkony, Y. Shiloach and D. H. Smith, J. Chem. Inf. Comput. Sci., 19 (1979) 104.
4 R. E. Carhart, D. H. Smith and R. Venkataraghavan, J. Chem. Inf. Comput. Sci., 25 (1985) 64.
5 Y. Takahashi, Y. Satoh, H. Suzuki, H. Abe and S. Sasaki, Anal. Sci., 2 (1986) 321.
6 Y. Takahashi, Y. Satoh, H. Suzuki and S. Sasaki, Anal. Sci., 3 (1987) 23.
7 P. Gund, in F. E. Hahn (Ed.), Progress in Molecular and Subcellular Biology, Vol. 5, Springer-Verlag, New York, 1977, p. 117.
8 N. C. Cohen, in E. C. Olson, R. E. Christoffersen (Eds.), Computer-Assisted Drug Design, American Chemical Society, Washington, DC, 1979, p. 377.
9 G. R. Marshall, C. D. Barry, H. E. Bosshard, R. A. Dammkoehler and D. A. Dunn, in E. C. Olson, R. E. Christoffersen (Eds.), Computer-Assisted Drug Design, American Chemical Society, Washington, DC, 1979, p. 205.
10 C. W. Crandell and D. H. Smith, J. Chem. Inf. Comput. Sci., 23 (1983) 186.
11 V. E. Golender and A. B. Rozenblit, Logical and Combinatorial Algorithms for Drug Design, Research Studies Press, New York, 1983.
12 G. M. Crippen, Distance Geometry and Conformational Calculations, Research Studies Press, New York, 1981.
13 T. F. Havel, I. D. Kuntz and G. M. Crippen, Bull. Math. Biol., 45 (1983) 665.
14 F. Harary, Graph Theory, Addison-Wesley, Reading, MA, 1969.
15 F. S. Kuhl, G. M. Crippen and D. K. Friesen, J. Comput. Chem., 5 (1984) 24.
16 C. Bron and J. Kerbosch, Commun. ACM, 16 (1973) 575.
17 A. G. Michel, G. Evrard, M. Schiltz, F. Durant and M. H. J. Koch, Acta Crystallogr., Sect. B, 32 (1976) 2507.
18 M. H. J. Koch, J. P. Declercq, G. Germain and M. Van Meerssche, Acta Crystallogr., Sect. B, 33 (1977) 2945.
19 L. Barino, Comput. Chem., 5 (1981) 85.
20 Y. Takahashi and S. Sasaki, Unpublished program.
21 D. A. Dobosh, CNINDO program, QCPE No. 141, Carnegie-Mellon University, 1968.
22 P. G. Waser, Pharmacol. Rev., 13 (1961) 465.
23 F. Jellinek, Acta Crystallogr., 10 (1957) 277.
24 C. Chothia, R. W. Baker and P. Panling, J. Mol. Biol., 105 (1976) 517.
25 C. Chothia and P. Pauling, J. Chem. Soc. D, (1969) 626.
26 H. R. Ing, Science, 109 (1949) 264.
27 J. G. Cannon, in M. E. Wolff (Ed.), Burger's Medicinal Chemistry, Part III, 4th edn., Wiley-Interscience, New York, 1980, p. 339.

Analytica Chimica Acta, 200 (1987) 379—385
Elsevier Science Publishers B.V., Amsterdam — Printed in The Netherlands

APPLICATION OF MULTICOMPONENT SPECTROPHOTOMETRY IN ANALYSIS OF COPPER ELECTROPLATING BATH SOLUTIONS

MATTHIAS OTTO* and TATJANA GEORGE

Department of Chemistry, Bergakademie Freiberg, Leipziger Strasse, 9200 Freiberg (German Democratic Republic)

(Received 8th April 1987)

SUMMARY

Multiwavelength multicomponent analysis for copper and nickel is explored within the spectral range 230—900 nm in order to enable copper (≥ 0.2 g l^{-1}) and nickel to be determined simultaneously even at high (20 g l^{-1}) nickel concentrations in industrial electroplating baths. Calibration based on pure-component spectra is compared to multivariate calibration based on data reduction with principal component analysis with the partial least-squares algorithm. By use of multivariate calibration techniques, sulphuric acid can also be determined indirectly by its effect on the absorbance of the metal ions. The performance of the method is evaluated for different spectral ranges and the experimental results are related to the selectivity of the different systems quantified by the condition number of the actual absorptivity matrix.

A recent development in spectrophotometric analysis is related to fiber optic-based photometers that are used as sensors for industrial process control. Such a fibre-optic absorption sensor for monitoring copper in electroplating baths was introduced by Freeman et al. [1]. The sensor was constructed from a near-infrared light-emitting diode (LED) as the radiation source (820 nm) connected to a photomultiplier for measuring the absorbance of highly concentrated solutions of copper. Interferences from sulphuric acid could be overcome by two-wavelength measurements. The proposed sensor cannot be used, however, in electroplating baths containing nickel at high concentrations because nickel absorbs in the same spectral range as copper.

In order to make fiber-optic sensing feasible for the determination of

---

*Prof. Dr. M. Otto is Professor for Analytical Chemistry at the Bergakademie Freiberg. Educated as a chemist (1973 Diplom) he holds Ph.D. (Dr.rer.nat.) and the Doctor of Sciences (Dr.sc.nat.) degrees from the Karl-Marx-University, Leipzig. For specialization in analytical chemistry he worked as a Postdoctoral Fellow at the University in Sofia, the Technical University in Graz and at UWIST, Cardiff. He has coauthored a book on "Catalytic Methods in Trace Analysis" (Weinheim). His specific research interests are in the application of computers and mathematics in analytical chemistry, particularly in respect to spectroscopy, chromatography (HPLC), kinetic/catalytic methods and to chemical sensors.

0003-2670/87/$03.50

copper in the presence of high nickel concentrations, a thorough study of the simultaneous spectrophotometric determination of copper and nickel in the visible/near infrared spectral range is reported here. Multiwavelength multicomponent analysis is based on calibration with pure component spectra as well as on multivariate calibration and data reduction with the partial least-squares algorithm (PLS) [2, 3].

EXPERIMENTAL

Absorption spectra were recorded on a Specord M40 two-channel spectrophotometer (VEB Carl Zeiss Jena) in 0.2, 0.5 and 1.0-cm cuvettes, in the range 230–900 nm.

For computations, the digitized spectra were transferred to a digital computer BC A5120 (VEB Robotron, G.D.R.) for processing with the Householder algorithm [4] (pure component calibration) or by the PLS method [2, 3]. The programs were run in a compiled BASIC version. For computing the condition number of the absorptivity matrix, the eigenvalues were determined according to the algorithm given by Wilkinson and Reinsch [4].

A conventional recipe for preparing the copper electroplating solutions was based on weighed amounts of $CuSO_4 \cdot 5H_2O$, $NiSO_4 \cdot 7H_2O$ and sulphuric acid. The metal ion solutions were standardized by titrimetric methods [5]. For studying the effects of chloride, arsenic and antimony, hydrochloric acid, arsenic(III) oxide and potassium antimonyl tartrate were used.

THEORY

Multiwavelength spectrophotometric analysis is based on Beer's law according to $\mathbf{A} = \mathbf{C}\,\mathbf{K}$, where $\mathbf{A}$ stands for the matrix of absorbances that consists of n rows (number of calibration mixtures) and p columns (number of wavelengths), $\mathbf{C}$ represents the matrix of concentrations with n rows and m columns (number of components), and $\mathbf{K}$ is the matrix of absorptivities consisting of m rows and p columns.

Calibration based on pure component spectra is done by conventional regression analysis. After the absorptivities have been measured for every component under study (i.e., matrix $\mathbf{K}$), the sought concentrations $\mathbf{c}_o$ are obtained from the sample absorption spectrum $\mathbf{a}_o$ by the least-squares solution [4]:

$$\mathbf{c}_o = (\mathbf{K}\,{}^t\mathbf{K})^{-1}\,\mathbf{K}\,{}^t\mathbf{a}_o$$

where the subscript o stands for the analysis phase and t means the transpose of a matrix.

Multivariate calibration is based on preparing mixtures of all components of the system and recording the absorption spectra of these mixtures. The calibration factors are estimated in the present work by means of a principal component analysis based on the PLS algorithm [2, 3]. With this method

the matrices of absorbances and of concentrations are decomposed into principal components (latent variables) giving

$$\mathbf{A} = \mathbf{F}_A \mathbf{L}_A + \mathbf{E}_A \quad (1)$$

$$\mathbf{C} = \mathbf{F}_C \mathbf{L}_C + \mathbf{E}_C \quad (2)$$

where $\mathbf{F}_A$ and $\mathbf{F}_C$ are the abstract absorbance and concentration matrices, respectively, of dimensions n (mixtures) $\times$ d (number of abstract components), $\mathbf{L}_A$ is the $d \times p$ loading absorbance matrix, $\mathbf{L}_C$ the $d \times m$ loading concentration matrix, and $\mathbf{E}_A$ and $\mathbf{E}_C$ are the residual matrices having the same dimensions as the original absorbance and concentration matrices, respectively.

With the PLS method, the decomposition of the matrices A and C is done by correlating mutually the latent variables in the course of their estimation. Thus, regression of the concentration matrix on the absorbance matrix is done as follows:

$$\mathbf{F}_C = \mathbf{F}_A \mathbf{V} + \mathbf{E}_d \quad (3)$$

where V is a diagonal regression matrix of dimension d and $\mathbf{E}_d$ is the $n \times d$-dimensional error matrix. With use of the calibration factors from Eqns. 1–3, analysis with the PLS method is done from

$$\mathbf{c}_o = \mathbf{a}_o (\mathbf{F}_C {}^t\mathbf{A})^t \mathbf{V} \mathbf{L}_C \quad (4)$$

where $\mathbf{c}_o$ and $\mathbf{a}_o$ are again the concentration vector and the absorption spectrum vector of the sample, respectively, and the other matrices are known from the calibration step.

RESULTS AND DISCUSSION

Samples with comparable copper and nickel concentrations

In the first part of the study, electroplating solutions with similar concentrations of copper and nickel in sulphuric acid were investigated. The spectra of copper and nickel in sulphuric acid are shown in Fig. 1. The spectra were digitized every 25 nm between 400 nm and 900 nm and were used as the pure component spectra for analyzing samples of different metal ion concentrations. The compositions of the analyzed samples and the estimated concentrations for copper and nickel are given in Table 1. Sulphuric acid cannot be estimated with the pure-component calibration technique because it does not absorb in the spectral range investigated. The relative mean error of 1.6% is satisfactory for determination of copper, whereas that of 5.4% for the determination of nickel is unsatisfactory.

In order to improve the performance of the method and to make the estimation of sulphuric acid feasible, analysis was based on calibrating the system with mixtures of metal ions in sulphuric acid of various concentrations. The calibration matrix for the mixtures is given in Table 2. It was based on a full two-level three-factor experimental design [6] with an additional point

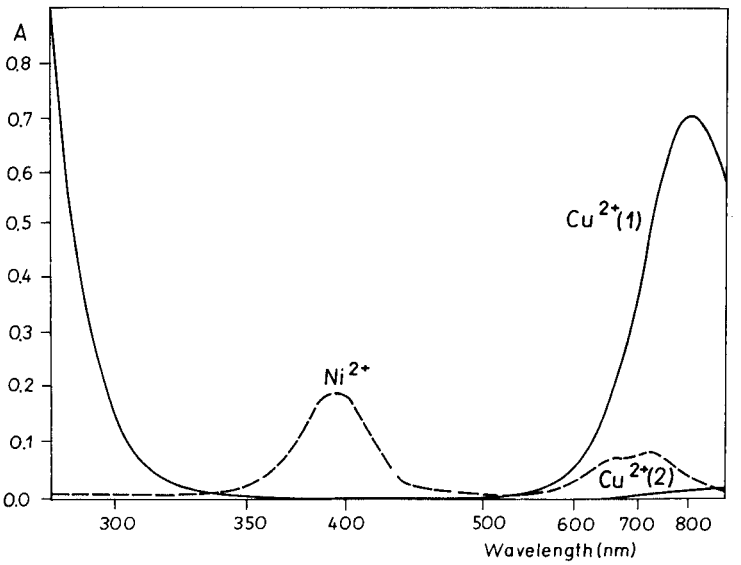

Fig. 1. Absorption spectra of copper and nickel ions in sulphuric acid (200 g l^{-1}). Concentrations are 20 g Ni l^{-1}; (1) 30 g Cu l^{-1}; (2) 0.8 g Cu l^{-1}.

TABLE 1

Determination of similar concentrations of copper and nickel and of sulphuric acid based on calibration with pure-component spectra (A) or component-mixture spectra (B)

Sample	Conc. taken (g l^{-1})			Conc. found (g l^{-1})				
				A		B		
	Cu	Ni	H_2SO_4	Cu	Ni	Cu	Ni	H_2SO_4
I	18.0	6.5	150	17.64	7.22	17.62	6.50	162
II	12.0	13.0	250	12.22	13.26	12.00	13.29	245
III	15.0	7.5	200	15.00	7.96	14.92	7.61	208
	Relative mean error[a] (%)			1.6	5.4	1.5	1.9	4.4

[a]Calculated for sample i as 100 $(\Sigma_{l=1}^{l=3} \Sigma_{l=1}^{l=3} (c_{ij} - c_{ij,\mathrm{act}}^2)/\Sigma_{l=1}^{l=3} c_{ij,\mathrm{act}}^2)^{1/2}$ where c_{ij} is the result found and $c_{ij,\mathrm{act}}$ is the true result.

in the centre of the design. The results for analysis of the three samples with this calibration are also given in Table 1. With use of this multivariate calibration technique, the results for nickel are improved to a relative error of 1.9%. In addition, sulphuric acid can be indirectly determined, by its effect on the metal ion spectra, with a relative error of 4.4%.

Determination of copper in the presence of excess of nickel

A special problem in controlling copper electroplating solutions lies in analyzing copper-depleted solutions that still contain a high nickel concentra-

TABLE 2

Concentrations of mixtures for calibrating the three-component system

Mixture no.	Concentrations (g l^{-1})			Mixture no.	Concentrations (g l^{-1})		
	Cu(II)	Ni(II)	H_2SO_4		Cu(II)	Ni(II)	H_2SO_4
1	20	5	150	6	20	5	250
2	10	5	150	7	10	15	250
3	10	15	150	8	20	15	250
4	20	15	150	9	15	10	200
5	10	5	250				

TABLE 3

Precision of the method for determination of low copper concentrations at high nickel concentrations (200 g l^{-1} sulphuric acid) measured at 13 wavelengths (A) and at 30 wavelengths (B)

Cu(II)			Ni(II)		
Actual conc. (g l^{-1})	Error[a] (%)		Actual conc. (g l^{-1})	Error[a] (%)	
	A	B		A	B
Mixture calibration					
0.2	−5.6	−9.7	18	−2.8	−2.4
2.0	−3.0	−4.0	22	−3.5	−2.9
2.0	1.2	−2.7	18	5.0	3.9
0.2	12.8	22.2	22	1.8	1.7
Pure-component calibration					
0.2	−48.1	−22.0	18	2.3	1.4
2.0	−22.2	−19.2	22	−7.8	−9.6
2.0	−14.1	−19.0	18	−4.4	−4.4
0.2	−22.5	−71.3	22	1.0	1.7

[a]Relative deviation calculated as $100\ (c_i - c_{i,\text{act.}})/c_{i,\text{act.}}$.

tion. Typically, copper has to be evaluated from the absorbance shown in Fig. 1 for 0.8 g l^{-1} copper in the presence of 20 g l^{-1} nickel. To enable copper concentrations to be determined under these conditions, the method was tested with respect to pure and mixture calibration and to exploiting different spectral ranges. Table 3 summarizes the experimental results obtained for analyzing samples at the lowest copper concentration (0.2 g l^{-1}) that can be determined with the multicomponent method, at various nickel concentrations. The experimental design for mixture calibration was based on a 2^2 system with the same concentration levels as given for the analysis of samples in Table 3. As can be seen, calibration by component mixtures again gives better precision for analysis than does pure-component calibration. With respect to the determination of copper, it is evident that for six out of the eight deter-

minations better precision is obtained if the wavelength range between 600 nm and 900 nm (13 wavelengths) is used rather than the full spectral range between 230 nm and 900 nm (30 wavelengths). This tendency was confirmed for further samples not given in the Table. In order to establish the reason for this difference, the selectivity of the systems was estimated.

The selectivity can be characterized quantitatively by the condition number cond(K) of the matrix of absorptivities as shown earlier [7]. A condition number of 1 would represent a fully selective system; the lower the selectivity, the higher is the condition number. The condition numbers for combinations of different parts of the spectra are given in Table 4. As can be seen, there are only marginal differences between the condition numbers computed for the different spectral ranges if the absorptivity data are scaled to unit variance at every wavelength. The worst condition number is observed in the spectral range between 600 and 900 nm, which is to be expected from the spectra given in Fig. 1. From Table 4, it is also evident that the conditioning of the system is decreased if the data are used without scaling. This is especially true if the ultraviolet range (230–300 nm) is used for analysis because in this range the absorptivities are evidently higher than in the visible range, leading to a poorly-conditioned data matrix. For that reason, all computations were performed with scaled absorbance and concentration data.

From these results, the better prediction errors for determination with use of 13 instead of 30 wavelengths cannot be attributed to the selectivity of the different systems (Table 4) but is most probably due to higher measurement precision in the near-infrared range compared to the ultraviolet range. Thus, the near-infrared range between 600 and 900 nm can be advantageously used for constructing fiber-optic sensors because light-emitting diodes are readily available for this spectral range. The limit of the method for determination of low copper concentrations is reached if the nickel concentration exceeds 22 g l^{-1}. Then, even with the use of mixture calibration, the relative error for copper may be as great as 50%.

TABLE 4

Selectivity of the system for different spectral ranges characterized by the condition number [7]

Wavelength range (nm)	Number of wavelengths	Cond(K)[a]	
		With scaling	Without scaling
230–300, 360–440, 600–900	30	1.05	36.9
360–440, 600–900	22	1.45	3.0
230–300, 600–900	21	1.03	77.4
230–300, 360–400	17	1.05	41.8
600–900	13	2.59	8.8

[a]Cond(K) = $[\mathrm{Cond}(K\,{}^{t}K)]^{1/2}$.

As possible interferences the influence of chloride, arsenic and antimony were investigated up to the following concentrations: 60 mg Cl l^{-1}, 1.5 g As l^{-1} and 0.5 g Sb l^{-1}. No significant effect, however, was found so that these species do not interfere at these concentrations.

Conclusions

Simultaneous analysis for copper and nickel in electroplating baths can be done spectrophotometrically or with fiber-optic absorbance sensors [1] down to copper concentrations of 0.2 g l^{-1} in the presence of up to 22 g l^{-1} nickel with reasonable accuracy and precision. Multivariate calibration is to be preferred to pure-component calibration, and is best in the near-infrared range between 600 and 900 nm. With use of the multivariate calibration method, the non-absorbing component, sulphuric acid, can be determined simultaneously as a third component, and better precision for nickel determinations can be achieved.

The authors thank H. Bombach (Department of Metallurgy) for helpful discussions and S. Zimmermann (Department of Chemistry, both Bergakademie Freiberg) for experimental assistance.

REFERENCES

1 J. E. Freeman, A. G. Childers, A. W. Steele and G. M. Hieftje, Anal. Chim. Acta, 177 (1985) 121.
2 W. Lindberg, J.-A. Persson and S. Wold, Anal. Chem., 55 (1983) 643.
3 M. Otto and W. Wegscheider, Anal. Chem., 57 (1985) 63.
4 J. H. Wilkinson and C. Reinsch, Handbook for Automatic Computation, Vol. II, Springer, New York, 1980, p. 21.
5 E. Merck, Komplexometrische Bestimmungsmethoden mit Titriplex, Merck, Darmstadt, 1976.
6 S. N. Deming and S. L. Morgan, Data Handling in Science and Technology, Vol. 3, Elsevier, Amsterdam, 1987, p. 187.
7 M. Otto and W. Wegscheider, Anal. Chim. Acta, 180 (1986) 445.

Analytica Chimica Acta, 200 (1987) 387—396
Elsevier Science Publishers B.V., Amsterdam — Printed in The Netherlands

THE DEPENDENCE OF THE VARIANCES OF THE PARAMETERS IN NON-LINEAR REGRESSION ANALYSIS ON THE NUMBER OF DATA POINTS

LOUIS MEITES*

Department of Chemistry, George Mason University, 4400 University Drive, Fairfax, VA 22030 (U.S.A.)

NICOLANGELO FANELLI and PAOLO PAPOFF**

C.N.R. Istituto di Chimica Analitica Strumentale, Dipartimento di Chimica e Chimica Industriale dell'Università, Via del Risorgimento, 35, 56100 Pisa (Italy)

(Received 10th February 1987)

SUMMARY

In designing an experiment in which non-linear regression analysis is used to evaluate the physicochemical parameters that characterize the behavior of the system being studied, it would be useful to be able to predict how the number of data points affects the reliabilities of the values obtained. The relation between these depends on how the points are distributed as well as on the nature of the equation to which the data are fitted. Weighted non-linear regression analysis has been applied to six common equations involving a total of fourteen parameters, using a number n of points that was varied from 4 to

*Professor Meites received his Ph.D. degree in 1947 from Harvard University, where his thesis was supervised by James J. Lingane. He has served on the faculties of Princeton University (1947—48), Yale University (1948—55), and the Polytechnic Institute of Brooklyn (1955—68), and is now chairman of the Department of Chemistry of George Mason University. His research has concentrated successively on polarography, controlled-potential electrolysis and coulometry, differential thermometry and thermometric titrations, and techniques for analyzing and interpreting physicochemical data. He has about 230 scientific publications to his credit, including the Handbook of Analytical Chemistry, Polarographic Techniques, and the multivolume CRC Handbook Series on organic and inorganic electrochemistry, was the founding editor of CRC Critical Reviews in Analytical Chemistry, and was the winner in 1984 of the Benedetti-Pichler Award of the American Microchemical Society.

**Paolo Papoff took his first degree in chemistry in 1946 at the University of Padua after five years of army service; he became an associate professor in electrochemistry and general inorganic chemistry in 1957 at the University of Modena and full professor in analytical chemistry in 1962 at the University of Bari. At present, he is full professor in instrumental analytical chemistry at the University of Pisa and director of the Istituto di Chimica Analitica Strumentale (C.N.R.). He has worked in the laboratories of Prof. Semerano (Padua), Prof. Riccoboni (Modena) and Prof. Delahay (Baton Rouge); his research team is presently engaged in international cooperation with the Heyrovsky Institute, the George Mason University and the University of Lund. Author of about one hundred publications, he is a member of many international societies in the field of analytical chemistry.

0003-2670/87/$03.50

100 for each equation. The relative standard deviations of the parameters V_i conformed roughly to the equation $\sigma_{V_i}/V_i = a/n^b$, but the values of b ranged unpredictably from 1.20 to 0.465. They conformed much more closely to the equation $\sigma_{V_i}/V_i = a/(n-c)^b$, in which thirteen of the fourteen "best" values of b lay between 0.496 and 0.546.

It is well known that the standard error of the mean, $\bar{y}$, of n replicate measurements of a constant quantity is given by the equation

$$\sigma_{\bar{y}} = a/n^{1/2} \tag{1}$$

where a represents the standard deviation of an individual value of y. If the values of y are fitted to the equation $y = m_1 + m_2x$ for a straight line, the variance of the slope m_2 is given by

$$V_{m_2} = \sigma_y^2/\sum(x_i - x)^2 \tag{2}$$

where σ_y is the population standard deviation of y about the line. The value of σ_y is assumed to be independent of x. Because a finite number of measurements does not provide a value of σ_y, its estimator s_y is generally combined with Student's t to establish a confidence interval for the slope of any desired level of confidence [1—4]. A confidence interval for the intercept may be established in a generally similar way.

The variance described by Eqn. 2 clearly depends both on the number of measurements that are made and on the way in which they are distributed. The same thing can be expected to be true in non-linear regression, where the nature of the relationship between y and x seems no less likely to be important. There appears to have been no previous study of the problem, and those who design experiments are handicapped by the lack of any reliable indication of what to expect. The work described here was undertaken in the hope of providing a basis for expectation.

THEORY AND PROCEDURE

Six relationships, each corresponding to a fairly common experimental problem, were selected for study and are described in Table 1, which also lists the values that were assumed for the parameters, the standard errors of measurement that were assigned to the independent and dependent variables, and the ranges over which the experimental data were taken to extend. Four of the six relationships involved two parameters, while each of the other two involved three.

In each computation it was assumed that n data points, equally spaced with respect to the independent variable except as otherwise stated, had been obtained. The value of n was varied from 4 to 100 in different computations, each of which was begun by synthesizing n points corresponding to the assumed values of the parameters. The resulting set of "data" was combined with the computer program VARPWR, which has been described previously [5]. For convenience, its operation will be described here with reference to Relation 1, which is based on the equation

TABLE 1

Relationships examined

Number	Chemical situation	Algebraic relationship	Values of the parameters	Standard errors of measurement	Range of values of the independent variable
1	Absorbance of a substance undergoing first-order decay	$A = A^0 \exp(-kt)$	$A^0 = 2$, $k = 0.01$	$\sigma_t = 0.1$, $\sigma_A = 0.001$	$\Delta t \leqslant t \leqslant 400$ (98.2% reaction)
2	Absorbance of a product of a first-order reaction	$A = A_\infty [1 - \exp(-kt)]$	$A_\infty = 2$, $k = 0.01$	$\sigma_t = 0.1$, $\sigma_A = 0.001$	$\Delta t \leqslant t \leqslant 400$ (98.2% reaction)
3	Same as 1, but with a constant background absorbance	$A = A^0 \exp(-kt) + c$	$A^0 = 2$, $k = 0.01$, $c = 0.05$	$\sigma_t = 0.1$, $\sigma_A = 0.001$	$\Delta t \leqslant t \leqslant 400$ (98.2% reaction)
4	Absorbance of a substance undergoing second-order decay	$A = A^0/(1 + ktA^0)$	$A^0 = 2$, $k = 0.08$	$\sigma_t = 0.1$, $\sigma_A = 0.001$	$\Delta t \leqslant t \leqslant 400$ (98.5% reaction)
5	Polarographic wave	$i = i_d/\{1 + \exp[(E - E_{1/2})/S]\}$	$i_d = 2$, $E_{1/2} = -600$, $S = 25.687$	$\sigma_E = 0.5$, $\sigma_i = 0.01$	-450 ($i/i_d = 0.0029$) $\leqslant E \leqslant$ -750 ($i/i_d = 0.9971$)
6	Absorbance of a complex ML	$K = [ML]/[M][L]$, $[M] + [ML] = c_M$, $[L] + [ML] = c_L$, $A = \epsilon [ML]$	$K = 10$, $\epsilon = 100$, $c_M = 0.01$	$\sigma_{c_L} = 0.0005$, $\sigma_A = 0.001$	0.01 (8.4% ML) $\leqslant c_L \leqslant$ 1 (90.8% ML)

$$A = A^0 \exp(-kt) \tag{3}$$

where A is the absorbance at time t produced by a substance that has an initial absorbance equal to A^0 and disappears by a first- or pseudo-first-order reaction having a rate constant equal to k. For any assumed combination of the standard errors of measurement σ_A and σ_t of the absorbance A and the time t, respectively, it estimates the variances of the parameters A^0 and k in the following way. It applies an increment $\Delta t = M \sigma_t$ to the time for each point in turn. The quantity M is a constant that is chosen by the operator at the time of execution. Small values of M exaggerate the importance of round-off errors, while large ones compromise the accuracy of the finite-difference approximation described below. Every use of the program must therefore include an examination of the effect of varying M so that an appropriate value can be selected [5]. All of the results reported in Tables 2 and 4 are the averages of values obtained with two different values of M, one twice as large as the other. As expected, the optimum values of M increased as the number of points increased, and the results reported for Relation 1 with $n = 4$ are therefore based on computations with $M = 1$ and 2 while those reported for the same relation with $n = 100$ are based on computations with $M = 4$ and 8. The two values that were averaged to obtain the reported results almost always agreed within 0.3%.

For each of the perturbed sets of data thus produced, the program computes the best values of the parameters V_i by weighted non-linear regression and finds the differences ΔV_i between these and the corresponding values used in generating the data. Values of $\Delta V_i/\Delta t$ are stored as estimators of the partial derivatives $\partial V_i/\partial t$ at the point under consideration, the original value of t at that point is restored, and the next point is treated in the same way. After the values of $\Delta V_i/\Delta t$ have been obtained and the original value of t has been restored for the last point, an increment $\Delta A = M\,\sigma_A$ is applied to the absorbance for each point in turn, and estimates of the partial derivatives $\partial V_i/\partial A$ are obtained and stored in the same way. Finally, the values of the derivatives are combined to yield estimates of the variances of the parameters.

In weighted regression, one must minimize the quantity Q defined by the equation

$$Q = \sum (A_{\mathrm{meas}} - A_{\mathrm{calc}})^2/[\sigma_t^2(\mathrm{d}A/\mathrm{d}t)^2 + \sigma_A^2] \qquad (4)$$

An expression for $\mathrm{d}A/\mathrm{d}t$ is needed to evaluate the weighting factor within square brackets, and was easily obtained by differentiating Eqn. 3. Computation was speeded by writing the result in the form

$$\mathrm{d}A/\mathrm{d}t = A^0\ [-k\exp(-kt)] = -kA_{\mathrm{calc}} \qquad (5)$$

Partly to permit examining the effects of round-off errors, partly to guide the choice of a value of M as was described above, and partly to ensure that the arbitrary conditions for termination were sufficiently stringent, a few replicate computations were made with different starting points, different values of M, and different conditions for termination. They led to the conclusion that the results given below are generally reliable within about 0.2%.

The computations were made in BASIC on Radio Shack TRS-80 Model II microcomputers.

RESULTS AND DISCUSSION

Table 2 shows how the standard or relative standard errors of all the parameters depend on n under the conditions summarized in Table 1 and with data-acquisition algorithms that gave rise to points evenly spaced along the independent-variable axes over the ranges specified in Table 1. The values given for $E_{1/2}$ and S in Relation 5 are the standard errors in mV, while all the other values represent the relative standard errors and are expressed as percentages. As long as the nature of the algorithm is unchanged, increasing the number n of data points always causes the standard error of a parameter to decrease. However, the magnitude of the effect resulting from any change of n depends on the relation between the independent and dependent variables and differs from one parameter to another.

Table 3 gives the results obtained by fitting the values for each parameter listed in Table 2 to two arbitrarily selected equations:

TABLE 2

Standard errors of the parameters for different values of n. (All these values are relative standard errors and are expressed as percentages, except those for $E_{1/2}$ and S in Relation 5, which are absolute standard errors and are expressed in mV)

n	Standard errors						
	Relation 1		Relation 2		Relation 3		
	A^0	k	A_∞	k	A^0	k	c
4	0.644	0.484	0.0654	0.2131	0.874	0.982	4.44
6	0.366	0.313	0.0559	0.1772	0.432	0.598	3.39
8	0.271	0.2464	0.0497	0.1554	0.302	0.460	2.88
10	0.2232	0.2095	0.0452	0.1402	0.2418	0.388	2.56
15	0.1634	0.1606	0.0378	0.1163	0.1725	0.296	2.076
20	0.1347	0.1350	0.0330	0.1008	0.1403	0.2485	1.797
30	0.1051	0.1077	0.0271	0.0825	0.1083	0.1967	1.469
40	0.0885	0.0918	0.02340	0.0714	0.0914	0.1690	1.275
60	0.0708	0.0740	0.01926	0.0588	0.0729	0.1363	1.031
80	0.0609	0.0637	0.01660	0.0507	0.0626	0.1171	0.891
100	0.0543	0.0569	0.01485	0.0455	0.0555	0.1042	0.794
	Relation 4		Relation 5			Relation 6	
	A^0	k	i_d	$E_{1/2}$	S	K	ϵ
4	60.8	3.241	0.748	1.705	0.834	0.874	0.2128
6	25.9	1.943	0.611	1.110	0.816	0.737	0.1862
8	14.80	1.403	0.550	0.951	0.732	0.648	0.1673
10	9.91	1.109	0.500	0.845	0.649	0.574	0.1511
15	5.29	0.758	0.418	0.686	0.526	0.457	0.1233
20	3.68	0.597	0.366	0.592	0.453	0.385	0.1026
30	2.477	0.449	0.302	0.481	0.368	0.315	0.0833
40	1.969	0.375	0.263	0.417	0.318	0.272	0.0734
60	1.504	0.297	0.2158	0.339	0.260	0.2232	0.0614
80	1.251	0.253	0.1870	0.293	0.2246	0.1920	0.0526
100	1.095	0.2239	0.1677	0.262	0.2010	0.1813	0.0495

$$\sigma_{V(I)}/V(I) \text{ [or } \sigma_{V(I)}] = a/n^b \quad (6)$$

$$\sigma_{V(I)}/V(I) \text{ [or } \sigma_{V(I)}] = a/(n-b)^c \quad (7)$$

It was assumed that the relative (rather than the absolute) deviations from these equations were randomly distributed, and a few of the results given in Table 2 for the smallest values of n (e.g., those for $n = 4$ and 6 for Relation 4) were omitted from the computations based on Eqn. 7 to ensure that $(n - b)$ would always be positive.

Although a small majority of the values of b in Eqn. 6 were close to the expected value of 0.5, many others were considerably larger, ranging up to 1.20 (for A^0 in Relation 4). Large values of b appear to be associated with situations in which, when n is small, the data-acquisition schedule produces

TABLE 3

Values of the parameters in Eqns. 6 and 7

Relation number	Parameter	Values of the parameters in Eqn. 6 and relative standard deviations of the fits			Values of the parameters in Eqn. 7 and relative standard deviations of the fits			
		a	*b*	RSD, %	*a*	*b*	*c*	RSD, %
1	A^0	1.31	0.720	13.6	0.644	3.02	0.545	1.92
	k	0.965	0.632	8.6	0.581	2.58	0.508	0.48
2	A_∞	0.130	0.466	2.2	0.161	−1.77	0.516	0.28
	k	0.423	0.482	0.98	0.459	−0.642	0.501	0.30
3	A^0	1.26	0.699	9.7	0.609	4.11	0.527	1.15
	k	1.60	0.603	5.2	1.01	3.12	0.496	0.18
	c	8.34	0.511	0.67	7.95	0.42	0.500	0.53
4	A^0	189	1.20	31	22.1	6.28	0.673	5.57
	k	7.71	0.803	14	2.63	4.91	0.543	1.61
5	i_d	1.45	0.465	1.6	1.78	−2.03	0.511	0.263
	$E_{1/2}$	2.75	0.511	0.46	2.62	0.429	0.500	0.10
	S	2.06	0.506	0.99	2.15	−0.365	0.515	0.98
6	K	1.81	0.509	2.5	1.81	0.010	0.509	2.64
	ϵ	0.436	0.478	3.2	0.492	−0.936	0.506	3.09

no, or disproportionately few, points in the region that exerts the greatest influence on the value of a parameter. The user of Relation 4 has made periodic measurements of the absorbance of a reactant that is being consumed by a second- or pseudo-second-order reaction, and is attempting to evaluate both the initial absorbance A^0 and the rate constant k of the reaction. It is obvious that data obtained near the start of the reaction influence the value of the initial absorbance much more than data obtained at any later time. Under the conditions assumed in these calculations, a data-acquisition schedule that produces only ten points at times equally spaced between 40 and 400 s contains no information whatever about the first 86% of the reaction. As a result, the value of the initial absorbance is very uncertain, just as it would be if it were obtained by employing a very long extrapolation in a graphical treatment of the data. As more points are secured, the first portion of the curve becomes better defined, and the value of A^0 rapidly becomes more precise.

Similar things are true [6] if the decay is first- or pseudo-first-order, but, because the concentration then changes less rapidly near the start of the reaction, the important data at short times are less poorly represented if only a few points are secured. The ten-point data-acquisition schedule just described would yield its first point at an instant when the reaction was only 33% complete, rather than 86%. There is less room for improvement as the number of points increases, and the value of b in Eqn. 6 (0.720) is much more nearly equal to 0.5 than it is if the decay is second- or pseudo-second order. It may be inferred that reasonable precisions would be difficult or

impossible to secure in kinetic (differential-reaction-rate) analyses based on pseudo-second-order reactions of the substances being determined.

The values of c obtained from the fits to Eqn. 7 cluster much more closely around the expected value of 0.5: the mean of all fourteen of these values is 0.525 and its standard deviation is 0.045. Four of the fourteen values (those for A^0 and k in Relation 4 and for A^0 in Relations 1 and 3) are clearly anomalous for the reasons discussed in the last two paragraphs. The mean and standard deviation for the remaining ten, in which regions of great influence are not unduly slighted by the data-acquisition schedule if n is small, are 0.506 and 0.006, respectively.

Anomalous values of c are accompanied by anomalous values of b. The mean and standard deviation of all fourteen values of b are 1.366 and 2.612, but for the ten described in the last sentence of the preceding paragraph they are 0.081 and 1.676, respectively.

Other data-acquisition schedules are of course available, and it was of interest to examine their behaviors. Three alternatives to the schedule given in Table 1 for Relation 1 were examined, and are described in Table 4. Although they do so in different ways, each yields a larger fraction of the points in the initial portion of the curve. Table 5 shows how the number of points affects the standard errors of the parameters for each of these schedules, and should be compared with the first two columns of Table 2. The comparison shows why the data-acquisition schedule deserves more attention than it has generally received: in the same chemical situation and for the same values of the physicochemical parameters that characterize the system being studied, it is possible to effect a fivefold improvement of the precision with which one of those parameters can be evaluated merely by adopting a different algorithm for obtaining the data. In slightly different words, an experiment in which

TABLE 4

Alternative data-acquisition schedules for Relation 1. [These schedules were employed in computations based on Relation 1 with the same values of the parameters (A^0 = 2, k = 0.01 s^{-1}) and of the standard errors of measurement (σ_t = 0.1 s, σ_A = 0.001), and with the same maximum value of t (400 s) as those given in Table 1 and employed to obtain the values in Table 2]

Schedule[a]	Algorithm	Values of t_i for i = 1, 6, 11, and 16 with n = 20
A	$t_i = 400^{i/n}$	1.349, 6.034, 26.99, 120.7
B	$A_i = 2 - 1.96337\ i/n$	5.033, 34.89, 77.64, 153.9
C	$t_i = 80\ i/n$ until $i = 3\ n/4$, then $t_i = 60 + 340\ (4\ i - 3\ n)/n$	4, 24, 44, 128

[a]Schedule A gives values of t_i that increase exponentially with i. Schedule B gives equally spaced values of A_i. Schedule C gives three-quarters of the points equally spaced until t_i = 60 s (or approximately 60 s if n is not evenly divisible by 4) and the remaining quarter of the points equally spaced from that time to 400 s.

TABLE 5

Standard errors of the parameters in Relation 1 for different values of n and different data-acquisition schedules. (All these values are relative standard errors and are expressed as percentages)

n	Standard errors					
	Schedule A		Schedule B		Schedule C	
	A^0	k	A^0	k	A^0	k
4	0.1371	0.332	0.2344	0.345	0.2430	0.576
6	0.1030	0.2485	0.1663	0.252	0.1502	0.313
8	0.0871	0.2138	0.1353	0.2088	0.1232	0.285
10	0.0771	0.1909	0.1174	0.1833	0.1062	0.2292
15	0.0619	0.1554	0.0920	0.1457	0.0834	0.1873
20	0.0531	0.1341	0.0785	0.1249	0.0710	0.1632
30	0.0430	0.1094	0.0629	0.1011	0.0574	0.1296
40	0.0371	0.0949	0.0538	0.0870	0.0493	0.1138
60	0.0302	0.0776	0.0437	0.0705	0.0402	0.0925
80	0.0262	0.0670	0.0378	0.0611	0.0348	0.0801
100	0.02337	0.0598	0.0338	0.0546	0.0310	0.0714

only four data points are obtained (by Schedule A) can yield a value of A^0 that is no less precise than the one obtained from another experiment in which twenty points are obtained under exactly the same conditions (by the schedule described in Table 1), while the experimenter who must achieve even better precision can do so by acquiring either twenty points (by Schedule A) or a hundred (by the schedule described in Table 1).

On the basis of calculations relating to titrations of strong acids with strong bases, and with an entirely different criterion of utility, Meites et al. [7] suggested that data equally spaced with respect to the dependent variable are preferable to those equally spaced with respect to the independent variable. This suggestion is confirmed by the results obtained here, for the relative standard errors of the parameters are much smaller for data obtained by Schedule B (in which the points are equally spaced along the absorbance axis) than for data obtained by the schedule given in Table 1 (in which the points are equally spaced along the time axis). For most purposes, however, Schedule A is superior to either of these others: for all but the smallest values of n, it yields values of A^0 that are slightly less precise than those obtained from Schedule B, but this small difference is more than compensated by the much better precisions of the values of k obtained from Schedule A. The superiority of Schedule A in this situation reflects the properties of pointwise-variance-analysis plots [8] based on Relation 1, and it cannot be inferred that this schedule will always, or often, be superior to others.

It has been shown [8] that the optimum data-acquisition schedule for evaluating any single parameter is the one according to which the probability of acquiring a point at any given value of the independent variable is

proportional to the relative influence of that point on the calculated value of that parameter. The way in which the relative influence is affected by the independent variable is portrayed by what has been called a "pointwise-variance-analysis plot", which is a plot of the relative influence (or, for convenience, its logarithm) against the independent variable. Averaging the relative influences of a point on the values of two or more different parameters gives an "overall pointwise-variance-analysis plot", which depicts the overall utility of that point if the values of all the parameters are considered to be equally interesting. (Of course, that may not be true in any particular experiment: the physical chemist attempting to evaluate k has much less interest in the value of A^0, whereas in differential-reaction-rate analysis the value of A^0 is far more interesting than that of k. This important difference between the purposes of two different workers conducting identical experiments will be ignored here.) A set of data conforming to Relation 1 was synthesized by taking a total of ten points: four at times equally spaced from 6 to 24 s, and six more at times equally spaced from 136 to 291 s. The average of the relative influences of an individual point on the values of A^0 and k, deduced from the results of calculations with 100 points equally spaced along the time axis, has a maximum value of 1 at the first point (where t = 4 s), decreases rapidly to a minimum of 0.087 at t = 92 s, passes through a very broad maximum at t = 210 s, and then decreases continuously as t increases further. The ten-point schedule thus constitutes a crude approximation to one in which the probability of acquiring any given point is proportional to its overall influence.

The resulting set of ten points gave relative standard errors of 0.0933% for A^0 and 0.1483% for k. Both of these figures are substantially superior to the corresponding ones for three of the other four schedules examined. The relative standard error of A^0 is slightly larger than for Schedule A (which places heavy emphasis on the initial portion of the curve, where the relative influences of the points are much higher for A^0 than for k) but that of k is much smaller than it is for Schedule A. A subsequent paper will describe a procedure for effecting the automated acquisition of data in such a way as to conform closely to the optimum schedule.

Table 6 gives the results obtained by fitting the values listed in Table 5 to Eqns. 6 and 7. Since all of these schedules emphasize the first portion of the curve to a larger extent than the schedule described in Table 1, they all yield values of b in Eqn. 6 that are well below the anomalously high figure (0.720) given in Table 3, although they are all substantially above 0.5. There is no evident explanation of the fact that all six of the values of c in Eqn. 7 are below 0.5.

Unless any particular situation has been examined in as much detail as is exemplified by Tables 2 and 5, and especially if the shape of its pointwise-variance-analysis plot is unknown, there seems to be very little basis for attempting to use anything more complicated than Eqn. 6 to predict how changing the value of n will affect the precisions of the parameters evaluated

TABLE 6

Effect of the data-acquisition schedule on the values of the parameters in Eqns. 6 and 7

Schedule	Parameter	Values of the parameters in Eqn. 6 and relative standard deviations of the fits			Values of the parameters in Eqn. 7 and relative standard deviations of the fits			
		a	*b*	RSD, %	*a*	*b*	*c*	RSD, %
A	A^0	0.271	0.537	2.7	0.222	1.29	0.490	0.49
	k	0.640	0.517	2.5	0.540	1.16	0.477	1.18
B	A^0	0.469	0.582	5.3	0.330	2.02	0.497	0.21
	k	0.682	0.556	4.0	0.515	1.71	0.489	0.37
C	A^0	0.451	0.596	8.9	0.268	2.75	0.469	1.15
	k	0.988	0.585	11.4	0.545	3.08	0.439	4.1

from a set of experimental data. In the absence of any other information, it would seem prudent to assume an average value of 0.55–0.60 for *b*, and to adopt a somewhat skeptical attitude toward the results of this rather crude approximation. Situations that are clearly anomalous should not be difficult to recognize in the light of the discussion presented here.

This work was aided by the generous support of the Consiglio Nazionale delle Richerche (C.N.R.) and the M.P.I., to which one of us (L.M.) is indebted for a visiting fellowship during the summer of 1986.

REFERENCES

1 A. G. Worthing and J. Geffner, Treatment of Experimental Data, Wiley, New York, 1943, p. 249.
2 C. A. Bennett and N. L. Franklin, Statistical Analysis in Chemistry and the Chemical Industry, Wiley, New York, 1954, p. 227.
3 J. Mandel, The Statistical Analysis of Experimental Data, Interscience, New York, 1964, p. 277.
4 G. W. Snedecor and W. G. Cochran, Statistical Methods, Iowa State University Press, Ames, IA, 6th Edn., 1967, p. 153.
5 L. Meites, The General Non-Linear Regression Program CFT4A, The George Mason Institute, Fairfax, VA, 1985, pp. 218–222.
6 E. D. Johnson, J. P. Weber and L. Meites, Anal. Chim. Acta, 178 (1985) 263.
7 L. Meites, M. P. Colombini, L. Lampugnani and P. Papoff, Anal. Chim. Acta, 152 (1983) 53.
8 L. Meites, Anal. Chim. Acta, 74 (1975) 177.

Analytica Chimica Acta, 200 (1987) 397—410
Elsevier Science Publishers B.V., Amsterdam — Printed in The Netherlands

ESTIMATION OF ESTER HYDROLYSIS PARAMETERS BY USING FOURIER-TRANSFORM INFRARED SPECTROSCOPY AND THE EXTENDED KALMAN FILTER

STEPHEN L. MONFRE and STEVEN D. BROWN*
Department of Chemistry, University of Delaware, Newark, DE 19716 (U.S.A.)
(Received 7th April 1987)

SUMMARY

Fourier-transform (FTIR) spectroscopy has found a wide range of applications. Attempts have been made to make FTIR spectroscopy a reliable quantitative technique for obtaining chemical information from complex systems, but it is often difficult to obtain even qualitative information about a complex system because of matrix, interaction, and background effects on the infrared spectra. In this study, FTIR spectroscopy was used in conjunction with the extended Kalman filter, a recursive digital filter, to investigate the simple, neutral hydrolysis of two esters in aqueous solutions. Interactions between the solvent, reactants and products of the hydrolysis perturb the spectrum, making a single-wavelength kinetic analysis impractical. With the extended Kalman filter, a range of frequencies where severe perturbation does not occur is processed to obtain not only the rate constant but also the initial reactant concentrations.

Kinetic methods have received extensive study over the past twenty years. Much of the work has involved the monitoring of changes in ultraviolet-visible spectra over the course of a reaction in the liquid phase. Although this approach is useful for many compounds, some compounds do not show substantial absorption in these spectral regions. Most compounds show some absorption in the infrared region, however. Kinetic analyses based on infrared spectroscopy have been restricted to rapid, gas-phase reactions, which are followed by Fourier-transform infrared (FTIR) spectrometry. Typically, the growth or disappearance of a single peak in the infrared spectrum is used to calculate kinetic information [1]. The use of FTIR in following chemical reactions in solution is less straightforward, because of the changes in component spectra arising from the interaction, matrix and background effects [2, 3]. These changes make following reaction kinetics by monitoring a single wavelength difficult, especially when the product and reactant species interact to perturb the infrared spectrum of each. Such interaction is common in the polar solvents used for many liquid-phase kinetic studies.

The work reported here involves the use of an extended Kalman filter for the investigation of the kinetics of the neutral aqueous hydrolysis of ethyl trifluoroacetate and ethyl trichloroacetate. Not only do the spectral responses of the reactants and products overlap in many regions of the infrared

0003-2670/87/$03.50

spectrum, but there is also substantial interaction between the ethanol, trihaloacetic acids and the solvent, causing time-dependent shifts in the infrared spectra observed for the product mixture. It is demonstrated that, if these effects are not severe, fitting the kinetic data to a first-order model is possible, and accurate concentration estimates can be obtained.

THEORY

The general rate expression for the hydrolysis of esters is

$$-d[R'COOR]/dt = [R'COOR](k_0 + k_{H^+}[H_3O^+] + k_{OH^-}[OH^-]) \quad (1)$$

However, when very weakly basic esters, such as the trihaloacetates, are hyrolyzed in dilute aqueous solutions, the system becomes pH-independent, and it follows first-order kinetics [4]. This is termed neutral hydrolysis. Now the concentration of the ester determines the rate of the reaction, as shown by the rate expression

$$-d[R'COOR]/dt = k_1[R'COOR] \quad (2)$$

Ideally, the determination of the rate constant in Eqn. 2 is made by making a measurement which is proportional to the concentration of the ester (absorbance vs. time). However, the nature of the reaction usually prevents such direct measurements from being made. Therefore, a more realistic case is when the measurement includes the contribution of all reactants, products, and solvents. In the case of a first-order neutral hydrolysis of an ester, this would correspond to

$$Z(j) = \epsilon_{R'COOR}(j)[R'COOR] + \epsilon_{H_2O}(j)[H_2O] + \epsilon_{R'COOH}(j)[R'COOH] + \epsilon_{ROH}(j)[ROH] + \epsilon_{solvent}(j)[solvent] \quad (3)$$

where ϵ is the product of the molar absorptivity and cell pathlength in accordance with Beer's law, and Z is the absorbance, both at a given wavelength, j. When several measurements are made, each at a different time, t, the expression becomes [5]

$$Z(j,t) = \epsilon_{R'COOR}(j)[R'COOR](t) + \epsilon_{H_2O}(j)[H_2O](t) + \epsilon_{R'COOH}(j)[R'COOH](t) + \epsilon_{ROH}(j)[ROH](t) + \epsilon_{solvent}(j)[solvent](t) \quad (4)$$

where $Z(j,t)$ is the infrared absorbance measured at wavelength j and time t.

By using nonlinear estimation techniques, it is possible to estimate the first-order rate constant, k_1, and the initial concentration of the ester, $[R'COOR]_0$. This is done by fitting several responses, $Z(j)$, as a function of time. One method used to estimate kinetic parameters is the extended Kalman filter. The extended Kalman filter has previously been applied to first-order kinetic studies in the ultraviolet-visible region of the spectrum [5]. Another study used the extended Kalman filter to describe three dimensional data (wavelength/absorbance/time) collected on an enzyme-catalyzed

reaction [6]. The extended Kalman filter is ideal for such estimations because it provides for time-dependent changes in models. As with non-linear regression methods, the extended Kalman filter can also include the spectral contributions of all reactants and products as part of the model.

Extended UDU^T Kalman filter

The extended Kalman filter uses a non-linear model which describes the system dynamics and the measurement process. The model is generally expressed in two equations: a time propagation of the states being estimated, and a measurement model relating states to measurable quantities. When the system is nonlinear with respect to the parameters, the model equations are expressed as

$$\mathbf{X}(j) = f[\mathbf{X}(j), \mathbf{X}(j-1)] + \mathbf{w}(j) \tag{5}$$

$$Z(j) = h^T[\mathbf{X}(j)] + v(j) \tag{6}$$

where $\mathbf{X}(j)$ is the vector containing the states to be estimated, $f[\mathbf{X}(j), \mathbf{X}(j-1)]$ is a non-linear function describing the propagation of these states in time, $h^T[\mathbf{X}(j)]$ is a non-linear function describing the measurement process, and $\mathbf{w}(j)$ and $v(j)$ are white-noise contributions [7]. In this specific case, the state vector is described as $\mathbf{X}^T = ([\text{R'COOR}]_0, k_1, [\text{solvent}])$. Because the elements of the state vector are time-independent for the application reported here, Eqn. 5 can be reduced to the linear equation

$$\mathbf{X}(j) = \mathbf{I}\,\mathbf{X}(j-1) + \mathbf{w}(j) \tag{7}$$

The measurement function used in this study is based on the integrated form of the rate expression [5]. It parallels Eqn. 4 and is based on three parameters: the first-order rate constant for the hydrolysis, k_1, the initial concentration of the ester, and the concentration of solvent. When the integrated rate expression and stoichiometry of the reaction are used, the measurement function becomes

$$h^T[\mathbf{X}(j)] = \{\epsilon_{\text{R'COOR}}(j) - \epsilon_{\text{R'COOH}}(j) - \epsilon_{\text{ROH}}(j)\}[\text{R'COOR}]_0 \exp(-k_1 t) + [\text{R'COOR}]_0\{\epsilon_{\text{R'COOH}}(j) + \epsilon_{\text{ROH}}(j)\} + \epsilon_{\text{solvent}}[\text{solvent}](j) \tag{8}$$

When the response of the solvent is removed prior to filtering by subtracting the spectrum of the solvent from each hydrolysis spectrum and each reactant and product model spectrum, the contribution of the solvent to the measurement function is set to zero, and the state vector reduces to $\mathbf{X}^T = ([\text{R'COOR}]_0, k_1)$.

Various algorithms have been implemented [8] for the estimation of the state, $\mathbf{X}$, by using a Kalman filter. Some of these algorithms have been found to be numerically unstable because of filter divergence [9, 10]. Filter divergence occurs when the estimated covariances predicted by theory are smaller than those calculated by the Kalman filter. Sources of divergence include roundoff error, modeling errors, system observability problems, and loss of

nonnegativity during computation of covariance matrices [7, 11]. Potter [12] replaced the conventional Kalman measurement update with a more numerically stable square-root measurement update. Another method of measurement updating, which has been found to be numerically stable based upon the Givens orthogonal transformation, is the U-D factorization method [9, 13, 14], which is used in this study. The U-D factorization is arranged in such a way to minimize computation. Comparison of the U-D factorization method to the square-root information filter has shown that for n estimated parameters, the square-root information filter requires n scalar square roots and n extra divisions for each scalar observation that is to be processed [15]. The use of the U-D factorization method also yields the same attributes which are available from the square-root information filter. Such attributes include variable dimension filtering, "sensitivity" computations, and improved error covariance computation [16].

The U-D factorization of the extended Kalman measurement update algorithm implies that the a priori covariance matrix, P, is given in the factored form as

$$\mathbf{P} = \mathbf{U}\mathbf{D}\mathbf{U}^{\mathrm{T}} \tag{9}$$

where U is an upper triangular matrix and $\mathbf{D} = \mathrm{diag}(d1, \ldots, dn)$. The matrix U and vector D are called the U-D factors of P. The extended Kalman update algorithm is now developed using the U-D factors of the updated covariance matrix, P. In the conventional Kalman filter, the systems dynamics noise, Q, is added at the point of error covariance extrapolation [7]. In the U-D factorization method, it is incorporated in the U-D factors [8, 9, 15]. This is done by extending the matrix diagonal D to include $\mathbf{Q} = \mathrm{diag}(q1, \ldots, qn)$ on the diagonal, such that $\mathbf{D} = \mathrm{diag}(D, \mathbf{Q})$. Table 1 provides the algorithm for the factorization of P.

The key feature to this approach of covariance matrix computation is that the updated values of D retain positivity. Another feature is that roundoff errors are avoided, and the accuracy is enhanced because the updated terms are obtained as fractional multiples of their previous construction [8]. These features are particularly important for this study because of the large number of data points which are filtered. For kinetic analysis of the absorbance/wavelength/time arrays obtained here, approximately 20 000 points are filtered. Roundoff error can become a significant problem over the course of such an extensive calculation; however, by using the $\mathrm{UDU}^{\mathrm{T}}$ filter, this problem is minimized, and filter divergence does not occur. Also, because the values of D remain positive, optimal evaluation of the states may be obtained, provided that systematic errors are minimized. Other advantages associated with the use of the $\mathrm{UDU}^{\mathrm{T}}$ filter are increased computational speed and decreased storage requirements. The square-root filters previously used for kinetic analysis have similar roundoff properties, but these filters have significantly larger storage requirements and computational burdens, making their use with large data sets inconvenient [8, 9].

TABLE 1

Covariance factoring algorithm equations

For $p = n, n-1, \ldots, 2$, cycle through eqns. 10—12: $D_p = \mathbf{P}_{p,p}(0\vert 0)$	(10)
for $i = 1, \ldots, p-1$ cycle through eqn. 11: $\mathbf{U}_{i,p} = \mathbf{P}_{i,p}/D_p$	(11)
for $k = 1, \ldots, i$ cycle through eqn. 12: $\mathbf{P}_{l,i} = \mathbf{P}_{k,i} - \mathbf{P}_{i,p}\mathbf{U}_{k,j}$	(12)
$D_1 = \mathbf{P}_{1,1}$	(13)
for $i = 1, \ldots, n$: $\mathbf{U}_{i,i} = D_i$	(14)

Although the use of these alternative algorithms in this study did not produce significantly different results because of the simplicity of the problem, they were substantially slower; this difference in computational speed is a consequence of the computational burdens previously mentioned.

Table 2 gives the algorithm used to implement the extended $\mathbf{UDU}^T$ Kalman filter. The algorithm is presented in a modified state-space notation, similar to that used to describe this filter in the aerospace literature [8, 9]. The first step in the extended Kalman filter involves updating the a priori estimate and the a priori covariance matrix. This includes the computation of the Kalman gain. The next step involves projecting the old estimate and covariance onto a new estimate and covariance.

EXPERIMENTAL

Reagents and procedures

Ethyl trichloroacetate and trichloroacetic acid were obtained from Eastman Kodak. Ethyl trifluoroacetate was prepared from trifluoroacetic acid (Aldrich Chemical Company) and ethanol (Fischer Scientific). Each reagent was purified using fractional distillation procedures described in the literature [17, 18]. Acetone was of reagent grade. The water was passed through a mixed-bed ion exchange column and further purified by glass distillation.

Both hydrolyses were done by addition of the ester to the solvent after all solutions were equilibrated to the cell chamber temperature (25°C). After careful mixing, a 1-ml portion of the solution was placed into the sample holder and permitted to react. The initial ester concentrations were 0.164 M and 0.134 M for ethyl trifluoroacetate and ethyl trichloroacetate, respectively.

Equipment

Spectra were obtained by using a Digilab FTS-40 Fourier-transform infrared spectrometer, equipped with a nitrogen-cooled mercury cadmium-telluride (MCT) detector. A 24-μl attenuated total reflectance CIRCLE cell (Spectra-Tech) with a zinc selenide crystal was used as the sample holder. Prior to the kinetic run, an appropriate background spectrum was

TABLE 2

Extended UDU^T Kalman filter

Algorithm equations

State estimate extrapolation:

$$\mathbf{X}(k|k-1) = \mathbf{F}_{k,k-1}\,\mathbf{X}(k-1|k-1) \tag{15}$$

Error covariance extrapolation: U-D time update

$$D_i(k) = \mathbf{U}_{i-1,\,i-1}(k);\ i = 1 \ldots n. \tag{16}$$

(compute new U-D factors)

For $p = n,\ n-1, \ldots, 2$ cycle through Eqns. 17—19

$$D_p(k|k-1) = \sum_{i=0}^{N} \mathbf{Y}_{p,i} D_i(k|k) \mathbf{Y}_{p,i} \tag{17}$$

for $i = 1, \ldots, p-1$ cycle through Eqns. 18—19

$$\mathbf{U}_{i,p}(k|k-1) = \sum_{i=0}^{N} [\mathbf{Y}_{i,l} D_p(k|k) \mathbf{Y}_{p,l}]/D_p(k|k-1) \tag{18}$$

$$\mathbf{Y}_{i,(n-p+1)} = \mathbf{Y}_{i,(n-p)} - \mathbf{U}_{i,p}(k|k-1)\mathbf{Y}_{p,(n-p)} \tag{19}$$

$$D_1(k|k-1) = \sum_{i=0}^{N} \mathbf{Y}_{1,i} D_1(k|k) \mathbf{Y}_{1,i} \tag{20}$$

State estimate update:

$$\mathbf{X}(k|k) = \mathbf{X}(k|k-1) + K(k) * [Z(j,k) - H^{\mathrm{T}}\mathbf{X}(k|k-1)] \tag{21}$$

Covariance update: U-D measurement update algorithm

$$g = H\mathbf{U} \tag{22}$$

$$s = D(k|k-1)g \tag{23}$$

$$\alpha_1 = R(k) + s_1 g_1 \tag{24}$$

$$D_1(k|k) = D_1(k|k-1)R(k)/\alpha_1 \tag{25}$$

$$b_1 = s_1 \tag{26}$$

For $p = 2, \ldots, n$ cycle through equations 27—32

$$\alpha_p = \alpha_{p-1} + g_p s_p \tag{27}$$

$$D_p(k|k) = D_p(k|k-1)\alpha_{p-1}/\alpha_p \tag{28}$$

$$b_p = s_p \tag{29}$$

$$\lambda = -g_p/\alpha_{p-1} \tag{30}$$

For $i = 1, \ldots, p-1$ compute recursively Eqns. 31—32
(update of column p of the U matrix factor)

$$\mathbf{U}_{i,p}(k|k) = \mathbf{U}_{i,p}(k|k-1) + b_i\lambda \tag{31}$$

$$b_i = b_i + \mathbf{U}_{i,p}(k|k-1)s_p \tag{32}$$

Kalman gain:

$$\mathbf{K}_p(k) = b_p/\alpha_n \tag{33}$$

where $\mathbf{Q}(k) = E[\mathbf{w}(k)\mathbf{w}^{\mathrm{T}}(i)]\delta_{ik}$; $R(k) = E[v(k)v(i)]\delta_{ik}$; $\mathbf{F}_{k,k-1} = \partial f[\mathbf{X}(k),\ \mathbf{X}(k-1)]/\partial \mathbf{X}|\mathbf{X} = \hat{\mathbf{X}}$; $H(k) = \partial h[\mathbf{X}(k)]/\partial \mathbf{X}|\mathbf{X} = \hat{\mathbf{X}}$; $N = n + n_q$; $\mathbf{Y} = [\mathbf{FU}(k|k), \mathbf{G}]$

TABLE 2 (continued)

Definitions of variables			
$\mathbf{D}(k\|k)$	**D** vector updated ($N \times 1$)	**Q**	System dynamic noise vector ($n \times 1$)
$\mathbf{D}(k\|k-1)$	**D** vector extrapolated	$R(k)$	Measurement variance
D_i	ith column of **D**	t_k	time k
$f[\mathbf{X}(k), \mathbf{X}(k-1)]$	Non-linear function describing the system dynamics	$\mathbf{U}(k\|k)$	Extrapolated unit upper triangular matrix of $\mathbf{P}(n \times n)$
F	Linearized state transition matrix		
G	Process noise matrix		
$h^{\mathrm{T}}(X(k))$	Non-linear function describing the measurement function	$\mathbf{U}(k\|k-1)$	Extrapolated unit upper triangular matrix
H	Linearized measurement function	$v(k)$	Measurement noise vector
		$w(k)$	System noise vector ($n \times 1$)
I	Identity matrix	X	State variable ($n \times 1$)
$\mathbf{K}(k)$	Kalman gain vector ($n \times 1$)	**Y**	Matrix composed of a D-orthogonal vector set
n	Number of states		
n_q	Dimension of system covariance vector	$Z(j,k)$	Measurement at wavelength j and time k
P	Error covariance matrix ($n \times n$)	$\mathbf{A}^{\mathrm{T}}$	Transpose of **A**
		$\mathbf{A}(k\|i)$	kth estimate of **A** based on the ith measurement
		$\mathbf{A}_i$	ith element of vector **A**

taken for each chemical system. Data were collected, and the autosubtraction software available on the Digilab 3200 Data Station was used to subtract the background from each spectrum. This was done to eliminate the contribution of the solvent in the measurement function of the filter. The data were transferred from the data station to a Celerity supermini computer running under the UNIX BSD 4.2 operating system. The data transfer was done under the u.u.c.p. communications protocol.

Spectra

To account for most of the spectral perturbation caused by the solvent, the model spectra for the products were taken in the appropriate solvent for each hydrolysis system. For the ethyl trichloroacetate hydrolysis, this was a 40/60 (v/v) mixture of ethanol and water. The ethyl trifluoroacetate hydrolysis was done in a 50/50 (v/v) mixture of acetone and water. The model spectra for the esters were obtained by using the first spectral measurement of the hydrolysis. That measurement contained negligible amounts of product species.

Ethyl trichloroacetate hydrolysis. Spectra for the ethyl trichloroacetate system were taken from 4400 cm^{-1} to 450 cm^{-1}. The initial time of the hydrolysis was carefully noted, with spectral measurements taken every 563 s. Each measurement was formulated by signal-averaging 64 scans. The time to complete the scans (ca. 28 s) constituted a change in concentration of less than 0.1%, as estimated using either the rate constant published [17], or the value obtained in these studies.

Ethyl trifluoroacetate hydrolysis. Spectra for the ethyl trifluoroacetate

system were taken from 2000 cm^{-1} to 975 cm^{-1}. The initial time of the hydrolysis was noted, with spectral measurements taken every 45 s. For this system, 32 scans were averaged to yield each spectral measurement. The time required to complete this set of scans (ca. 14 s) constituted a change in concentration of less than 0.4%, again as calculated using either the rate constant published [18], or the value obtained in these studies.

Both hydrolyses had reaction times which were appropriate for a real-time kinetic analysis. Because the filtering could be accomplished at a rate of one spectrum of 1024 points every 4 s, the time-consuming aspect of real-time analysis of such infrared data is the conversion of each interferogram into an absorbance spectrum, followed by data transfer. The data-transfer software provided with the 3200 Data Station for the transfer of data files between the data station and the Celerity supermini computer required 95 s for the file transfer, thus restricting this investigation to post-run analyses. Efforts are underway to improve the file-transfer software and remove this limitation.

RESULTS AND DISCUSSION

Previous studies of the hydrolysis of these esters have shown them to follow pseudo-first-order kinetics at concentrations less than 0.2 M [4, 17, 18]. Thus, a model of the form given in Eqn. 8 was used for all data analysis.

The data sets were filtered with and without prior subtraction of the large solvent background. From earlier work [5, 6], it would seem reasonable that filtering should account for the sizable, but linear, contribution of the solvent, in addition to deconvoluting the nonlinear effects of the chemical kinetics. When the solvent background was included in the filter measurement model, it was convenient to use the solvent spectrum as one of the components of the filter measurement model. In this case, the solvent state value used was a relative "concentration", with pure solvent having a "concentration" of unity. Permitting the solvent state to vary produced state values of 1.5 to 3.0, with poor covariance values, and poor values for the initial ester concentration and the first-order rate constant. Constraining the solvent state to a value of unity (by giving an initial guess for the state as unity and for the covariance of zero) gave results which agreed very well with those found by autosubtracting the solvent response from each of the spectra taken on the reaction mixture, and then filtering with the model not containing the solvent response. The poor results obtained when allowing the solvent state to vary may be attributed to the fact that the response of the solvent is very large compared to that of the reactants and products, and there may be several possible solvent state values giving rise to solutions which show an apparent minimum in the fit variance. These false minima are avoided by either constraining the solvent state to the true value, which is known prior to the collection of data, or by the subtraction of the solvent response before data analysis. In essence, these are equivalent operations, although the constrained filter offers some advantages for real-time use in

the analysis of systems with a large, linear contribution from solvent or some other "spectator" species. When the solvent response is removed prior to filtering, large negative spectral peaks result. Figures 1—4, the models used for filtering after removal of solvent response, demonstrate the poor background subtraction which occurred. This is attributed to shifts in the solvent peaks which are caused by the presence of the ester and ester hydrolysis products. The presence of negative peaks will have a deleterious effect on the state estimations calculated by the filter. As a consequence of the presence of these peaks, it is necessary to select regions of the data for filtering. The regions selected must be free of negative responses, but must be regions where the reactants and/or products absorb, so that the observability criterion can be satisfied [5]. Thus, the regions selected will depend on the spectra of reactants, products and solvents. When the data are filtered without prior removal of the solvent response, other regions may be appropriate, because there are no large negative peaks, and it is necessary to insure that the solvent state is also observable.

For all studies reported here, the initial estimates for the parameters $[RCOOR]_0$ and k_1 were set to zero, with the variance in the estimate set to a worst case value of unity. The measurement variance was set to a value of 10^{-6}.

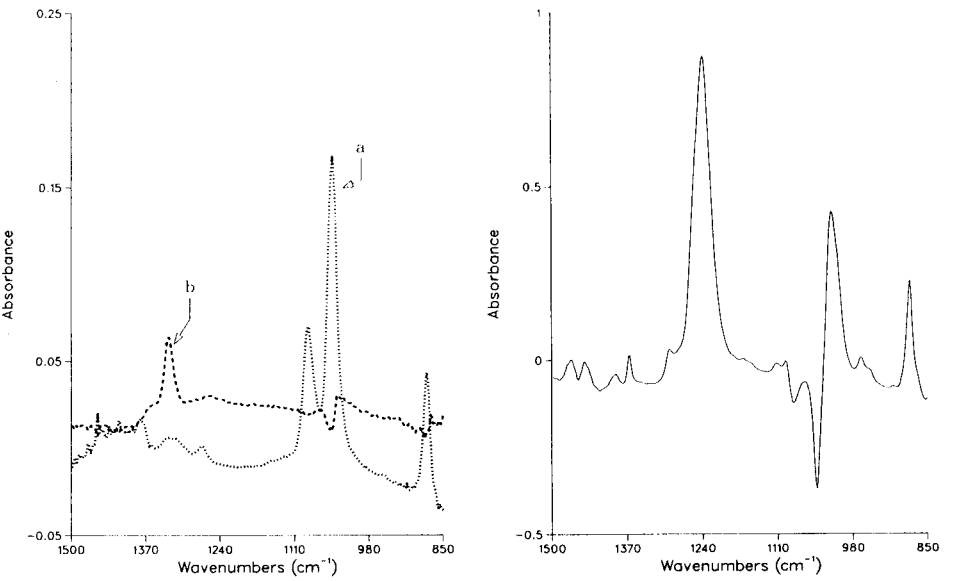

Fig. 1. Spectra: (a) ethanol (0.360 M) and (b) trichloroacetic acid (0.135 M) in 40% ethanol/water. Solvent response has been removed by autosubtraction.

Fig. 2. Spectrum of ethyl trichloroacetate in 40% ethanol/water at time 00:01:45. Solvent response has been removed by autosubtraction.

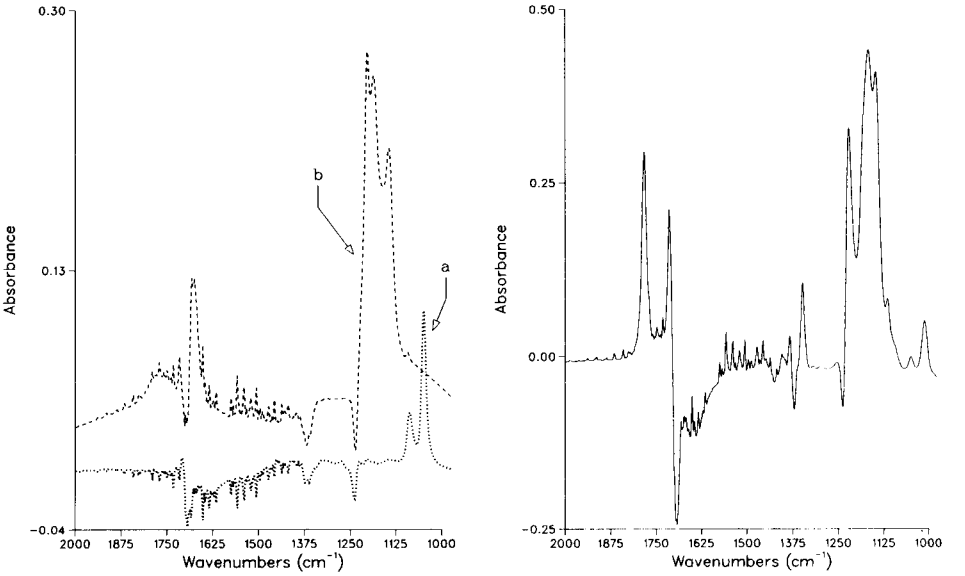

Fig. 3. Spectra: (a) ethanol (0.360 M) and (b) trifluoroacetic acid (0.267 M) in 50% acetone/water. Solvent response has been removed by autosubtraction.

Fig. 4. Spectrum of ethyl trifluoroacetate in 50% acetone/water at time 00:01:45. Solvent response has been removed by autosubtraction.

Filtering of ethyl trichloroacetate hydrolysis spectra

The hydrolysis data were examined over various spectral ranges and times of hydrolysis. A typical spectrum, taken at 11:45:30 after initiation of the reaction, is shown in Fig. 5. Filtering over the entire wavelength range (4000 cm^{-1} to 500 cm^{-1}) of the spectral set produced unsatisfactory results, a consequence of the poor background subtraction of the solvent in the high-frequency area of the spectrum (>2000 cm^{-1}). Table 3 shows typical results of filtering, after removal of solvent, for the spectral data over wavelengths from 1500 cm^{-1} to 850 cm^{-1}. The results indicate acceptable estimation of the rate constant. The reported value of k_1 in the literature, in a solvent mixture of 40/60 (v/v) ethanol and water at 25°C, is 2.8×10^{-5} s^{-1} [17]. The accuracy of estimation of the initial ester concentration was poor at early points of the hydrolysis. Table 3 also shows the results of filtering the data set over the region 1225 cm^{-1} to 900 cm^{-1}. Less solvent interference occurs in this region of the spectrum; therefore, better results would be expected.

Filtering of ethyl trifluoroacetate hydrolysis spectra

Because of the strong interaction between solvent, reactants and products, it was necessary to correct the baselines of the model spectra used in the study of the ethyl trifluoroacetate hydrolysis. A linear correction was used to prevent a negative rate constant being calculated, which could cause the failure of the extended Kalman filter.

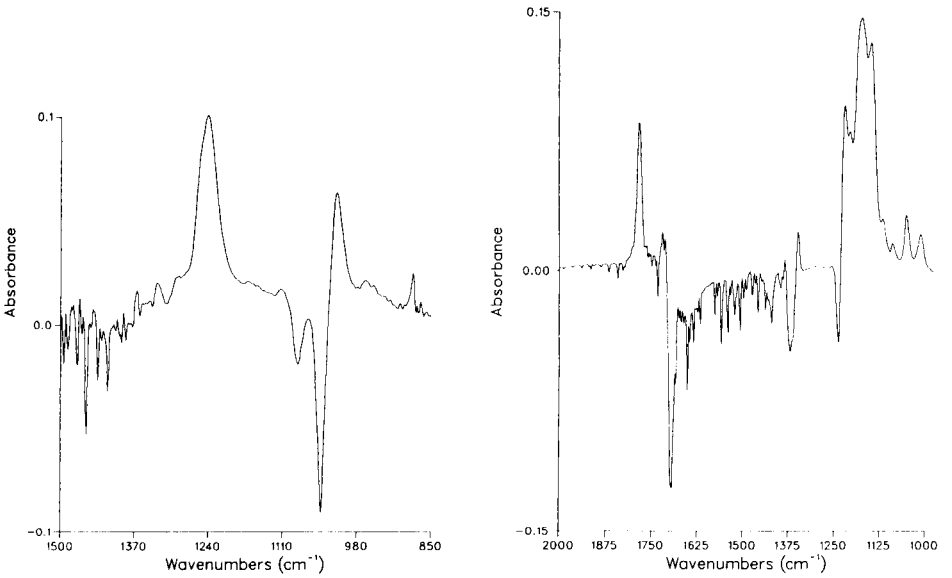

Fig. 5. Spectrum of ethyl trichloroacetate and hydrolysis products in 40% ethanol/water solvent at 11:45:30 after start of reaction. Solvent response has been removed by auto-subtraction.

Fig. 6. Spectrum of ethyl trifluoroacetate and hydrolysis products in 50% acetone/water solvent at 01:12:15 after start of reaction. Solvent response has been removed by auto-subtraction.

TABLE 3

Hydrolysis of ethyl trichloroacetate

Time[a] h:min:s	Spectral range (cm^{-1})	Calc. k_1 (10^{-5} s^{-1})	Calc. conc. (mol l^{-1})	Relative error in conc. (%)
06:17:05	1500—850	3.69	0.151	+12.0
	1225—900	2.61	0.144	+7.0
07:50:55	1500—850	3.86	0.150	+11.0
	1225—900	2.74	0.140	+4.0
11:45:30	1500—850	3.93	0.143	+6.0
	1225—900	2.72	0.131	—3.0
13:47:29	1500—850	3.86	0.139	+3.0
	1225—900	2.62	0.126	—7.0

[a]Time of hydrolysis reaction.

The hydrolysis data in this system were also filtered over various spectral ranges and times of reaction. The spectrum in Fig. 6 shows the hydrolysis at 1:12:15 after initiation of the reaction. Because only 32 scans were averaged to minimize the time spent in collecting data, a decrease in the signal-to-noise ratio is expected; Fig. 6 indicates that decreased signal-to-noise was

observed. Table 4 shows typical results of filtering, after removal of solvent, for the infrared data set over the wavelength range 2000—975 cm^{-1}. Filtering over this spectral region required analyzing the data sets through 00:58:45 of the hydrolysis reaction before consistent results were obtained. Analysis of the data sets through 00:25:00 produced inconsistent results for estimating the rate constant, probably because of the incomplete removal of background components from model and mixture spectra. In this reaction, the strong interactions between product and solvent which occurred were not well modeled, and the poor results are not surprising. The reported value of the rate constant in the literature, determined in a 50/50 (v/v) acetone/water solvent at 25°C, is 2.57×10^{-4} s^{-1} [18]. Table 4 also summarizes the results of filtering the data set from 1230 cm^{-1} to 975 cm^{-1}. Estimation of the initial ester concentration and the rate constant is less satisfactory, unless spectra collected late in the reaction are included in the filtering. Filtering over the larger spectral range was more suitable for estimating initial ester concentrations because regions where little apparent change occurred contributed significantly to the estimates. Because little change in the spectral response occurs, these regions might be excluded from a conventional data analysis, but they are important in making the system observable, as the filtering results indicate.

Interactions between solvent, reactants and products make generation of accurate models for filtering infrared data sets obtained on reacting mixtures difficult, but a careful choice of the spectral range minimizes these effects. There are two other possible contributors to the difficulties experienced in filtering these data sets. One is the effect of the time spent in collecting averaged spectra. Because the reaction causes changes in the spectra as the data are collected, there is a distortion of the spectrum of the reaction mixture. In essence, this spectrum describes a convolution of the reaction

TABLE 4

Hydrolysis of ethyl trifluoroacetate

Time[a] h:min:s	Spectral range (cm^{-1})	Calc. k_1 (10^{-4} s^{-1})	Calc. conc. (mol l^{-1})	Relative error in conc. (%)
00:25:00	2000—975	—	0.162	—1.0
	1230—975	0.87	0.203	+24.0
00:40:00	2000—975	0.72	0.164	0.0
	1230—975	1.42	0.198	+21.0
00:58:45	2000—975	1.94	0.162	—1.0
	1230—975	2.28	0.185	+13.0
01:12:15	2000—975	2.59	0.157	—4.0
	1230—975	2.66	0.170	+4.0

[a]Time of hydrolysis reaction.

kinetics and the sampling parameters used to generate the averaged multicomponent spectrum. This effect should be especially pronounced early in the course of a first-order reaction, because reactant and product concentrations are changing rapidly. This "integration effect" is a systematic error which is not accounted for in the Kalman filter model. When data are collected at times which are appreciably beyond the start time of the reaction, the estimation of the initial concentration should improve, because the contribution of this systematic error decreases. Although the estimates of initial concentration improve when spectra taken later in the reaction are filtered, integration effects are not likely to be significant in these systems because few scans were averaged and rate constants were relatively small.

The second contributor may be fluctuations in the instrument, caused by changes in temperature, source, and scan properties. It is assumed in the Kalman filter model used here that no significant change in temperature arose from solution warming by the source. This is a reasonable assumption, because the reactants were brought to the temperature of the cell chamber before the reaction was started, and because the infrared beam does not contact the bulk of the solution. Even at constant temperature, however, there is a possibility of significant drift occurring in a set of spectra collected over long periods of time, owing to fluctuations in source, interferometer or detector behavior. To determine the magnitude of the long-term drift contribution, the same instrumental conditions were used to measure the spectrum of a stable reference material over a 24-h period. The drift contribution to the spectrum was very small, being confined to small changes in the spectral offset. Because more significant changes in this offset were produced by the interaction of products with the solvent, the drift contribution to spectral measurements was neglected in the data analysis. Short-term fluctuations were noticeable, however. These fluctuations were attributed to the change in instrument properties generated by the cycling of the air dryer used to provide air for purge and for operation of the air bearing in the interferometer. These fluctuations manifest themselves in changes in the height of absorbance peaks as well as changes in the spectral offset. These changes contributed to the uncertainty in estimates generated in the data analysis; they are believed to limit the precision and accuracy of the method at this time.

Conclusions

Infrared spectroscopic measurements are suitable for use in kinetic analysis of reactions in condensed media, provided that several important restrictions can be met. First, the spectral integration time must be small compared to the time over which the reaction is observed, otherwise, the data are distorted by the changes in reactant and product concentrations occurring over the data-collection period. Second, accurate correction of all background effects or careful choice of the filtering range is necessary to avoid errors in the estimation of the rate constant and initial concentrations which are

produced by defects in the multicomponent model used to fit the spectral response observed as a function of time. Minimizing spectral integration time is possible by use of rapid-scan interferometric techniques used in gas-phase studies, or by preprocessing of fewer, "slow-scan" interferograms to enhance the signal-to-noise ratio prior to filtering. Correction of models to improve performance in kinetic analysis will be the subject of another communication. In either case, it is critical that care is taken to ensure the short-term stability of the instrument, as the filter model is sensitive to unmodelled, short-term fluctuations in the instrument. These fluctuations degrade the accuracy and the precision of extended filters used for kinetic analysis.

This work was supported by the U.S. Department of Energy, under Grant DE-FG02-86ER13542.

REFERENCES

1 P. Zuman and R. C. Patel, Techniques in Organic Reaction Kinetics, Wiley-Interscience, New York, 1984, p. 25.
2 D. W. Green and G. T. Reedy, in J. R. Ferraro and L. J. Basile (Eds.), Fourier Transform Infrared Spectroscopy, Vol. 1, Academic, New York, 1978, p. 1.
3 T. Hirschfeld, in J. R. Ferraro and L. J. Basile (Eds.), Fourier Transform Infrared Spectroscopy, Vol. 2, Academic, New York, 1978, p. 193.
4 A. J. Kirby, in C. H. Bamford and C. P. H. Tipper (Eds.), Comprehensive Chemical Kinetics, Vol. 10, Elsevier, Amsterdam, 1979, p. 153.
5 S. C. Rutan and S. D. Brown, Anal. Chim. Acta, 167 (1985) 23.
6 S. C. Rutan and S. D. Brown, Anal. Chim. Acta, 175 (1985) 219.
7 A. Gelb (Ed.), Applied Optimal Estimation, M.I.T. Press, Cambridge, MA, 1974.
8 G. J. Bierman and C. L. Thornton, Automatica, 13 (1977) 23.
9 G. J. Bierman and C. L. Thornton, in C. T. Leondes (Ed.), Control and Dynamic Systems, Vol. 16, Academic, New York, 1980, p. 177.
10 W. M. Gentlemen, J. Inst. Math. Appl., 12 (1973) 329.
11 A. H. Jazwinski, Stochastic Processes and Filtering Theory, Academic, New York, 1970.
12 J. E. Potter, Instrumentation Lab., M.I.T. Press, Cambridge, MA, 1963.
13 W. M. Gentlemen, J. Linear Alg. Appl., 10 (1975) 189.
14 P. G. Kaminski, A. E. Bryson and S. F. Schmidt, IEEE Trans. Autom. Control, 16 (1971) 727.
15 G. J. Bierman, Factorization Methods for Discrete Sequential Estimation, Academic, New York, 1977, p. 77.
16 G. J. Bierman, Automatica, 12 (1976) 375.
17 W. P. Jencks and J. Carriolo, J. Am. Chem. Soc., 83 (1961) 1743.
18 A. Moffatt and H. Hunt, J. Am. Chem. Soc., 79 (1957) 54.

Analytica Chimica Acta, 200 (1987) 411—419
Elsevier Science Publishers B.V., Amsterdam — Printed in The Netherlands

SELEX: AN EXPERT SYSTEM FOR EVALUATING PUBLISHED DATA ON SELENIUM IN FOODS

D. W. BIGWOOD

Program Resources, Inc., Model and Database Coordination Laboratory, Agricultural Research Service, U.S. Department of Agriculture, Beltsville, MD 20705 (U.S.A.)

S. R. HELLER*

Model and Database Coordination Laboratory, Agricultural Research Service, U.S. Department of Agriculture, Beltsville, MD 20705 (U.S.A.)

W. R. WOLF, A. SCHUBERT and J. M. HOLDEN

Nutrient Composition Laboratory, Agricultural Research Service, U.S. Department of Agriculture, Beltsville, MD 20705 (U.S.A.)

(Received 8th April 1987)

SUMMARY

Providing consistent and objective evaluation of published data on nutrient composition is critical for planning future analytical studies and for effective use of data. Based on a commercial expert system shell, a computer system of approximately 200 rules has been created to evaluate and rate quantitatively published data on selenium in foods. The evaluation scheme uses five general categories for its rule-making process: number of samples, analytical method, sample handling, sampling plan, and analytical quality control. For each selenium value to be evaluated, ratings are assigned in each category by the expert system based on input which is derived from the information reported in a given paper. A quality index, which is derived from the ratings, is a measure of the reliability of a given selenium value over all categories for a given study. The concepts used in developing SELEX have the potential of establishing criteria for evaluation of proposed analytical methods prior to their publication.

Increasing interest in the selenium intake of Americans is due to the potential relationship of selenium to cancer prevention and has generated a need for the compilation, evaluation, and improvement of data on selenium

*Stephen R. Heller received a B.S. in chemistry in 1963 at the State University of New York—Stony Brook and a Ph.D. in organic chemistry in 1967 at Georgetown University. He is presently the research leader of the Model and Database Coordination Laboratory at the U.S. Department of Agriculture, Agricultural Research Service, in Beltsville, Maryland. Previously, he has served as a chemist at the U.S. Environmental Protection Agency and as a Senior Staff Fellow at the National Institutes of Health (1970—1973). He also served for 6 months with the U.S. House Subcommittee on Health and Environment (1979—1980) and as a Lady Davis Visiting Professor of Chemistry at the Hebrew University, Jerusalem (1981). He has published over 100 papers and books during the past 20 years and is currently a member of the IUPAC Committee on Chemical Databases.

in foods. Reasons for undertaking this work include some concern with the uneven quality of the data and the lack of support documentation. A set of criteria was developed to evaluate the quality of existing, peer-reviewed, published selenium data [1]. A manual system for post-publication evaluation of selenium data [2] based on these criteria proved successful in identifying foods for which the quality of data was poor or for which there were no acceptable data. However, this manual system was more tedious, more time-consuming, and less consistent than desired. Consequently, an expert system, SELEX, was developed to automate the evaluation process. Developed directly from the previously established criteria, this expert system provides users with several advantages over the manual system. These include speeding the evaluation process and production of more consistent numeric ratings. Development of the expert system also allows users who have less expertise than the domain experts to generate ratings.

Figure 1 shows an overview of the entire evaluation procedure, including the selection of the selenium core foods as well as the individual rating process which is addressed by SELEX. For each food within a study, a rating is assigned in each of five different categories. These five categories are: number of samples, analytical method, sample handling, sampling plan, and analytical quality control. The ratings assigned by SELEX, the selenium mean, and ancillary information from the publication are written into a computer file which can be read by a SAS (Statistical Analysis System) program which evaluates the Quality Index (QI), selenium mean, and Confidence Code (CC) for each particular food. The QI is evaluated from the five ratings, and with a few exceptions, is equal to the simple mean of the five numbers. The ratings and QI range from 0 to 3. A QI of 1.0 or greater indicates that the selenium mean is considered acceptable. All acceptable means for a particular food are averaged to yield a grand selenium mean for that food. The CC (A, B, or C), derived from the sum of the QIs, represents the confidence that can be attributed to the grand selenium mean.

Using the concepts and methods created for the development of the process of evaluating published selenium data, we have considered the broader implications of these methods. It is hoped that the concepts, principles, and rules developed for the selenium data evaluation system will be considered by journal editors and their reviewers for use in their prepublication review process. At the least, this work indicates that well-defined procedures are possible for evaluation of analytical chemical data. With use of such techniques, it is considered that a better dialog could be developed between journal editors and authors.

It is well known that the quality of much of the scientific literature is often lower than desired. There is probably far more poor and irreproducible research being published than there should be. As Lide [3] rather bluntly points out the "scientific literature contains vast amounts of data collected for a specific purpose and presented by authors to support their conclusions . . .. Unfortunately, the quality of the data preserved in the literature

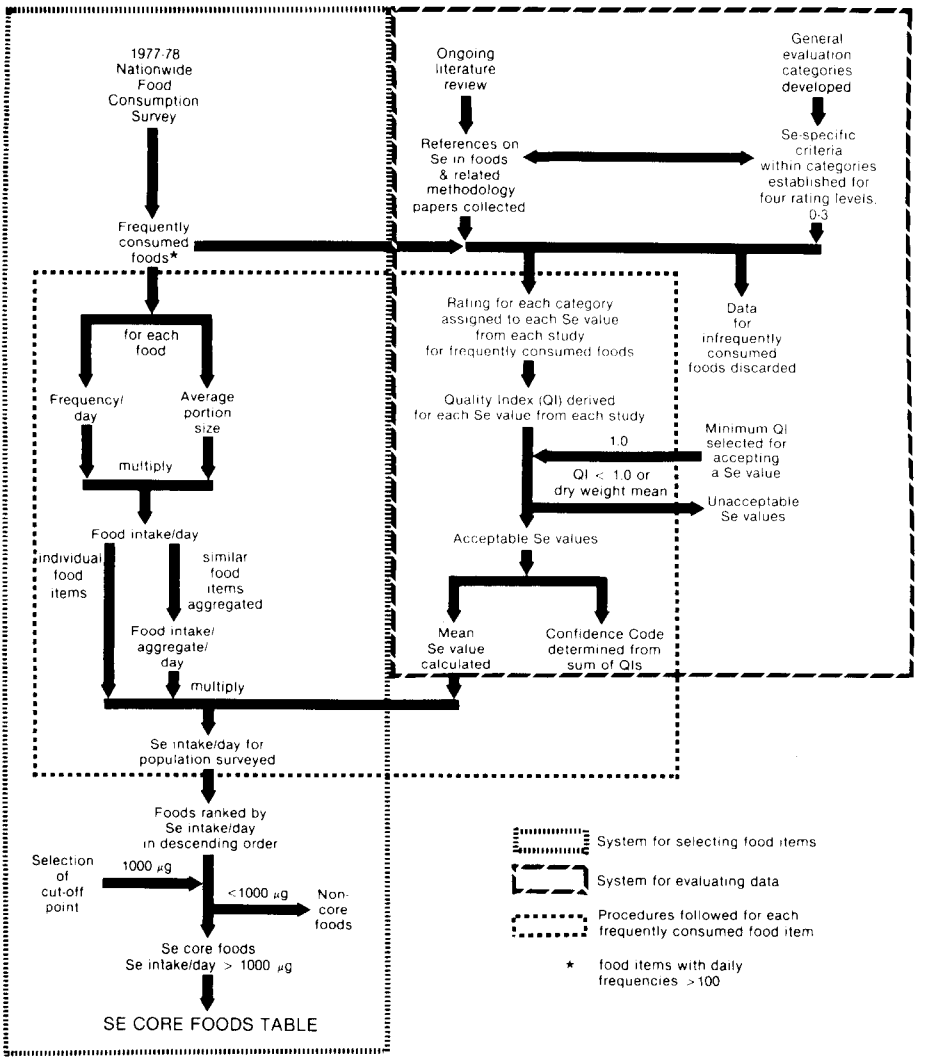

Fig. 1. System overview of the selection of selenium core foods and evaluation of published data.

leaves much to be desired. This becomes apparent when data on a much-studied subject are systematically retrieved . . .. The measurements for (about 200 values of the thermal conductivity of copper as a function of temperature) were analyzed by the Center for Information and Numeric Data Analysis and Synthesis at Purdue University. The scatter of these data illustrates the pitfalls of relying on a single value retrieved from the literature". The scientific community needs to find a way to improve the peer review process. Based on this system for published data on selenium in foods, it appears this is a goal that is achievable in certain cases at least.

DATA QUALITY CRITERIA

For each of the five areas or categories used in the evaluation process [1], a detailed description of the criteria was prepared based on knowledge of accepted analytical methodology, sample-handling procedures, and quality control measures for selenium, as well as a knowledge of statistical methods, including statistically based sampling methods. As stated above, the ratings ranged from 3 (highest and most desirable) to 0 (lowest and unacceptable). For example, the evaluation criteria for the analytical method category are described in the following paragraphs.

Rating 3 (highest). The official fluorimetric method (reference provided) or other method was used and is documented by a complete write-up with validation studies for the foods analyzed. Validation includes use of an appropriate Standard Reference Material where available, 95—105% recoveries on a food similar to the samples analyzed which were reported in the same or another paper, and the selenium concentration above the quantitation limit of the method.

Rating 2. A modified fluorimetric or other method was used and is partially documented, but validation studies for the foods analyzed are incomplete. There must be at least 90—110% recoveries on a food similar to the samples analyzed which were reported in the same or another paper, or good recoveries but no statistics are given in the paper, and/or the authors have used another method (official fluorimetric, isotope dilution, or neutron activation method) on the same sample with good agreement (which is defined as within 10% relative).

Rating 1. A non-fluorimetric method was used and is only partly described. Recoveries were either 80—90% or >110% on a food similar to the samples analyzed, or even better recoveries were obtained, or a comparison method was used on food samples with only a somewhat related nature to the sample in question.

Rating 0 (lowest). The method used for the determination of selenium was not documented or referenced or the reference was inaccessible. No validation studies were conducted or selenium levels found in the food sample by the test method compared poorly to those found by the comparison method (>10%).

With the above definitions, it is expected that trained evaluators will derive the same ratings. Table 1 reproduces a manual worksheet for raw egg white which shows the ratings assigned to each of eight selenium values found in the literature. It is disappointing to note that measures to achieve analytical quality control were rarely reported.

SELEX IMPLEMENTATION

The initial SELEX implementation was written in ART (Automated Reasoning Tool) on a VAX Station II. The main inferencing mechanism was

TABLE 1

Manual worksheet for rating data on raw egg whites

Description	Data quality criteria ratings						
	Number of samples	Analytical method	Sample handling	Sampling plan	Analytical quality control	Quality index	Comments
White	1	2	1	2	0	1.2	Duplicates; no QC documentation
Albumen	1	1	1	0	0	0.6	No sampling plan or QC documentation
White	2	2	2	2	0	1.6	No QC documentation
White	1	0	1	2	0	0	No method validation
White	3	2	1	0	0	1.2	—
White part	1	2	2	0	0	1.0	Triplicates
White	2	0	0	1	0	0	No method validation
White	1	1	0	0	0	0	Mercury-contaminated feed
Confidence code[a] = B							

[a]The confidence code is derived from the sum of the quality indexes of the acceptable studies (QI $\geqslant$ 1). In this case the sum is equal to 5.0.

backward-chaining (deductive reasoning), although approximately 10% of the rules were forward-chaining (inductive reasoning). The system was driven backwards from the so-called "rating rules" which generated an integer rating from 0 to 3 for each of five major categories. The system was rewritten as completely forward-chaining because the automatic goal-generating mechanism of ART produced unacceptable slowness in response time to users. The forward-chaining ART version was then converted to CLIPS (the C Language Interfacable Production System) [4], a forward-chaining rule-based system which uses the Rete pattern-matching algorithm also used by ART and the computer language OPS5. Examples of two rules and their English translations are given in Table 2.

CLIPS was written by the NASA Artificial Intelligence Section [4]. CLIPS provided three immediate benefits. First, the CLIPS syntax is based closely on ART syntax so that SELEX could be ported quickly. Second, because CLIPS is written in standard C, it will run on any machine which has a suitable C compiler. This is particularly important in light of the fact that ART runs on a limited number of computers. Third, the source code was provided along with a built-in mechanism for adding functions so that extending and customizing CLIPS for SELEX was easily accomplished. For example, two extensions to CLIPS provide SELEX with the capabilities of verifying user input and keeping an audit trail file which contains the sequence of questions and the user's input for each session. The final system consists of approxi-

TABLE 2

Two rules used to determine a rating for sample handling. The first rule asserts a rating from information that has been obtained from the user. The second rule is an example of a rule which queries the user for information. Each rule is followed by an English translation

```
(defrule Rating-sample-handling-10
        (declare (salience 100))
        (seeking-rating sample-handling)
        (homogenization-validation-data optimal)
        (moisture-level-documented false)
        = >
        (assert (rating sample-handling 2)))
```

Translation of rule Rating-sample-handling-10[a]:

If you are seeking a rating for sample handling and the homogenization validation data are optimal and the moisture level was not documented, then the rating for sample handling is 2.

```
(defrule Food-preparation-documented
        (seeking-rating sample-handling)
        (or (perishable-food false)
            (shipping-and-storage-appropriate true)
            (shipping-and-storage-documented false))
        (not (food-preparation-documented ?))
        = >
        (if (y-or-n-p 3060 0 "Was the food preparation documented")
            then (assert (food-preparation-documented true))
            else (assert (food-preparation-documented false))
                 (assert (food-preparation-appropriate true))))
```

Translation for rule Food-preparation-documented:

If you are seeking a rating for sample handling and either the food is not perishable or the shipping and storage procedures were appropriate or the shipping and storage procedures were not documented and it is not known whether or not the food preparation was documented, then ask the yes-or-no question "Was the food preparation documented?". If the answer is yes then assert that the food preparation was documented or else assert that the food preparation was not documented and assume that the food preparation was appropriate.

[a]This rule has a declared salience of 100. The system will "fire" this rule ahead of rules with lower salience. In this case, rating rules must be fired ahead of information-gathering rules such as the second rule given (rules with no declared salience are assigned a default salience of 0) because once SELEX can determine a rating, no further information is needed. This exemplifies one key element of expert systems: intelligent questioning.

mately 200 rules and currently is implemented on VAX VMS and IBM PC MS-DOS machines, such as the IBM AT and Toshiba 3100.

As already stated, SELEX derives ratings for five major categories of evaluation: number of samples, analytical method, sample handling, sampling plan, and analytical quality control. Information is gathered by SELEX by a process of intelligent questioning of the user. The system was designed so

that only pertinent questions are asked. The responses are provided in accordance with information derived from the publication containing the selenium value to be rated. Depending on the responses, SELEX can produce a rating for each category from as few as 6 or as many as 65 answers. Approximately 90% of the questions require only a yes or no response with the remaining 10% requiring numeric input. A portion of a sample session with SELEX is shown in Table 3. As soon as SELEX has enough information to determine a rating for each of the five categories, the ratings are written to a file along with associated information such as a publication reference number and a description of the food. Periodically, this file is merged with a master file containing information from previously evaluated data. The master file is then analyzed with a SAS program which calculates a QI, a mean selenium value for each food, and a Confidence Code (CC) for that mean. The CC is derived from the QIs for all acceptable selenium values pertaining to a particular food.

VALIDATION AND BENEFITS OF SELEX

During development, SELEX was validated in two distinct ways. First, several of the 65 post-1960 selenium publications which reported original analytical selenium data for foods (from 33 different journals, reports, pro-

TABLE 3

Part of a typical session with SELEX. This portion represents the rating process for sample handling for a hypothetical example

Now seeking a rating for sample-handling for selenium
Was the sample handling procedure documented?
Response (Y or N): y
Was the sample food perishable?
Response (Y or N): y
Were the shipping and storage procedures documented?
Response (Y or N): n
Was the food preparation documented?
Response (Y or N): y
Was the method of food preparation appropriate?
Response (Y or N): y
Was only the edible portion of the food analyzed?
Response (Y or N): y
Was homogenization of the sample required?
Response (Y or N): n
Was the sample moisture level documented?
Response (Y or N): y
Was the moisture level of the sample appropriate?
Response (Y or N): y
The rating for sample-handling is 2.

ceedings, and books) which had been evaluated manually by the domain experts were run through SELEX. In instances where there was a difference between the manual rating assignments and the computer expert system ratings, the differences were compared. When necessary, existing rules were clarified or changed. Also, if needed, additional rules were written to assure a correct evaluation. Second, hypothetical cases were run through the system to validate decision paths which were not encompassed by actual data from the publications. Ongoing validation will continue until the domain experts are satisfied that SELEX performs at an acceptable level.

SELEX has several benefits over the original manual rating system. The manual system and the rules developed for SELEX incorporate knowledge from several domain experts who have complementary expertise. Therefore, the knowledge base is both broader and deeper than if only one expert had been used. With these rules incorporated in SELEX, publications can be rated by users who have less expertise than the domain experts.

During the process of formally defining the rating criteria as a rule set for SELEX, it was necessary to refine or restate some of the original criteria in more detail. Therefore, SELEX should produce more consistent results. The formalization of the knowledge base facilitates its transfer to other users. SELEX speeds the evaluation process and automatically maintains detailed records (audit trail) for each session. SELEX also reduces the "human error" factor by minimizing transcription, data entry, and calculation errors. The determination of a rating for a category, e.g., analytical method, results from the synthesis of several pieces of information. SELEX minimizes the errors that may be caused by the omission of information.

Because new publications with selenium data are evaluated intermittently, SELEX eliminates the need for the users to refamiliarize continually themselves with the complex set of heuristics.

The overall benefit, of course, is that SELEX will improve the definition and evaluation of the quality of the information available to identify any selenium/cancer correlation, because the results will be more accurate when an automated (objective) method is used rather than a manual method.

Although SELEX reduces the need for domain expertise, the user must have a certain level of understanding of analytical chemistry and nutrition science. Further refinement should reduce the level of expertise required by the user. SELEX will be generalized so that it is valid for the evaluation of published data from areas outside the United States. SELEX will provide the foundation of an expert system which can be adapted to evaluate data for a variety of nutrients. Part of this effort will include the engineering of an expert system which will automatically build rule sets for each nutrient. Such an expert system is possible because the structure of SELEX can be utilized as the template for new rules; the five categories and the rating process for each will be similar for many, if not most, nutrients. For example, the rating criteria for analytical methods will always include the use of a standard analytical method or methods, the description of non-standard

analytical methods, validation of these analytical methods, and the use of reference materials. The expert system will be able to query the user about the specific details for each nutrient and generate a rule set which is analogous to the SELEX rule set.

REFERENCES

1 J. M. Holden, A. Schubert, W. R. Wolf and G. R. Beecher, Food and Nutrition Bulletin, 9 (Suppl. — Food Composition Data: The User's Perspective), 1987.
2 A. Schubert, J. Holden and W. R. Wolf, J. Am. Diet. Assoc., 87 (1987) 285.
3 D. R. Lide, Jr., Science, 212 (1981) 1343.
4 G. Riley and C. Culbert, NASA/Johnson Space Center, Mission Planning and Analysis Division, Artificial Intelligence Section — FM72, Houston, TX 77058.

Analytica Chimica Acta, 200 (1987) 421—430
Elsevier Science Publishers B.V., Amsterdam — Printed in The Netherlands

CLASSIFICATION OF CHINESE TEA SAMPLES ACCORDING TO ORIGIN AND QUALITY BY PRINCIPAL COMPONENT TECHNIQUES

XIANDE LIU, P. VAN ESPEN and F. ADAMS*

Department of Chemistry, University of Antwerp (U.I.A.), Universiteitsplein 1, B-2610 Wilrijk (Belgium)

SHOU HE YAN and M. VANBELLE

Department of Animal Biology and Agriculture, Catholic University of Leuven, B-1348 Louvain La Neuve (Belgium)

(Received 10th April 1987)

SUMMARY

Three categories of tea, black, green and oolong tea, with two varieties in each category were analyzed for their contents of cellulose, hemicellulose, lignin, polyphenols, caffeine and amino acids. The data were subjected to multivariate analysis. Principal component analysis and principal component classification provide discrimination between the different categories and varieties. The quality index, assigned to these tea standards by experts, could be predicted from the principal component scores.

Tea is one of the most important and probably also one of the oldest beverages. Apart from its economic value, tea has also some religious and cultural significance. The total annual production of tea is about 2 million tons, of which 80% is produced in Asia. For a commercial product of this importance, it is necessary to use objective means for the quality control.

Chemical analysis in combination with multivariate data interpretation provides an interesting framework for the study of the quality and the origin of foodstuffs. Kwan and Kowalski [1] investigated wines from France and from the United States and used multivariate techniques to classify them according to the geographical origin and to evaluate the scores of a panel of experienced tasters [2]. Forina et al. [3] used pattern recognition methods to classify olive oils based on their fatty acid composition. A good overview of the possibilities and the application of multivariate data analysis in food science is available [4].

In this paper, principal component analysis and cluster analysis are applied to data from the chemical analysis of various tea samples in order to establish why and how the tea samples are different and how teas from different origin can be recognized, and to investigate the relation between the quality of the tea and its chemical composition.

0003-2670/87/$03.50

EXPERIMENTAL

Samples

Three categories of tea of Chinese origin were used in this study: green tea, black tea and oolong tea. Green tea is produced by drying and roasting of the leaves. To obtain black tea, the leaves are additionally fermented. Oolong tea is made by partial fermentation of the leaves. In each category, two varieties were available: Chunmee and Hyson for green tea, Keemun and Feng Quing for black tea, Tikuanyin and Se Zhong for oolong tea. The samples in each group were assigned a number according to their quality; the best quality has number 1. This quotation is given by tea experts on the basis of taste. All samples are reference samples produced by Chinese Tea Institutes. The information on the samples is summarized in Table 1. The names of the samples consist of the first letter of the name of the variety, followed by the number indicating the quality.

Chemical analysis

All samples were dried at 105°C to constant weight. The ash content was determined by heating the sample at 550°C for 6 h in a muffle furnace.

The fiber content was determined by a method developed by Van Soest and Wine [5, 6]. Approximately 1 g of dried sample was extracted by refluxing for 60 min with a neutral detergent solution. This aqueous solution contained 30 g of sodium lauryl sulfate, 18.61 g of Na_2 EDTA · 2 H_2O, 6.81 g of $Na_2B_4O_7$ · 10 H_2O, 4.56 g of Na_2HPO_4 and 10 ml of 2-ethoxyethanol per liter; the pH of the solution was adjusted with sodium hydroxide or hydrochloric acid to between 6.9 and 7.1. The residual material was rinsed with water and acetone, the latter to remove pigments and lipids. After subtraction of the ash content, the remaining weight is the total cellulose content or neutral detergent fiber (NDF) (cellulose, hemicellulose and lignin). In a similar way, the acid detergent fiber (ADF) was obtained by using a solution containing 27.8 ml of concentrated sulfuric acid and 20 g of acetyltrimethylammonium bromide in 1 l of water. Finally, the lignin content was determined by treating the residue of the ADF with a 72% (w/v) solution of

TABLE 1

Data on the tea samples studied

Category	Variety	Samples	Source
Green tea	Chunmee	C1, C2, C3, C4, C5, C6, C7	Shanghai Tea Institute
	Hyson	H1, H2, H3, H4, H5	Shanghai Tea Institute
Black tea	Keemun	K1, K2, K3, K4	Shanghai Tea Institute
	Feng Quing	F1, F2, F3, F4, F5, F6, F7	Yunnan Tea Institute
Oolong tea	Tikuanyin	T1, T2, T3, T4	Xia Men Tea Institute
	Se Zhong	S1, S2, S3, S4	Xia Men Tea Institute

sulfuric acid for 3 h. The residue is called the acid detergent lignin (ADL). The cellulose content is determined by subtracting the weight of the ADL residue from the weight of the ADF residue and hemicellulose content is obtained by subtracting the weight of the ADF residue from that of the NDF residue.

The polyphenol content was determined as in the AOAC methods [5, 6]; caffeine was determined by ultraviolet spectrophotometry and the amino acid content was obtained spectrophotometrically after reaction with ninhydrin [5–7].

TABLE 2

Results of chemical analysis of the standard tea samples

Sample	Concentration (% w/w, dry weight)					
	Cellulose	Hemicellulose	Lignin	Polyphenols	Caffeine	Amino acids
C1	9.50	4.90	3.53	29.03	4.44	3.82
C2	10.06	5.11	3.57	27.84	4.29	3.70
C3	10.79	5.46	4.62	26.53	3.91	3.46
C4	11.31	4.92	5.02	25.16	3.72	3.29
C5	11.50	6.08	5.48	23.28	3.50	3.10
C6	12.10	5.64	5.61	22.23	3.38	3.02
C7	13.30	5.68	6.32	21.10	3.14	2.87
H1	9.07	5.33	4.42	27.23	4.20	3.18
H2	10.75	5.80	5.29	25.99	4.00	3.00
H3	10.78	5.72	5.79	24.77	3.86	2.91
H4	12.00	6.68	7.20	24.05	3.49	2.81
H5	12.17	5.86	7.71	23.02	3.42	2.60
K1	10.32	10.66	5.07	21.55	4.23	4.43
K2	10.99	10.11	5.60	20.64	4.14	4.35
K3	12.32	10.12	6.53	20.06	4.02	4.12
K4	13.04	7.70	7.70	19.34	3.74	3.45
F1	10.95	7.84	5.22	26.68	5.03	5.32
F2	10.70	7.80	5.82	24.45	4.32	4.72
F3	10.81	8.43	6.00	23.74	4.11	4.50
F4	10.65	8.41	6.40	23.21	3.99	4.28
F5	11.24	8.13	7.61	22.68	3.81	4.09
F6	11.11	8.53	7.97	22.54	3.75	3.97
F7	11.83	9.78	8.67	22.16	3.59	3.88
T1	12.15	12.84	9.95	20.65	3.09	2.97
T2	12.13	12.35	10.55	20.61	2.97	2.49
T3	11.90	15.83	11.18	20.52	2.94	1.90
T4	11.92	15.58	11.87	20.42	2.83	1.79
S1	12.11	14.02	10.99	18.96	2.87	2.80
S2	12.74	14.23	11.16	18.64	2.72	2.23
S3	12.01	14.45	12.08	18.86	2.66	1.84
S4	11.85	14.42	12.60	18.84	2.64	1.76

All analyses were done in triplicate. The average concentrations found are listed in Table 2. Some replicate analyses indicated that the average uncertainty caused by random errors was ca. 1.5% (relative standard deviation) for the NDF, ADF and ADL determinations and ca. 2% for the determinations of polyphenols, amino acids and caffeine.

DATA ANALYSIS

The concentrations of the six chemical components measured on the 31 samples form a data matrix $\mathbf{X}_{(N \times M)}$; x_{nm} is the value of variable m measured on sample n. Mean and standard deviation for each variable were calculated as usual:

$$\bar{x}_m = (1/N) \sum_{n=1}^{N} x_{nm} \text{ and } s_m^2 = [1/(N-1)] \sum_{n=1}^{N} (x_{nm} - \bar{x}_m)^2$$

The data were autoscaled to zero mean and unit variance by subtracting from each variable the mean and dividing by the standard deviation:

$$z_{nm} = (x_{nm} - \bar{x}_m)/s_m$$

Hierarchical cluster analysis

The basic idea of cluster analysis is to find similar samples based on their closeness in the multidimensional space spanned by the variables [8]. In hierarchical clustering, the two samples that are closest together form a cluster. The distances between all the remaining samples and the newly formed cluster are recalculated. Then, two other samples form a new cluster, a sample is added to the existing cluster or clusters merge depending on the proximity of samples and clusters. This process is repeated until all individual samples are grouped in one cluster. The similarity measure used here was the Euclidian distance based on the autoscaled data. The distance between each pair of samples was calculated from

$$d_{ij} = (1/M) \sum_{m=1}^{M} (z_{im} - z_{jm})^2$$

The distance between a cluster i and a newly formed cluster, resulting from the merging of cluster j and k was calculated from

$$d_{i,j+k} = \frac{n_i + n_j}{n_i + n_j + n_k} d_{ij} + \frac{n_i + n_k}{n_i + n_j + n_k} d_{i,k} - \frac{n_i}{n_i + n_j + n_k} d_{j,k} \quad (1)$$

where n_i is the number of objects in cluster i. This procedure is known as Ward's error sum clustering method [8]. The result of the clustering process can be depicted as a branching-tree diagram.

Principal component analysis

In principal component analysis [9], new variables Y, called principal components (PC), are calculated as linear combinations of the original variables

in such a way that the first PC takes up as much as possible of the variance present in the original variables, the second PC accounts for as much as possible of the remaining variance, and so on. The principal components formed are orthogonal (uncorrelated):

$$y_{nk} = \sum_{m=1}^{M} z_{nm} b_{mk} \tag{2}$$

where y_{nk} is the value of the kth PC for object n and b_{mk} is the mth term of the kth eigenvector of the $(M \times M)$ matrix of correlations between the variables. The principal component scores calculated in this way have zero mean and variance equal to the corresponding eigenvalue λ_k. Standardized scores are calculated from $y'_{nk} = y_{nk}/\lambda_k^{1/2}$. From the eigenvectors, principal component loadings are calculated from $l_{mk} = b_{mk}\ \lambda_k^{1/2}$; l_{mk} reflects the correlation between the original variable m and the calculated principal component k and can be used to interpret the component.

Because the first principal components often account for a large fraction of the total variance of the original data set, an effective reduction of the dimensionality of the latter is achieved. The structure present in the data matrix can be visualized by plotting the first two or three principal components. The fraction of the variance explained by each principal component, k, is given by $\lambda_k/\Sigma_{m=1}^{M} \lambda_m$. Further, when principal components are calculated from autoscaled data, the total variance is equal to the number of variables: $\Sigma_{m=1}^{M} = M$. If K components are retained, the fraction of the total variance explained by the K components is given by $\Sigma_{k=1}^{K} \lambda_k/\Sigma_{m=1}^{M} \lambda_m$ and the fraction of the variance of each variable m in the original data set explained is $h_m^2\ \Sigma_{k=1}^{K} l_{mk}^2$; this is known as the communality.

Principal component classification

In this method, also known as SIMCA [10], a principal component model is built for each separate class of objects. The data in each class q are autoscaled by using the mean and the standard deviation calculated over the objects in the class:

$$\bar{x}_m^{(q)} = (1/N_q) \sum_{n=1}^{N_q} x_{nm}^{(q)}\ ;\ s_m^{2(q)} = [1/(N_q - 1)] \sum_{n=1}^{N_q} (x_{nm}^{(q)} - \bar{x}_m^{(q)})^2$$

so that $z_{nm}^{(q)} = (x_{nm}^{(q)} - \bar{x}_m^{(q)})/s_m^{(q)}$

Analogously to Eqn. 2, the principal component model becomes

$$y_{nk}^{(q)} = \sum_{m=1}^{M} z_{nm}^{(q)} b_{mk}^{(q)} \tag{3}$$

If K_q components are retained in model q, the data can be described in terms of the principal component model by

$$z_{nm}^{(q)} = \sum_{k=1}^{K_q} y_{nk}^{(q)} b_{mk}^{(q)} + e_{nm}^{(q)}$$

because the eigenvectors are orthogonal; $e_{nm}^{(q)}$ are the residuals of the fit of the data to the model. The residual variance in class q:

$$s_0^{2(q)} = [1/(N_q - K_q - 1)(M - K_q)] \sum_{n=1}^{N_q} \sum_{m=1}^{M} e_{nm}^2$$

is a measure of the overall fit or tightness of the class.

Any object t can then be tested to establish if it fits any of the Q models. The principal component scores y_{tk} are calculated from $y_{tk}^{(q)} = \Sigma_{m=1}^{M} z_{tm}^{(q)} b_{mk}^{(q)}$ $(k = 1 \ldots K_q)$ where $z_{tm}^{(q)}$ is the data vector of object t, scaled to zero mean and unit variance by using the mean and the standard deviation of class q. The prediction of this data vector by the model is then given by $\hat{z}_{tm}^{(q)} = \Sigma_{k=1}^{K_q} y_{tk}^{(q)} b_{mk}^{(q)}$ $(m = 1 \ldots M)$.

The goodness of fit to this model is given by

$$s_t^{2(q)} = [1/(M - K_q)] \sum_{m=1}^{M} (z_{tm}^{(q)} - \hat{z}_{tm}^{(q)})^2 \qquad (4)$$

If $s_t^{2(q)}$ is of the same magnitude as $s_0^{2(q)}$, the object t is considered as a member of class q. The F-test provides a quantitative measure for the classification: $F = s_t^{2(q)}/s_0^{2(q)}$, with $(M - K_q)$ and $(N_q - K_q - 1)(M - K_q)$ degrees of freedom.

All calculations were done with the data-analysis program DPP [11], running on a VAX computer.

RESULTS AND DISCUSSION

Table 3 summarizes the statistics for each variable; the mean, the standard deviation, the highest and lowest value and the sample having that value are given. The cellulose content is fairly constant and independent of the category and the variety. The hemicellulose and lignin contents are very variable and their concentrations tend to be lower for the high-quality tea samples (low numbers) in each group. The caffeine and amino-acid contents are highest for the good-quality teas in each group. The same observation can be made for the polyphenol concentration except for the oolong teas which have a nearly constant content of polyphenols.

TABLE 3

Summarized statistics for the tea data

Constituent	Mean	Standard deviation	Highest value and sample	Lowest value and sample
Cellulose	11.4	1.0	13.3 (C7)	9.1 (H1)
Hemicellulose	9.0	3.6	15.8 (T3)	4.9 (C1)
Lignin	7.3	2.7	12.6 (S4)	3.5 (C1)
Polyphenols	22.7	2.9	29.0 (C1)	19.0 (S1)
Caffeine	3.6	0.6	5.0 (F1)	2.6 (S4)
Amino acid	3.3	0.9	5.3 (F1)	1.8 (S4)

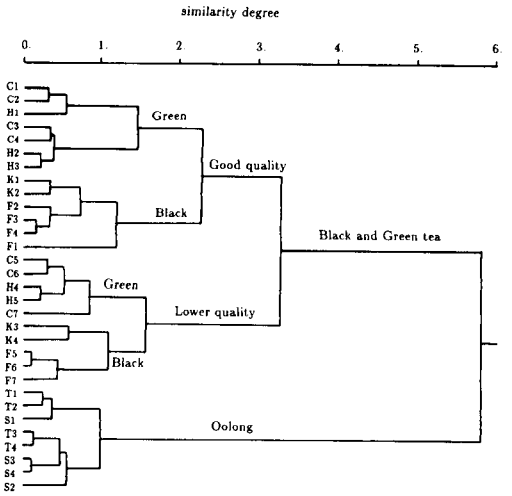

Fig. 1. Hierarchical clustering of the tea samples.

Hierarchical cluster analysis was used to investigate the possibility of classifying the tea samples according to their category or variety. The results of the clustering are shown in Fig. 1. At the highest level of dissimilarity (5.8) two distinct groups are formed. The smaller group contains all the oolong teas. In this group, no separation is obtained between the Tikuanyin and Se Zhong varieties. The larger group consists of the green and black tea samples, and is divided into two subgroups at a dissimilarity level of 3.3. The tea samples of good quality, both green and black, join the first subgroup, while the second subgroup contains all the green and black tea samples of lower quality. The cluster of high-quality teas finally breaks down at a dissimilarity level of 2.3 to give a group of green and a group of black teas. In the same way, the group of lower-quality teas is split into green and black teas at dissimilarity of 1.56. No direct clustering occurs on the basis of the variety. The results of the hierarchical clustering indicate that information on the category and quality of the tea is present in the results of the chemical analysis.

To investigate this further, principal component analysis was applied to the data. Table 4 summarizes the results. In the upper part of Table 4, the loadings, l_{mk}, of the first three principal components are given; they show the relation between the original variables and the components. The communality expresses how much of the variance of each variable is explained by these first three components. The eigenvalues in Table 4 show that about 96% of the variance in the original data is explained by the first three components. Component 3 has nearly the same eigenvalue as the second, whereas the fourth eigenvalue is only 0.1 (<2%), therefore only three components were retained. The correlation of the first principal component with the fiber material is highly positive but its correlation with the other constituents is

TABLE 4

Results of principal component analysis of the tea data in Table 2

Variable	Loading of PC 1–3			Communality
	1	2	3	
Cellulose	0.77	0.11	−0.61	0.98
Hemicellulose	0.82	0.33	0.44	0.97
Lignin	0.95	0.07	0.21	0.95
Polyphenols	−0.89	−0.36	0.14	0.94
Caffeine	−0.94	0.29	0.03	0.97
Amino acids	−0.76	0.63	−0.08	0.98
Eigenvalue	4.42	0.74	0.64	
% Eigenvalue	73.6	12.4	10.6	
Cumulative %	73.6	86.0	96.6	

negative. This typical pattern may be due to the partial closure in the data; a high fiber content necessarily results in lower concentrations of the other constituents. The second principal component is significant for amino acids, and the third component for cellulose. Figure 2 shows a plot of the first three components. Three well-separated groups, one containing the green tea, one containing the black tea and one containing the oolong tea samples are formed. The separation is also clear on the projection to the first two components (Fig. 3). Further, it seems that the first principal component is indicative of the quality of the tea. Indeed, the samples in each group are ordered from high quality to lower quality along the projection to the first axis. Some structuring in the plot, related to the variety in each category, can be seen.

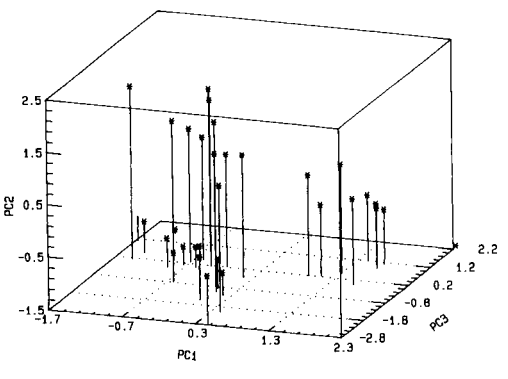

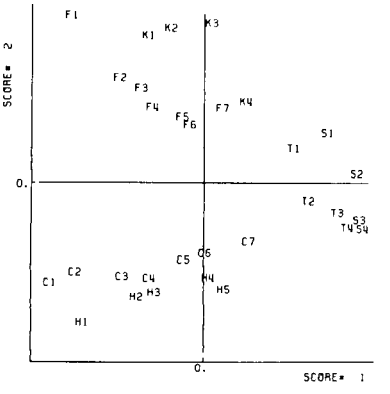

Fig. 2. Plot of the tea samples in the space of the first three principal components.

Fig. 3. Projection of the tea samples in the plane of the first two principal components.

Classification of tea samples

Figures 2 and 3 show that the three categories of tea are well separated in the principal component space, but it is not clear if any distinction can be made between the two varieties in each category. In order to investigate this, a separate principal component model was built for each of the six groups. Data in each group were corrected for the mean of the group and standardized to unit variance by dividing by the group standard deviation. Based on cross-validation [10], it was found that each group could be fitted to a model with one principal component. Next, the distances, as given by Eqn. 4, of all the tea samples to each of the models were calculated. The distance plots are given in Fig. 4. In Fig. 4A, the line parallel to the x-axis is the critical distance of the Hyson model; samples below this line are considered as belonging to the Hyson variety. In a similar way, samples to the left of the line parallel to the y-axis are classified as Chunmee teas. The critical distance was calculated at a 95% confidence level (F-test) based on the residual variance of the model considered. As can be seen, all samples are classified correctly and there is no overlap (lower left part of the figure) between the tea samples. Figure 4B shows a similar plot for the Keemun and Feng Quing black teas. Similar results, with complete separation, were found for the oolong teas. Because this data set consists of a unique set of samples, division of the samples in a training set and an "unknown" set was not viable. The results, however, indicated that the chemical results provided a basis for distinguishing not only between the different categories of tea but also between the two varieties within each category.

Prediction of quality

As mentioned above, Fig. 2 shows the ordering of the samples along the first principal component axis, related to the quality of the tea (low number have high quality). It must be stressed that the assignment of quality by the

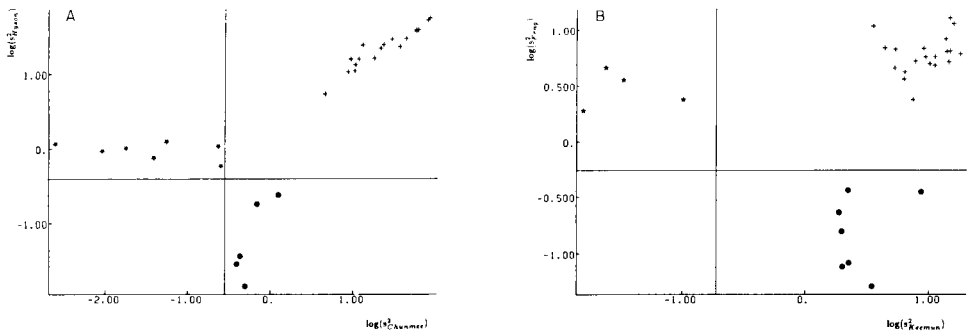

Fig. 4. Distance plots. (A) Green teas: x-axis is the distance of the sample from the Chunmee model; y-axis is the distance from the Hyson model; (⋆) Chunmee samples, (•) Hyson samples, (+) other samples. (B) Black teas: x-axis is the distance of the sample from the Keemun model; y-axis is the distance from the Feng Quing model; (⋆) Keemun samples, (•) Feng Quing samples, (+) other samples.

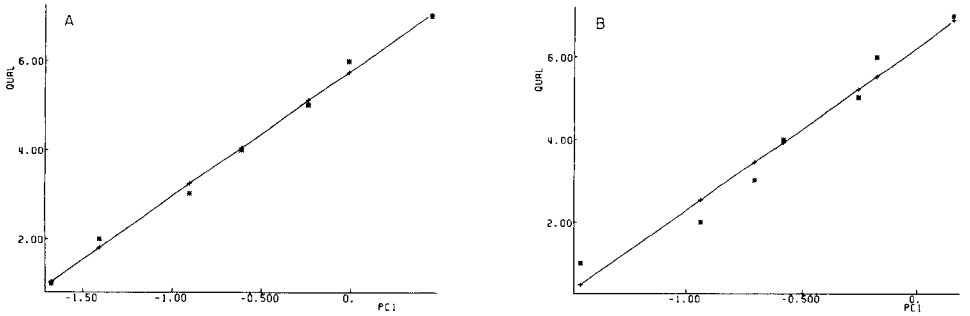

Fig. 5. Regression of the quality index of different samples with the scores of the first principal component: (A) Chunmee samples (green tea); (B) Feng Quing samples (black tea).

tea experts is valid only for samples belonging to the same category and variety. Further, the quality index is a simple ordinal scale; a tea with a quality index 2 is not necessarily twice as good as a tea with quality index 4. Nevertheless, an attempt was made to predict the quality index based on the principal component scores.

For each tea variety, a straight-line regression was calculated with the quality index as dependent variable and the scores of the first principal component as independent variable. The standardized principal components calculated for the entire data set were used. Figure 5 shows the results for the Chunmee and the Feng Quing samples. In both cases, there is an excellent fit between the quality index and the first principal component, with correlation coefficients of 0.997 (Fig. 5A) and 0.983 (Fig. 5B). Similar results were obtained for the Hyson, Keemun and Tikuanyin varieties. For the Se Zhong variety, no meaningful results were obtained; samples S2, S3 and S4 had nearly the same scores on the first principal component.

The procedure described apparently allows accurate prediction of the quality scores given by the tea experts.

REFERENCES

1 W. O. Kwan and B. R. Kowalski, Anal. Chim. Acta, 122 (1980) 215.
2 W. O. Kwan and B. R. Kowalski, J. Agric. Food Chem., 28 (1980) 356.
3 M. Forina, C. Armanino, S. Lanteri and E. Tiscornia, in H. Martens and H. Russwurm (Eds.), Food Research and Data Analysis, Applied Science Publishers, London, 1983, pp. 189—214.
4 Food Research and Data Analysis, H. Martens and H. Russwurm (Eds.), Applied Science Publishers, London, 1983.
5 P. J. Van Soest and R. H. Wine, J. Off. Anal. Chem., 50 (1967) 50.
6 P. J. Van Soest and R. H. Wine, J. Off. Anal. Chem., 51 (1968) 780.
7 S. H. Yan, Tea Quarterly Sinica, 1 (1978) 13; Acta Biochim. Biophys. Sinica, 8 (1979) 225; Acta Agr. Sinica, 2 (1983) 45.
8 D. L. Massart and L. Kaufman, The Interpretation of Analytical Chemical Data by the Use of Cluster Analysis, Wiley, New York, 1983.
9 M. A. Sharaf, D. L. Illman and B. R. Kowalski, Chemometrics, Wiley, New York, 1986.
10 S. Wold, Pattern Recognition, 8 (1976) 127.
11 P. Van Espen, Anal. Chim. Acta, 165 (1984) 31.

Analytica Chimica Acta, 200 (1987) 431—445
Elsevier Science Publishers B.V., Amsterdam — Printed in The Netherlands

FAST-ATOM-BOMBARDMENT AND TANDEM MASS SPECTROMETRY FOR DETERMINING STRUCTURES OF FATTY ACIDS AS THEIR PICOLINYL ESTER DERIVATIVES

LEESA J. DETERDING and MICHAEL L. GROSS*

Midwest Center for Mass Spectrometry, Department of Chemistry, University of Nebraska, Lincoln, NE 68588 (U.S.A.)

(Received 2nd February 1987)

SUMMARY

Picolinyl ester derivatives of common fatty acids can be readily desorbed by fast atom bombardment (FAB) as positive ions and then collisionally activated. Collisionally activated spectra of the $(M + H)^+$ ions of the derivatives reveal that structurally informative remote-charge-site fragmentations occur. The presence of substituents such as double bonds, branch points, cyclopropane rings, hydroxy groups, and epoxy rings interrupts the fragmentation process in such a way that the substituent can be identified and its location on the alkyl chain can be determined. This method is also applicable to the picolinyl esters of short-chain fatty acids and to the analysis of mixtures of fatty acid derivatives. The approach is advantageous because the picolinyl ester derivatives are also amenable to gas chromatography/mass spectrometry (GC/MS). Therefore, the FAB-MS/MS approach developed here is complementary to GC/MS.

Many structurally modified fatty acids exist as part of complex lipids. The structural modifications, such as double bonds, branch points, hydroxy and epoxy groups, and cyclopropane rings, are of interest because they are characteristic of the organism [1—5]. Because these fatty acids exist as complex mixtures, it is necessary to use some type of separation coupled with structural analysis to study a particular acid [5—7].

Gas chromatography is useful for dealing with mixtures, and when combined with mass spectrometry (GC/MS), much structural information can be obtained [8]. Unfortunately, free fatty acids cannot be examined directly by GC/MS, and some kind of derivatization is necessary.

*Michael L. Gross is 3M Alumni Professor of Chemistry at the University of Nebraska, Lincoln. He received his Ph.D. in Organic Chemistry in 1966 at the University of Minnesota and was a postdoctoral fellow at the University of Pennsylvania and at Purdue University. He joined the faculty at the University of Nebraska as Assistant Professor in 1968. His research interests include chemistry of gas-phase ions, development of tandem MS and Fourier-transform MS instrumentation and their application to biomolecules, and the analysis for traces of chlorinated dioxins, dibenzofurans, and related compounds in environmental and biological samples. He is the author or coauthor of over 180 publications and has edited one book.

0003-2670/87/$03.50

The mass spectrometric analysis of many derivatized fatty acids reveals useful structural information. Derivatization is usually focussed either at the acid function or at the structural modification (e.g., double bond or hydroxyl function). Most common of the former are the methyl ester or trimethylsilyl (TMS) ester derivatives [9—11]. These ester derivatives are very amenable to GC/MS, but problems such as the low abundance of high-mass ions and loss of information about double-bond positions as a result of migration of double bonds along the alkyl chain of the molecular ion have limited their use.

Recently, new derivatization methods of the acid function involving preparation of pyrrolidides [12—18] and picolinyl esters [19, 20] have been used to advantage. Probably because of the ability of the derivatizing group to localize the charge, these molecules fragment under electron-ionization (EI) conditions more selectively than other derivatives. Not only are these derivatives useful for locating double bonds, but also they are valuable for determining the location of other structural modifications. The fragmentation pattern of pyrrolidides and picolinyl esters are similar because both yield fragments 14 mass units apart. The location of double bonds can be determined because intervals of 12 mass units appear in the spectra. Although pyrrolidide derivatives have been most often studied, the picolinyl ester derivatives are more advantageous because they yield more abundant high-mass ions and are easier to prepare. The usefulness of these two derivatives for the structural elucidation of fatty acids was recently compared [21].

More recently, it was established that fast atom bombardment (FAB) in conjunction with tandem mass spectrometry is very useful for the structural determination of both free fatty acids and mixtures of fatty acids and related materials [22, 23]. FAB-desorbed ions, either carboxylate anions [24—30] or lithiated species [31, 32], undergo remote-charge-site fragmentations upon collision activation, and these fragmentations produce information for locating a variety of structural modifications.

A hybrid approach is described in this paper and utilizes the advantages of both the method involving derivatives and the FAB-MS/MS methods. Picolinyl ester derivatives of common fatty acids are not only amenable to GC/MS but also can be readily desorbed by FAB as positive ions and then collisionally activated. Collisionally activated decomposition spectra of the $(M + H)^+$ ion of the derivatized fatty acids reveal that structurally informative remote-charge-site fragmentations occur just as they do for fatty acid carboxylates [25] and for metal-ion cationized acids [31]. This method was developed as an alternative approach or as a means for confirming interpretations drawn from GC/MS results. Moreover, a study of the collisional activation of fatty acid derivatives presents an opportunity to understand and expand the scope of charge remote decompositions.

EXPERIMENTAL

Samples

Capric, myristic, lauric, oleic, ricinelaidic, vaccenic, linolelaidic, 12-hydroxydodecanoic, 12-hydroxystearic, erucic, 4,8,12,15-octadecatetraenoic, n-valeric, palmitoleic, n-caproic, heptanoic, 3-methyl-n-valeric, α-hydroxyisocaproic, 4-pentenoic, α-hydroxyisovaleric, n-butyric and propionic acids were purchased from Sigma Chemical Co. Stearic, 2-octenoic, palmitic, 4-methylvaleric, *trans*-2-pentenoic, 2-methylhexanoic, *trans*-2-methyl-2-pentenoic, 2-methylbutyric, 3,3-dimethylacrylic acids were purchased from Aldrich Chemical Co. The following fatty acids were purchased from Foxboro/Analabs (North Haven, CT): eicosanoic, 9,10-epoxyoctadecanoic, 2-hydroxytetradecanoic, 2-hydroxyhexadecanoic, docosahexaenoic, 2-hydroxydecanoic, *trans*-9-hexadecenoic, erucic, *trans*-9,10-methyleneoctadecanoic, linolenic, phytanic, 14-methylhexadecanoic, 16-methylheptadecanoic, 16-methyloctadecanoic, and 18-methylnonadecanoic acids. Hexadecanoic-7,7,8,8-d_4 and hexadecanoic-16,16,16-d_3 acids were from MSD Isotopes (Montreal, Canada), and oleic-9,10-d_2 acid was from Cambridge Isotopes (Woburn, MA). Vaccenic epoxide was prepared by allowing a mixture of vaccenic acid, 3-chloroperoxybenzoic acid and acetone to stand in a reaction vial at room temperature.

Derivatization and mass spectrometry

The picolinyl esters were prepared by the method previously described by Harvey [20]. The acid (ca. 1 mg) was placed in a reaction vial and was converted to its acid chloride by reaction with an excess of thionyl chloride. A stream of nitrogen was used to blow off the excess of thionyl chloride, and the residue was reacted with ca. 500 μl of a 10% solution of 3-(hydroxymethyl)pyridine in acetonitrile. The resulting solution was then purified by liquid chromatography by using a short silica column prepared in a disposable Pasteur pipet. Ethyl acetate was used to elute the fatty acid derivative. The sample was collected, and the excess solvent was blown off with a stream of nitrogen.

For unsaturated fatty acids and some epoxy acids, chlorination at the functional group may result if an excessive amount of thionyl chloride is used in the synthesis. Ions of these chlorinated materials, if present, are seen in the full mass spectrum. Upon collisional activation, the loss of one and two molecules of HCl, some water loss, and a few fragmentations proximate to the charge site (discussed below) are the only decompositions that result. The problem of unwanted chlorination is easily remedied by avoiding large excesses of the thionyl chloride.

Mass spectra of the derivatized fatty acids were obtained with a Kratos MS-50 triple analyzer mass spectrometer [33]. The instrument consists of a high-resolution MS-I followed by an electrostatic analyzer used as MS-II. An Ion-Tech atom gun and a standard Kratos FAB source were used. The

samples were dissolved in dithiothreitol/dithioerythritol matrix, and a small drop was placed on the tip of the FAB direct-insertion probe. The sample was bombarded with 6—8-keV argon atoms. Full mass spectra were acquired at a resolution of ca. 3000 by scanning MS-I and leaving MS-II fixed. The mass-selected ions were activated by colliding them with helium gas (50% beam suppression) in the collision cell between MS-I and MS-II. Collisionally-activated dissociation (CAD) spectra of the resulting daughter ions were obtained by scanning MS-II, and the spectra were signal-averaged and processed with a Kratos DS-55 data system using software written in this laboratory [34].

RESULTS AND DISCUSSION

Mass spectra of the positive ions of saturated, unsaturated, polyunsaturated, branched, cyclopropane, epoxy, and hydroxy acids that were converted into picolinyl esters and desorbed by FAB contain the $(M + H)^+$ ion and typically the low-mass matrix ions. Little or no information regarding structure can be obtained from these spectra because the desorption is accompanied by little fragmentation except for the loss of water from some hydroxy and epoxy acids.

Although fast atom bombardment was chosen to prepare $(M + H)^+$ ions of the derivatized fatty acids, another means for generating these ions is chemical ionization. Chemical-ionization mass spectrometry has also been applied to fatty acids for structural determination [35—40]. For the problem of double-bond location, derivatization is necessary and may be accomplished either by an ion-molecule reaction in the mass spectrometer or by derivatization prior to analysis. Chemical ionization and other methods were recently reviewed [41].

If the $(M + H)^+$ ions of the picolinyl ester derivatives of the acids are selected by using MS-I and collisionally activated, then distinctive remote-charge-site fragmentation [25] occurs producing information for identifying structurally modified fatty acids. This is to be contrasted with the collisional activation of the $(M + H)^+$ ions of the fatty acids and their methyl esters. Here, carbocation intermediates are formed by charge-mediated processes. The usual isomerizations of carbocations cause loss of structural information. Typical charge-mediated processes are the losses of water and methanol from $(M + H)^+$ ions of acids and methyl esters, respectively, to give acylium ions (RCO^+). These latter ions fragment to carbocations by undergoing losses of carbon monoxide and water, for example. The decomposition chemistry of the $(M + H)^+$ ions of the picolinyl ester derivatives is discussed in the following paragraphs in terms of the various classes of fatty acids.

Saturated fatty acids

Collisionally activated dissociation (CAD) spectra of the $(M + H)^+$ ion of derivatized fatty acids reveal two types of fragmentation: (1) remote-charge-

site fragmentation, and (2) fragmentation proximate to the charge site. The latter produces characteristic ions as those of *m/z* 93, 109, 152, and 164. The CAD spectrum (Fig. 1) of the $(M + H)^+$ ion of the stearic acid derivative is illustrative and presents likely structures of these fragments.

For charge-remote fragmentation to occur, a stable charge site must be present in the molecule [29]. The picolinyl ester moiety apparently is sufficiently basic and provides a stable site where the proton can be localized such that remote-charge-site fragmentation occurs. The fragmentations involve the parallel losses of C_nH_{2n+2} elements beginning at the alkyl terminus. This unique fragmentation pattern is highly reproducible in the CAD spectra of these saturated fatty acid derivatives and resembles that found for saturated fatty acid carboxylates [25] and for metal-cationized fatty acids [31].

Unsaturated fatty acids

Mono-unsaturated fatty acids, such as erucic acid, fragment in much the same way as saturated acids. However, cleavage of double bonds is not readily accomplished; thus, an interruption in the remote-charge-site fragmentation pattern occurs at the location of the double-bond position. Mono-unsaturated fatty acids fragment by losing the elements of C_nH_{2n+2} from the hydrocarbon terminus until the allyl bond is reached. Allyl bond cleavage accompanied by H-transfer gives a facile loss of C_nH_{2n+2}. Cleavage of

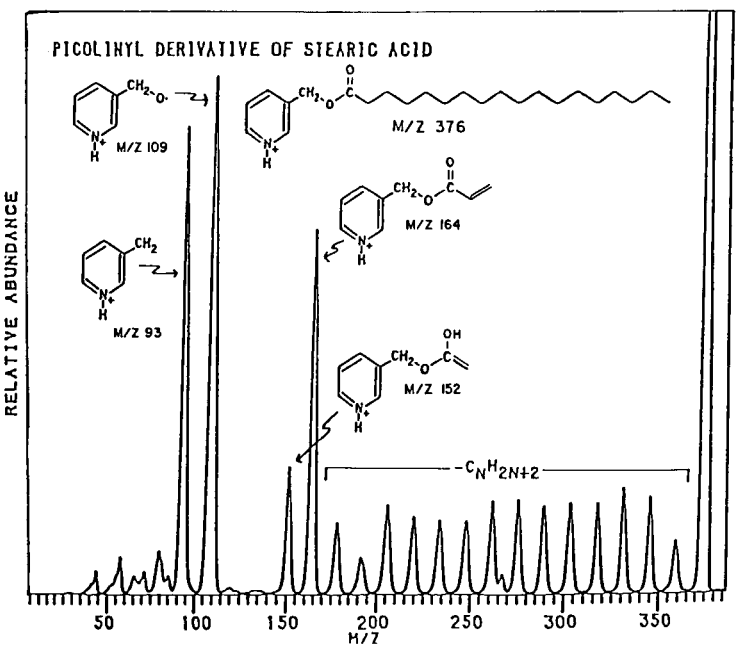

Fig. 1. CAD spectrum of the $(M + H)^+$ ion of *m/z* 376 of the picolinyl ester of stearic acid.

the other allyl bond, the one proximate to the ester function, is also facile and is accompanied by the loss of C_nH_{2n}. Structurally isomeric unsaturated fatty acids, for example oleic and vaccenic acid, may be easily determined by interpreting the CAD spectra of the $(M + H)^+$ ions (Fig. 2A and B).

Polyunsaturated fatty acids

Establishing the location of double bonds in polyunsaturated acids is possible for cases of two and three double bonds, linolelaidic and linolenic acid (Fig. 3A and B), respectively, but becomes more difficult for acids containing four or more sites of unsaturation. For polyunsaturated acids, the abundances of the fragment ions relative to the $(M + H)^+$ are lower than those of fragment ions of saturated and monounsaturated fatty acids. Introduction of multiple double bonds strengthens the hydrocarbon chain and decreases the opportunity of charge-remote fragmentation.

Branched fatty acids

The methyl branch positions in phytanic acid (3,7,11,15-tetramethylhexadecanoic acid) are easily located from the CAD spectrum of the $(M + H)^+$ ion of the picolinyl derivative (Fig. 4A). The remote-charge-site fragmentation is observed with nearly total suppression of the fragments that involve the losses of the alkyl and methyl branches. Branched fatty acids (iso and anteiso), such as 16-methylheptadecanoic acid and 16-methyloctadecanoic acid, respectively, are easily distinguished by this characteristic fragmentation pattern (Fig. 4B and C).

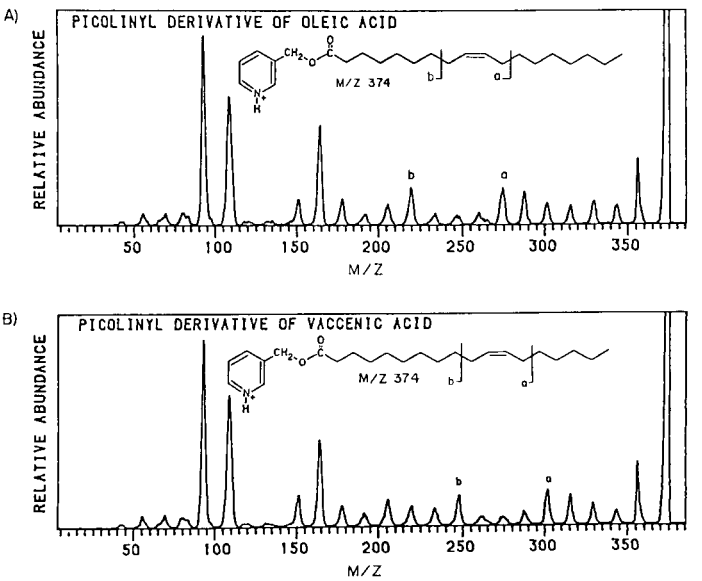

Fig. 2. CAD spectra of the picolinyl ester $(M + H)^+$ ions of oleic acid (A) and vaccenic acid (B).

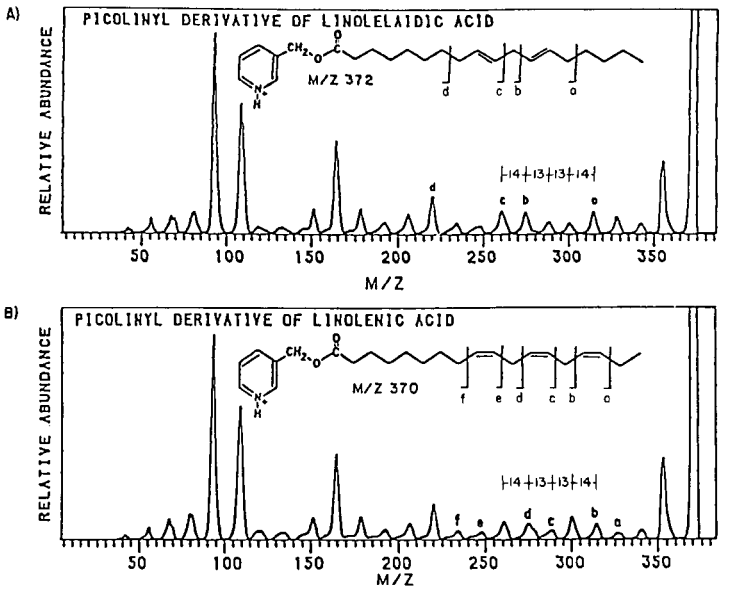

Fig. 3. CAD spectra of the picolinyl ester $(M + H)^+$ ions of polyunsaturated linolelaidic acid (A) and linolenic acid (B).

Cyclopropane-substituted fatty acids

From the CAD spectrum of *trans*-9,10-methyleneoctadecanoic acid (Fig. 5), location of the position of the cyclopropane ring is possible, but the location is not as readily determined from the general appearance of the spectrum as are other substituents. However, the loss of 13 mass units at the site of the substitution rather than the typical loss of 14 mass units along the alkyl chain makes location of the cyclopropane ring possible. The remote-charge-site fragmentation pattern is similar to, but less pronounced than, that observed for unsaturated acids. Fragmentations at the site of the ring are somewhat suppressed as compared to the other fragmentations.

Hydroxy fatty acids

Hydroxy groups on fatty acids can be located at any position on the alkyl chain. Fatty acids containing terminal hydroxy functions such as 16-hydroxyhexadecanoic acid (Fig. 6A) show an abundant loss of water and the loss of $C_nH_{2n+2}O$ fragments such as CH_3OH, C_2H_5OH, etc. These fragmentations are regarded as occurring without intervention of the charge site.

Mid-chain hydroxy acids such as 12-hydroxystearic acid (Fig. 6B) undergo primarily the loss of water upon collisional activation. Nevertheless, remote charge-site fragmentations still occur and allow the location of the hydroxy substituent to be determined. Fragmentation on either side of the substituted carbon is particularly facile whereas fragmentation at the point of substitution is suppressed. This MS fragmentation pattern is very similar to

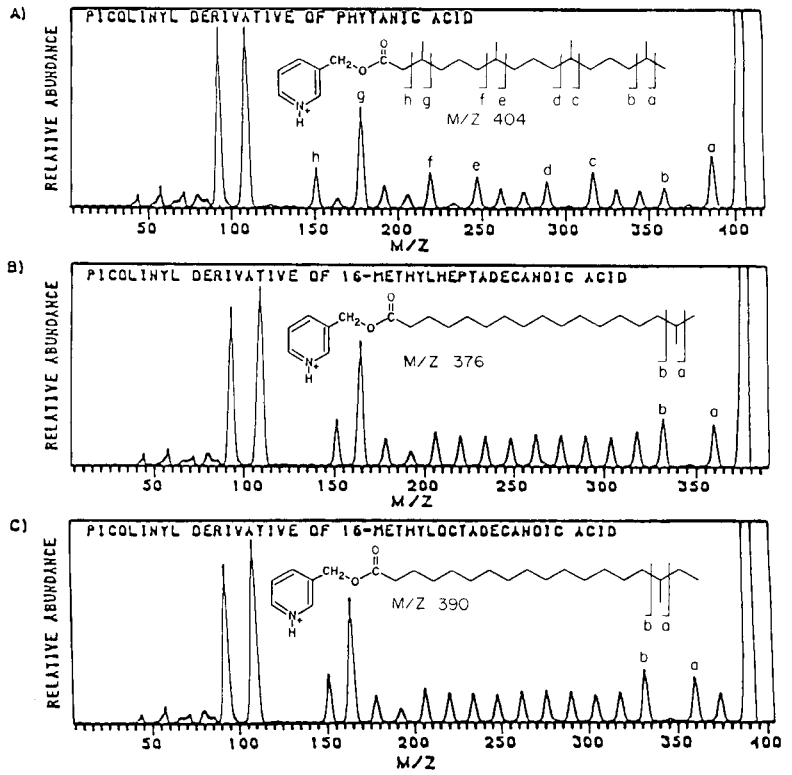

Fig. 4. CAD spectra of the picolinyl ester $(M + H)^+$ ions of branched fatty acids: (A) phytanic acid; (B) 16-methylheptadecanoic acid; (C) 16-methyloctadecanoic acid.

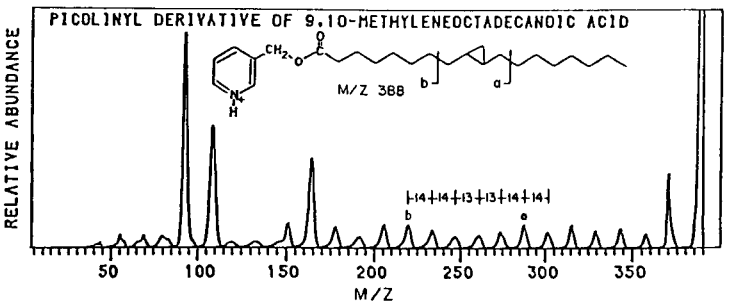

Fig. 5. CAD spectrum of the picolinyl ester $(M + H)^+$ ion of 9,10-methyleneoctadecanoic acid.

those of methyl-branched acids but is immediately distinguishable by the abundant loss of water from the $(M + H)^+$ ions of derivatized hydroxy acids, and the fact that the mass difference between peaks *a* and *b* (Figs. 4 and 6) is 30 mass units for hydroxy acids and 28 mass units for branched acids.

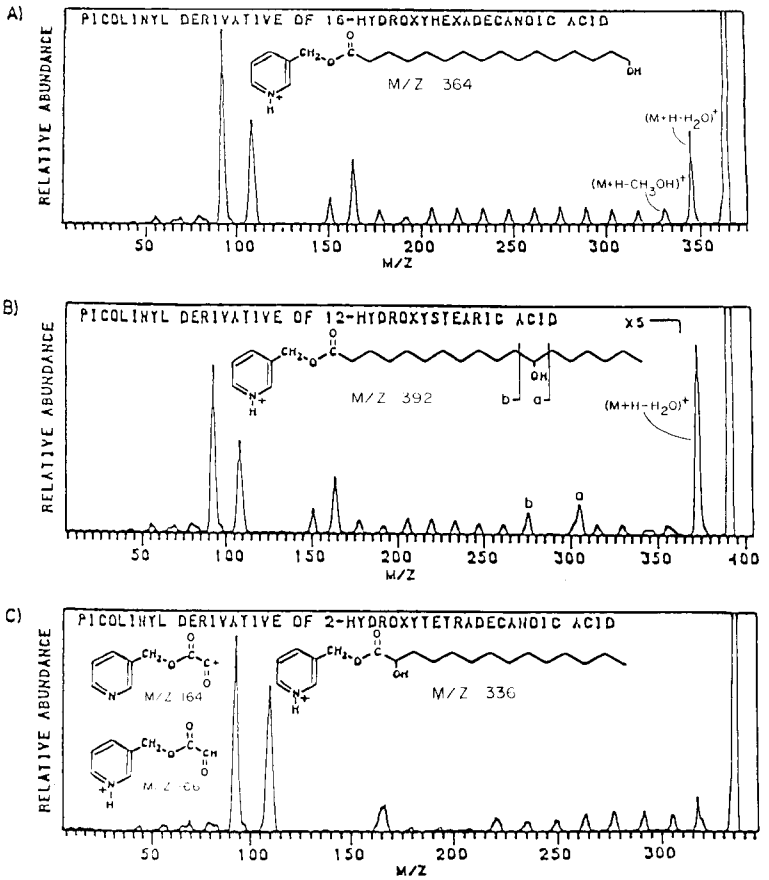

Fig. 6. CAD spectra of the picolinyl ester $(M + H)^+$ ions of hydroxy-substituted acids: (A) 16-hydroxyhexadecanoic acid; (B) 12-hydroxystearic acid; (C) 2-hydroxytetradecanoic acid.

Picolinyl ester derivatives of 2-hydroxyhexadecanoic acid and 2-hydroxytetradecanoic acid (Fig. 6C) fragment upon collisional activation to give an abundant ion at approximately *m/z* 166 and three adjoining ions with low abundance at *m/z* 180, 194, and 208. Narrow scans over the region of *m/z* 166 reveal that the peak is actually a doublet consisting of the ions of *m/z* 164 and *m/z* 166 (proposed structures are given in Fig. 6C). Other charge-remote fragments that are also observed in the spectra are due to the losses of the elements of C_nH_{2n+2}. This fragmentation pattern is unique for 2-hydroxy acids.

Epoxy-substituted fatty acids

The CAD spectrum of the $(M + H)^+$ ion of derivatized *cis*-9,10-epoxyoctadecanoic acid (Fig. 7) is representative of fatty acids containing epoxy

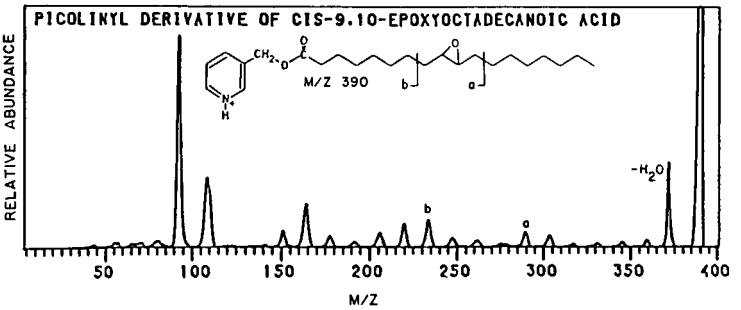

Fig. 7. CAD spectrum of the picolinyl ester $(M + H)^+$ ion of *cis*-9,10-epoxyoctadecanoic acid.

substituents. The ion formed by the loss of water is more abundant than those produced by other remote-charge-site fragmentations. However, the parallel losses of the elements of C_nH_{2n+2} are observed as fragmentation moves along the alkyl chain. The epoxy substituent can be located by the relatively more facile cleavages at points *a* and *b* (see Fig. 7), which correspond to the fragmentations at the C—C bond that is one bond removed on either side of the three-membered ring. In general, the presence of an epoxy substituent in fatty acids is located by identifying a spectral region having a very intense peak on either side of three adjoining peaks with low intensity.

Short-chain fatty acids

The FAB-MS/MS method is also useful for identifying short-chain fatty acids. One example in which characterization of short-chain fatty acids is important is in the diagnosis of inherited metabolic diseases in children. Typically, excessive amounts of short-chain acids are found in these children [42]. Hunt et al. [43] also used MS/MS for the identification of short-chain carboxylic acids found in metabolic abnormalities. Upon collisional activation, remote-charge-site fragmentations are still observed for picolinyl esters of small saturated acids such as *n*-valeric acid and heptanoic acid (Fig. 8A). The ions resulting from the familiar losses of C_nH_{2n+2} elements from the alkyl terminus are relatively abundant. Low-mass ions owing to fragmentations proximate to the charge site are also observed. Because the alkyl chain length is relatively short (4—8 carbons), it is difficult to locate double bonds, but the CAD spectrum of the $(M + H)^+$ ion of the picolinyl ester of 4-methylvaleric acid (Fig. 8B) shows that it is possible to locate branch points on short-chain fatty acids. In general, it is more difficult to define structural features on short-chain acids by examining charge-remote fragmentation than on long-chain acids, but this approach involving picolinyl esters may be useful for confirming GC/MS data of short-chain fatty acids produced by metabolic diseases.

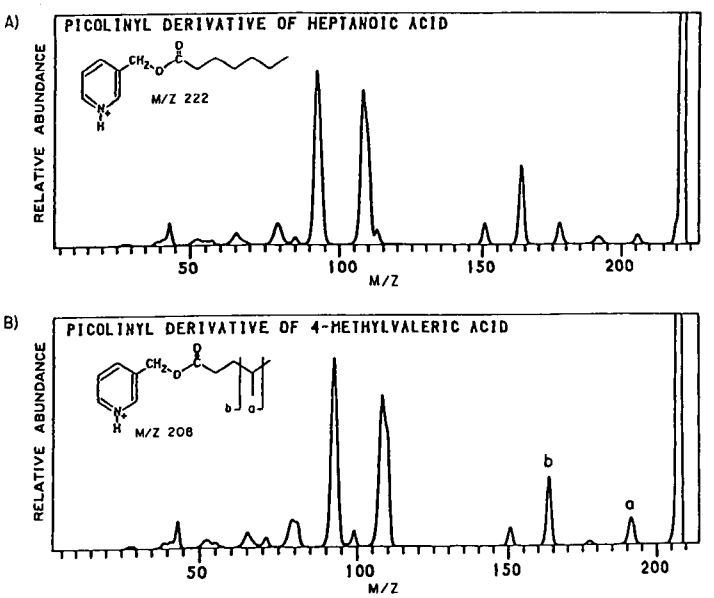

Fig. 8. CAD spectra of the picolinyl ester $(M + H)^+$ ion of short-chain acids: (A) heptanoic acid; (B) 4-methylvaleric acid.

Mixture of fatty acid derivatives

A mixture of five different fatty acids was prepared by placing the free fatty acids together in a reaction vial and preparing the picolinyl ester derivatives as previously described. Two separate experiments were done. The first involved the picolinyl derivatives of erucic, eicosanoic, 14-methylhexadecanoic, 12-hydroxystrearic, and linolenic acids; the second was the same except that linoleic acid was used instead of linolenic acid. Ions formed by the FAB desorption of the picolinyl derivative $(M + H)^+$ ions of the different acids were all observed in the mass spectra. The eicosanoic and erucic acid derivatives showed equal response factors within 25% in the two separate experiments. However, the experiments were slightly more sensitive to the 14-methylhexadecanoic acid derivative in the early scans, but in later scans, this derivatized acid was not observed. Apparently, this acid derivative is preferentially desorbed and ultimately depleted with respect to the other acids.

Lower response factors were observed for the $(M + H)^+$ ions of the derivatized 12-hydroxystearic acid and linoleic or linolenic acid. These lower response factors may be attributed to the fact that the more hydrocarbon-like acids (i.e., eicosanoic, erucic, and 14-methylhexadecanoic acids) are less polar than the hydroxy and polyunsaturated acids, and therefore, are less tightly bound to the matrix. As a result, these hydrocarbon-like acids are more surface-active and thus are more readily desorbed and detected [44, 45]. The less hydrocarbon-like acids (i.e., 12-hydroxystearic, linolenic and linoleic acids) are more polar and, therefore, prefer to exist in the bulk of

the matrix. These more polar acids are desorbed less readily. This explanation is under further investigation.

Selection of any given $(M + H)^+$ ion of the picolinyl ester derivatives of the mixture with MS-I followed by collisional activation and mass analysis with MS-II was successful. The CAD spectra obtained in the mixture analysis are identical to those obtained from the $(M + H)^+$ ions of the individual fatty acid derivatives.

Mechanism and comparison with the collisional activation of $(M - H)^-$ anions and $(M + 2Li - H)^+$ ions

Upon collisional activation, the $(M + H)^+$ ions of the picolinyl ester derivatives of fatty acids undergo remote-charge-site fragmentation as do carboxylate anions [24—30] and the lithiated species $(RCOOLi_2)^+$ [31] of these fatty acids. Collisional activation of the $(M + H)^+$ ions of the derivatized hexadecanoic-7,7,8,8-d_4 acid leads to a set of fragments (Table 1) that show that the mechanism is consistent with a 1,4-hydrogen elimination as was proposed previously for carboxylate anions [25] and lithiated ions [31].

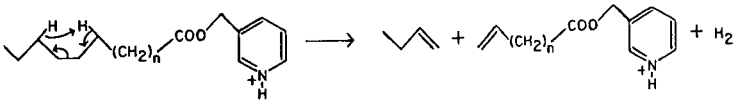

It was impossible to resolve, for example, $(M + H - C_7H_{15}D)^+$ and $(M + H - C_7H_{16})^+$. Nevertheless, it is certain that the amount of the latter ion formed, if any, is no more than 5% of the former.

Although the decomposition reactions of the ions of $RCOO^-$, $RCOOLi_2^+$, and $(M + H)^+$ of picolinyl ester derivatives are generally similar, there are a few differences. The major difference is the relatively high abundance of low-mass ions present in the decomposition spectra of the $(M + H)^+$ ions of

TABLE 1

Relative abundances of ions formed in the CAD spectrum of the picolinyl ester derivative of hexadecanoic-7,7,8,8-d_4 acid

m/z	Fragment	Relative abundance (%)	*m/z*	Fragment	Relative abundance (%)
336	$(M + H - CH_4)$	18	222	$(M + H - C_9H_{18}D_2)$	17
322	$(M + H - C_2H_6)$	18	206	$(M + H - C_{10}H_{18}D_4)$	19
308	$(M + H - C_3H_8)$	18	192	$(M + H - C_{11}H_{20}D_4)$	7
294	$(M + H - C_4H_{10})$	23	178	$(M + H - C_{12}H_{22}D_4)$	16
280	$(M + H - C_5H_{12})$	21	164	$(C_9H_{10}NO_2)$	61
266	$(M + H - C_6H_{14})$	18	152	$(C_8H_{10}NO_2)$	25
251	$(M + H - C_7H_{15}D)$	14	109	(C_6H_7NO)	100
237	$(M + H - C_8H_{17}D)$	13	93	(C_6H_7N)	82

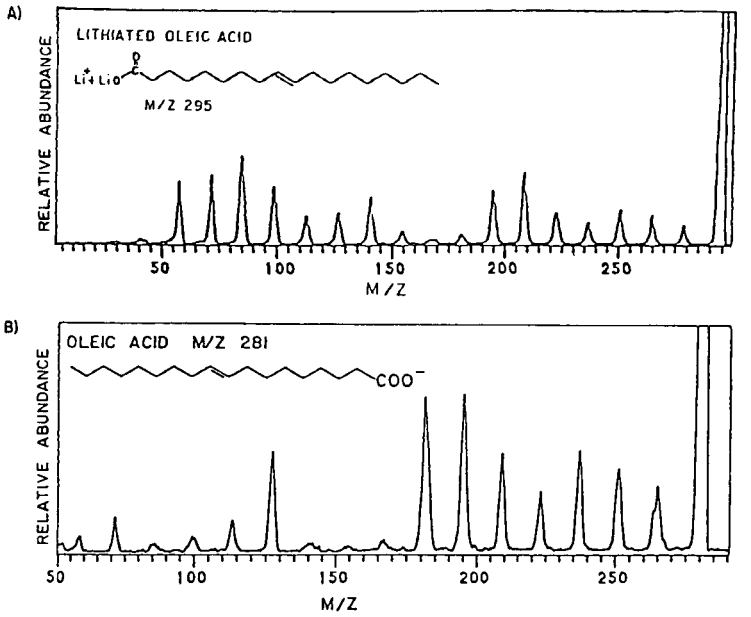

Fig. 9. CAD spectra of $(M + 2Li - H)^+$ ion of oleic acid (A) and $(M - H)^-$ ion of oleic acid (B).

the derivatives (Fig. 2A) and of the $(M + 2Li - H)^+$ ions (Fig. 9A). Carboxylate anions (Fig. 9B) give, by way of comparison, low abundances of low-mass ions upon collisional activation.

For polyunsaturated fatty acids, the lithiated species can be activated to provide information for locating up to six double-bond positions [31] whereas the $(M + H)^+$ ions of the picolinyl esters are useful for locating up to four sites of unsaturation. The CAD spectra of $(M - H)^-$ anions for acids containing two and three double bonds are difficult to interpret, and for acids containing four or more sites of unsaturation, the spectra are largely uninformative because the anion undergoes only the loss of 45 mass units [24]. If the carboxylate anions must be studied, then it is necessary to reduce the double bond with deuterium and then to activate collisionally the $(M - H)^-$ anion of the saturated deuterated acid [26].

Another difference is that picolinyl ester $(M + H)^+$ ions of cyclopropane-containing fatty acids give CAD spectra that are not as distinctive as the CAD spectra of the $(M - H)^-$ anions and $(M + 2Li - H)^+$ ions. However, mass assignments permit location of the cyclopropane ring even if the pattern in the CAD spectrum is less pronounced.

Remote-charge-site fragmentation is observed in the CAD spectra of the picolinyl ester derivative $(M + H)^+$ ions of short-chain (4—8 carbons) fatty acids (Fig. 8). Although it is difficult to locate double bonds on the short alkyl chains by examining charge-remote fragmentation, many other struc-

tural features (i.e., branch points, location of hydroxy functions, etc.) of short-chain acids can be determined. Yet, remote-site fragmentation diminishes upon collisional activation of $(M - H)^-$ anions of fatty acids having alkyl chains that contain fewer than ten carbons [25] and of $(M + 2Li - H)^+$ ions of fatty acids containing fewer than five carbons in the alkyl chain [31].

The final comparison between the CAD spectra of picolinyl ester $(M + H)^+$ ions, $(M - H)^-$ anions and $(M + 2Li - H)^+$ ions involves the detection limits. For the picolinyl derivative of stearic acid, the amount of material needed to obtain a CAD spectrum is approximately 50 ng for a S/N of approximately 35:1 for the base peak. The detection limit for the CAD of oleic acid for both the $(M - H)^-$ anions and the $(M + 2Li - H)^+$ ions is ca. 10 ng at a S/N of ca. 4. Thus, the detection limits are similar for all three methods. The choice of ion, $(M - H)^-$, $(M - H + 2Li)^+$, or $(M + H)^+$, of the picolinyl ester is principally one of convenience. If a crude mixture of fatty acids has been already derivatized, one may consider FAB combined with MS/MS for the picolinyl esters as a means of providing complementary information to that of the electron-ionization GC/MS method.

We thank N. J. Jensen for the preparation of vaccenic epoxide. This research was supported by the National Science Foundation (Grant CHE-8320388) and by the Midwest Center for Mass Spectrometry, an NSF Instrumentation Facility (Grant CHE-8620177).

REFERENCES

1 Y. Katayma-Fujimura, N. Tsuzaki and H. Kuraishi, J. Gen. Microbiol., 128 (1982) 1599.
2 B. Bøe and J. Gjerde, J. Gen. Microbiol., 116 (1980) 41.
3 M. Goodfellow, M. D. Collins and D. E. Minnikin, J. Appl. Microbiol., 48 (1980) 269.
4 J. Asselineau, The Bacterial Lipids, Holden-Day, San Francisco, CA, 1966.
5 J. Asselineau, Bull. Inst. Pasteur, 81 (1983) 367.
6 W. W. Christie, Lipid Analysis, Pergamon, New York, 1982.
7 L. D. Bergelson, Lipid Biochemical Preparations, Elsevier, Amsterdam, 1980.
8 G. Odham, L. Larsson and P.-A. Mårdh, Gas Chromatography/Mass Spectrometry Applied to Microbiology, Plenum, New York, 1984.
9 R. Ryhage and E. Stenhagen, J. Lipid Res., 1 (1960) 361; Ark. Kemi, 15 (1960) 291, 545.
10 S. Abrahamsson, S. Stallberg-Stenhagen and E. Stenhagen, in R. T. Holman and T. Malkin, (Eds.), The Higher Saturated Branched Chain Fatty Acids, Pergamon, Oxford, 1963, pp. 41—59.
11 R. Ryhage, S. Stallberg-Stenhagen and E. Stenhagen, Ark. Kemi, 18 (1961) 179.
12 W. Vetter, W. Walther and M. Vecchi, Helv. Chim. Acta, 54 (1971) 1599.
13 B. A. Andersson, W. H. Heimermann and R. T. Holman, Lipids, 9 (1974) 443.
14 B. A. Andersson and R. T. Holman, Lipids, 9 (1974) 185.
15 B. A. Andersson, W. W. Christie and R. T. Holman, Lipids, 10 (1975) 215.
16 W. M. D. Wijekoon, E. Ayanoglu and C. Djerassi, Tetrahedron Lett., 25 (1984) 3285.

17 E. Ayanoglu, S. Popov, J. M. Kornprobst, A. Aboud-Bichara and C. Djerassi, Lipids, 18 (1983) 830.
18 E. Ayanoglu, R. D. Walkup, D. Sica and C. Djerassi, Lipids, 17 (1982) 617.
19 D. J. Harvey, Biomed. Mass Spectrom., 9 (1982) 33; 11 (1984) 340.
20 D. J. Harvey, Biomed. Mass Spectrom., 11 (1984) 187.
21 W. W. Christie, E. Y. Brechany, S. B. Johnson and R. T. Holman, Lipids, 21 (1986) 657.
22 P. A. Lyon, W. L. Stebbings, F. W. Crow, K. B. Tomer, D. L. Lippstreu and M. L. Gross, Anal. Chem., 56 (1984) 8.
23 P. A. Lyon, F. W. Crow, K. B. Tomer and M. L Gross, Anal. Chem., 56 (1984) 2278.
24 K. B. Tomer, F. W. Crow and M. L. Gross, J. Am. Chem. Soc., 105 (1983) 5487.
25 N. J. Jensen, K. B. Tomer and M. L. Gross, J. Am. Chem. Soc., 107 (1985) 1863.
26 N. J. Jensen, K. B. Tomer and M. L. Gross, Anal. Chem., 57 (1985) 2018.
27 N. J. Jensen and M. L. Gross, Lipids, 21 (1986) 362.
28 M. L. Gross, N. J. Jensen, D. L. Lippstreu-Fisher and K. B. Tomer, in A. L. Burlingame and N. Castagnoli, Jr., (Eds.), Mass Spectrometry in Health and Life Sciences, Elsevier, Amsterdam, 1985, pp. 209—238.
29 N. J. Jensen, K. B. Tomer, M. L. Gross and P. A. Lyon, in P. A. Lyon, (Ed.), Desorption Mass Spectrometry — Are SIMS and FAB the Same?, American Chemical Society, Washington, DC, 1985, pp. 194—208.
30 K. B. Tomer, N. J. Jensen and M. L. Gross, Anal. Chem., 58 (1986) 2429.
31 J. Adams and M. L. Gross, Anal. Chem., 59 (1987) 1576.
32 J. Adams and M. L. Gross, J. Am. Chem. Soc., 108 (1986) 6915.
33 M. L. Gross, E. K. Chess, P. A. Lyon, F. W. Crow, S. Evans and H. Tudge, Int. J. Mass Spectrom. Ion Phys., 42 (1982) 243.
34 F. W. Crow and R. L. Lapp, Abstract of the 29th Annual Conference on Mass Spectrometry and Allied Topics, Minneapolis, MN, May, 1981, pp. 448—449.
35 J. H. Tumlinson, R. D. Heath and R. E. Doolittle, Anal. Chem., 46 (1974) 1309.
36 R. D. Plattner, H. W. Gardner and R. Kleinman, J. Am. Oil Chem. Soc., 60 (1983) 1298.
37 H. Stan and M. Scheutwinkel-Reich, Fresenius' Z. Anal. Chem., 296 (1979) 400; Lipids, 15 (1980) 1044.
38 M. Scheutwinkel-Reich and H. Stan, Biochem. Med., 6 (1980) 45.
39 H. W. Gardner, D. Weisleder and E. C. Nelson, J. Org. Chem., 49 (1984) 508.
40 M. Bambagiotti A., S. A. Coran, F. F. Vincieri, T. Petrucciani and P. Traldi, Org. Mass Spectrom., 21 (1986) 485.
41 N. J. Jensen and M. L. Gross, Mass Spectrom. Rev., 6 (1987), in press.
42 I. Matsumoto and T. Kuhara, Mass Spectrom. Rev., 6 (1987) 77.
43 D. F. Hunt, A. B. Giordani, G. Rhodes and D. A. Herold, Clin. Chem., 28 (1982) 2387.
44 M. Barber, R. S. Bordoli, G. J. Elliot, R. D. Sedwick and N. J. Tyler, J. Chem. Soc., Faraday Trans. 1, 79 (1983) 1249.
45 S. Naylor, A. F. Findeis, B. W. Gibson and D. H. Williams, J. Am. Chem. Soc., 108 (1986) 6359.

Analytica Chimica Acta, 200 (1987) 447—458
Elsevier Science Publishers B.V., Amsterdam — Printed in The Netherlands

DIRECT SECONDARY-ION MASS SPECTROMETRIC ANALYSIS OF MIXTURES SEPARATED BY THIN-LAYER CHROMATOGRAPHY AND ELECTROPHORESIS

M. S. STANLEY, K. L. DUFFIN, S. J. DOHERTY and K. L. BUSCH*
Department of Chemistry, Indiana University, Bloomington, IN 47405 (U.S.A.)
(Received 7th April 1987)

SUMMARY

Secondary-ion mass spectrometry (SIMS) is used to sputter ions directly from thin-layer chromatograms in which components in a mixture have been separated. Mixtures of phenothiazine drugs and small peptides have been separated and detected by the chromatography/SIMS method. Phosphonium salts have been separated by thin-layer chromatography and imaged in situ by the mass spectrometer. Organometallic compounds such as the transition metal acetylacetonates have been similarly determined. Mixtures that have been separated by gel electrophoresis are transferred by using a standard blotting procedure to a nitrocellulose support, which is then examined by secondary-ion mass spectrometry. A mixture of organic dyes was separated by gel electrophoresis, and characterized by secondary-ion mass spectrometry. The use of the mass spectral information to deconvolute overlapping components on the chromatogram is discussed, and the ultimate spatial resolution for molecular mapping is estimated as about 1 μm.

The direct analysis of planar chromatograms by secondary-ion mass spectrometry was recently demonstrated [1—3], and the analytical advantages of such a combination were discussed. The extension of the technique to the analysis of planar electrophoretograms has also been reported [4]. A result of these developments is an increased analytical confidence in the identification and quantitation of components in mixtures separated by these forms of chromatography, based on the ability of the mass spectrometer to measure the unique mass spectra of the components, and the ability to chart the abundances of mass-selected ions in the x/y plane of chromatographic separation.

In secondary-ion mass spectrometry, ions are sputtered from a solid or a liquid surface by the impact of an energetic primary ion beam. The ions are

*Kenneth L. Busch obtained his B.S. (Chemistry) at the University of Maryland and his Ph.D. (Analytical Chemistry) in 1979 from the University of North Carolina at Chapel Hill. After working at the National Institute of Environmental Health Sciences and at Purdue University, he became Assistant Professor of Chemistry at Indiana University in 1983. His research interests include the conjunction of planar chromatography with secondary-ion mass spectrometry, MS/MS, and the gas-phase chemistry of organometallic ions.

0003-2670/87/$03.50

drawn into the mass spectrometer and analyzed by their mass-to-charge ratio. Two analytical characteristics of secondary-ion mass spectrometry are of interest in its interface with planar chromatography. First is the absence of any requirement that the sample molecules be evaporated prior to ionization; nonvolatile and thermally fragile samples can be determined without thermal decomposition. Second is that the ionization method is not only surface-sensitive, but further that ions are sputtered only from that area of the surface bombarded by the primary ion-beam. Secondary-ion mass spectrometry can thus provide a planar spatial distribution of ions sputtered from a surface, as evident in the classical ion microprobe instruments.

It is also appropriate to review the analytical aspects of planar chromatography. In planar chromatography, the separation of compounds is spatial in nature; compounds are separated by their differential migration along the development axis or axes. Separated compounds are identified by comparison of the R_f value for the sample to that of the pure compound, assuming that a detection system can chart the location of the spots by a color development or a fluorescence-based spectroscopic system. Mass spectrometric identification is not only more accurate, but eliminates the need to chromatograph pure standard samples that may be costly or impossible to obtain. Samples cannot be lost in a planar chromatogram as can occur in gas or liquid chromatography. Components of a mixture that do not migrate under the chosen conditions can be retrieved from the point of initial sample deposition. In the combination of planar chromatography with secondary-ion mass spectrometry, the time domain in which the mass spectrometer operates is independent of chromatographic development. Rather than have each component present in the mass spectrometer source only within the elution window of gas chromatography, for instance, the secondary-ion mass spectrometer can integrate the signal for any sample spot that remains within the point of instrument focus, provided that a stable and persistent flux of ions can be maintained. Therefore, shorter data acquisition intervals can be assigned to higher level components, or components of lesser interest.

The ability to access any of the components in a mixture separated within a planar chromatogram in an independent order, the ability to store the sample as well as the data, and the ability to re-analyze the sample at a later time, are also advantages of the chromatography/secondary-ion mass spectrometry system. Independence of access order is an advantage in analyses of complex mixtures when targeted components are sought. A chromatogram can be rescanned many times to establish the required level of analytical accuracy in spatial profile and sample identification. This is apparent when a non-destructive detection technique such as fluorescence spectrometry is used. That secondary-ion mass spectrometry can be a non-destructive technique is less obvious. The material sputtered from the top surface of the sample is consumed in the analysis; sample that remains in the underlying bulk chromatogram can be recovered.

Finally, the chromatography/SIMS experiment is unique in that the data

in the mass spectrum are used not only to identify the components separated within a planar chromatogram, but can be interpreted to provide on-line control of the spatially resolved experiment. Different spatial profiles of organic ions can be used to deconvolute spectra from mixtures of compounds, and the effective resolution of the chromatographic separation is thereby increased. Such use of the mass spectral data is demonstrated in this paper. Mass spectral data in x and y dimensions can also be used in a feedback mechanism that decreases the beam diameter to precisely that necessary to deconvolute overlapping chromatographic components.

Several mixtures have been separated by thin-layer chromatography and by electrophoresis, with a spatial analysis by secondary-ion mass spectrometry. Phenothiazines are commonly used drugs with psychotherapeutic properties. Several common assays involve a thin-layer chromatographic separation [5]. Incomplete separation is sometimes noted, and mass spectrometric data are useful in establishing the presence of overlapping sample spots on the chromatogram. Phosphonium salts are widely used not only as organic synthetic intermediates, but as photo-initiators. An example will be discussed in which the data from mass spectrometry were used to show the co-migration of closely related, but mass-spectrometrically distinct, phosphonium salts. Small peptides can be separated by thin-layer chromatography, and results of an in situ analysis of such a separation will be presented. Similarly, the first results for the thin-layer chromatographic/mass spectrometric analysis of simple metal acetylacetonates are presented.

Direct analysis of paper electrophoretograms by secondary-ion mass spectrometry is also discussed. Planar (slab) electrophoresis with aqueous gels is widely used in biochemical and clinical separations. The vapor pressure of water even at reduced temperatures makes the direct analysis of these chromatographic substrates impossible under usual instrument conditions. Persistent secondary-ion signals from dried gels could not be obtained. Results are presented here that show the spatially-resolved mass spectral data obtained from an electrophoretic gel separation with an intermediate transfer step onto a nitrocellulose support. Blotting techniques such as that described here are commonly used in the electrophoretic separation and analysis of deoxyribonucleic acids, ribonucleic acids, and small peptides [6].

EXPERIMENTAL

Positive secondary-ion mass spectra were obtained on a custom-built secondary-ion mass spectrometer [1] based on an Extrel quadrupole mass analyzer. Neat samples were introduced on a copper platform attached to the direct-insertion probe. The primary beam consisted of 8—10-keV cesium ions emitted from a thermionic source. The primary-ion current density at the sample surface was approximately 10^{-6} A cm^{-2} with a beam diameter of approximately 0.5 mm for the spatially resolved experiments. Spectra

were recorded directly on an xy recorder at a scan speed of 0.5 dalton s^{-1}; neither spectral averaging nor background subtraction was used. Thin-layer chromatography plates used were aluminum-backed, 0.2-mm thick silica gel, commercially prepared (Merck), with a fluorescent indicator. They were pre-eluted by prior development with the solvent system. All reagent-grade solvents were obtained from Mallinkrodt.

For most spatially resolved data, phase-transition matrices [2] were used to extract the sample from the chromatogram, and to minimize lateral spreading of the sample in the chromatogram during analysis. Spatially resolved selected-ion monitoring data were acquired by setting the quadrupole to pass the ion of interest, and adjusting the x and y manipulators to move the chromatogram into the point of instrument focus. The secondary-ion mass spectrum persists in most cases for more than 30 min, and sometimes for more than an hour, with no changes in the relative abundance of the ions. Based on the amount of sample present in the spot, very low rates of sample removal (on the order of pg s^{-1}) from the surface are indicated. For samples of the peptides, changes in the relative abundances of the fragment ions of about 20% were noted between analysis of a discrete sample and analysis of the same sample sputtered directly from a silica-gel thin-layer chromatogram. No regular pattern to these changes has yet been noted. These changes are distinct from those that might be expected as a result of beam-induced reactions of the sample. Ion abundances in the secondary-ion mass spectrum, recorded as a function of x and y, were manipulated by the plotting routines of ASYST scientific software, which produced the axonometric and contour plots.

RESULTS AND DISCUSSION

Determination of phenothiazine drugs

Phenothiazine-derived drugs are a pharmacologically diverse group of substances possessing antiemetic, antipsychotic, sedative, antipruritic, antidyskinetic, analgesic, and antihistamine properties. Separation of the drugs from their metabolites, or from other components present in a biological matrix, often involves thin-layer chromatography. The x-y-mapped absolute abundance of the protonated molecule of acepromazine separated in a thin-layer chromatogram is given in Fig. 1. The total amount of sample in the oval spot is 1 μg. Liquid threitol was used as the extracting solvent. The spectrum persists for over 30 min, ample time for the manual recording of the xy spectral intensities, for adjustment of the instrumental parameters, and for rescanning of the spot along other x,y lines. The dip in ion abundance shown in the figure is real, and reflects an inhomogeneous distribution of the sample in the thin-layer chromatogram. The localization in the xy plane of the signal for this particular ion at m/z 327 is apparent; adjacent areas of the chromatogram do not produce an ion at this mass-to-charge value. Because the signal-to-noise (S/N) ratio for any ion from the mass spectrum of the

sample at that spot is high, the spot boundaries are clearly defined. Figure 2 is a plot of spatially resolved mass spectral data for overlapped spots of two phenothiazine drugs partially separated by thin-layer chromatography [5]. Contours A and B correspond, respectively, to data from the protonated molecules of promethazine at *m/z* 285 and of trimeprazine at *m/z* 299. For ions that are common to both secondary-ion mass spectra (ions at *m/z* 198 and *m/z* 180, for example), double-lobed contour plots would be generated.

Phosphonium salts

The secondary-ion mass spectra and fast-atom-bombardment mass spectra of phosphonium salts have been studied previously [7, 8]. The positive-ion secondary-ion mass spectra typically contain an abundant ion corresponding to the intact cation of the phosphonium salt, and fragment ions with relative abundances of 10 to 20% that can be related to the structure of the cation. The predominance of the intact cation suggests that this "molecular" ion would be ideal for charting the distribution of phosphonium salts separated by planar chromatography. Mixtures of phosphonium salts were separated by thin-layer chromatography under conditions similar to those developed for the separation of sulfonium salts [9]. Figure 3 contains the spatially resolved selected-ion monitoring data for phosphonium salts with cation masses of 335 and 339 daltons that have been separated by thin-layer chromatography. The *x* and *y* coordinates for both parts of the figure are the same, and in fact, one of the phosphonium salts with a mass of 335 daltons co-migrates with the phosphonium salt with a cation mass of 339

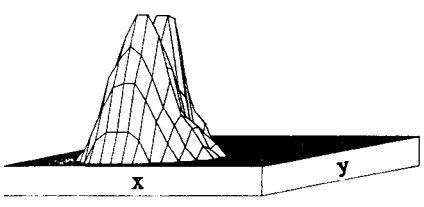

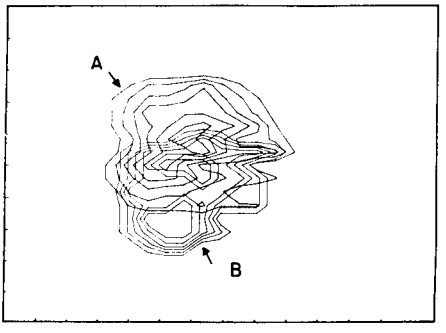

Fig. 1. Spatially resolved selected-ion monitoring of the protonated molecule of acepromazine (*m/z* 327) by secondary-ion mass spectrometry, charting the location of the acepromazine separated from a phenothiazine drug mixture by thin-layer chromatography on silica gel.

Fig. 2. Iso-abundance contour plots for the protonated molecules of trimeprazine and promethazine. Contour A is the plot of ion-abundance data from the protonated molecule of promethazine at *m/z* 285. Contour B is the plot of ion-abundance data from the protonated molecule of trimeprazine at *m/z* 299.

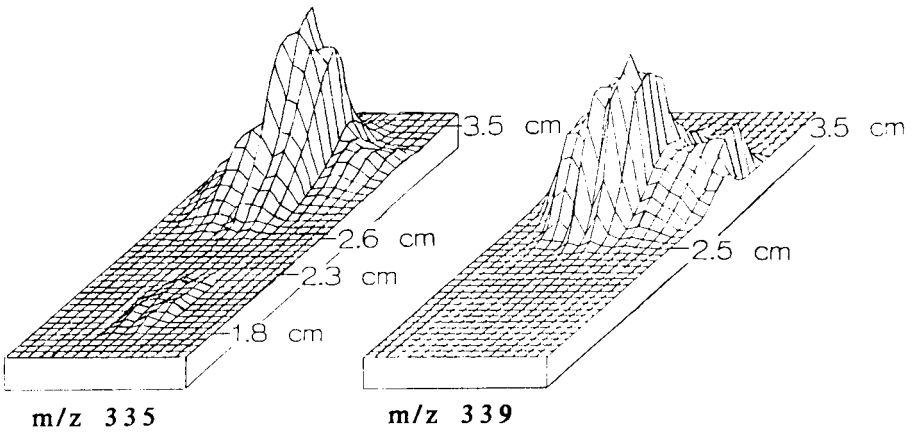

Fig. 3. Spatially resolved selected-ion monitoring for phosphonium salts separated by thin-layer chromatography. Two salts that provide signals for the intact cation at *m/z* 335 can be seen in discrete locations in the left plot. The right plot, which overlays that on the left, provides the location of the phosphonium salt that provides an intact cation at *m/z* 339.

daltons. The mass-spectral data allow the individual contours of these separated compounds to be distinguished on the basis of the different mass ions in their respective mass spectra. In the plot on the left, two abundance maxima for the ion at *m/z* 335 are noted. That in the foreground represents the location of a second phosphonium salt with a cation mass of 335 daltons with a lower R_f value. For these experiments, each phosphonium salt was present at the 10 μg level, and a total of 2 h was required manually to record the mass spectra of each point across the entire intact chromatogram introduced into the mass spectrometer. No technique other than mass spectrometry was used to establish the locations of the spots. The S/N ratio for ion current at these masses relative to background is higher than 20, even for the minor peak in the chromatogram.

Small peptides

The mass range of the quadrupole mass analyzer currently in use is 1300 daltons, allowing the molecular ions of peptides of up to about ten amino-acid residues to be measured directly. Still larger peptides can be determined, but only those ions with masses of less than 1300 daltons can be separated and measured. Sufficient information often remains, however, for the sample spot identity and homogeneity to be established. In this section, a few examples of the separation by thin-layer chromatography and direct determination of small peptides are presented.

The direct sputtering of glycylphenylalanine from a thin-layer plate to produce an imaged secondary-ion mass spectrum was an early example of this work. Sorbitol was used in the phase-transition matrix. The protonated

molecule at *m/z* 223 is a large peak in the mass spectrum, with the ion at *m/z* 166 corresponding to the loss of glycine from the protonated molecule, and another large ion at *m/z* 120 representing loss of carbon monoxide from the phenylalanine residue. Any of the ions from the peptide can be charted in *x* and *y* spatial distributions to provide the spatially resolved image of this particular peptide on the thin-layer chromatogram. In our experience, small peptides that contain the —GLY—PHE— sequence (but not the —PHE—GLY— sequence) produce an ion at *m/z* 166, and a scan across the entire chromatogram for local maxima in the abundance of the ion at *m/z* 166 will provide the spatial coordinates of all such peptides. Likewise, a scan across the entire chromatogram for local maxima of the ion at *m/z* 223 will provide coordinates of peptides of the general sequence GLY—PHE—R, with *N*-terminal glycylphenylalanine as the target sequence. This procedure is called a selected sequence monitoring experiment.

As mentioned above, peptides with up to about ten amino-acid residues can be examined. Figure 4A is the positive-ion secondary-ion mass spectrum of a nonapeptide, bradykinin, illustrating the protonated molecule and the fragment ions that are integrated to provide the sequence. The matrix was melted with sorbitol, with a small amount of *p*-toluenesulfonic acid added to increase the abundance of $(M + H)^+$. Mapped *xy* abundances of any of the ions can be used to create the three-dimensional plot of a bradykinin spot; however, for maximum sensitivity, one would prefer more of the ion current concentrated in the protonated molecule. Such an effect is noted when the bradykinin is supported on a nitrocellulose matrix

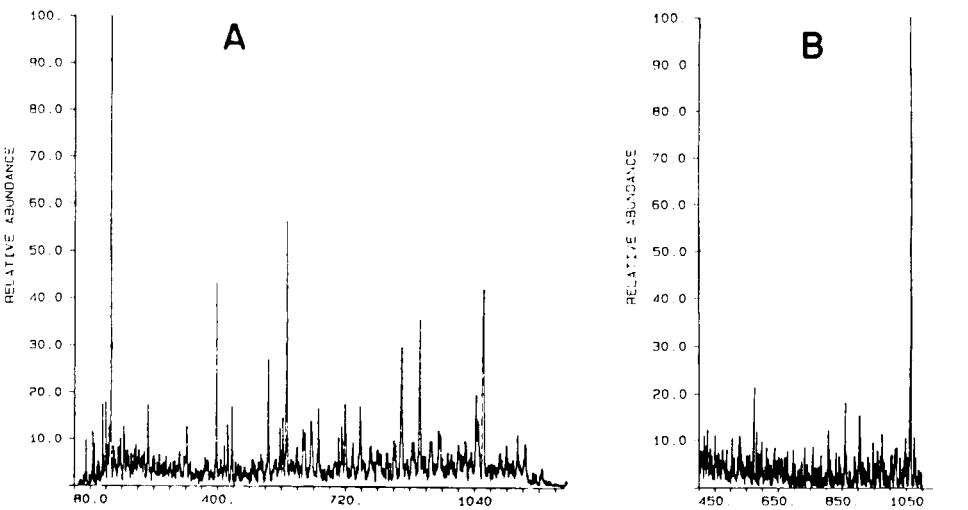

Fig. 4. Positive-ion secondary-ion mass spectra of bradykinin: (A) a matrix of melted sorbitol acidified with *p*-toluenesulfonic acid; (b) supported on a nitrocellulose backing, with glycerol as the solvent.

(Fig. 4B), here with glycerol as the solvent. The use of the nitrocellulose matrix is an integral part of the sample-transfer methods described later in the electrophoresis section of this paper. Nitrocellulose has been noted to increase the secondary ion yields of compounds ionized by plasma-desorption mass spectrometry [10].

Lysine-containing peptides can be derivatized with a pyrylium salt reagent to transform the lysine residues into pyridinium salts that produce very abundant secondary ions in the positive-ion mass spectrum [11]. As in the experiments described above, a scan of this ion across all x and y of the chromatogram produces the spatial distribution of ions that contain lysine residues. As the mass of the selected ions increases to R—LYS$^+$, any lysine-containing ion can be identified on the basis of the variance in R, and its distribution across the chromatogram investigated. Derivatization reagents are now being developed for disulfides and thiols, and these reagents should be helpful in establishing the locations of the peptides that contain the cystine and cysteine residues. Larger peptides are typically separated by electrophoretic methods, and the interface of electrophoresis with secondary-ion mass spectrometry is discussed below.

Organometallic compounds

Organometallic and coordination compounds have been examined by secondary-ion and fast-atom-bombardment mass spectrometry [12—14], both of which provide spectra for these nonvolatile compounds. Thin-layer and paper chromatography are often used to separate synthetic mixtures of organometallic compounds [15]. As in the analysis of organic and biochemical mixtures, the secondary-ion mass spectrometer can also be applied to the direct determination of organometallic and coordination compounds separated by planar forms of chromatography. Figure 5 is the positive-ion secondary-ion mass spectrum of iron(III) acetylacetonate (acac) separated by thin-layer chromatography, extracted from the chromatogram with an 18-crown-6/crown ether matrix, and sputtered from the surface of the chromatogram with a primary ion beam. Two large ions in the mass spectrum correspond to $Fe(acac)_2^+$ and $Fe(acac)^+$, at m/z 254 and 155, respectively. Ions from the solvent are labeled S. In a thin-layer chromatographic separation of the metal acetylacetonates, sample spots from chromium and iron tris acetylacetonates overlapped. Monitoring ion-abundance data for $Cr(acac)_2^+$ and $Fe(acac)_2^+$ ions in one dimension of chromatographic development yields the plots given in Fig. 6, which documents the overlap in the sample spots. The key to the successful secondary-ion mass spectrometric analysis of these systems is use of the correct phase-transition matrix. Crown ethers can be used to extract some organometallic compounds from the polar silica gel without excessive lateral diffusion, but preliminary results indicate that extraction with the crown ethers is not universal.

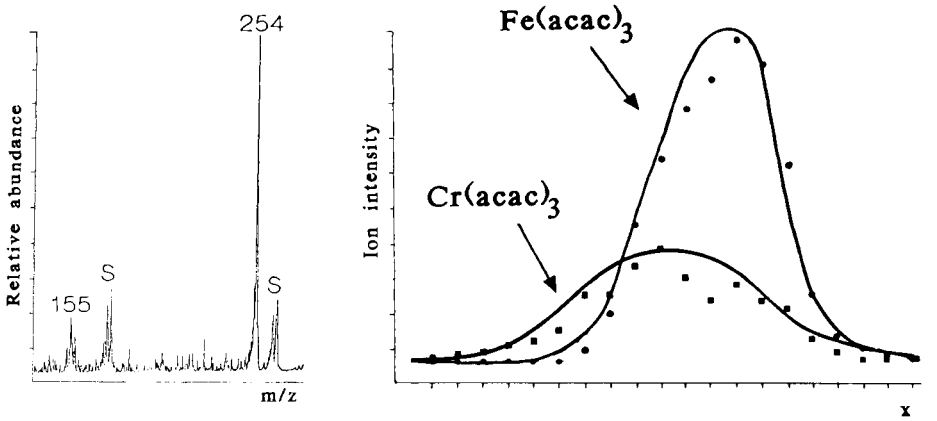

Fig. 5. The positive-ion secondary-ion mass spectrum of iron acetylacetonate separated by thin-layer chromatography and extracted from the chromatographic matrix with a crown ether phase-transition matrix. The ions at *m/z* 254 and 155 represent $Fe(acac)_2^+$ and $Fe(acac)^+$, respectively, where (acac) is the acetylacetonate ligand.

Fig. 6. Spatially resolved secondary-ion mass spectrum for overlapped spots of $Fe(acac)_3$ and $Cr(acac)_3$ separated on a thin-layer chromatogram. The ions $Fe(acac)_2^+$ and $Cr(acac)_2^+$ were monitored in the dimension of chromatographic development. The full width at the base of each spot is 2 mm.

Electrophoresis

Separation of larger biomolecules is often accomplished with electrophoretic techniques. As described in the introduction, an intermediate transfer step is required to move the sample material, with the spatial resolution of the separation retained, from an aqueous electrophoresis gel onto a medium compatible with the vacuum of the secondary-ion mass spectrometer. Blotting by capillary action, by electrophoresis, and by application of a vacuum have all been described. The medium to which the sample compounds are transferred is typically nitrocellulose, although for special applications, a treated paper support can be used to increase the binding. Our initial investigations have used electrophoresis to separate mixtures of organic dyes which are maintained in their charged forms by a buffer. The bands of separated dye are easily seen on the electrophoretic plate, and the transfer of the dye to the nitrocellulose is also visually monitored. The development of the gel results in a band of the dye. Figure 7 is the positive-ion, secondary-ion mass spectrum of methylene blue separated from a dye mixture by electrophoresis and transferred onto a nitrocellulose support by capillary action. The protonated molecule at *m/z* 284 is monitored in *x* and *y* dimensions. The shape of the elongated band as shown by mass-spectral data contrasts with the symmetric sample spots observed in the images from thin-layer chromatograms.

Small peptides and steroid sulfates have also been separated by electrophoresis and transferred onto the nitrocellulose support by an electro-

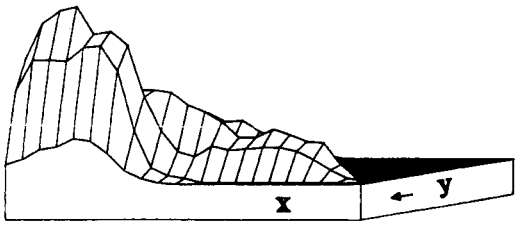

Fig. 7. Methylene blue is separated from other dyes with gel electrophoresis, transferred to a nitrocellulose support, and extracted with glycerol. The "band" shape of the sample is confirmed by the ion-abundance imaging for the intact cation at *m/z* 284. The direction of electrophoretic gel development is noted.

blotting procedure. The secondary-ion mass spectra of those samples so prepared are identical to those measured for the discrete samples measured in the extraction solvent directly. An example of the quality of the data upon which the imaging is based is given in Fig. 8, obtained for 10 μg of androsterone sulfate. The negative ion at *m/z* 369 is the anion of the sulfate salt itself. Despite reports that the positive-ion mass spectra of these compounds are irreproducible and of low quality [16], such is not the case in our experience. The positive ion at *m/z* 289 is formed by loss of the sulfonate and its associated cation, and addition of hydrogen to the unsaturated site; this ion represents the intact steroid skeleton. Both the positive and the negative ions are used to create the image of this particular compound on the nitrocellulose support.

Spatial resolution

It is worthwhile to consider the limits of spatial resolution of the chromatography/SIMS technique. The ultimate spatial resolution of the hardware used in assembly of the secondary-ion mass spectrometer permits a spatial resolution in the *xy* plane of 1 μm. Although this is much finer than that typically required for a gross siting of the spots on a chromatogram, spatial resolution on this scale may be necessary to image overlapped sample components. For a spot size of 100-μm diameter, 20 μm in depth, with a sample

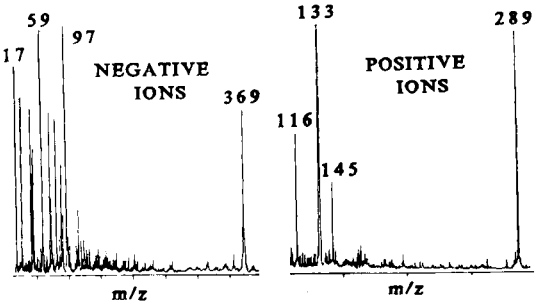

Fig. 8. Positive and negative secondary-ion mass spectra of androsterone sulfate. The negative ion at *m/z* 359 is loss of the cation, and represents the intact sulfonate.

density of 0.1 g ml^{-1}, approximately 10^{14} molecules of a compound with a 300-dalton molecular weight are present. Assuming an instrumental transmission efficiency of 10^{-4}, an ionization efficiency of 10^{-3}, and an effective sampling depth of 5 nm, approximately 2×10^7 ions will reach the detector of the mass spectrometer. A spot size of 10-μm diameter will result in 10^5 ions at the detector, and a 1-μm spot size will provide 10^3 ions at the detector. The same figures show that a 0.1-μm spot size (within the limits of the current primary-ion gun) will provide ten ions at the detector. Allowing some variation in the numbers, an order-of-magnitude estimate for the lower limit of attainable spatial resolution is 1 μm. Attempts to equate the chromatography/secondary-ion mass spectrometer with a "molecular microprobe" are premature, although the spatial resolution is ideal for chromatographic imaging. Extension of the capability to finer spatial dimensions depends on more careful control of the sample, in terms of both the chemical state of the analyte (a neutral versus a preformed ion), and in its physical location (the ability to maneuver the sample ions from the bulk to the surface from which they can be sputtered).

Conclusions

The secondary-ion mass spectrometer can be used to analyze mixtures of compounds separated by planar chromatography, including thin-layer chromatography, paper chromatography, and electrophoresis. The use of a phase-transition matrix is required to provide a steady supply of sample to the surface from which the secondary ions are sputtered. The choice of the extraction matrix is important, because an efficient extraction must occur without excessive lateral diffusion of the analyte. Applications to phenothiazines, small peptides, organometallic compounds, and steroid sulfates are described. The limit of spatial resolution based on sample density within a chromatographic matrix is shown to be about 1 μm.

This work was supported by the Whitaker Foundation, the National Institutes of Health, and the National Science Foundation. Derivatization experiments for SIMS were supported by the Donors of the Petroleum Research Fund, administered by the American Chemical Society. Lisa Detter catalyzed our interest in the organometallic chromatography experiment.

REFERENCES

1 J. W. Fiola, G. C. DiDonato and K. L. Busch, Rev. Sci. Instrum., 57 (1986) 2294.
2 G. C. DiDonato and K. L. Busch, Anal. Chem., 58 (1986) 3231.
3 M. S. Stanley and K. L. Busch, Anal. Chim. Acta, 194 (1987) 199.
4 K. L. Busch, Trends. Anal. Chem., 6 (1987) 95.
5 C. Korczak-Fabierkiewicz and G. Cimbura, J. Chromatogr., 53 (1970) 413.
6 M. Bittner, P. Kupferer and C. F. Morris, Anal. Biochem., 102 (1980) 459.
7 A. Ba-isa, K. L. Busch, R. G. Cooks, A. Vincze and I. Granoth, Tetrahedron, 39 (1983) 591.
8 K. J. Kroha and K. L. Busch, Org. Mass Spectrom., 21 (1986) 507.

9 A. A. Bornstein, J. Chromatogr., 238 (1982) 258.
10 G. P. Jonsson, A. B. Hedin, P. L. Hakansson, B. U. R. Sundqvist, B. Goran, S. Save, P. F. Nielsen, P. Roepstorff, K. E. Johansson, I. Kamensky and M. S. L. Lindberg, Anal. Chem., 58 (1986) 1084.
11 K. L. Busch and R. A. Flurer, Adv. Mass Spectrom., 10 (1986) 1529.
12 J. Pierce, K. L. Busch, R. A. Walton and R. G. Cooks, J. Am. Chem. Soc., 103 (1981) 2583.
13 J. L. Pierce, K. L. Busch, R. G. Cooks and R. A. Walton, Inorg. Chem., 21 (1982) 2597.
14 L. D. Detter and R. A. Walton, Polyhedron, 5 (1986) 1321.
15 J. C. MacDonald (Ed.), Inorganic Chromatographic Analysis, Wiley, New York, 1985.
16 S. J. Gaskell, B. G. Brownsey, P. W. Brooks and B. N. Green, Biomed. Mass Spectrom., 10 (1983) 215.

Analytica Chimica Acta, 200 (1987) 459—468
Elsevier Science Publishers B.V., Amsterdam — Printed in The Netherlands

STUDIES OF ALKOXYSILANE HYDROLYSIS AND CONDENSATION BY FOURIER-TRANSFORM INFRARED SPECTROSCOPY WITH A CYLINDRICAL INTERNAL-REFLECTION CELL

D. E. LEYDEN*, R. S. SHREEDHARA MURTHY, J. B. ATWATER and J. P. BLITZ

Condensed Matter Sciences Laboratory, Department of Chemistry, Colorado State University, Fort Collins, CO 80523 (U.S.A.)

(Received 23rd April 1987)

SUMMARY

The relative concentrations of unhydrolyzed and hydrolyzed forms of (3-trimethoxysilyl)propyloctadecyldimethylammonium chloride (SiQAC) were determined in aqueous solutions as functions of pH and time. Subtraction of the concentrations of these two forms of SiQAC from the total concentration of SiQAC was assumed to give the concentration of the "condensed" form of SiQAC irrespective of its extent of oligomerization. The silane, SiQAC, is used to modify a variety of surfaces to impart antimicrobial properties. Knowledge of the speciation of SiQAC is required to understand its effect on the efficiency and durability of such chemically modified surfaces. The cylindrical internal-reflection/FTIR spectroscopy was also used to determine the rate constants for hydrolysis and condensation of monomethoxytrimethylsilane (MTMS) in 10% (v/v) water/acetone medium as a function of hydrogen-ion concentration. The hydrolysis of MTMS was found to be first order in both silane and water concentrations. The condensation of trimethylsilanol to form hexamethyldisiloxane was second order in silanol concentration.

Alkoxysilanes with the general formula, $(RO)_n SiR'_{(4-n)}$ (where $n = 1, 2$ or 3), represent an important class of compounds used for chemical modification of a variety of surfaces. The alkoxy groups (usually methoxy or ethoxy) are merely intermediates in the formation of silanol groups for bonding to suitable surfaces. When extensive bonding of the silane with the surface is desired, trialkoxysilanes perform better than dialkoxy- or monoalkoxy-silanes [1, 2]. The organofunctional R′ group determines the ultimate use of properties of the modified surface. It may be $-C_{18}H_{37}$ to render silica surfaces highly hydrophobic for reversed-phase high-performance liquid chromatographic (HPLC) columns [3], or $-(CH_2)_3N^+(CH_3)_2C_{18}H_{37}$ Cl^- to provide the surface with antimicrobial properties [4]. Because of the wide range of applications to such surfaces, many investigations have been performed to characterize them using infrared [5], nuclear magnetic resonance [6] and photoacoustic [7] spectroscopies. Blitz et al. [8] have found the diffuse reflectance sampling technique coupled with Fourier-transform infrared (FTIR) spectroscopy to be superior to transmission studies of

0003-2670/87/$03.50

modified Cab—O—Sil samples. It is also useful to obtain absolute [9] and relative [2, 10] silane concentration data from room-temperature [9] and variable-temperature [10] investigations.

During our detailed study of the reaction of methoxymethylsilanes with Cab—O—Sil [2], the need for determining the structure of silanes in solution before they react with the silica surface became apparent. Ongoing research [11] into the characterization of a variety of surfaces modified with the antimicrobial silane, (3-trimethoxysilyl)-propyloctadecyldimethylammonium chloride (SiQAC), required the capability of routinely monitoring the concentration and speciation of SiQAC in aqueous or organic solutions. Kinetic and mechanistic data regarding hydrolysis and condensation were also required.

Few techniques have been applied to study the hydrolysis and condensation of alkoxysilanes in aqueous solutions, even though it is the solvent most often used for commercial surface reactions. Plueddemann's "eyeball test" [12] gave an indication of the relative rates of hydrolysis as well as a measure of ultimate solubility of an alkoxysilane in water. Laser Raman and FTIR spectroscopies [13, 14] have been used to obtain information about the structures of aryl- and alkyl-trialkoxysilanes in aqueous solutions. These techniques were not used to acquire quantitative data from which kinetics of condensation of silanetriols to siloxane bonds could be determined. Pohl and Osterholtz [15] used infrared spectroscopy, after extraction of the unhydrolyzed silane into hexane, to determine the rates of hydrolysis as a function of pH. The rates of condensation of alkylsilanetriols were followed by ^{13}C-NMR spectroscopy [15, 16]. Savard et al. [17] used ^{1}H-NMR spectroscopy to follow the rates of hydrolysis and condensation of 3-methacryloxypropyltrimethoxysilane as a function of pH. The need to use deuterated solvents for NMR spectroscopy does not permit it to be used as a technique for routine determination of the behavior of silanes in aqueous solutions. Transmission infrared spectroscopy has not been used extensively to study aqueous solutions of silanes because of the solubility of common window materials in water and the difficulty in obtaining cells of extremely short path lengths. Among other sampling techniques, attenuated total reflection (ATR) provides path lengths of 5—15 μm. Detailed theory of the internal reflection process is provided by Harrick [18]. The internal reflection element of high refractive index (such as KRS-5 or germanium) with which the sample comes in contact is insoluble in water. The signal-averaging and spectral-subtraction capabilities of an FTIR spectrometer have been coupled with ATR to obtain spectra of aqueous solutions [19]. It has also been used to monitor the adsorption of proteins on the internal reflection element with a time resolution of 0.8 s [20] and for quantitative purposes [21]. A rhombohedral internal-reflection element (with dimensions that match the rectangular slit image of a dispersive infrared spectrometer) was used in those studies. The introduction of a cylindrical internal-reflection cell (CIRCLE; Spectra-Tech) with optical arrangement

that matches the circular beam of an FTIR spectrometer has made the ATR technique more popular for studying aqueous solutions [22] even at high pressures and temperatures [23]. Studies in this laboratory have been directed at the use of the cylindrical internal-reflection sampling technique coupled with rapid scanning capabilities of FTIR spectrometry for speciation of alkoxysilanes in solution. This paper describes the results obtained from the speciation studies of SiQAC in aqueous solutions, and studies done to determine the rates of hydrolysis and condensation of monomethoxytrimethylsilane (MTMS) in aqueous acetone.

EXPERIMENTAL

Reagents

The SiQAC was obtained from Dow Corning Corporation as a 40% solution in methanol. A suitable aliquot of this solution was diluted to 10 ml with distilled water and its infrared spectrum was recorded immediately. Although the methanol could be rotary-evaporated to isolate solid SiQAC, it was found that this leads to hydrolysis and condensation [11]. Monomethoxytrimethylsilane (MTMS; Petrarch Systems) was distilled in vacuum just prior to use. A solution-phase ^{13}C-NMR spectrum of MTMS showed little or no methanol, suggesting negligible hydrolysis of the methoxy group. Solutions of SiQAC in water and MTMS in 10% water/acetone medium were prepared just before use. An acetic acid/sodium acetate buffer was used for studies with SiQAC. For studies with MTMS, a HCl/KCl buffer was used.

Instrumentation

A Nicolet 60SX FTIR spectrometer (Nicolet Analytical Instruments) purged with dry air and equipped with a wide-band mercury cadmium telluride detector cooled with liquid nitrogen was used to obtain infrared spectra. Data collection parameters were optimized to obtain one scan per 0.18 s at a nominal resolution of 8 cm^{-1}. The additional time required for data handling and storage permitted the acquisition of one spectrum per 1.52 s. The time resolution available was found adequate for most purposes.

Spectrum acquisition and data treatment

The boat configuration of the microcylindrical internal-reflection cell (Spectra-Tech) with a ZnSe internal reflection element was used. For cases in which the pH of the solution had to be changed rapidly, 70 μl of a suitable buffer was injected into 1 or 2 ml of the silane solution while spectra were being acquired. The time required to mix the solutions was not more than 2 s. At pH values where the hydrolysis was not expected to be fast, the buffer solution was added to the silane solution in a volumetric flask prior to the start of spectrum acquisition. The hydrolysis and/or conden-

sation of the silane was followed by acquiring spectra at suitable intervals of time. After subtraction of the solvent spectrum, the bands arising from $Si—OCH_3$, Si—O—C, Si—OH groups and methanol were integrated. For studies with MTMS in 10% (v/v) water/acteone medium, the hydrogen ion concentration was varied from 0.56 to 2.88×10^{-4} M while the ionic strength was maintained at 10^{-3} M with KCl.

The infrared spectrum of SiQAC recorded immediately after diluting a methanolic solution with water was assumed to represent the trimethoxysilane. The pH of this solution was lowered to 3 to hydrolyze all the methoxy groups rapidly, resulting in an increase in methanol concentration. After subtraction of a spectrum of water, the concentration of net methanol produced was obtained by reference to a calibration graph. The concentrations of trimethoxy-SiQAC and silanetriol-SiQAC were assumed to be equal to one-third the concentration of the net methanol produced. This experiment was repeated with various initial concentrations of SiQAC. This indirect approach to determine the concentration of SiQAC was essential because solid SiQAC which has not undergone partial hydrolysis and/or condensation was not available [11]. A spectrum of methanol was used to subtract its contribution from each SiQAC spectrum regardless of its state of hydrolysis. The concentration of unhydrolyzed SiQAC was related to the asymmetric Si—O—C stretch and $Si—OCH_3$ rock-band areas. The concentration of completely hydrolyzed SiQAC was related to the Si—OH band area. The concentration of SiQAC, irrespective of its state of hydrolysis, was related to the symmetric CH stretch-band area. With these calibration graphs, it was possible to determine the contribution of total, unhydrolyzed and hydrolyzed forms of SiQAC in each spectrum. The percent of condensed SiQAC was obtained by difference.

The initial concentration of MTMS was calculated to be 0.36 M from the volume taken and the density of the liquid. After complete hydrolysis at room temperature (typically 25 ± 2°C), the concentration of methanol produced ($[MeOH]_f$) agreed with the concentration of MTMS taken to within ±5%. At any given time, t, the concentration of unhydrolyzed MTMS was obtained from ($[MeOH]_f - [MeOH]_t$). A calibration graph relating Si—OH band area with the concentration of trimethylsilanol was also prepared. The MTMS solutions were allowed to hydrolyze at different concentrations of hydrogen ion. The concentration of methanol produced as a function of time was used to fit standard rate expressions to evaluate first- or second-order rate constants. The decrease in Si—OH band area as a function of time was used to obtain the second-order rate constant for condensation.

RESULTS AND DISCUSSION

Speciation studies of SiQAC

Figure 1 shows the infrared spectrum of SiQAC in unhydrolyzed (A), completely hydrolyzed (B) and partially condensed (C) forms in aqueous

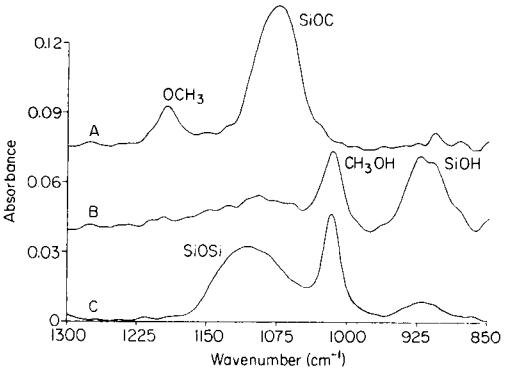

Fig. 1. Infrared spectra of an aqueous 0.025 M solution of SiQAC in its (A) unhydrolyzed, (B) completely hydrolyzed and (C) partially condensed forms. See Table 1 for band assignments.

medium. A methanol spectrum was used to subtract the contribution of solvent methanol from these spectra. The band at 1015 cm^{-1} is from methanol produced by hydrolysis alone. The assignments of other bands of SiQAC are based on those reported by Smith [24] and are summarized in Table 1. The symmetric CH stretch band at 2853 cm^{-1} (not shown) after methanol subtraction was used to obtain total SiQAC concentration irrespective of its state of hydrolysis. The methoxy rock-band area was used to measure the extent of hydrolysis and the Si—OH-band area was used to determine the concentration of silanetriol that was not condensed. By reference to calibration graphs prepared as described in the experimental section, it was possible to determine the concentration of total, unhydrolyzed, and hydrolyzed SiQAC. It was not possible to distinguish between the dimer, trimer or higher oligomers of the condensed SiQAC. The difference given by [total — (unhydrolyzed + hydrolyzed)] was assumed to account for all "condensed" forms of SiQAC. Even though the three methoxy groups of a trimethoxysilane are known to hydrolyze at different rates [25]. It was assumed that only either trimethoxy or silanetriol forms of SiQAC had to be considered. This assumption was valid from a practical point of view as the SiQAC was always prehydrolyzed at low pH before being applied onto a surface. Because the condensation of silanetriols to siloxane bonds is also acid-catalyzed [15, 16], it was essential to know the extent of condensation that has occurred in the hydrolyzed SiQAC solution as a function of time. If all the silanols are condensed, they are not available for bonding to reactive surfaces such as rayon, silica gel etc. On the contrary, extensive condensation is essential for physically depositing SiQAC on non-reactive surfaces such as poly(vinyl acetate), teflon, etc., to render bactericidal properties to them.

Figure 2 shows a plot of the percentage hydrolyzed (A) and condensed (B) forms of SiQAC in a solution with a pH value lowered to 4.2 as a function of time. Zero for the time axis was taken to be the moment when

TABLE 1

Assignments of infrared bands for SiQAC and MTMS

Band assignments	Band maximum (cm^{-1})	
	SiQAC in water	MTMS in 10% water/acetone
Si—OCH_3 rock	1192	—[a]
Si—O—Si asym. str.	1100	1043
Si—O—C asym. str.	1072	1083
C—O str. of methanol	1015	1031
Si—OH str.	917	896
Si—O—C sym. str.	—[b]	865

[a]Obscured by solvent band. [b]Obscured by absorption from water and ZnSe.

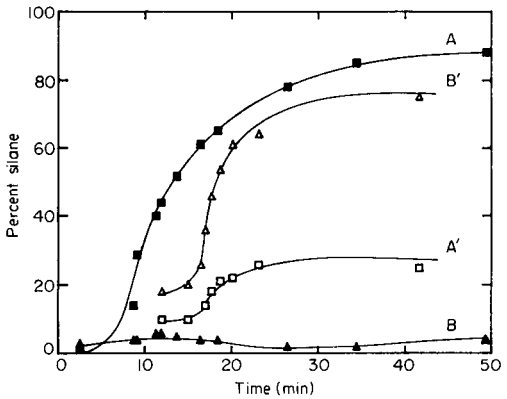

Fig. 2. The relative concentrations of (A) hydrolyzed and (B) condensed forms of SiQAC in an aqueous solution at pH 4.2. A′ and B′ are the corresponding curves for SiQAC in a solution at pH 7.3.

water was added to an aliquot of the methanolic solution of SiQAC. A 70-μl aliquot of a buffer was injected to lower the pH after about 9 min while spectra were being acquired. The percent of condensed form remains less than 10% for up to 50 min when nearly 90% of the silane is in the hydrolyzed form. When spectra of this solution were taken 5 days later, 78% of the silane was found to be in the condensed form and yet the solution was clear. Whether such a condensed form of SiQAC modifies a reactive surface to the same extent as that of a freshly hydrolyzed SiQAC is now being investigated. Curves A′ and B′ in Fig. 2 show the percent hydrolyzed and condensed forms of SiQAC, respectively, when the pH of the solution was raised to 7.3. For this study, water was added to a weighed quantity of solid SiQAC. Dissolution of the solid took more time before the buffer could be added. The percentage condensed form of SiQAC (Curve B′), even before the buffer was added, was 18% which is consistent with earlier solid-state

^{29}Si NMR data [11] which shows that removal of methanol to isolate the SiQAC solid results in hydrolysis and condensation. After the pH of the solution was raised, both hydrolysis and condensation proceeded, resulting in 75% of condensed form of SiQAC after 40 min. The percent condensed form did not change even after 150 min. The final composition of the SiQAC solution after raising the pH to 7.3 and that of the prehydrolyzed SiQAC after 5 days were approximately the same. Investigations are now underway to compare the antimicrobial properties of surfaces modified with these solutions.

Because the assumption that all three methoxy groups of SiQAC hydrolyze at the same rate is not correct [25], it was not possible to fit the data for the rate of production of methanol to obtain rate constants for hydrolysis and condensation. Hence, it was decided to use the cylindrical internal-reflection cell to follow the hydrolysis and condensation of the simplest alkoxy-alkylsilane, monomethoxytrimethylsilane (MTMS).

Kinetics of hydrolysis and condensation of MTMS

The MTMS was not soluble in water and hence all studies were done in 10% (v/v) water/acetone medium. Figure 3 shows the infrared spectrum of MTMS in the unhydrolyzed (A), completely hydrolyzed (B) and partially condensed (C) forms. The band assignments and positions are summarized in Table 1. The rate of hydrolysis was extremely slow. Even at 72 h after mixing the silane with the solvent (wherein the mole ratio of silane to water was 1:15), only 50% of MTMS had hydrolyzed. However, the hydrolysis was fast when the hydrogen ion concentration was increased. For example, spectrum B in Fig. 3 was obtained 60 s after increasing the $[H^+]$ of the solution to 2.88×10^{-4} M. The rate of production of methanol as a function of time was followed at different hydrogen ion concentrations. The concentration of methanol at any instant was used to calculate the concentration of unhydrolyzed MTMS.

The hydrolysis of alkoxysilanes in water has been shown to follow a first-order rate law [15, 17]. Even though water was in 15-fold excess in the present studies, a plot of ln $([MTMS]_t)$ vs. time did not give a linear relationship. Because water is consumed during the hydrolysis of MTMS, as shown in the following reaction

$$CH_3OSi(CH_3)_3 + H_2O \rightarrow HOSi(CH_3)_3 + CH_3OH$$

a rate expression involving water also was used. When the hydrolysis of MTMS was considered to be first order in both silane and water concentrations, the following expression resulted:

$$k_2t = (1/[MTMS]_0[H_2O]_0) \ln ([MTMS]_t[H_2O]_0/[H_2O]_t[MTMS]_0) \quad (1)$$

where the subscripts 0 and t refer to the concentration of the species at times zero and t, respectively. A plot of the expression on the right-hand side of Eqn. 1 (abbreviated to ln S) vs. time should be a straight line with slope

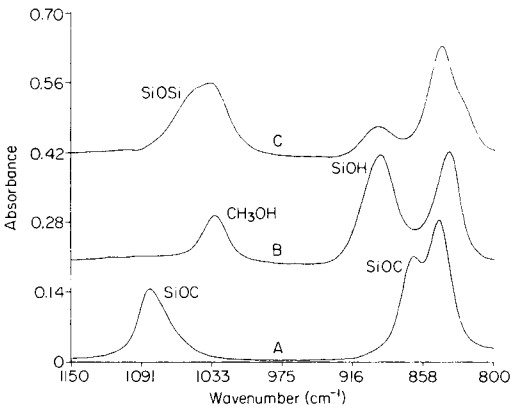

Fig. 3. Infrared spectra of 0.36 M MTMS in 10% (v/v) water/acetone medium in its (A) unhydrolyzed, (B) completely hydrolyzed and (C) partially condensed forms. See Table 1 for band assignments.

equal to the second-order rate constant, k_2. Figure 4 shows such plots at hydrogen ion concentrations of 2.88, 1.66, 0.89 and 0.56×10^{-4} M as A, B, C, and D, respectively. Regression lines with correlation coefficients larger than 0.995 and slopes of 6.85, 1.75, 0.88 and 0.19×10^{-3} M^{-1} s^{-1} for A, B, C and D, respectively, were obtained.

At hydrogen ion concentrations greater than the 2.88×10^{-4} M used to produce plot A in Fig. 4, hydrolysis was too rapid to be followed at the data-acquisition speed used. In addition, the process of increasing the hydrogen ion concentration by adding a buffer to the silane solution in the cylindrical internal-reflection cell had a time constant which became similar to $t_{1/2}$ of

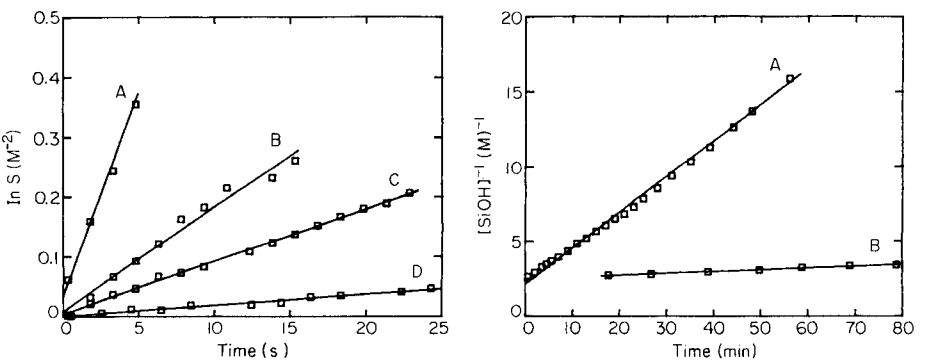

Fig. 4. Kinetics of hydrolysis of MTMS in 10% (v/v) water/acetone medium at different hydrogen ion concentrations: (A) 2.88×10^{-4} M; (B) 1.66×10^{-4} M; (C) 0.89×10^{-4} M; (D) 0.56×10^{-4} M.

Fig. 5. Kinetics of condensation of trimethylsilanol in 10% (v/v) water/acetone medium at two hydrogen ion concentrations: (A) 3.98×10^{-3} M; (B) 0.29×10^{-3} M.

the hydrolysis reaction. Different means of mixing the silane solution and the buffer (or use of stopped-flow technique) and the use of the rapid-scanning mode of the Nicolet 60SX FTIR spectrometer which easily permits 15—20 scans per second at 8 cm^{-1} resolution [26] are needed to follow the hydrolysis at higher hydrogen ion concentrations.

Once the methoxy groups have been hydrolyzed, the silanols can condense to form siloxane bonds to give hexamethyldisiloxane. Because of the large difference in the rates of hydrolysis and condensation, the two events could be easily observed in sequence for MTMS. The methanol produced after complete hydrolysis of MTMS was always equal to the concentration of MTMS taken to within ±5%. The silanols began to condense only after complete hydrolysis. Thus, the rate of condensation could be followed by the disappearance of Si—OH band area (spectrum C in Fig. 3). The rate of condensation was extremely slow at low $[H^+]$. Hence, rate constants for condensation could not be obtained in the time frame of measurement used (30 min) for hydrolysis done at hydrogen ion concentrations of 1.66, 0.89 and 0.56×10^{-4} M. Only in a solution at $[H^+] \leqslant 0.88 \times 10^{-4}$ M could the rates of both hydrolysis (plot A in Fig. 4) and condensation be measured. As observed by others [15—17], condensation was found to be second order in silanol concentration. This was proved by plotting (1/[Si—OH]) vs. time to obtain the plots shown in Fig. 5. The regression lines had correlation coefficients better than 0.995 with slopes giving the second-order rate constants for condensation. Even though the rate of hydrolysis could not be measured at $[H^+] = 3.98 \times 10^{-3}$ M because it was too rapid, the rate constant for condensation was 4.0×10^{-3} M^{-1} s^{-1}. The slope of line B in Fig. 5 gave the rate constant for condensation as 2.0×10^{-4} M^{-1} s^{-1} at $[H^+] = 2.88 \times 10^{-4}$ (same conditions as plot A in Fig. 4).

Conclusions

The circular internal-reflection sampling technique coupled with FTIR spectroscopy is clearly useful for quantitative monitoring of the rapid hydrolysis and condensation of even simple silanes such as MTMS. With suitable calibration graphs, it is possible to quantify the changes in speciation of silanes in aqueous and aqueous organic media. Other solvents found useful for such studies are methyl ethyl ketone, dimethylsulfoxide, dimethylformamide, dioxane and toluene. The methoxysilanes are particularly suitable for such a study as their infrared spectra in the 1300—800 cm^{-1} region are relatively simple. Ethoxy and other alkoxy silanes may not be easily amenable to this technique because of their complex spectra in this region.

This work was supported in part by Research Grant CHE 85-13247 from the National Science Foundation. The Nicolet 60SX FTIR spectrometer was purchased in part by an instrumentation grant from the National Science Foundation (CHE 83-17079). The suggestions of J. D. Vaughan, B. Ladanyi, and A. Rachetti contributed significantly to this work.

REFERENCES

1 T. G. Waddell, D. E. Leyden and M. T. DeBello, J. Am. Chem. Soc., 103 (1981) 5303.
2 J. P. Blitz, R. S. Shreedhara Murthy and D. E. Leyden, J. Colloid Interface Sci., in press.
3 R. K. Gilpin and M. E. Gangoda, J. Chromatogr. Sci., 21 (1983) 352.
4 J. R. Malek and J. L. Speier, J. Coated Fabr., 12 (1982) 38.
5 H. Ishida and J. L. Koenig, J. Polym. Sci., Polym. Phys. Ed., 17 (1979) 615.
6 M. L. Miller, R. W. Linton, G. E. Maciel and B. L. Hawkins, J. Chromatogr., 319 (1985) 9.
7 M. W. Urban and J. L. Koenig, Appl. Spectrosc., 40 (1986) 513.
8 J. P. Blitz, R. S. Shreedhara Murthy and D. E. Leyden, Appl. Spectrosc., 40 (1986) 829.
9 R. S. Shreedhara Murthy and D. E. Leyden, Anal. Chem., 58 (1986) 1228.
10 R. S. Shreedhara Murthy, J. P. Blitz and D. E. Leyden, Anal. Chem., 58 (1986) 3167.
11 R. S. Shreedhara Murthy, G. S. Caravajal and D. E. Leyden, in D. E. Leyden (Ed.), Chemically Modified Surfaces, Vol. 1, Gordon and Breach, New York, 1986, pp. 141—155.
12 E. P. Plueddemann, SPI 24th Annual Conference Reinf. Plast. Comp. Div. 19A, Washington, DC, February, 1969.
13 H. Ishida and J. L. Koenig, Appl. Spectrosc., 32 (1978) 462.
14 H. Ishida and J. L. Koenig, Appl. Spectrosc., 32 (1978) 469.
15 E. R. Phol and F. D. Osterholtz, in H. Ishida and G. Kumar (Eds.), Molecular Characterization of Composite Interfaces, Plenum, New York, 1985, pp. 157—170.
16 E. R. Pohl and F. D. Osterholtz, in D. E. Leyden (Ed.), Chemically Modified Surfaces, Vol. 1, Gordon and Breach, New York, 1986, pp. 481—500.
17 S. Savard, L. P. Blanchard, J. Leonard and R. E. Prudhomme, Polym. Composites, 5 (1984) 242.
18 N. J. Harrick, Internal Reflection Spectroscopy, Harrick Scientific, New York, 1967.
19 F. M. Mirabella, Jr. and N. J. Harrick. Internal Reflection Spectroscopy: Review and Supplement, Harrick Scientific, New York, 1985.
20 R. M. Gendreau, Appl. Spectrosc., 36 (1982) 47.
21 D. J. Fink and R. M. Gendreau Anal. Biochem., 139 (1984) 140.
22 E. G. Bartick and R. G. Messerschmidt, Am. Lab., 16(11) (1984) 56.
23 W. R. Moser, J. E. Cnossen, A. W. Wang and S. A. Krouse, J. Catal., 95 (1985) 21.
24 A. L. Smith, Analysis of Silicones, Wiley, New York, 1974, p. 269.
25 E. P. Plueddemann, in D. E. Leyden and W. T. Collins (Eds.), Silylated Surfaces, Gordon and Breach, New York, 1980, pp. 31—53.
26 R. Rosenthal, Nicolet Analytical Instruments, Madison, WI, private communication.

Analytica Chimica Acta, 200 (1987) 469—480
Elsevier Science Publishers B.V., Amsterdam — Printed in The Netherlands

STUDIES OF SAMPLE PREPARATION FOR SURFACE-ENHANCED RAMAN SPECTROMETRY ON SILVER HYDROSOLS

J. J. LASERNA[a], E. L. TORRES[b] and J. D. WINEFORDNER*
Department of Chemistry, University of Florida, Gainesville, FL 32611 (U.S.A)
(Received 21st January 1987)

SUMMARY

Surface-enhanced Raman spectra (SERS) on silver hydrosols of *p*-nitrobenzoic acid, *p*-aminobenzoic acid and aniline are reported. Several theoretical and practical aspects of the hydrosol preparation protocols and sample preparation procedures, and their effects on the sensitivity and reproducibility of the Raman signals are discussed. The effect of acidity on SERS signal intensity is shown to depend on the time of observation of the Raman spectra, illustrating the relevance of time to quantitative SERS data. The identification power of SERS at trace levels for closely related compounds (*p*-nitrobenzoic acid, *p*-aminobenzoic acid and aniline) is illustrated.

It is well established that the electromagnetic properties of nonflat surfaces of certain materials can radically alter the spectroscopic properties of mol-

---

*James D. Winefordner received his B.S., M.S., and Ph.D. degrees in chemistry from the University of Illinois in 1954, 1955, and 1958, respectively. His research advisor was Professor H. V. Malmstadt. After a year as a postdoctoral fellow, he was appointed Assistant Professor of Chemistry at the University of Florida in 1959, and, in 1965, was promoted to Full Professor. He was appointed Graduate Research Professor of Chemistry in 1976 and is currently Chairman of the Analytical Division of the Department of Chemistry. His research interests include: atomic and molecular emission, absorption, and fluorescence in flames and other hot gases; molecular fluorescence and phosphorescence of species in the condensed phase; development of sensitive, selective gas and liquid chromatographic detectors; and development of spectroscopic instrumentation for analysis. He has published over 500 scientific papers and chapters on the above topics. He is a member of the American Chemical Society, Society of Applied Spectroscopy, Phi Lambda Phi, Alpha Chi Sigma, and American Association for Advancement of Sciences. He received the 1971 Sigma Xi University of Florida Research Award, the 1968 Meggers Award, the 1973 ACS Award in Analytical Chemistry (Fisher Award), the 1973 Pittsburgh Society of Applied Spectroscopy Award, and the 1978 ACS Chemical Instrumentation Award. He was also the recipient of the 1980 ANACHEM Award, the 1981 Theophilus Redwood Lecture Award, the 1982 ACS Florida Section Award, the 1982 Southern Chemist Award, the 1983 SAS Honorary Membership Award, as well as the 1984 University of Florida Teacher/Scholar of the Year Award, the 1984 Golden Key Honorary Membership and the 1985 Blue Key Distinguished Faculty Award, 1986 Honorary Member Japan Society of Analytical Chemistry, 1987 Torbern Bergman Award, and 1987 ACS Analytical Division Spectroscopy Award.

[a]On leave from: Department of Analytical Chemistry, Faculty of Sciences, University of Malaga, 29071 Malaga, Spain.
[b]Present address: Smith Kline & French Lab. Co., Cidra, Puerto Rico.

0003-2670/87/$03.50

ecules located nearby; normal and resonant Raman scattering, fluorescence and absorption are among the phenomena involved. Extensive overviews on the subject have been reported by Metiu [1] and Gersten and Nitzan [2]. From an analytical point of view, it is of particular importance to establish those circumstances under which the intensity of Raman scattering of molecules near a surface (surface-enhanced Raman scattering) is enormously increased with respect to that in solution. Under such conditions, surface-enhanced Raman spectrometry (SERS) becomes an analytical technique with a sensitivity comparable with that of conventional molecular absorption or fluorescence spectrometry, with the additional major advantage of selectivity inherent in vibrational spectroscopies. The sensitivity of SERS can be further enhanced by the amplification process of Raman scattering which occurs usually in parallel with the quenching of luminescence by adsorption on surfaces [3, 4]. Thus, the difficulties caused by fluorescence in normal Raman applications are often no longer a problem in SERS.

Both electromagnetic [5—8] and chemical theories [9—11] have been developed to explain the enormous increase in Raman cross-sections. Briefly, the electromagnetic theory relies upon the plasma resonance model which is related to optical properties of free electron systems such as metals. The electric field at such a surface becomes greatly enhanced if the incident photon energy is in resonance with a normal mode of conduction electrons in the metals, which leads to enhanced Raman scattering for those molecules which are close to the metal surface. The chemical enhancement theory involves enhanced cross-sections which arise from adsorption-induced resonant intermediate states in the scattering process, by analogy to resonance Raman scattering. Chemisorption and charge transfer are clearly important features of this mechanism. Sufficient experimental evidence now exists for each of these theories to suggest that more than one mechanism is responsible for the overall enhancement [12].

Various substrates have been used for the observation of SERS, involving a restricted number of metals, such as silver, gold, copper, platinum and nickel. Among the substrates, vacuum-deposited films, electrodeposited metals and electrodes, and colloidal particles have been mostly used. Several analytical applications of SERS for trace characterization on all three types of substrates have been reported. Detection of low concentrations of diphenylthiocarbazone adsorbed on a silver electrode was reported [13]. Concentrations as low as 10^{-9} M were reported to give spectra with acceptable signal-to-noise ratio. Copper and zinc phthalocyanine complexes were determined on silver island films [14], while silver hydrosols have been used in the liquid phase [15, 16] or deposited on filter paper [17] or silica gel plates [18] for the detection of dyes [17] and organic bases [15, 16, 18]. Chemically prepared silver films were used for the detection of bipyridine [19] and silver particles deposited on quartz substrates were used for the detection of polyaromatic compounds [20]. Metal island films provide perhaps the most reproducible substrate. In contrast, electrodes have been

mostly used for theoretical studies because favorable conditions are given for supporting the electromagnetic and the chemical models. However, one disadvantage of these static substrates is that the intense laser fields associated with SERS can destroy the surface morphology which gives rise to surface enhancement and/or induced molecular desorption and even molecular decomposition [21—23]. In addition, careful attention must be given to geometric factors in order to maximize classical field enhancements and light collection.

Colloidal hydrosols provide a number of advantages for SERS observation including ease of formation and manipulation, simple characterization by absorptiometric techniques and a definite dependence of the enhancement on particle size and shape. Disadvantages are that the analyte (sample)-induced coagulation of the colloidal dispersion eventually causes instability of the entire system and the SERS activity of a given analyte depends to a certain extent on the means of hydrosol preparation and on the exact protocol used for a given preparation [24—26]. The present work is an effort to obtain better characterization of silver hydrosols and of their usefulness for SERS observation with analytical purposes. *p*-Nitrobenzoic acid, *p*-aminobenzoic acid and aniline are used as model compounds in this study.

EXPERIMENTAL

Instrumentation

The Raman system has been described by Torres and Winefordner [16]. Basically, it consisted of a Spectra-Physics, model 171, argon-ion laser and a Spex Industries, model 1680B, double monochromator. The detector was a thermoelectrically cooled Hamamatsu model R-928 photomultiplier tube, with a photon-counting system (SSR Instruments, model 1105/1120). Conventional 1×1 cm^2 quartz cells and 90° geometry were used for Raman sampling.

Procedures

Silver hydrosols were prepared by reduction of 1×10^{-3} M silver nitrate with 2×10^{-3} M sodium tetrahydroborate in a volume ratio of 1:3. Three different procedures were used. In the first procedure, 20 ml of the silver nitrate solution was added dropwise to 60 ml of vigorously stirred, ice-cooled sodium tetrahydroborate solution. The resulting sol was allowed to reach room temperature for 2 h with occasional stirring at ca. 15°C. The second procedure was essentially the same as the first except that after mixing the silver nitrate and ice-cooled sodium tetrahydroborate solutions, the hydrosol was allowed to reach room temperature with constant stirring for 2 h. In the third procedure, 1 ml of silver nitrate solution was added to 3 ml of sodium tetrahydroborate solution at room temperature and the resulting hydrosol was vortex-mixed to give complete homogenization.

Stock solutions of *p*-nitrobenzoic acid (PNBA), *p*-aminobenzoic acid (PABA) and aniline were prepared in ethanol. Sample solutions were prepared in 16-mm × 125-mm disposable plastic test tubes by mixing 0.1 ml of an ethanolic solution of analyte with 4 ml of the prepared silver hydrosol (first and second procedures) or with 3 ml of sodium tetrahydroborate and 1 ml of silver nitrate solution (third procedure). Microliter volumes of acid or salt solutions were added for activation when required.

The cleanliness of the glassware and the purity of materials were important factors which determined the reproducibility and stability of the sol systems. All glassware was soaked in (1 + 1) nitric acid solution and rinsed thoroughly with deionized water (Barnstead Sybron) before use. Analytical-reagent grade chemicals were used throughout. Except, when otherwise stated, all spectral data reported were obtained by using freshly prepared solutions of analytes, silver nitrate, sodium tetrahydroborate, salts and acids.

RESULTS AND DISCUSSION

Preparation procedures

Most of the procedures for the preparation of silver hydrosols involve several stages which may result in systems of different stability against aggregation. One of the commonest protocols used for the observation of SERS involves the slow addition of a silver nitrate solution to an ice-cooled solution of sodium tetrahydroborate with vigorous stirring (first procedure) [27]. When this method was used, it was found that in the process of thermal equilibration to room temperature, a considerable aggregation of the hydrosol can take place, which may result in a totally useless sol for the observation of SERS. The aggregation process was found to take place at ca. 15°C; one can observe how the system changes its color from the initial bright yellow (4°C) to brown and finally black, indicating the aggregation process. The aggregation process can be essentially "stopped" by stirring the hydrosol several times until the system stabilizes. After this, the hydrosol remains stable for several weeks. The hydrosol is characterized by an absorption spectrum with a maximum at 400 nm, which depends on the extent of stirring during thermal equilibration and has a shoulder at 420 nm (spectrum a, Fig. 1). This spectrum characterizes the surface plasma resonance absorption for silver spheres of ca. 20-nm diameter, although a certain degree of polydispersity or aggregation is manifested by the spectral feature at 420 nm [28, 29].

In an attempt to minimize the polydispersity, the hydrosol was allowed to reach room temperature with constant stirring for 2 h (second procedure). This process resulted in a bright yellow hydrosol with a single absorption maximum at 380 nm (spectrum b, Fig. 1), indicating that under these conditions, the particle size obtained is much smaller. (A silver hydrosol peaking at 384 nm has been reported to correspond to an average particle diameter of 7.5 nm as measured by transmission electron microscopy [30].)

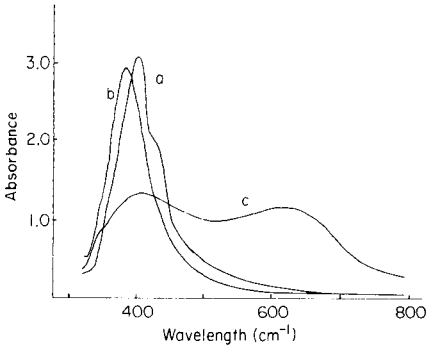

Fig. 1. Adsorption spectra: (a) Silver hydrosol at room temperature (first procedure); (b) silver hydrosol allowed to reach room temperature with constant stirring (second procedure); (c) silver hydrosol in (b) after addition of 10 μg ml^{-1} PABA and activation with 0.15 M acetic acid.

Both these hydrosol procedures can be used for the observation of SERS from PABA, PNBA, and aniline but they showed different resistance to aggregation. Thus, with the hydrosol peaking at 400 nm, addition of 10 μg ml^{-1} PABA resulted in the SERS spectrum shown in Fig. 2, with a signal-to-noise ratio of 20 for the Raman band at 1359 cm^{-1}. With the hydrosol with its absorption maximum at 380 nm, the production of a SERS signal-to-noise ratio similar to that in Fig. 2 required a PABA concentration 10-fold greater. Also, it is possible to obtain a similar signal-to-noise ratio with 10 μg ml^{-1} PABA by activating the hydrosol with electrolytes (sodium nitrate or sodium acetate) or acids (nitric acid or acetic acid). In all cases, the Raman spectrum of PABA showed intensity distribution and vibrational modes identical to those shown in Fig. 2; the absorption spectrum which peaked at 380 nm had a broad band between 500 and 800 nm (spectrum c, Fig. 1) after the addition of 10 μg ml^{-1} PABA and activation with 0.15 M acetic acid. The peak wavelength of this broad band depends on a variety of parameters, such as

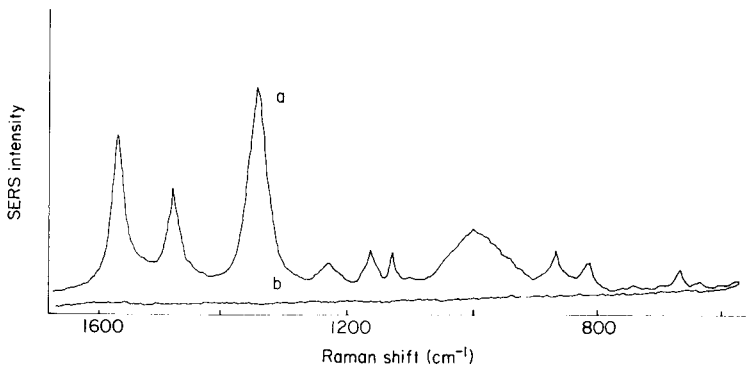

Fig. 2. (a) Surface-enhanced Raman spectrum of 10 μg ml^{-1} PABA on silver hydrosol; (b) normal Raman spectrum of the hydrosol blank.

acidity, concentration of adsorbate and activating species (such as salts) and time between activation and measurement (see below).

While it is well established that the observation of SERS requires an aggregation process induced by the adsorption of analyte on the colloidal particles [31], the results above indicate also that a high analytical sensitivity is facilitated by a hydrosol partially coagulated prior to the addition of analyte. In other words, for an unaggregated sol, the adsorbate plays a double role: firstly, it causes hydrosol activation, i.e., the compression of the electrical double layer surrounding the sol particles, and secondly, it causes adsorption and subsequent aggregation needed for strong Raman scattering. Therefore, observation of SERS at low adsorbate concentrations is possible when coagulation is caused by an external activating species such as an electrolyte or an acid or when the hydrosol is previously coagulated to some extent in the process of thermal equilibration. In the latter case, because string-like particle aggregation is known to be a requisite for large Raman signals, the pre-aggregation must have a practical limit because this process results in compact cluster formation which is known to be detrimental to SERS observation [24]. It is thus expected that a definite degree of pre-aggregation will result in maximum sensitivity. Unfortunately, it proved impossible to determine such a practical limit owing to difficulties in controlling the process of thermal equilibration.

A hydrosol preparation equally useful for SERS observation can be prepared by mixing sodium borohydride and silver nitrate at room temperature (third procedure). This hydrosol also shows an absorption maximum at 380 nm with no other spectral features in the long wavelength side of this band, indicating considerable monodispersity, small-sized particles and resistance to aggregation by added adsorbates. Figure 3 shows the activation effect as well as the additive character of acid and electrolyte in promoting SERS from PNBA.

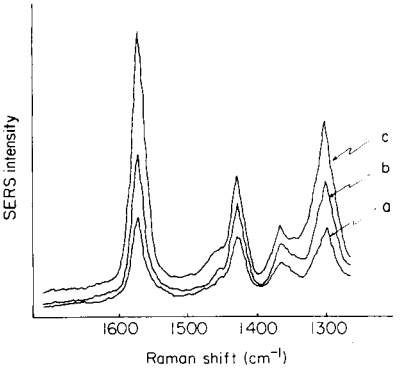

Fig. 3. Surface-enhanced Raman spectra of 10 μg ml^{-1} PNBA on silver hydrosols after addition of (a) 10 μl of 0.3 M nitric acid; (b) 20 μl of 0.3 M nitric acid; (c) 20 μl of 0.3 M nitric acid and 10 μl of 1 M sodium nitrate. All measurements taken 5 min after the addition of activating agent.

One of the greatest problems in the application of silver hydrosols for analytical purposes is the poor batch-to-batch reproducibility. This is of practical importance because of the limited time after preparation in which the hydrosols provide stable spectra [16]. The low precision is caused by the poor control that can be exercised over the several stages involved in the preparation procedures, as discussed above. It was found, however, that it is possible to reproduce to within ±10% the signal in the SERS spectrum of PABA with the hydrosol prepared at room temperature and activation with nitric acid. Nevertheless, it is necessary to maintain strict control of the timing in the measurement, as discussed below. Unless otherwise stated, the following data refer to hydrosols prepared at room temperature (third procedure).

Aging of the solutions

To obtain reproducible SERS signals, it is important to use freshly prepared solutions of analyte, acids, electrolytes, as well as the solutions used in hydrosol preparation. In the case of PABA, it was found that changes in spectral characteristics can also take place. Figure 4 shows the spectrum obtained without activation when one or more of the following solutions are employed: (i) a hydrosol aged for 24 h or more; and (ii) the silver solution used in the hydrosol preparation or the PABA solution are more than approximately one week old.

Comparison of the spectra in Figs. 2 (spectrum a) and 4 shows that when aged solutions were used, the following major changes occurred: intensification of the Raman mode at 1127 cm^{-1}; a red shift in the vibrational mode at 1359 cm^{-1}; and the appearance of two new vibrations at 1446 cm^{-1} and 1620 cm^{-1}. The 1127 cm^{-1} and 1620 cm^{-1} modes can be assigned to the NH_2 vibrations [16], while the 1446 cm^{-1} mode is assignable to the benzene ring-stretching vibration. The shift of the 1359 cm^{-1} Raman mode as well as the appearance of the vibration at 1446 cm^{-1} are clearly visible in the expanded spectra in the 1300—1500 cm^{-1} range (Fig. 5). When freshly prepared solutions were used, the peak was centered at 1359 cm^{-1} and this was shifted to 1389 cm^{-1} when aged solutions were used. Suh et al. [25] have

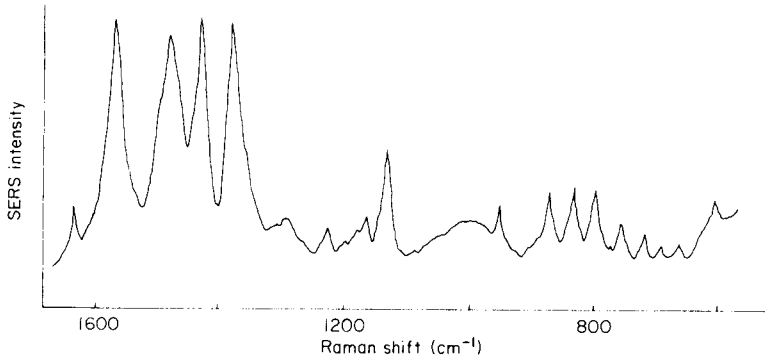

Fig. 4. Surface-enhanced Raman spectrum of PABA from aged solutions.

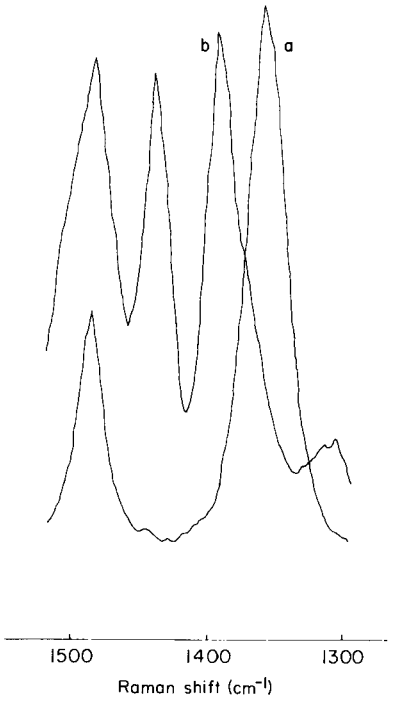

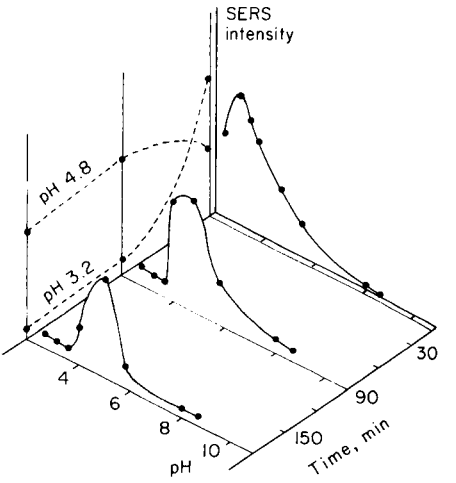

Fig. 5. Expanded surface-enhanced Raman spectra of PABA showing the age-dependent shift and growing of vibrational modes: (a) from freshly prepared solutions; (b) from aged solutions.

Fig. 6. Effects of acidity and time on the SERS signal intensity of PABA at the 1359 cm^{-1} peak.

reported similar changes in the spectrum of PABA on silver particles as a function of concentration. At low PABA concentrations, the adsorbed PABA molecules are isolated on the surface; as the PABA concentration is increased, the molecules link together by hydrogen bonds between NH_2 and COO^- groups [25].

The changes in the surface-enhanced Raman spectrum upon aging of the solutions is interpreted here also to reflect the molecular reorientation taking place on the silver surface. In other words, with freshly prepared solutions, PABA molecules are preferentially adsorbed through the carboxylate group giving rise to the 1359 cm^{-1} peak. When aged solutions are used, the PABA molecules adopt a flat position on the surface, being then adsorbed through both the carboxyl and the amino groups. The result is the shift to 1389 cm^{-1} and the strengthening of the vibrations at 1127 cm^{-1} and 1620 cm^{-1}. Whether or not the PABA molecules are then associated through hydrogen bonds is not unambiguous, but the molecule has to be close to the surface as manifested by the general enrichment of vibrational modes in the region below 900 cm^{-1}, almost all of which are assignable to benzene ring modes.

The occurrence of these spectral changes as well as the intensity variations when aged solutions were used, was found to be dependent to some extent on the order of mixing of reagents as well as on the time after sample preparation or sol activation (see below). Because the aging effect has been found [16] to be more the result of changes in the silver sol particles than changes in the analyte itself, the phenomenon can be expected to be quite general. Thus, to obtain reproducible results, it is strongly recommended that freshly prepared solutions should be used.

Effect of acidity

Figure 6 shows the pH dependence of the SERS intensity of PABA, as well as the temporal behavior of the Raman signal. Nitric acid was used to increase the acidity of the medium. Data reported are for a Raman shift of 1359 cm^{-1}, but equivalent results were obtained at the other main Raman peaks. As shown, for the measurements done 5 min after addition of nitric acid, the maximum SERS intensity is obtained at a pH of 3.2, with a decrease in Raman signal at both sides of this value. However, when the samples were measured 90 min or more after acid addition, the maximum intensity was obtained at pH 4.8. These observations can be understood by observing the kinetic behavior of the 1359 cm^{-1} Raman band at both pH values. This is depicted in Fig. 6 as the dashed lines drawn in the intensity/time plane. The Raman intensity decays quickly at a pH of 3.2 as a result of the instability of the sol system. However, at this acidity, the activation of the hydrosol is very fast. The decrease in Raman intensity at pH lower than 3.2 is probably more the result of measuring the scattering intensity in latter stages of the SERS decay (see Fig. 6) than a real decrease in intensity with acidity. At a pH of 4.8, however, the signal increases with time and, after 90 min of acid addition, this pH value becomes that of maximum intensity (Fig. 6). No measurable SERS signals could be detected at pH > 7, even 3 h after sample preparation.

An interesting observation in this study is that the absorbance of the solutions decreased faster than the Raman signals. At a pH of 5.5, the sample showed considerable sedimentation 12–14 h after preparation. The SERS spectrum of the supernatant solution was only ca. 20% less intense than that 30 min after sample preparation, while the absorption spectrum of the same solution indicated essentially no absorbance at any of the significant wavelengths mentioned above. These results suggest that most of the Raman scattering for the adsorbed PABA molecules is caused by a small portion of the aggregates, probably from those formed by a small number of primary silver particles. In agreement with this observation, Kerker et al. [32] have recently calculated that with only 0.5% aggregates formed by two primary silver particles and 0.02% aggregates formed by three primary particles, a strong SERS signal equivalent to a 10^4 enhancement is possible.

Another interesting observation arising in the pH study is the persistence of the SERS bands of the carboxylate form of PABA at pH values lower

than the pK_a of this group. The pH of the PABA/hydrosol solution before acidification is 8.6, and the activation with nitric acid in all the pH range studied results in identical surface-enhanced spectra. The constancy with respect to pH changes of the intensity distribution and vibrational pattern already exclude a primary effect of nitric acid on PABA. However, because the pK_a for the protonation of the carboxyl group is 4.9, one would expect that for pH values lower than this, the Raman mode at 1700 cm^{-1} corresponding to vibration of the COOH group [33] would be present. The lack of this vibrational mode at pH < 4.9 can be explained if the kinetics of adsorption are faster than the kinetics of protonation; before addition of acid, PABA is not expected to be adsorbed on the silver particles. However, this explanation is unlikely because acid-base reactions are known to be among the fastest reactions in solution. A possible explanation is that PABA is already adsorbed on the colloidal particles through the carboxyl group prior to the addition of acid, although this adsorption cannot cause the coagulation needed for SERS observation. In fact, the absorption spectrum of the solution at pH 8.6 does not show any sign of aggregation. Addition of nitric acid causes coagulation by compression of the electrical double layer with the PABA molecules remaining adsorbed through the carboxylate group, independent of the final acidity reached. This is probably further evidence that the SERS emanates from the chemisorbed (coordinated) molecules to surface silver atoms and accounts for the chemical mechanism of SERS.

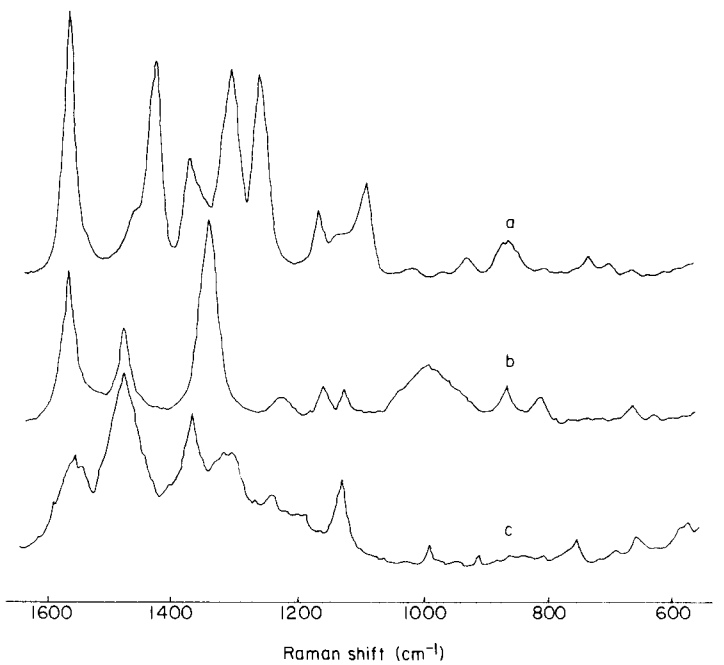

Fig. 7. Surface-enhanced Raman spectra: (a) 10 $\mu g\ ml^{-1}$ PNBA; (b) 10 $\mu g\ ml^{-1}$ PABA; (c) 100 $\mu g\ ml^{-1}$ aniline.

TABLE 1

Surface enhanced Raman bands of *p*-nitrobenzoic acid, *p*-aminobenzoic acid and aniline on silver hydrosols

Raman shift (cm^{-1})			Raman shift (cm^{-1})		
PNBA	PABA	Aniline	PNBA	PABA	Aniline
—	662	667	—	1231	1242
753	—	765	1262	—	—
857	852	—	1306	—	1305
938	—	—	—	1359	—
—	979	977	1375	—	1362
1088	—	—	1425	—	—
—	1127	1126	—	1495	1495
1175	1167	—	1587	1582	1577

Identification study

The surface-enhanced Raman spectrum is a result of the interaction between the incident photons and the vibrational energy levels of the particular molecule being irradiated, and so it is, like the conventional Raman spectrum, unique to the compound that produces it. Hence, these spectra can be used in much the same way as normal Raman spectra for the characterization and identification of unknown samples. This is illustrated in Fig. 7 for three closely related compounds. For clarity, the baseline of the spectra have been shifted. Spectrum (a) corresponds to *p*-nitrobenzoic acid, PNBA; spectrum (b) corresponds to *p*-aminobenzoic acid, PABA; and spectrum c corresponds to aniline. As shown in Table 1, the three compounds exhibit a common Raman band near 1580 cm^{-1} corresponding to the stretching vibration of the benzene ring. The band near 1125 cm^{-1} can be due to NH_2 bending, and it is shown by both PABA and aniline. The band of PABA at 1359 cm^{-1}, which has been repeatedly assigned to stretching vibration of the COO^- group [16, 25], is not shown by PNBA. Instead, a band at 1305 cm^{-1} in PNBA may indicate a different orientation of this group on the silver surface. The band at 1262 cm^{-1} in PNBA can be assigned to NO_2 stretching vibration.

Conclusions

On the basis of this study, several conclusions can be drawn. First, colloidal suspensions can be used as substrates for analytical studies by surface-enhanced Raman spectrometry especially if a better understanding of the interaction between analytes and colloidal particles is gained. Secondly, silver hydrosols prepared at room temperature (third procedure) are very convenient for the observation of SERS from several adsorbates, because samples can be prepared as required by mixing sequentially analyte, sodium tetrahydroborate and silver nitrate. Thirdly, high analytical sensitivity requires activation of the resulting system and careful attention to the timing in the measurement process. Finally, cleanliness of the glassware, use of freshly prepared solutions, purity of reagents and solvents, and adherence to a strict procedure for sample preparation are key factors for the reproducibility of

the Raman signals. The data obtained in this work are confined to qualitative identification of several closely related analytes, but the results are encouraging enough to suggest that activation of hydrosols can be developed comparable to other substrates for quantitative studies. The relevance of the time-dependent factor to activation processes deserves the introduction of some kind of automation scheme for quantitative studies, such as those inherent to flow-injection systems or post-column derivatization in liquid chromatography.

This research was supported by NIH-5-R01-GM11373-23.

REFERENCES

1 H. Metiu, Prog. Surface Sci., 17 (1984) 153.
2 J. I. Gersten and A. Nitzan, Surface Sci., 158 (1985) 165.
3 G. Ritchie and C. Y. Chen, Pure Appl. Chem., 52 (1980) 361.
4 C. Y. Chen, I. Davoli, G. Ritchie and E. Burstein, Surface Sci., 101 (1980) 363.
5 J. I. Gersten and A. Nitzan, J. Chem. Phys., 73 (1980) 3023.
6 M. Kerker, D. S. Wang and H. Chew, Appl. Opt., 19 (1980) 415.
7 T. E. Furtak and J. Reyes, Surface Sci., 93 (1980) 351.
8 P. W. Barber, R. K. Chang and H. Massoudi, Phys. Rev. B, 27 (1983) 7251.
9 A. Otto, Appl. Surface Sci., 6 (1980) 309.
10 J. Billman, G. Kovacs and A. Otto, Surface Sci., 92 (1980) 153.
11 E. Burstein, Y. J. Chen, C. Y. Chen, S. Lundquist and E. Tossatti, Solid State Commun., 29 (1979) 567.
12 T. E. Furtak, in B. A. Garetz and J. R. Lombardi (Eds.), Advances in Laser Spectroscopy, Vol. 2, Wiley, New York, 1983, p. 175.
13 J. E. Pemberton and R. P. Buck, Anal. Chem., 53 (1981) 2263.
14 C. Jennings, R. Aroca, A. M. Hor and R. O. Loutfy, Anal. Chem., 56 (1984) 2033.
15 E. Gautner, D. Steinart and J. Reinhardt, Anal. Chem., 57 (1985) 1658.
16 E. L. Torres and J. D. Winefordner, Anal. Chem., 59 (1987) 1626.
17 C. D. Tran, Anal. Chem., 56 (1984) 824.
18 J. M. L. Sequaris and E. Koglin, Anal. Chem., 59 (1987) 526.
19 F. Nin and T. Cotton, Anal. Chem., 58 (1986) 3159.
20 T. Vo-Dinh, M. Meier and A. Wokaun, Anal. Chim. Acta, 181 (1986) 139.
21 R. P. Cooney, M. R. Mahoney and M. H. Howard, Langmuir, 1 (1985) 273.
22 R. P. Cooney and T. P. Mernagh, J. Electroanal. Chem., 168 (1984) 67.
23 J. P. Davies, S. J. Pachuta, R. G. Cooks and M. J. Weaver, Anal. Chem., 58 (1986) 1290.
24 H. D. Stidham and S. M. Harris, J. Raman Spectrosc., 16 (1985) 193.
25 J. S. Suh, D. P. Dilella and M. Moskovits, J. Phys. Chem., 87 (1983) 1540.
26 J. A. Creighton, in R. K. Chang and T. E. Furtak (Eds.), Surface Enhanced Raman Scattering, Plenum, New York, 1982, p. 315.
27 J. A. Creighton, C. G. Blatchford and M. G. Albrecht, J. Chem. Soc. Faraday Trans. II, 75 (1979) 790.
28 M. Kerker, D. S. Wang, H. Chew, O. Siiman and L. A. Bumm, in R. K. Chang and T. E. Furtak (Eds.), Surface Enhanced Raman Scattering, Plenum, New York, 1982, p. 109.
29 P. C. Lee and D. Meisel, J. Phys. Chem., 86 (1982) 3391.
30 R. L. Garrell and R. H. Schultz, J. Colloid Interface Sci., 105 (1985) 483.
31 C. G. Blatchford, J. R. Campbell and J. A. Creighton, Surface Sci., 120 (1982) 435.
32 M. Kerker, O. Siiman and D. S. Wang, J. Phys. Chem., 88 (1984) 3168.
33 J. Klein, A. Leger, M. Berlin, D. Defourneau and M. J. L. Sangster, Phys. Rev. B, 7 (1973) 2336.

Analytica Chimica Acta, 200 (1987) 481—490
Elsevier Science Publishers B.V., Amsterdam — Printed in The Netherlands

IDENTIFICATION AND DETERMINATION OF AROMATIC NITRO COMPOUNDS BY ELECTRON SPIN RESONANCE SPECTROMETRY

D. THORBURN BURNS**, MOHAMED A.-Z. ELTAYEB and BRIAN D. FLOCKHART*
Department of Pure and Applied Chemistry, The Queen's University, Belfast BT9 5AG Northern Ireland (Great Britain)

(Received 2nd April, 1987)

SUMMARY

Aromatic nitro compounds are quantitatively converted to the corresponding anion-radical form by electron transfer at the surface of thermally activated magnesium oxide. The radicals are stable in the adsorbed state, and the reaction is useful for the identification and determination of the parent compound. The method is applied to detect and quantify various nitrobenzenes, nitrotoluenes and tetryl by electron spin resonance spectrometry. For 2,4,6-trinitrotoluene (TNT), the detection limit was ca. 10 ng; the r.s.d. at the 2 μg level was ±1.8%. The analysis of hand-swab extracts that contained TNT at the trace level demonstrates a potentially important application of the method.

The determination of aromatic nitro compounds, particularly at the trace level, is a growing problem. Many compounds in this group exhibit various degrees of mutagenicity and/or carcinogenicity [1]; many are used as drugs, cosmetic ingredients and perfumes [2]; others are potentially explosive. Those in the last category are clearly of particular interest in forensic science. The unequivocal detection and identification of explosive residues in samples such as hand-swab extracts or post-blast debris can be very difficult. Whereas explosives in the pure state can often be satisfactorily determined by a variety of methods, the determination of these chemicals in contaminated samples usually exposes the lack of selectivity of the analytical procedure, making an initial sample clean-up obligatory [3—5]. Although many tech-

---

*Brian Duncan Flockhart has been a Senior Lecturer in Physical Chemistry at The Queen's University of Belfast since 1967. His research interests include the study of the redox activity and catalytic properties of oxide catalysts, free-radical studies in fluid solution, and applications of n.m.r. spectrometry and e.s.r. spectrometry to analytical chemistry.

**Duncan Thorburn Burns has been Professor of Analytical Chemistry at The Queen's University, Belfast since 1975, before which he was Reader at the University of Technology, Loughborough. He was the Royal Society of Chemistry Theophilus Redwood Lecturer in 1982, and their Perkin-Elmer medallist in the same year. In 1984 he was elected as a Member of the Royal Irish Academy and a Fellow of the Royal Society of Edinburgh. He is the President-Elect of the Analytical Division of the RSC. His main analytical research interests lie in ion-pair extraction and in historical aspects.

0003-2670/87/$03.50

niques have been evaluated for the determination of organic explosive compounds and their residues [6—9], no application of electron spin resonance (e.s.r.) spectrometry to the problem has been reported. The data presented herein demonstrate the potential of the e.s.r. technique for the identification and determination of aromatic nitro compounds at submicrogram levels in both clean and contaminated samples. The method is based on anionic radical formation through adsorption of the parent nitro compound on the surface of a thermally activated oxide. Concentrations of the analyte in solution are determined by direct comparison of the e.s.r. signal obtained on the addition of the oxide with that of standard solutions similarly treated. The *g* value of the adsorbed radical, the shape of the e.s.r. spectrum, and the colour developed on the oxide surface are used to identify individual nitro compounds.

EXPERIMENTAL

Apparatus

The e.s.r. spectra were obtained with a Varian E-109 spectrometer operated at ca. 9.45 GHz with a magnetic field modulation of 100 kHz. Samples were put in either quartz or Pyrex tubes (4 mm i.d.). A Pye 104 (Model 74) gas chromatograph was used for comparative examinations of hand-swab extracts of 2,4,6-trinitrotoluene (TNT). The chromatograph was fitted with an electron-capture detector (10 mCi ^{63}Ni held at 250°C, pulse space 150 μs) and it had a glass column (0.9 m × 4 mm i.d.) packed with 7% SGR E301 (Perkin-Elmer) on 100—120 mesh Chromosorb W-HP and operated at 170°C; nitrogen was used as carrier gas (60 ml min^{-1}).

Reagents

Magnesium oxide was prepared from magnesium hydroxide as follows. Magnesium sulphate (AnalaR, BDH, 100 g) was dissolved in deionized water. Ammonia solution (AnalaR; BDH) was added with constant and vigorous mechanical stirring until the solution reached pH 11. The precipitate was allowed to settle, filtered through hardened filter paper (Whatman No. 542), and washed thoroughly with deionized water until free from sulphate. The magnesium hydroxide was dried at 100°C overnight and then ground to a fine powder. Active magnesium oxide was obtained by heating the hydroxide in air for 1 h at 400°C (see below) in an electric muffle furnace, followed by cooling at 1 Pa over phosphorus(V) oxide for 30 min.

Aluminium oxide was essentially of the gamma-type (Laporte Industries); the principal contaminants were Na_2O (0.5%), SiO_2 (0.03%) and Fe_2O_3 (0.01%). Optimum activation of this oxide for present purposes was achieved by heating at ca. 800°C for 3 h. Active calcium oxide was prepared by thermal decomposition of calcium carbonate (AnalaR). The optimum decomposition temperature was found to be ca. 600°C. After activation, the oxides were cooled at 1 Pa over phosphorus(V) oxide for 30 min.

Nitrobenzene, *o*- and *p*-dinitrobenzene, *o*- and *p*-nitrotoluene and 2,4-dinitrotoluene were all general-purpose reagents and were used as received. *m*-Dinitrobenzene, 2,6-dinitrotoluene and 1,3,5-trinitrobenzene were also general-purpose reagents and were recrystallized from ethanol. 2,4,6-Trinitrotoluene (TNT) and 2,4,6-*N*-tetranitro-*N*-methylaniline (tetryl) were gifts from the Northern Ireland Forensic Science Laboratory, Belfast; the TNT was recrystallized from ethanol/benzene. 2,4,5-Trinitrotoluene was prepared [10] in this laboratory by nitration of *m*-dinitrotoluene, and was recrystallized from acetone.

Toluene (AnalaR), acetone (AnalaR) and n-hexane (Spectrosol grade; BDH) were used as solvents; the toluene was treated with sodium wire and distilled before use.

Procedure for e.s.r.

Aliquots of the solution of the nitro compound were measured into separate tubes (4 mm i.d.) by means of an Agla micrometer syringe. Solvent was added to bring the level of solution in each tube to about the same height (ca. 35 mm). Activated oxide catalyst was added from a glass spoon and funnel until the depth of solid sample was 22—23 mm. The contents of the tubes were stirred with clean brass wires to ensure homogeneous mixtures. The tubes were stoppered and allowed to stand for 10—15 min, and the e.s.r. spectra were then recorded.

Relative concentrations of radicals were obtained by measuring changes in peak-to-peak height of the first derivative curves, because the line shape remained unchanged. (If the shape changes, double integration must be used to give the areas under the absorption curves which can then be used for comparison.) Absolute concentrations were determined by comparing the areas under the absorption curves for the analyte and a standard solution of 1,1-diphenyl-2-picrylhydrazyl in toluene. The *g* values of the adsorbed nitro radicals were obtained by comparison with that of the perylene radical generated on a silica/alumina (ca. 13% Al_2O_3) surface [11] taken as 2.0026.

Preparation of hand-swab extracts

The stock solution was 10 μg TNT μl^{-1} in acetone. A ten-fold dilution of this solution was made and a 200-μl portion of the diluted solution (200 μg of TNT) was applied evenly to the palm of a hand from a syringe; the solvent evaporated quickly. Hand-swabbing [12] was begun after 30 min. The swab (ca. 25 mg of cotton wool tied to a wooden stick) was dipped in ca. 2 ml of toluene, rubbed over a small area of the hand, and rinsed in the toluene. The process was repeated until the whole palm had been swabbed six times. After the final rinse, the swab was squeezed out and discarded. The solution was diluted to 25 ml with toluene and examined by both gas chromatography (g.c.) and e.s.r. spectrometry.

RESULTS

2,4,6-Trinitrotoluene

Adsorption of TNT at room temperature from solution in toluene on pre-heated magnesium oxide produced a violet surface coloration. The system gave a three-line e.s.r. spectrum (Fig. 1a) with a g value of 2.0052 and extreme splitting of 52 G. Electron transfer has been shown to occur at the surfaces of clean magnesium oxide [13], partially dehydrated catalytic aluminas [14, 15], amorphous silica/aluminas of high alumina content [15] and zeolite aluminosilicates [16] to produce the anion radicals of various mono-, di- and tri-nitro aromatic compounds. TNT was not included among the adsorbates used in those investigations, but the characteristics of the spectrum shown in Fig. 1(a), and the conditions under which it was obtained, point clearly to the adsorbed species being the mono-negative ion radical of the parent compound. The reducing activity of magnesium oxide depends markedly on the temperature of activation. Heating of the oxide below 200°C produced neither a surface coloration nor an e.s.r. signal when a solution of TNT in toluene was added at room temperature. Maximum reducing power was exhibited at an activation temperature of ca. 400°C. The required activation period was relatively short. A sample of magnesium oxide that had been heated at 400°C for 50 min was just as active for the reduction of TNT as a sample heated for 18 h. For the remainder of the work involving magnesium oxide, an activation period of 1 h was therefore used.

A study of the effect of contact time of TNT with magnesium oxide on the reducing ability of the oxide showed that adsorption of the nitro compound from dilute solution in toluene was rapid and complete. A strong signal was obtained when the measurement was made about 10 min after the initial contact, and the amplitude of the signal changed little over the following 24 h. A plot of signal amplitude (peak-to-peak height of the central line of the spectrum) as a function of the amount of TNT initially present in the supernatant solution is shown in Fig. 2. A linear relationship exists up to ca. 260 μg of TNT, and the line passes through the origin, as is emphasized

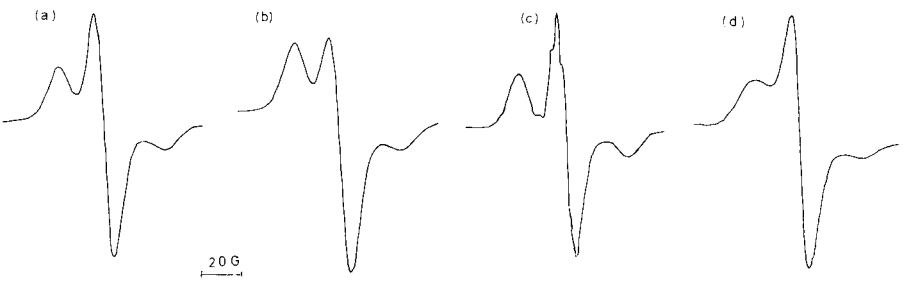

Fig. 1. E.s.r. spectra (first derivative) of aromatic nitro compounds adsorbed from toluene at 20°C on MgO activated at 400°C: (a) TNT; (b) *o*-nitrotoluene; (c) 1,3,5-trinitrobenzene; (d) tetryl.

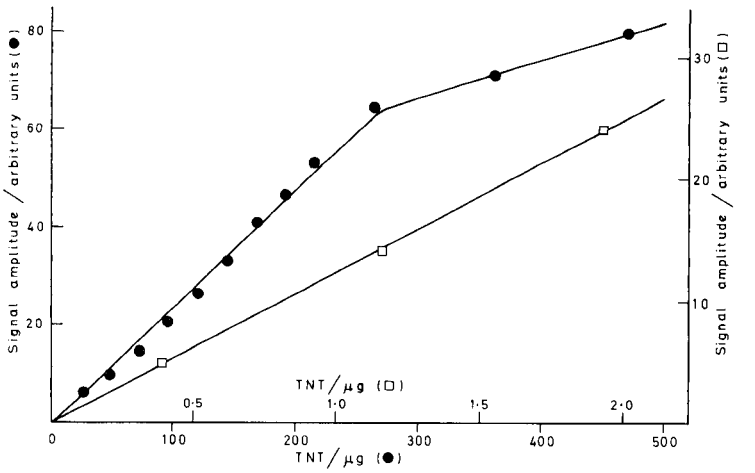

Fig. 2. Signal amplitude as a function of the amount of TNT initially present in the supernatant solution.

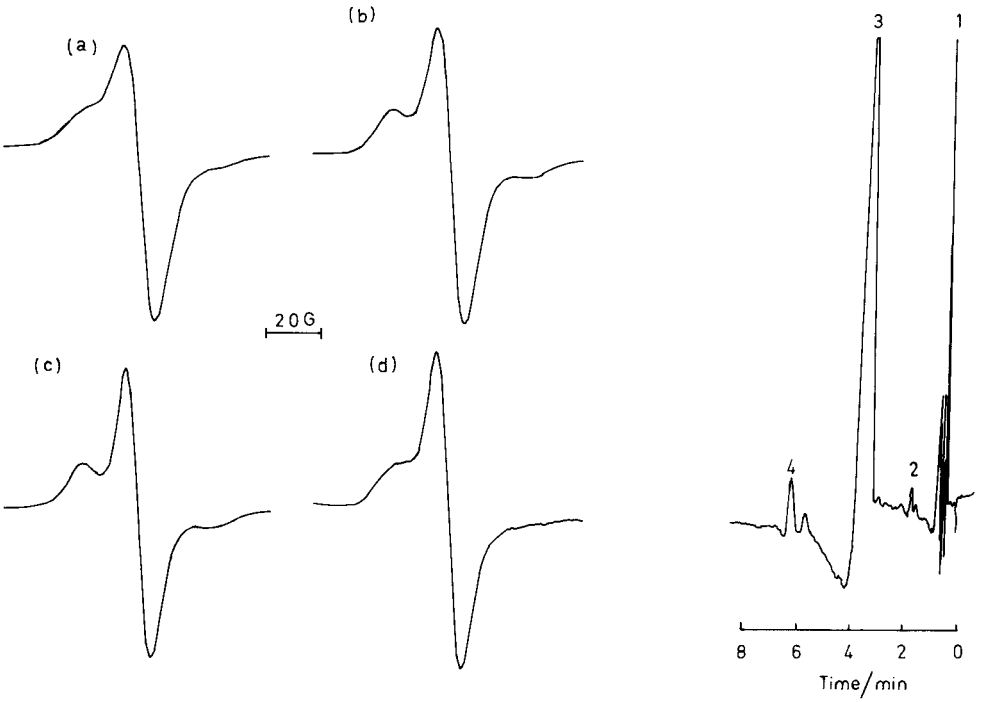

Fig. 3. E.s.r. spectra of TNT on MgO at different temperatures: (a) —100°C; (b) —50°C; (c) 100°C; (d) 180°C.

Fig. 4. Gas chromatogram (electron-capture detection) of a hand-swab extract of TNT. Peaks: (1) toluene; (2, 4) contaminants; (3) TNT.

by the linear plot obtained for low concentrations. Samples with low concentrations were contained in quartz tubes as this material shows a lower dielectric loss than glass at microwave frequencies. The practical detection limit for TNT was ca. 10 ng. Five replicate measurements at the 2 μg level gave a relative standard deviation (r.s.d.) of 1.8%.

The solubility of TNT is lower in n-hexane than in toluene; otherwise, either solvent may be used for the measurements. The effect of temperature on the anionic radical spectrum of TNT is shown in Fig. 3. The three-line structure is apparent in the spectra recorded between −100°C and 100°C. The width of the central line decreased from ca. 12.0 G at −100°C to ca. 9.0 G at 50°C; between 50°C and 180°C, it remained constant. A decrease in the separation of the outer peaks occurred between 20°C and 100°C (52 G to 48 G). This splitting could not be measured satisfactorily in the spectrum recorded at 180°C because of poorer resolution. The fact that a relatively strong signal was still observable at 180°C demonstrates the remarkable stability of the adsorbed species.

Hand-swab extracts, prepared as described, were examined by g.c. and e.s.r. spectrometry. As might be expected, the extracts contained TNT and other substances, a fact clearly demonstrated by the chromatogram shown in Fig. 4. Some of these contaminants would obviously have to be removed before a reliable estimate could be made of TNT by g.c. This problem did not arise, however, when the e.s.r. method was applied. Addition of magnesium oxide to the extract produced a spectrum identical to that shown in Fig. 1(a), thus allowing the nitro compound to be determined by direct measurement of signal amplitude. Moreover, the colour assumed by the oxide surface and the *g* value of the adsorbate were identical to those cited for TNT in Table 1, making identification possible had this been necessary.

Other nitro compounds

The possibility of applying the e.s.r. technique to the determination of other aromatic nitro compounds was investigated. Figure 1 shows the spectra arising from the anionic radicals of *o*-nitrotoluene, 1,3,5-trinitrobenzene and tetryl, adsorbed on magnesium oxide. The central line of the 1,3,5-trinitrobenzene anion spectrum (Fig. 1c) exhibited structure which, although poorly defined, indicated five components. The spectra of the other anionic radicals (including those not shown in Fig. 1) displayed three lines without additional splitting. Table 1 summarizes information derived from the present study that could be useful in qualitative analysis. The relation between signal amplitude and the amount of nitro compound initially present in the supernatant solution was examined for nitrobenzene, *p*-dinitrobenzene, *o*-nitrotoluene and 2,6-dinitrotoluene. Linear plots were obtained over the range investigated (0−30 μg). Determination of these compounds by e.s.r. spectrometry is therefore also possible.

TABLE 1

Aromatic nitro compounds adsorbed on magnesium oxide activated at 400°C

Adsorbate	Colour of oxide surface	*g* value of adsorbed species	Extreme splitting (G)
Nitrobenzene	Brownish yellow	2.0045	59
o-Dinitrobenzene	Orange	2.0064	54
m-Dinitrobenzene	Brownish yellow	2.0051	51
p-Dinitrobenzene	Yellow	2.0051	—
1,3,5-Trinitrobenzene	Reddish purple	2.0046	55
o-Nitrotoluene	Green	2.0057	52
p-Nitrotoluene	Blue	2.0062	42
2,4-Dinitrotoluene	Brownish blue	2.0052	48
2,6-Dinitrotoluene	Blue	2.0052	50
2,4,5-Trinitrotoluene	Black	2.0048	—
2,4,6-Trinitrotoluene	Violet	2.0052	52
Tetryl	Red	2.0057	54

Other adsorbents

Adsorption of TNT from solution in toluene or n-hexane on active aluminium oxide resulted in a three-line spectrum similar to that shown in Fig. 1(a). The amplitude of the signal increased with time and reached a steady value after ca. 12 h. The plot of signal amplitude (spectra recorded after 12 h) versus amount of TNT initially present in the supernatant solution was linear over the range 3—160 μg. A weak signal was observed when the solvent alone was brought into contact with the alumina surface and this prevented measurements of TNT being made below ca. 3 μg.

The signal amplitude/concentration plot for TNT with calcium oxide as adsorbent was linear over the range 20—160 μg and the line passed through the origin. Measurements were not made below 20 μg of TNT. An increase in the receiver gain to facilitate the measurement of low radical concentrations revealed a large background signal from this adsorbent.

DISCUSSION

The nitro group is strongly electron-attracting so that polynitro aromatic compounds have acceptor properties. Previous work [14, 15] has shown that the anionic radicals of these molecules can be generated by electron transfer at the surface of partially dehydrated catalytic aluminium oxides and that, in contrast with the relative instability of the nitro anions in solution, the adsorbed species are remarkably stable. The present study has shown that these anion radicals are also formed on the surface of thermally activated magnesium oxide and that a strong signal from the adsorbed species is still observable at 180°C. Conversion to the radical form is quantitative. The concentration of an aromatic nitro molecule in solution can

therefore be determined by direct comparison of the e.s.r. signal which accompanies the addition of magnesium oxide with that obtained from a standard solution of the same compound similarly treated.

The lower limit for quantitation depends on the compound being determined and the nature of the container. The use of quartz rather than glass tubes minimizes the reduction in the Q value of the cavity on introduction of the sample. With TNT contained in quartz tubes, quantitative measurements were possible down to ca. 10 ng. For five replicate measurements of 2 μg of TNT, the r.s.d. was 1.8%. Identification of a particular aromatic nitro compound (within the group of twelve examined) is possible based on the g value of the adsorbed anion, the shape of the spectrum, and the colour imparted to the oxide surface. Nitrate esters are not amenable to this method of analysis. Thus, the addition of magnesium oxide to solutions of nitroglycerine or pentaerythritol tetranitrate produces no resonance absorption.

Analysis, both qualitative and quantitative, for trace amounts of explosives present in heavily contaminated extracts from hand-swabs and post-explosion debris is required in forensic science. Figure 4 shows the gas chromatogram (7% SGR column at 170°C) of a mildly contaminated hand-swab extract of TNT. Clearly, detection of the nitro constituent in such a sample would be straightforward. A clean-up procedure that removed at least some of the co-extracted compounds would be required, however, before accurate quantitation of the analyte by this technique would be possible. In contrast, the impurities present in this particular sample had no adverse effect on the resonance method of analysis. The e.s.r. spectrum of the hand-swab extract was identical to that obtained from pure TNT. Contaminants in the extracts can only prevent satisfactory analysis through e.s.r. spectrometry by either poisoning the magnesium oxide surface or generating signals which overlap that arising from the nitro compound. A further advantage of the e.s.r. method in the forensic context is that the compound of interest is not destroyed. A polar liquid such as water or ethanol will remove the nitro radical from the oxide surface and allow the parent compound to be recovered unchanged.

With one exception (1,3,5-trinitrobenzene), the spectra obtained when the mono- and poly-nitro aromatic compounds are adsorbed on the surface of activated magnesium oxide are similar, an asymmetric triplet showing no additional structure; the high-field half is broader than the low-field half, and the intensity of the central line is much greater than that of the wing lines. The three-line structure would indicate that the unpaired electron is highly localized on only one nitrogen. Such a localization might be expected; adsorption not only results in quantitative conversion of the nitro compound to its anionic radical form, but also accounts for the continuing stability of the radical species. If the electron/nitrogen interaction is anisotropic, the shape of the observed spectra can be explained readily. Because the ^{14}N nucleus has a spin of 1, three lines of equal intensity might be expected. When hyperfine anisotropy is present, however, the lines corresponding to $m_I = \pm 1$ (+1, low-field line) will be broadened in powders compared to the

line with $m_I = 0$ (central line). If the adsorbed radical possesses axial symmetry and $g_\perp > g_\parallel$, the overall effect on the spectrum will be to move the low-field portion of the spectrum towards the central line and the high-field side to higher fields. This will tend to sharpen the low-field line and broaden the high-field line [13]. Such effects are evident in the present spectra (Fig. 1). The presence of an additional hyperfine structure of five components in the central line of the spectrum arising from the adsorbed 1,3,5-trinitrobenzene radical suggests that in this case the unpaired electron is delocalized over all the radical, the two other nitrogen nuclei interacting more weakly with the uncoupled spin.

Electron-donor centres on the magnesium oxide surface that have the capacity to reduce aromatic nitro compounds are probably O^{2-} ions in sites of low coordination [13]. Another centre consisting of an O^{2-} ion associated with a nearby hydroxyl ion may also be responsible for the reduction of the same molecules [17]. Adsorbed molecules of oxygen cannot obtain electrons from the surface of magnesium oxide for negative-ion formation [13, 17]. The electron affinities of nitrobenzene and molecular oxygen are $\geqslant 0.7 \pm 0.2$ eV [18] and 0.440 ± 0.008 eV [19], respectively. This suggests that the lattice O^{2-} ions on the surface of magnesium oxide may act as electron donors to adsorbed molecules with electron affinities not less than ca. 0.5 eV.

The determination of aromatic nitro compounds by the e.s.r. method is not limited to the use of magnesium oxide. However, the two other adsorbents used in this investigation had drawbacks. The amplitude of the signal arising from TNT adsorbed on aluminium oxide increased with time and reached a steady value only after ca. 12 h. A background signal from the calcium oxide sample prevented quantitative measurements of TNT below 20 μg.

REFERENCES

1 N. I. Sax, Dangerous Properties of Industrial Materials, Van Nostrand, 6th edn., New York, 1984.
2 I. S. Krull, M. Swartz, R. Hilliard, K.-H. Xie and J. N. Driscoll, J. Chromatogr., 260 (1983) 347.
3 D. G. Higgs, P. N. Jones, J. A. Markham and E. Newton, J. Forensic Sci., 18 (1978) 137.
4 J. M. F. Douse, J. Chromatogr., 328 (1985) 155.
5 J. B. F. Lloyd, J. Chromatogr., 330 (1985) 121.
6 J. Yinon, Crit. Rev. Anal. Chem., 7 (1977) 1.
7 I. S. Krull and M. J. Camp, Am. Lab., May (1980) 63.
8 T. C. Castorina, Analytical Chemistry of 2,4,6-Trinitrotoluene, Special Publication ARLCD-SP-80007, U.S. ARRADCOM, Dover, NJ, 1980.
9 J. Yinon and S. Zitrin, The Analysis of Explosives, Pergamon, Oxford, 1981.
10 P. Hepp, Annalen, 215 (1882) 344.
11 B. D. Flockhart and R. C. Pink, Talanta, 9 (1962) 931.
12 J. D. Twibell, J. M. Home, K. W. Smalldon and D. G. Higgs, J. Forensic Sci., 27 (1982) 783.
13 A. J. Tench and R. L. Nelson, Trans. Faraday Soc., 63 (1967) 2254.

14 B. D. Flockhart, I. R. Leith and R. C. Pink, Chem. Commun., (1966) 885.
15 B. D. Flockhart, I. R. Leith and R. C. Pink, Trans. Faraday Soc., 66 (1970) 469.
16 B. D. Flockhart, L. McLoughlin and R. C. Pink, J. Catal., 25 (1972) 305.
17 D. Cordischi, V. Indovina and M. Occhiuzzi, J. Chem. Soc. Faraday Trans. I, 74 (1978) 456.
18 C. Lifshitz, T. O. Tiernan and B. M. Hughes, J. Chem. Phys., 59 (1973) 3182.
19 R. J. Celotta, R. A. Bennett, J. L. Hall, M. W. Siegel and J. Levine, Phys. Rev. A, 6 (1972) 631.

Analytica Chimica Acta, 200 (1987) 491—502
Elsevier Science Publishers B.V., Amsterdam — Printed in The Netherlands

REMOTE SENSING IN AN OPTICALLY DENSE ENVIRONMENT BY USING TWO-PHOTON EXCITED FLUORESCENCE AND A SINGLE MULTIMODE FIBER OPTIC

RAY L. STEFFEN and FRED E. LYTLE*
Department of Chemistry, Purdue University, West Lafayette, IN 47907 (U.S.A.)
(Received 11th May 1987)

SUMMARY

The feasibility of remote sensing by means of two-photon excited molecular fluorescence was investigated by using a single 115-m multimode optical fiber. Because of modal dispersion and reflection of Rayleigh scatter, time-resolved detection was required to resolve the weak fluorescence from the relatively intense laser background. The bare-ended probe, which both delivered the excitation radiation and collected the fluorescence emission, was employed to detect an analyte in an optically dense environment. For a fixed amount of fluorophore, the solvent was continuously changed from 90% (w/w) ethanol (non-absorbing) to 100% acetone (absorbing). The result was a fluorescence signal constant to within 5%. Quantitation via one-photon excitation using a 50-cm optical fiber demonstrated the characteristic inner filter roll-off of optically dense systems. Because of the large attenuation of the waveguide in the ultraviolet range, remote sensing via one-photon excited fluorescence proved impossible. However, linear calibration plots for the nonlinear excitation process were obtained from micromolar to near saturation levels. Sources of interference were isolated, and the extension to a single-mode fiber was made.

The use of optical fibers as chemical sensors is becoming increasingly widespread and diverse, ranging from probes for determining enzyme activities [1] to detecting contaminants in underground water [2]. By their very nature, optical fibers are well suited as sensors involving such methodologies as absorbance [3–5], Raman [6], infrared [7], and near-infrared spectroscopy [8]. Reviews by Seitz [9], Peterson and Vurek [10] and Wolfbeis [11] have summarized many of the recent spectroscopic advances in fiber-optic sensor development.

---

*Fred E. Lytle received his B.S. degree in chemistry from Juniata College in 1964 and earned his Ph.D. degree in analytical chemistry at The Massachusetts Institute of Technology in 1968. He joined the faculty at Purdue University that same year, being promoted to Associate Professor in 1974 and Professor in 1979. During his tenure at Purdue he has been awarded the Merck Company Faculty Development Award; was voted the Outstanding Teacher in the School of Science for 1979; and received the Amoco Undergraduate Teaching Award in 1985. In 1986 he was the recipient of the American Chemical Society Division of Analytical Chemistry Award in Chemical Instrumentation sponsored by the Dow Chemical Company.

0003-2670/87/$03.50

Of particular interest to this research group is the area of fiber-optic fluorosensing. In this field, the probe is typically a bifurcated fiber bundle, where part of the bundle is used to transport the excitation radiation to the sample, and the remaining fibers deliver the emission to the detector, with the common end of the bundle placed in or near the sampled environment [9, 11–13]. Alternatively, because the detected radiation can be distinguished from the probe radiation by wavelength, fluorescence sensing is compatible with a single optical fiber configuration. Specific fluorescence-based sensors (optrodes) are made by immobilizing chemical reagents at or in the vicinity of the distal end of the single-stranded fiber. These reagents can either enhance the natural fluorescence of the analyte of interest [14], react with the analyte to form a highly fluorescent product [1, 15], or change its fluorescence intensity in response to changes in sample composition [16].

Apart from the chemically-modified optrodes, the simplest fluorescence-based sensor is the plane termination, or photometric, fiber which is used to measure naturally fluorescing samples. Fluorescence is excited at the fiber terminus and collected by the same fiber in a 180° back-scattering configuration. The sensitivity of this probe depends on the numerical aperture (NA) of the fiber [17]; the larger the numerical aperture, the greater the excitation/observation volumes, the more emission collected. In this work, a single, bare-ended fiber (NA = 0.2) was used to ascertain the feasibility of two-photon excited fluorescence for remote sensing in an optically dense environment. Because of the trade-off between numerical aperture and pulse-broadening, a gradient-index optical fiber with a relatively small core diameter (50 μm) was chosen in order to minimize pulse dispersion but still provide relative coupling ease and a respectable probe volume. Only naturally fluorescent species were examined.

Tromberg et al. [18] have previously demonstrated two-photon excited fluorescence using a single optical fiber by quantifying the organic scintillator 2-(4-biphenylyl)-5-phenyl-1,3,4,-oxadiazole in both blood and cerebral spinal fluid matrices. Although the authors failed to mention the length of fiber used, it is inferred from their instrumental diagram that the fiber waveguide was relatively short. Here, two-photon spectroscopy is performed with fiber lengths comparable to that required in process-control applications (>100 m). Because two-photon excited fluorescence has previously been shown to be a useful analytical tool for probing fluorophore concentrations in the presence of other absorbing species [19], it may prove to be an ideal technique for analysis in-line, where relatively high analyte concentrations and strong impurity/solvent absorbances would render a one-photon quantitation ineffective. Conversely, in the nonlinear case, where the incident radiation is not attenuated by absorbers, there is no inner-filter effect and the measured emission intensity is directly proportional to analyte concentration.

EXPERIMENTAL

Chemicals

The 2-(1-naphthyl)-5-phenyloxazole (α-NPO) and *p*-bis(*o*-methylstyryl)-benzene (bis-MSB) were Eastman Kodak scintillation grade. All chemicals were used without further purification. In order to approximate the chemical quality of a process stream, pure-grade (99%) acetone, cyclohexane, and ethanol were used rather than the corresponding high-purity solvents. Note, however, that the difference in fluorescence intensities from two-photon excitation between the high-purity and pure-grade solvents was less than 0.1% in the wavelength range of interest.

Optical arrangement

A schematic diagram of the instrument is shown in Fig. 1. A mode-locked Nd:YAG laser (Spectra-Physics, Model 3460), producing a 900-mW train of 532-nm radiation, was used to pump rhodamine-6G in a synchronously-pumped, cavity-dumped dye laser configuration (Spectra-Physics, Model 375B broadband dye laser and Model 344 cavity dumper). For experiments involving simply a current-measuring mode of detection, the dye laser was dumped at 4 MHz, resulting in 27-nJ pulses at 590 nm. Because of the triggering

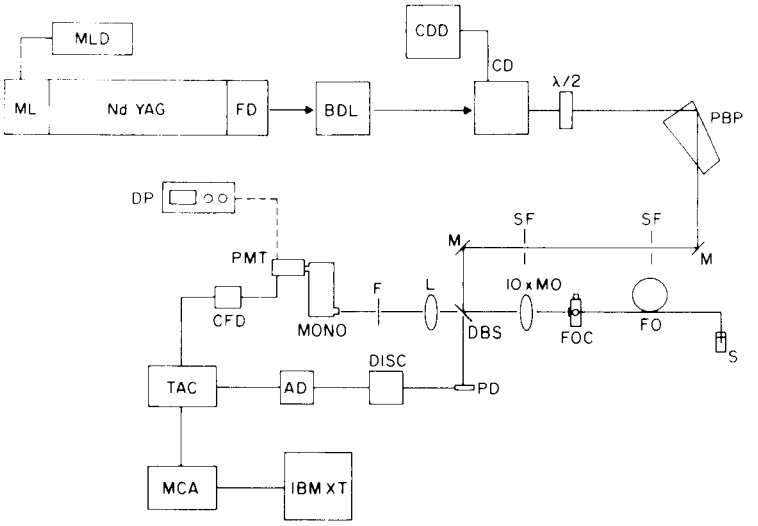

Fig. 1. Schematic diagram of experimental arrangement for remote two-photon excited fluorimetry. AD, adjustable delay; BDL, broadband dye laser; CD, cavity dumper; CDD, cavity dumper driver; CFD, constant fraction discriminator; DBS, dichroic beam-splitter; DISC, discriminator; DP, digital photometer; F, broadband filter; FD, frequency doubler; FO, fiber optic; FOC, fiber optic coupler; IBM XT, computer; L, focussing lens; M, mirror; MCA, multichannel analyzer; ML, mode-locker; MLD, mode-locker driver; 10 × MO, 10× microscope objective; MONO, monochromator; Nd:YAG, laser source; PBP, Pellin-Broca prism; PD, photodiode; PMT, photomultiplier; S, sample; SF, spatial filter; TAC, time-to-amplitude converter; λ/2, half-wave plate. See text for a description of the system.

limitations of the time-to-amplitude converter, the repetition rate of the dye laser was lowered to 150 kHz for the time-resolved experiments, producing 110-nJ pulses at 590 nm. In both cases, the pulse width, as measured with a Coherent Radiation Model CR-290 autocorrelator, had a FWHM of approximately 15 ps.

In order to overcome the spectral interferences arising from the dye laser (e.g., superradiance), a Pellin-Broca prism/spatial filter combination (PBP/SF) was placed after the dye laser to "clean-up" the laser output. A dichroic beam-splitter (DBS; from OLCI, Inc., percentage transmission at red and violet wavelengths of approximately 2% and 90%, respectively) was used simultaneously to reflect the excitation radiation and to transmit the fluorescence emission. The sum of the percentage transmission and percentage reflectance is close to 100% at the wavelengths used. A 10× microscope objective (10× MO) was used to launch the excitation light into either a 10- or 115-m multimode optical fiber (50-μm core diameter). A coupling throughput of 65–70% was obtained routinely through the 10-m fiber optic (FO; Newport Research Corp. Model F-MSD), 50–55% for the 115-m sensor. The fiber collected the fluorescence emission (acceptance angle of 17° in acetone) and directed it back to the detection system.

The collimated return beam was passed through the dichroic beam-splitter (DBS), which also acted as a prefilter, and was subsequently focussed by a lens (L) through a Corning 7-59 broadband blue filter (F) and into a double holographic grating monochromator (MONO; Instruments SA, Model DH-10) with a 6-nm bandpass. For the analog experiments, the fluorescence signals were detected with a thermoelectrically cooled RCA 31034 photomultiplier tube (PMT) operated at 1520 V. The high voltage and current amplification were provided by a Pacific Photometric Instruments Model 124 digital photometer (DP). In the time-resolved work, the blue-shifted emission was detected with the higher-gain RCA 8850 photomultiplier operated at 2150 V and in a single-photon counting mode. A trigger pulse from a photodiode (PD), illuminated by the laser leakage through the dichroic beamsplitter, was sent into a discriminator (DISC) and then passed to the "Start" port of a time-to-amplitude converter (TAC; EG & G Ortec 457). Because of the time lag (μs) experienced by the fluorescence signal in passing through the fiber, the adjustable (35 ns to 1 s) delay (AD) of a Hewlett-Packard pulse generator (Model 8013B) was used to locate the fluorescence in time. The PMT signal, in turn, was passed through a constant-fraction discriminator (CFD; Tennelec TC 455) and input into the "Stop" terminal of the TAC. A multichannel analyzer (MCA; Nuclear Data), operated in a pulse-height analysis mode, was used to reconstruct the fluorescence decay curve. Data storage and manipulation were done on an IBM XT personal computer.

RESULTS AND DISCUSSION

For continuous measurements of the concentration of components in a process stream, fluorimetric methods are very useful. Often, however, the

solvent matrix or interfering chromophores exhibit absorption bands at or near the excitation wavelength, absorbing the exciting radiation and obscuring the required signal. Also, the amount of analyte in the process environment may be considerable, giving rise to a nonlinear response between solute concentration and signal intensity (inner-filter effect). Few techniques have been developed to solve such interferences. Current methods use internal reflection spectroscopy [20–23], in which the evanescent wave present at the crystal/solution interface penetrates into the surrounding medium and produces a spectrum of the sample in contact with the crystal. Because the depth of penetration of the excitation radiation is small ($\approx$10 μm), excessive attenuation of the incident beam is avoided. But, because the measured signal in internal reflection techniques occurs near the surface of the crystal, it is highly susceptible to contamination. In addition, the concentration information obtained from attenuated internal reflection pertains to the solution within the first few micrometers of the crystal, which may or may not be indicative of the composition of the bulk solution.

Alternatively, two-photon excited fluorescence has been shown to be most effective at quantifying species in optically dense media [19]. The high peak powers required in two-photon spectroscopy, however, typically mandate the use of pulsed lasers, systems which are not readily conducive to the rigors of a processing environment. In order to apply two-photon spectroscopy to a quality-control situation, optical fibers are necessary to isolate the source, detector, and data-acquisition equipment in a central laboratory while the light is piped to and from various sensor locations within the fiber light-guides. The fact that the information is carried optically rather than electronically enhances the noise immunity, ruggedness, and corrosion resistance of this or any remote-sensing scheme based on fiber optics.

Studies with short optical fibers

In order to test the remote-sensing feasibility of two-photon excited fluorescence spectroscopy, a single 10-m gradient index fiber optic was used in preliminary experiments. In a two-photon absorption process, the energy of the resultant excited state equals the sum of the energies of the incident photons. The fraction of light absorbed is directly proportional to the square of the incident power [19]. Thus, a plot of fluorescence signal divided by optical power versus optical power yields a straight line for a simultaneous two-photon absorption event. The fraction of light absorbed is also directly proportional to fluorophore concentration.

Bis-MSB in cyclohexane was used to ascertain both the power and concentration dependence of the emission signal. A reliable means of making the power-squared calibration mentioned above is to vary the intensity incident to the sample with a half-wave plate/polarization-based beam-splitter combination. By using a rotatable polarizer to attenuate the excitation radiation (λ_{ex} = 600 nm), the problem of changing the beam alignment through the ensuing optics was minimized. In the present study, the Pellin-Broca prism,

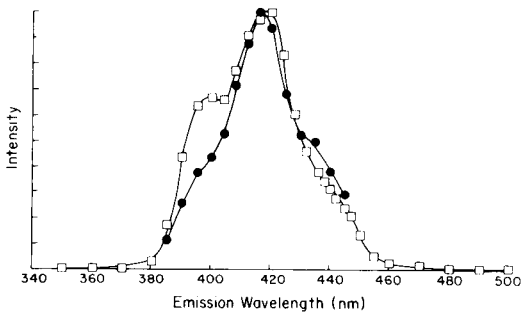

Fig. 2. Emission spectrum of 1.3 mM bis-MSB in cyclohexane taken via fluoroprobe sampling with a 10-m (□) and 115-m (•) optical fiber. Note the distortion, especially in the blue spectral region, caused by the wavelength-dependent attenuation of the optical fiber.

which is polarization-dependent, served as the birefringent beam-splitter. The power was measured after reflection off the dichroic beam-splitter with a pyroelectric radiometer (Laser Precision Corp., Model Rk-5100). The sample and background signals (λ_{em} = 419 nm) were measured consecutively. A plot of background-corrected fluorescence intensity divided by average input power versus average input power was linear (slope 127 ± 7 W^{-2}; intercept 0.5 ± 0.4 W^{-1}; relative standard error of the estimate, σ_{se} = 0.5%; 8 points), indicating a nonlinear absorption event at the fiber terminus [24]. The working curve for bis-MSB was also linear (slope 74 ± 1 M^{-1}; intercept 0.00 ± 0.01; σ_{se} = 1.9%; 10 points) with a limit of detection (LOD) of 90 μM at a signal-to-noise ratio (S/N) of three.

To check the quality of the data, a point-by-point emission scan of a 1.30 mM solution of bis-MSB in cyclohexane was obtained via two-photon fluoroprobe sampling for the 10-m fiber waveguides. The emission curve, given in Fig. 2, has peaks centered around 395 nm, 400 nm, and 425 nm and is consistent with previously reported spectra [25]. This demonstrates the reliability of the short fluoroprobe for obtaining spectra in regions where the optical fiber is transparent.

Studies with long optical fibers

There was some skepticism as to whether two-photon spectroscopy could be used in conjunction with relatively long fibers as a remote-sensing technique. The modal dispersion present in multimode fibers decreases the peak power of a pulse traversing the fiber, reducing quadratically any nonlinear spectroscopic processes that may occur at the distal end of the fiber waveguide. For example, in going from 10 m of gradient index optical fiber to 115 m, the pulse width (FWHM), as measured with an optical autocorrelator, increased from 30 ps to over 120 ps. Because of both pulse dispersion and increased fiber attenuation, the fluorescence signal from two-photon excitation was seen to decrease by more than a factor of sixteen. As a result, in a

current-measuring mode, the Rayleigh scattering from the front and rear fiber interfaces overwhelmed the fluorescence emission in the 115-m fiber experiments, making quantitation with the longer fiber optic nearly impossible. This occurs even with the broadband filter and monochromator in place. Two-photon excited fluorescence produces a large anti-Stokes signal, unlike a one-photon process where fluorescence and excitation are commonly near one another. Because of this large blue shift between excitation and emission wavelengths, chromatic dispersion was able to separate cleanly, within the fiber, the fluorescence emission and laser background in time. As such, time resolution offset the deleterious effects of pulse dispersion and permitted quantitation at extended distances from the excitation source.

With the aid of time-resolved detection, results comparable to the 10-m fiber optic were found for the 115-m photometric probe. The fluorescence emission from the sensor was collected for a period of 5—10 min at a sampling rate of 150 kHz. The area under the emission profile was taken to be a measure of the relative fluorescence intensity. It should be noted that the time-averaged signal was not strictly the fluorescence decay, but a convolution of the decay with the chromatic dispersion of the fiber optic. Both the power-squared calibration (slope 132 ± 4 W^{-2}; intercept 0.3 ± 0.2 W^{-1}; σ_{se} = 1.4%; 5 points) and working curves (slope 75 ± 2 M^{-1}; intercept 0.01 ± 0.01; σ_{se} = 2.2%; 6 points) for bis-MSB were linear. The limit of detection was calculated to be 60 μM for a *S/N* ratio of three. Although the pulse width increased by a factor of four and the fluorescence intensity dropped by more than a factor of sixteen in going to the longer fiber, the time resolution provided by photon counting yielded a better detection limit than that obtained by a current-measuring mode of detection.

Figure 2 also shows a point-by-point emission scan of a 1.30 mM solution of bis-MSB in cyclohexane acquired by two-photon fluoroprobe sampling for the 115-m fiber optic. Again, emission peaks at 395, 400 and 425 nm are apparent. Because of wavelength-dependent attenuation [26], however, distortion of the emission curve, especially toward the blue spectral region, occurs with the longer fiber. As such, the reliability of this bare-ended fluoroprobe for obtaining spectra in regions where the fiber optic is "transparent" is limited to shorter fibers where spectral distortion is not so prevalent.

When the sensing end of the 115-m multimode fiber was suspended in air, a blue background emission was observed. This interference remained after the fiber terminus was freshly cleaved, eliminating memory effects from fluorophore contamination as the cause. An emission spectrum of the interference is given in Fig. 3. After some study, it is thought that the blue background is due to the excitation of germanium dopants present in the core of the fiber. Ultraviolet-excited fluorescence of germanium-silicate optical fiber preforms [27] demonstrates an emission maximum near 420 nm. Time-filtered detection was used in acquiring the data shown in Fig. 3. The spectrum results from the backward-generated fluorescence which was obtained by integrating, as a function of wavelength, the signal area between the laser

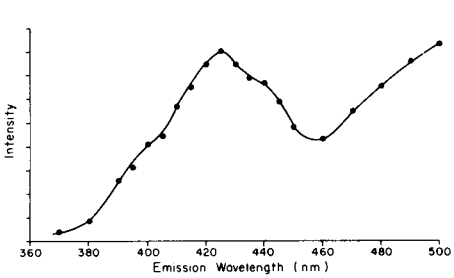

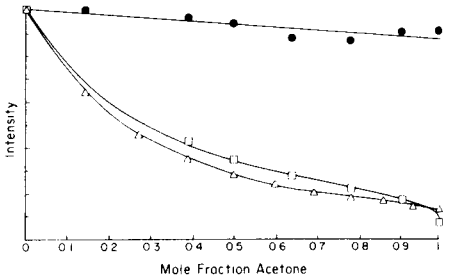

Fig. 3. Emission spectrum of the fluorescence background generated by two-photon absorption from the germanium dopant inside the fiber-optic core. The spectra were similar for the backward-generated and forward-generated/back-reflected cases.

Fig. 4. Fluorescence intensity of 1.5 mM α-NPO in a cyclohexane/acetone mixed solvent as a function of acetone concentration. Intensity resulting from two-photon (•) and one-photon (□) excitation. Also shown is the theoretically predicted one-photon intensity (△).

pulses reflected off the proximal and distal ends of the fiber optic. A similar emission curve was obtained when the forward-generated fluorescence was examined, which was done by adjusting the detection electronics to look at the back-reflected light from the sensing terminus. Because the background has emission bands in the same spectral region as the fluorophores of interest, chromatic dispersion could not separate background and analyte fluorescence. Fortunately, because it is only the back-reflected light which directly interferes with the analysis, placing the sensing terminus in solution more closely matches the refractive indices of fiber core and sensing medium, decreasing the amount of Rayleigh scattering from the distal end. For solutions used in this study, less than 0.3% of the background emission was reflected back along the length of the fiber to the detector. Thus, the blue interference, although present, did not represent a serious impediment to the multimode fiber experiments.

Because the excitation radiation was in the red (λ_{ex} = 600 nm), the blue interference would have to be the result of nonlinear excitation of the germanium dopant followed by fluorescence emission. A plot of signal divided by input power versus input power proved to be linear (slope 490 ± 7 W^{-2}; intercept 4.1 ± 0.2; σ_{se} = 0.1%; 10 points), supporting this proposition. The exact nature of the nonlinear excitation process is not presently known. Two-photon absorption [28], stimulated four-wave mixing [29], and three-wave sum-frequency generation [30] are known to produce frequencies in glass optical fibers with anti-Stokes shifts large enough to access an absorption band of the germanium oxide dopant (at 200–350 nm). For the moment, the background does not present a major interference to this analytical technique. However, the question as to its origin will be examined if studies with longer fibers are hindered.

Optically dense system

A common problem facing fluorimetric methods is the presence of one or more chromophores with absorption bands which coincide with those of the

analyte. If the total absorption of such a system is small, all species have independent responses. The result is an emission intensity related only to fluorophore concentration. However, if the system is optically dense, interfering chromophores decrease the amount of radiation exciting the fluorophore by the ratio of its absorbance to the total solution value. Unlike the situation with pure substances, diluting the solution is not a practical alternative. Upon dilution, the signal will often fall below the limits of detection or the nature of the fluorophore could be changed because of a shifted equilibrium. Also, the resulting inner-filter effect changes the intensity along the cell path length, producing a nonlinear response between fluorescence intensity and concentration. This is usually true even in situations involving small observation volumes like that used by a fiber-optic probe [31]. As such, it is difficult to quantitate such a system reliably by one-photon excitation. A two-photon process is required.

In order to test the feasibility of using two-photon excited fluorescence as a remote-sensing technique for highly absorbing matrices, α-NPO and acetone were used to prepare a suitable photophysical environment. The one-photon absorption bands of acetone lie in the same spectral region as those for α-NPO; α-NPO is a reasonably efficient two-photon absorber at the excitation wavelength (λ_{ex} = 585 nm), whereas acetone absorbs very little in the yellow by either a one-photon or two-photon process. In the following experiments, acetone serves both as an interfering chromophore in an acetone/cyclohexane/α-NPO solution and as an optically dense solvent with α-NPO alone.

The situation where acetone serves as an interfering chromophore was studied initially with the 115-m fiber sensor. For a fixed amount of fluorophore (1.5 mM α-NPO), the solvent was continuously varied from 90% by weight cyclohexane (non-absorbing) to 100% acetone (absorbing). The result was a fluorescence signal constant to within 13% (slope —0.13 ± 0.04; intercept 1.01 ± 0.03; σ_{se} = 3.3%; 7 points). The results from the 115-m fiber optic are given in Fig. 4 along with the theoretically predicted one-photon excitation intensity as described by the equation

$$F_{obsd} \propto A_f\,(1 - T)/(A_f + A_c)$$

where A_f and A_c are the absorbances of the fluorophore and chromophore, respectively, and T is the total solution transmittance [32]. A path length of 1 mm was used in the above calculations. This length was selected by observing, with a microscope, the extent from the fiber terminus at which the generated fluorescence was visible. For solutions of differing chromophore concentration, the average path length for which the blue emission could be seen extending into the solution was on the order of 1 mm. In addition, preliminary computer calculations, which modeled the acceptance capability of the optical fiber, gave path lengths similar to that determined empirically.

Also shown in Fig. 4 is the corresponding one-photon excitation response using 50 cm of the multimode optical fiber. Although less than 2% coupling

efficiency could be achieved with the short probe, there was sufficient ultraviolet radiation emerging from the optical fiber to obtain quantitative results (S/N = 10 for 1.5 mM α-NPO solutions). Extension to longer fibers proved unsuccessful due to attenuation in the ultraviolet. In the one-photon studies, because a single fiber configuration was used, the dichroic beam-splitter of Fig. 1 was replaced by an ultraviolet grade 50/50 beam-splitter (Melles Griot, Model 08BSQ005/805). The output of the dye laser was frequency doubled (Inrad, Model 5-011), reflected off the beam-splitter, and focused with a quartz lens (f/1) into the fiber waveguide. Approximately half of the returning fluorescence signal passed through the beam-splitter and entered the monochromator as the signal.

For a fixed amount of α-NPO and varying acetone concentrations, the one-photon excited fluorescence intensity varied with the absorbance ratio as predicted. The slight discrepancy may be due to changes in fiber collection efficiency or path length as a function of solution refractive index. From the experimental results presented, it can be seen that with unknown levels of chromophore, the fluorophore concentration is lost for one-photon excitation. In two-photon excited molecular fluorescence, however, the inner-filter effect is nonexistent because the excitation wavelength is in a transparent spectral region of the solution, and the amount of power extracted by any nonlinear process is negligible [19]; the intensity of the diverging beam is uniform throughout the observation region.

It should be noted that the presence of chromophores absorbing the emitted radiation will interfere with the analysis regardless of the method of excitation. Reabsorption of emission is a limitation in fluorescence spectroscopy and cannot be suppressed by changes in the excitation process as long as the same final state is populated. The self-absorption effect can be suppressed, however, by using a single-fiber configuration, which exhibits efficient collection of the emitted radiation because of the complete overlap of the relatively small excitation and observation volumes at the fiber tip.

The slightly negative slope evident in Fig. 4 is thought to be due to a refractive index effect and not the matrix absorbance. Because acetone (η = 1.357) has a smaller refractive index than cyclohexane (η = 1.424), the transverse area of the exciting beam enlarges as the mole fraction of acetone is increased. Because the two-photon excitation signal is inversely proportional to the transverse area, increasing the acetone concentration decreases the fluorescence intensity. To test this hypothesis, the solvent system was changed to an acetone/ethanol matrix, because ethanol (η = 1.359) has a refractive index almost identical to acetone. For a fixed amount of fluorophore, the fluorescence intensity from two-photon excitation was independent of acetone concentration and was constant to within ca. 5% (slope 0.002 ± 0.003; intercept 0.95 ± 0.02; σ_{se} = 1.8%; 5 points), indicating that the gradual decline in emission intensity for the acetone/cyclohexane system was indeed a refractive index phenomenon.

Finally, for the situation where acetone was used as an optically dense solvent, a plot of emission intensity against α-NPO concentration was linear

over a dynamic range extending from hundreds of micromolar to near the saturation concentration, nearly three orders of magnitude. Unlike one-photon excitation, no curvature in the calibration graph caused by the absorbance of the analyte was seen at high concentrations. The response was linear (slope $9.8 \pm 0.8\ M^{-1}$; intercept -0.0006 ± 0.0003; $\sigma_{se} = 0.07\%$; 6 points) with a limit-of-detection ($S/N = 3$) of 110 μM.

Preliminary studies with single-mode fibers

Because of modal dispersion, remote sensing via two-photon excited fluorescence is not likely to be feasible for multimode optical fiber distances much greater than 200 m. Because single-mode fibers are designed to support one transverse mode at their operating wavelength, they do not suffer the extensive pulse-broadening effects of modal dispersion, and thus demonstrate bandwidths larger than those found with most low-loss multimode fibers. As such, single-mode fibers are capable of delivering larger peak powers to the fiber terminus.

To test the applicability of a two-photon excited fluorescence/monomode sensor combination, a single-mode fiber optic with a 4-μm diameter core (Newport Research Corp., Model F-SV) was used in place of the multimode fiber shown in Fig. 1. Because the excitation wavelength ($\lambda_{ex} = 600$ nm) was higher in energy than the operating wavelength ($\lambda_{op} = 633$ nm) of the fiber, several bends (ca. 3/4 in. diameter) were placed near the proximal end in order to strip away any spurious modes, allowing only the fundamental to propagate. Because of the larger coupling losses (<20% coupling efficiency) and the reduced excitation/observation volumes incurred in going to the smaller core waveguide, the signal-to-noise ratio of a typical fluorescence signal was much lower for the single-mode probe ($S/N = 2$) than for the multimode one ($S/N = 40$) at the same fluorophore concentration (1.5 mM α-NPO). Nonetheless, in the single-mode regime, quantitation of naturally fluorescent species was still possible 200 m from the laser source. For the experiment involving a fixed amount of α-NPO in varying concentrations of acetone, the fluorescence intensity was again constant to within 13% (slope 0.03 ± 0.06; intercept 0.90 ± 0.04; $\sigma_{se} = 4.7\%$; 7 points).

When the output of the single-mode fiber was directed off a grazing-angle grating, a relatively large amount of frequency-shifted light, caused primarily by self-phase modulation [33], was observed extending from the yellow-green to the deep red. No such spectrum was seen emerging from the multimode fiber, because of the much lower power density in the larger core fiber. Because excitation and emission in one-photon excited fluorescence are spectrally close, the presence of the picosecond continuum in combination with Raman shifting and impurity fluorescence would seriously interfere with a one-photon spectroscopic approach using long, narrow-radius fibers. Conversely, the emission in two-photon excited fluorescence occurs on the anti-Stokes side of the pump, and thus, appears in a relatively dark portion of the spectrum. As such, the limitations mentioned above present little in-

terference to the analysis. Also, because the frequency spreading is approximately symmetric about the excitation wavelength, it is expected that the sensitivity of the signal is not decreased by the frequency shifting. Light emerging from the fiber is still relatively coherent and can couple into the excited state of the molecule, in this case, by a two-color, two-photon process.

This work was supported by Dow Chemical Corporation and National Science Foundation Grant CHE-8320158.

REFERENCES

1 O. S. Wolfbeis, Anal. Chem., 58 (1986) 2874.
2 W. A. Chudyk, M. M. Carrabba and J. E. Kenny, Anal. Chem., 57 (1985) 1237.
3 J. T. Coleman, J. F. Eastham and M. J. Sepaniak, Anal. Chem., 56 (1984) 2249.
4 K. Newby, W. M. Reichert, J. D. Andrade and R. E. Benner, Appl. Opt., 23 (1984) 1812.
5 M. A. Arnold and T. J. Ostler, Anal. Chem., 58 (1986) 1137.
6 R. L. McCreery, M. Fleischmann and P. Hendra, Anal. Chem., 55 (1983) 146.
7 L. A. Hilliard, Anal. Proc. (London), 22 (1985) 210.
8 T. Hirschfeld, Fresenius' Z. Anal. Chem., 324 (1986) 618.
9 W. R. Seitz, Anal. Chem., 56 (1984) 16A.
10 J. I. Peterson and G. G. Vurek, Science (Washington, D.C.), 224 (1984) 123.
11 O. S. Wolfbeis, Trends Anal. Chem., 4 (1985) 184.
12 E. D. Lee, T. C. Werner and W. R. Seitz, Anal. Chem., 59 (1987) 279.
13 O. S. Wolfbeis and H. E. Posch, Anal. Chim. Acta, 185 (1986) 321.
14 F. Milanovich and T. Hirschfeld, Adv. Instrum., 38 (1983) 407.
15 F. Milanovich, D. G. Garvis, S. M. Angel, S. M. Klainer and L. Eccles, Anal. Instrum., 15 (1986) 137.
16 C. Munkolm, D. R. Walt, F. P. Milanovich and S. M. Klainer, Anal. Chem., 58 (1986) 1427.
17 S. M. Angel, Spectroscopy, 2 (1987) 38.
18 B. J. Tromberg, J. F. Eastham and M. J. Sepaniak, Appl. Spectrosc., 38 (1984) 38.
19 M. J. Wirth and F. E. Lytle, Anal. Chem., 49 (1977) 2054.
20 P. A. Wilks, Ind. Res. Dev., 9 (1982) 132.
21 W. N. Hansen, Anal. Chem., 35 (1963) 765.
22 F. M. Mirabella, Jr., Appl. Spectrosc. Rev., 21 (1985) 45.
23 E. G. Bartick and R. G. Messerschmidt, Am. Lab., 16 (1984) 56.
24 R. R. Birge, in D. S. Kliger (Ed.), Ultrasensitive Laser Spectroscopy, Academic, New York, 1983, p. 165.
25 I. B. Berlman, Handbook of Fluorescence Spectra of Aromatic Molecules, Academic, New York, 1971, p. 327.
26 J. H. D. Eland, Chem. Phys. Lett., 93 (1982) 318.
27 H. M. Presby, Appl. Opt., 20 (1981) 701.
28 R. H. Stolen, C. Lin, in S. S. Mitra and B. Bendow (Eds.), Optical Properties of Highly Transparent Solids, Plenum, New York, 1975, p. 307.
29 C. Lin and M. A. Bosch, Appl. Phys. Lett., 38 (1981) 479.
30 J. M. Gabriagues, Opt. Lett., 8 (1983) 183.
31 E. H. Ratzlaff, R. G. Harfmann and S. R. Crouch, Anal. Chem., 56 (1984) 342.
32 J. F. Holland, R. E. Teets, P. M. Kelley and A. Timnick, Anal. Chem., 49 (1977) 706.
33 R. H. Stolen and C. Lin, Phys. Rev. A, 17 (1978) 1448.

Analytica Chimica Acta, 200 (1987) 503—514
Elsevier Science Publishers B.V., Amsterdam — Printed in The Netherlands

ON/OFF CHEMICAL DETERMINATION OF REACTIVE AMINO GROUPS IMMOBILIZED ON SILICA SURFACES

RICKY E. SNELLING and HORACIO A. MOTTOLA*

Department of Chemistry, Oklahoma State University, Stillwater, OK 74078-0447 (U.S.A.)

(Received 20th March 1987)

SUMMARY

Reaction of silica frameworks with aminosilanes to generate reactive amino groups on the surface of solid supports is a widely used step in the chemical modification of such surfaces. These reactive amino groups can aid in the chemical attachment of proteins (enzymes and/or antibodies) or chelating agents. Analytical accounting of the reactive groups generated is of interest in method optimization and in reactor design when these materials are used. A nondestructive method for the determination of reactive amino groups after attachment to silica surfaces is presented; it can be used for in-situ determinations in reactors. The method involves on/off chemistry based on the attachment of a chromophoric probe (*p*-dimethylaminocinnamaldehyde), its subsequent detachment under different experimental conditions, and spectrophotometric measurement of the released probe at 390 nm. Aspects of covalent attachment of amino groups to silica surfaces are also discussed.

Chemical modification of silica surfaces to attach reactive amino groups is generally accomplished by reaction with an aminosilane. The modified surface can be used directly for analytical purposes (e.g., x-ray fluorescence determination of orthophosphate [1], ion-pair extraction of uranium in mining samples prior to x-ray fluorescence spectrometry [2], preconcentration of metal ions also prior to x-ray fluorescence spectrometry [3], and chromatographic separations [4]) or can be modified by attachment of enzymes [5] or chelating agents [6] for further use as analytical reagents. The performance of chemically immobilized reagents and chemical reactors depends on the effectiveness of attachment procedures; this, in turn, can be improved by gaining quantitative understanding of each reaction step in the immobilization sequence. In covalent attachment of enzymes via glutaraldehyde spacing (one of the simplest, gentlest, fastest and most efficient methods for chemical immobilization of enzymes), procedures are available to determine reactive aldehyde groups [7] and protein [8] immobilized on silica materials.

The reaction of silica surfaces with an aminosilane has been the subject of numerous physical as well as chemical studies to characterize and/or

0003-2670/87/$03.50

quantify surface modification. Methods such as ^{13}C- and ^{29}Si-nuclear magnetic resonance, calorimetry, Fourier-transform infrared spectrometry, and photoacoustic spectrometry have been used [9, 10]. These methods were ruled out here because they require physical destruction of the sample and thus cannot be used if the physical form of the modified surface (by extension, the overall reactor) needs to be kept intact, and if the reactive groups have to be measured in a manner that does not disqualify them for further immobilization purposes. When these nondestructive requirements are considered, one attractive alternative is the use of "on/off" chemical methods based on the quantitative attachment of a probe (preferably chromophoric, e.g., copper(II) extraction [3], although other labeling may be used), subsequent detachment of the immobilized probe by changing experimental conditions, and final measurement of the released probe. Colorimetric determinations of aminosilanes on glass [11] with 1-chloro-2,4-dinitrobenzene have been described. This method is destructive because it measures the absorbance of the aminosilane-dinitrobenzene released in solution. More recently, ninhydrin was used to determine terminal amino groups on glass [12, 13]; this method, however, is also destructive [14].

The reaction of silica surfaces with an aminosilane produces an aminated surface which is treated with glutaraldehyde in the most commonly used procedure for immobilizing enzymes. Ideally, the chromophoric probe should react chemically with the "reactive" group under determination in the same fashion and under the same experimental conditions to be used in successive immobilization steps. *p*-Dimethylaminocinnamaldehyde (DACA) was chosen as the probe in the method described here because it reacts with primary amines to form an α,β-unsaturated imine similar to that postulated for the glutaraldehyde/amine immobilization/reaction product [15—18]. The chemical method for determination of reactive amino groups after surface modification by use of DACA, and several considerations of relevance to the chemistry of immobilization by the glutaraldehyde spacing, are the subject of this paper.

EXPERIMENTAL

Apparatus. A Perkin-Elmer Lambda 3840 UV/visible linear-diode-array spectrophotometer operated by a Perkin-Elmer 7300 computer was used for collection, manipulation, and output of spectral and photometric measurements.

The probe was attached by using either of two inverting shakers for mixing. For reactions at room temperature a Universal Oscillating Shaker (Model 2095, Lab-Line Instruments, Melrose Park, IL) was used, and for reactions at elevated temperatures, a Multi-Blok Heater (Model 2093, Lab-Line Instruments) was mounted on a custom-made air-driven shaker.

Detachment of the probe was studied by placing 30-ml glass vials containing DACA-reacted controlled-pore glass and the appropriate hydrolysis

medium in a test-tube rack located within the well of an ultrasonic mixer. The temperature of the hydrolysis reaction mixture was controlled (±0.1°C) by water circulated from a Haake R-22 water bath (PolyScience Corp., Evanston, IL). The extent of hydrolysis as a function of time was determined by adding to the setup a Gilson Minipuls 2 peristaltic pump (Gilson Medical Electronics, Middleton, WI) to pump the hydrolysis medium through a gas dispersion tube (to filter out suspended glass from the vial) to a flow-through cell in the spectrophotometer and back into the capped vial.

Reagents and glass supports

All chemicals used were of analytical-reagent grade. Solutions were prepared in deionized water distilled from an all borosilicate-glass still with a quartz immersion heater (Wheaton Instruments, Millville, NJ). Anhydrous reagents were prepared by drying over type 4A molecular sieves (Union Carbide Corp., Linde Division, Danbury, CT). The buffer solutions used for detachment were 0.050 M in total phosphate and 0.10 M in sodium chloride. Controlled-pore glass and aminopropyl controlled-pore glass were obtained from Electro-Nucleonics (Fairfield, NJ) and used without further treatment. Piperidine and DACA were obtained from Aldrich Chemical Co.

Procedures

Attachment of chromophoric probe. About 50 mg of aminopropyl controlled-pore glass was placed in a 30-ml glass vial with an excess (40 mg) of DACA and 20 ml of reaction solvent. (For the recommended procedure, the solution was 1.0×10^{-3} M piperidine in anhydrous ethanol.) The vial was then capped and mechanically shaken for 60 min. The reacted controlled-pore glass was separated from the mixture by aspirated filtration, sequentially washed with four 10-ml portions of anhydrous ethanol, and finally allowed to dry under air flow.

Detachment of chromophoric probe. At least 10.0 mg of the reacted glass was carefully weighed into each of three 30-ml glass vials and each weight was recorded because all determinations are on a weight/weight basis. Hydrolysis medium (25.00 ml) was pipetted into the vial and the vial was placed in a thermostated (±0.1°C) ultrasonic bath for 60 min. (For the recommended procedure the hydrolysis solution was 95% ethanol kept at 40° C.) Suspended glass particles were removed by centrifugation and the absorbance was measured at 390 nm.

Reaction vs. time studies. The reaction of DACA with the aminated glass as a function of time was monitored in a variety of solvents by stopping the reaction at designated times and subjecting the reacted material to hydrolysis.

Detachment of probe as a function of time was studied in a closed-loop continuous-flow system. The hydrolysis medium was circulated between the reaction vial and a flow cell located in the spectrophotometer. Absorbance measurements were made every 30 s and used to locate an absorbance plateau.

Evaluation of limit of detection. Non-aminated controlled-pore glass was treated with DACA and piperidine in anhydrous ethanol for 1 h and the glass was then filtered out, rinsed, dried, and weighed into portions of about 30 mg. Each portion was subjected to hydrolysis at 40.0°C with 95% ethanol. The limit of detection was taken as the average of ten blank readings plus three times the standard deviation of those readings.

Solutions and procedure for titrations. Anhydrous titrant was prepared by adding 200 μl of 70% perchloric acid (Mallinckrodt) and 450 μl of acetic anhydride (Mallinckrodt) to about 1.00 l of anhydrous acetic acid (J. T. Baker). Care was taken to avoid an excess of acetic anhydride because it reacts with primary amines. The indicator solution was prepared by dissolving 0.25 g of methyl violet 2B (Matheson Co., East Rutherford, NJ) in 100 ml of anhydrous acetic acid.

Aminated controlled-pore glass (20 mg) was placed in 25 ml of anhydrous acetic acid and 2 drops of the 0.25% (w/v) indicator solution was added. The mixture was titrated [19, 20] until the last tinge of purple color disappeared; the end-point is from purple to green.

RESULTS AND DISCUSSION

The reversible addition of a chemical probe to an immobilized chemical species with the subsequent quantitative removal and measurement of the released probe is referred to herein as "on/off chemistry" [21]. Formations of Schiff bases (imination) are good candidates for use in such procedures. Product formation is easily reversed by hydrolysis of the imine and a wide range of conditions can be selected to favor the forward reaction. Dimethylaminocinnamaldehyde has been proposed as a colorimetric reagent for detecting amines [22] and was selected for the work reported here in preference to iodine or chloranil, two other potential probes tested, because it provided better behavior for the type of application sought.

Iodine is released slowly during the exposure of samples to air; this results in very poor reproducibility. Chloranil is attached practically irreversibly; neither concentrated solutions of the bases morpholine or piperidine, nor hydrochloric acid or sodium hydroxide were effective in removing chloranil. Iodine was studied because it has been used to enhance the ultraviolet detectability of *N,N*-dimethylbenzylamine in liquid chromatography [23], and chloranil because it has been proposed for the spectrophotometric determination of surface-bound amines [24].

Imine formation can be either acid-catalyzed or base-catalyzed, in general [25], and piperidine has been proposed as a basic promoter of imine formation [26]. Base-promoted imine formation can be considered to occur as follows:

$$R{-}NH_3^+ + B: \rightleftharpoons R{-}NH_2 + BH^+ \qquad (1)$$

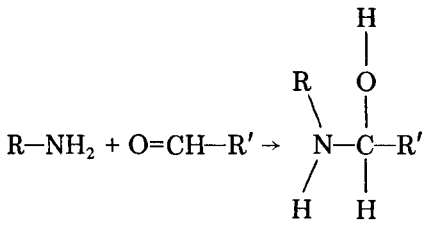

(2)

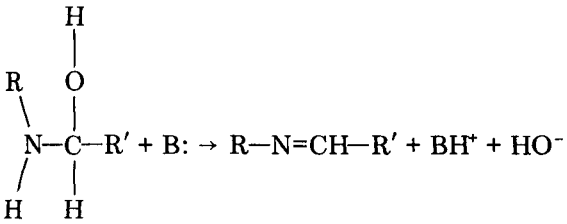

(3)

Piperidine as a basic promoter (B:) first shifts the amine protonation equilibrium (Reaction 1) to the unprotonated primary amine; then it removes a proton from the carbinolamine intermediate during the dehydration step (Reaction 3). Table 1 shows results in presence and absence of piperidine and of acetic acid as potential promoters of imine formation. Acetic acid as a potential promoter shows no effect at all except at relatively high concentrations when a detrimental rather than a beneficial effect is observed. If contact times are extended to 4.5 h, the results obtained with acetic acid are identical to those obtained without acetic acid present. Piperidine, however, shows a definite promoting effect; results after only 1 h in anhydrous ethanol in the presence of piperidine, for instance, are similar to those obtained in its absence but after overnight contact. Hence the recommended procedure calls for piperidine in anhydrous absolute ethanol, room temperature, and 60-min contact time.

The piperidine-promoted reaction reaches a yield plateau after a 60-min contact time and longer times are not justified. Water as a reaction solvent was discarded because the equilibrium constant for imination in aqueous media does not favor product formation [27]; the results for absolute ethanol and anhydrous absolute ethanol (stored over molecular sieves) in Table 1 are lower when water is present in the solvent. Methanol can be used because it gives higher values; however, the use of less expensive ethanol was justified in a comparative study. In another experiment, 18 times as much probe was attached in 95% ethanol as in deionized/distilled water under otherwise identical conditions. In pH 5.00 phosphate buffer, conditions were even worse because 44 times as much probe was attached when 95% ethanol was used as solvent.

Detachment of the chromophoric probe

The conjugated system of double bonds present in DACA is energetically unfavorable to tautomerization (Reaction 4), this ensures recovery of the

TABLE 1

Effect of different solvents and piperidine or acetic acid added as potential promoters of the attachment of DACA to aminosilane controlled-pore glass. (Temperature 25.0 ± 0.2°C; DACA concentration 0.01 M)

Solvent	Amount attached (μmol NH_2 per g of glass)[a]					
	No promoter added		Piperidine added (1.0×10^{-3} M)		Acetic acid added	
	60 min[b]	19 h[b]	60 min[b]	19 h[b]	5.7×10^{-2} M 60 min[b]	5.7×10^{-4} M 60 min[b]
Ethanol (absolute)	32.7 ± 0.4	50.0 ± 0.3				
Anhydrous ethanol[c]	39.1 ± 0.6	53.9 ± 0.9	51.8 ± 0.5	61.2 ± 0.6	29.5 ± 0.8	39.0 ± 0.2
Anhydrous methanol	44.7 ± 1.0	61.6 ± 1.1	58.4 ± 1.7	63.9 ± 1.0		

[a]Average of three determinations on the same sample of aminosilane controlled-pore glass. [b]Contact time. [c]Absolute ethanol dried over molecular sieves.

original amine and aldehyde when the probe is detached by rupture of the imine bond.

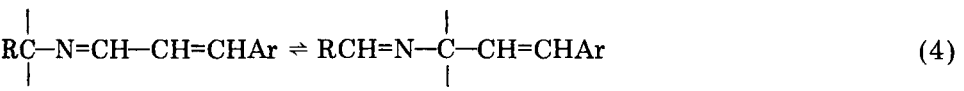

$$\text{RC(=CH–CH=CHAr)–N=CH–CH=CHAr} \rightleftharpoons \text{RCH=N–C(=CH–CH=CHAr)–CH=CHAr} \quad (4)$$

The hydrolysis of the imine is spontaneous and rapid in the presence of water [25, 27, 28]. To drive this reaction to completion in a reasonable length of time, however, it was necessary to elevate the temperature to 40.0°C and efficient mixing was required. The detachment step was done immediately after attachment was completed because a decrease in the amount of probe recovered was observed after extended storage time of DACA-reacted controlled-pore glass. Over a period of ten days, for instance, the amount of DACA detached from portions of the same DACA-reacted glass decreased from 176 ± 6 to 142 ± 3 μmol g^{-1}.

A continuous, closed-loop, flow system was used for photometric monitoring of the progress of probe detachment. Plots of absorbance (from DACA released) vs. time indicated a decrease in time needed to reach the absorbance plateau as the temperature was increased. Time required to detach the same amount (μmol g^{-1}) of probe was less than 10 min at 70.0°C, 30 min at 50.0°C, and about 1 h at 36.0°C. Figure 1 summarizes the results collected in the temperature study.

Figure 2 shows the detachment of the probe as a function of pH of the hydrolysis medium. Aminopropyl controlled-pore glass and DACA were allowed to react for 5 h in anhydrous ethanol; the modified material was then exposed to the hydrolysis medium for 30 min at 70.0°C. The wide plateau observed in Fig. 2 indicates that temperature plays a more important role than hydrogen ion concentration (at pH 4—7) in the detachment process. The recommended conditions for detachment of probe are 60 min at 40.0°C (at 70°C the method is destructive) in 95% ethanol. Detachment in aqueous buffers proved to create destructive conditions (i.e., irreproducible results and loss of amino groups in repeated determinations on one portion of the material). For one-time determinations in which sample destruction is unimportant, aqueous hydrolysis works well.

Blank value, limit of detection and reproducibility

Non-aminated glass showed no visual evidence of adsorption of the probe when exposed to DACA under reaction conditions. No peak at 390 nm was observed in the spectrum of the hydrolysis medium when non-aminated glass was used. The average of ten blank determinations was 0.079 ± 0.014 μmol g^{-1}; thus a limit of detection (3σ) of 0.12 μmol g^{-1} was calculated.

To evaluate the reproducibility, four different portions of the same glass sample were separately subjected to identical attachment/detachment procedures. The probe was attached to a particular portion of the glass in one reaction and that portion was then split into thirds; thus the hydrolysis and spectrophotometric measurement steps were done in triplicate for each por-

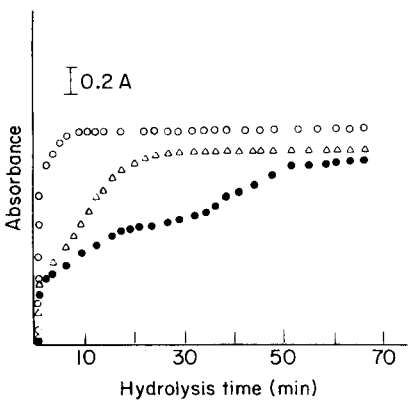

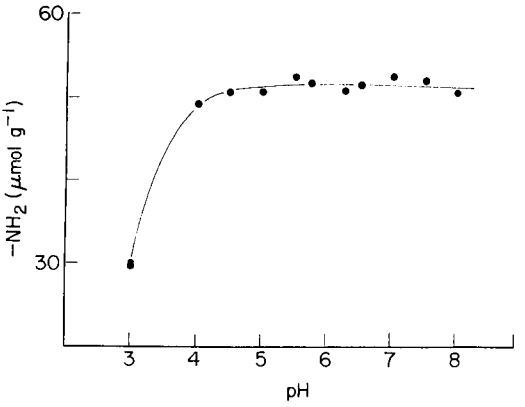

Fig. 1. Effect of temperature on DACA release from aminopropyl controlled-pore glass: (•) 26° C; (△) 36° C; (○) 70° C. Detachment medium, 95% ethanol; absorbance measured at 390 nm.

Fig. 2. Effect of pH on DACA detachment from aminopropyl controlled-pore glass. Experimental conditions: DACA attached by 5-h reaction in anhydrous ethanol; detachment for 30 min at 70°C.

tion. Each result reported in Table 2 is the average of those three measurements. A comparison of the amount of reactive amino groups found (Table 2) shows that this on/off chemical method has acceptable uncertainty (i.e., less than 2%) from run-to-run under a given set of conditions.

Repetitive determinations on one portion of a glass sample were done under conditions found to be nondestructive (Table 3). After each determination (in triplicate as above) the glass was recovered, pooled, rinsed repeatedly with anhydrous ethanol, then subjected again to the attachment/detachment

TABLE 2

Results of determination of amino groups on four different portions of controlled-pore glass

Portion	NH_2 groups found[a] (μmol g^{-1})	
	Method A	Method B
1	52.2 ± 2.7	63.7 ± 0.9
2	52.1 ± 0.6	65.5 ± 2.7
3	51.5 ± 0.5	63.2 ± 0.8
4	51.9 ± 0.6	64.1 ± 0.4

[a]Method A: attachment for 5 h in anhydrous ethanol; detachment for 30 min in pH 7.50 buffer, 70°C. Method B: attachment for 1 h in ethanol/piperidine medium; detachment for 1 h at 40°C in 95% ethanol.

TABLE 3

Results of successive determinations of amino groups on the same portion of controlled-pore glass[a]

Determination	1	2	3	4
NH_2 found[b] (μmol g^{-1})	54.2 ± 2.1	55.4 ± 1.5	59.3 ± 1.9	53.5 ± 0.7

[a]Attachment for 1 h in ethanol/piperidine medium; detachment for 1 h at 40°C in 95% ethanol. [b]Average and standard deviation for 3 replicates.

procedure. The uncertainty of these successive determinations is higher because of the difficulty of quantitative removal of water from the silica by rinsing. This results in rather poor reproduction of the anhydrous environment for the subsequent attachment/detachment procedure.

When aqueous buffers were used as hydrolysis media, sequential determinations made on the same portion of aminated glass showed continuously decreasing amounts of reactive amino groups (Table 4). The loss of such groups is more pronounced at higher temperatures. Detachment in alkaline aqueous buffers and elevated temperatures favors the hydrolytic scission of the siloxane bond, detaching the organosilane from the glass backbone [29]. In the essentially organic matrix of 95% ethanol and under milder conditions (40.0°C), the imine is preferentially cleaved.

Comparison with results obtained by nonaqueous titration

Titration of amines in anhydrous acetic acid medium with perchloric acid is well documented [19, 20] and has been applied for quantitative information on amino groups immobilized on glass [30]. Results obtained by nonaqueous titration, an optimized form of DACA attachment/detachment (which, unfortunately, is nonrepetitive), and the DACA attachment/detachment procedure that is nondestructive are compared in Table 5. Each application of the optimized conditions for the DACA/amine reaction involved attachment of a certain amount of probe that was not recoverable by the hydrolysis conditions used. The variation in the results observed in Table 5 points to differences in relative accessibility of surface amino groups on different samples of controlled-pore glass.

A trend can be seen between the reported surface area and the results obtained when DACA is used as the probe. The number of reactive amino groups increases with increasing surface area and doubling the surface area roughly doubles the amount of amino groups found. The fact that the acid-base titration in anhydrous acetic acid yields higher results hints at a dependence on probe size. Uneven surface distribution of amino groups can produce areas with clusters and areas with relatively wide separation between amino groups. The proximity of adjacent groups may hinder the molecules of DACA from binding all amino groups on the surface. By this logic, the results from nonaqueous titration will always be equal to or larger than those

TABLE 4

Results of successive determinations of amino groups on one portion of controlled-pore glass with aqueous hydrolysis medium[a]

Determination	NH_2 groups found (μmol g^{-1})	
	70.0°C	40.0°C
1	52.1 ± 0.6	51.9 ± 0.6
2	24.6 ± 0.1	35.2 ± 2.2
3	19.5 ± 0.7	28.5 ± 2.8
4	8.28 ± 0.50	—

[a]Attachment for 5 h in anhydrous ethanol, using glass B (see Table 5); detachment at pH 7.50 buffer at indicated temperature.

TABLE 5

Comparison of amino group contents determined by "on/off" methods and nonaqueous titrations

Glass sample	Particle size (mesh)	Pore size (Å)	Surface area (m^2 g^{-1})	NH_2 groups found (μmol g^{-1})		
				Nonaqueous titration[a]	Optimized on/off method[b]	Repetitive on/off method[c]
A	80/120	1273	24	91.3 ± 1.9	76.5 ± 2.2	65.2 ± 0.7
B	200/400	1273	24	70.4 ± 0.9	72.0 ± 1.3	58.7 ± 1.4
C	80/120	530	43	268 ± 5	123 ± 2	89.9 ± 4.2
D	80/120	547	44.5	298 ± 4	159 ± 4	123 ± 2
E	80/120	156	91	314 ± 3	289 ± 3	266 ± 4

[a]Results reported are the average of triplicate perchloric acid titrations as described in text. [b]Optimized on/off method: attachment 4 h, 40 ± 1°C in piperidine/ethanol media; detachment 1 h, 40.0°C, 95% ethanol. [c]Repetitive on/off method: attachment 1 h, 25°C in piperidine/ethanol media; detachment 1 h, 40.0°C, 95% ethanol.

obtained with larger probes. This observation is relevant to the availability of reactive amino groups for glutaraldehyde attachment because glutaraldehyde is not a small entity. The aldehyde group of DACA, which mimics the reactive ends of glutaraldehyde, makes a better probe to map reactive amino groups because it has only one way to bond. The presence of the double bond and the benzene ring gives DACA a stiffness which ensures the absence of intramolecular interactions (hydrogen bonding, cyclization, etc.).

The ratio of the results obtained by using the larger probe, DACA, to the results obtained from the nonaqueous titration can be used as a measure of accessibility of immobilized amino groups to this particular probe. Table 5 shows that controlled-pore glasses B and E appear to have very accessible

surface amino groups. The variation in accessible groups with different glass samples can be illustrated by comparing two samples from the same manufacturing lot; samples B and A have the same surface area and pore size, but sample B has smaller particles and a greater percentage of the amines are accessible to DACA under the conditions used. A pattern by which to generalize aminated glass characteristics has not emerged because of the heterogeneous nature and the lot-to-lot variation of this material. For instance, sample E, which has approximately 1/10 the pore size of sample A, has a larger percentage (from the DACA and titration results) of its amino groups available to react with the DACA probe. Samples C and D, which have similar surface areas and pore sizes, give results with DACA probe that show less than 50% of the amino groups that were determined by titration.

These observations underscore the fact that the amount of amino groups immobilized on controlled-pore glass surfaces may not be the amount available for subsequent chemical reactions. The microscopic physical characteristics of controlled-pore glasses as well as the surface distribution of immobilized groups may preclude a particular probe from binding with all "available" amino groups. Chemical interactions of the immobilized amine with surface silanols or other species may render an otherwise available amino group unreactive to a particular probe. The measurement of total amino groups by spectroscopic methods may not take into account these physical and/or chemical factors. The measurement of reactive groups by "on/off" chemistry, however, is dependent on the accessibility of the amino groups, as well as the probe size, type of bonding, contact time, and reaction conditions.

Comparative studies need only to yield reproducible relative results to permit conclusions about the chemistry being studied. The method described here for the batch determination of immobilized amino groups on controlled-pore glass particles is nondestructive, repeatable, and readily adaptable to determinations within the actual reactors to be used in flow systems [7, 8, 31].

This research was supported in part by the National Science Foundation (Grant CHE-8312494).

REFERENCES

1 D. E. Leyden, W. K. Nonidez and P. W. Carr, Anal. Chem., 47 (1975) 1449.
2 B. B. Jablonski and D. E. Leyden, in C. S. Barrett, D. E. Leyden, J. B. Newkirk and C. O. Rund (Eds.), Advances in x-ray Analysis, Vol. 21, Plenum, New York, 1978, pp. 59, 60.
3 D. E. Leyden, G. H. Luttrell, A. E. Sloan and N. J. DeAngelis, Anal. Chim. Acta, 84 (1976) 97.
4 N. H. C. Cooke, R. L. Viavattene, R. Eksteen, W. S. Wong, G. Davies and B. L. Karger, J. Chromatogr., 149 (1978) 391.
5 H. A. Mottola, Anal. Chim. Acta, 145 (1983) 27.
6 M. A. Marshall and H. A. Mottola, Anal. Chem., 55 (1983) 2089.
7 M. C. Gosnell and H. A. Mottola, Anal. Chem., 58 (1986) 631.

8 M. C. Gosnell, Ph.D. Dissertation, Oklahoma State University, 1986.
9 R. S. S. Shreedhara Murthy and D. E. Leyden, Anal. Chem., 58 (1986) 1228 (and references therein.)
10 D. E. Leyden, Chemically Modified Surfaces, Vol. 1, Gordon and Breach, New York, 1985.
11 J. R. Ritter and O. R. Strauch, Ger. Offen., 2343899, 1974; Chem. Abstr., 81 (1974) 121829.
12 O. D. Shapilov, V. G. Kayumov and A. I. Krashenyak, Zh. Anal. Khim., 38 (1981) 564; J. Anal. Chem. USSR (Engl. Transl.), 38 (1983) 436.
13 Z. Machacek and J. Nemecek, Czech. CS 195896, 1982; Chem. Abstr., 98 (1983) 144383.
14 D. McCaldin, Chem. Rev., 60 (1960) 39.
15 P. Monsan, G. Puzo and H. Mazarquil, Biochemie, 57 (1975) 1281.
16 P. Monsan, G. Puzo and H. Mazarquil, in D. Thomas and J.-P. Kerneyez (Eds.), Anal. Control Immobilized Enzyme Syst., Proc. Int. Symp. 1975, North-Holland, Amsterdam, 1976, p. 275.
17 P. Monsan, J. Mol. Catal., 3 (1978) 371.
18 D. T. Cheung and M. E. Nimni, Connect. Tissue Res., 10 (1982) 187.
19 J. S. Fritz, Acid-Base Titrations in Nonaqueous Solvents, Allyn & Bacon, Boston, MA, 1973.
20 S. Siggia and J. G. Hanna, Quantitative Organic Analysis via Functional Groups, 4th edn., Wiley-Interscience, New York, 1979, p. 545.
21 H. A. Mottola, R. E. Snelling and M. C. Gosnell, 13th Annual Meeting of the Federation of Analytical Chemistry and Spectroscopy Societies, St. Louis, MO, October 1, 1986, Abstr. 369.
22 F. Feigl, Spot Tests in Organic Analysis, 7th edn., Elsevier, Amsterdam, 1966, p. 243.
23 C. R. Clark, C. M. Darling, Jen-Lee Chan and A. C. Nichols, Anal. Chem., 49 (1977) 2080.
24 R. E. Smith and W. R. Davis, Anal. Chem., 56 (1984) 2345.
25 P. Y. Sollenberger and R. B. Martin, in S. Patai (Ed.), Chemistry of the Amino Group, Interscience, New York, 1968, pp. 349—406.
26 F. A. Adam, M. T. El-Haty and A. A. Ibrahem, J. Chin. Chem. Soc. (Taipei), 31 (1984) 345.
27 E. H. Cordes and W. P. Jencks, J. Am. Chem. Soc., 84 (1962) 832.
28 R. W. Layer, Chem. Rev., 63 (1963) 489.
29 W. H. Scouten in D. E. Leyden (Ed.), Chemically Modified Surfaces, Gordon and Breach, New York, 1985, pp. 59—72.
30 Y. Wong, Electronucleonics Inc., Fairfield, NJ, personal communication, 1986.
31 M. C. Gosnell, R. E. Snelling and H. A. Mottola, Anal. Chem., 58 (1986) 1585.

Analytica Chimica Acta, 200 (1987) 515—521
Elsevier Science Publishers B.V., Amsterdam — Printed in The Netherlands

SIMULTANEOUS DETERMINATION OF IRON AND COPPER IONS BY FLOW-INJECTION ANALYSIS WITH A MULTICHANNEL PHOTODIODE-ARRAY DETECTOR

HIROKO WADA**, TOMOAKI MURAKAWA and GENKICHI NAKAGAWA*

Department of Applied Chemistry, Nagoya Institute of Technology, Gokiso-cho, Showa-ku, Nagoya (Japan)

(Received 30th March 1987)

SUMMARY

Iron(II) and copper(II) ions are determined simultaneously in a simple manifold by using a multichannel photodiode-array detector. 1-(2-Pyridylazo)-2-hydroxy-7-sulfonaphthalene (PAN-7S) is used as the sole chromogenic reagent. The absorbance at 550 nm is related to the PAN-7S chelates of iron(II) and copper(II) and that at 764 nm to the iron(II) chelate alone. Calibrations are linear over the range 0—8.0 × 10^{-6} M for each metal. Interference from zinc is avoided by addition of nitrilotriacetic acid; nickel interferes. Application to the determination of iron and copper ions in blood serum is discussed.

Numerous methods have been developed for the simultaneous determination of two or more species by flow-injection analysis. Several detectors, splitting of the stream for a single detector, multi-injections, zone sampling, differential kinetics, etc. have been used [1]. Recently, the multichannel photodiode-array detector has been widely used for high-performance liquid chromatography. In flow-injection analysis (FIA), iron and copper ions were determined simultaneously by using a mixture of 1,10-phenanthroline and neocuproine with a multichannel photodiode-array detector [2]. The absorbances at two wavelengths for the iron(II) and copper(I) chelates (512 and 454 nm) were monitored, and iron (1– 8 μg ml^{-1}) and copper (15– 30 μg ml^{-1}) were determined. A computer program was needed for calculation of the results. The sensitivity for the copper determination was lower than that of the conventional method.

In clinical analysis, determinations of iron and copper ions are very important, because both ions play important roles in many body processes.

*Genkichi Nakagawa has been Professor of Analytical Chemistry at Nagoya Institute of Technology since 1968, where he has taught since 1958. He received his B.S. from Nagoya Institute of Technology (1949) and his doctoral degree from The University of Tokyo (1960).

**Hiroko Wada has been Professor of Analytical Chemistry since 1982 at Nagoya Institute of Technology, where she has taught since 1960. She received her B.S. from the Nagoya City University (1960) and her doctoral degree from Nagoya University in 1969.

0003-2670/87/$03.50

Several methods have been reported for sequential determinations of iron and copper in a single aliquot of serum by batch methods [3–7]. However, no methods are available for simultaneous determination with a single chromogenic reagent.

In the present work, a single chromogenic reagent, 1-(2-pyridylazo)-2-hydroxy-7-sulfonaphthalene (PAN-7S), which is soluble in water and more sensitive than 1,10-phenanthroline and neocuproine, is applied. The iron(II)/PAN-7S chelate has two absorption maxima around 530 and 750 nm, while the copper(II) chelate has an absorption maximum around 545 nm. Absorbances at two wavelengths are monitored by means of a multichannel photodiode-array detector. The method is applied to the simultaneous determination of iron and copper ions in serum.

EXPERIMENTAL

Reagents

The chromogenic reagent, 1-(2-pyridylazo)-2-hydroxy-7-sulfonaphthalene (PAN-7S), was synthesized as described previously [8]. Its sodium salt was dissolved in water as required.

The copper(II) stock standard solution (1×10^{-3} M) was prepared by dissolving copper (99.99% purity) in dilute nitric acid (1 + 1), and diluting appropriately. The iron(III) stock standard solution (1×10^{-3} M) was prepared by dissolving iron(III) ammonium sulfate in dilute hydrochloric acid, and diluting to the required volume. The concentration of iron(III) was determined by EDTA titration.

All the reagents used were of analytical-reagent grade. The water was redistilled from a hard-glass vessel.

Manifold and recommended procedure for iron and copper

A diagram of the flow-injection manifold is shown in Fig. 1. The reciprocating pump used was a Sanuki Kogyo DM2U-1026 model. Samples were injected via a rotary valve (Oyo-Bunko Kiki) with an 80-μl loop. The reaction

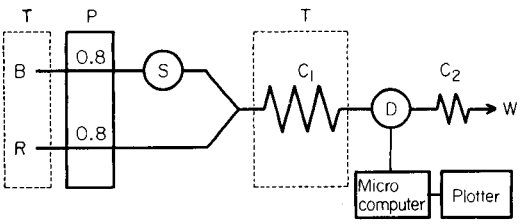

Fig. 1. Flow diagram: P, reciprocating pump with indication of flow rate (ml min^{-1}); S, sample injector with loop (80 μl); C_1, mixing coil (0.5 mm i.d., 200 cm long); C_2, back-pressure coil (0.25 mm i.d., 100 cm long); D, multichannel photodiode-array detector equipped with flow cell (volume 8 μl, light path 10 mm); B, carrier solution; R, chromogenic reagent solution; T, thermostat (40°C).

coil and the containers for the chromogenic reagent and carrier solutions were kept in a thermostat at 40°C. The multichannel photodiode-array detector (Union-Giken; Model MCPD-350PC) was equipped with a flow cell (10-mm light path, 8-μl volume).

The reagent solution consisted of 10^{-4} M PAN-7S in acetic acid/sodium acetate buffer (0.4 M, pH 5.0) containing 2×10^{-4} M sodium nitrilotriacetate. The carrier solution consisted of acetic acid/sodium acetate buffer (0.4 M, pH 5.0) with L-ascorbic acid (10^{-2} M). The flow rate for each solution was 0.80 ml min^{-1}. The sample solutions (80 μl) were injected into the carrier stream. The samples and reagents were mixed in a double coil (see below). The signals at 550 and 764 nm were recorded. Iron was determined from the absorbance at 764 nm, and copper from the difference between the absorbances at 550 nm and 764 nm.

Procedure for blood serum

Freeze-dried normal control serum (Control Serum I, Wako) was dissolved by adding 5 ml of water in a glass container. An aliquot (2 ml) of the solution was transferred to a test tube, and 1 ml of 0.1 M hydrochloric acid was added. The solution was heated in a water bath at 80–90°C for 2 min, and then 2 ml of 10% (w/v) trichloroacetic acid (TCA) and 0.6 ml of 0.01 M ascorbic acid were added. The solution was mixed well and then centrifuged and the supernatant liquid was transferred to a 10-ml volumetric flask. To the residue, 1 ml of 5% (w/v) TCA solution was added and, after centrifugation, the supernatant liquid was again transferred to the volumetric flask. Then the pH was adjusted to about 4.5 by adding 1 ml of 2 M sodium acetate and the solution was diluted to the mark with water. An 80-μl aliquot of this solution was injected into the flow-injection system.

RESULTS AND DISCUSSION

Characteristics of absorption spectra

Figure 2 shows the absorption spectra of PAN-7S and of the copper(II), iron(II) and zinc(II) chelates measured with a multichannel photodiode-array detector by delivering each solution separately. The absorbance of the copper(II) chelate was negligible at wavelengths greater than 700 nm, while the absorption maximum of iron(II) chelate was around 750 nm. The absorbances of iron(II) chelate were the same at 550 and 764 nm. Thus the signals at 550 and 764 nm were selected for the simultaneous determination of iron and copper.

Optimization of reaction and instrumental conditions

The effect of pH was examined by the batch method. As shown in Fig. 3, the absorbance of iron(II) chelate was almost constant in the pH range 4–9.5. In contrast, the absorbance of the copper(II) chelate increased with pH because the 1:1 copper(II)/PAN-7S chelate formed in the lower pH range

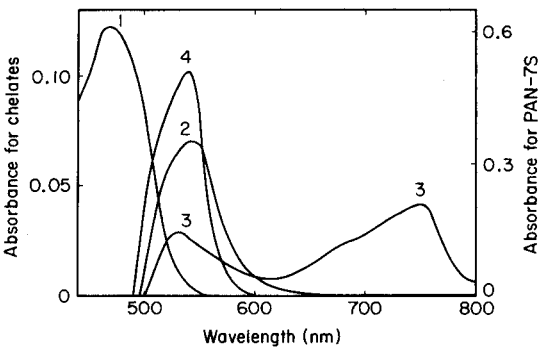

Fig. 2. Absorption spectra of PAN-7S and its Cu(II), Fe(II) and Zn(II) chelates: (1) PAN-7S (4×10^{-5} M) against water; (2) 1×10^{-5} M Cu(II), pH 9; (3) 1×10^{-5} M Fe(II), pH 9; (4) 1×10^{-5} M Zn(II), pH 9; (2—4) measured against PAN-7S solution, 1×10^{-4} M.

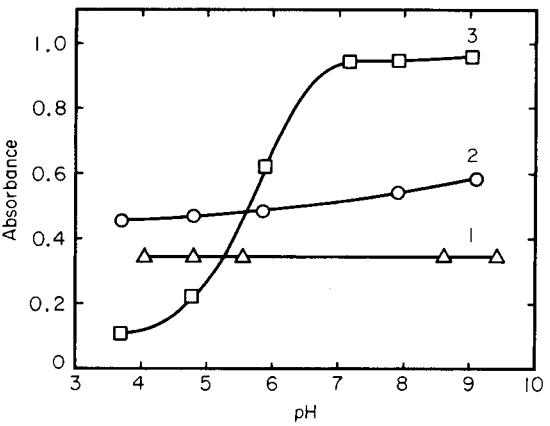

Fig. 3. Effect of pH on the absorbances of the PAN-7S chelates: (1) Fe(II); (2) Cu(II); (3) Zn(II). Conditions: PAN-7S, 2×10^{-4} M; metal ions, 2×10^{-5} M.

changed to the 1:2 chelate with increasing pH. The flow-injection system was run at pH 5.0 where the buffer capacity of acetate buffer was large and the interferences from other metal ions were small, except for nickel [8].

The concentration of PAN-7S was varied from 2.0×10^{-5} to 1.0×10^{-4} M. Maximum peak height was obtained with more than 6.0×10^{-5} M reagent, thus a 1.0×10^{-4} M PAN-7S solution was chosen.

The effects of the length and shape of the reaction coil were examined for various flow rates; the flow rates of the chromogenic reagent solution and carrier solution were the same in all cases. Single and double coils with helix diameters of 4—30 mm were tested. Single coils were wound in the conventional manner; double coils were wound in a figure-of-eight fashion. The peak heights were larger with the coils of small helix diameter. The results obtained with coils of 4-mm helix diameter are given in Table 1. On using a double coil

TABLE 1

Effect of mixing coil and flow rate on the peak height for 8×10^{-6} M iron(II) at 750 nm

Length of mixing coil	Absorbance[a] at total flow rate (ml min^{-1})			
	1.0	1.6	2.0	3.0
Single coil				
2 m	0.029	0.026	0.023	0.019
3 m	0.022	—	0.016	0.014
Double coil				
1 m	0.026	—	0.021	0.017
2 m	0.028	0.028	0.026	0.023
3 m	0.024	—	0.023	0.021

[a]Absorbance 0.01 corresponds to a 2.7-cm peak height.

with helix diameters of 4 mm, the peak height was largest and the peak width smallest. A 2-m double coil and a total flow rate of 1.6 ml min^{-1} were found to give the best reproducibility. The reaction between PAN-7S and iron(II) was somewhat slow, thus the reaction coil was warmed at 40°C.

Calibration

A three-dimensional calibration output for iron(II) is shown in Fig. 4 as an example. Calibration outputs for iron(II) and copper(II) are shown in Fig. 5. Both calibrations were linear over the range 0– 8.0×10^{-6} M. The detection limits (S/N = 3) were 0.03 μg ml^{-1} for both iron and copper ions. The cali-

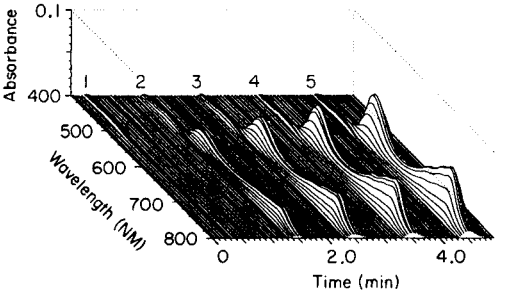

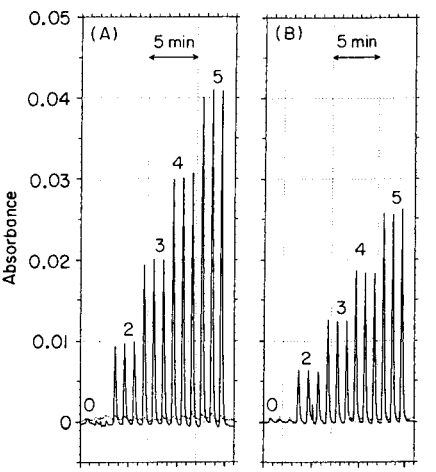

Fig. 4. Three-dimensional output for different iron concentrations ($\times 10^{-6}$ M): (1) 0, (2) 2.0, (3) 4.0, (5) 6.0, (5) 8.0.

Fig. 5. Calibration outputs: (A) Cu(II) at 550 nm; (B) Fe(II) at 764 nm. Concentrations of Cu(II) and Fe(II) ($\times 10^{-6}$ M), (1) 0; (2) 2.0; (3) 4.0; (4) 6.0; (5) 8.0.

bration graphs for iron and copper were not affected by the presence of ascorbic acid. Iron and copper did not interfere with each other within the specified ranges.

Application to the simultaneous determination of copper(II) and iron(II, III) in serum

Among the metal ions likely to be present in serum, only zinc(II) ion interferes with the method. Because the differences between the absorption spectra of the copper and zinc chelates with PAN-7S were small (Fig. 2), the simultaneous determination of iron, copper and zinc was impossible. Sodium iminodiacetate and sodium nitrilotriacetate were examined for masking zinc(II). By using a chromogenic reagent solution containing 2×10^{-4} M sodium nitrilotriacetate, up to 1.3 μg ml^{-1} zinc(II) could be masked. Therefore, 6.5 μg ml^{-1} zinc in serum was tolerable.

The procedure outlined in the Experimental part was applied in the analysis of blood serum. The results are shown in Table 2. For comparison, various procedures for the pretreatment of the serum were examined. When the serum was treated with TCA solution in the absence of ascorbic acid, the recovery of iron was low, while that of copper ion tended to be high. When ascorbic acid was added only to the treated sample solution, the recovery of iron was still low. When TCA and potassium periodate were used, the recovery of copper was only slightly higher than that by treatment with TCA with or without ascorbic acid, but the iron result was very low. When the serum was decomposed with nitric acid and perchloric acid in a teflon vessel at 140°C, the recoveries of both iron and copper ions were higher than those obtained by pretreatment with TCA and ascorbic acid. Iron and copper in the serum

TABLE 2

Results for the determination of iron and copper ions in a control serum by the proposed flow-injection method with PAN-7S

Sample[a]	Found (mg l^{-1})		Remarks
	Fe	Cu	
1—5	1.62 ± 0.019[b]	1.01 ± 0.037[b]	Pretreated with TCA and ascorbic acid
6	1.60	2.30	(With 1.27 mg l^{-1} Cu added to serum)
7	1.45	1.03	Pretreated with TCA only
8	0.99	1.26	
9	1.04	1.03	Ascorbic acid added after TCA treatment
10	1.01	1.05	
11	0.29	1.10	Pretreated with TCA and KIO_4
12	1.91	1.38	Oxidative decomposition
13	1.86	1.19	Fe by ICP/AES, Cu by AAS

[a]Reported values (mg l^{-1}): Fe 1.51—1.87, Cu 1.03—1.39. [b]Mean and standard deviation for 5 separate determinations.

were also determined by inductively-coupled plasma atomic emission spectrometry (ICP/AES) and by atomic absorption spectrometry (AAS), respectively.

Although the results by the proposed method were somewhat lower than those obtained by the same flow-injection procedure after oxidative decomposition of the serum and by ICP/AES and AAS, the method could readily be standardized against a standard serum for satisfactory routine work.

REFERENCES

1 M. D. Luque de Castro and M. V. Cases, Analyst, 109 (1984) 413.
2 F. Lázaro, A. Ríos, M. D. Luque de Castro and M. Valcárcel, Anal. Chim. Acta, 179 (1986) 279.
3 B. Zak and N. Ressler, Clin. Chem., 4 (1958) 43.
4 D. Wilkins and G. F. Smith, Anal. Chim. Acta, 9 (1953) 538.
5 A. Schilt and P. Taylor, Anal. Chem., 42 (1970) 220.
6 H. Y. Yee and J. F. Goodwin, Clin. Chem., 20 (1974) 188.
7 H. L. Williams, D. J. Johnson and M. J. Haut, Clin. Chem., 23 (1977) 237.
8 K. Ohshita, H. Wada and G. Nakagawa, Anal. Chim. Acta, 140 (1982) 291.

Analytica Chimica Acta, 200 (1987) 523—531
Elsevier Science Publishers B.V., Amsterdam — Printed in The Netherlands

AN AUTOMATED SPECTROPHOTOMETRIC FIELD MONITOR FOR WATER QUALITY PARAMETERS
Determination of Nitrate

J. RICHARD CLINCH and PAUL J. WORSFOLD*

Department of Chemistry, University of Hull, Hull HU6 7RX (Great Britain)

HARRY CASEY

Freshwater Biological Association, River Laboratory, East Stoke, Wareham, Dorset BH20 6BB (Great Britain)

(Received 18th April 1987)

SUMMARY

An automated spectrophotometric field monitor is described for the determination of nitrate in river water. The bias, precision and linear calibration range of the monitor were determined in the laboratory. Samples taken from six locations on the River Frome in Dorset were analyzed for nitrate content by the monitor, and the results obtained were in good agreement with those obtained by two spectrophotometric reference methods. The relative standard deviation for 672 replicate injections of a 7.7 mg l^{-1} NO_3-N standard over a 14-day period was 1.4%, during which time 2.5 l of the colour reagent and 2.5 l of the ammonium chloride solution were consumed. The linear calibration range of the procedure was 0—12 mg l^{-1} NO_3-N. Results are also presented for a four-day field trial on the River Frome.

The current generation of process analyzers is restricted primarily to monitoring physical parameters, e.g., temperature, pressure and flow rate. There is, however, an increasing desire to conduct chemical on-line analysis, with a view to controlling a process more efficiently, for reasons of economy and of environmental and product quality [1]. One laboratory technique that could be modified for on-line use is flow injection analysis (f.i.a.). It is easily automated, will accept samples delivered directly from a process stream, is reliable and easy to maintain, has a rapid sample throughput for pseudo-continuous measurement, and is extremely flexible in terms of manifold design.

This paper focuses attention on the design and operation of a flow-injection-based process analyzer with spectrophotometric detection as a field monitor for the water industry, where sampling and sample transport can introduce significant errors [2] and where concern about water quality is increasingly being supplemented by EEC legislation and stricter limits for "consent to discharge". This public concern was emphasized in a recent survey [3] which showed that more of the people questioned were worried about chemicals put into rivers and the sea (86%) than about any other

0003-2670/87/$03.50

environmental issue, including disposal of nuclear waste (82%), destruction of wildlife (82%) and acid rain (68%).

Potential applications for such a water-quality monitor include pollution control, water-intake protection, effluent monitoring and nutrient budget studies. If spectrophotometric detection is used, a wide variety of species can potentially be determined; a procedure for phosphate has already been reported [4]. The determination of nitrate in surface waters, however, is of wider importance because of its known link with methaemoglobinaemia and its possible link with stomach cancer and hypertension [5—8]. With this in mind, the EEC has set a guideline level of 5.65 mg l^{-1} NO_3-N (nitrate as nitrogen) and a maximum admissible concentration of 11.3 mg l^{-1} NO_3-N for surface waters abstracted for drinking water supply [9].

The nitrogen content (as nitrate, nitrite or ammonia) of lakes, rivers and streams usually arises from the groundwater, sewerage effluent or drainage and leaching from agricultural land [10]. The last is the most significant input and nitrate levels have increased substantially over the last 40 years because of the increased use of nitrogen-based fertilizers [10—12]. There is also some concern about the rise in nitrogen levels in the English Channel, presumably arising from the same sources [13].

Several methods are available for the determination of nitrate in waters [14], including direct ultraviolet spectrophotometry, derivatization with sulphosalicyclic acid, use of a nitrate-selective electrode and reduction to nitrite followed by derivatization, e.g., with *N*-1-naphthylethylenediamine dihydrochloride (N1NED) and sulphanilamide. In this paper, the design of a fully automated spectrophotometric field monitor based on f.i.a. is described for the determination of nitrate in surface waters by reduction with copperized cadmium and derivatization by N1NED and sulphanilamide. Results are presented here for nitrate budget studies on the River Frome in Dorset.

EXPERIMENTAL

Reagents

All solutions were prepared in distilled deionized water and all reagents were AnalaR (BDH) except the cadmium powder (Johnson-Matthey Metals). A stock nitrate solution containing 100 mg l^{-1} NO_3-N was prepared by dissolving 0.7220 g of potassium nitrate (dried for 2 h at 105°C) in 1 l of water. Six working nitrate standards covering the range 0—10 mg l^{-1} NO_3-N were prepared by serial dilution of the stock solution. A 5 mg l^{-1} NO_3-N standard was used for all the manifold optimization experiments.

The ammonium chloride carrier stream was prepared by dissolving ammonium chloride (10 g) in 1 l of water. The *N*-1-naphthylethylenediamine dihydrochloride (N1NED) reagent was prepared by dissolving 0.5 g of the compound in 1 l of 10% (v/v) orthophosphoric acid. The sulphanilamide (*p*-aminobenzenesulphonamide) reagent was prepared by dissolving 25 g of

the compound in 1 l of 10% (v/v) orthophosphoric acid. A working colour-reagent solution was prepared by mixing equal volumes of the sulphanilamide and N1NED reagents and was stored in a brown glass bottle. The cadmium reactor columns were prepared by adding 5 g of cadmium powder (100 mesh, 0.15-mm diameter) to 50 ml of a copper sulphate solution (10 g l^{-1}) and stirring for 2 min. The resultant copperized cadmium was washed with 2 M hydrochloric acid and ammonium chloride solution (10 g l^{-1}), packed into glass tubes (40 mm long, 2 mm i.d.) and plugged with glass wool. The columns were stored in ammonium chloride solution (10 g l^{-1}) until required and connected to the PTFE tubing of the manifold by short lengths (10 mm) of red/red pump tubing (Anachem).

Instrumentation and procedures

The manual flow injection manifold used to optimize the system is shown in Fig. 1. A peristaltic pump (Ismatec Mini S-820) was used to propel both the ammonium chloride carrier stream and the colour-reagent stream through PTFE tubing (0.5 mm i.d.) at 0.8 ml min^{-1}. Nitrate standards and samples (30 μl) were manually injected into the ammonium chloride carrier stream via a PTFE rotary valve (Rheodyne 5020), passed through the reductor column (to reduce nitrate to nitrite) and merged with the colour-reagent solution in a 200-cm mixing coil. The absorbance was monitored by a solid-state photometric detector furnished with a green LED (Radio Spares 588-285) [1] and the analogue output was relayed to a chart recorder (Tekman Labwriter) set at 1-V full scale deflection.

Automated field monitor

A block diagram of the automated field monitor is shown in Fig. 2. A single-board microcomputer (Control Universal, Cambridge) was used to control a 12-V solenoid-activated injection valve (Chemlab Instruments), a 12-V two-way solenoid valve (Lee, Westbrook, CN) and two 240-V peristaltic pumps (Ismatec Mini S-820). The signal obtained from the detector was digitized via a 13-bit analogue/digital converter (Control Universal), and the output was sent to a miniature printer (24 characters per line) and a 24 X 2 character liquid-crystal display. The reaction manifold and the detector were as described above.

Control software, which was written in-house in BBC BASIC, was designed to introduce a sample in duplicate followed by a 10 mg l^{-1} NO_3-N standard in duplicate, every 30 min. The nitrate level was calculated by

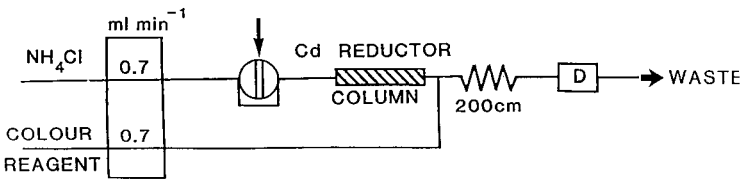

Fig. 1. Manual flow-injection manifold for the determination of nitrate.

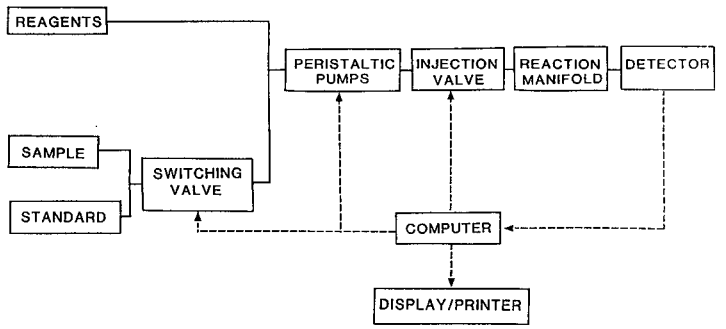

Fig. 2. Block diagram of the automated field monitor.

ratioing the means of the sample and standard signals, and the most recent reading was displayed on the liquid-crystal display. The date, time and nitrate concentration were recorded on the mini-printer. The software was stored on a read-only memory device and was configured to start up whenever the microcomputer was powered up.

RESULTS AND DISCUSSION

Characteristics of light-emitting diodes

The three light-emitting diodes (LEDs) most commonly available with emission in the visible region of the electromagnetic spectrum are red, green and amber. All are available at a minimal cost (Radio Spares) with emission intensities of 125, 120 and 140 mcd, respectively, and a typical current requirement of 20 mA. The spectral characteristics of each of the LEDs were obtained with a silicon-intensified-target vidicon detector (B & M Elektronik OSA-500) and are shown in Fig. 3. Their maximum emission wavelengths and bandwidths, respectively, were 635 nm and 38 nm (red), 583 nm and 26 nm (amber) and 565 nm and 30 nm (green). The major limitation of LEDs as sources for photometric detectors, therefore, is the restricted wavelength range covered. However, for the determination of nitrate by the formation of an azo dye [λ(max) = 542 nm], a green LED is acceptable.

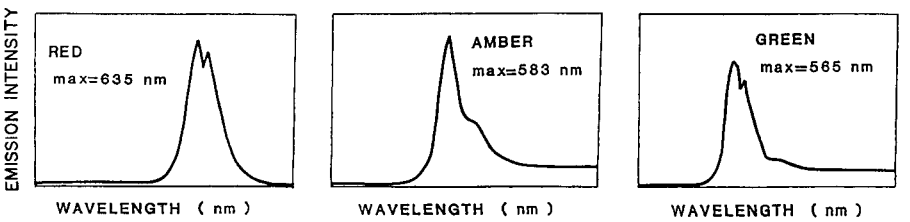

Fig. 3. Emission spectra of red, amber and green LEDs.

Manifold optimization

Experimental parameters for the manually operated two-channel manifold (Fig. 1) were optimized by a univariate approach. The minimum concentrations of N1NED and sulphanilamide in 10% orthophosphoric acid that produce maximum signals were 0.5 and 25 g l^{-1}, respectively. The optimum ammonium chloride concentration was 10 g l^{-1}; above this level, the response decreased because chloride ions inhibited the derivatization reaction and the reduction step [15], whereas below this level the response was erratic because of the decreased buffering capacity of the carrier stream.

The response increased with increasing sample volume (15—180 μl), but a sample volume of 30 μl was chosen for all further experiments in order to prolong the lifetime of the cadmium column and therefore extend the unattended operating lifetime of the monitor. The effect of overall flow rate on the response is given in Fig. 4 and shows a maximum response at 1.4 ml min^{-1} (0.7 ml min^{-1} per channel). The reduction in response at higher flow rates is due to incomplete reaction and at lower flow rates is due to increased dispersion in the cadmium column. The optimum reaction coil length was 200 cm.

The cadmium column is the critical component of the manifold with regard to unattended operating lifetime. The effect of varying the length of the column (Table 1) shows that shorter columns give higher sensitivity because the sample is less dispersed, but the longer columns obviously have a greater reducing capacity and therefore a longer lifetime. A 40-cm column was used for all further experiments.

Calibration

Six nitrate standards covering the range 0—10 mg l^{-1} NO_3-N were analyzed in the laboratory by the optimized manifold (Table 2). A linear calibration graph was obtained (r = 0.9995) which was described by the equation

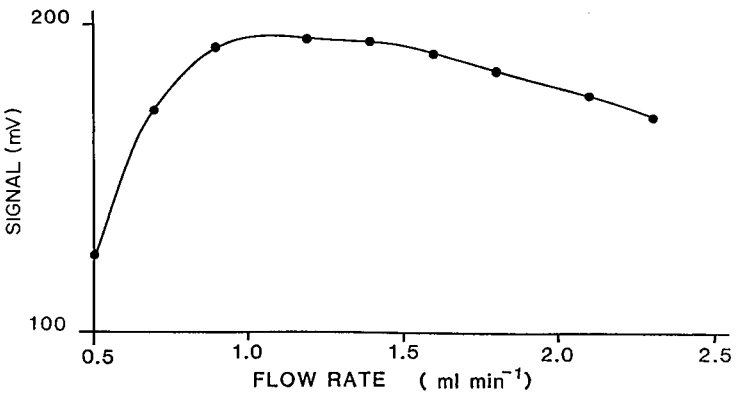

Fig. 4. Effect of total flow rate on signal.

TABLE 1

Effect of length of the cadmium column on sensitivity

NO_3-N (mg l^{-1})	Mean[a] peak height (mV) for various cadmium-column lengths		
	10 mm	20 mm	40 mm
2	156.7	149.2	127.5
5	348.3	336.7	295.0
7	451.7	438.3	400.0
10	615.0	590.8	565.0
r[b]	0.9970	0.9968	0.9988

[a]n = 4. [b]Correlation coefficient.

TABLE 2

Calibration data for nitrate

NO_3-N (mg l^{-1})	0	1	2	5	7	10
Peak height[a] (mV)	1.0	63.1	127.5	295.0	400.0	565.0

[a]Mean of six measurements.

$$\text{signal (mV)} = 56.1\ C(NO_3\text{-N}) + 8.4$$

where C is the concentration in mg l^{-1}. The relative standard deviation (r.s.d.) was in the range 0.0—0.7% (n = 6) and the limit of detection (2σ) was 24 μg l^{-1} NO_3-N. The linear calibration range was 0—12 mg l^{-1} NO_3-N when the optimized manifold was used. A 7.7 mg l^{-1} NO_3-N standard was analyzed every 30 min for two weeks (n = 672) by ratioing the response with that of a 10.0 mg l^{-1} NO_3-N standard. The r.s.d. over that period was 1.4%.

The proposed method will also measure nitrite and therefore is strictly a measure of total oxidized nitrogen (TON), but the concentration of nitrite in surface waters and groundwaters is normally too low to affect the nitrate result significantly. Other oxidizing and reducing species will have an effect on the reduction step but again this is not normally a significant problem. Estuarine and seawater samples, however, would need special attention owing to the inhibiting effect of salt on both the reduction and the diazotization steps [15].

Operational lifetime

The monitor is designed to operate unattended for a minimum of one week, after which time the cadmium column should be changed and the reagent solutions replenished.

The stability of the reagents used is of crucial importance in deciding the applicability of a proposed method for field use. The ammonium chloride solution was stable for 30 days in the laboratory at room temperature (20°C) after which time microbial growth was observed in the reagent container. Similarly, the colour reagent was stable for 20 days, after which time oxides of nitrogen absorbed from the atmosphere [16] gave the solution a pink tinge.

The consumption of reagents and 10 mg l^{-1} standard over a two-week period, involving duplicate sample and standard determinations every 30 min, was 2.5 l each of the colour reagent and the ammonium chloride solution and 1.0 l of the standard.

The reducing capacity of the cadmium column was investigated by repeated injections of a 10.0 mg l^{-1} NO_3-N standard. There was no decrease in signal after 5 days (1600 injections). After a further 400 injections, a 30% decrease in signal was observed.

Comparison of methods

Six river-water samples were collected from various locations in the River Frome (Dorset) catchment area in PTFE bottles on 25 June 1986. On the same day, each sample was filtered through a 0.45-μm glass fibre filter (Whatman GF/C) and examined for nitrate content by the proposed flow-injection procedure and two reference methods. The reference methods were a manual spectrophotometric procedure based on derivatization with phenoldisulphonic acid [17] and an automated laboratory-based flow-injection procedure based on the same chemistry as the proposed method [16]. Both of these procedures have been used by one of the authors for nitrate budget studies on the River Frome for several years. The results obtained (Table 3) show good agreement between all three methods.

TABLE 3

Comparative results for water samples from the River Frome catchment area

Location	Grid reference	NO_3-N content (mg l^{-1})		
		Proposed method	Automated method [16]	Manual method [17]
Sydling Water	SY 637947	3.6	3.5	3.4
South Winterbourne	SY 712889	5.0	4.9	4.9
River Hooke	SY 592976	3.4	3.4	3.2
Woodsford	SY 769909	4.6	4.7	4.5
Empool	SY 763874	5.5	5.6	5.2
Broomhill Bridge	SY 811881	4.8	4.9	4.8

Field trial

The fully automated monitor was installed on the River Frome at East Stoke, Dorset (SY 867868) for a 4-day period in November 1986. River water was pumped into a 50-l constant-head polypropylene container by a submersible pump situated on the river bed. The container was flushed with water every 15—20 s and was sampled every 30 min, as described above, by pumping water to the monitor via PTFE tubing (0.8 mm i.d.). The results obtained are shown in Fig. 5, together with flow data and calculated nitrate load (kg h^{-1}) for the same period. During the trial, no sample filtration was used although a glass column packed with glass wool has been shown to be necessary when the suspended solids content of the river is high.

The short-term field trial clearly demonstrates the potential of the field monitor for the determination of nitrate. Future work will include a long-term field trial, improvements in sample introduction and data transmission,

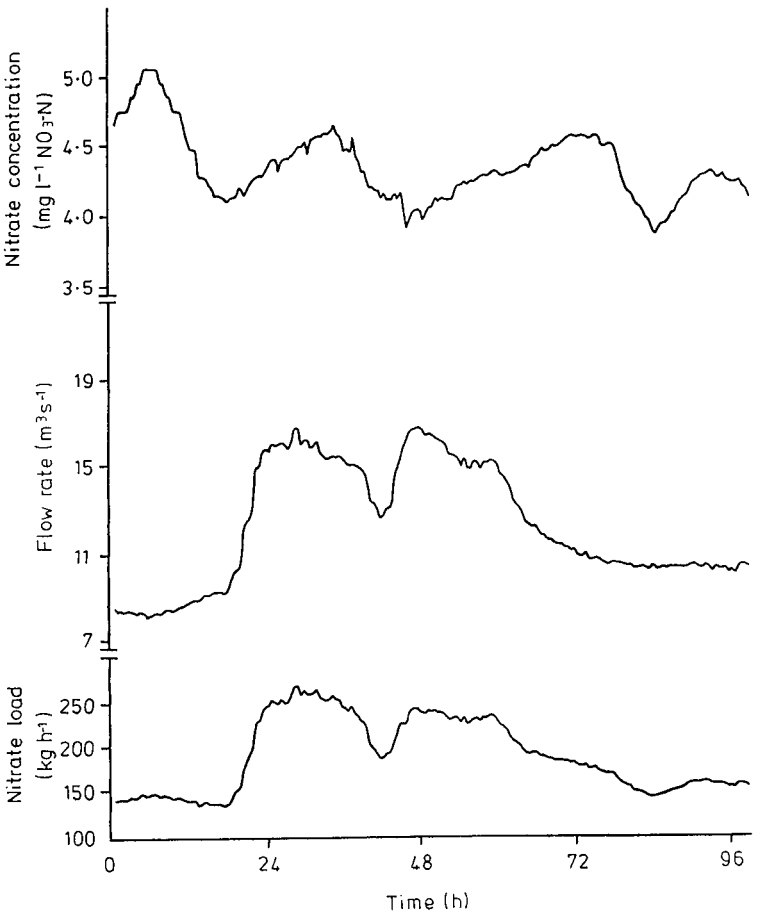

Fig. 5. The variation in nitrate concentration, flow rate and nitrate load in the River Frome from 12.00 a.m. (starting time) on 10 November 1986 to 3.00 p.m. on 14 November 1986.

and the extension of the technique to monitoring other species, e.g., total ammonia, aluminium and total iron, and other sample types, e.g., industrial effluents, water intakes.

The authors thank Wessex Water for financial support and one of us (J.R.C.) thanks the Science and Engineering Research Council for a scholarship. The Freshwater Biological Association is a grant-in-aid body of the Natural Environment Research Council.

REFERENCES

1 W. E. Van der Linden, Anal. Chim. Acta, 179 (1986) 91.
2 D. T. E. Hunt and A. L. Wilson, The Chemical Analysis of Water: General Principles and Techniques, Royal Society of Chemistry, London, 1986.
3 Department of the Environment, Digest of Environmental Protection and Water Statistics, HMSO, London, 1986.
4 P. J. Worsfold, J. R. Clinch and H. Casey, Anal. Chim. Acta, 197 (1987) 43.
5 R. J. Burden, N.Z. J. Sci., 25 (1982) 205.
6 P. N. Magee, Ambio, 6 (1977) 123.
7 E. R. Jaffe, Clin. Hemat., 10 (1981) 99.
8 P. N. Magee, Phil. Trans. R. Soc. London, Ser. B, 296 (1982) 543.
9 J. Gardiner and G. Mance, U.K. Water Quality Standards Arising from EEC Directives, WRC Technical Report TR204, Medmenham, Great Britain, 1984.
10 S. S. D. Foster, L. R. Bridge, A. K. Geake, A. R. Lawrence and J. M. Parker, The Groundwater Nitrate Problem: A summary of research on the impact of agricultural land-use practices on ground-water quality between 1976 and 1985, Hydrogeol. Rep. Br. Geol. Survey, No. 86/2, 1986.
11 H. Casey and R. T. Clarke, Freshwater Biol., 9 (1979) 91.
12 The Nitrogen Cycle of the United Kingdom, Royal Society, London, 1983.
13 I. Butler, Marine Biological Association, private communication.
14 Department of the Environment, Methods for the Examination of Waters and Associated Materials, Oxidised Nitrogen in Waters, HMSO, London, 1982.
15 F. Nydahl, Talanta, 23 (1976) 349.
16 Tecator Application Note ASN 62-02/83.
17 Standard Methods for the Examination of Water and Waste Water, American Public Health Association, New York, 1960.

Analytica Chimica Acta, 200 (1987) 533–538
Elsevier Science Publishers B.V., Amsterdam — Printed in The Netherlands

THE APPLICATION OF STRONGLY REDUCING AGENTS IN FLOW INJECTION ANALYSIS
Part 6. Molybdenum(III)

W. Th. KOK, D. T. THUY[a], T. V. NGHI[a] and G. DEN BOEF*

Laboratory for Analytical Chemistry, University of Amsterdam, Nieuwe Achtergracht 166, 1018 WV Amsterdam (The Netherlands)

(Received 3rd April 1987)

SUMMARY

The application of molybdenum(III) as reducing agent in flow injection analysis is described. Molybdenum(III), which is unstable to oxidation by air, is generated in-line from the stable molybdenum(VI) by means of a Jones reductor column. With spectrophotometric detection, iodate, uranium(VI), vanadium(V) and nitrite can be determined in the concentration range 5×10^{-5}—5×10^{-3} M at an injection rate of 3 min^{-1}. Amperometric detection of nitrite is also described.

A series of publications [1—5] has been devoted to the application of strongly reducing agents in flow injection analysis (FIA). The instability of reducing agents with respect to oxidation by air has been an impediment for their application in analysis. However, when these agents are produced in-line in a flow-injection system, their instability is no longer a problem, because the time interval between their production and use is short and fixed. In-line generation can be achieved by chemical or electrochemical reduction of a species in a stable higher-valency state.

In the work presented in this paper, the application of Mo(III) is described. Molybdenum(III) was generated from Mo(VI) in acidic medium by means of a Jones reductor, a column of amalgamated zinc particles, as described by Headridge and Taylor [6]. From Table 1, in which are listed some values of the relevant standard potentials reported in the literature, it appears that Mo(III) is a less strong reducing agent than the agents studied previously, so that it may be applied more selectively than, for example uranium(III).

*Gerrit den Boef is a graduate of the University of Amsterdam. He was appointed Lecturer in Chemistry in 1961, Professor of Analytical Chemistry in 1970 and is currently Head of the Chemistry Department. He served as Rector Magnificus of the University of Amsterdam from 1976 to 1979. He has been Secretary of the Analytical Chemistry Division of IUPAC since 1983.

[a]Present address: Analytical Department, Chemistry Faculty, University of Hanoi, Vietnam.

0003-2670/87/$03.50

TABLE 1

Standard potentials of molybdenum in aqueous solutions

Half-reaction	$E^{0\prime}$ (V vs. NHE)	Reference
$HMoO_4^- + 7H^+ + 3e^- \rightleftharpoons Mo^{3+} + 4H_2O$	+0.39	7
$MoO_2^+ + 4H^+ + 2e^- \rightleftharpoons Mo^{3+} + 2H_2O$	~0.0	8
$Mo^{5+} + 2e^- \rightleftharpoons Mo^{3+}$ (2 M HCl)	−0.25	9
MoO_2 (s) $+ 4H^+ + e^- \rightleftharpoons Mo^{3+} + 2H_2O$	+0.311	10

The application of spectrophotometric and amperometric detection in FIA is described.

EXPERIMENTAL

The experimental set-up is shown schematically in Fig. 1. A Gilson Minipuls 2 peristaltic pump was used, delivering a flow rate of 0.75 ml min^{-1} through each line. The Rheodyne injector was equipped with a 30-μl loop. Both single-bead-string reactors (SBSR) were 100 mm × 1.0 mm i.d., packed with 0.6-mm glass beads.

For the preparation of the Jones reductor, 5 g of zinc particles (0.18–0.60 mm diameter) was washed with 1 M hydrochloric acid and stirred for 15 min in a solution of 0.34 g of mercury(II) chloride in 10 ml of 0.1 M HCl. After amalgamation, the particles were washed with water and with 2% (v/v) sulphuric acid and packed into a 150 mm × 4 mm i.d. glass column.

The spectrophotometer for flow-through detection was a Zeiss M4Q-III with a home-made flow cell. Amperometric flow-through detection was done with a Princeton Applied Research (PAR) 310 flow cell and a PAR 174A potentiostat/amplifier.

Absorbance spectra were recorded with a Beckman Acta double-beam spectrophotometer. Polarograms were recorded with a PAR 303 polarographic stand. All potentials were measured against an Ag/AgCl/1 M KCl (SSCE) reference electrode.

Molybdenum(VI) solutions, from molybdenum trioxide, and test solutions were prepared in 0.5 M sulphuric acid, except for the sodium nitrite

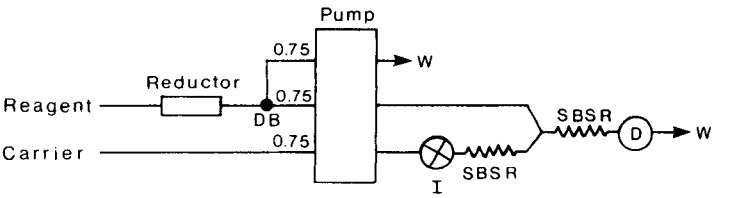

Fig. 1. Flow diagram. DB, debubbler; I, injector; D, detector.

solutions which were prepared in distilled water. Oxygen was removed from all solutions before and during use by purging with nitrogen.

RESULTS AND DISCUSSION

Polarography

In the present work, the use of hydrochloric acid media for the generation of Mo(III) from Mo(VI), as described by Headridge and Taylor [6], resulted in excessive hydrogen evolution and occasionally in the breakdown of the reductor column. Therefore, 0.5 M sulphuric acid solutions were used as solvent instead of hydrochloric acid.

Figure 2 shows polarograms of molybdenum solutions before and after passage through the reductor column. The electrochemical reduction of Mo(VI) to Mo(V) gives a well-defined polarographic wave with a halfwave potential at +0.10 V. Reduction to Mo(III) occurs in two overlapping, irreversible waves at about −0.35 and −0.60 V, respectively. According to the literature [11], these two waves are related to the occurrence of two different species of Mo(VI) in sulphuric acid solutions. From the fact that no cathodic wave is observed for the molybdenum solution that has passed the reductor (Fig. 2, curve e), it may be concluded that the conversion to Mo(III) is complete. Molybdenum(III) is oxidized to Mo(IV) with a half-wave potential of −0.28 V; oxidation to Mo(VI) occurs in two irregular waves at about −0.05 and +0.12 V.

Attempts were made to establish what the main product is when Mo(III) is partly oxidized in solution. For this purpose, polarograms of mixtures of Mo(III) and Mo(VI) solutions in different ratios were recorded. When an excess of Mo(VI) is present, the typical Mo(VI) waves remain visible in the polarogram (Fig. 2, curve b). At the same time, when an excess of Mo(III) is present, the typical Mo(III) waves are observed (Fig. 2, curve d). Only when Mo(VI) and Mo(III) are mixed in a 1:1 ratio are the original waves absent from the polarogram (Fig. 2, curve c). Though it is clear that neither Mo(IV) nor Mo(V) is formed exclusively, these experiments are not conclusive. The results may be explained by the simultaneous existence of more than two species with different valency states. The existence of a species with a valency state between +4 and +5 (cf. molybdenum blue) can, however, be postulated.

When a small amount of sodium nitrite, which is not electroactive itself in the potential range studied, was added to a Mo(III) solution, polarograms were obtained as in Fig. 2 (curve d). However, with an excess of nitrite, typical Mo(VI) polarograms were obtained.

Spectrophotometry

Figure 3 shows the ultraviolet-visible absorbance spectra of Mo(VI) and Mo(III) solutions and of a mixture of the two. The Mo(III) solution has an absorbance maximum at 360 nm with $\epsilon = 300$ l mol^{-1} cm^{-1}. When Mo(III)

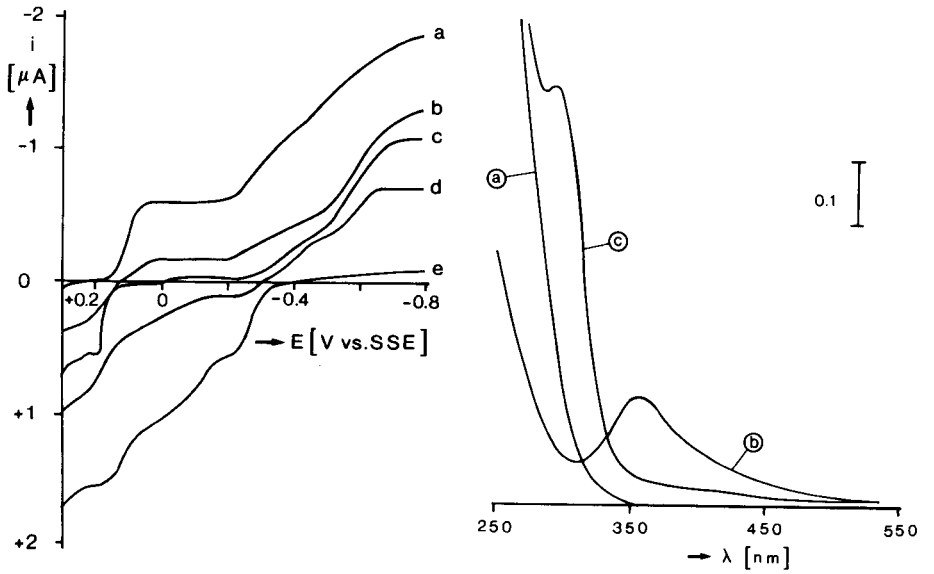

Fig. 2. Polarograms of molybdenum solutions in 0.5 M sulphuric acid. Sampled DC; drop time, 1 s; total Mo concentration, 5×10^{-4} mol l^{-1}. Polarographic curves: (a) Mo(VI); (b) Mo(VI) + Mo(III), 2:1; (c) Mo(VI) + Mo(III), 1:1; (d) Mo(VI) + Mo(III), 1:2; (e) Mo(III).

Fig. 3. UV-visible absorbance spectra of molybdenum solutions. Total Mo concentration, 5×10^{-4} mol l^{-1}. Spectra: (a) Mo(VI); (b) Mo(VI) + Mo(III), 2:1; (c) Mo(III).

is oxidized by addition of Mo(VI), this maximum disappears and a new maximum (or shoulder) is observed at 290 nm. The addition of other reducible substances to Mo(III) resulted in similar absorbance spectra as with Mo(VI).

Flow injection analysis

In principle, it is possible to monitor the increase of absorption in the 250—300 nm region when Mo(III) is oxidized in FIA. However, interferences have to be expected from test components that absorb themselves at these wavelengths. Therefore, the decrease of the Mo(III) absorption was monitored at 360 nm. The highest signal-to-noise ratios were obtained when the tungsten lamp of the spectrophotometer was used.

No reaction was observed with potassium dichromate, potassium bromate, sodium nitrate or *o*-nitrophenol. Compared to uranium(III), which does react with nitrate and *o*-nitrophenol in acidic medium, Mo(III) is a more selective but therefore less widely applicable reagent.

Calibration curves were obtained for iodate, V(V), U(VI) and nitrite. As expected, the upper limit of linearity depends on the reagent concentration. Figure 4 shows calibration plots for iodate obtained by using different con-

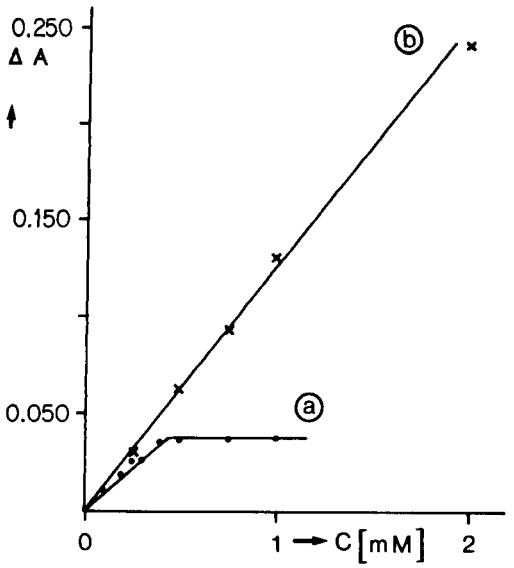

Fig. 4. Calibration plots for iodate with different reagent concentrations obtained with the flow-injection spectrophotometric system. Mo(VI) concentrations in stock solution: (a) 6.25×10^{-3} mol l^{-1}; (b) 1.25×10^{-3} mol l^{-1}. Peak heights are given as the change in absorbance (ΔA) from the baseline.

centrations of molybdenum. However, not only the linear range but the baseline noise increases with the reagent concentration, thus the lower limit of detection is also affected. Regression data are summarized in Table 2.

No significant changes in signals (or noise) were observed when the flow rates were decreased from the values stated in Fig. 1. It can be assumed that for the analytes that react, steady state is reached within the available reaction time, i.e., 2 s. Because of the short residence time and the effective mixing properties of the SBSR, a sample through-put up to 3 min^{-1} is possible.

The use of amperometric detection was also studied for the determination of nitrite, which is not electroactive itself at moderate potentials. Either the increase of the cathodic current of Mo(VI) or Mo(V), or the decrease of the anodic current of Mo(III) can be monitored. The latter method is to be preferred by reason of selectivity. The best results were obtained with sampled DC measurements at a potential of −0.15 V. Results are included in Table 2. A major disadvantage of the polarographic detector is its slow response. The sample through-put had to be limited to 1 min^{-1}.

Conclusions

Molybdenum(III) can be easily and effectively generated in-line from Mo(VI) for application as a reducing agent in FIA. Compared to U(III), its reactivity is more selective. The range of analyte concentrations that can be measured can be adapted to the demands of the analysis by adjusting the

TABLE 2

Regression data for the calibration plots in FIA, with a molybdenum concentration of 6.25×10^{-3} mol l^{-1}

Sample	Regression line $y = a + bC$[a]		Limit of detection[b] (mol l^{-1})	Limit of linearity[c] (mol l^{-1})
	$a \pm S_a$	$b \pm S_b$		
Spectrophotometric detection				
KIO_3[d]	0.0 ± 0.6	84 ± 3	2×10^{-5}	4×10^{-4}
KIO_3	2 ± 2	122 ± 2	5×10^{-5}	2×10^{-3}
$UO_2(CH_3COO)_2$	−6 ± 2	79 ± 2	1×10^{-4}	2×10^{-3}
NH_4VO_3	13 ± 3	22 ± 1	4×10^{-4}	8×10^{-3}
$NaNO_2$	14 ± 4	54 ± 1	2×10^{-4}	4×10^{-3}
Amperometric detection				
$NaNO_2$	13 ± 3[e]	51 ± 2[f]	2×10^{-4}	2×10^{-3}

[a] y and a are given as changes in absorbance; C, analyte concentration in mol l^{-1}. [b] Calculated as 3 S_a/b. [c] Evaluated by F-testing. [d] With Mo concentration of 1.25×10^{-3} mol l^{-1}. [e] $\times 10^{-8}$ A. [f] $\times 10^{-8}$ A mol^{-1} l.

reagent concentration. Limits of detection are in the order of 10^{-4} mol l^{-1}. For the determination of nitrite, amperometric detection offers no advantages over spectrophotometric detection.

REFERENCES

1 R. C. Schothorst, J. M. Reijn, H. Poppe and G. den Boef, Anal. Chim. Acta, 145 (1983) 197.
2 R. C. Schothorst and G. den Boef, Anal. Chim. Acta, 153 (1983) 133.
3 R. C. Schothorst, J. J. F. van Veen and G. den Boef, Anal. Chim. Acta, 161 (1984) 27.
4 R. C. Schothorst, M. van Son and G. den Boef, Anal. Chim. Acta, 162 (1984) 1.
5 R. C. Schothorst and G. den Boef, Anal. Chim. Acta, 175 (1985) 305.
6 J. B. Headridge and M. S. Taylor, Analyst, 88 (1963) 590.
7 M. Pourbaix, Atlas of Electrochemical Equilibria in Aqueous Solutions, Pergamon, Oxford, 1966.
8 W. M. Latimer, The Oxidation States of the Elements and their Potentials in Aqueous Solutions, Prentice-Hall, New York, 1952.
9 F. Foerster, E. Fricke and R. Hausswald, Z. Phys. Chem., Abt. A, 146 (1930) 177.
10 Th. Heumann and N. D. Stolica, in A. J. Bard (Ed.), Electrochemistry of the Elements, M. Dekker, New York, 1976.
11 J. J. Wittick and G. A. Rechnitz, Anal. Chem., 37 (1965) 816.

Analytica Chimica Acta, 200 (1987) 539—550
Elsevier Science Publishers B.V., Amsterdam — Printed in The Netherlands

THE USE OF DISCHARGE LAMPS AS DIRECTLY MODULATED ATOM RESERVOIRS FOR SELECTIVE LINE MODULATION IN ATOMIC EMISSION SPECTROMETRY

J. C. MITCHELL, A. W. STEELE and G. M. HIEFTJE*
Department of Chemistry, Indiana University, Bloomington, IN 47405 (U.S.A.)
(Received 24th April 1987)

SUMMARY

A simple method is described for selectively modulating the atomic or ionic resonance lines emitted by an excitation source. A modified discharge lamp with a cylindrical hollow cathode is used to generate a modulated atom cloud. The emission from the excitation source is then imaged through the modulated atom cloud within the cylindrical cathode lamp, to yield a selectively modulated signal. The ability of the system to reduce spectral interferences in inductively-coupled plasma emission spectrometry is assessed and discussed.

Inductively-coupled plasma/atomic emission spectrometry (ICP/AES) is one of the most popular methods for elemental determinations. High sensitivity, ease of operation, reliability and simultaneous multi-element detection capability are features of ICP/AES. An additional advantage of the method is a high degree of freedom from the interelement interferences that are

*Gary M. Hieftje is Distinguished Professor of Chemistry at Indiana University in Bloomington, Indiana. He received the A.B. degree from Hope College, Holland, Michigan in 1964 and the Ph.D. in 1969 from the University of Illinois under the direction of H. V. Malmstadt. From 1964 to 1965 he served as a research associate in physical chemistry at the Illinois State Geological Survey in Urbana, Illinois. In 1969, he was appointed assistant professor of chemistry at Indiana University, was promoted to associate professor in September, 1973, to full professor in July, 1977. He received a special appointment to a Distinguished Professorship in April, 1985. His research interests include the investigation of basic mechanisms in atomic emission, absorption, and fluorescence spectrometric analysis, and the development of atomic methods of analysis. He is also interested in the on-line computer control of chemical instrumentation and experiments, the use of time-resolved luminescence processes for analysis, the application of information theory to analytical chemistry, near-infrared reflectance analysis, and the use of stochastic processes to extract basic and kinetic chemical information. In 1983, he was the co-recipient of an IR-100 award for the development of the atomic absorption background-correction technique that bears his name, and in the summer of 1983, he received a senior guest fellowship from the Science and Engineering Research Council of Great Britain. He has received the 1984 Meggers Award, the 1984 Lester W. Strock Award, and the 1984 Anachem Award, the 1985 American Chemical Society Chemical Instrumentation Award, the 1986 Pittsburgh Analytical Chemistry Award, the 1986 Theophilus Redwood Award from the Royal Society of Chemistry, and the 1987 American Chemical Society Award in Analytical Chemistry sponsored by the Fisher Scientific Company. He is a past chairman of the Analytical Division of the American Chemical Society.

0003-2670/87/$03.50

common in flame atomic-emission spectrometry. However, the high temperature of the ICP generates an intense background composed of both a strong continuum and a highly structured line spectrum from atomic and ionic emission of the plasma supporting gas. In addition, intense molecular band emission arising from air entrainment is present. Moreover, multi-element samples are usually run in ICP/AES, a situation which leads to possible spectral-line overlap between the analyte and concomitant sample species. For these reasons, spectral interference remains one of the most troublesome aspects of ICP/AES.

Methods used to reduce the severity of spectral interferences in AES have traditionally involved high-resolution dispersion systems. Along with the high cost and complexity of such optical systems, light throughput is substantially reduced. Modulation schemes have also been successful in reducing spectral interferences in atomic spectrometry; these methods include wavelength modulation [1—6], sample modulation [7—16] and selective spectral-line modulation [17—22]. The most readily apparent advantage of such techniques is that they can often utilize a medium-resolution, high-speed spectral-dispersion device. More importantly, however, they can reduce both the detected background emission and the additive background noise. This noise reduction can result in an improvement in detection limits if the analytical signal is not attenuated appreciably.

Selective spectral-line modulation (SLM) functions by passing source radiation through an atom reservoir or zone that intermittently contains a high concentration of atoms and ions identical to the analyte species. Absorption of the source radiation at the atomic line then produces a modulated signal at the detector only for species common to both sources. The advantage of SLM over the alternative modulation methods is that discrimination from both source background and sample concomitant emission is achieved. The difficulty in improving detection limits is that the SLM signal will always be somewhat smaller than the corresponding direct-current emission signal because of the limited efficiency of the atomic absorption process. Also, additional background noise sources are added to the SLM system by the modulating atom reservoir.

This study explores the use of the kind of modulating atom reservoir originally used by Sullivan and Walsh for isolating resonance lines from a hollow-cathode lamp [23]. This device, a discharge lamp, can be electronically rather than mechanically modulated. The ability of the system to reduce the spectral interference of palladium (324.3 nm) on copper (324.7 nm) with a low-resolution monochromator was examined. It was found that the SLM system reduces the effective bandpass of the optical system to a level equivalent to the absorption linewidth of the atom cloud in the modulating reservoir.

EXPERIMENTAL

Figure 1 is a schematic diagram of the SLM system used in this study; Table 1 lists the various components that were required. A low-flow optimized

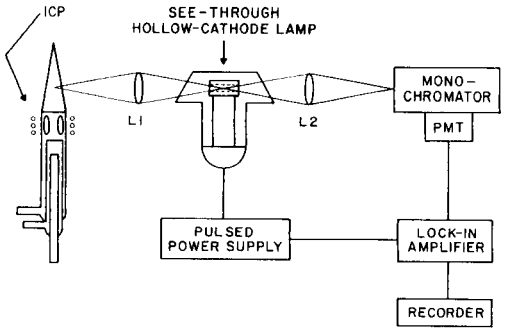

Fig. 1. Block diagram of the SLM system.

torch [24] was supplied with sample aerosol from a glass concentric nebulizer and a Scott double-pass spray chamber. The modulated atom reservoir was a pulsed hollow-cathode lamp of special design (cylindrical cathode lamp, CCL), intended by Hamamatsu Corp. (Middlesex, NJ) for optogalvanic wavelength calibration of dye lasers. The device used in this study was custom-fabricated but is available from the manufacturer as a "see-through hollow-cathode lamp". The cathode of this lamp is a cylinder with a bore of 2-mm diameter. The present CCL is a multi-element lamp with silver and copper in the cathode and a Ne/Kr mixture for a fill gas. A direct-current high-voltage power supply was modified for pulsed operation by a simple transistor switch circuit and used to drive the lamp in a modulated fashion. The pulsing waveform and frequency were controlled by an external function generator and were varied depending on the desired demodulation scheme.

For comparison, conventional emission data were collected by mechanically chopping the emission from the ICP. This chopping allowed the same detection electronics to be used for all data collected in the study and also permitted the use of double modulation, to be described later. For the double-modulation experiments, the chopper was placed between the ICP and lens L1 whereas for the conventional measurements, it was located between lens L2 and the monochromator. The mechanical chopper was operated at 27 Hz. For the double-modulation experiment, the signal was collected at the sum frequency which was generated by multiplying the CCL modulation waveform and the chopper-modulation waveform in an analog multiplier circuit. The entire optical system was mounted on a single, eight-foot optical-rail bed system as described by Walters [25].

Stock solutions were prepared from reagent-grade metals, salts and acids following standard procedures [26].

RESULTS AND DISCUSSION

The performance of the SLM system was evaluated by determining its ability to reduce spectral interferences commonly found in atomic spectrometry. These interferences include those from source background (both line and broad band), and from line overlap with sample-matrix elements.

TABLE 1

System components and operating conditions

Inductively-coupled plasma	
ICP	Model HFP-5000F, 5 kW, 27.12 MHz with model AMN-PS-1 automatic impedance matcher (Plasma Therm, Kresson NJ)
Applied r.f. power	750 W
Gas flows (Ar)	Coolant 10 l min^{-1}; plasma 0.5 l min^{-1}; nebulizer 0.5 l min^{-1}
Gas handling	Bulk liquid Ar, (Mineweld Co., Indianapolis, IN) controlled by needle valves, monitored by calibrated rotameters (Matheson Co., Jioliet, IL)
Sample solution uptake	1.0 ml min^{-1} delivered by peristaltic pump (Minipuls 2, Gilson Medical Electronics, Middleton, WI)
Nebulizer	Concentric glass
Torch	Optimized low-flow torch [24]
Modulated atom reservoir	
Cylindrical cathode lamp	See-through hollow-cathode lamp (Hamamatsu Corp., Middlesex, NJ)
Optics	
Monochromator	EU-700 GCA/McPherson Instruments (Acton, MA), 0.35-m Czery-Turner mount, slit width 75 μm, 0.15-nm spectral bandpass
Chopper	Constructed in-house, butterfly configuration, operated at 27 Hz
Lenses	150-mm focal length, 5-cm diameter, quartz (Melles Griot, Irvine, CA)
Detection	
Photomultiplier	1P28A (RCA Lancaster, PA), operated at 400—800 V
PMT power supply	EU-42A (Heath Co., Benton Harbor, MI)
Pre-amplifier	High-speed current amplifier, model 427 (Keithley Instruments, Cleveland, OH)
Boxcar integrator	Model 162 with two model-164 gated integrator modules (Princeton Applied Research Corp., Princeton, NJ)
Lock-in amplifier	Model 128 (Princeton Applied Research Corp., Princeton, NJ)
Frequency-selective amplifiers	Model 210A (Princeton Applied Research Corp.)
High-pass active filter	Model 3342 (Krohn-Hite Corp., Avon, MA)
Analog multiplier	AD 533J (Analog Devices, Norwood, MA)
Function generator	Model 1600 (Krohn-Hite Corp., Avon, MA)
Recorder	Model 3091 digital storage oscilloscope (Nicolet Instrument Corp., Madison, WI)
Microcomputer	COMPAQ portable (Compaq Computer Corp., Houston, TX)

To produce a high concentration of free atoms in the CCL, a high operating current (10—150 mA) is required. As a consequence, strong emission from the lamp is produced at the analytical wavelength. To overcome this background-emission problem, several different modulation and demodulation schemes were explored.

Boxcar demodulation

The first method involved pulsing the CCL with a low duty-cycle (2%), high current (20—150 mA) pulse and using a boxcar integrator for demodulation. This scheme generated a dense atom cloud (via the large current) and also allowed the SLM process to be studied at different times along the pulse waveform. The pulse repetition rate was 20 Hz with a pulse duration of 1 ms. Figure 2 shows four traces obtained with the boxcar integrator used in the scanning mode with a 0.5-μs aperture. Trace A is the CCL trigger pulse from the function generator. Traces B and C are the SLM signals obtained at the Cu I (324.7 nm) line with a blank solution being aspirated into the plasma and with CCL driving-current pulses of 20 mA and 150 mA, respectively. Trace B was recorded with a factor of five greater gain than trace C. The signal pulse apparent in traces B and C is caused by copper emission from the lamp. Not surprisingly, the emission is much weaker when a lower lamp current is used. Traces B and C show that the atom cloud emission from the lamp requires a finite time to reach a steady state, and that the emission takes a noticeable time to decay after the lamp is turned off.

Trace D in Fig. 2 is the output waveform that is obtained when a 150-mA lamp-current pulse is used and when a 1000 μg ml^{-1} copper solution is aspirated into the plasma. The baseline (delay marked *a*) of this trace corresponds to the emission from copper in the plasma, which is at a much higher absolute level than the baseline of traces B and C, which represent the background emission from the ICP. The pulse height in trace D is noticeably less than that in trace C, also taken with a peak CCL current of 150 mA.

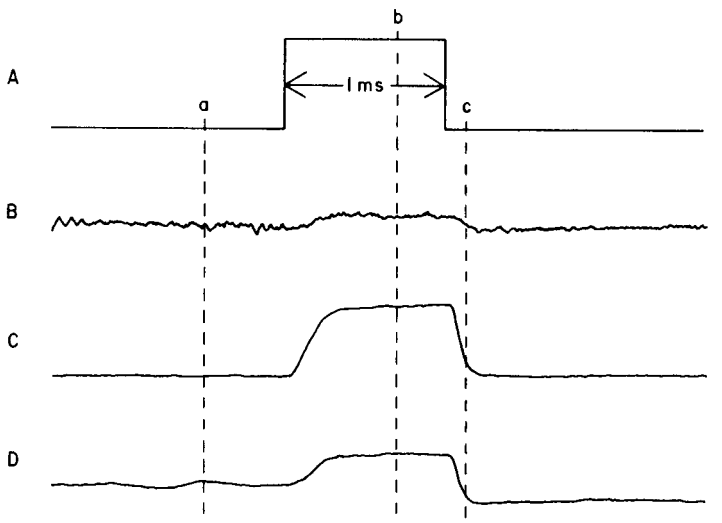

Fig. 2. Boxcar scans of: A, the lamp trigger pulse; B and C, the signal while a blank solution was aspirated into the ICP with lamp currents of 20 and 150 mA, respectively; D, the signal when a 1000 μg ml^{-1} copper solution was aspirated into the plasma with a lamp current of 150 mA. Delays marked *a*, *b* and *c* are discussed in the text.

This reduction is caused by absorption of the copper emission from the plasma by free atoms in the lamp. Also, the baseline in trace D is depressed after the lamp emission has decayed (point *c*), indicating that the modulating atom cloud is still present and absorbing analyte emission from the plasma. It was found that the atom cloud decays to the baseline level within 5 ms after the termination of CCL driving current. Conveniently, the boxcar integrator can be used in a differential mode, so that the recorded output signal corresponds to the net pulse height (i.e., signals collected at the delays marked *b* or *c* minus the background collected at the point marked *a*). Subtracting the blank reading from the analytical signal then results in a voltage proportional to analyte concentration in the plasma.

The waveforms in Fig. 2 suggest several approaches to conducting the SLM experiment with a boxcar integrator. If a boxcar sampling aperture much shorter than the pulse duration of the lamp is used, the detected signal can be obtained from any point along the waveforms shown in Fig. 2. Two sampling points were investigated. The first was in the middle of the pulse (delay marked *b*) after the atom concentration in the CCL has reached a steady state. Figure 3A shows that for this mode of operation, increasing the current level of the CCL pulse increases the background-corrected signal. Raising the current level of the CCL increases the atom concentration in the cathode aperture and thereby increases absorption of the analyte emission from the ICP. However, because emission from the lamp also rises with higher lamp currents, additive flicker noise from the lamp emission similarly increases, and degrades the overall performance of the system. This behavior is shown in Fig. 3B, where the signal-to-noise ratio decreases rapidly at peak lamp currents above 20 mA. The results shown in Fig. 3 are for the SLM experiment done with a 100 μg ml^{-1} silver sample in the ICP; similar results were obtained for copper.

Trace D in Fig. 2 suggests a second measurement approach. A significant atom concentration remains in the viewing region of the lamp for several

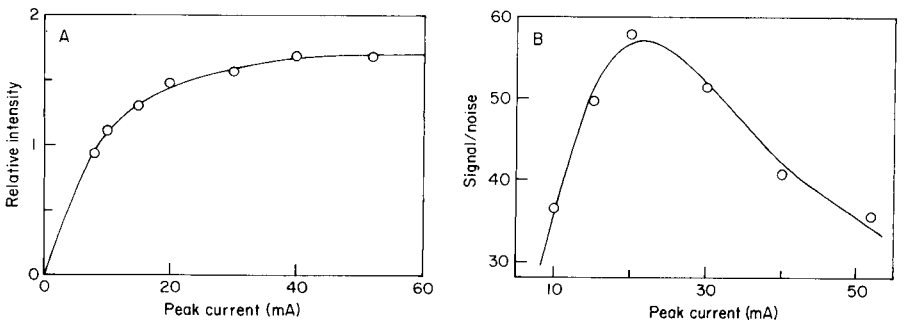

Fig. 3. The effect of increasing peak CCL current on background-subtracted signal magnitude (A) and on the signal-to-noise ratio (B). Signal measured as the difference between points *a* and *b* in Fig. 2. Signal derived from a 100 μg ml^{-1} silver solution introduced into the ICP.

microseconds after the lamp is turned off. Because the atomic emission decays more rapidly than the free-atom cloud, a significant reduction in the background emission from the lamp could be obtained if the signal were collected after the emission decayed but before the atom cloud dissipated. Higher lamp currents could be used in this mode of detection with minimal interference from the intense background emission of the CCL.

Figure 4 shows working curves obtained in this mode and constructed from data obtained at two lamp-current levels (20 and 150 mA). For each current level, signals were collected with the sampling aperture positioned at the middle of the CCL pulse (point *b* in Fig. 2) and 0.02 ms after the end of the pulse (point *c* in Fig. 2). Background (point *a* in Fig. 2) was subtracted in all cases.

A comparison of signal-to-background (S/B) ratios (see Table 2) shows that there is a significant reduction in background level for signals collected after the current pulse. The S/B ratios obtained for these two sampling positions show the expected trends. The 20-mA S/B ratio is quite high as expected because of the low CCL emission, while the 150-mA S/B ratio is much smaller, indicative of the relatively intense background present. Interestingly, the signal obtained just after the 150-mA pulse (curve B in Fig. 4) is nearly equal to that obtained at the middle of the 20 mA pulse (curve A). The signals measured with the sampling aperture at the end of the 20-mA pulse and in the middle of the 150-mA pulse are significantly lower. The atom concentration will understandably be lowest at the end of the 20-mA pulse, and will result in the smallest signal. The low signal levels obtained with the sampling aperture in the middle of the 150-mA pulse are probably caused by a significant amount of copper ion production, which depletes the neutral-atom concentration.

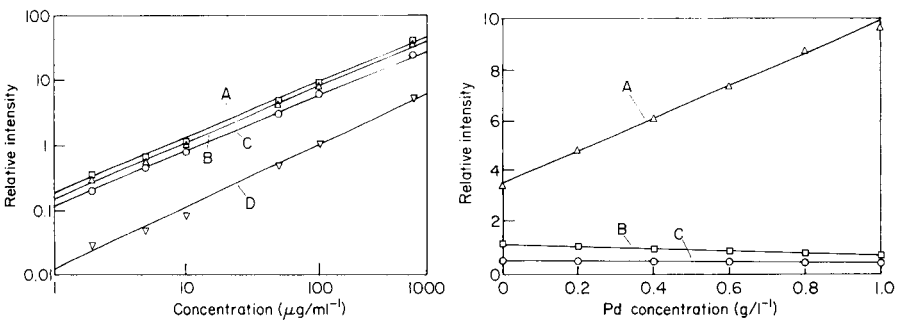

Fig. 4. Working curves for copper obtained with the boxcar-demodulation system. The curves correspond to measurements at different delays (as depicted in Fig. 2) and different CCL currents. Curves A and D: signal collected at delay *b* depicted in Fig. 2 (with peak CCL currents of 20 mA and 150 mA, respectively). Curves B and C: signal collected at delay *c* depicted in Fig. 2 (with peak CCL currents of 150 mA and 20 mA, respectively).

Fig. 5. Spectral interference of palladium (324.3 nm) on copper (324.7 nm, 10 μg/ml) emission: A, conventional chopped emission; B, double modulation; C, single modulation. Vertical axis is apparent signal from copper emission.

TABLE 2

Detection limits and S/B ratios obtained with the boxcar-integrator detector system

CCL peak driving current (mA)	Sampling position on waveform	S/B (at 10 $\mu g\ ml^{-1}$)		Detection limits ($\mu g\ ml^{-1}$)	
		Cu	Ag	Cu	Ag
20	Current pulse center[a]	0.34	0.38	1.3	1.6
20	0.02 ms after pulse[b]	9.20	—	2.7	—
150	Current pulse center[a]	0.02	—	29.0	—
150	0.02 ms after pulse[b]	2.66	—	1.6	—

[a]Point *b* on Fig. 2. [b]Point *c* on Fig. 2.

Table 2 also shows detection limits for copper obtained at different current levels and sampling times. The detection limits follow the trends expected from the previous discussion. The best results were obtained by sampling in the middle of the 20-mA pulse, with very similar detection limits obtained by sampling at the end of the 150-mA pulse. Signals sampled at the end of the current pulse showed more noise than those obtained by sampling in the middle. The reason for this behavior is not clear at present.

Lock-in demodulation

The SLM experiment was repeated with a lock-in amplifier and 20-mA current pulses, with a 50% duty cycle (100-Hz repetition rate). In addition, a double-modulation scheme was used, in which the lamp current was modulated with a 110-Hz square wave and with an optical chopper operated at 27 Hz inserted between the ICP and the CCL. Double modulation can be detected at either the sum or difference between the two modulation frequencies; it discriminates against any event (here, CCL emission and unmodulated ICP emission) that is not affected by both modulation processes. The SLM signal was demodulated at the sum frequency. For high modulating current and low signal levels, the modulating-atom-cloud emission can produce the limiting noise in the SLM technique. It was for this reason that the double modulation scheme was investigated.

The ability of the SLM system to discriminate between analyte emission and overlapping emission lines of matrix concomitants is shown in Fig. 5, which examines the spectral interference of the Pd I 324.27-nm line on Cu I emission at 324.75 nm. For the conventional (chopper-based) emission experiment (curve A), the spectral interference is substantial. In contrast, double- and single-modulation SLM experiments (curves B and C, respectively) are free from the spectral interference.

Spectral interference from ICP background emission can be eliminated similarly. The spectral bandpass of an SLM system is limited by the absorption linewidth of the atoms in the modulating atom reservoir, and not by that of the spectral dispersion device that is used. This fact is illustrated in Fig. 6.

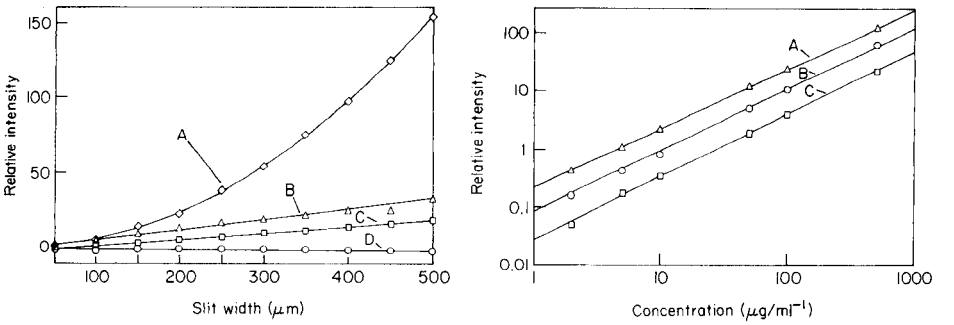

Fig. 6. The effect of slit width on various signals (324.7 nm). A and D, blank aspirated with conventional chopped emission and SLM systems, respectively; B and C, 100 μg ml^{-1} Cu aspirated with conventional chopped emission and SLM systems, respectively. Curves B and C have been background-corrected.

Fig. 7. Working curves for copper: A, with conventional chopped emission; B, with double modulation; C, with single modulation.

Curve A is the conventional (chopper-based) background signal measured at the Cu I wavelength (324.75 nm) and with a blank aspirated into the ICP; the signal increases approximately with the square of slit width as expected for broad-band emission. Curve B is the background-corrected conventional signal from a 100 μg ml^{-1} copper solution, and shows the linear relationship with slit width expected for line emission. Curves C and D are the results of similar experiments done with the SLM system. Curve D shows that the SLM-detected background signal does not increase, indicating that the effective spectral bandpass of the SLM system is limited by the absorption line-width of the modulating atoms. The slight negative slope of curve D is due to emission from the modulating atoms (in the CCL), which occurs 180° out-of-phase with the SLM signal. This phase shift causes any residually detected emission from the modulating atoms to appear as a negative background signal. Curve C is the background-corrected SLM signal that arises from a 100 μg ml^{-1} copper solution aspirated into the ICP, and again shows the linear dependence on slit width expected for a line source.

Figure 7 compares working curves obtained with the single-modulation and double-modulation detection schemes. For comparison, a conventional working curve generated with the optical chopper operated at 27 Hz is also shown. All curves show good linearity over the concentration range studied. A comparison of curves A (chopper) and C (single modulation) shows that the signal level is much lower for the SLM system. This behavior is apparent also in Fig. 6. The chopper data were obtained with the CCL left in the optical path, so that the difference in signals is not attributable to the limiting aperture of the CCL. Instead, the lower SLM signal is caused by a necessarily limited degree of absorption, which is a result of the small volume of the atom cloud in the CCL. The larger signal levels shown for curve B (double modulation) are a result of increasing the PMT gain. Increased PMT gain was

TABLE 3

Detection limits and S/B ratios obtained with the single- and double-modulation systems

Detection method	S/B (at 10 μg ml^{-1})		Detection limits (μg ml^{-1})	
	Cu	Ag	Cu	Ag
Double modulation	116.1	29.9	0.27	0.33
Single modulation	0.3	0.3	0.43	0.18
Chopped emission	37.6	25.0	0.04	0.10

possible with the double-modulation system because of the significantly reduced background signal. Table 3 lists detection limits and signal-to-background ratios for the single- and double-modulation arrangements.

The ability of the double-modulation system to reject the background emission of the CCL is clearly shown by the S/B ratios in Table 3. The S/B ratios for double modulation are over two orders of magnitude higher than for the single modulation, but detection limits are not greatly improved for reasons explained earlier [17]. The S/B ratios are improved also over those of the optical chopper, although the improvement is slight because of the much larger signals obtained with the chopper-based detection system.

Conclusions

The performance of a simplified device for producing selective spectral-line modulation (SLM) has been explored. The device is much simpler in terms of equipment and operation than any of the previous SLM arrangements. Some of the advantages of SLM systems include easier spectral-line identification, an absolute lock to desired analytical wavelengths, and reduction of the detrimental effect of spectral interferences from both source background and sample concomitants [17].

Because the modulation here is controlled electronically, higher modulation frequencies (limited only by the atom cloud decay time) can be used. Also, the modulation waveform can be easily varied. However, the aperture through the CCL cathode in the current system is very small (2 mm) and limits the optical throughput of the device. Sensitivity is consequently sacrificed.

The boxcar integrator performed well in the SLM system, but suffered from several drawbacks. The dynamic range of the boxcar integrator was very limited, and the instrument had no provision for offset. In addition, the boxcar integrator detected only a very small temporal segment of the CCL pulse; increasing the duty cycle of the lamp should raise signal levels and lead to improved detection limits. The system with the lock-in amplifier did yield better detection limits; however, the sensitivity of the SLM system was still lower than that of the optically-chopped system.

The prominent feature of the CCL/SLM system is its simplicity and ruggedness. The device lends itself well to the concept of a very simple

direct-reading spectrometer that could be used for the routine analysis of multi-element samples. The idea is again similar to the concept of Sullivan and Walsh [23] and would incorporate an array of lamps and detectors. A separate detector would be placed behind each CCL for monitoring the desired elemental signal, or a multiplexed system of fiber-optic cables, each leading from an individual CCL, could be used with a single detector. Because the absorption linewidth of the modulating atoms will determine the effective spectral bandpass of the optical system, bandpass filters placed between the lamps and the detectors could be used to eliminate much of the excess of radiation from the emission source and would obviate the need for a monochromator. The double-modulation system could be easily constructed by surrounding the emission source with a cylindrical chopper.

The CCL is interesting also from a fundamental point of view. This lamp design is ideally suited for the study of atom-cloud formation by sputtering processes. These processes could easily be probed by spatially and temporally resolving the absorption phenomena in the bore of the cylinder.

The authors greatly appreciate the generosity of the Hamamatsu Corp. who provided the cylindrical cathode lamp used in this study. This study was supported in part by the National Science Foundation through grant CHE 83-20053, the Office of Naval Research, and American Cyanamid.

REFERENCES

1 L. Bezur, J. Marshall and J. M. Ottaway, Spectrochim. Acta, Part B, 39 (1984) 787.
2 M. S. Epstein and T. C. O'Haver, Spectrochim. Acta, Part B, 30 (1975) 135.
3 T. C. Rains and O. Menis, Anal. Lett., 7 (1974) 715.
4 J. S. Maines, D. G. Mitchell, J. M. Rankin and B. W. Bailey, Spectrosc. Lett., 5 (1972) 251.
5 S. R. Koirtyohann, E. D. Glass, D. A. Yates, E. J. Hinderberger and F. E. Lichte, Anal. Chem., 49 (1977) 1121.
6 W. Snelleman, T. C. Rains, K. W. Yee, H. D. Cook and O. Menis, Anal. Chem., 42 (1970) 394.
7 V. G. Mossotti, F. N. Abercrombie and J. A. Eakin, Appl. Spectrosc., 25 (1971) 331.
8 M. Marinkovic and T. J. Vickers, Anal. Chem., 42 (1970) 1613.
9 V. Bojovic and A. Antić-Jovanovic, Spectrochim. Acta, Part B, 27 (1972) 385.
10 A. Antić-Jovanovic, V. Bojovic and M. Marinkovic, Spectrochim. Acta, Part B, 25 (1970) 405.
11 W. Trampish and R. Herrmann, Spectrochim. Acta, Part B, 24 (1969) 215.
12 K. Rudiger, B. Gutsche, H. Kirchhof and R. Herrmann, Analyst, 94 (1969) 204.
13 W. Lang, Spectrochim. Acta, Part B, 23 (1967) 471.
14 J. E. Patterson, Anal. Chim. Acta, 125 (1981) 193.
15 A. W. Steele and G. M. Hieftje, Appl. Spectrosc., 40 (1986) 1110.
16 A. W. Steele and G. M. Hieftje, Appl. Spectrosc., 40 (1986) 1127.
17 S. W. Downey and G. M. Hieftje, Anal. Chim. Acta, 141 (1982) 193.
18 S. W. Downey, J. G. Shabushnig and G. M. Hieftje, Anal. Chim. Acta, 121 (1980) 165.
19 R. L. Cochran and G. M. Hieftje, Anal. Chem., 50 (1978) 791.
20 R. L. Cochran and G. M. Hieftje, Anal. Chem., 49 (1977) 98.
21 C. T. J. Alkemade and J. M. W. Milatz, Appl. Sci. Res., 4 (1955) 289.

22 A. W. Steele and G. M. Hieftje, Appl. Spectrosc., 40 (1986) 1117.
23 J. V. Sullivan and A. Walsh, Appl. Opt., 7 (1968) 1271.
24 R. Rezaaiyaan, G. M. Hieftje, H. Anderson, H. Kaiser and B. Meddings, Appl. Spectrosc., 36 (1982) 627.
25 J. P. Walters, in D. M. Hercules, G. M. Hieftje, L. R. Snyder and M. A. Evenson (Eds.), Contemporary Topics in Analytical and Clinical Chemistry, Vol. 3, Plenum, New York, 1978, Chap. 3.
26 J. A. Dean and T. C. Rains, Flame Emission and Atomic Absorption Spectrometry, Vol. II, M. Dekker, New York, 1969, Chap 13.

Analytica Chimica Acta, 200 (1987) 551—557
Elsevier Science Publishers B.V., Amsterdam — Printed in The Netherlands

MULTI-ELEMENT SIMPLEX OPTIMIZATION FOR INDUCTIVELY-COUPLED PLASMA/ATOMIC EMISSION SPECTROMETRY WITH A PLASMA TORCH HAVING A WIDE-BORE INJECTOR TUBE
Part 1. Conditions for Optimum Detection Limit

LES EBDON*

Department of Environmental Sciences, Plymouth Polytechnic, Drake Circus, Plymouth PL4 8AA (Great Britain)

ROBERT C. CARPENTER[a]

Central Research Establishment, Home Office Forensic Science Service, Aldermaston, Berkshire RG7 4PN (Great Britain)

(Received 27th April 1987)

SUMMARY

An objective function, based on signal-to-background ratio measurements, with a variable step-size simplex procedure is used to optimize operating conditions for multi-element determinations by inductively-coupled plasma/atomic emission spectrometry. When a typical 10-element solution was used, the optimization produced small but significant improvements in limits of detection. The ease with which optimal multi-element instrumental conditions were identified is attributed to the compact analytical zone of the plasma produced when a wide-bore (2 mm i.d.) injector tube is used.

Inductively-coupled plasma/atomic emission spectrometry (ICP/AES) is a multi-element technique which is generally operated with a single set of analytical conditions. In practice, true multi-element optimization is rarely applied and compromise conditions obtained from the literature, manufacturers or as a result of single-element studies are preferred. The versatility of the ICP source is such that good performance can generally be obtained.

---

*Les Ebdon obtained his B.Sc. and Ph.D. at Imperial College, London, the latter on analytical atomic spectroscopy under the supervision of Professor T. S. West and (the late) Professor G. F. Kirkbright. He later worked at the University of Makerere, Uganda, and at Sheffield City Polytechnic. He was appointed Reader in Analytical Chemistry at Plymouth Polytechnic in 1981 and given the personal title of Professor of Analytical Chemistry in 1986. He was awarded the 13th SAC Silver Medal by the Analytical Division of the Royal Society of Chemistry in 1986. The author or joint author of about 100 research papers and books, his research interests include plasma and atomic absorption spectrometry, chromatography (for trace metal speciation), sensors and environmental monitoring.

[a]Present address: Home Office Forensic Science Laboratory, Aldermaston, Berks RG7 4PN, Great Britain.

0003-2670/87/$03.50

However, only a comprehensive multi-element optimization can ensure that the best performance is achieved for a particular application.

The establishment of compromise conditons for multi-element optimization has been reported by several workers. Boumans and De Boer [1] commented on the ideal nature of (argon) ICP/AES for simultaneous multi-element determinations and presented a set of compromise conditions. Greenfield and Burns [2] compared the performance of argon-cooled and nitrogen-cooled torches under optimized conditions. Berman and McLaren [3] advocated the use of "ion-line" conditions as a good compromise for obtaining optimum limits of detection and reduction of interference. Similar conclusions were also drawn by Boumans and Lux-Steiner [4] and Bamiro et al. [5]. There has been considerable controversy concerning optimal conditions for ICP/AES. In part, this arose because of the interrelated nature of the operating parameters in the ICP and the consequent need to use multivariate techniques for rigorous optimization. Ebdon et al. [6, 7] showed that the variable step-size simplex procedure was well suited to the true optimization of ICP/AES. In their studies, the argon ICP appeared to be more suitable for multi-element analysis as optimal conditions for different elements were more similar than those obtained with a nitrogen-cooled plasma. Montaser et al. [8] reached similar conclusions in their studies.

Moore et al. [9] conducted univariate searches on a nitrogen-cooled argon plasma and identified optimum conditions for atomic and ionic lines and for compromise analysis. The application of simplex optimization for establishing simultaneous multi-element conditions such as are required when a polychromator is used was pioneered by Leary et al. [10]. They reported the application of an objective function for the multi-element simplex optimization of an argon plasma. The forward power and observation height were optimized for a set of five elements and the simplex was terminated after 30 moves. This technique was used by Montaser et al. [11] to optimize a torch with a low gas-flow. Six parameters were optimized for a set of 20 elements and the performance of this torch shown to be comparable to that of a conventional ICP. Moore et al. [12] optimized a nitrogen-cooled argon ICP with the same objective function but added a second stage for minimization of ionization interference effects. These workers achieved an analytically useful plasma which combined good detection limits and minimum interference effects.

The potential of a wide-bore injector tube for multi-element determinations under compromise conditions has been demonstrated [13]. The more compact analytical region produced in the ICP by using a 2-mm-bore injector tube in an otherwise conventional Fassel torch decreased the variation in optimal conditions for different elements. Given the importance of multi-element analysis by ICP/AES using a polychromator and direct-reading spectrometer, an investigation of this configuration by simplex optimization appeared timely. This paper reports the evaluation of a 10-element, 3-parameter simultaneous multi-element simplex optimization study for this torch.

EXPERIMENTAL

An argon ICP (Plasma-Therm, Kreesson, NJ) was used. Signal detection was by means of a 1-m 32-channel polychromator (Optical Emission Services, Milton Keynes, England) fitted with a holographic diffraction grating. A graphite-loaded plastic (Ryton) cross-flow nebulizer and spray chamber were used with a demountable torch fitted with an alumina injector tube (Perkin-Elmer).

Multi-element test solutions were prepared from 1000 mg l^{-1} stock solutions (BDH) in nitric acid (5% v/v).

OPTIMIZATION

A number of optimization schemes could be selected but the one chosen for this work was that the element concentrations in a test solution should be similar to the particular samples requiring analysis. This plan is obviously weighted towards the trace elements, whereas the major element responses can change markedly without the overall performance being affected.

Successful multi-element optimization requires the selection of a suitable objective function to represent the composite response from the group of elements of interest. The general weighted-average incorporating the reciprocal of the signal-to-background ratio (SBR^{-1}), as reported by Leary et al. [10], appeared simple to apply and as elegant as the simplex optimization itself. This calculation takes the form:

$$F = n / \sum_{i=1}^{n} (\mathrm{SBR})_i^{-1}$$

where F is the objective function and n is the number of analyte elements.

Preliminary experiments were done with a 4-element, 3-parameter simplex optimization (observation height, power and injector gas flow); as in previous work [13] the auxiliary gas flow was set at zero and the plasma gas flow at 18 l min^{-1}. It was established that the SBR^{-1} function was very sensitive to a 10% change in trace-element response but insensitive to a 50% change in minor-element response. Incorporation of a $SBR^{-0.7}$ function was slightly less sensitive to the trace-element change but responded to the minor-element change. Therefore, the following calculation was used, as its performance appeared more appropriate for these studies:

$$F = n / \sum_{i=1}^{n} (\mathrm{SBR})_i^{-0.7}$$

A set of ten elements was selected to test the optimization routine. These were not derived from a particular sample type but represent a compilation of elements encountered in forensic analyses. The element set is shown in Table 1 together with concentrations and other fundamental data. It can be

TABLE 1

Element set for multi-element simplex optimization

Element	Line and wavelength (nm)		Concentration ($\mu g\ ml^{-1}$)	Difficulty of excitation (eV)	Classification [14]
Tl	I	351.9	1	4.5	Soft
Zn	I	213.8	1	5.8	Hard
Pb	II	220.3	10	14.7	Hard
Mn	II	257.6	0.005	12.2	Hard
Fe	II	259.9	0.05	13.0	Hard
Mg	I	285.2	0.5	4.3	Soft
Al	I	308.2	5	4.0	Soft
Ti	II	334.9	0.05	11.1	Hard
Sr	II	407.8	0.05	8.7	Soft
Ba	II	455.4	0.01	7.9	Soft

seen that these elements range from a difficulty of excitation of 4.0 eV for aluminium to 14.7 eV for lead. In addition, five of these element lines could be classified as "soft" and five as "hard", according to the criteria of Boumans and Lux-Steiner [14].

As in previous work [13], a 3-parameter optimization was used and three optimization experiments were conducted over a 3-week period. As the plasma gas flow rate has little effect on the optimal SBR this was set at 18 l min^{-1}. As an auxiliary or intermediate gas degrades the optimal performance, it was omitted [13]. The power quoted represents the indicated forward power, and the height of observation is the distance from the top of the load coil to the centre of a 4-mm vertical-slit viewing window [13]. An average time of 3.5 h was required for manual optimizations consisting of about 18 moves. The simplex conclusions are shown in Table 2 and demonstrate acceptable precision.

In order to test the performance of the simplex optimization, the limits of detection were evaluated on three days under both the mean simplex conditions and the compromise conditions previously used in this laboratory (Table 3). The multi-element simplex conditions demonstrate an overall improvement in limits of detection, though only minimal improvements were obtained for manganese and thallium, which were the trace elements. In all probability, the data obtained for these elements, with both sets of conditions, are approaching the single-element optimum obtainable for this particular configuration of sample introduction/torch/spectrometer (see below). Under the simplex optimized conditions, the limits of detection at the "soft" lines were improved by an average of 26% and the "hard" lines by 14%. This could be a characteristic of the low observation region in this plasma but the overall improvement confirms the earlier observations that this compact argon plasma is very appropriate for compromise multi-element determinations.

TABLE 2

Optimal conditions found in three separate multi-element simplex optimization experiments

Injector flow rate (l min^{-1})	Power (kW)	Height (mm)
0.89	0.55	11
0.85	0.55	9.5
0.85	0.50	9.5
Mean 0.87	0.55	10

TABLE 3

Comparison of limits of detection

Element	Limit of detection[a] (μg ml^{-1})		Element	Limit of detection[a] (μg ml^{-1})	
	Multi-element simplex conditions[b]	Laboratory compromise conditions[c]		Multi-element simplex conditions[b]	Laboratory compromise conditions[c]
Tl	0.18	0.19	Mg	0.0015	0.002
Zn	0.0015	0.002	Al	0.035	0.05
Pb	0.045	0.055	Ti	0.001	0.001
Mn	0.0008	0.001	Sr	0.00009	0.0001
Fe	0.004	0.005	Ba	0.0004	0.001

[a]Mean of 3 determinations, 3σ criterion. [b]See Table 2. [c]Injector flow rate 1.15 l min^{-1}; power 1.0 kW; height 18 mm.

An alternative to the multi-element simplex routine could be simplex optimization for the most demanding of the trace elements in a test solution and the subsequent use of these "single-element" conditions for the full multi-element procedure. Both thallium and manganese (the least prominent elements in the multi-element study) were individually optimized in this way. The optimal conditions together with limits of detection obtained are shown in Table 4. These results are similar to those previously obtained with the multi-element simplex and thus confirm its successful operation. The limits of detection obtained for the individual optimizations suggest that this approach could be a viable alternative to a full multi-element optimization. However, the time required for two individual optimizations (ca. 3 h) is only slightly shorter than for the full 10-element optimization which is inherently superior for multi-element work.

The results obtained from the individual simplex optimizations are very interesting because of the similarity in optimum conditions for a "soft" line with a "difficulty of excitation" (sum of the ionization potential, where appropriate, and the excitation potential) of 4.5 eV (Tl I) and a "hard"

TABLE 4

Individual simplex optimization for two trace elements

Element	Injector flow rate ($l\ min^{-1}$)	Power (kW)	Height (mm)	Detection limit ($\mu g\ ml^{-1}$)
Mn	0.86	0.65	11.5	0.0008
Tl	0.89	0.55	11.0	0.15

line with a "difficulty of excitation" of 12.2 eV (Mn II). The maximum intensities of "hard" lines have been reported at higher positions in plasmas than "soft" lines [15, 16]. Spectral studies by Kawaguchi et al. [15] and Blades and Horlick [16] indicated the presence of two regions in the aerosol channel of an argon plasma. A lower, thermal region was identified where "soft" line behaviour was observed and a higher, non-thermal region where "hard" line behaviour was observed.

The optimizations reported here are all based on measurements of the signal-to-background ratio (SBR), which is of greater analytical value than maximum intensity. The relationship between maximum signal and maximum SBR depends on the plasma background and thus similar optimum regions may not be obtained. However, the argon plasma used here is unlikely to differ from the previously reported systems except in its more compact useful region as a result of the larger-bore injector tube.

Occasional difficulties were experienced in terminating these simplex optimization experiments, mainly because of the gently sloping response surfaces which enabled similar performance to be obtained for different instrumental conditions. These problems were investigated further by examining the response surfaces for several elements. The injector flow rate (0.87 $l\ min^{-1}$) obtained from the multi-element optimization was used; the observation height was varied between 8 and 12 mm and the power was varied between 0.4 and 0.9 kW. The response surfaces (using SBR) obtained for manganese and thallium are shown in Fig. 1. These (and other) element maps confirmed the presence of gently sloping response surfaces, except below 0.5 kW where the response decreased rapidly. Ridges and plateaux could be identified, which explained the similar performances obtainable at differing instrumental conditions. Multiple optima were not detected during these experiments, which agrees with the findings of numerous simplex optimization experiments with this plasma system. Response surface mapping is not a viable alternative to simplex optimization because of the large number of parameters involved. However, the technique can be used to visualize a section of the response surface to assist the interpretation of results.

Conclusions

An ICP torch fitted with a wide-bore injector tube has been shown to be most appropriate for multi-element analysis because of its compact useful region. By using a suitable objective function, a 10-element 3-parameter

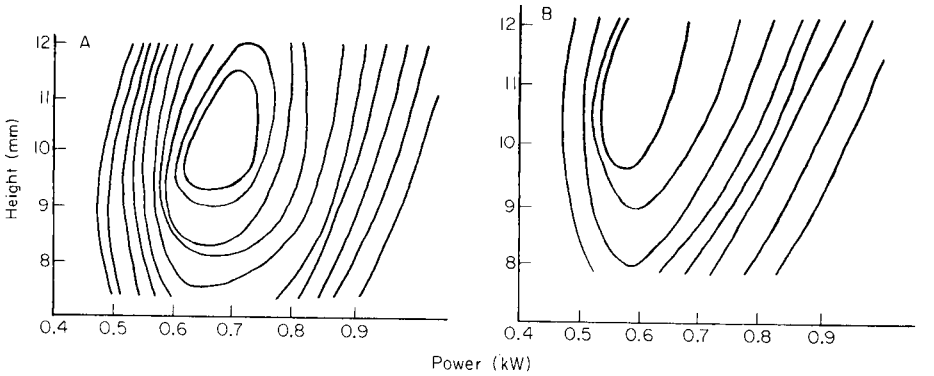

Fig. 1. Response surfaces showing the influence of observation height and power on the signal-to-background ratio: (A) manganese; (B) thallium. Injector-gas flow rate 0.87 l min^{-1}.

simplex optimization can be achieved for this system. The multi-element conditions are reproducible and provide small but consistent improvements in limits of detection compared to previous data. The manual optimization routine required ca. 3.5 h for completion. A suitable computer program would ensure more rapid optimization particularly if it was part of a suite of programs supplied by the instrument manufacturer.

REFERENCES

1 P. W. J. M. Boumans and F. J. De Boer, Spectrochim. Acta, Part B, 30 (1975) 309.
2 S. Greenfield and D. T. Burns, Anal. Chim. Acta, 113 (1980) 205.
3 S. S. Berman and J. W. McLaren, Appl. Spectrosc., 32 (1978) 372.
4 P. W. J. M. Boumans and M. Ch. Lux-Steiner, Spectrochim. Acta, Part B, 37 (1982) 97.
5 F. O. Bamiro, D. Littlejohn, J. Marshall and J. M. Ottoway, Anal. Proc., 20 (1983) 602.
6 L. Ebdon, M. R. Cave and D. J. Mowthorpe, Anal. Chim. Acta, 115 (1980) 179.
7 L. Ebdon, in R. M. Barnes (Ed.), Developments in Atomic Plasma Spectrochemical Analysis, Heyden, London, 1981.
8 A. Montaser, V. A. Fassel and J. Zalewski, Appl. Spectrosc., 35 (1981) 292.
9 G. L. Moore, A. E. Watson and G. M. Russel, NIM Report 2116, Council for Mineral Technology, Randbury, South Africa, 1981.
10 J. J. Leary, A. E. Brookes, A. F. Dorrzapf and D. W. Golightly, Appl. Spectrosc., 36 (1982) 37.
11 A. Montaser, G. R. Huse, R. A. Wax, S. K. Chan, D. W. Golightly, J. S. Kane and A. F. Dorrzapf, Anal. Chem., 56 (1984) 283.
12 G. L. Moore, P. J. Humphries-Cuff and A. E. Watson, Spectrochim. Acta, Part B, 39 (1984) 915.
13 R. Carpenter and L. Ebdon, J. Anal. At. Spectrom., 1 (1986) 265.
14 P. W. J. M. Boumans and M. Ch. Lux-Steiner, Spectrochim. Acta, Part B, 37 (1982) 97.
15 H. Kawaguchi, T. Ito and A. Mizuike, Spectrochim. Acta, Part B, 36 (1981) 615.
16 M. W. Blades and G. Horlick, Spectrochim. Acta, Part B, 30 (1975) 309.

Analytica Chimica Acta, 200 (1987) 559—571
Elsevier Science Publishers B.V., Amsterdam — Printed in The Netherlands

CHROMATOGRAPHIC RETENTION OF MOLYBDENUM, TITANIUM AND URANIUM COMPLEXES FOR REMOVAL OF SOME INTERFERENCES IN INDUCTIVELY-COUPLED PLASMA MASS SPECTROMETRY

S.-J. JIANG, M. D. PALMIERI, J. S. FRITZ and R. S. HOUK*

Ames Laboratory, U.S. Department of Energy, and Department of Chemistry, Iowa State University, Ames, IA 50011 (U.S.A.)

(Received 1st April 1987)

SUMMARY

Complexes of molybdenum(VI) or titanium(IV) with *N*-methylfurohydroxamic acid (*N*-MFHA) are retained on a column packed with polystyrene/divinylbenzene. At the pH values chosen, copper, zinc and cadmium are washed rapidly through the column and are detected by inductively-coupled plasma mass spectrometry (i.c.p./m.s.) without interference from metal oxide ions of titanium or molybdenum. Detection limits are 1 to 2 $\mu g\ l^{-1}$, and analyte recoveries are essentially 100%. The resin capacity for the titanium and molybdenum complexes is sufficient for several hundred injections, and the complexes can be readily washed from the column. Uranium(VI) also forms a stable complex with *N*-MFHA, and ionization interference caused by excess of uranium can be avoided by chromatographic removal of the uranium complex. Various other potentially interfering elements with aqueous oxidation states of +4 or higher (e.g., Sn, W, Hf or Zr) could also be separated by this technique.

Inductively-coupled plasma mass spectrometry (i.c.p./m.s.) is a very sensitive technique for elemental and isotopic determinations [1, 2]. Most elements yield primarily singly charged, monatomic ions (M^+) so that analyte spectra are simple with limited overlap between peaks of different elements. The most abundant molecular species observed from analytes are the diatomic oxide ions, MO^+, which cause overlap interferences with analytes 16—18 *m/z* units above M^+. Formation of metal oxide ions is a problem mainly for elements such as tungsten and the rare earths that form refractory oxide species in high-temperature media. Such elements that are also multi-isotopic generate the worst interference problems. Two particular interferences that have been noted are the overlap of MoO^+ with all the useful isotopes of cadmium [3], and overlap of TiO^+ with both copper isotopes and the most abundant zinc peak [4]. Some elements also yield metal hydroxide ions (MOH^+), which further complicate matters [5—7].

At present, operating conditions can generally be identified for which the observed ratio MO^+/M^+ is 4% or less for elements that form the more stable oxide ions [1, 2, 8]. As a rule of thumb, therefore, the error induced by oxide or hydroxide ion formation is significant only when the analyte is

0003-2670/87/$03.50

present at a concentration of a few percent or less relative to that of the interfering element. In many cases, the oxide contribution can be evaluated and subtracted from the total signal at the analyte *m/z* value to correct for the interference [6]. Another conceivable approach is to find plasma operating conditions that completely suppress MO^+. This measure may be realistic for "dry" sample introduction devices such as laser ablation [9] or arc nebulization [10]. For introduction of aqueous aerosols, it is difficult to reduce the refractory metal-oxide ions to less than 0.1% of the M^+ peak without having the plasma discharge strongly to the sampling orifice. A strong discharge generates ions from the orifice, yields excessive numbers of doubly charged ions, and causes high ion-kinetic energies and other problems [5, 11, 12]. It has recently been reported that use of a cooled spray chamber, aerosol desolvation, and/or a mixed argon/nitrogen plasma [13—15] helps reduce metal oxide levels somewhat. However, with the present performance of i.c.p./m.s. instrumentation, the analyst simply tolerates metal oxide ions. The resulting interferences are usually not severe, but they sometimes limit the accuracy achievable for some elements in certain types of samples.

An alternative approach to alleviating oxide interferences is to separate the interfering element(s) chemically or chromatographically so that they never reach the plasma. Use of chromatographic conditions that retain only the interferent and allow the analyte to flow freely through the column would accomplish this on a rapid time-scale. The previous work of Al-Biaty and Fritz [16] on the properties of the chelating reagent *N*-methylfurohydroxamic acid (*N*-MFHA) indicates that this compound is potentially useful for these separations. Conditions can be adjusted such that only ions with metals in highly positive oxidation states (usually +4 or higher) are complexed by *N*-MFHA. Under these conditions, ions with metals in lower oxidation states are complexed only to a slight extent or not at all. The metal complexes are readily retained by a short column containing polystyrene/divinylbenzene resin; the uncomplexed metal ions are not retained and wash rapidly through the column [16]. Several metals that can cause significant oxide interference in i.c.p./m.s. also form stable complexes with *N*-MFHA at pH values that are sufficiently acidic that other potential analyte elements are not complexed. In the present work, titanium(IV) and molybdenum(VI) are selectively removed from analytical samples by complexation with *N*-MFHA and sorption on a resin column. Interference from TiO^+ and MoO^+ in the determination of copper, zinc, and cadmium by i.c.p./m.s. is thereby avoided.

Complexation of metals with *N*-MFHA is also potentially valuable for attenuating so-called "ionization interferences" in i.c.p./m.s. [15, 17—21]. Although virtually any element is capable of inducing such an interference, uranium can be one of the worst interferents [18, 19, 21]. Furthermore, uranium oxide tends to deposit on the sampling cone and plug the sampling orifice to a greater extent than many other elements. If these deleterious

effects could be circumvented, then i.c.p./m.s. would be very valuable for determination of trace impurities in uranium [21] because the mass spectrum of uranium is far simpler than its optical emission spectrum [22]. The present work also shows that uranium(VI) can be readily complexed by *N*-MFHA and retained at a pH value that permits elution and determination of analyte elements such as rare earths.

EXPERIMENTAL

Apparatus

The i.c.p./m.s. device (ELAN Model 250, Sciex) has been described previously [21, 23]; for the present work, the upgraded ion-optical system provided by Sciex was used. Operating conditions (Table 1) were optimized by the procedure described previously [21] and were generally similar to those used for other liquid chromatographic (l.c.) separations with i.c.p./m.s. detection [24].

The sample introduction system consisted of a dual-piston pump (Model 2010, Varian), an injection valve and loop (50 μl unless stated otherwise), and a Hamilton PRP-1 column (150 mm long, 4.1 mm i.d., 10-μm diameter particles). The effluent from the column (1.2 ml min^{-1}) flowed into a continuous-flow ultrasonic nebulizer [26]; the resulting aerosol was desolvated with a heating chamber at 200°C and a condensor at 0°C before being injected into the plasma. The dead volume after the column was approximately 13 μl in the liquid phase [24].

TABLE 1

Experimental parameters

ICP torch	Ames Laboratory design [25]. Outer tube extended to 40 mm from inner tubes
Argon flow rates (l min^{-1}): outer	14
auxiliary	0.8
aerosol	1.2
Forward power	1.25 kW
Sampling position	22 mm from load coil, on center
m/z Values monitored	
Ti	48
Cu	63
Zn	64 or 66
Mo	98
Cd	114
Tb	159
U	238
Data acquisition	Multiple ion monitoring [21]. Three measurement positions per peak spaced 0.1 *m/z* unit about peak top. Dwell time, 0.1 s at each measurement position. Total measurement time, 0.5 s per peak.

Reagents, solvents, standards and samples

N-MFHA was prepared by the procedure outlined previously [16]. The starting material was 2-furoyl chloride, which is a volatile irritant and should be handled with eye protection in a hood with adequate ventilation.

Solutions of molybdenum, titanium, cadmium, copper, and zinc were prepared by diluting aliquots of commercial stock solutions (Fisher Scientific). For isotope-dilution experiments, isotopically enriched cadmium (as CdO, 96.53 atom % ^{116}Cd) and copper (as copper metal, 99.70 atom % ^{65}Cu) were obtained from Oak Ridge National Laboratory and dissolved in 1% (v/v) nitric acid in deionized-distilled water. Aliquots of these stock solutions were mixed with the standard solutions in known amounts. Uranium solutions were prepared from $UO_2(NO_3)_2$ (Fisher Scientific). Rare-earth solutions were diluted from stock nitrate solutions supplied by Ames Laboratory.

Deionized-distilled water with 2% (v/v) methanol (HPLC grade, Fisher Scientific) and *N*-MFHA was used as the eluent for the titanium and molybdenum separations. The *N*-MFHA concentration was generally 0.003 M, unless stated otherwise; in some experiments, a higher concentration of *N*-MFHA was necessary to keep the complexes in solution. The pH of the eluent was adjusted by adding concentrated nitric acid and/or ammonia liquor prior to the analysis. Molybdenum was separated from cadmium at pH 1.0; titanium was separated from copper and zinc at pH 2.2.

For uranium separations, the uranium(VI) complex with *N*-MFHA was retained at pH 5.0. The eluent was 1% methanol in distilled-deionized water with 0.001 M *N*-MFHA, 0.01 M pyridine, and sufficient nitric acid to achieve the desired pH. Excess of *N*-MFHA (2.4×10^{-3} M) was added to the samples before injection. EDTA (1×10^{-4} M) was also added to the samples to mask rare-earth analytes from the *N*-MFHA.

Several standard reference materials (SRM), for which oxide-ion interferences had been noted in previous i.c.p./m.s. studies [3, 4], were analyzed in the present work. These SRMs were the nickel base alloy BAS-346 (Bureau of Analyzed Samples, U.K.), and the marine sediments BCSS-1 and MESS-1 (National Research Council of Canada). The procedure used to dissolve the nickel base alloy required redistilled, concentrated aqueous nitric acid and hydrochloric acid and has been described elsewhere [27]. A similar procedure was used for the sediments. Naturally, the silica in these latter samples was not fully dissolved, so these digests were filtered and the filtrates were washed with 1 M HNO_3 several times.

After dissolution, the sample digests were diluted with deionized water so that the sample concentration was 0.4%. Quantification was done by standard additions to correct for any ionization interferences that may have occurred [4]. The sample and three spiked samples were analyzed in each case. Calibration was done by using the net heights of the chromatographic peaks.

Determination of the titanium concentration in the sediment solutions

indicated that only approximately 20% of the titanium was dissolved by the digestion procedure [28]. Analysis of these digests yielded good agreement between the certified and found results for copper and zinc, but the concentration of interferent was artificially low (approximately 3 mg l^{-1} titanium). To provide a more rigorous test of the separation procedure, fresh samples were digested and analyzed after being spiked with a titanium stock solution to bring the total titanium concentration to approximately 27 mg l^{-1}. This level was 10 mg l^{-1} higher than what would have been obtained if all the titanium in the original sample had dissolved.

Measurement of recovery and combining ratio of complex and metal

Solutions of copper, zinc and cadmium (250 ml, 1 mg l^{-1} each element) were complexed with *N*-MFHA (0.42 mM) at the desired pH. These solutions were passed through the column and the eluents collected. The collected eluents were then introduced continuously into the i.c.p. (i.e., the column was bypassed), and the concentrations of copper, zinc and cadmium were determined by m.s. The recovery was defined as the ratio of the count rate for the original solution to that for the solution that had gone through the column.

The combining ratio of *N*-MFHA with molybdenum(VI) was measured at pH 1.0 by a Job's plot method [29] using a conventional spectrophotometer (Model 552, Perkin-Elmer). The ratio of *N*-MFHA to titanium(IV) could not be determined at the pH value used (2.2) because of hydrolysis of titanium in those solutions containing an excess of this metal.

RESULTS AND DISCUSSION

Multiple ion chromatograms for titanium and molybdenum separations

For the operating conditions used for the plasma and mass spectrometer, the ratios TiO^+/Ti^+ and MoO^+/Mo^+ were 0.2% and 0.5%, respectively. A multiple ion chromatogram obtained for a sediment sample spiked with additional titanium is shown in Fig. 1. At the pH value indicated, the titanium (shown at $m/z = 48$) was efficiently retained by the column so that there was no overlap of TiO^+ isotope peaks with the copper and zinc peaks. For these chromatographic conditions, zinc eluted in the void volume slightly before copper. This difference was also apparent from Fig. 2, which shows multiple ion chromatograms for two zinc isotopes and one copper isotope for several injections of sample and spiked samples of the MESS-1 sediment for the standard additions experiment.

As shown in Fig. 3, cadmium at 0.1 mg l^{-1} was readily detected in the presence of a large excess of molybdenum (100 mg l^{-1}) because the *N*-MFHA complex of the latter was retained by the column. This separation was con-

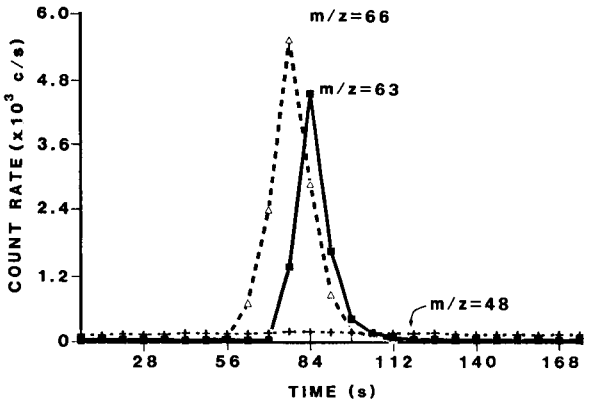

Fig. 1. Multiple ion chromatogram for single injection of MESS-1 spiked with additional titanium at pH 2.2. Concentrations (in mg l^{-1}) are Zn (0.76), Cu (0.10), Ti (27). Curves: (△) m/z = 66 (Zn); (■) m/z = 63 (Cu); (+) m/z = 48 (Ti). The sample was injected at zero time.

ducted under more acidic conditions than the titanium/copper/zinc separation for reasons described below. The retention time for cadmium in Fig. 3 was approximately the same as that for zinc in Fig. 2, indicating that both elements eluted with the void volume. At a pH of 1.0, the Job's plot study showed that the molar ratio of *N*-MFHA to molybdenum(VI) was 0.92/1, i.e., essentially 1/1. Injections of copper, zinc, and cadmium without *N*-MFHA present yielded the same peak heights as those shown in Figs. 1—3, i.e., the presence of *N*-MFHA in the eluent did not affect the signal for Cu^+, Zn^+, or Cd^+. For these 50-μl injections, the chromatographic peak heights were approximately 30% of the steady-state count rates, i.e., those obtained during continuous introduction of copper, zinc, or cadmium standards.

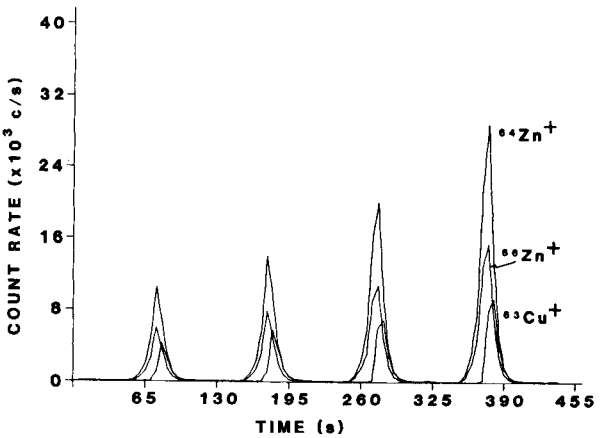

Fig. 2. Multiple ion chromatogram for one injection of MESS-1 (left) followed by injections of three MESS-1 samples with spikes added for standard additions.

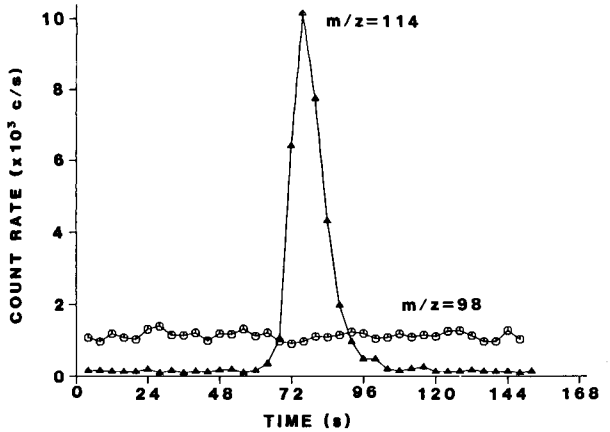

Fig. 3. Multiple ion chromatogram for single injection of solution containing 0.1 mg l^{-1} Cd and 100 mg l^{-1} Mo at pH 1.0. Curves: (▲) m/z = 114 (Cd); (○) m/z = 98 (Mo) with 120 counts s^{-1}.

The slightly elevated count rates at m/z = 48 in Fig. 2 and at m/z = 98 in Fig. 3 were due mainly to small amounts of titanium and molybdenum eluting continuously from the column. This was verified by observing the correct isotope ratios for these elements when the appropriate m/z regions were scanned. In addition, a very small peak was eluted for titanium (approximately 30 counts s^{-1} net).

Analysis of sediments and nickel base alloy

Several standard reference materials were analyzed by the chromatographic i.c.p./m.s. procedure. The results are compared with the certified values in Table 2. The results found for copper were slightly high and those for zinc were somewhat low for both sediments (MESS-1 and BCSS-1), but the deviations were within the uncertainties both for this particular measurement and those quoted by the suppliers of the reference materials. The cadmium in the final solution of the nickel base alloy (BAS-346) was only a factor of five above the detection limit (see below), yet the agreement with the certified value was reasonable. Except for the cadmium determination near the detection limit, the ranges cited in Table 2 were 2—4% relative to the mean. In each case, the standard additions curves were linear (correlation coefficient = 0.995—0.999).

An additional "analysis" was done by standard additions for a synthetic sample containing 500 mg l^{-1} titanium, 0.29 mg l^{-1} zinc, 300 mg l^{-1} molybdenum, and 0.020 mg l^{-1} cadmium. Five injections were made for each solution. The concentrations found were 0.30 mg l^{-1} for zinc and 0.021 mg l^{-1} for cadmium, also in good agreement with the expected values. The agreement in this experiment and in the analysis of the reference materials (Table 2) indicated that the small leakage of titanium and molybdenum from the column did not yield significant TiO^+ or MoO^+.

TABLE 2

Elemental analysis of standard reference materials with separation of Ti and Mo complexes

Sample	Element	Analyte concentration in original sample ($\mu g\ g^{-1}$)		Interferent concentration in final solution ($mg\ l^{-1}$)
		Found[a]	Certified	
BCSS-1 (sediment)	Cu	19.6 (18.9—20.0)	18.5 ± 2.7[b]	Ti[c] (27)
	Zn[d]	107 (105—111)	119 ± 12[b]	
MESS-1 (sediment)	Cu	26.8 (26.1—27.3)	25.1 ± 3.8[b]	Ti (27)
	Zn[d]	183 (181—187)	191 ± 17[b]	
BAS-346 (Ni base alloy)	Zn[e]	30 ± 1	29 ± 2[f]	Ti (200)
	Cd	0.48 ± 0.06	0.4 ± 0.05[f]	Mo (120)

[a]Mean of 3—4 determinations for all values found; ranges are given in parentheses. [b]Uncertainties are 95% confidence limits. [c]Titanium spike (ca. 24 mg l^{-1}) added to compensate for incomplete dissolution (see text). [d]Zinc monitored at m/z = 64. [e]Zinc monitored at m/z = 66 because of interference from $^{64}Ni^+$ and/or $^{32}S^{16}O_2^+$. [f]Uncertainties are absolute standard deviations; the data supplied with SRM use this measure of precision.

Calibration curves were obtained for a series of cadmium standards (0.01—50 mg l^{-1}), each with 500 mg l^{-1} molybdenum. These calibration curves were linear (correlation coefficient 0.999 or better) up to the maximum cadmium concentration injected. Similar calibration curves were obtained for copper and zinc in the presence of titanium. For repetitive injections of solutions at concentrations similar to those for the peaks shown in Figs. 1—3, the peak heights were reproducible to within a relative standard deviation of 3—7%, which is similar to the precision obtained in previous i.c.p./m.s. experiments with l.c. separations [24]. These calibration curves were extrapolated to evaluate detection limits, which were the solution concentrations necessary to yield net peak heights equivalent to three times the standard deviation of the background at each m/z value of interest. The detection limits were 2 $\mu g\ l^{-1}$ for copper, 1 $\mu g\ l^{-1}$ for zinc, and 1 $\mu g\ l^{-1}$ for cadmium at their most abundant isotopes. For zinc, the detection limit was a bit better than for copper because the background for copper at m/z = 63 was about 60 counts s^{-1} compared to 20 counts s^{-1} for zinc at m/z = 64 or 66, and the standard deviation of the background was higher by a factor of approximately three at m/z = 63 as well. The detection limits were poorer by a factor of approximately 20 than what would be obtained for continuous nebulization of aqueous standards under similar operating conditions. The reasons for this degradation of detection limits when l.c. separations are used with i.c.p./m.s. detection include injection of a discrete sample, dilution by the eluent, and use of methanol in the eluent [24].

Isotope-ratio determinations

Separation techniques are also of potential value for isotope-ratio determinations, in which all the isotopes of interest should be free of overlap interference. Therefore, some isotope-dilution experiments were done for copper, zinc, and cadmium both with and without the potential interferent present. These results are shown in Table 3. In each case, the evaluated isotope ratios were the same whether titanium or molybdenum was present or not, which further indicated that oxide ion interferences were indeed negligible. The precision (1—2.5% r.s.d.) was similar to that achieved previously during multiple ion monitoring of individual chromatographic peaks [24] but was poorer than the 0.5—1% r.s.d. typically obtained for isotope-ratio measurements for metals at mg l^{-1} levels during continuous introduction of aqueous solutions [23]. Somewhat poorer precision in isotope-ratio measurements is to be expected when transient sample-introduction techniques are used because the ions of interest are observed for a shorter time and averaging of nebulizer fluctuations, etc., is less efficient. The slight but reproducible differences between the found and expected values are similar to those commonly seen in isotope-ratio measurements with i.c.p./m.s. [23, 30] and were probably caused by some mass discrimination in ion extraction, focusing, mass analysis, and/or detection. This experiment indicated that copper, zinc and cadmium could be readily quantified in the presence of excess of titanium and molybdenum by isotope dilution [31] using the chromatographic i.c.p./m.s. procedure.

TABLE 3

Isotope-ratio determinations with separation of Ti and Mo complexes

Elements injected (concentration, mg l^{-1})	Ratio	Isotope ratios		
		Found[a]	R.s.d. (%)[a]	Expected[b]
Natural Cu (5)	$^{63}Cu/^{65}Cu$	2.28	2.0	2.24
Natural Cu (5) + Ti (200)	$^{63}Cu/^{65}Cu$	2.26	1.4	2.24
Natural Cu (5) + enriched Cu (2) + Ti (200)	$^{63}Cu/^{65}Cu$	0.983	0.9	0.978
Natural Zn (5)	$^{64}Zn/^{66}Zn$	1.82	2.4	1.76
Natural Zn (5) + Ti (200)	$^{64}Zn/^{66}Zn$	1.82	2.6	1.76
Natural Cd (5)	$^{114}Cd/^{116}Cd$	3.68	1.7	3.79
Natural Cd (5) + Mo (200)	$^{114}Cd/^{116}Cd$	3.69	2.4	3.79
Natural Cd (5) + enriched Cd (1) + Mo (200)	$^{114}Cd/^{116}Cd$	1.05	1.4	1.08

[a]Mean and relative standard deviation of five separate injections. [b]Based on accepted natural abundances.

Column capacities and recoveries

Capacities for titanium and molybdenum complexes were evaluated by performing multiple injections of standards at 1000 mg l^{-1} and obtaining the resulting breakthrough curves [16] by monitoring Ti^+ or Mo^+ with the mass spectrometer. The concentration of *N*-MFHA was 0.01 M. The measured capacity for molybdenum at pH 1 was 200 μmol; for titanium at pH 2.2, the capacity was 360 μmol. These values corresponded to approximately 400 injections of molybdenum and 360 of titanium for each element at 1000 mg l^{-1}. The actual mass of resin in this commercially obtained column was not known accurately but probably was about 0.5 g. After these capacity experiments, the resin was readily regenerated by rinsing with 1 M HNO_3 in methanol at a flow rate of 1 ml min^{-1} for approximately one hour.

Several injections were also made with very high concentrations of molybdenum or titanium. For these experiments, the concentration of *N*-MFHA was increased to 0.03 M to keep the complexes in solution. The resin retained nearly all (99%) of the metal complexes for single injections of 11 300 mg l^{-1} molybdenum or 2000 mg l^{-1} titanium. However, the higher concentration of complexing agent in the mobile phase plugged the torch tip (not the sampling orifice of the mass spectrometer), so that the ability of the resin to retain very large amounts of molybdenum or titanium was not of much practical value in the present study. The 1000 mg l^{-1} concentrations used in the capacity experiment represent a practical upper limit to the molybdenum and titanium levels that can be used with i.c.p./m.s. detection.

The recoveries for analyte elements were evaluated by the procedure described in the experimental section. For the molybdenum separation (at pH 1), the cadmium complex was 100% recovered. For the titanium separation (at pH 2.2), the recoveries were 104% for copper and 101% for zinc. The titanium complex was also retained efficiently at pH 3, but recoveries for copper and zinc were only 92—93%, so separations at pH 3 were not utilized further.

Alleviation of interference from uranium

A multiple ion chromatogram for several injections of terbium standards that also contained 100 mg l^{-1} uranium (as the complex in 1 mM *N*-MFHA) is shown in Fig. 4. The U^+ signal would have been over 5×10^6 counts s^{-1} for each injection without the complexing agent present. However, the count rate at $m/z = 238$ was indistinguishable from the background (20 counts s^{-1}), which indicated that the uranium was retained very efficiently by the column. For the operating conditions chosen, the Tb^+ count rate would have been suppressed by 40% (relative to the levels shown in Fig. 4) if the standards had been injected without prior complexation and removal of the uranium. The terbium standards for Fig. 4 also contained EDTA at 1×10^{-4} M; terbium recoveries were essentially quantitative with the EDTA present but were very low (<10%) without EDTA. The peak heights shown in Fig. 4 yielded a calibration plot that was linear with a correlation

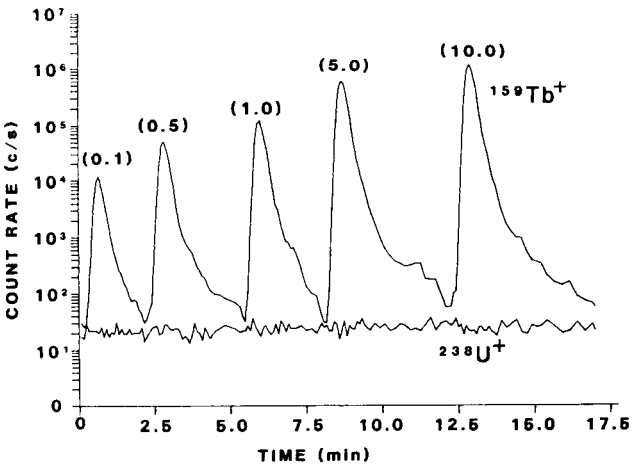

Fig. 4. Multiple ion chromatogram for injections of various terbium standards (Tb concentrations in mg l^{-1} given in parentheses on the peaks). Each standard also contained uranium at 100 mg l^{-1}, which provided a mean count rate of 20 s^{-1}. Note logarithmic scale on vertical axis.

coefficient of 0.9998. For these 200-μl injections, the maximum Tb^+ signal reached approximately 60% of the steady-state level. For the latter two injections in Fig. 4, the Tb^+ signal did not quite decay completely to the background in the 4-min rinse interval used. The rinse-out time requirement could be reduced by use of a fast flow cycle as shown by Fassel and Bear [26].

Similar results were obtained for the other rare-earth elements, and many other potential analytes (e.g., thorium) are either not complexed by *N*-MFHA at pH 5.0 [16] or would be masked by EDTA. This chromatographic separation should facilitate determination of a variety of elements in the presence of moderate amounts of uranium by i.c.p./m.s. (or i.c.p. emission spectrometry, for that matter). The maximum solubility of the complex between *N*-MFHA and uranium(VI) corresponds to a uranium concentration of 470 mg l^{-1}, which limits the amount of uranium that can be present in the sample solution.

Other possible uses of N-*MFHA*

Complexation of interfering elements with *N*-MFHA may well be useful for avoiding other interferences encountered by i.c.p./m.s. Iron(III) can be efficiently retained at pH 2.2. This capability could be used to prevent ionization interference [18] or oxide ion overlap [6] induced on analyte ions by excess of iron. Tin(IV) can also be efficiently retained at pH 0.5. Tin has the largest number of stable isotopes (ten) of any element. The combination of Sn^+ with any appreciable oxide or hydroxide ions would obscure most of the region m/z = 112—140 (or 141). These ions would interfere with one or more isotopes of cadmium, In, Te, Cs, Ba, Ce and Pr. However, these analyte elements would be in oxidation states +3 or lower and should

be easily separable from the tin(IV) complex with *N*-MFHA. Various other elements that form stable oxide ions (e.g., zirconium, hafnium, and tungsten) can also be separated from potential analyte elements as *N*-MFHA complexes [16].

Finally, the plasma operating conditions used were chosen by our normal process [21, 23], in which minimizing oxide ions was an important criterion. These conditions generally yield rather less than the maximum M^+ count rates obtainable [4, 21, 23, 32]. With the Sciex i.c.p./m.s. device, the M^+ count rate can often be increased substantially by increasing the aerosol gas flow rate. These measures can also increase the abundance of oxide or hydroxide ions [4, 32, 33]. If the oxide-forming elements can be removed chromatographically, plasma conditions that yield maximum M^+ signal and best detection limits could be used without severe interference from oxide ions of other elements. However, operation at relatively high aerosol-gas flow rates also tends to yield worse ionization interferences [15, 18] and poorer signal stability, the latter of which may require mass-flow control of the flow rate of the aerosol gas.

Ames Laboratory is operated for the U.S. Department of Energy by Iowa State University under Contract No. W-7405-Eng-82. This research was supported by the Director for Energy Research, Office of Basic Energy Sciences. One of the authors (M.D.P.) was supported by the Institutional Supporting Research and Development Program of the Los Alamos National Laboratory, which is operated by the University of California. The authors thank Timothy Brown for synthesizing the *N*-MFHA, Joseph J. Thompson for helpful discussions, and Jack E. Powell for providing the rare-earth stock solutions.

REFERENCES

1 R. S. Houk, Anal. Chem., 58 (1985) 97A.
2 A. L. Gray, Spectrochim. Acta, Part B, 40 (1985) 1525.
3 C. W. McLeod, A. R. Date and Y. Y. Cheung, Spectrochim. Acta, Part B, 41 (1986) 169.
4 J. W. McLaren, D. Beauchemin and S. S. Berman, J. Anal. At. Spectrom., 2 (1987) 277.
5 R. S. Houk, H. J. Svec and V. A. Fassel, Appl. Spectrosc., 35 (1981) 380; Dynamic Mass Spectrom., 6 (1981) 234.
6 A. R. Date, Y. Y. Cheung and M. E. Stuart, Spectrochim. Acta, Part B, 42 (1987) 3.
7 M. A. Vaughan and G. Horlick, Appl. Spectrosc., 40 (1986) 434.
8 R. S. Houk, Plasma Ionization Techniques for Elemental Analysis by Mass Spectrometry, in L. R. P. Butler (Ed.), Analytical Chemistry in the Exploration, Mining, and Processing of Materials, Blackwell, Oxford, 1986, p. 25.
9 A. L. Gray, Analyst, 110 (1985) 551.
10 S.-J. Jiang and R. S. Houk, Anal. Chem., 58 (1986) 1739; Spectrochim. Acta, Part B, 42 (1987) 93.
11 A. L. Gray, R. S. Houk and J. G. Williams, J. Anal. At. Spectrom., 2 (1987) 13.
12 D. J. Douglas and J. B. French, Spectrochim. Acta, Part B, 41 (1986) 197.

13 R. Hutton, Winter Conference on Plasma and Laser Spectrochemistry, Lyon, France, 1987.
14 G. Horlick, Winter Conference on Plasma and Laser Spectrochemistry, Lyon, France, 1987.
15 G. Horlick, S. H. Tan, M. A. Vaughan and J. Lam, Pittsburgh Conference and Exhibition on Analytical Chemistry and Applied Spectroscopy, Atlantic City, NJ, 1987, Paper No. 922.
16 I. A. Al-Biaty and J. S. Fritz, Anal. Chim. Acta, 146 (1983) 191.
17 J. A. Olivares and R. S. Houk, Anal. Chem., 58 (1986) 20.
18 J. J. Thompson and R. S. Houk, Appl. Spectrosc., 41 (1987) 801.
19 D. Beauchemin, J. W. McLaren and S. S. Berman, Spectrochim. Acta, Part B, 42 (1987) 467.
20 D. C. Gregoire, Appl. Spectrosc., 41 (1987) 897.
21 M. D. Palmieri, J. S. Fritz, J. J. Thompson and R. S. Houk, Anal. Chim. Acta, 184 (1986) 187.
22 R. K. Winge, V. A. Fassel, V. J. Peterson and M. A. Floyd, Inductively-Coupled Plasma/Atomic Emission Spectroscopy: An Atlas of Spectral Information, Elsevier, Amsterdam, 1985, Appendix A.
23 R. E. Serfass, J. J. Thompson and R. S. Houk, Anal. Chim. Acta, 188 (1986) 73.
24 J. J. Thompson and R. S. Houk, Anal. Chem., 58 (1986) 2541.
25 R. H. Scott, V. A. Fassel, R. N. Kniseley and D. E. Nixon, Anal. Chem., 46 (1974) 75.
26 V. A. Fassel and B. R. Bear, Spectrochim. Acta, Part B, 41 (1986) 1089.
27 H. Diehl, D. C. Johnson and R. R. Walters, Laboratory Manual for the Course in Quantitative Analysis, Oakland Street Science Press, Ames, IA, 1985 edn., p. 15-2.
28 J. W. McLaren, S. S. Berman, V. J. Boyko and D. S. Russell, Anal. Chem., 53 (1981) 1802.
29 D. A. Skoog and D. M. West, Principles of Instrumental Analysis, Holt, Rhinehart and Winston, New York, 1971, p. 103.
30 G. P. Russ and J. M. Bazan, Spectrochim. Acta, Part B, 42 (1987) 49.
31 J. W. McLaren, D. Beauchemin and S. S. Berman, Anal. Chem., 59 (1987) 610.
32 G. Horlick, S. H. Tan, M. A. Vaughan and C. A. Rose, Spectrochim. Acta, Part B, 40 (1985) 1555.
33 M. A. Vaughan and G. Horlick, Appl. Spectrosc., 40 (1986) 434.

Analytica Chimica Acta, 200 (1987) 573—579
Elsevier Science Publishers B.V., Amsterdam — Printed in The Netherlands

IMPROVEMENT OF THE DETECTION POWER IN ELECTROTHERMAL ATOMIC ABSORPTION SPECTROMETRY BY SUMMATION OF SIGNALS
Determination of Traces of Metals in Drinking Water and Urine

H. BERNDT*, G. SCHALDACH and R. KLOCKENKÄMPER

Institut für Spektrochemie und angewandte Spektroskopie, Bunsen-Kirchhoff-Strasse 11, D-4600 Dortmund 1 (Federal Republic of Germany)

(Received 8th December 1986)

SUMMARY

In electrothermal atomic absorption spectrometry, the signals corresponding to total absorption (TA), background (BG) and the required atomic absorption signal (TA — BG) show good temporal reproducibility. For improvement of the detection power, the time-resolved signals can be summed with the aid of a microcomputer. The summed signal height is exponentially related to the number (N) of measurements up to $N = 40$. The detection power is improved according to the $N^{1/2}$ law with a practical limit at summation of ca. 20 signals. Concentrations which are around the detection limit in single measurements (lead and cadmium in drinking water or lead in urine) can readily be determined by summation of signals from, for example, sixteen 20-μl injections of urine. Resulting high summed backgrounds, giving absorbances > 5, can be compensated.

The term atomic absorption spectrometry (AAS) covers a group of different techniques, all of which possess the same measuring principle. The most familiar variants are flame atomic absorption spectrometry, electrothermal AAS and the hydride technique, as well as the special cold-vapour method for mercury determination. In flame AAS, a laminar flame serves as the absorption volume; in electrothermal AAS, an electrically-heated graphite tube is normally used and in hydride techniques, an electrically heated quartz cell. In flame techniques, the solution is usually drawn up by continuous suction and nebulized. Apart from this continuous nebulization, it is also possible in flame AAS to work with small discrete volumes [1, 2]; sample volumes of 40—100 μl are fed to the nebulizer from a microlitre pipette, during which injection the signal pulses are recorded. When electrothermal AAS is used only small discrete volumes or masses of sample can be used; the volumes commonly utilized are between 10 and 25 μl. During the atomization step,

[a]Harald Berndt has several engineering and chemical degrees and obtained his doctoral degree from the University of Bochum in 1975. He has wide analytical experience in the steel industry and joined ISAS in 1971. His main research interests are in micro- and trace analysis of high-purity and biological materials, with particular regard to atomic absorption spectrometry and sample introduction in spectroscopic sources.

0003-2670/87/$03.50

the transient signal is recorded, with a chart recorder when "older" equipment is used, or in modern equipment on a video in a time-resolved mode.

In order to determine small concentrations of metal ions in real matrices (e.g., urine), enhancements of the detection power are always sought. In flame AAS, this is usually achieved by longer measuring times (integration times). The precision of the results then depends on the integration time and the corresponding relative standard deviation is inversely proportional to the square root of the integration time [3]. Longer measuring times, t, improve the signal-to-noise ratio and the limit of detection by a factor of $t^{1/2}$; this is the well-known law of time which is quite general for spectroscopic methods. The validity of this law has also been confirmed for the injection method of flame AAS. With 16 injections, Bekjarov et al. [4] achieved a 4-fold enhancement of the detection power; this was achieved by computer-assisted summation of the signals. However, 16 injections correspond to a 16-fold sample volume and thus a 16-fold measuring time. If the total sample volume required for the signal addition were nebulized continuously, the same result would be achieved. Thus, no advantage would be gained for the flame AAS by the elaborate computer-assisted signal summation for the injection mode in comparison to the continuous suction mode with the same integration time.

In electrothermal AAS, however, longer measuring times are not possible, and the summation mode should bring significant advantages. Barzev et al. [5] have demonstrated a reduced noise level of the corrected signals by a signal-summation mode. In their method, the separate signals which are insignificantly different from the noise level, are smoothed by ensemble summation and presented graphically; a better visual control of the optimal conditions for peak-area calculation is then possible [5].

Signal summation is well known for other spectroscopic methods, e.g., in infrared spectroscopy with multiple-scan techniques. During the multiple scans and summation, the peaks grow out of the background noise and after N repetitions, the signal-to-noise ratio is enhanced by a factor $N^{1/2}$.

In previous work [6, 7], it was shown that the signals of electrothermal AAS can be rendered time-resolved with the aid of a minicomputer; when this mode was used, details of the vaporization and atomization behaviour could be observed. It became evident that the signals relating to the atomic absorption and to the background each possessed a surprisingly good temporal reproducibility for the repetition of a measurement. Consequently, it was expected for electrothermal AAS, that the signal height would increase with the number N of the measurements, while the noise level would only increase according to $N^{1/2}$. Generally, it was concluded that the well-known $N^{1/2}$ law is valid for enhancement of the detection power. The study reported in this paper is concerned with the extent to which signal heights are proportional to the number of repetitions and with evaluating the improvement in the detection power that can be reached in actual practice, i.e., for routine work with real samples such as drinking water and urine.

EXPERIMENTAL AND RESULTS

Instrumentation

The atomic absorption spectrometer used was a Perkin-Elmer model 4000 equipped with a graphite-tube cuvette, HGA-500. This spectrometer works with a chopping frequency of 50 Hz corresponding to a cycle time of 20 ms. During a single cycle, four intensity values are measured: the radiation of the hollow-cathode lamp, its reference radiation, the radiation of the deuterium lamp and the corresponding reference radiation. The different signals can be collected by a microcomputer with an interface developed in this laboratory.

The computer (CBM 8096) takes over the entire evaluation of the signals: (a) the graphical presentation of the absorbance as a function of time for the total signal (TS), the background signal (BG) and the required atomic-absorption signal (TS − BG) with selectable axial intercepts for video, printer and plotter; (b) setting of temporal windows, signal-area integration and identification of the maximum of the signal height; (c) output of the corresponding signal data at any chosen moment; (d) storage of data on discs; and (e) superposition of different time-resolved signals [6]. The values are stored as the logarithms of the intensity ratios (i.e., absorbances). For the repetition of measurements, a program was developed in which time-identical values of the absorbance are summed. Data transfer is started by a read command of the unit controlling the graphite furnace (HGA 500); with this, all measurements within a furnace program are recorded at the same time and are thus exactly comparable.

Preliminary tests

Additivity of the absorbance. These investigations were conducted with pure aqueous and matrix-containing solutions. As an example, Fig. 1A shows the signal for a single measurement of lead (25 ng ml^{-1}) in a weak solution of nitric acid. Figure 1B shows the summed signal established from 16 measurements; the absorbance is 16-fold the size of the single signal. Strict propor-

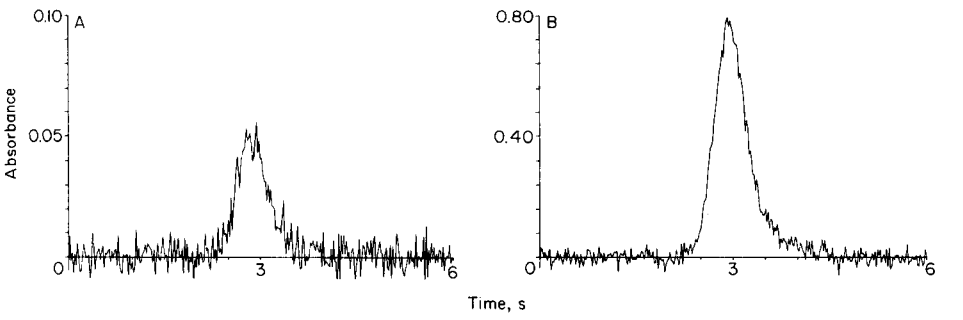

Fig. 1. (A) Corrected signal for 0.5 ng Pb (20 μl of 25 ng ml^{-1} Pb solution) in very dilute nitric acid. (B) The sum of 16 signals for 0.5 ng Pb from very dilute nitric acid (16 × 20 μl of 25 ng ml^{-1} Pb solution, corresponding to 8 μg Pb/320 ml).

tionality between the signal height and the number N of measurements was found between $N = 1$ and $N = 40$ (controlled working range). Depending on the concentration of the solution and the number N, values between 2 and 20 were obtained for the total absorbance.

Signal-to-noise ratio and the power of detection. Figure 2A shows the reduction in the limit of detection for traces of lead in a weak nitric acid solution; for the individual measurements, 20-μl injections were used. In Fig. 2B, similar results are presented for cadmium in drinking water. Both curves show that after about 16–20 measurements, no further significant improvement of the detection power is achieved. These practical measurements illustrate the limitation of the $N^{1/2}$ law. This appearance of a boundary limit is also known from other spectroscopic techniques, such as x-ray fluorescence spectrometry [8].

Analytical applications

In numerous cases, the signal of the element to be determined lies below the limit of detection; it cannot be distinguished significantly from the background noise. Moreover, in real samples, the spectral background can be very high, e.g., in the determination of trace metals in urine, and this requires very elaborate background correction.

Determination of traces of lead in drinking water. In this determination, the concentration is around the limit of detection. Figure 3A shows the corrected signal for the traces of lead in drinking water from a single measurement. The signal lies at the limit of detection, so that a precise determination is not possible. Figure 3B shows the computer-assisted signal established from summation of 16 measurements; this signal is easily evaluated, corresponding to an absorbance of 0.45, and is obviously well above the limit of detection. The signal enhancement by summation is clearly valuable in this example.

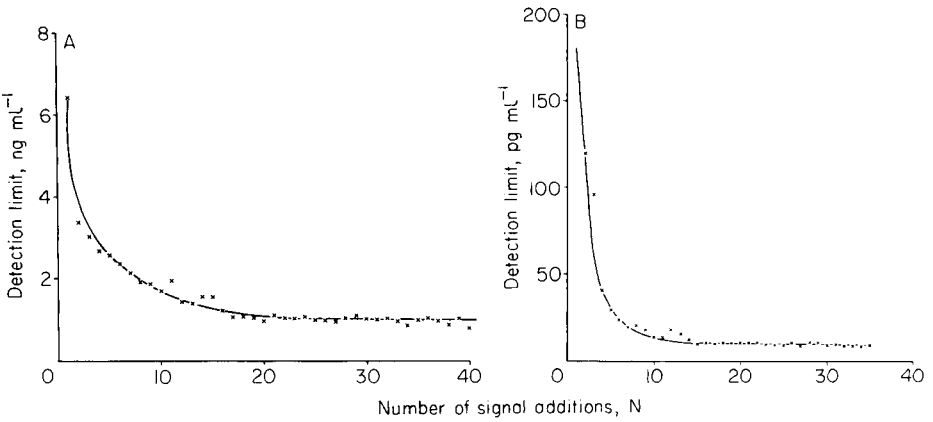

Fig. 2. Dependence of the detection limit on the number of signal additions: (A) for the determination of lead traces in very dilute nitric acid (20 μl of sample solution); (B) for the determination of cadmium in drinking water.

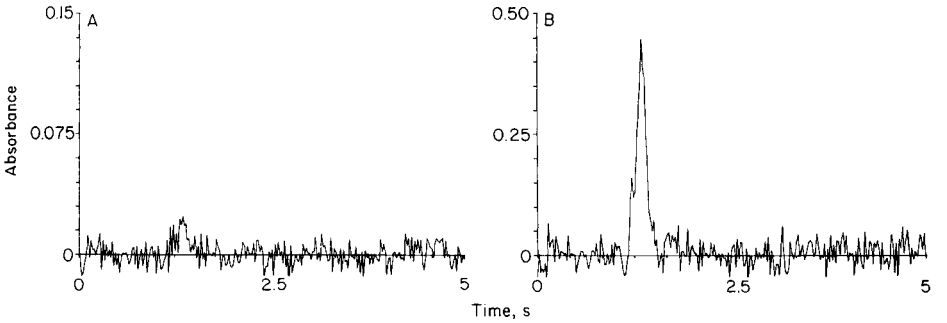

Fig. 3. Determination of lead in drinking water: (A) single measurement showing the signal indistinguishable from the limit of detection (20 μl of sample solution); (B) signal summed from 16 repeated measurements (16 × 20 μl of sample solution).

Determination of traces of lead in urine. Again, the expected concentration lies around the limit of detection. Figure 4A depicts the lead signal and the background signal for a urine sample from an occupationally unexposed person. The lead signal is very small in relation to the background signal, being of the same order as the noise. The background signal comprises two

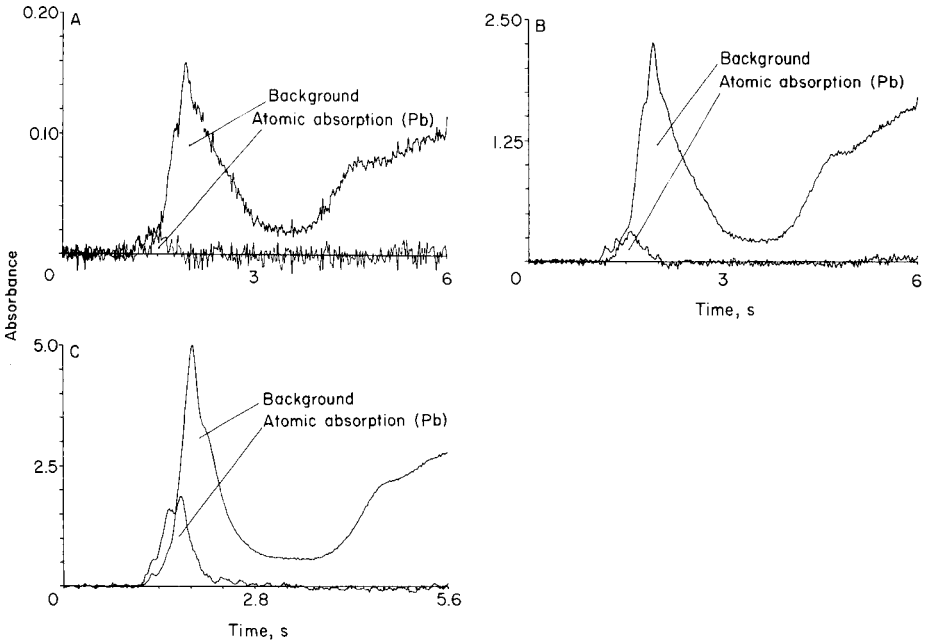

Fig. 4. The determination of lead in urine from an occupationally unexposed person: (A) signals from 20 μl of sample solution showing the atomic absorption at the limit of detection; (B) signals summed for 16 repeated measurements (16 × 20 μl of sample solution); (C) signals summed for 16 repeated measurements of a urine specimen with an additive background absorbance of 5 (16 × 20 μl of sample solution).

larger signals, as already shown in previous measurements [6]; the lead signal appears immediately at the start of the first large background signal. The computer-assisted signal summed from 16 individual measurements is presented in Fig. 4B; this signal can readily be evaluated despite the background corresponding to an absorbance of 2–3. The figure demonstrates that this additive background is properly compensated as the corrected signal retreats to zero.

If the background of a single measurement is compensated properly, the considerably higher additive background is also well corrected. Figure 4C shows the outputs for the determination of traces of lead in a urine specimen from an occupationally exposed person. The atomic absorption signal shows the characteristic stepwise vaporization of lead from the urine matrix while the additive background reaches an absorbance of 5. The proper correction can be recognized even here and this was possible only by means of the summation of repeated signals. In AAS, a background absorbance of 5 cannot be compensated in a single measurement because of the physical conditions; modern systems for background correction (Zeeman AAS) have a limit at absorbances around 1.5—1.8.

DISCUSSION

The summed signal height is proportional to the number of measurements; this was confirmed up to $N = 40$. In electrothermal AAS, as in other spectrometric techniques, the limit of detection obeys the well-known $N^{1/2}$ law so that the limit of detection decreases with the inverse square root of the number of the signals summed. A practical limitation was found at about twenty signal additions.

Figure 3 illustrates the peak heightening of the lead signal above the background for the determination of lead in drinking water. A comparative summation of the signal heights and signal areas in this case showed that there are significant advantages in the evaluation of peak heights; much lower signal-to-noise ratios were obtained for area integration. Figure 4C shows the signal corresponding to the introduction of a total of 320 μl of a urine specimen (16 × 20 μl injections). The proposed sequential summation of the signals is the only possibility to compensate properly for the background (absorbance ≈ 5) caused by this large volume of urine.

For calibration, the addition of signals is not essential. Calibration can be done with single samples and based on mass (e.g., micrograms).

With the computerized summation of signals, it is possible directly to determine concentrations of trace elements which otherwise could be determined only by chemical preconcentration and separation techniques. A significant advantage, apart from saving of time, is that the sample is merely subjected to repeated measurements which can be done without risk of contamination. Thus, the well-known problems of blanks in chemical preconcentration methods can be avoided.

When very low trace concentrations of an element have to be determined in the presence of any high matrix concentration which overexerts the background-correction system even in an individual measurement, a pre-dilution step is possible. Such a dilution may restore the measurement to a region where background compensation is viable and the resulting loss in sensitivity of the analytical signal can be negated by summation of the signals.

In this work, background correction was done only with the aid of deuterium compensation. In this case, a proper background correction can be assumed up to an absorbance of 0.5, so that compensation for background absorbances up to 8 should be possible for the summed signals from 16 measurements. This is in good agreement with the results of Fig. 4C. If a more effective background compensation system were used, perhaps by line splitting in the magnetic field (Zeeman AAS), it should be possible to work with higher individual backgrounds (absorbance up to 2) for which the summed background from 16 measurements would reach values of around 30.

For samples producing a low spectral background, the known technique of multiple-step drying of the sample in the graphite tube may be applied for improvement of the detection limit. If the standard deviation at the detection limit is caused essentially by signal noise, improvement is possible by increasing the number of drying steps (practically 2–5). A combination of the multiple drying technique with the summation mode described above would produce better enhancement of detection power.

In principle, the method described can be made fully automatic. The sample changers currently available provide fully automatic, programmable multiple injections and some commercial spectrometers provide exits for data transmission to external computers. The proposed mode of signal summation is then quite viable insomuch as appropriate software is easily developed for the particular computer available.

This work was supported by the "Bundesministerium für Forschung und Technologie" and by the "Ministerium für Wissenschaft und Forschung des Landes Nordrhein-Westfalen".

REFERENCES

1 S. Greenfield and P. B. Smith, Anal. Chim. Acta, 59 (1972) 341.
2 H. Berndt and E. Jackwerth, Spectrochim. Acta, Part B, 30 (1975) 169.
3 B. Welz, Atomabsorptionsspektrometrie, 3. Aufl., Verlag Chemie, Weinheim, 1985, p. 103.
4 G. L. Bekjarov, L. Futekov and G. N. Andreev, Fresenius' Z. Anal. Chem., 322 (1985) 563.
5 A. Barzev, D. Dobreva, L. Futekov, V. Rusev, G. Bekjarov and G. Toneva, Fresenius' Z. Anal. Chem., 325 (1986) 255.
6 J. Baasner, H. Berndt and R. Eiermann, Fortschritte atomspektroskopischer Spurenanalytik, Band 2, Herausgeber: Welz B, VCH Verlagsgesellschaft, Weinheim, 1986.
7 H. Berndt, J. Baasner and J. Messerschmidt, Anal. Chim. Acta, 180 (1986) 389.
8 R. Klockenkämper and H. Bubert, Fresenius' Z. Anal. Chem., 323 (1986) 112.

Analytica Chimica Acta, 200 (1987) 581—591
Elsevier Science Publishers B.V., Amsterdam — Printed in The Netherlands

LASER-EXCITED MOLECULAR FLUORESCENCE SPECTROMETRY FOR THE DETERMINATION OF TRACES OF NONMETALS
Part 1. Determination of Traces of Fluoride, Chloride and Bromide based on Diatomic Molecules in a Graphite Furnace

KLAUS DITTRICH* and HANS-JOACHIM STÄRK

Chemistry Section, Karl Marx University, Leipzig Talstr. 35, Leipzig, 7010 (German Democratic Republic)

(Received 7th May 1987)

SUMMARY

For the determination of fluoride, chloride and bromide, a suitable metal ion is added in a modified graphite tube atomizer. After drying and ashing, the substances are vaporized and diatomic molecules between the metal and nonmetal are formed. These molecules are excited by a pulsed dye laser and the resulting fluorescence is measured. At constant metal concentration, the fluorescence is proportional to the halide concentration. The diatomic molecules used are MgF, InCl and AlBr. The detection limits are 11 pg of fluoride, 15 pg of chloride and 70 pg of bromide in the 10-μl injections, corresponding to 6×10^{-8} mol l^{-1} fluoride, 4×10^{-8} mol l^{-1} chloride and 9×10^{-8} mol l^{-1} bromide.

The most sensitive atomic spectrometric technique for determination of trace metals is laser-excited atomic fluorescence spectrometry (LEAFS). Absolute detection limits in the femtogram range have been achieved for many metals when this technique is used in combination with a graphite rod atomizer [1–3]. Considering the poor thermal characteristics of carbon rod atomizers, attempts were made to apply the conventional carbon tube atomizer, which has better thermal characteristics, for this purpose. The results were described earlier [4, 5]. It was shown that the detection limits could be improved for some metals, particularly for refractory elements such as vanadium and iridium. Depending on the element, improvement factors of 1–3 orders of magnitude in comparison with rod atomization were achieved.

Until now this sensitive technique has not been used for the determination of nonmetals, because the wavelengths needed lie in the vacuum or far ultraviolet range, and intense lasers are not available for this spectral region. Some work on the determination of elements of the sixth periodic group (Se, Te) by atomic fluorescence spectrometry has been reported, in which less intense light sources such as hollow-cathode lamps or, better, electrodeless-discharge lamps were applied [6].

Some years ago a new technique, molecular absorption spectrometry (MAS) with electrothermal evaporation was introduced for the determination

0003-2670/87/$03.50

of traces of nonmetals [7]. In this technique, diatomic molecules comprising the non-metal and an added metal were formed by simultaneous evaporation in a hot graphite tube. The molecular absorption of these molecules under the chosen conditions (excess of metal) was proportional to the concentration of the non-metal. It was especially useful for halide determination. The detection limits are at the nanogram level. This technique has recently been reviewed [8].

There is some information about the fluorescence of such diatomic molecules in flames and plasmas; fluorescence of OH, S_2, SH and other molecules has been observed, but no analytical applications have been reported [9]. Some other publications [10–13] have described metal halide fluorescence, including that of InCl and GaCl [13], again without any analytical application. Only Fowler and Winefordner [14] have used molecular fluorescence in this way, to determine phosphate in flames based on PO fluorescence.

In this paper, a new technique is described for the determination of traces of some halides by laser-excited molecular fluorescence spectrometry (LEMFS) of diatomic molecules. These molecules are formed in carbon tube atomizers by electrothermal evaporation of the nonmetallic and metallic components. The aim of this work was to improve the detection limits of molecular absorption spectrometry to allow analyses for very low traces of nonmetals.

EXPERIMENTAL

Apparatus and solutions

A diagram of the arrangement of the spectrometer for laser-excited molecular fluorescence is shown in Fig. 1.

The nitrogen pulsed-laser system gives laser pulses at 337.13 nm with a duration of about 8 ns and a pulse energy of about 2 mJ. The maximum power (250 kW) is given at a pulse frequency of 5—7 Hz. The dyes C462 (562—594 nm/265—285 nm) and C611/4 (670–750 nm/340–370 nm) were available. The maximum laser energy for second-harmonic generation at 280 nm and 367 nm were 9 and 0.3 μJ, respectively. The durations of these pulses were ca. 4 ns. Particularly, the latter energy is too small for achieving saturation of the excited levels. The carbon tubes of the modified tube atomizer had two slits nearly in the middle of the tube. The laser beam was focussed through these holes.

Stock solutions were prepared by dissolution of sodium fluoride, sodium chloride or sodium bromide in water (X^- = 1 mg ml^{-1}). Magnesium nitrate, indium nitrate and aluminium nitrate (M^{n+} = 1 mg ml^{-1}) were dissolved in 0.01 M nitric acid, and barium hydroxide (10 mg Ba ml^{-1}) was dissolved in water. Working solutions were prepared by suitable dilution.

Procedure

The sample solution containing the anion (X^-) to be determined was mixed with an excess of an added substance (M) with which this ion can form stable

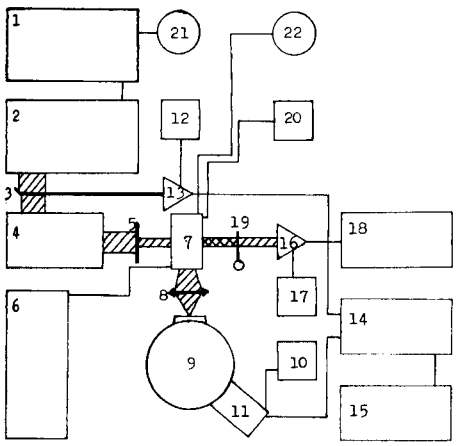

Fig. 1. Schematic diagram of the spectrometer: (1) power supply for the nitrogen pulsed-laser, type IGT-300 (ZWG, AdW, Berlin, G.D.R.); (2) nitrogen laser, type IGT-1000 (ZWG); (3) mirror for light for triggering the measurement; (4) dye laser, type FLGR 2 (Carl Zeiss, Jena); (5) filter for ground vibration of laser radiation; (6) power supply for tube atomizer (home-made); (7) modified tube atomizer (tube dimensions as in HGA-500, Perkin-Elmer, and EA3, Carl Zeiss); (8) quartz lens; (9) monochromator, type SPM-1 (Carl Zeiss); (10) power supply for PMT; (11) photomultiplier tube, M-11 FVC-520 (Werk für Fernsehelektronik, Berlin, G.D.R.); (12/13) trigger system; (14) boxcar integrator, type BCI-280 (ZWG); (15) X, Y recorder, type "endim 620.01" (Meßgerätewerk Schlotheim, G.D.R.); (16/17/18) pyroelectric joulemeter, power supply, oscillograph (ZIE, AdW, Berlin, G.D.R.); (19) mirror for doubling the excitation laser energy; (20) thermostat for cooling the atomizer; (21) nitrogen; (22) argon.

diatomic molecules (MX) in the gaseous phase. Small volumes of these solutions were introduced into the graphite tube furnace. To avoid precipitate formation, separate reagent addition may be made into the furnace. After deposition, the controlled heating program normally used for drying, ashing and vaporization with carbon tube furnaces was applied (see, e.g. [4]). In the vaporization phase, the M and X components evaporate together and form MX molecules in the gas phase. These molecules are excited by laser irradiation and the intensity of the fluorescence is measured. The intensity is proportional to the concentration of X^-.

RESULTS AND DISCUSSION

Because the purpose was to determine fluoride, chloride and bromide, it was necessary to choose stable diatomic molecules containing these species. The most stable diatomic molecules which could be used for determination of halides by electrothermal MAS were the AlX molecules which have the following dissociation energies: E_D (AlF) = 6.8 eV, E_D (AlCl) = 5.1 eV, and E_D (AlBr) = 4.1 eV. The maximum absorbances of these molecules lie at 227.5, 261.4 and 279.0 nm, respectively. The available laser system, there-

fore, allowed only the AlBr fluorescence to be studied. Accordingly, for fluoride and chloride, other stable molecules with maximum molecular absorbances at longer wavelengths were selected. For fluoride, only MgF was suitable, with a dissociation energy (E_D) of 4.8 eV and two absorbance maxima at 359.28 nm and 268.94 nm; the generation of CaF (E_D = 5.5 eV, maximum absorbance at 529.1 nm) was problematical in graphite tubes. For chloride, InCl was used (E_D = 4.5 eV, maximum absorbance at 267.2 nm). Other chlorides were considered: GaCl (E_D = 4.9 eV, λ_{max} = 249 nm) and MgCl (E_D = 3.2 eV, λ_{max} = 269.3/376.2 nm), but they had disadvantages. The dissociation energy of MgCl is relatively low and the GaCl molecule did not give very good results in electrothermal MAS [15]. The characteristics of the transitions of the molecules used are listed in Table 1. It was assumed that only when the laser energy was higher than 1 μJ would molecular fluorescence be observed.

Study of InCl by LEMFS

Choice of wavelength. Measurements of indium by LEAFS in the presence of some halides showed strong matrix interferences, which were explained by the formation of appropriate diatomic molecules [5] of the InX type [7, 8, 15]. As had been found earlier, the absorption coefficient in the C-system was appreciably higher than in the A- and B-systems which are commonly used for InCl molecular emission in flames, etc. Accordingly, molecular fluorescence was sought after absorption of radiation at 267.21 nm. The higher absorption probability of the C-system can be attributed to the ground and excited states both being singlets.

Fluorescence was detected by using one of three exciting wavelengths (Table 2). Because the detection system did not allow higher spectral resolution, it was impossible to determine accurately at which wavelength the highest fluorescence intensity was emitted; the spectral bandpass of the monochromator used was about ±3.5 nm. But, although the laser energy for the last two transitions (Table 2) was higher, the highest fluorescence intensity was found at the vibrational 0,0-transition, as would be expected from the

TABLE 1

Characterization of the transitions of molecules used in LEMFS with electrothermal vaporization

Molecule	Transition	Wavelength (nm)	Laser energy (μJ)
MgF	$A^2\Pi \leftrightarrow X^2\Sigma^+$	359.28	0.3
	$B^2\Pi \leftrightarrow X^2\Sigma^+$	268.94	6
InCl	$A^3\Pi^+ \leftrightarrow X^1\Sigma^+$	359.92	0.3
	$B^3\Pi^0 \leftrightarrow X^1\Sigma^+$	349.50	0.3
	$C^1\Pi^1 \leftrightarrow X^1\Sigma^+$	267.21	3.5
AlBr	$A^1\Pi \leftrightarrow X^1\Sigma^+$	278.91	5

TABLE 2

Fluorescence intensities for InCl in electrothermal LEMFS

Laser-excited wavelengths (nm)	Transition[a]		Laser energy (μJ)	Fluorescence intensity (%)
	v'	v''		
267.21	0	0	3.5	100
269.45	0	1	4.5	77
271.75	0	2	6	69

[a]Vibrational quantum number.

Franck—Condon principle. No resonance or nonresonance fluorescence at the A- or B-wavelengths could be found after irradiation at any of the three exciting wavelengths. This may have been due to the small laser energy at these wavelengths (Table 1).

Optimization of conditions. The influence of the indium concentration on the fluorescence intensity was measured for a chloride concentration of 10 ng/10 μl. The results are shown in Fig. 2, which indicates that maximal molecule formation was achieved in the presence of 1 μg In^{3+}/10 μl. Further increase in the indium concentration led only to more stray light. Therefore, 1 μg of indium(III) was used for the analytical studies.

The following thermal and electrical conditions were found to give the greatest sensitivity: drying at 150°C, ashing at 900°C, evaporation at 2800°C with gas stop; maximum heating rate at 3000 K s^{-1}; PMT voltage at 1300 V; boxcar integrator gate width at 400 ns.

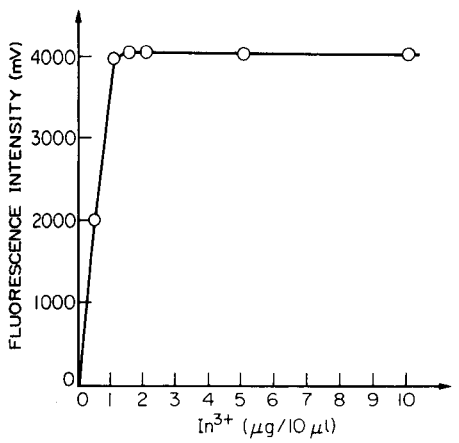

Fig. 2. Dependence of InCl signal for 10 ng Cl^{-1}/10 μl on the In^{3+} concentration.

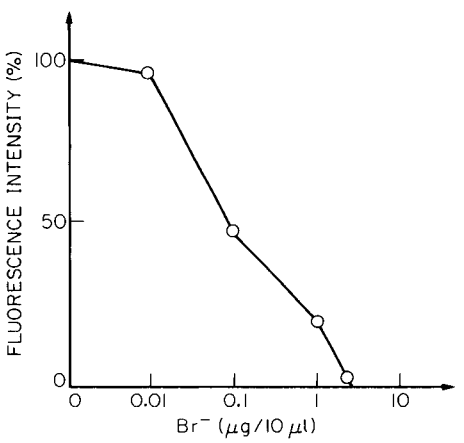

Fig. 3. Effect of bromide concentration on the InCl signal for 1 ng Cl^{-}/10 μl.

Calibration and interferences. The calibration equation for 0.1—10 ng of chloride in 10 μl of solution was $I = 28.5\ C^{0.54}$, where C is given in pg Cl^-/10 μl and I is the intensity in mV. The 3 σ detection limit was 15 pg Cl/10 μl (4×10^{-8} mol l^{-1}). As in the molecular absorption procedure [16], bromide affected the signal (Fig. 3) because of the shift of the equilibrium

$$InCl + Br \rightleftharpoons InBr + Cl$$

towards indium(I) bromide formation. Attempts to avoid this effect by increasing the indium concentration were unsuccessful because of increased light scattering by condensed particles. Nevertheless, it was possible, as in the MAS procedure [15], to determine chloride in the presence of 3000-fold amounts of bromide.

The effect of hydrofluoric acid was also tested. Because indium(I) fluoride is the most stable indium(I) halide, fluoride should interfere most strongly in the determination of chloride. The dissociation energies are 5.5 eV for InF, 4.8 eV for InCl, 4.2 eV for InBr and 3.5 eV for InI. However, no interference from fluoride was found, probably because of thermal hydrolysis with release of hydrogen fluoride during the ashing step, which left the chloride unaffected, for later vaporization as InCl.

Study of MgF by LEMFS

Choice of wavelength. Both transitions (Table 1) could be used for determination of fluoride by electrothermal MAS, but the A-system was more sensitive [17]. However, in the present work, the available laser energy was

TABLE 3

Characterization of LEMFS for MgF

Excitation laser wavelength (nm)	Transition vibration quantum number		Observed wavelength (nm)[a]	Fluorescence intensity[b] (%)	Laser energy (μJ)
	v'	v''			
268.94	0	0	269	100	6
268.65	1	1	269	73	6
268.38	2	2	269	47	6
268.13	3	3	269	31	6
273.46	2	3	273	4	7
273.14	3	4	273	3	7
268.94	0	0	360	30	6
268.65	1	1	360	25	6
268.38	2	2	360	16	6
273.14	3	4	360	17	7
359.28	0	0	360	6	0.3

[a]Spectral bandpass was about 8 nm. [b]The resonance fluorescence at 268.94 nm was set at 100%.

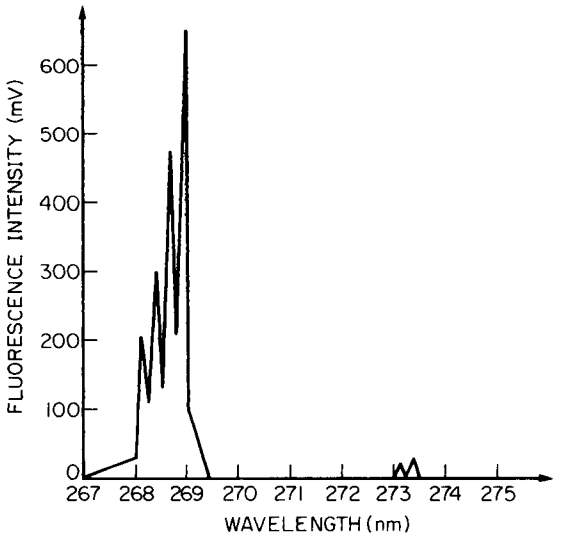

Fig. 4. Dependence of the MgF signal for 50 ng F^-/10 µl on the excitation wavelength with 50 µg Mg^{2+}/10 µl added.

higher for the B-system (Table 1). The effect of the exciting radiation wavelength is shown in Fig. 4 and Table 3. Table 3 shows that the 0,0-transition is the most sensitive. The ratio of the resonance and nonresonance fluorescence intensities was 3:1. For analytical purposes, the resonance and nonresonance fluorescences of the 0,0-transition were used (268.94/269 ± 4 nm and 268.94/360 ± 4 nm).

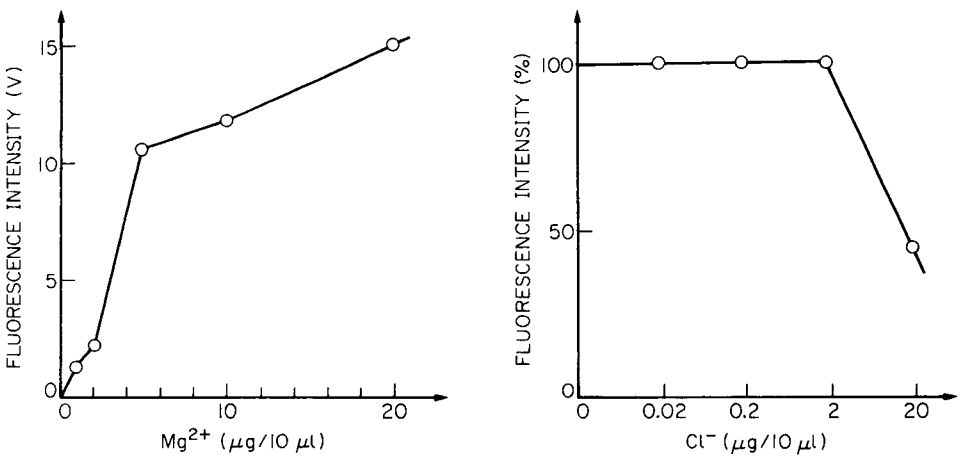

Fig. 5. Dependence of the MgF signal for 5 ng F^-/10 µl on the Mg^{2+} concentration.

Fig. 6. Effect of chloride concentration on the MgF signal (nonresonance fluorescence) for 10 ng F^-/10 µl with 5 µg Mg^{2+}/10 µl added.

Optimization of conditions. The effect of magnesium concentration at a fluoride concentration of 5 ng/10 μl is shown in Fig. 5. As in molecular absorption spectrometry [17], the concentration of magnesium ions has a strong effect. The highest sensitivity was achieved at a magnesium concentration of 50 μg/10 μl, but the stray radiation intensity was then very high. Accordingly, a concentration of 5 μg/10 μl is recommended. The thermal and electrical conditions were the same as for indium chloride.

Calibration and interferences. With the optimal chemical and thermal conditions, calibration graphs were obtained for resonance and nonresonance fluorescence. The equations of the plots over the fluoride range 0.1—20 ng/10 μl were as follows: for resonance, $I_F = 14.5 \times C^{0.8}$ and for non-resonance, $I_F = 6.3 \times C^{0.73}$ where C is given as pg/10 μl and the intensity is in mV. The 3 σ detection limits were 11 pg F^-/10 μl for resonance fluorescence and 45 pg F^-/10 μl for non-resonance fluorescence, i.e. 6×10^{-8} and 24×10^{-8} mol l^{-1} fluoride, respectively. The difference between these two values is not large and so it can be assumed that for real analytical problems the non-resonance fluorescence would be more suitable, because the background (stray light) is much less.

It was known from molecular absorption measurements [17] that chloride has a strong influence on the magnesium fluoride absorbance because the gas-phase equilibrium

$$MgF + Cl \rightleftharpoons MgCl + F$$

is shifted towards magnesium chloride formation at large chloride concentrations. The difference between the dissociation energies of these two molecules is relatively large (4.8 eV for MgF and 3.3 eV for MgCl). The effect of chloride concentration is shown in Fig. 6.

Considering a signal depression of 50% and the detection limits found, it can be calculated that the fluoride determination is possible in the presence of up to 10^5-fold amounts of chloride. This is a little better than in molecular absorption spectrometry (2×10^4); the difference can be explained by the improved detection limit in the present procedure.

Study of AlBr by LEMFS

Choice of wavelength. According to Table 1, only one transition is available for the study of AlBr. This molecule has a high dissociation energy (4.1 eV), and was found to give the best analytical results by molecular absorption spectrometry by comparison to GaBr (4.3 eV), InBr (4.2 eV) and TlBr (3.4 eV) [8, 18]. However, the wavelength of molecular bands of the other molecules (InBr, 284.5 nm; TlBr, 266.8 nm) also lie in a region in which high energy is available from the laser system used, and these molecules will be tested in the near future. As for indium chloride and magnesium fluoride, the excitation of the 0,0-transition of AlBr at 278.91 nm, according to the Franck—Condon principle, produced the highest fluorescence intensity and was therefore used for further studies.

Optimization of conditions. In molecular absorption spectrometry, aluminium bromide gave rise to some problems [18]. Because $Al(OH)_3$ is only a very weakly basic substance, use of only an excess of aluminium ions to bind bromide in the drying and ashing phases led to losses of hydrogen bromide by thermal hydrolysis. 0.025 M barium hydroxide was therefore used as matrix modifier. This solution has some advantages. Aluminium ions are soluble as $Al(OH)_4^-$ ions; barium hydroxide is a strong base and forms salts of the type Ba(OH)Br during the drying and ashing stages. Barium bromide (and also the basic salts) is thermally stable (b.p. 1900°C for $BaBr_2$) and does not undergo thermal hydrolysis in the drying and ashing phases; barium ions form thermally stable carbides. Thus it can be concluded that bromide ions are thermally stabilized by adding barium hydroxide. In the vaporization phase, readily volatile $AlO_x(OH)_y$ species evaporate together with the thermally stabilized bromide species, and AlBr molecules are formed by gas-phase reactions. Best sensitivity was obtained with 1 μg Al^{3+} and 35 μg Ba^{2+}/10 μl, but because of the large levels of stray radiation under these conditions, the following concentrations were found to be optimum (Fig. 7): 0.3 μg Al^{3+}/10 μl and 14 μg Ba^{2+}/10 μl.

The temperature of the ashing phase could be increased to 1500°C without bromide loss. Maximum heating in the evaporation phase gave the best results. The electrical conditions were the same as given above for InCl and MgF. The laser output was 5 μJ.

Calibration and interferences. The calibration graph for 0.5—50 ng Br^-/10 μl is described by the equation $I_F = 5.7 \times C^{0.68}$ where C is given in pg Br^-/10 μl

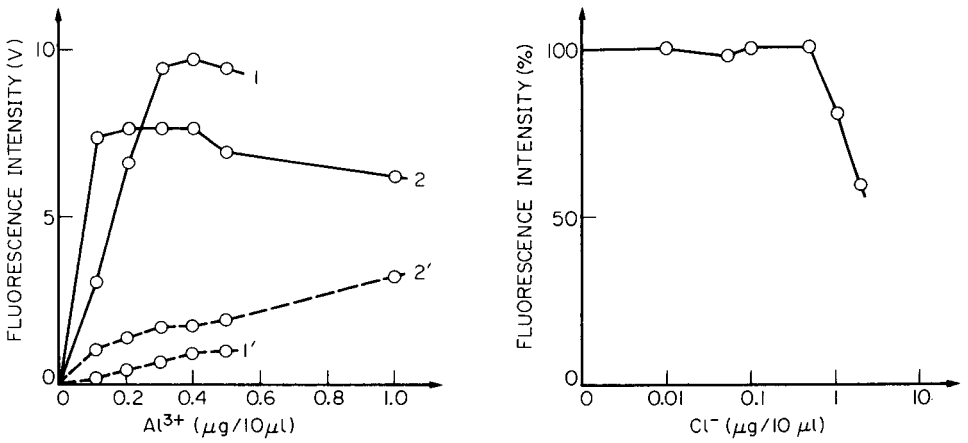

Fig. 7. Dependence of AlBr signal on the concentrations of $Al^{3+}/Al(OH)_4^-$ and $Ba^{2+}/Ba(OH)_2$: (1) 0.01 M $Ba(OH)_2$ (14 μg Ba^{2+}/10 μl); (2) 0.025 M $Ba(OH)_2$ (35 μg Ba^{2+}/10 μl); (1′, 2′) background signals.

Fig. 8. Effect of chloride concentration on the AlBr signal for 1 ng Br^-/10 μl with 0.3 μg Al^{3+}/10 μl and 14 μg Ba^{2+}/10 μl added.

and I_F as mV. The 3 σ detection limit for bromide was 70 pg (9×10^{-8} mol l^{-1}).

It was again known from the earlier data on molecular absorption spectrometry that other halides interfere. The effect of chloride in the present study is shown in Fig. 8. For a signal depression of 50% and the detection limit found, it was calculated that bromide can be determined in the presence of up to 2×10^4-fold amounts of chloride. This value is much better than that possible by MAS (10^2), largely because of the greatly improved detection limit for bromide.

Comparison of LEMFS with molecular absorption spectrometry

The detection limits for the two techniques are listed in Table 4. The improvement in the detection limit in electrothermal LEMFS is generally about two orders of magnitude. Further improvement would be possible by the application of a better laser system with pulse energies higher than 10 μJ. Thus it can be concluded that this method would be suitable for the determination of very low traces of nonmetals in very small samples. In spite of the interferences of some halides, it is still possible to determine some halides in presence of quite high concentrations of other halides.

TABLE 4

Comparison of detection limits for halides by electrothermal LEMFS and electrothermal molecular absorption spectrometry (MAS)

Molecule	Mode[a]	Halide detection limit (pg)		Improvement factor
		LEMFS	MAS	
MgF	RF	11	2000	182
	NRF	45	2000	44
InCl	RF	15	3000	200
AlBr	RF	70	18 000	257

[a](N)RF = (non)resonance fluorescence.

REFERENCES

1 M. A. Bolshov, A. V. Zybin and I. I. Smirenkina, Spectrochim. Acta, Part B, 36 (1981) 1143.
2 J. Tilch, H.-J. Paetzold, H. Falk and K.-P. Schmidt, Analytiktreffen 1982, Atomspektroskopie, Neubrandenburg, D.D.R., Abstr. Vol., Karl Marx University, Leipzig, 1982, DV 55.
3 H. G. C. Human, N. Omenetto, P. Cavalli and G. Rossi, Spectrochim. Acta, Part B, 39 (1984) 1343.
4 K. Dittrich and H.-J. Stärk, J. Anal. At. Spectrom., 1 (1986) 237.
5 K. Dittrich and H.-J. Stärk, J. Anal. At. Spectrom., 2 (1987) 63.
6 T. Nakahara, T. Wakisaka and S. Musha, Spectrochim. Acta, Part B, 36 (1981) 661.
7 K. Dittrich, Anal. Chim. Acta, 97 (1978) 69.
8 K. Dittrich, Crit. Rev. Anal. Chem., 16 (1986) 223.

9 D. R. Crosley (Ed.), Laser probes for Combustion Chemistry, A.C.S. Symposium Ser. No. 134, American Chemical Society, Washington, DC, 1980.
10 G. A. Capelle and H. P. Broida, J. Chem. Phys., 56 (1972) 149.
11 R. B. Green, L. Hanko and S. J. Davis, Chem. Phys. Lett., 64 (1979) 461.
12 P. Bonczyk and J. A. Shirley, Combust. Flame, 34 (1979) 253.
13 V. M. Donelly and R. F. Karlicek, J. Appl. Phys., 53 (1982) 6395.
14 W. C. Fowler and J. D. Winefordner, Anal. Chem., 49 (1977) 944.
15 K. Dittrich and P. Meister, Anal. Chim. Acta, 121 (1980) 205.
16 K. Dittrich, B. Hanisch and H.-J. Stärk, Fresenius' Z. Anal. Chem., 324 (1986) 497.
17 K. Dittrich and B. Vorberg, Anal. Chim. Acta, 140 (1982) 237.
18 K. Dittrich, B. Y. Spivakov, V. M. Shkinev and G. A. Vorobeva, Talanta, 31 (1984) 39.

Analytica Chimica Acta, 200 (1987) 593—607
Elsevier Science Publishers B.V., Amsterdam — Printed in The Netherlands

MICROWAVE SPECTRAL EMISSION FROM A GLOW DISCHARGE-FILLED 18—26 GHz FABRY-PEROT CAVITY SPECTROMETER

ANDREW S. DAVIS, ACHILLES N. LEONTAKIANAKOS, FARIDA BENMAKROHA, PING WANG, RABIA HAIDER and JOHN F. ALDER*

Department of Instrumentation and Analytical Science, UMIST, P.O. Box 88, Manchester M60 1QD (Great Britain)

GUNNAR THIRUP**

Kemisk Institut, Aarhus Universitet, Langelandsgade 140, DK-8000 Aarhus C (Denmark)

(Received 3rd April 1987)

SUMMARY

A Fabry-Perot semiconfocal cavity resonator containing air at reduced pressure forms part of a Stark-modulated microwave spectrometer operated near the water 22.235-GHz (6_{16}—5_{23}) and ammonia 23.870 GHz (J = 3, K = 3) absorption lines. A glow discharge is formed in the cavity by an 8.333-kHz sinusoidal electric field of strength up to 140 kV m^{-1}. Under these conditions in the pressure region near 0.01—1 mbar, microwave emission from water and ammonia is observed when microwave energy between 4 to 6 dBm (source output power) at frequencies near that of the line is coupled into the cavity. Spectral features indicate that the emitting molecules arise from recombination of H + OH and H + NH_2. Predischarge features indicate that H_2O is excited directly by electron impact with simultaneous dissociation to OH and its excitation. NH_3 appears to be excited indirectly by energy transfer possibly from a metastable state resulting in dissociation to radicals in the discharge. Significant signal/noise enhancement of the signals is found, compared with signals arising from conventional rotational (H_2O) or inversion (NH_3) absorption at these lines.

A glow in a gas at reduced pressure can be used to excite atomic or molecular species by electron impact, recombination or collisional energy transfer from other species. Collisional energy transfer between bromine and hydrogen cyanide has been used to excite maser action from hydrogen cyanide, emission occurring in the far-infrared spectral region [1]. Indeed, the first indication that population inversion could be achieved in a glow discharge of polyatomic molecules occurred in a pulsed discharge far-infrared water maser [2]. Polyatomic molecules that can be made to produce maser action are few. Coleman [3] suggested several possible reasons for this,

*John F. Alder is in charge of Analytical Science at the Department of Instrumentation and Analytical Science and has studied analytical chemistry and spectrometry over two decades, receiving his Ph.D. from the Imperial College of Science and Technology in 1971.
**Gunnar Thirup heads the electronics section, Kemisk Institut, Aarhus University, specialising in microwave spectrometry and ESR studies.

0003-2670/87/$03.50

including problems of relative cross-section, small transition moments, unfavourable relaxation rates and excessive distortion. The excitation is not specific so that all rotational levels within a vibrational state are pumped and selective relaxation would be required to produce a population inversion. Coleman [4] also suggested that lasing levels in water, hydrogen cyanide, hydrogen sulphide and sulphur dioxide may be associated with irregular perturbations of energy levels, arising for example from mixing of the levels. Kneubuhl [5] reported that the molecules capable of emitting in glow discharges comprised dideuterium oxide, water, formaldehyde, ammonia, hydrogen cyanide, hydrogen sulphide, sulphur dioxide and iodine cyanide/dihydrogen.

Amongst the most important energy-loss mechanisms for slow electrons in molecular gases is the excitation of molecular rotational and vibrational levels [6, 7]; indeed, the carbon dioxide laser relies for its action on electron-impact excitation. The electron may attach to the molecule forming a temporary intermediate state which can then decay by emission of the electron, leaving the molecule in an excited vibrational state. Alternatively, the intermediate may dissociate with loss of the electron and ultimately the free radicals may recombine. This phenomenon may be important: Price [8] noted that emission spectra of free radicals in a glow discharge would be expected to occur, but that with the exception of OH and a few others, the radical lifetimes are too short for large enough concentrations to accumulate. Only molecules with stable excited states or those which dissociate into radicals which recombine to give the original molecules show strong emission. Larger molecules may dissociate and reform to yield smaller stable molecules like H_2O, CO or CO_2.

The first maser [9] worked at the ammonia line with $J = 3$ and $K = 3$, 23.870 GHz, utilising a molecular beam. The first maser in a Fabry-Perot cavity also worked at this frequency [10]. The water emission line at 22.235 GHz, 6_{16}—5_{23} has only been detected as a galactic maser source [11] and Bluyssen et al. [12] resolved the hyperfine structure from this source into six lines. The 6_{16} level in H_2O is not metastable, yet the radiative lifetime is much greater than expected, and metastable-like properties have been reported [13]. Del Greco and Kaufman [14] indicated that the product of H_2O reactions in a water-vapour discharge are capable of various other reactions which continuously generate OH radicals and thereby falsely give the appearance of a long lifetime.

In this work, a semi-confocal Fabry-Perot cavity was used as a microwave spectrometer. The operation of this device has been discussed in detail elsewhere [15]. Briefly, the gas under investigation is diluted with air and maintained at reduced pressure (10^{-3}—10^{-1} mbar) whilst being subjected to a sinusoidal electric field (up to 12 kV p-p) and input microwave power up to +6 dBm (see Experimental). Ammonia and water exhibit a quadratic Stark effect and this gives rise to second and fourth harmonics of the Stark field frequency modulating the reflected microwave power from the cavity. A

relationship between the amplitude of the fourth-harmonic signal and the additive gas concentration was demonstrated [15]. The second harmonic of the Stark modulation frequency was preferred for measurements (rather than the fourth harmonic) because its amplitude and signal/noise (S/N) ratio are greater for a given set of conditions [15, 16]. The absorption intensity of the 22.235-GHz water line is 7.21×10^{-6} cm^{-1} [17] and the sensitivity of the spectrometer (S/N = 2) is ca. 7.7×10^{-10} cm^{-1} when the second harmonic is used compared with ca. 2×10^{-9} cm^{-1} for the fourth harmonic.

Theory of the response

If the absorbing gas is present in fractional abundance x in the gas contained in the cavity, the output of the detector diode will be proportional to x [15]. The detected signal is amplified and filtered to extract the second-harmonic component $V_D \cos(2\omega t + \phi)$ which is multiplied by a reference signal of the second harmonic of the Stark modulation, $V_R \cos 2\omega t$; here ω is the angular frequency of the Stark field and ϕ is the phase difference between the reference signal and the detected one. The output of the phase-sensitive detector is then

$$V_R \cos 2\omega t \, V_D \cos(2\omega t + \phi) = (V_R V_D/2) \cos(4\omega t + \phi) - (V_R V_D/2) \cos\phi \tag{1}$$

A low-pass filter after the multiplier is used to remove all but the d.c. component, $(V_R V_D \cos\phi)/2$, and the instrument automatically adjusts the phase angle ϕ to zero or π to maximize the output to $\pm V_R V_D/2$, which is therefore proportional to the amplitude of the second harmonic of the Stark modulation frequency and therefore to $x\gamma$, where γ is the absorption coefficient.

The fractional change in voltage amplitude ΔV of the reflected wave V from the cavity at resonance with the absorbing gas in the cavity is given by $\Delta V/V = x\gamma L$, where L is the equivalent pathlength of the cavity [15] with $\gamma = ANf\,S(\nu, \Delta\nu)$;

$$A = 8\pi^2 |\mu_{ij}|^2 \nu_0^2 / 3ckT\Delta\nu$$

where $|\mu_{ij}|^2$ is the squared transition dipole moment matrix for the transition i,j, ν_0 the line frequency, $\Delta\nu$ the line half-width, and c, k and T have their usual meanings.

$$S(\nu, \Delta\nu) = \Delta\nu^2 / [(\nu - \nu_0)^2 + (\Delta\nu)^2]^2$$

For a Lorentz profile line where ν_0 is the line-centre frequency and ν the frequency over the line profile.

It can be shown that

$$\Delta V/V = xANf\,\Delta V^2 \, [p/2 \cos 2\omega t + (\nu - \nu_0) - p/2]^2 + \Delta\nu^2 \tag{2}$$

where p is the product KE^2, E being the Stark field strength and K a term containing the transition dipole moment matrix [15].

Hershberger [16] showed that the second-harmonic amplitude can be described in terms of h:

$$h = (\nu - \nu_0 - p)/\Delta\nu \tag{3}$$

which is maximal when $h^2 = (p^2/4\Delta\nu^2) - 1$. Under these conditions, the function achieves its maximal value (except for the physically meaningless value $p/\Delta\nu = 0$), when $p/\Delta\nu = 4$. At this point, the two extremes occur when

$$(\nu - \nu_0)/\Delta\nu = 2 \pm 3^{1/2}$$

and the position of the unperturbed line is given by $(\nu - \nu_0)/\Delta\nu = 0$. Under these conditions, the d.c. output of the phase-sensitive detector, V_{dc}, is equal to

$$V_{dc} = V_R V_D x \gamma L/2$$

and the distance in frequency between the two peaks is therefore $2 \times 2^{1/2}\ \Delta\nu$.

The width of the second-harmonic amplitude vs. the frequency of the spectral line is therefore directly related to the half-width at half-height of the line, and the extreme amplitude to the product γx, i.e., to the fractional abundance of absorbing gas in the cavity. The observed width of the second-harmonic function will be a convolution of the line-width contribution and the cavity profile, so that one cannot simply measure linewidths directly, but trends in line width can be followed for a given set of cavity dimensions and Q values. There is also a degree of distortion imposed on the line profile by the cavity, which leads to asymmetry. For amplitude measurements, the two profiles must be carefully aligned.

EXPERIMENTAL

Instrumentation

A block diagram of the apparatus used for second-harmonic detection is shown in Fig. 1. The sinusoidal electric field and microwave power were provided by a Wiltron 6669A sweep generator with a residual frequency modulation of <15 kHz up to 26 GHz (Wiltron, Crowthorne, Berks., England).

The fundamental Stark modulation frequency, f, is generated from an oscillator running at $2f$ by binary division [15]. The signal f is amplified and filtered so that a pure sine wave is impressed on the Stark field electrode. The current in the detector diode circuit is modulated at $2f$ when the source oscillator frequency is near the line-absorption frequency. The $2f$ component is selectively amplified and multiplied with the originally generated $2f$ in an EG & G 5206 phase-sensitive detector. The phase of the signals is automatically adjusted with respect to each other to give maximum output measured at zero frequency and this signal is displayed.

Samples

Natural ammonia and water were studied. Ammonia was taken from a liquefied gas cylinder and blended with air dried over silica gel/molecular sieve 4A. Ambient air was used as the source of water; its relative humidity (which was generally 55 ± 15% relative humidity at 20–25°C) was measured

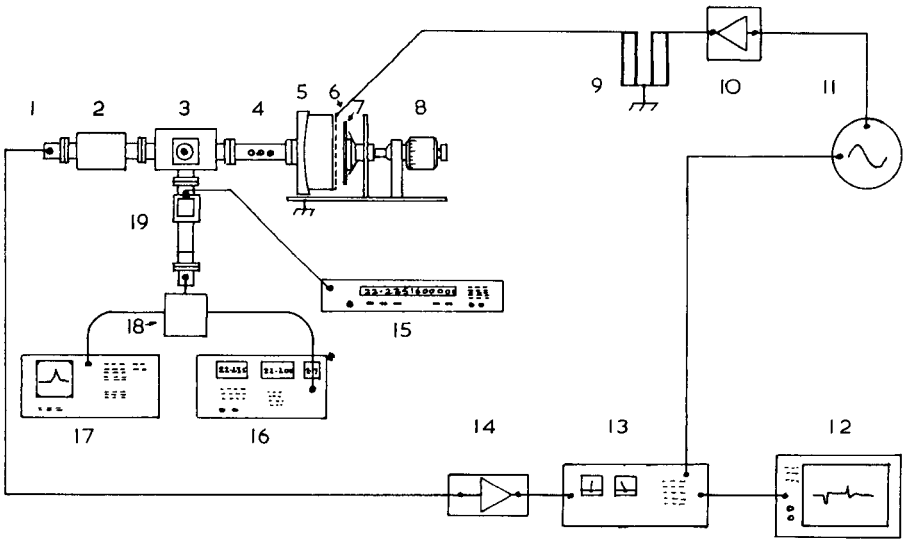

Fig. 1. Block diagram of the spectrometer. (1) Detector diode; (2) isolator; (3) hybrid-T; (4) 3-stub tuner; (5) Fabry-Perot cavity curved mirror with teflon cup; (6) serpentine wire Stark field electrode; (7) Fabry-Perot cavity flat mirror mounted on loudspeaker cone; (8) micrometer adjustment; (9) Stark field transformer; (10) Stark field transformer drive amplifier; (11) Stark field generator; (12) recorder; (13) phase-sensitive detector; (14) tuned high-gain amplifier; (15) microwave frequency counter; (16) microwave sweep generator; (17) scalar network analyzer; (18) microwave bridge; (19) directional coupler (10 dB).

with a wet-and-dry bulb hygrometer and the water content was deduced from Smithsonian tables [18]. The air was blended with dried air for lower concentrations.

RESULTS

Electrical measurements

Preliminary experiments were done to judge the effect of a glow discharge in the Fabry-Perot cavity. With the Wiltron 6669A sweep generator as source, phase and amplitude reflection measurements were made on the cavity and the quality factor Q was derived by plotting these data on a Smith chart. Three sets of data were obtained, for the empty Fabry-Perot cavity, the cavity with the teflon cup in place, and the cavity with a glow discharge in air contained in the teflon cup. The air glow discharge arises from the magnitude of the Stark electric field and not from the microwave field strength. The Q-factors for the first two cases were $Q = 5900$ for the empty cavity and $Q = 4600$ with the cup in place. In the presence of the discharge, the Smith chart plot was distorted but the estimated value for Q was approximately the same as without the discharge present. One might expect the presence of the discharge to alter the loading and coupling between oscillator and cavity, as

the discharge would be more lossy at most frequencies, but these experiments did not indicate any major electrical effects resulting from the presence of the glow discharge.

Behaviour in the pre-breakdown and post-breakdown regions with variation of pressure

Breakdown of a gas subjected to an increasing electric field is not instantaneous but is preceded by an increase in electron density leading eventually to discharge formation. The predischarge state was studied by adjusting the total gas pressure (measured on a Pirani gauge, located out of the discharge region) at constant electric field with a peak amplitude of 7 kV p-p (140 kV m^{-1}). The Stark field modulation frequency was 8.333 kHz and the sweep generator output power was +3.5 dBm. (dBm means decibels above 1 mW). The cavity pressure was varied over the range 0.003—1.0 mbar by varying the gas flow through the inlet valve. The results obtained are shown in Fig. 2. At pressures below 0.04 mbar, the normal second-harmonic signals arising from water and ammonia absorption at their respective frequencies were observed. The most significant point is that the peak-peak signal amplitude from water decreases with rising pressure whereas the signal from ammonia increases as the pressure rises towards the breakdown pressure. In neither case did the width of the spectral line, inferred from the width of the second-harmonic profile, increase, which suggests that the decrease in water intensity represents a depletion in the number of molecules undergoing the 5_{23}—6_{16} transition. For ammonia, however, the rise in the intensity indicates an increase in the number absorbing the radiation.

When the pressure in the cavity is increased, electrical breakdown of the

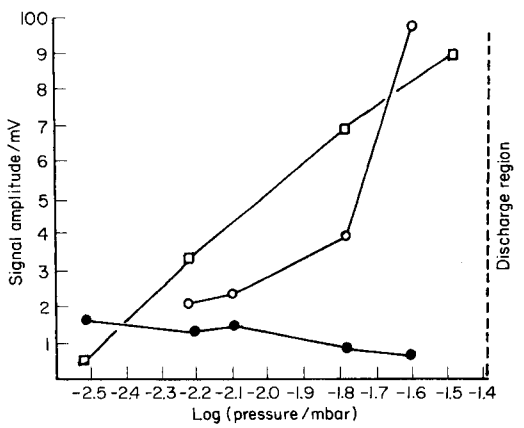

Fig. 2. Second-harmonic amplitude as a function of gas pressure in the cavity for ammonia and water mixtures in air: (□) 100% NH_3; (○) 3 μl l^{-1} NH_3 in air; (●) 1% (v/v) H_2O in air. The ordinate axis is the output of the phase-sensitive amplifier operated at different gain for the different mixtures.

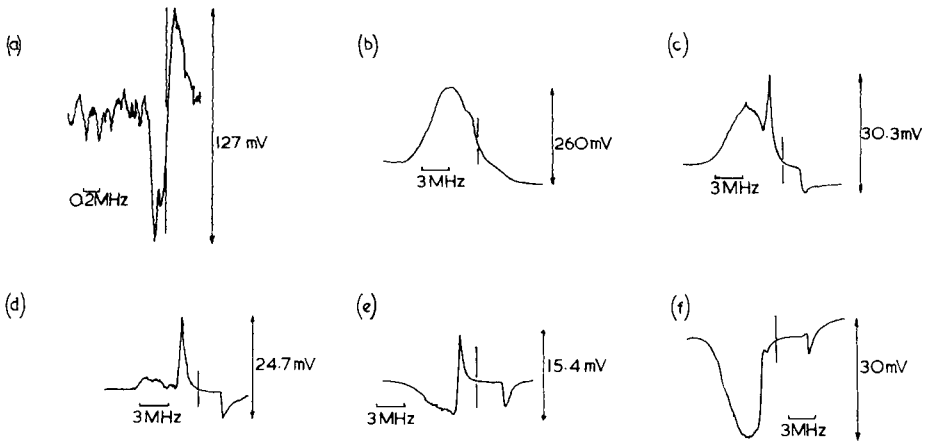

Fig. 3. Variation of the spectral features caused by water with pressure: (a) in the pre-discharge region, p = 0.01 mbar; (b) in the discharge, p = 0.04 mbar; (c) in the discharge, p = 0.07 mbar; (d) in the discharge, p = 0.08 mbar; (e) in the discharge, p = 0.09 mbar; (f) in the discharge, p = 0.10 mbar. The ordinate axes are on different scales and cannot be compared. The S/N ratio of (a) compared to (b—f) indicates the improvement in signal/noise for the emission signals. The vertical bars in the spectra indicate the position for 22.235 GHz.

gas occurs to give a glow discharge. The normal second-harmonic intensity spectra (Fig. 3a) are replaced by much larger, broader and more complex structures (Fig. 3, b—f). There are two major features: a broad profile, about 6 MHz wide and a second narrower feature which is resolved better by slightly increasing the pressure.

Variation of signal amplitude with Stark field strength in the discharge

The Stark field amplitude was varied between 2 and 7 kV (40—140 kV m^{-1}) at a pressure of 0.06 mbar for water and 0.6 mbar for ammonia. The oscillator output power was constant at 4.3 dBm. The concentration of ammonia was 15% (v/v) in air and that of water 0.9% (v/v) in air.

With the glow discharge present, the peak field strength attainable was 140 kV m^{-1} (7-kV peak potential on the Stark field electrode); the discharge could not support a higher field strength. The peak voltage across the primary winding of the Stark field transformer could be increased beyond this point, however, thus increasing the current induced in the secondary circuit through the plasma. This clearly has some influence on the spectral features for water above 140 kV m^{-1}, but rather less on those for ammonia (Fig. 4).

The spectral features undergo radical change over this range of field strengths. Of particular note is the stepped feature in the ammonia series (Fig. 4A), which grows into well-defined peaks reminiscent of the first derivative of a flat-top peak. A similar progression, though less well defined, occurs in the water series.

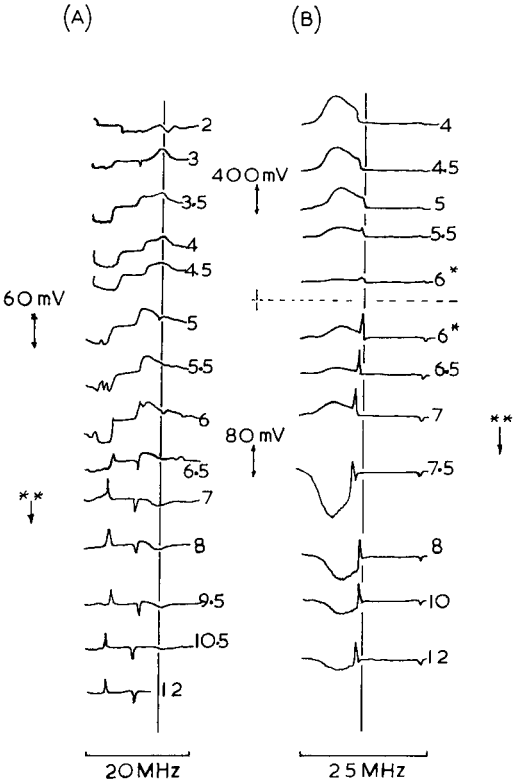

Fig. 4. Variation of spectral features with change in Stark field amplitude from 2 to 12 kV: (A) for 15% NH_3 in air; (B) for 0.9% H_2O in air. (*) A × 5 scale change was made between these points; (**) see text.

Variation of the emission with source oscillator power, and effect of cavity detuning

When a Stark field of 140 kV m^{-1} (7 kV p-p) was used with a pressure of 0.6 mbar for 15% ammonia in air or 0.06 mbar for 0.9% water in air, the output power of the source oscillator output power was changed over the range 0—5.8 dBm. The power threshold was 1.9 dBm for water and 4.3 dBm for ammonia, and the data obtained above these powers are shown in Fig. 5A, B. Below these thresholds, the plots were featureless. At the threshold power, the emission line has the appearance of a normal second-harmonic emission profile. Increasing the power causes the two peaks to separate. Above 6 dBm for the ammonia line, the amplitude of the peaks suddenly diminishes before disappearing; this was not observed for water.

The effect of detuning the cavity was studied by using a 140 kV m^{-1} Stark field at 0.6 mbar pressure and 4.7 dBm oscillator output power and adjusting the cavity mirror spacing to resonate at 23.870 GHz. This point was clearly observable by using the scalar network analyzer and frequency counter. The

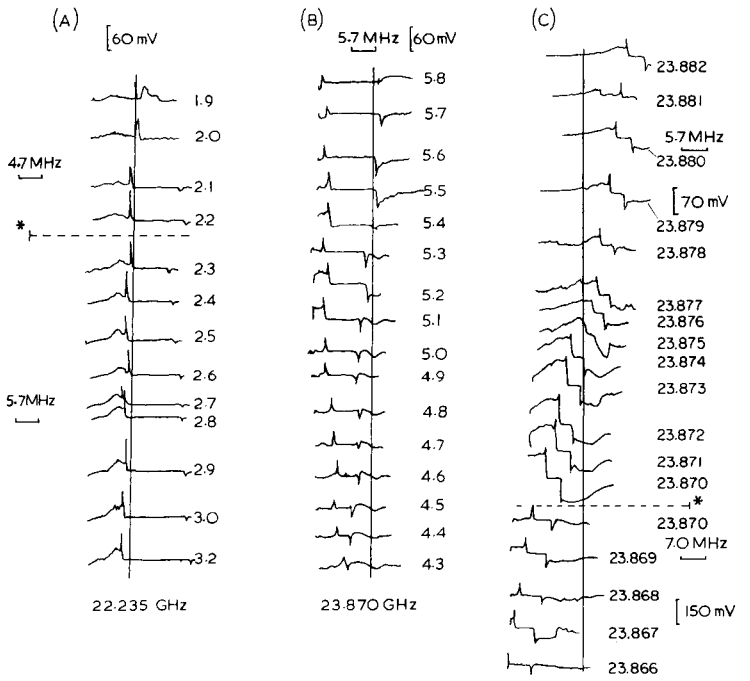

Fig. 5. Variation of emission signals with oscillator power (dBm): (A) for 0.9% H_2O in air; (B) for 15% NH_3 in air. (C) Effect of cavity resonance frequency on spectral profiles near the 23.870-GHz NH_3 line; the vertical line represents the cavity peak resonant frequency shown to the right of each trace, as measured on the counter using the network analyzer as indicator; (*) scale change.

cavity resonant frequency was then altered between 23.882 and 23.866 GHz and the source frequency swept as shown in Fig. 5C. The shape, width and central frequency of the spectral feature change as the cavity resonant frequency moves towards the feature frequency. When the two are coincident, the feature diminishes significantly in amplitude. When the cavity resonance is 70 MHz distant from the ammonia line and beyond, the features disappear.

Mixing of the emission signal with the source frequency

Microwave emission is identified by detecting an emission signal from the cavity at the spectral line frequency. Signals in the discharge region are inherently unlikely to be caused by enhanced absorption but with the detection system used here, it is difficult to discriminate between absorption and emission signals. One way of discriminating is to observe the phase of the detected signal compared with that of the Stark field frequency. A change of phase would be expected in a transition between an absorbing and an emitting cavity, and this was observed when the glow discharge commenced, associated with the increase in amplitude of the detected signal. It would appear from Fig. 5C that the frequency of the emission feature associated with

ammonia is pulled by the cavity and, if the cavity resonance and source frequency were set to coincide at the ammonia absorption line frequency of 23.870 GHz, mixing would occur in the detector diode with any emission signal giving a radiofrequency beat.

The output of the detector diode was connected to the input of a Takeda-Riken (type TR4172) or a Hewlett-Packard (8590A) 1.5-GHz bandwidth spectrum analyzer. With ammonia in the cavity, and appropriate settings, the trace from the spectrum analyzer was as shown in Fig. 6A. No other feature was discernible in the range 10 kHz to 1.5 GHz. The frequency of the feature in the centre of the sweep is 5 MHz, 22 dB above the background. The absolute amplitude of the signals is not important, as the detector response function was indeterminate. In some experiments, a wide-band amplifier was inserted between the detector diode and the spectrum analyzer to act as both buffer and amplifier; a small amount of breakthrough from what was probably local radio stations was then discernible in the 1—2 MHz band. The feature at 5 MHz, as well as the baseline structure, disappeared when the glow discharge was extinguished, or the microwave power was switched off or the Stark field was reduced to zero. The structure disappeared gradually after extinction of the glow discharge, probably because of the signal-averaging system, but perhaps partly because of residual discharge arising from the charge in the teflon cup. This effect was noted at both the ammonia and water line frequencies. The effect was not always reproducible and a considerable amount of adjustment of the various pressure, Stark field and power parameters was needed to establish the beat frequencies. The microwave source power was particularly important but the optimum characteristics have not so far been identified. When the source oscillator frequency was moved away from the 23.870 GHz line, the frequency of the beat changed along with the source oscillator frequency. The difference between

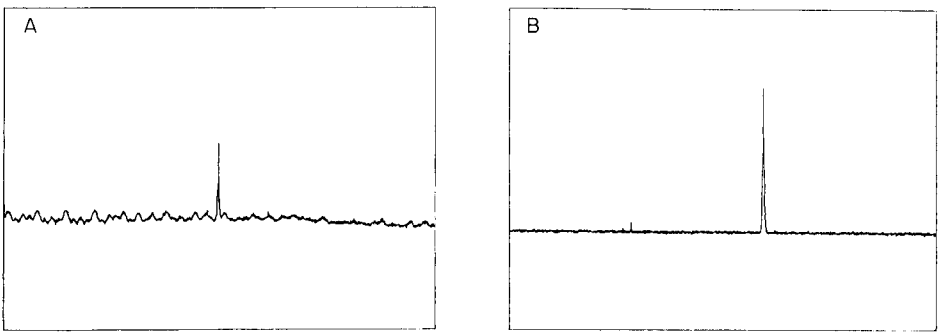

Fig. 6. Spectra with NH_3 in the cavity: (A) output from the detector diode over the range 4.4—5.6 MHz centred at 5.0 MHz, with source power 6 dBm, source frequency 23.870 GHz, pressure 0.2 mbar, Stark field 60 kV m^{-1}; (B) output from the detector diode over the range 141.4—142.6 MHz centred at 142.0 MHz, with source power 6 dBm, source frequency 23.722 GHz, pressure 0.07 mbar, Stark field 56 kV m^{-1}. The vertical axes correspond to 100 dB range.

the source oscillator frequency and the beat frequency gave an indication of the line frequency. The change in this difference with varying source oscillator frequency indicated, after computation, an apparent emission line frequency of 23.865 GHz; in these tests, the source frequency was adjusted between 23.805 and 23.900 GHz, in all cases. The apparent emission line lies about 5 MHz below the NH_3 (J = 3, K = 3) transition. In one experiment, the oscillator was set to 23.722 GHz which corresponds to the NH_3 (J = 2, K = 2) transition ($\gamma = 3.2 \times 10^{-4}$) [17]. A signal appeared at 142 MHz, 44 dB above the background (Fig. 6B); no other feature was observed in the range 10 kHz—150 MHz.

Similar experiments were done at the 22.235 GHz water line. Scans were recorded for various conditions of Stark field, pressure, microwave power input and source oscillator frequency. It was more difficult than had been found with ammonia, to generate conditions which resulted in beats being detectable in the spectrum between 10 kHz and 1.5 GHz. Nonetheless, beats were measured when the source oscillator was moved between 22.2347 and 22.242 GHz. In this instance, the apparent emission frequency changed from about 1.9 MHz below the water absorption line with the source oscillator set at 22.23572 GHz (Fig. 7A), to coincidence with the water absorption line when the source oscillator was at 22.2420 GHz (Fig. 7B). Other frequencies gave results indicating a line which varied gradually between 1.9 MHz below the line frequency and coincidence with the usual line frequency for water absorption.

DISCUSSION

The important finding is that when a glow discharge is present in the spectrometer cavity, spectral emission takes place associated with the 23.870-GHz NH_3 and 22.235-GHz H_2O lines. This may be due to stimulated emission of radiation from the molecular species involved [19] or possibly maser action.

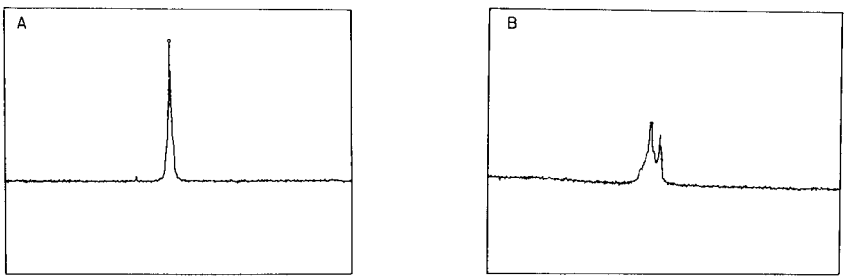

Fig. 7. Spectra with water in the cavity: (A) output from the detector diode over the range 0—5 MHz centred at 2.5 MHz, with source power 4.8 dBm, frequency 22.23572 GHz, pressure 0.14 mbar, Stark field 96 kV m^{-1}; (B) output from the detector diode over the range 4.5—9.5 MHz centred at 7.0 MHz, with source power 4.8 dBm, frequency 22.2420 GHz, pressure 0.14 mbar, Stark field 96 kV m^{-1}. The vertical axes correspond to 100 dB range.

In the pre-breakdown pressure region, the number of H_2O molecules undergoing the 22.235-GHz transition decreases as the pressure is increased towards the discharge pressure. The opposite behaviour is observed for the 23.870-GHz inversion transition of NH_3. Hence, although both species are contained in an air mixture, different mechanisms governing the populations of the transient levels must be involved.

Water is known to be excited by direct electron-impact in a discharge of this type. The excitation mechanism is thought to be the simultaneous dissociation of H_2O and excitation of OH by electron impact [20]:

$$H_2O \rightarrow H + OH\ (^2\Sigma^+)$$

$$OH\ (^2\Sigma^+) \rightarrow OH\ (^2\pi) + h\nu$$

Supporting evidence was provided from earlier work [21] on water-vapour electrical discharges; two predominant excited H_2O states were found of which the lower energy state was not the result of direct H_2O dissociation ($J \approx 5$ level); this agrees with the OH ($^2\pi$) state undergoing recombination. Benedict et al. [22] suggested that recombination of this type would lead to the formation of rotationally and vibrationally excited H_2O.

Ammonia exhibits different behaviour; the signal amplitude and pressure increase linearly for both NH_3 in air and 100% NH_3. The implication is that mechanisms associated with NH_3 excitation are only present sufficiently in the discharge and involve indirect excitation. NH_3 is efficient at deactivating the first metastable state of nitrogen [23] quenching some N_2 emission, and conversely [24] excited N_2 removes the lower NH_3 energy levels. Indirect excitation of NH_3, via interaction with, and deactivation of, the N_2 (A) metastable state (produced by direct electron-impact), could result in excitation and dissociation into radicals in the discharge. The major features of the spectra obtained in the discharge show marked similarity to the first derivatives of the cavity profile and molecular-beam maser profile observed by Gordy [9]. The broad spectral feature must be the cavity resonance because it can be obtained from an air discharge, with no ammonia present, when the cavity is tuned to 23.870 GHz. The narrower feature is an emission line caused by ammonia because a change of phase occurs compared to the pre-breakdown second harmonic, indicating a change from absorption to emission.

The flattened profile is similar to those obtained in square-wave Stark modulation, but such a profile cannot be obtained with sine-wave Stark modulation unless the fundamental emission profile is also flat. There is the possibility that an apparent instrument emission signal could have been generated. Heald and Wharton [25] found that under certain conditions the plasma can increase the coupling between two horn antennae, which could be confused with amplification. However, all the evidence and measurements in this work are against the possibility of non-spectral phenomena as the origin of these signals. A flat spectral line profile of this nature has been observed in the afterglow of a microwave discharge from neon; Biondi [26] associated this with a dissociative recombination mechanism.

Kneubuhl [5] among others has pointed out that a discharge provides non-selective excitation and that for H_2O, one of the easiest modes to excite is the bending mode. Stretching modes may be excited but these require higher energy. It is possible that excited H_2O formed by OH and H recombination will initially exist in a range of bond angles or bond lengths. If emission occurs before this distortion is relieved, then a range of emitted energies will arise which will be discrete because the distortion will be quantized. It is possible that the broad profile of the spectral feature in this work may be due to similar recombination mechanisms.

Both the cavity profile and the emission line amplitude pass through a minimum as the pressure is varied, before changing phase. This is not a property of the emitting species because both NH_3 and H_2O show the same behaviour in an air discharge. The same behaviour, but at higher pressure, was found in a helium-supported discharge, observing the 22.235-GHz H_2O transition.

The features in Fig. 4 associated with increase in Stark field amplitude support the general picture outlined above. The broad feature which changes sign and is particularly noticeable in Figs. 3 (b—f) and 4(B) is associated with the cavity, because it is present with no emitting species present when the cavity resonance is tuned to the source frequency. As the transformer primary drive current is increased, the plasma current and consequently the ionization rate will increase. This may affect the degree of excitation of the H_2O by electron impact, but would not affect the emission intensity, as both upper and lower levels would be equally affected. Direct comparison of the ammonia and water data in Fig. 4 is not possible because of the different pressures used but the same overall trends can be noticed.

The major effect of source oscillator power on the spectral characteristics is its strong influence on the line width, whilst the intensity of the signals is little altered. This is not likely to be a conventional power broadening effect, which one would expect to be associated with a decrease in signal amplitude. The effect of detuning the cavity on the emission feature is significant; when the two coincide, the amplitude of the emission from ammonia is significantly reduced and the linewidth narrows markedly. The reasons for this are not clear.

In some experiments, the concentration of ammonia in the discharge was varied from 3 to 3000 $\mu l\ l^{-1}$ ammonia in air; there did not appear to be any significant difference between the emission intensities with high or low concentrations of ammonia. Given the complex nature of the discharge, it may be that above a low concentration threshold, the effect of concentration on intensity is small, especially as the mechanism appears to be associated with recombination of H and NH_2 or H and OH. It seems likely [8] that only small molecules which produce radicals that can recombine to form their parents rather than stable fragments, will build up sufficient free-radical populations to give strong emission in this way. Potential candidates, are SO_2, H_2S, PH_3, HCN, CNCl, etc. The first time this phenomenon was noticed

[27] was with methanol in air. Analytically, these observations are important, because the signal/noise ratio of these emission features is at least 10—100-fold those of conventional absorption measurements.

When the spectrometer was used in the conventional absorption mode with second-harmonic amplitude measurement, the limits of detection for water and ammonia were 130 μl l^{-1} at the 22.235-GHz water line and 2 μl l^{-1} at the 23.870-GHz ammonia line (pressure 0.01 mbar, Stark field 100 kV m^{-1}) with working ranges up to at least 1% for water and 90% ammonia in air.

This work has been funded from many sources: A. S. D. and R. H. were funded by SERC, A. N. L. by Shell Internationale Petroleum Maatschappij BV, F. B. by the Algerian Government and by her family, P. W. by the Chinese Government and British Council. SERC, Imperial College, UMIST. British Petroleum International Ltd., Servomex Ltd., and the Royal Society of London have also contributed financial support. The original manuscript was read by J. Baker (Manchester University), A. C. Legon (Exeter University), R. Stephens (Dalhousie University) and a number of colleagues. We are most grateful for their helpful comments.

REFERENCES

1 A. B. Peterson and C. Wittig, Appl. Phys. Lett., 27 (1979) 305.
2 H. A. Gebbie, N. W. B. Stone and F. D. Findlay, Nature, 202 (1964) 685.
3 P. D. Coleman, IEEE J. Quantum Electron., 9 (1973) 130.
4 P. D. Coleman, J. Opt. Soc. Am., 67 (1977) 894.
5 F. Kneubuhl, Opt. Acta, 32 (1985) 1055.
6 K. Takayanagi and S. Geltman, Phys. Rev., 138 (1965) A1003.
7 J. C. Ingraham and S. C. Brown, Phys. Rev., 138 (1965) A1015.
8 W. C. Price, in M. Davies (Ed.), Infrared Spectroscopy and Molecular Structure, Elsevier, Amsterdam, 1963, Chap. 13.
9 J. P. Gordy, Phys. Rev., 161 (1967) 367.
10 D. C. Laine and G. D. S. Smart, J. Phys. D, 4 (1971) L23.
11 E. Churchwell, A. Witzel, W. Huchtmeier, I. Pauling-Toth, J. Roland and W. Sieber, Astron. Astrophys., 54 (1975) 969.
12 H. Bluyssen, A. Dymanus and J. Verhoeven, Phys. Lett., 24 (1967) 482.
13 D. M. Rank, Molecular Spectroscopy: Modern Research, Academic, 1971, p. 76.
14 F. P. del Greco and F. Kaufman, Discuss. Faraday Soc., 33 (1962) 128.
15 G. Thirup, F. Benmakroha, A. N. Leontakianakos and J. F. Alder, J. Phys. E., 19 (1986) 823.
16 W. D. Hershberger, J. Appl. Phys., 19 (1948) 411.
17 C. H. Townes and A. L. Schawlow, Microwave Spectroscopy, Dover, New York, 1975.
18 CRC Handbook of Chemistry and Physics, R. C. Weast (Ed.), 60th edn, CRC Press, Boca Raton, FL, 1979.
19 C. E. Hamilton, J. L. Kinsey and R. W. Field, Ann. Rev. Phys. Chem., 37 (1986) 493.
20 H. P. Broda and W. R. Kane, Phys. Rev., 89 (1953) 1053.
21 J. Niira, J. Phys. Soc. Jpn., 7 (1952) 193.
22 W. S. Benedict, M. A. Pollack and W. J. Tomlinson, IEEE J. Quantum Electron., 5 (1969) 108.

23 J. W. Dreyer, P. Pemer and C. R. Roy, J. Chem. Phys., 61 (1974) 3164.
24 R. Burnham, Appl. Phys. Lett., 33 (1985) 156.
25 M. A. Heald and C. B. Wharton, Plasma Diagnostics with Microwaves, Wiley, New York, 1965, p. 202.
26 M. A. Biondi, in E. Bekefi (Ed.), Principles of Laser Plasmas, Wiley, New York, 1976, p. 125.
27 G. Thirup and J. F. Alder, unpublished work (1982).

ANALYTICA CHIMICA ACTA, VOL. 200 (1987)

AUTHOR INDEX

INFORMATION FOR AUTHORS

ailed "Information for Authors" was published in Vol. 190, No. 2, pp. 375–378. A free reprint is available from the ors or from:

vier Editorial Services Ltd., Mayfield House, 256 Banbury Road, Oxford OX2 7DH (Great Britain)

ıes of contribution. The journal welcomes original research papers, short communications and reviews. iews are written by invitation of the editors, who welcome suggestions for subjects. Short communications are ally complete descriptions of limited investigations, and should generally not exceed six printed pages. Preliminary ımunications of important urgent work can be printed within four months of submission, if the authors are ɔared to forgo proofs.

nuscripts. The preferred language of the journal is English, but French and German manuscripts are also ɛptable. For authors whose first language is not English, French or German, linguistic improvement is provided as of the normal editorial processing. Authors should submit three copies of the manuscript in double-spaced typing ɔne side of the paper only, with a margin of 4 cm, on pages of uniform size. If any variety of machine copying is ɔ (e.g. xerox), authors should ensure that all copies are easily legible and that the paper used can be written on ı both ink and pencil. Authors are advised to retain at least one copy of the manuscript. Manuscripts should be ɛeded by a sheet of paper carrying (a) the title of the paper, (b) the name and full postal address of the person to ɔm proofs are to be sent, (c) the number of pages, tables and figures.

rmation on the *submission of papers* is given on the inside front cover.

nmary. Research papers and reviews begin with a Summary (50–250 words) which should comprise a brief ual account of the contents of the paper, with emphasis on new information. Short communications and iminary communications require summaries, which should not exceed 50 words. Uncommon abbreviations, on and reference numbers must not be used. The Summary should be suitable for use by abstracting services ıout rewriting. Papers in French or German require a Résumé or Zusammenfassung preceded by a Title and ımary in English; authors are encouraged to provide translations where necessary.

'oduction. The first paragraphs of the paper should contain an account of the reasons for the work, any essential ɔrical background (as briefly as possible and with key references only) and preliminary experimental work.

ures. Figures should be prepared in black waterproof drawing ink on drawing or tracing paper of the same size as on which the manuscript is typed. One original (or sharp glossy print) and two photostat (or other) copies are ıired. Attention should be given to line thickness, lettering (which should be kept to a minimum) and spacing on ɜ of graphs, to ensure suitability for reduction during printing. Axes of a graph should be clearly labelled, along the ɜ, and outside the graph itself.

igures should be numbered with Arabic numerals, and require descriptive legends. Explanatory information should ılaced not in the figure, but in the legend, which should be typed on a separate sheet of paper. Simple straight-line ɔhs are not acceptable, because they can readily be described in the text by means of an equation or a sentence. ms of linearity should be supported by regression data that include slope, intercept, standard deviations of the ıe and intercept, standard error, and the number of data points; correlation coefficients are optional.

tographs should be glossy prints and be as rich in contrast as possible; colour photographs cannot be accepted. In eral, line diagrams are more informative and less liable to dating than photographs of equipment, which are efore not usually acceptable.

ıputer outputs for reproduction as figures must be good quality on blank paper, and should preferably be ɲitted as glossy prints.

nenclature, abbreviations and symbols. In general, the recommendations of the International Union of Pure Applied Chemistry (IUPAC) should be followed, and attention should be given to the recommendations of the lytical Chemistry Division in the journal *Pure and Applied Chemistry* (see also *IUPAC Compendium of Analytical nenclature*, 1978).

erences. The references should be collected at the end of the paper, numbered in the order of their appearance in text (*not* arranged alphabetically), and typed on a separate sheet.

ıe list of references, the following forms should be adopted.

rnals

I. Lund and M. Salberg, Anal. Chim. Acta, 76 (1975) 131.

1. McDaniel, A. D. Shendrikar, K. D. Reizneir and P. W. West, Anal. Chem., 48 (1976) 2240.

title of the journal must be abbreviated as in the Bibliographic Guide for Editors and Authors.

ks

. D. Perrin, Masking and Demasking of Chemical Reactions, Interscience–Wiley, New York, 1970, p. 188.

. Hofmann, in G. Svehla (Ed.), Wilson and Wilson's Comprehensive Analytical Chemistry, Vol. 9, Elsevier, msterdam, 1979, p. 89.

s of papers are unnecessary. Citations of reports which are not widely available (e.g., reports from government arch centres) should be avoided if possible. Authors' initials should not be used in the text, unless real confusion d be caused by their omission. If the reference cited contains three or more names, only the first author's name wed by et al. (e.g., McDaniel et al.) should be used in the text; but the reference list must contain the initials and es of *all* authors.